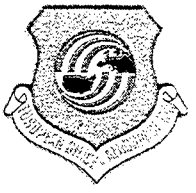
UNIVERSITY OF PARDUBICE

Faculty of Chemical Technology

and

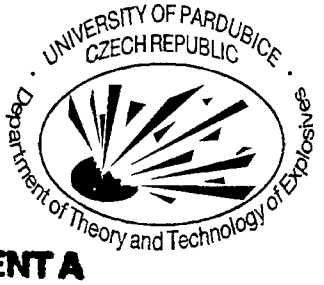
EUROPEAN OFFICE
OF AEROSPACE RESEARCH AND DEVELOPMENT





NEW TRENDS IN RESERCH OF ENERGETIC MATERIALS

PROCEEDINGS OF THE V. SEMINAR



DISTRIBUTION STATEMENT A
Approved for Public Release
Distribution Unlimited

Pardubice, Czech Republic

April 24 - 25, 2002

REPORT DOCUMENTATION PAGE

Form Approved OMB No. 0704-0188

Public reporting burden for this collection of information is estimated to average 1 hour per response, including the time for reviewing instructions, searching existing data sources, gathering and maintaining the data needed, and completing and reviewing the collection of information. Send comments regarding this burden estimate or any other aspect of this collection of information, including suggestions for reducing the burden, to Department of Defense, Washington Headquarters Services, Directorate for Information Operations and Reports (0704-0188), 1215 Jefferson Davis Highway, Suite 1204, Arlington, VA 22202-4302. Respondents should be aware that notwithstanding any other provision of law, no person shall be subject to any penalty for failing to comply with a collection of information if it does not display a currently valid OMB control number.
PLEASE DO NOT RETURN YOUR FORM TO THE ABOVE ADDRESS.

1. REPORT DATE *(DD-MM-YYYY)*	2. REPORT TYPE	3. DATES COVERED *(From – To)*
30-04-2002	Conference Proceedings	24 April 2002 - 25 April 2002

4. TITLE AND SUBTITLE

New Trends in Research of Energetic Materials, 5th Seminar

5a. CONTRACT NUMBER
F61775-02-WF049

5b. GRANT NUMBER

5c. PROGRAM ELEMENT NUMBER

6. AUTHOR(S)

Conference Committee, Prof Svatopluk Zeman

5d. PROJECT NUMBER

5d. TASK NUMBER

5e. WORK UNIT NUMBER

7. PERFORMING ORGANIZATION NAME(S) AND ADDRESS(ES)

University of Pardubice
CZ-532 10
Pardubice
Czech Republic

8. PERFORMING ORGANIZATION REPORT NUMBER

N/A

9. SPONSORING/MONITORING AGENCY NAME(S) AND ADDRESS(ES)

EOARD, ONRIFO
PSC 802 BOX 14 and BOX 39
FPO 09499-0014

10. SPONSOR/MONITOR'S ACRONYM(S)

11. SPONSOR/MONITOR'S REPORT NUMBER(S)
CSP 02-5049

12. DISTRIBUTION/AVAILABILITY STATEMENT

Approved for public release; distribution is unlimited.

13. SUPPLEMENTARY NOTES

14. ABSTRACT

The Final Proceedings for New Trends in Research of Energetic Materials, 5th Seminar, 24 April 2002 - 25 April 2002

The fifth consecutive Seminar on new trends in research of energetic materials is intended to be a worlds meeting of young people and university teachers working in the field of teaching, research, development, processing, analysing and application of all kinds of energetic materials. A subject of interest for this Seminar includes also explosions of the gaseous, dispersing and condensed systems. It will not be aimed only at the exchange of professional information but also to create pleasant meeting where young specialists from different countries will have the opportunity to meet and gain personal contacts.

15. SUBJECT TERMS

EOARD, Explosive Devices, Energetic Materials, Propellants

16. SECURITY CLASSIFICATION OF:			17. LIMITATION OF ABSTRACT	18, NUMBER OF PAGES	19a. NAME OF RESPONSIBLE PERSON
a. REPORT	b. ABSTRACT	c. THIS PAGE			Ingrid Wysong
UNCLAS	UNCLAS	UNCLAS	UL	470	19b. TELEPHONE NUMBER *(Include area code)* +44 (0)20 7514 4285

UNIVERSITY OF PARDUBICE
Faculty of Chemical Technology
Department of Theory & Technology of Explosives
CZ-532 10 Pardubice

EUROPEAN OFFICE OF AEROSPACE RESEARCH AND DEVELOPMENT
London NW1 5TH United Kingdom

PROCEEDINGS

of the fifth Seminar

„NEW TRENDS IN RESEARCH OF ENERGETIC MATERIALS"

held at the University of Pardubice,

Pardubice, the Czech Republic

April 24 – 25, 2002

20020531 117

intended as a meeting of students, postgraduate students, university teachers and young research and development workers concerned from the whole world

AQ F02-08-1613

NOTICE

This publication has not been submitted to language corrections
and contributions have not been reviewed.

The only distributor of the present publication is the
Department of Theory & Technology of Explosives, University of Pardubice,
CZ-532 10 Pardubice,
where the publication can be ordered or gained by exchange of similar publications.

Contributions of the Proceedings will be quoted in the Chemical Abstracts.

March 30th, 2002

Close

Editor:
Jiří Vágenknecht

Edition 1st, impression 150 issues
Pressed by the Edition Centre of University of Pardubice

© University of Pardubice, 2002

ISBN 80-7194-435-1

Seminar is held under the aegis of his magnificence,

Prof. Miroslav Ludwig, Ph.D.,
rector of the University of Pardubice

and in support of

European Office of Aerospace Research and Development,
Air Force Office of Scientific Research,
United States Air Force Research Laboratory,
and **United States Office of Naval Research.**

Chairman of the Seminar:

Prof. Svatopluk Zeman, D.Sc.

Scientific Committee:

Prof. José Campos (*Univ. of Coimbra, Portugal*)
Dr. Adam S. Cumming (*DSTL, Fort Halstead, Sevenoaks, U. K.*)
Dr. Stanislaw Cudziło (*Military Univ. of Technology, Warsaw, Poland*)
Prof. Li Bing-ren (*Inst. of Chem. Materials, CAEP, Sichuan, China*)
Prof. Boris Lur'e, D.Sc. (*Mendeleev's Univ. of Technology, Moscow*)
Prof. Andrzej Maranda, D.Sc. (*Military Univ.of Technol., Warsaw, Poland*)
Prof. Gurdip Singh (*DDU Gorakhpur Univ., Gorakhpur, India*)
Dr. Muhamed Sućeska (*Brodarski Inst., Zagreb, Croatia*)
Assoc. Prof. Pavel Vávra, Ph.D. (*Univ. Pardubice*)
Assoc. Prof. Boris Vetlický, Ph.D. (*Univ. Pardubice*)
Dr. Fred Volk, (*ICT Pfinztal, Germany*)
Dr. Woodward Waesche (*Office of Naval Res. Int. Field Office, USA*)
Prof. Ou Yuxiang (*Beijing Institute of Technology,Beijing China*)

Organizing Committee:

Jiří Vágenknecht, Ph.D. (*Univ. Pardubice*)
Zdeněk Jalový, Ph.D. (*Univ. Pardubice*)
Marcela Jungová, M.Sc. (*Univ. Pardubice*)
Břetislav Janovský, Ph.D. (*Univ. Pardubice*)
Miloslav Krupka, Ph.D. (*Univ. Pardubice*)
František Masař, M.Sc. (*Univ. Pardubice*)
Jiří Pachmáň, M.Sc. (*Univ. Pardubice*)
Robert Matyáš, M.Sc. (*Univ. Pardubice*)
Robert Matyáš, M.Sc. (*Univ. Pardubice*)
Martin Kouba, M.Sc. (*Univ. Pardubice*)

Financial Support:

EOARD, London
Dr. Machacek, president of the UTeC, Dallas
University of Pardubice

CONTENT

PREFACE 10

A S Cumming - Chairman CEPA 14
Defence Science and Technology Laboratory (Dstl), Sevenoaks, UK
CEPA 14 – A MECHANISM FOR EUROPEAN COLLABORATION ON ENERGETIC MATERIALS AND THEIR APPLICATIONS 11

B.P. Aduev, E.D. Aluker and A.G. Krechetov
Kemerovo State University, Krasnaya 6, Kemerovo, 650043, Russia
PRE-EXPLOSIVE PROCESSES IN HEAVY METAL AZIDES 18

Alexander M. Astachov *, Alexander D. Vasiliev **, Maxim S. Molokeev **,Ludmila A. Kruglyakova *, and Rudolf S. Stepanov *
* Siberian State Technological University Krasnoyarsk, Russia, 660049
** Institute of Physics RAS (Sib. branch) Krasnoyarsk, Russia, 660036
1,2-DINITROGUANIDINES: STRUCTURE – PROPERTY RELATIONSHIPS 29

Li Bing-ren and Li xianming
Insitute of Chemical Materilas, China Academy of Engineering Physics, Mianyang, 621900,Sichuan,China
STUDY ON THE DESENSITIZATION OF PLASTIC BONDED BIS(β,β,β-TRINITROETHYL- N-NITRO)ETHYLENEDIAMINE 42

Stanislaw Cudziło and Waldemar Andrzej Trzciński
Military University of Technology, Kaliskiego 2, 00-908 Warsaw 49, POLAND
THERMOCHEMICAL ANALYSIS OF COMBUSTION PROCESS OF GAS GENERANTS CONTAINING SODIUM AZIDE 48

Luisa Durães*, José Campos and António Portugal***
Laboratory of Energetics and Detonics
*Chem. and **Mech. Eng. Departments - Fac. of Sciences and Technology,
University of Coimbra - Polo II - 3030-290 Coimbra - PORTUGAL
IRON OXIDE/ALUMINUM FAST THERMITE REACTION DRIVEN PROPAGATION 56

Eisner A.*, Ventura K.* and Varga R.**
* Univerzity of Pardubice, Faculty of Chemical -Technology, Department of Analytical Chemistry,
Nám. Čs. Legií 565, Pardubice 532 10, CZ
** Univerzity of Pardubice, Faculty of Chemical - Technology,
Department of Theory and Technology of Explosives, Nám. Čs. Legií 565, Pardubice 532 10, CZ
DETERMINATION OF ADDITIVES FROM EXPLOSIVE MATERIALS WITH GC/MS (EI,NCI) 57

L. Čačić*, Z. Ester and M. Dobrilović****
*Ministry of Interior, Zagreb, Republic of Croatia
**Faculty of Mining, Geology and Petroleum University of Zagreb, Republic of Croatia
DETERMINATION OF THE DETONATION VELOCITY EMULSIONS EXPLOSIVES IN THE DIFFERENT THERMAL CONDITION 60

Gurdip Singh and Prem Felix S
Department of Chemistry, DDU Gorakhpur University, Gorakhpur -273 009, India
DETERMINATION OF THE DETONATION VELOCITY EMULSIONS EXPLOSIVES IN THE DIFFERENT THERMAL CONDITION THERMOLYSIS OF A PLASTIC BONDED EXPLOSIVE 69

Marcel Hanus
Military Institute for Weapon and Ammunition Technology, 763 21 Slavičín, CZ
NEW METHODOLOGIES FOR MILITARY EXPLOSIVE MATERIALS TESTING IN THE CZECH ARMY 78

Martina Chovancová, Peter Očko, Rastislav Ševčík, Ľuboš Čavojský, Jozef Lopúch
Military Technical and Testing Institute Záhorie, Slovak Republic
STABILITY INVESTIGATION OF PLASTIC EXPLOSIVES DURING THEIR AGEING PROCESS 87

Zdeněk Jalový, Robert Matyáš
University of Pardubice, Department of Theory and Technology of Explosives,
532 10 Pardubice, Czech Republic
THE INFLUENCE OF REACTION CONDITIONS ON TEX SYNTHESIS **93**

Marcela Jungová and Jiří Strnad
Department of Theory and Technology of Explosives,University of Pardubice, Czech Republic
INITIATION STRENGTH OF DETONATORS – AIR GAP TEST METHOD. A SURVEY OF EXPERIMENTAL RESULTS **100**

Jiří Kočí, Svatopluk Zeman, Jiří Majzlík and Jiří Strnad
Department of Theory & Technology of Explosives, University of Pardubice
CZ-532 10 Pardubice, Czech Republic
NOTICES TO DETERMINATION OF THE ELECTRIC SPARK SENSITIVITY OF ENERGETIC MATERIALS **111**

Miloslav Krupka and Svatopluk Zeman
Department of Theory & Technology of Explosives, University of Pardubice,
CZ-532 10 Pardubice, Czech Republic
STUDY OF THERMAL STABILITY AND COMPATIBILITY OF 2,3-DIMETHYL-2,3-DINITROBUTANE (DMDNB) **128**

A. Książczak* and T. Wolszakiewicz**
*Department of Chemistry, Warsaw University of Technology, Noakowskiego 3, 00 – 664 Warsaw, Poland *
**Institute of Organic Industrial Chemistry, Annopol 6, 03 – 236 Warsaw, Poland **
THERMODYNAMIC PROPERTIES OF BINARY SYSTEM NITROCELLULOSE + 2,4,6 – TRINITROTOLUENE **136**

Andrzej Maranda*, Katarzyna Lipińska and Marek Lipiński****
*Military University of Technology, 2 Kaliskiego str. 00-908 Warsaw, Poland
**Institute of Industrial Organic Chemistry 6 Annopol str. 03-236 Warsaw Poland
APPLICATION IN MINING BLASTING AGENTS **146**

V.A. Malchevsky, N.A. Zarytovskaya and T.A. Mikhailikova
D.I. Mendeleev Russian Chemical Technological University, Miusskaya pl. 9, Moscow, 125047
MECHANICAL DESTRUCTION OF ENERGETIC POLYMERIC COMPOSITES (EPC) **151**

Andrzej Maranda*, Barbara Gołąbek and Johann Kasperski****
*Military University of Technology, Warsaw, POLAND
**BLASTEXPOL, Duninów, POLAND
DETONATION AND APPLICATION CHARACTERISTICS OF THE LATEST GENERATION OF EMULSION EXPLOSIVES **159**

Pavel MAREČEK and Kamil DUDEK
ALIACHEM a.s., Division SYNTHESIA, Research Institute of Industrial Chemistry (RIIC),
532 17 Pardubice - Semtín, Czech Republic
CAST TNAZ MIXTURES **165**

František Masař, Pavel Vávra and Jiří Vágenknecht
University of Pardubice, KTTV, 530 12 Pardubice, CZ
DETERMINATION OF PHYSICAL CHARACTERISTICS OF DETONATION PRODUCTS **170**

Alevtina S. Medvedeva*, Luybov P. Safronova, Maria M. Demina, Galina S. Lyashenko,Vladimir V. Novokshonov, Andrei V. Afonin and Galina I. Sarapulova
A. E. Favorsky Irkutsk Institute of Chemistry, Siberian Branch of the Russian Academy of Sciences,
664033 Irkutsk, Russian Federation
SYNTHESIS OF NEW HETEROCYCLIC AZIDONITRAMINES **175**

R. Mendes, J. Campos, I. Plaksin and J. Ribeiro
LEDAP - Lab. of Energetics and Detonics, Mech. Eng. Dept., Fac. of Sciences and Technology,
Polo II, University of Coimbra, 3030-201 Coimbra, Portugal
DEVELOPMENT OF THE DIVERGENT DETONATION WAVE IN PBX BASED ON RDX **178**

Milka Matejic Grguric
Tehnicki opitni center, Vojvode Stepe br. 445, 11000 Belgrade, Serbia, Yugoslavia
ON THE STABILITY OF EMULSION SLURRY EXPLOSIVES 185

Maciej Miszczak, Eugeniusz Milewski, Jan Szymanowski, Jacek Borkowski, Andrzej Marczuk and Beata Śmigielska
Research Department of Combat Means, Military Institute of Armament Technology,
Wyszyńskiego Str .7, 05-220 Zielonka, POLAND
A CONTACT COMPATIBILITY INVESTIGATIONS BETWEEN SMOKELESS POWDERS AND EPOXIDE PAINT BY MEANS OF TGA, DSC THERMAL ANALYSIS AND ISOTHERMAL HEATING AT 75°C 190

Maciej Miszczak, Jacek Borkowski, Eugeniusz Milewski, Jan Szymanowski, , Andrzej Marczuk and Beata Śmigielska
Research Department of Combat Means, Military Institute of Armament Technology,
Wyszyńskiego Str. 7, 05-220 Zielonka, POLAND
CONTACT COMPATIBILITY INVESTIGATIONS OF HIGH-ENERGETIC MATERIALS USED IN MORTAR AUGMENTING PROPELLING CHARGES 200

Joel Morgado*, Luisa Durães, José Campos* and António Portugal****
Laboratory of Energetics and Detonics
* Mech. and Chem.** Eng. Departments - Fac. of Sciences and Technology
University of Coimbra - Polo II – 3030 Coimbra - PORTUGAL
IRON OXIDE/ALUMINUM FAST THERMITE REACTION USING NITRATE ADITIVES 208

Sanja Matečić Mušanić, Muhamed Sućeska and Bakija Sanko
Brodarski institut – Marine Research & Special Technologies, Av. V. Holjevca 20, 10020 Zagreb, Croatia
INFLUENCE OF TESTING CONDITIONS ON RESULTS OF DYNAMIC MECHANICAL ANALYSIS OF DOUBLE BASE ROCKET PROPELLANTS 223

Aleš Nepovím*, Radka Podlipná*, Hartmuth Thomas, Andre Gerth**, Zdeněk Jalový***, Svatopluk Zeman*** and Tomáš Vaněk***
*Dept. of Plant Tissue Cultures, Institute of Organic Chemistry and Biochemistry, AS CR, Flemingovo nám. 2, 166 10 Praha 6, Czech Republic.
**Bioplanta GmbH, Delitzsch, Germany
*** Dept. of Theory and Technology of Explosives, University of Pardubice, 532 10 Pardubice, Czech Republic
STUDY OF BIODEGRADATION OF SELECTED EXPLOSIVES BY PLANTS - ALTERNATIVE WAY OF SOIL AND WATER DECONTAMINATION 234

Andrzej Orzechowski[*], Witold Pągowski[*] and Andrzej Maranda[**]
[*]Institute of Industrial Organic Chemistry
[**]Military Academy of Technology
RESEARCH OF PHYSICOCHEMICAL PROPERTIES OF PLASTIC EXPLOSIVE 238

Ou Yuxiang, Liu Lihua, Chen Boren and Lijin
School of Chemical Engineering & Material Science, Beijing Institute of Technology,Beijing 100 081, China
SYNTHESIS AND CRYSTAL STRUCTURE OF TETRAACETYLDICHLOROACETYLHAXAAZAISOWURTZITANE TRIHYDRATE 247

Jiří Pachmáň*, Marcel Hanus and Jakub Šelešovský***

*University of Pardubice, Dept. Theory and Technology of Explosives, 532 10 Pardubice, CZ
**Military Institute for Weapon and Ammunition Technology (VTÚVM), 763 21 Slavičín, CZ
SOME ASPECTS OF SERVICE LIFE EVALUATION OF COMPOSITE ROCKET PROPELLANTS 252

Miroslav Pospíšil*, Pavla Čapková*, Pavel Vávra and Svatopluk Zeman[**]**
* Department of Chemical Physics and Optics, Faculty of Mathematics and Physics,
Charles University Prague, Ke Karlovu 3, 12116 Prague 2, Czech Republic
** Department of Theory and Technology of Explosives, University of Pardubice,
53210 Pardubice, Czech Republic.
CHARACTERISATION OF EXPLOSIVE MATERIALS USING MOLECULAR DYNAMICS SIMULATIONS 263

Maša Rajić and Muhamed Sućeska
Brodarski institut - Marine Research & Special Technology, Av. V. Holjevca 20, 10000 Zagreb, Croatia
THERMAL PROPERTIES OF A NITROCELLULOSE PROPELLANT UNDER ACCELERATED AGEING CONDITION 272

Tadeusz J. Rychter, Andrzej Teodorczyk
Warsaw University of Technology, ITC, Nowowiejska 25, 00-665 Warszawa, Poland
PARAMETERS IN CLOSED AND VENTED VESSELS 281

Camilla Sandberg*, Nikolaj Latypov*, Patrick Goede*, Rolf Tryman* and Anthony J. Bellamy**
* FOI, Swedish Defence Research Agency, Department of Energetic Materials, S-147 25 Tumba, Sweden
** Department of Environmental and Ordnance Systems, Cranfield University,
Royal Military College of Science, Shrivenham, Swindon, Wilts SN6 8LA, England.
ACID-BASE CHARACTERISTICS OF FOX-7 AND ITS MONOHYDRAZO ANALOGUE 293

Sergey Smirnov and Boris Lurie
Mendeleev University of Chemical Technology, Miusskaya sq. 9, Moscow, 125047, Russia
KINETICS AND MECHANISM OF TRIAMINOGUANIDINE NITRATE THERMAL DECOMPOSITION 301

Muhamed Sućeska
Brodarski institut - Marine Research & Special Technologies, Av. V. Holjevca 20, 10000 Zagreb, Croatia
ON RESULTS OF PROPELLANTS SELF-IGNITION NUMERICAL MODELING 309

Andrzej Teodorczyk
Warsaw University of Technology,
ITC, Nowowiejska 25, 00-665 Warszawa, Poland
AN ANALYSIS OF LARGE SCALE ETHYLENE RELEASE AND EXPLOSION 324

Waldemar Andrzej Trzciński, Radosław Trębiński and Stanisław Cudziło
Military University of Technology, Kaliskiego 2, 00-908 Warsaw, POLAND
ANALYSIS OF THE MOTION OF METAL PLATES IN MODEL REACTIVE ARMOURS 331

Miroslava Trchová*, Irina Sapurina and Jaroslav Stejskal*****
* Charles University Prague, Faculty of Mathematics and Physics, 180 00 Prague 8, CZ
** Institute of Macromolecular Compounds RAS, St. Petersburg 199004, RUS
*** Institute of Macromolecular Chemistry AS CR, 162 06 Prague 6, CZ
FTIR SPECTROSCOPIC STUDY OF THE PROTONATION OF CONDUCTING POLYMER WITH ENERGETIC COMPOUND 339

Jiří Vágenknecht*, Zbyněk Akštein and Pavel Vávra***
* University of Pardubice, Department of Theory and Technology of Explosives, 530 12 Pardubice, CZ
** Research Institute of Industrial Chemistry (RIICH), 532 17 Pardubice - Semtin, CZ
MEASUREMENT OF DETONATION VELOCITIES OF FORMED LINEAR CHARGES 349

Pavel Vávra*, Miroslav Pospíšil, Jarmila Repáková****
* Department of Theory and Technology of Explosives Faculty of Chemical Technology,
University of Pardubice, 53210 Pardubice, Czech Republic
** Department of Chemical Physics and Optics, Faculty of Mathematics and Physics, Charles University
12116 Prague, Czech Republic
EFFECT OF INTERMOLECULAR FORCESON SOME PROPERTIES OF EXPLOSIVES 358

Richard Wild
Diehl Munitionssysteme GmbH & Co. KG, Werk Maasberg, MML, D-66620 Nonnweiler, Germany
ENERGETIC MATERIALS FOR INSENSITIVE MUNITIONS 384

Fred Volk
Fraunhofer Institut Chemische Technologie (ICT), D-76327 Pfinztal-Berghausen
PERFORMANCE PARAMETERS OF EXPLOSIVES: EQUILIBRIUM AND NONE-EQUILIBRIUM REACTIONS 385

Stephan Wilker, Uldis Ticmanis, Gabriele Pantel
WIWEB Außenstelle Heimerzheim, Großes Cent, 53913 Swisttal, Germany
HEAT CONDUCTIVITY MEASUREMENTS OF EXPLOSIVES

Shu Yuanjie, Dong Haishan, Liu Shijun, Liu Yonggang, Song Huajie, Hao Ying, Zhan Chunhong and Chen Jie
Institute of Chemical Materials CAEP, 621900, Mianyang, Sichuan, China
EFFECT OF MOLDING POWDER PRODUCTION, CHARGE PRESSING AND AGING ON PARTICLE SIZE OF EXPLOSIVES **400**

Svatopluk Zeman and Miloslav Krupka
Department of Theory & Technology of Explosives, University of Pardubice, CZ-532 10 Pardubice, Czech Republic
STUDY OF THE IMPACT REACTIVITY OF POLYNITRO COMPOUNDS PART I. IMPACT SENSITIVITY AS "THE FIRST REACTION" OF POLYNITRO ARENES **407**

Svatopluk Zeman and Miloslav Krupka
Department of Theory & Technology of Explosives, University of Pardubice,
CZ-532 10 Pardubice, Czech Republic
STUDY OF THE IMPACT REACTIVITY OF POLYNITRO COMPOUNDS PART II. IMPACT SENSITIVITY AS A FUNCTION OF THE INTERMOLECULAR INTERACTIONS **416**

Svatopluk Zeman*, Zdeněk Friedl and Radim Huczala***
* Department of Theory & Technology of Explosives, University of Pardubice,
CZ-532 10 Pardubice, Czech Republic
** Faculty of Chemistry, Brno University of Technology, CZ-612 00 Brno, Czech Republic
STUDY OF THE IMPACT REACTIVITY OF POLYNITRO COMPOUNDS PART III. RELATIONSHIP BETWEEN ELECTRONIC CHARGES AT NITROGEN ATOMS OF PRIMARILY SPLIT OFF NITRO GROUPS AND IMPACT SENSITIVITY OF SOME POLYNITRO ARENES **427**

Svatopluk Zeman
Department of Theory & Technology of Explosives, University of Pardubice,
CZ-532 10 Pardubice, Czech Republic
STUDY OF THE IMPACT REACTIVITY OF POLYNITRO COMPOUNDS PART IV. ALLOCATION OF POLYNITRO COMPOUNDS ON THE BASIS OF THEIR IMPACT SENSITIVITIES **435**

Product Education Session

Jiří Chládek
Jiří Chládek - AALL, Sulova 1247, CZ-156 00 Prague
EXPLOSIVE AND METAL DETECTORS **445**

J. Zeman and J. Chládek
ZEMAN Co., Otrokovice, Czech Rep.
AM - BLAST PROTECTIVE BOOTS **446**

PREFACE

This is the fifth seminar "New Trends in Research of Energetic Materials" and the fourth in the series of seminars organised by the Department of Theory and Technology of Explosives (DTTX) at the University of Pardubice. The original purpose of these meetings was to teach young research workers how to present their results in front of scientific audience. Starting with the second seminar, these meetings have become international – at first Czech-Polish-Slovak (the second seminar in 1999) and then Czech-Polish-Slovak-Croatian (the third meeting in 2000). The fourth seminar in 2001 was already conceived a worldwide meeting of young research workers and university teachers. The original aim of these meetings was thus complemented by not only the exchange of findings and experience but in particular making friendly contacts between the members of the beginning young generation of experts in the area of energetic materials coming from many countries all over the world.

With regard to economic situation of the middle European countries, Balkan and former Soviet Union, no fee was and is asked from the participants. The main load of financing was always on DTTX. In one case this load was partially shared by Research Institute of Industrial Chemistry (Synthesia Pardubice) and Military Institute for Weapon and Ammunition Technology (Slavičín). A significant financial support was regularly provided by the long-term co-worker of DTTX – Austin Detonator Comp. (Vsetín). In the case of the fourth seminar, also DTTX members contributed from their private sources.

The activities of this year fifth seminar is sponsored by European Office of Aerospace Research and Development, Air Force Office of Scientific Research, United States Air Force Research Laboratory, and United States Office of Naval Research, Europe. A certain financial support was also provided by Dr. Machacek, president of the Universal Tech. Corporation, Dallas. The efficient help in ensuring smooth and successful course of the meeting obtained from all these institutions is gratefully acknowledged. We greatly appreciate that thanks to this sponsoring all the above-mentioned specifics of earlier seminars could be maintained.

On the eve of this fifth seminar there was held a two-day session of the steering committee of CEPA 14 (group of energetic materials) of Western Europe Armaments Group in the Congress Hall of the University of Pardubice. This session as well as the subsequent participation of its members in our seminar has contributed to publicity of the seminar and, last but not least, also publicity of our University. Cordial thanks are due to the organisers of the said session.

Finally, I wish to thank the members of the Scientific Committee, the authors of all the seminar papers and lastly but not the least, you, the participants of this seminar, for its success and its influence on the continued success and growth of all future meetings at our University of *young* people and university teachers working in the field of teaching, research, development, processing, analyzing and application of all kinds of energetic materials.

The next sixth seminar of this type is intended to be dedicated to the 50th anniversary of the beginning of teaching of the science of explosives at the Faculty of Chemical Technology of the University of Pardubice. Allow me to use this opportunity for inviting you in the name of my co-workers and myself: we are looking forward to meet you at the sixth seminar in the second half of April 2003 in the Aula Magna of our University.

Pardubice, March 30th, 2002



Svatopluk Z e m a n

CEPA 14 – A MECHANISM FOR EUROPEAN COLLABORATION ON ENERGETIC MATERIALS AND THEIR APPLICATIONS

A. S. Cumming
Chairman CEPA 14

Defence Science and Technology Laboratory (Dstl), Sevenoaks, UK

Abstract:

In a world where science and technology develops rapidly, and where there is need to maintain credible defence capability, there is a real need for collaborative mechanisms to enable allies to work together on Research and Technology. Only in this way can limited budgets be used most effectively, while maintaining an awareness and involvement in the state-of-the-art. CEPA 14, one of the Western European Armament Group CEPAs, covers Energetic Materials and their Applications and provides a means for such collaboration. It history and purpose are outlined together with a description of the programmes both under way and planned. Future strategy is also described.

1. INTRODUCTION

The official history of the WEAG is quoted below (1).

In 1976, the Defence Ministers of the European NATO nations (except Iceland) established a forum for armaments co-operation, the Independent European Programme Group (IEPG). The Declaration agreed by the WEU Ministers in Maastricht on 10 December 1991 called for further examination of the possibilities for enhanced co-operation in the field of armaments, with the aim of creating a European Armaments Agency. At their meeting in Bonn in December 1992, the Defence Ministers of the 13 countries of the IEPG decided upon the transfer of the functions of the IEPG to the WEU.

Furthermore they agreed six basic principles for the transfer, principal among which were:

- All 13 nations should be entitled to participate fully and with the same rights and responsibilities, in any European armaments co-operation forum.
- There should be a single European armaments co-operation forum.
- Armaments co-operation in Europe should be managed by the National Armaments Directors of all the 13 nations, who will be accountable to the Ministers of Defence of those governments.
- The existing links with NATO and European Defence Industry Group should be maintained.

At the meeting of the WEU Council of Ministers in Rome in May 1993, the Defence Ministers of the IEPG reaffirmed the six key principles on which armaments co-operation should be based, and in particular that all decisions on these matters within the WEU framework should be taken by the 13 nations. They agreed on a number of organisational

aspects of the transfer which were subsequently adopted formally by the Council at 13. Since that meeting the WEU armaments co-operation forum has been known as the Western European Armaments Group (WEAG).

At their meeting in Marseilles in November 2000, WEAG Defence Ministers agreed to the accession to WEAG full membership of six new nations: Austria, the Czech Republic, Finland, Hungary, Poland and Sweden.

WEAG numbers now 19 full members each enjoying the same rights and responsibilities.

The objectives of the WEAG are the following:

- more efficient use of resources through, increased harmonisation of requirements;
- the opening up of national defence markets to cross-border competition;
- to strengthen the European defence technological and industrial base;
- co-operation in research and development.

As part of the initial approach to R&T co-operation, Technical Areas were set up. One of these, called TA25, concentrated on explosives and their processing. This TA contained three programmes covering injection moulding, pressed shaped charges and energetic binders. These were successful, not only scientifically, but also in bringing together the various partners.

When IEPG was replaced by the Western European Armaments Group 1992, a more comprehensive structure was produced aimed at allowing industry more formal participation in programmes and to provide an overarching agreement to ease the agreement process.

The areas of activity were originally called Common European Priority Areas (CEPAs), and the first of these were set up in the late eighties. Some 82 specific Projects which are part of the 13 Common European Priority Areas (CEPAs) now active, have been agreed

CEPA 14 was one of the second group of CEPAs, set up in 1994 to address a perceived need. Its original remit was to seek ways of collaborating on Energetic Materials, and it built on the success of the earlier TA programmes already mentioned. There was a significant amount of research on Energetic Materials within Western Europe, and since the TA mechanism had shown that there were opportunities for collaboration, it seemed appropriate to investigate the possibilities. Since then several programmes have been started, and the existing TA programmes have been drawn to successful conclusions. The WEAG organisation is shown in the diagram below.

The WEAG Organisation

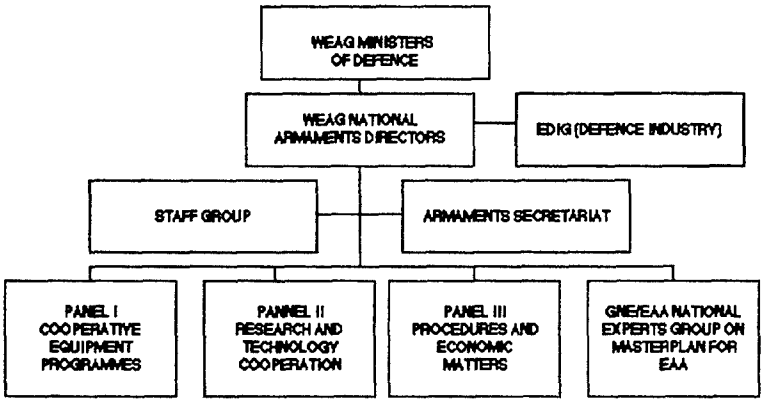


Fig 1. Panel II is responsible for oversight of the CEPA research activities.

CEPA 14 membership has grown and it now contains twelve nations. It is led by the UK. The current members are:

Denmark Finland France Germany Italy Netherlands Norway Portugal Spain Sweden Turkey ***United Kingdom***

Not all of the members are involved in all the programmes, nor might all stay within the CEPA, but it does provide a large and flexible group from which to draw for research. As mentioned earlier industry is heavily involved as a full participant, and this adds significantly to the range of experience and abilities available to the CEPA.

Industry has a significant role through CEPA Industry Group (CIG) 14, which formally links the various communities. In reality, most CEPA meetings are joint CEPA/CIG meetings.

The CEPA is supported by a Research Cell in Brussels, which organises the formal approval of the programmes by National Armament Directors, and provides contract and administrative support.

2. AIMS AND OBJECTIVES

Energetic materials cover Explosives, Gun and Rocket propellants and Pyrotechnics. The CEPA covers not only the manufacture but also the assessment and use of these materials, including performance and vulnerability assessment. This requires that CEPA 14 also covers Terminal Effects, in particular performance prediction, design of applications, as well as their behaviour under stimulus. The increase in the breadth has provided opportunities to develop more integrated research programmes.

The aim of the CEPA is to develop and manage collaborative programmes, within its technical area, amongst the participants to meet common military needs and fill capability

gaps. It requires that its members be aware of these military needs and of the available technology which might answer the requirements. Future strategy and planning is also required.

3. MILITARY FUNCTION AND APPLICATIONS

Energetic Materials are the basis of almost all weapons systems and their reliable and safe performance is crucial for weapon effectiveness. Their funding is also essentially military specific. The major themes of direct military application are being addressed by the CEPA and can be listed as

- Improved performance
- Reduced vulnerability through Hazard Assessment (in particular for Insensitive Munitions)
- Higher Quality coupled with reduced cost of manufacture
- Cost Effectiveness in Development, Production and Lifetime Management
- Demilitarisation and Environmentally Acceptable Disposal
- Novel Concepts to improve characteristics, eg Signature, Erosion, Production etc

These technologies have application in almost all systems: missile propulsion, gun propulsion, warheads, and related applications such as gas generators and electro-thermal systems. Ignition and proper functioning are also covered. A specific aim is to develop sufficient understanding to provide performance prediction for use in all types of systems. The ability to provide high quality, low cost materials of known and satisfactory performance and vulnerability is the goal of much European research.

CEPA 14 aims to review national needs; national capabilities and devise programmes to fill the gap. The CEPA also provides a means to compare needs and technology and to ***identify*** gaps. The CEPA involves industry as well as government and offers the opportunity to learn form each other, ***and to apply what we have learned.***

The area consists of enabling technology, and so suffers from distance from the application BUT proper use will provide improved performance and ownership cost and joint consideration of needs will provide novel solutions for applications.

4. PROJECTS TO DATE AND IN DEVELOPMENT

There are two main mechanisms for collaboration, based round separate Memoranda of Understanding. The original or EUCLID Memorandum involves a contract with an industrial consortium, and the programmes are designated RTPs. The single contract is let and overseen by the Research Cell, though payments and money is controlled by the participating nations. The second mechanism is under the THALES MoU, which produces JPs. These are more like traditional collaborative programmes where much of the work is undertaken by government institutes. In addition there is a formal means of seeking industrial proposals under EUCLID. This EUROFINDER process involves a conference once a year in Brussels where proposals are invited and the options discussed.

The CEPA strategy is to be as pragmatic and flexible as possible, within the procedures, remembering that these exist to enable the CEPA to deliver applicable solutions to the military users. The CEPA operates by mutual briefings followed by Workshops on areas of significant common interest. These Workshops not only provide in depth briefings, but could also produce a programme proposal, and include government, industry and academia. Part of the role of the CEPA is to review the progress of such programmes.

At present any such programmes are open to any member of WEAG. As some areas are subject to commercial or other sensitivities, this could limit activity. A new MoU, EUROPA, allows for closed groupings, and this should expand the possible activities significantly. The CEPA will be attempting to determine how this affects its procedures during the next year.

The CEPA has already addressed some of the areas identified as important by the participating nations. A summary was given at the 4th WEAG R&T Symposium(2). The following programmes are already running or nearing commencement. The lead nation is given in bold. A paper on RTP 14.1 will be given in Bordeaux. Other papers deriving from the CEPA programme will be given from time to time.

greener. — reduced signature

RTP14.1	[**FR** IT NL NO PO SP TU UK]	Clean Rocket Propellants
RTP14.2	[FR IT NL PO **UK**]	Insensitive Munitions, Modelling and Testing
JP14.4	[NL **PO** UK]	Ignition Systems
JP14.5	[NL IT SP TU **UK**]	Low Vulnerability Charge Systems
RTP14.6	[DE **UK**]	Demilitarisation of Conventional Munitions
JP14.7	[FR **GE** IT UK]	Submarine Vulnerability Codes
RTP14.8	[**FR** NO]	Anti-bunker shell
JP14.9	in development	Flare Compositions
RTP14.10	in development	Synthesis of organic nitrocompounds
RTP14.11	in development	Bullet and Fragment Attack
RTP14.12	under consideration	Reclamation of Land contaminated by explosives

Further programmes are under discussion and cover micro-detonics and thermochemistry of pyrotechnics.

CEPA 14 also responsible for management of one TA of the IEPG programmes

TA29	[FR GE IT UK]	Submarine warhead performance

All these programmes include a sharing of the understanding and risk amongst the partner nations.

And include the sharing of the research base and costs. They build on common understanding and pursue its development into common technology. However, they need to be further developed into common applications

This is the challenge for CEPA 14!

5. OPPORTUNITIES FOR FURTHER WORK

There have been several changes in priority and capability since CEPA 14 was formed. The addition of new nations has extended the likely interest significantly, and the addition of application areas has necessitated a change in approach. These additions also mean that other industrial partners are available, so it is essential to review and consider the options available, and this is under way.

If this approach is to be taken successfully, it will be necessary to include industry and academia as fully as possible. Industry will have its own priorities, which should extend and complement those of government. They may also clash with governmental priorities, so a mechanism to deal with this is essential. Academia is equally important as a source of innovation and basic research able to supplement both governmental and industrial capabilities. This input will be more significant for the longer term viability of the CEPA.

Industry is becoming increasingly global, which will affect how the CEPA does its business. There is the possibility of increasing interdependence amongst the nations, but this will not happen rapidly. It is clear that a flexible and dynamic approach is essential.

Most participants in CEPA 14 are in the process of reviewing their national priorities and technical bases, and it is essential that this debate informs the CEPA activities, and that the CEPA provides timely and effective briefings to inform the national and international debate. This information can be in the form of briefings, studies or the results of collaborative programmes. What is required is that a flexible and inclusive approach is adopted to ensure that all parties can contribute, and that proper and timely advice is presented.

Despite the longer term developments, a healthy CEPA requires that new programmes and areas are developed to meet changing needs. Several areas are being investigated at present. These include:

- Development of Equations of State for Next Generation Explosives
- The study of Terminal Effects as a means of assessing Energetics effectiveness and providing research targets
- The study of cost effective explosives processing for a whole range of applications
- Warhead studies
- Gun and Rocket propulsion studies

RTP 14.10 will add Czech Rep

6. FUTURE DIRECTIONS

It is essential that the CEPA evolves to meet requirements, and provides information to help define those requirements.

The Strategy has been developing rapidly in recent months, including the formal adoption of applications areas. The extension of the CEPA's interests help focus the strategy, allowing the CEPA to examine applications of technology as well as the technology itself.

Part of the overall strategy of WEAG is to propose demonstrator programmes aimed at proving the technology etc in a European context, and CEPA 14 intends to be part of this.

The developing strategy includes closer industrial/institutional links and the CEPA has proven a useful forum for developing a small strategy group, tentatively called ENERG, with membership from France, Germany, Sweden, The Netherlands and the UK. The aim of the group is to 'create a coordination group in order to develop their cooperation and to promote, on a European basis, the development and use of Energetic Materials, the associated skills, tools and expertise, and the related research and technology activities.'

The advent of EUROPA will give greater impetus to the development of closer links, possibly leading to degrees of interdependence, and it will be essential that the CEPA manages this properly. It is equally important that the WEAG develops some mechanism for more formal links with other nations, for example the USA.

7. CONCLUSIONS

CEPA 14 has proven to be a useful and effective vehicle for European collaboration. This is largely due to the commitment and enthusiasm of the participants. The flexibility and pragmatism already demonstrated must continue if the CEPA is to achieve its goals.

Acknowledgments

Thanks are due to the members of CEPA 14 for their enthusiasm, and hard work. This must include the members of the WEAG Research Cell, whose support has been invaluable. In particular, thanks must go to the Secretary of CEPA 14, Peter Flower, now of QinetiQ.

REFERENCES

[1] WEAG Web site; www.weu.int/weao

[2] Proceedings of the 4th WEAG R&T Symposium, Naples, March 2001

© Crown Copyright, Dstl 2001

PRE-EXPLOSIVE PROCESSES IN HEAVY METAL AZIDES[1]

B.P. Aduev, E.D. Aluker and A.G. Krechetov

Kemerovo State University, Krasnaya 6, Kemerovo, 650043, Russia

Abstract

The results of the investigations of the processes of slow and explosive decomposition of heavy metal azides are summarized. A new class of chemical reactions – solid-phase chain reactions involving quasi-particles has been discovered on the basis of numerous experimental data.

1. INTRODUCTION

Chain reactions has been of great interest for researchers for more than a half of century. It is a well-developed field of chemical and nuclear physics including explosion, nuclear energetics and nuclear weapons.

A wealth of experimental data on mechanisms for chemical chain reactions in gases and liquids has been accumulated [1]. A common feature for all these reactions is the presence of active particles (free atoms or radicals) providing chain reactions resulting from real migration causing impacts and reactions with actual molecules of gases and liquids. Neutrons are active particles in chain reactions of heavy nuclei fission.

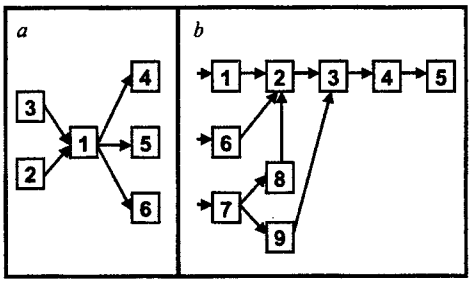


Fig. 1. The scheme of apparatus for the investigating the explosive decomposition.
a – the general scheme of apparatus:
1 –sample, 2 – excitation source (laser, electron accelerator) 3 –source of probing light, 4, 5, 6 –registration channels of optical, acoustic and electrical signals, respectively.
b – the scheme of signal registration channels:
1 – acoustic detector, 2 – oscillograph, 3 – television reading device, 4 – interface, 5 – computer, 6 – conductivity measuring cell, 7 – spectral device (monochromator, spectrograph) 8 – photomultiplier, 9 –streak camera.

The same process in solids remains much more ambiguous so far. Firstly, the number of processes having a chain nature as has been experimentally verified is rather limited. Secondly, there exists a number of fundamental difficulties as to understanding the nature of active particles providing for chain reactions in solids. Actually, a real migration of active particles such as atoms (or radicals) along the crystal lattice can only result from rather slow diffusion processes. Hence, it may be assumed that in this case electron excitations of the crystal lattice, viz. electrons, holes and excitons are active particles providing for the chain nature of the process [2-4]. However, it is still

[1] The present work was supported by the Russian Fund for Basic Research (01-03-32015a).

unknown in what way the energy released during the chemical reaction provides for the multiplication of electron excitations.

A fundamental aspect of the problem is to make use of quasi-particles (electrons, holes and excitons) in solids as active particles providing for the chain nature of the process.

The applied aspect of the problem is to prove the chain nature of the explosive decomposition of explosives (primary explosives first of all) [5].

That is why a number of investigations aimed at discovering and studying chain reactions involving electron excitations in primary explosives (HMAs) has been lately carried out at Kemerovo State University. The results of the investigations make up the content of the present paper.

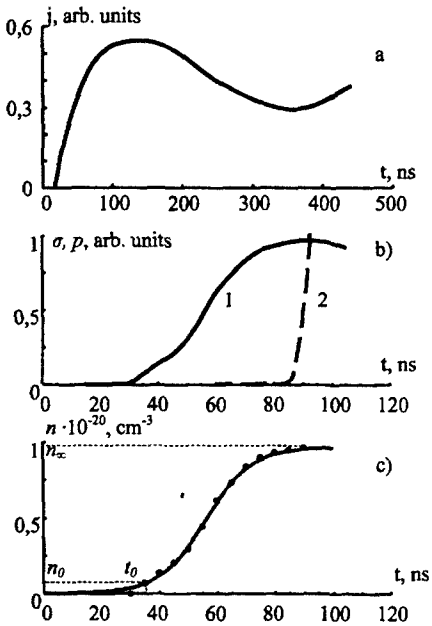


Fig. 2. Kinetics of AgN_3 whiskers explosive conductivity.
a – complete oscillogram of the current pulse,
b – initial site of explosive conductivity pulse (pre-explosive conductivity)
1 – conductivity
2 – leading edge of acoustic signal
c – kinetics approximation by equation (3).
(solid line – the calculation according to the expression (3),
points show the n values calculated on the basis of experimental σ values , t_0, n_0 are the time and concentration corresponding to the appearance of reliable registered current signal.

2. OBJECTS AND PROCEDURE

Silver azide (AgN_3), thallium azide (TlN_3) and lead azide (PbN_6) were synthesized by the dual-jet crystallization [6]. The concentrations of the main impurities (Fe, Si, Ca, Mg, Al, Na) were determined by polarographic and complexometric analysis and did not exceed $10^{16} \div 10^{17}$ cm^{-3}. The investigated PbN_6 and TlN_3 samples as pressed tablets and the AgN_3 samples as whiskers with characteristic dimensions 0,1 × 0,05 × 10 mm^3 and macrocrystals (0,5 × 3 × 3 mm^3) were used The density of cation vacancies did not exceed 10^{16} cm^{-3} [6].

The basic principles of both pulse radiolysis and photolysis [7-10] were the basis for the instrument configuration for this study (Fig.1).

3. EXPLOSIVE CONDUCTIVITY

The explosion was initiated by a laser pulse. Uniform initiation was ensured by covering the interelectrode gap by a laser beam, the energy of exciting photons (λ = 1064 nm) being in the optical transparence range (the optical width of the band gap in silver azide ~3,5 eV, the thermal width ~1,5 eV [11]).

A typical profile of the explosive conductivity pulse is shown in Fig.2[a]. The simplest explanation for the observed kinetics is that the rise of conductivity in the first peak is assotiated with the still intact crystal (predetonation conductivity), the decay of the first peak corresponds to rupture of discontinuity of the sample due to growing stresses induced by decomposition and the next rise is related to the conductivity of explosion products (plasma).

In order to verify the above assumption the following series of experiments was carried out. The sample was mounted by its lateral face against the input window of the acoustic detector to allow one to synchronically measure both the acoustic signal and the conductivity signal. The onset of the sample deformation resulting in its mechanical fragmentation was determined from the leading edge of the acoustic detector signal. The sample conductivity preceding the leading edge of the acoustic signal (Fig.2[b]) corresponds to the intact sample, i. e. it can be identified as predetonation conductivity.

The concentration of conductivity electrons in the crystal $n \approx 5 \cdot 10^{20}$ cm^{-3} [14] corresponds to the maximum values of the recorded conductivity 1000 $\Omega^{-1} \cdot$cm^{-1} (Fig.2[c]) at $\mu = 10$ cm^{2}V$^{-1} \cdot$s^{-1} [12,13]. The resulting estimate of n as an approximation of characteristic values for metals indicates a very unusual state of the material in the predetonation phase, which can probably be regarded as a special kind of phase transition. It can serve as a reference point for an experimentally justified choice between the concepts of thermal and chain explosions of HMAs [1].

As the thermal width of silver azide band gap is ~1,5 eV [11], the equilibrium concentration of electron-hole pairs is about 10^{-10} cm^{-3} at 523 K (the melting point of AgN_3 [2]). Consequently, the experimental values of σ in the predetonation state unequivocally rule out the thermal mechanism of explosive decomposition and can be regarded as direct experimental proof that the explosion of HMAs is a chain reaction.

A series of experiments on the effect of external electromagnetic fields on slow decomposition of HMAs is of special importance [12,13]. Most of the interesting and unexpected effects obtained in the experiments have not been satisfactorily interpreted so far. However, that the processes of slow decomposition of HMAs is also of a chain nature leaves no doubt on the basis of the above papers.

The simplest quantitative description of the kinetics of the type in Fig.2[c] is represented as:

$$\frac{dn}{dt} = \alpha \cdot n - \beta \cdot n^2 \qquad (1)$$

where n is the density of holes (electrons).

The solution of Eq. (1) at $n(t_0) = n_0$ is:

$$n(t) = \frac{\exp[\alpha \cdot (t - t_0)]}{n_\infty^{-1} \cdot \{\exp[\alpha \cdot (t - t_0)] - 1\} + n_0^{-1}} \qquad (2)$$

where n_∞ is the density on the plateau, and t_0 and n_0 are the time and density at which the density attains a value that can be reliably measured. The value of n in Fig 1[c] is calculated from the relation: $\sigma = e \cdot n \cdot \mu$ with $\mu \approx 10$ cm^{2}V^{-1}s^{-1}. It should be emphasized that parameters t_0, n_0 and n_∞ in Eq. (2) have been evaluated directly from the experimental curve and the only fitting parameter is α. For all the investigated samples the values α and β lie in the intervals $10^8 - 10^9$ s^{-1} and $10^{-11} - 10^{-12}$ cm^3 s^{-1}, respectively.

The simplest interpretation for Eq. (1) whose solution is given by Eq. (2) is as follows. The growth (branching) of the chain is governed by a monomolecular process (αn), and its breaking by a bimolecular process (βn^2). It is reasonable to analyze the experimental values α and β in order to advance the a sensible hypothesis concerning the nature of corresponding processes. The simplest approach is to start with $\beta = \upsilon \cdot S_r$, where υ is thermal electron (hole) velocity, and S_r – the cross-section of the process inducing the breaking of the chain. For $\upsilon \approx 10^7$ cm s^{-1} we have $S_r \approx 10^{-18} \div 10^{-19}$ cm^2. These values are typical of indirect interband recombination [15], i.e., the simplest interpretation of bimolecular breaking of the chain, ($\beta \cdot n^2$), is the interband recombination of electrons and holes.

The simplest interpretation of the linear branching of a chain ($\alpha \cdot n$) is the trapping of a hole by a point defect. In this case $\alpha = \upsilon \cdot S_l N$, where υ is the thermal velocity, S_l – the capture cross-section, and N – the density of defects. For $\upsilon \approx 10^7$ cm s^{-1} and $N \approx 10^{15}$ cm^{-3} (the typical density of cation vacancies in AgN_3 whiskers) S_l was ~ 10^{-14} cm^2, i.e. the characteristic capture cross-section for trapping by the attractive center [16]. Thus, the branching of the chain may be related to the trapping of a hole by the cation vacancy (the attractive center).

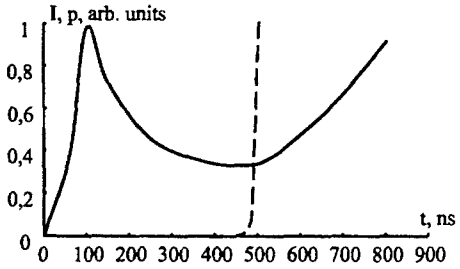


Fig. 3. Kinetics of AgN_3 whisker explosive luminescence (λ = 550 nm, the initiation was performed by laser pulse, crystal was mounted on a flat cell in contact with acoustic detector), solid line – light signal, dotted line - leading edge of acoustic signal..

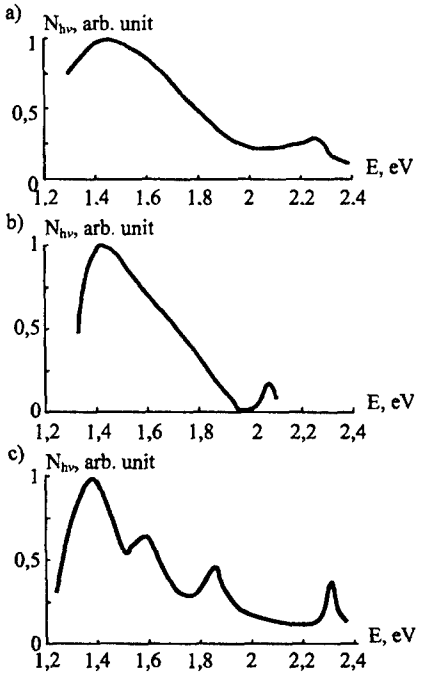


Fig. 4. HMA predetonation luminescence spectra of AgN_3 (a), $Pb(N_3)_2$ (b), TlN_3 (c)

4. EXPLOSIVE LUMINESCENCE

The shape of the light pulse accompanying the explosive decomposition of HMAs (Fig.3) resembles that of the current pulse (Fig.2[a]) and suggests that this luminescence consists of two components: predetonation luminescence (the first maximum) and luminescence of the explosion products (the next rise). At any rate, the part of the luminescence preceding the onset of the acoustic signal (Fig.3) is undoubtedly associated

with the intact sample and can be identified as predetonation luminescence. This conclusion has been confirmed by the luminescence spectral composition at different stages of explosive decomposition [11,17,18].

Predetonation luminescence is of major interest. The spectrum of this luminescence (Fig. 4[b]) or at least part of it cannot be described by the Planck formula, attesting to its nonthermal nature and identifying the light radiation as predetonation luminescence [10,19,20].

Certain properties of this luminescence necessary for better understanding the nature and mechanism of explosive decomposition are as follows.

1. In all the objects the short-wavelength boundary of the luminescence lies in the optical transparency region. This result allows one to eliminate the photomultiplication process as a probable mechanism of hole multiplication discussed elsewhere [3].
2. A large part of the predetonation luminescence spectrum corresponds to photon energies grater than the HMA thermal band gap width (1÷1,5eV). Thus, the luminescence discussed is hot luminescence [21].
3. Synchronous measurements of the predetonation conductivity and predetonation luminescence show that this luminescence is observed in the range of very high band charge carriers densities (~10^{20} cm^{-3}) [10].
4. It has been shown that the mechanical fragmentation of a sample is preceded by partial melting. Consequently, predetonation luminescence is observed at close to melting point temperatures, at which luminescence is usually extinguished [21,22].

The reabsorption-corrected luminescence kinetics is represented by a curve leveling off into a plateau (Fig. 5) and is very similar to the kinetics of the predetonation conductivity (Fig.2). This similarity is more than outward appearance. The corrected luminescence kinetics as is the case for the predetonation conductivity kinetics is well approximated by the solution of the equation:

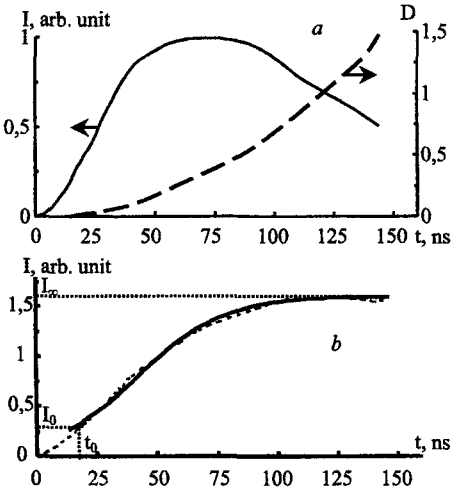


Fig. 5. *Kinetics of AgN_3 whisker explosive luminescence (λ = 550 nm, the initiation was performed by laser pulse)*
a – luminescence signal (solid line) and optical absorption (dotted line),
b – luminescence kinetics corrected for reabsorption. Dotted line shows the calculation of luminescence signal and optical density by experimental values, solid line – the calculation by equation (4), t_0 is the time at which luminescence signal is a reliable registered I_0 value.

$$\frac{dI}{dt} = \alpha \cdot I - \beta \cdot I^2 \tag{3}$$

which has the form

$$n(t) = \frac{\exp[\alpha \cdot (t - t_0)]}{I_\infty^{-1} \cdot \{\exp[\alpha \cdot (t - t_0)] - 1\} + I_0^{-1}} \tag{4}$$

where t_0 is the time at which I(t) attains a value I_0 that can be reliably measured, and I_∞ is the value of $I(t)$ on the plateau. As in the case of the predetonation conductivity, the value of the constant α in Eqs. (3) and (4) lie in the interval $\alpha = 10^8 \div 10^9$ s^{-1} for different samples.

The present authors suppose that the coincidence of both predetonation luminescence and predetonation conductivity kinetics is very important fact confirming that they reflect the kinetics of the basic process: explosive decomposition. This must be taken into account in constructing a model of predetonation luminescence and explosive decomposition on the whole.

The predetonation luminescence properties enable one to considerably limit the range of possible model of this phenomenon.

Above all, the condition $\hbar\omega > E_g$ and the absence of the temperature extinction of this luminescence rule out all types of luminescence associated with local centers [21,22].

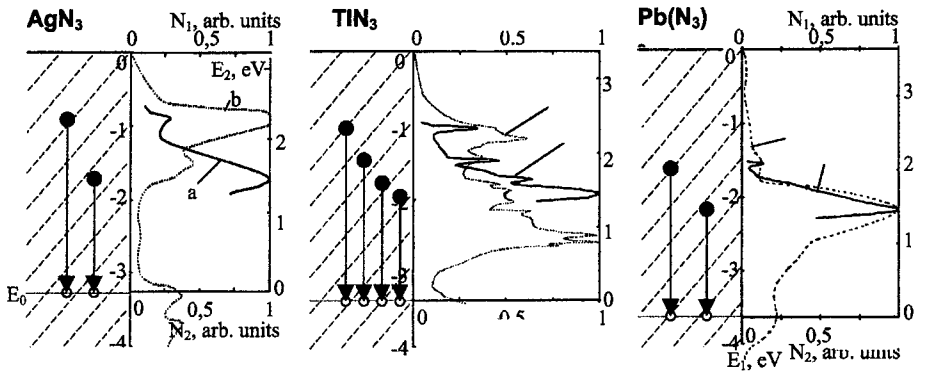
The comparison of the spectra of predetonation luminescence with the band structure data [16,23,24] also serves to rule out such types of fundamental luminescence as edge, exciton and cross-luminescence [21,22,25].

Thus, the only luminescence we should discuss is the intraband luminescence due to radiative transitions of hot electrons and holes in the conduction and the valence bands, respectively. However, the present authors failed to discern any reasonable correlation between the band structure of the objects under investigation and the predetonation luminescence spectra, which is one of the basic approaches used to identify the intraband luminescence [26].

An altogether different picture emerges when the valence band is , assumed to contain quasi-local hole states. If a level corresponding to a quasi-local hole state is present in the interior of the valence band at a distance of 3,2 eV for AgN_3, at 3,4 eV for TlN_3, and at 3,6 eV for PbN_6 from the top of the valence band, a distinct correlation is observed between the luminescence maxima and the density-of-state peaks (Fig.6). The present authors have failed to obtain an analogous correlation, for a level corresponding to a quasi-local state in the conduction band.

All this has enabled us to propose intraband radiative transitions of valence band electrons into quasi-local hole states situated in the depth of the valence band as a model of predetonation luminescence (Fig.6). Inasmuch as the lifetime of hole in quasi-local state is at most ~ 10^{-14} s [27] these states must be continuously generated during explosive decomposition.

It should be also mentioned that the detrapping of holes from a quasi-local state produces hot holes, which can cause hole multiplication as a result of impact ionization and, hence, the development of a chain reaction.



n of the predetonation luminescence (a) and the density-of-states in the valence band (b)
for *$(N_3)_2$.*
E_1 *or density-of-states*
E_2 and N_2 - the scale for the predetonation luminescence spectrum, E_0 - the position of a quasi-local level corresponding to the best correlation between the predetonation luminescence spectrum maxima and the density-of-states peaks. Optical transitions of electrons from the valence band into a quasi-local state are shown by arrows.

5. MODEL OF HMA EXPLOSIVE DECOMPOSITION

The following basic principles must serve as the basis of the model of explosive decomposition.

1. The chain nature of explosive decomposition has been proved experimentally. The decomposition kinetics is described on the assumption that the branching of the chain is linear and its breaking is quadratic [10].
2. Experimental estimates of the cross-sections allow one to assume that the branching of the chain (hole multiplication) is due to the trapping of holes by cation vacancy and the chain breaking is caused by indirect interband recombination [10].
3. The branching of the chain is not sufficiently affected by photomultiplication of holes. The main mechanism of hole multiplication is the impact ionization with hot holes generated during their detrapping from quasi-local states.
4. Molecular nitrogen in the crystal is not formed in the chain reaction of HMA decomposition. [12,13].

A proposed mono-hole model for AgN_3 chain link, satisfying the above requirements is presented in Fig.7, which shows only the basic processes underlying the chain branching, and terminating the production of a hot hole and the restoration of a local level in the band gap.

It is convenient to divide the process into 3 stages.

1. Hole trapping at a cation vacancy (Fig.7).
2. The parameters of the process ($S_l \sim 10^{-14}$ cm^2, $\tau \sim 10^{-9}$ s) are given in section 3. The end result of this stage is the transformation of detrapped state (band hole) into a radical trapped at a cation vacancy, i. e., the formation of a nonequilibrium ($V_c N_3^0$) cluster. It is this stage that is responsible for the kinetics of the process because the duration of this stage sufficiently exceeds that of the subsequent stages.

3. Formation of quasi-local states due to the reconstruction of the $(V_c N_3^0)$ cluster in the interaction with neighboring N_3^- and Ag^+ ions.

One can assume that the reconstruction process begins with the formation of molecular bond between a N_3^0 radical trapped at a vacancy and a neighboring N_3^- ion ($N_3^0 + N_3^- \rightarrow N_6^-$). This process is similar to the well-studied process of the hole self-trapping for alkali-halides [16,22]. However, unlike alkali-halide crystals the completion of the reconstruction process apparently has the effect of "smearing" the hole wave-function throughout a (V_c,N_6,Ag) cluster. An analogous process occurs in AgCl, where the self-trapped hole is a $(AgCl_6)^{4-}$ cluster [28].

Unfortunately, calculations that could be to estimate at least approximately the energy released at this stage are nonexistent at the present time. But taking into account the fact that the resultant state is close to N_6^0, and relying on the results of the calculations of the reaction $N_3^0 + N_3^0 \rightarrow N_6^0$ in [2] it can be stated that the process involved is exothermic.

The released energy is stored as the potential energy of a hole in a quasi-local state (Fig.7).

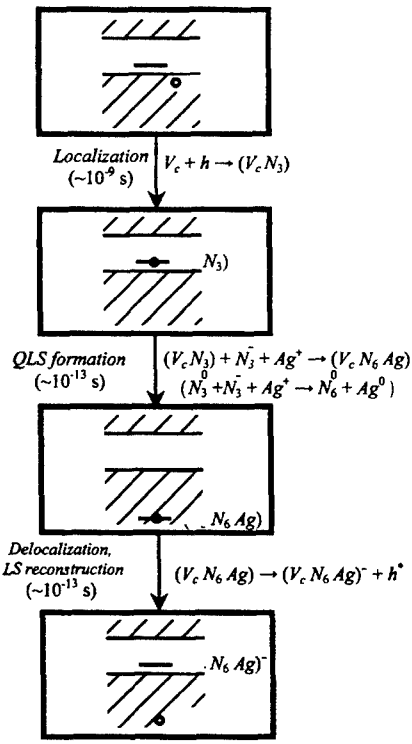


Fig. 7. Main stages of the chain reaction of AgN_3 explosive decomposition.

According to the data obtained in the investigation of predetonation luminescence (Fig.6) the depth of this state is 3 ÷ 3,5 eV. According to the proposed model the density of quasi-local states is proportional to the density of band holes, thereby reconciling the kinetics of predetonation luminescence and predetonation conductivity.

It should be emphasized that because the intraband luminescence yield does not exceed 10^{-5} [26], it serves as a convenient indicator of the decomposition process without influencing its overall energetics.

The slowest process at this stage is the displacement of heavy particles during reconstruction, i.e., the duration of the stage is ~ 10^{-13} s.

3. Hole detrapping (Fig.7)

The lifetime of holes in the quasi-local state does not exceed 10^{-14} s [27]. A hot band hole with the energy 3 ÷ 3,5 eV arises from the hole detrapping.

This process can be considered as transfer of the potential energy of a hole in a quasi-local state into the kinetic energy of a hot hole. Thus, hot holes with the energy sufficiently exceeding the width of the HMA band gap (1 ÷ 1,5 eV [11] are generated. The energy is expended in two ways: impact ionization leading to the multiplication of band holes and electrons and phonon emission causing heating of a sample.

A fundamental question arises: What happens at the local density- of-state peak corresponding to a quasi-local state before hole detrapping? In other words, where will the level corresponding to the $(V_c,N_6,Ag)^-$ cluster be? (Fig.7). First of all, it should be noted that the (V_c,N_6,Ag) cluster maintaining the presence of the quasi-local state in the depth of the valence band is neutral with respect to the lattice, while the $(V_c,N_6,Ag)^-$ cluster arising from the detrapping has a single negative charge, i. e. this cluster has the same charge as the cation vacancy. As a rule, the position of the defect energetic level in the band diagram is strongly dependent of its charge [16]. Therefore it can be stated that the position of the $(V_c,N_6,Ag)^-$ cluster level does not sufficiently differ from the position of the original cation vacancy. Since the transition of the cluster into the equilibrium state is accompanied by the displacement of heavy particles, the duration of this stage is also about 10^{-13} s.

Consequently, the detrapping of a hole from a quasi-local state eradicates the density-of-states peak from the valence band and introduces a local level in the band gap in a position close to the level of the isolated cation vacancy. The emergence of such a level provides for the conditions for the above chain of the processes to be repeated, i. e. for the chain reaction to go on.

It must be emphasized that the kinetics of explosive decomposition described by Eq. (1) is referred to the "already developed" explosion process, when the density of band electrons and holes is 10^{18} cm^{-3} It is the high band charge carrier densities that lead to saturation of the processes caused by the trapping of holes by local centers and account for the simplicity of the observed kinetics of the process.

Under low excitation, i.e. slow decomposition the processes caused by biography defects can play a decisive role (section 2). In the framework of formal kinetics α can be written as $\alpha = f - g(t)$, where f and $g(t)$ are the rate constants of hole detrapping by cation vacancies and by competing centers, respectively. The dependence $g(t)$ could be supported by the "burnout" of these centers during initiation. Since a chain can grow only when $\alpha > 0$, (i.e., $g < f$), the threshold character of initiation can be attributed to the need to maintain sufficiently "complete burnout" ($g < f$) under the effect of initiating pulse.

6. CONCLUSION

By way of conclusion the present authors would like to call attention to a certain fundamental aspect of the problem, which far transcends the problem of elucidating the mechanism of HMA explosive decomposition. The information presented convincingly demonstrates a very interesting possibility for chemical reactions to be realized in solids. A necessary condition for the chemical reaction in liquids and gases is a real migration of reactants towards each other. In solids it is quite different. Electron excitations migrate and their trapping at certain sites of the crystal lattice (at structural or impurity defects) gives rise to actual radicals at the necessary site. Thus, a sufficiently lengthy migration of real heavy particles (usually by diffusion) is replaced by a faster migration of electron excitations. Far-going prospects to utilize this promising possibility have not been fully appreciated in modern solid-state physics and chemistry.

REFERENCES

[1] N.N. Semenov, *Tsepnye reaktsii.*- Moskva, 1986, p. 533 (in Russian).

[2] H.D. Fair, R.F. Walker (Ed.), *Energetic Materials.*- New York, Plenum Press, V. 1, 1987, p. 501.

[3] Kriger V. and Kalensky A. *Chem. Phys. Reports*, **14**(4), 556 (1995).

[4] Aduev B.P., Aluker E.D., Belokurov G.M., Zakharov Yu.A. and Krechetov A.G. *Izv. VUZov. Fizika* **11**, 162 –175 (1996)

[5] B.P. Aduev, E.D. Aluker, V.G. Kriger, Yu.A. Zakharov. *Solid State Ionics*, **101-103**, 33 (1997).

[6] Kurakin S.I., Diamant G.M., Pugachev V.M. *Izv. AN SSSR. Neorganicheskie materialy*, **26**(11), 2301 (1990).

[7] E.D. Aluker, V.V. Gavrilov, R.G. Deich, S.A. Chernov, *Bystroprotekayushcie radiatsionno-stimulirovannye protsessy v shcelochnogaloidnykh kristallakh*, - Riga. Zinantne. 1987, p. 183.

[8] Aduev B.P., Belokurov G.M., Krechetov A.G and Shvayko V.N. *In the book Proceedings of IX International congress Radiation Solid-State Physics*, - Moscow, MGIEM, 1999, v.2, p.1124-1133.

[9] B.P. Aduev, E.D. Aluker, A.G. Krechetov and A.Yu. Mitrofanov. *Phys. Stat. Sol. B*, **207**, 535 (1998).

[10] B.P. Aduev, E.D. Aluker, G.M. Belokurov, Yu.A. Zakharov, A.G. Krechetov, *JETP* **116**, 5 (11) p. 1676 – 1693, (1999) (in Russian).

[11] Gordienko A.B., Zhuravlev Yu.N., Poplavnoi A.S. *Phys. Stat. Sol. B*, **198** 707 –719 (1996).

[12] Krascheninin V.I., Kuzmina L.V. and Zakharov Yu.A. *Journal of Applied Chemistry* (in Russian), **69** (1), 21-24, (1996).

[13] Krascheninin V.I., Kuzmina L.V., Zakharov Yu.A. and Stalinin A.Yu. *Chem. Phys. Reports*, **14**(4), 126-135 (1995).

[14] Aduev B.P., Aluker E.D., Belokurov G.M., Krechetov A.G. *JETP Lett.* (in Russian) **62 (3)**, p.203-204 (1995).

[15] Ya. E. Pokrovskiy (Ed.) *Radiative recombinations in semiconductors.* - Moscow, Nauka. 1972, p.304.

[16] A.M. Stoneham. *Theory of Defects in Solids*, Clarendon Press, Oxford, 1975, p. 731.

[17] Aduev B.P., Aluker E.D., Belokurov G.M. and Krechetov A.G. *Khimitcheskaya fizika.* **16** (8), p.130-136 (1997)

[18] Aduev B.P., Aluker E.D., and Krechetov A.G. *Khimitcheskaya fizika.* **17** (3), p.59-64 (1998)

[19] B.P. Aduev, E.D. Aluker, Yu.A. Zakharov, A.G. Krechetov and I.V. Chubukin, *JETP Lett (in Russian)*, **66**(2), p.101-103 (1997).

[20] B.P. Aduev, E.D. Aluker, A.G. Krechetov, Ju.P. Saharchuk, *Proceedings of I All-Russian Congress Solid-State Detectors of ionizing radiation*,- Ekaterinburg, 1998, p.110-117

[21] V.P. Gribkovskii *Teoriya pogloshcenia i ispuskaniya sveta v poluprovodnikakh.* - Minsk. Nauka i tekhnika. 1975. p. 463.

[22] E.D. Aluker, Lusis D.Yu., Chernov S.A. *Elektronnye vozbuzhdeniya i radioluminestsentsiya shcelochnogaloidnykh kristallov.* - Riga. Zinatne. 1979. p. 251.

[23] B.P. Aduev, E.D. Aluker, A.G. Krechetov, A.Yu. Mitrofanov, Gordienko A.B. and Poplavnoy A.S. *Pisma v ZhTF*, **25**(9), 28-30 (1999).

[24] E.H. Younk, A.B. Kunz. *Int. Journ. of Quant. Chem.*, **63**, (1997) 615-621.

[25] Rodnyi P.A. *Fisika tverdogo tela* **34**(7), 1975-1996 (1992)

[26] B.P. Aduev, E.D. Aluker, V.V. Gavrilov, R.G. Deich, and S.A. Chernov. *FTT*, 12, 3521-3530, (1996).

[27] F. Bassani, G.P. and Parravicini. *Electronic States and Optical Transitions in Solids.* - Pergamon Press. New York. 1975, p. 391.

[28] Spoonhower J.P. and Morcetti A.P. *J. Phys. Chem. Solids*, **51**(7), (1990) 793-804.

1,2-DINITROGUANIDINES: STRUCTURE – PROPERTY RELATIONSHIPS

Alexander M. Astachov *, Alexander D. Vasiliev **, Maxim S. Molokeev **, Ludmila A. Kruglyakova * and Rudolf S. Stepanov *

* Siberian State Technological University
Krasnoyarsk, Russia, 660049

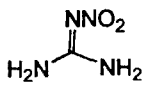
** Institute of Physics RAS (Sib. branch)
Krasnoyarsk, Russia, 660036

Abstract:

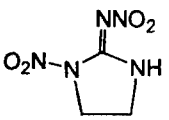
Structure and some properties of two 1,2-dinitroguanidines, 1-nitro-2-nitrimino-imidazolidine and 1-methyl-1,2-dinitroguanidine, have been investigated. Their crystal and molecular structures were found by X-ray analysis. The structure data have been compared with thermal stability and impact sensitivity. Detonation parameters of the compounds were calculated by thermodynamic and correlation methods.

1. INTRODUCTION

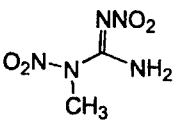
Nitrimines are of interest as explosives and components of propellants [1-7]. The 2-nitroguanidine (NQ, I) is the most known among the compounds. NQ is the insensitive high explosive compound of middle power and is used as explosive compositions' and propellants' component. [6,7]. Structure and some properties of two derivatives of (I), 1-nitro-2-nitriminoimidazolidine (II) and 1-methyl-1,2-dinitroguanidine (III), are considered in the present work.



(I)



(II)



(III)

Due to second nitro group insertion in the molecule, energetic parameters of 1,2-dinitroguanidines (II) and (III) are higher than those of (I). So, as shown in [8], the efficiency of (II) is 1.3 times greater than of TNT in a ballistic-mortar method and 1.5 times greater according to Trauzl lead block test. In spite of moderate value of oxygen balance (–41.1%) the brisance of (II) is comparable with that of more balanced explosive compound of RDX (oxygen balance is –21.6%). At the same time the compound (II) 2.8 times more sensitive to impact and 1.6 times more sensitive to friction than RDX [8].

At first, one supposes that sensitivity to mechanical influence increases with increasing of oxygen balance [9] within limits of one class of energetic compounds. RDX and (II) both are N-nitrocompounds. A question arises accordingly as to why the compound (II) with worse oxygen balance shows comparative brisance and essentially higher impact sensitivity than RDX?

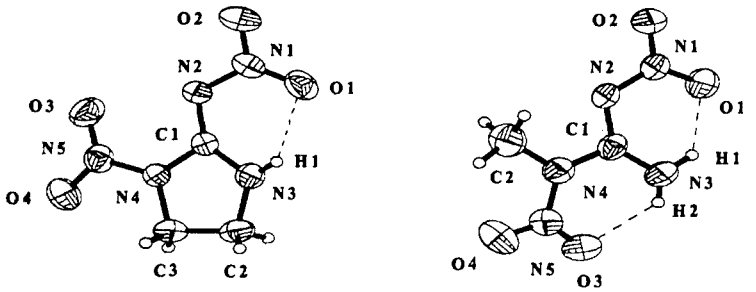
Presently, the most widespread theory is the hot-spot theory of initiation of explosions by impact [9,10]. In agreement with this theory, impact produces hot spots, where the thermal decomposition of an explosive happens. Many different physical and chemical factors influence the impact sensitivity: a heat yielded at decomposition, heat capacity, heat conduction, crystals size and shape, crystal lattice energy and so on. Nevertheless, thermal stability of an explosive (that is, kinetics of initial, rate-determining step and mechanism of thermal decomposition) plays main, determining role. The thermal decomposition of N-nitrocompounds starts with rupture of the least stable N–NO_2 bond [11]. Investigation of thermal decomposition of compound (II) fulfilled in the present work showed that thermal stability of (II) is essentially less than of RDX; this fact agrees with the relative impact sensitivity of both explosives. It's unlikely that the bond N–NO_2 of the nitrimine group is responsible for low thermal stability and high impact sensitivity of (II). For instance, NQ has comparatively high thermal stability and is one of less impact sensitive explosive of IHE class (insensitive high explosives) [6,7,12-14]. Therefore, one may suppose that the bond N–NO_2 of the second nitramine group triggers thermal decomposition in (II). One may expect that the bond will be longer and, consequently, its strength will be less than strength of analogous bonds in RDX. In agreement with aforesaid it appears to be imperative to study structure of compound (II). In addition, the compound (III) has been investigated: explosive performances of the compound are even somewhat higher than those of compound (II). But, unlike (II), compound (III) has low impact sensitivity (level of TNT).

2. X-RAY CRYSTALLOGRAPHY

Molecular structures of (II) and (III) are shown in Fig. 1. These structures correspond in many respects to conformations of the nitrimines investigated before [13,15-23]. Similar to other nitrimines, the molecules of (II) and (III) have planar nitroguanyl fragment with intermolecular hydrogen bond. Because of delocalization of π-electron density in the nitrimine fragment, bond lengths C–N, N–N and N–O have intermediate values. These values are somewhere in between the values characteristic for corresponding single and double bonds (Tables 1,2; Fig. 2). The molecular geometry of (II) is close to planar. Deviations from the least-squares plane through the non-H atoms are 0.078(3) Å (r.m.s.) and 0.202(3) Å (maximum). On the whole, the molecule (III) is less planar than that of (II) (r.m.s. deviation 0.126(4) Å, max. deviation 0.284(4) Å, the torsion angle N5–N4–C1–N3 17.8°). However, conformation of nitroguanyl fragment of (III) is close to planar (r.m.s. deviation 0.087(4) Å, max. deviation 0.139(4) Å).

The bond C1–N2 [1.322 Å for (II) and 1.333 Å for (III)] that is technically 'double', is, in fact, slightly longer than bond C1–N3 [1.308 Å for (II) and (III)] that is technically 'single'. Strong electron-acceptor substituent, the nitrogroup connected with N4 atom, decreases electron density on this atom. Possibility of its participation in a nitrimine conjugation is diminished, and, as a consequence, the C1–N4 bond length increases [1.379 Å for (II) and 1.392 Å for (III)]. Similar situation takes place in other nitrimines, which have electron-acceptor substituents: 1-methyl-2-nitro-1-nitrosoguanidine [17,21] and nitroguanyl azide [23]. In these compounds analogous bond length C–N is equal to 1.389–1.408 Å. The N4 atom has planar conformation (sum of valence angles is 359.8°). This fact in

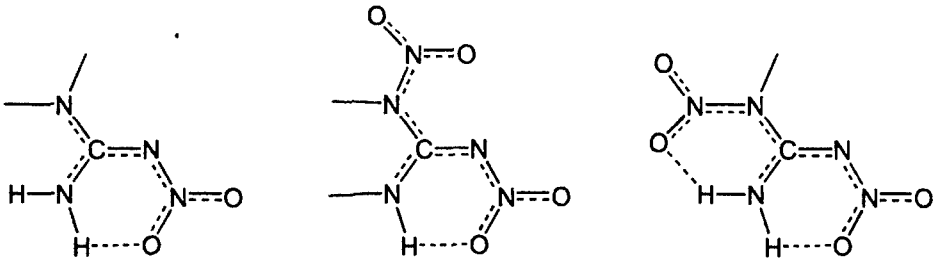
combination with N4–N5 bond length (1.373 Å for (II) and 1.380 Å for (III)) testifies about this atom participation in a conjugation not only with the nitroguanyl group but also with the nitrogroup.



(II) (III)

Fig 1. Molecule of (II, III) shows the atom-numbering scheme and displacement ellipsoid at the 50% probability level. H atoms are drawn as small spheres of arbitrary radii.

Therefore, the nitrimine conjugation spreads in 1,2-nitroguanidines on other nitrogroup (Fig. 2). Molecular conformation analysis of (II) and (III) shows different orientation of nitrogroups with regard to nitrimine fragments. However, this does not influence a strength of N4–N5 bonds. Methylene groups in (II) and methyl group in (III) are not involved in any conjugation and, therefore, lengths of corresponding bonds are close to observed values in compounds with single C–N bond [15].



(I) (II) (III)

Fig 2. The delocalization of π-electron density in the nitrimine fragment of (I–III) is shown.

In Fig. 3 the molecular packing in crystal lattices is shown. Molecules of the compound (II) in a crystal are connected with one another in pairs by weak hydrogen bonds. Interesting feature of the compound (III) crystal structure is the absence of intermolecular H-bonding. This fact is not typical for nitrimines, which usually have developed intermolecular H-bonds net [15-23]. Table 3 contains geometrical parameters of inter- [crystal (II)] and intramolecular H-bonds.

The consequence of intermolecular H-bonds absence in a crystal (III) is low crystal lattice energy and melting temperature (m.p. 80–81°C) and high solubility both in polar (water, alcohols) and in low polar (benzene) solvents [25].

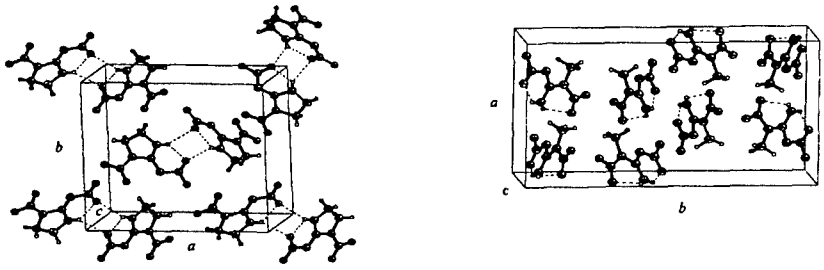
Table 1. *Bond lengths (Å) and angles (°) for compound (II).*

N1–N2	1.358(4)	N3–C2	1.455(4)	N1–O1	1.242(4)
N2–C1	1.322(3)	N4–C3	1.460(3)	N1–O2	1.224(4)
C1–N3	1.308(4)	C2–C3	1.499(4)	N5–O3	1.206(3)
C1–N4	1.379(3)	N4–N5	1.373(3)	N5–O4	1.213(3)
N1–N2–C1	115.6(2)	N3–C2–C3	104.0(2)	O1–N1–O2	121.7(2)
N2–C1–N3	133.2(2)	N4–C3–C2	101.9(2)	O3–N5–N4	119.5(2)
N2–C1–N4	120.2(2)	C1–N4–N5	127.5(2)	O4–N5–N4	114.4(2)
N3–C1–N4	106.6(2)	C3–N4–N5	119.4(2)	O3–N5–O4	126.1(2)
C1–N3–C2	114.2(2)	O1–N1–N2	123.6(2)		
C1–N4–C3	112.9(2)	O2–N1–N2	114.5(2)		

Table 2. *Bond lengths (Å) and angles (°) for compound (III).*

N1–N2	1.341(3)	N4–C2	1.471(3)	N5–O3	1.212(4)
N2–C1	1.333(3)	N4–N5	1.380(3)	N5–O4	1.212(4)
C1–N3	1.308(3)	N1–O1	1.229(3)		
C1–N4	1.392(3)	N1–O2	1.225(3)		
N1–N2–C1	118.6(2)	C1–N4–N5	122.6(2)	O3–N5–N4	119.0(3)
N2–C1–N3	128.4(2)	C2–N4–N5	115.1(2)	O4–N5–N4	115.6(3)
N2–C1–N4	110.0(2)	O1–N1–N2	123.9(2)	O3–N5–O4	125.4(3)
N3–C1–N4	121.5(2)	O2–N1–N2	115.1(2)		
C1–N4–C2	122.0(2)	O1–N1–O2	120.9(2)		

One considers that the presence of strong intermolecular H-bonds, which absorb inputted energy, is the necessary condition that provides explosive with low sensitivity to external influences. One supposes that just because of developed net of intermolecular H-bonds the NQ is an insensitive high explosive [13]. At the same time, the compound (II) doesn't have such a developed net (Fig. 3). On the other side, the compound (III), which has low impact sensitivity, does not have intermolecular H-bonds at all.



(II) (III)

Fig 3. The molecular arrangement of (II, III) in the crystal.

Table 3. . *Hydrogen-bonding geometry (Å, °) for compounds (II, III).*

Compound	*D*–H···*A*	*D*–H	H···*A*	*D*···*A*	*D*–H···*A*
II	N3–H1···O1	0.77(4)	2.02(4)	2.569(4)	128(4)
	N3–H1···O1′ *	0.77(4)	2.37(4)	3.033(4)	145(4)
III	N3–H1···O1	0.85(4)	1.90(4)	2.561(2)	133(3)
	N3–H2···O3	0.76(4)	2.02(4)	2.557(2)	128(3)

* O1′ = (1-x, 1-y, z)

Values of N–NO_2 bond lengths in (II) do not exceed values of analogous bonds in RDX (1.351, 1.392 and 1.398 Å) [27]. And what is more, because of conjugation in a dinitroguanyl fragment, N4–N5 bond length (1.373 Å) in a molecule (II) turned out even smaller than the length of the weakest N–N bond in RDX. Supposition about heightened value of N4–N5 bond length has not been confirmed. Therefore, one cannot explain essential difference in thermal stability and impact sensitivity of (II) and RDX based on the chemical bonds strength in molecules considered. The knowledge of molecular structure does not help either. Nevertheless, the performed investigation allows excluding from consideration one of the most probable factors and directs our efforts to search other possible reasons of high impact sensitivity of the compound (II).

Established structures of (II) and (III) allow to select some features of dinitroguanidines reaction possibility. The increased value of C1–N4 bond length in this compounds and in other nitrimines, which have electron-acceptor substituents, is correlated with the easiness of reaction of nucleophilic substitution with C1–N4 bond cleavage, observed in experiment [1,24-26]. When nitrimines do not contain electron-acceptor substituent, e.g. (I), they have shorter analogous C–N bond (1.330 Å and less) and, consequently, smaller reaction ability in the substitution nucleophilic reactions [1].

More detailed crystallographic structure data of (II) and (III) will be considered in other publications.

3. THERMAL DECOMPOSITION

Thermal decomposition of (II) and (III) has been studied by manometric method [11] in a condensed state [solid phase of (II) and melted phase of (III)] and in diluted solutions of low polar aprotic inert solvents (phenyl benzoate and *m*-dinitrobenzene). In addition there were performed TGA and DTA studies (heating rate 2.5–5°C/min).

Both (II) and (III) compounds do not show high thermal stability. According to data of nonisothermal study, decomposition of (II) occurs in a solid state without melting (the endothermal effects, which precede an exothermal peak on the DTA curve, are absent). Temperature of onset of decomposition is 152.5°C. The decomposition proceeds sharply, explosion-like. So, at 156°C the mass loss makes up 0.6% of initial mass while at 157°C the mass loss makes up already 67.2%. The DTA curve of (III) has endothermal peak of melting with maximum at 81°C. The TGA data show that the decomposition begins from the temperature of 116°C; it proceeds more smoothly than in case of (II). The temperature of intensive decomposition is near 166°C.

For both compounds, the isothermal kinetic curves of thermal decomposition in a condensed state have an S-shape appearance and were described satisfactorily by a first-order equation in solutions. In a case with S-shape appearance kinetic curves, rate constants of thermal decomposition reactions were defined via initial rates of decomposition with assumption of first-order reaction. The activation parameters of thermal decomposition are presented in Table 4.

Table 4. *Kinetic parameters of thermal decomposition of compounds (II, III).*

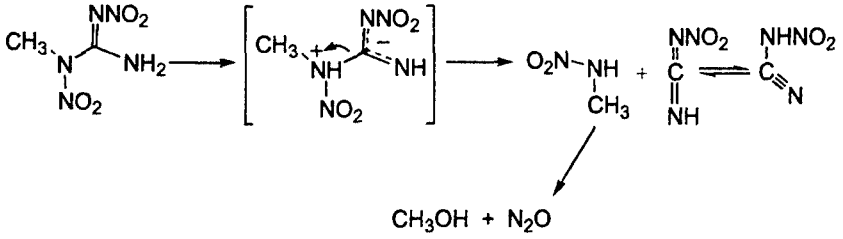
Compound	Thermolysis condition	ΔT, °C	E_a, kJ/mole	lg$A$	R
II	Solid phase	120–140	191.4	19.98	–0.9948
	1% sol. in PhB	100–140	132.1	13.27	–0.9999
	1% sol. in *m*-DNB	110–140	132.4	13.36	–0.9913
III	Melt	100–140	99.8	8.68	–0.9838
	1% sol. in PhB	110–160	120.4	11.32	–0.9932
	1% sol. in *m*-DNB	110–150	100.6	8.86	–0.9904

An analysis of kinetic data and decomposition products allow proposing a mechanism of the compound (III) thermal decomposition. Temperature dependencies of rate constants of (III) thermal decomposition in a melt and in solutions are presented in Fig. 4. In spite of some different values of activation parameters, in Fig. 4 one can see that rates of thermal decomposition in solutions, which are different by the nature of solvent, and in a melt turned out close to one another. They are in a good agreement with temperature dependence of rate constants of methylnitramine thermal decomposition (E_a = 106.3 kJ/mole, lg$A$ = 9.55 [28,29]).

After full decomposition in a melt and in solutions there was generated approximately 2 moles of gaseous products per one mole of (III) (with the exception of temperatures of 130–140°C in a melt, when full amount of gas formed reaches 2.3 mole). The residue after the decomposition of (III) in a melt at 100–120°C has been FTIR identified as nitrocyanamide

[30]. The subsequent decomposition of nitrocyanamide takes place at higher temperature (m.p. 137–138°C with dec.).

The decomposition of (III) one can describe by next scheme:



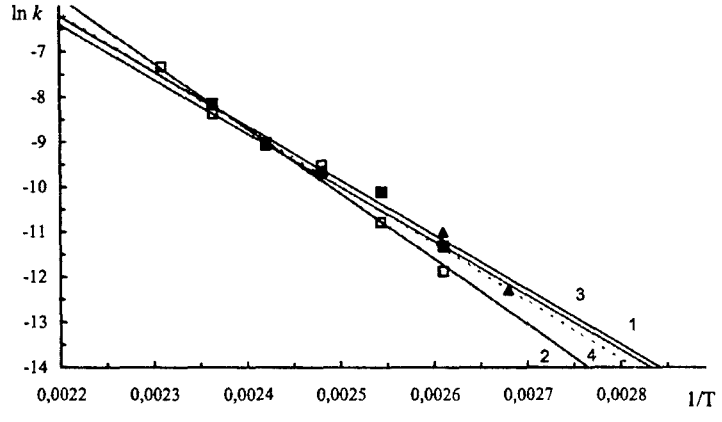


Fig 4. Arrhenius plot for the rate constants of thermal decomposition of (III) in a melt (1) and in solutions [phenyl benzoate (2), *m*-dinitrobenzene (3)]. The dashed line shows data for methylnitramine in a melt (4).

At first, an intramolecular proton transfer from nitroguanyl part of a molecule (III) to methylnitramine group takes place. One can imagine a mechanism of the process only speculatively. It is possible that a transfer of proton from N3 atom to O3 atom occurs via the H-bond O3...H2 (Fig.1, Table 3). Later on there may occur either elimination of *aci*-form of methylnitramine (the latter must transform itself to usual nitramine form [31,32]) or subsequent proton transfer to N4 atom and elimination of 'usual' nitramine form of methylnitramine. Whatever it is, when protonation of methylnitramine group occurs, possibility of its conjugation with nitroguanyle part is diminished and weakest bond C1–N4 of a molecule (III) becomes even weaker. Then this bond will break and molecules of methylnitramine and nitrocyanamide are generated. Molecule of methylnitramine in considered experimental conditions is unstable and, in turn, is decomposed to CH_3OH and N_2O [28,29]. Close kinetic parameters of (III) and methylnitramine thermal decomposition show that for (III), destruction itself proceeds more quickly than decomposition of methylnitramine. Therefore, as a result of manometric study we fix the process of decomposition of methylnitramine and, as a result, cannot judge about details of a process preceding the methylnitramine decomposition on a base of observed kinetic parameters. The proposed scheme allows explaining the S-shape appearance of kinetic curves of compound

(III) thermal decomposition by acid catalysis in a melt. The methylnitramine decomposition is accelerated under the influence of nitrocyanamide, a strong acid. In 1% solutions of aprotic solvents the acid catalysis by nitrocyanamide is difficult. As a result, first order of reaction is observed and influence of solvent's nature on the reaction rate is not shown.

The S-shape appearance of kinetic curves of solid phase thermal decomposition of compound (II) probably has topochemical nature. Thermal decomposition in a solid phase proceeds with lower rate than in solutions (Table 4, Fig. 5). One can explain both facts by the influence of crystal lattice, whose energy increases thermal stability of a molecule (II). This is usual regularity, which is observed for many nitrocompounds [11]. As in the case of (III), a solution change has almost no influence on decomposition rate. In comparison with (III) the decomposition in solutions proceeds with higher rate (by several times). At full decomposition in solutions nearly 2 moles of gaseous products per mole of (II) are formed and at full decomposition in a solid phase the maximum gas formation reaches 2.2-2.3 moles.

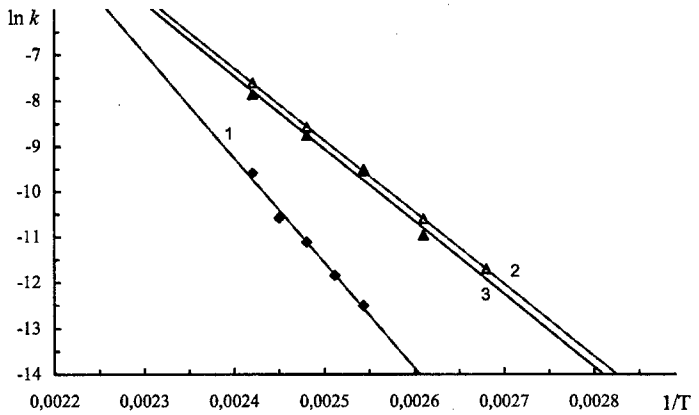
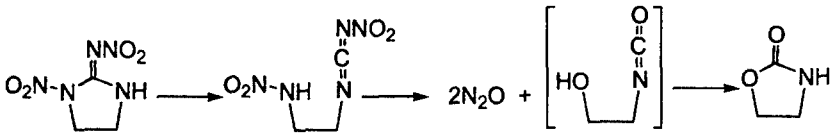


Fig 5. Arrhenius plot for the rate constants of thermal decomposition of (II) in a melt (1) and in solutions [phenyl benzoate (2), *m*-dinitrobenzene (3)].

Today's we could not identify a condensed residue after the decomposition of (II), but following FTIR spectroscopy, the compound contains the molecular fragments of –NH– and –O–C(=O)– (which is a solid decomposition product and not pure 2-oxazolidone). For this reason we could not offer proven thermal decomposition mechanism for the compound (II). Nevertheless, basing on decomposition scheme for similar compound (III), that was proposed before, and taking into consideration X-ray analysis data, which show low possibility of primary breaking of N–NO_2 bond (and preference of C1–N4 bond breaking), we consider that the thermal decomposition of (II) proceeds similar to the compound (III) decomposition. Therefore, the trigger for thermal decomposition is the breaking of C1–N4 bond after transfer of a proton.



Taking this into consideration, we may emphasize once more that the mechanism proposed is only hypothetical, although it allows explaining the observed regularities of thermal decomposition reasonably.

4. IMPACT SENSITIVITY

In addition to [8] data in the present work an impact sensitivity of (II) was established by so-called 'Russian probe' with K-44-II drop-weight machine (m=10 kg, h=25 cm) by state standard 4545–88/99. In this conditions a sensitivity of (II) makes up 100% of explosions. For other high explosives the explosion percent is such: PETN 100%, RDX 72±12%, Tetryl 48±8%. The compound (III) gives 12% of explosions, which corresponds approximately to sensitivity level of TNT (4-28%).

Besides, on the basis of obtained kinetic parameters of thermal decomposition we tried to estimate critical parameters of initiation by impact (critical temperature, pressure, layer thickness) using the theoretical model [10], which is in a good agreement with experimental results for many of high explosives. In order to use the model, however, we need to know some physical and chemical characteristics of explosives and a number of them for (II) and (III) are unknown at present. We used approximate values for heat capacity c_p=1.25 J/(g·K) (it is changed in limits 1.0–1.5 J/(g·K) for most high explosives) and ultimate strength σ_{ult} (it was calculated using $\sigma_{ult}=0.42T_{m.p.}$ [33]). For heat of decomposition reaction, like in [10], we used heat of explosion Q_{expl} (calculated in the next chapter). Variation of the above-mentioned characteristics by 20% limits does not in principle influence the results obtained. The main factors, which strongly influence the values of critical parameters of initiation obtained, are activation parameters of thermal decomposition. These parameters we established with experiment. The main difficulty arose with determination of melting point value for (II), which is decomposed (following TGA and DTA data) in a solid phase without melting. In this ambiguous situation we executed calculation for two possible extreme hypothetical melting points. 152.5°C was chosen as low limit (temperature of onset of decomposition by TGA data) and 300°C as reasonable high limit. Increase in the high explosives melting point on the same other conditions diminishes a value of critical pressure of initiation.

The calculated values of critical parameters of initiation by impact for compounds (II) and (III) and for comparison RDX and TNT are presented in Table 5. In spite of our assumptions, the calculation shows that the compound (II) has considerably lower critical pressure of initiation ($190 < P_{cr.} < 460$ MPa) than RDX (700 MPa) and sensitivity of (II) is the same as of TNT (P_{cr} = 1100 MPa).

Table 5. *The some constants and calculated values of critical parameters of initiation by impact for compounds (II,III).*

	II	III	RDX*	TNT*
$T_{m.p.}$, °C	152.5 300	81	204.5	81
c_p, J/(g·K)	1.25	1.25	1.26	1.465
β, K/MPa	0.2	0.2	0.2	0.3
$\sigma_{ult.}$, MPa	64 126	34	82	40
$Q_{expl.}$, MJ/kg	5.20	5.44	5.40	4.23
E_a, kJ/mole	191.4	120.4	174	144
lg$A$	19.8	11.32	15.55	11.4
$P_{cr.}$, MPa	456 184	1087	692 (700)	1018 (1100)
$T_{cr.}$, K	626	866	787	1070
$\delta_{cr.}$, mm	0.314 4.120	0.062	0.258 (0.25)	0.078 (0.08)

* Experimental data given in brackets [10].

So, the numerical model [10] allows explaining experimentally observed high impact sensitivity of (II) and low impact sensitivity of (III), which may look contradictory on the face of it. More simple correlation models, like proposed in [9], are not suitable in this case.

5. ENERGETIC AND DETONATION PROPERTY

Energetic and detonation parameters of (II) and (III) were calculated using thermodynamic method with BKW equation of state [34] at various sets of parameters (BKW-RDX [34], BKW-R [35], BKW-RR [36], BKW-C [37]) and, also, by simple correlation methods [38-41]. Table 6 shows averaged converging values obtained by various methods. The calculation was performed at maximum possible density of compounds (the density of single crystal was found from X-ray data). The condensed carbon forming by detonation was taken into consideration in diamond and graphite phases and in a model BKW-RR as the graphite and the ultra-disperse diamond [42]. In all the cases the calculation shows that diamond phase is preferable in Chapman-Jouguet point. The values for standard enthalpies of formation, necessary for the calculation of detonation parameters, were found from experimentally determined calorimetric heats of combustion. Accuracy of used ΔH_f^0 values is not high because heat of combustion was determined with error near 1%. However, this fact has little effect on the calculated values of detonation parameters. Known experimental values of detonation parameters for RDX [43] are shown in table 6 for comparison.

Table 6. *Some energetic and detonation parameters of compounds (II,III).*

	II	III	RDX
Formula	$C_3H_5N_5O_4$	$C_2H_5N_5O_4$	$C_3H_6N_6O_6$
Molecular weight	175.10	163.09	222.12
Oxygen balance, %	–41.1	–24.5	–21.6
ΔH_f^0, kJ/mole	+19.7	–6.6	+61.5
ρ_0, g/sm^3	1.746	1.644	1.71 1.80
$Q_{expl.}$, MJ/kg	5.20 $^{\pm 1.2\%}$	5.44 $^{\pm 1.2\%}$	5.40 (1.70 g/sm^3)
V_0, m^3/kg	0.738 $^{\pm 1.1\%}$	0.794 $^{\pm 1.3\%}$	0.762 (calc. 1.70 g/sm^3)
D_{CJ}, km/s	8.19 $^{\pm 1.8\%}$	8.18 $^{\pm 1.2\%}$	8.39 8.77
P_{CJ}, Gpa	28.0 $^{\pm 4.6\%}$	27.1 $^{\pm 4.3\%}$	31.4 36.1
T_{CJ}, K	2325–3600	2455–3780	3740 3520
γ	3.20 $^{\pm 7.9\%}$	3.06 $^{\pm 6.5\%}$	2.83 2.83

From Table 2 data it follows that compound (II) somewhat yields to RDX in detonation parameters. The latter possesses lesser cartridge density and has bigger values of detonation velocity and pressure. Detonation parameters of (III) on equal cartridge density surpass that of (II) and close to RDX parameters. However, comparatively low single crystal density of (III) restricts maximal values of these parameters on a level of lesser balanced but possessing bigger density compound (II)

6. CONCLUSION

It is obvious that physical, chemical and explosive properties of (II) and (III) in combination cannot compete with many explosives used in practice, in particular with RDX. Compound (II) yields to RDX by all characteristics, important for energetic compounds (detonation parameters, thermal stability, impact sensitivity). Compound (III) is comparable with RDX by detonation parameters (on equal cartridge density) and has essentially lesser sensitivity to mechanical influences. However, its low thermal stability and comparatively low density also does not allow this compound to compete with RDX.

Despite the fact, that neither of compounds (II) and (III) are of practical interest, the fulfilled study is useful for understanding the molecular and crystal structure peculiarities and reaction ability of compounds containing 1,2-dinitroguanyle fragment. The revealing of relationships 'structure – properties' in a series of known compounds is quite necessary for the prognosis of properties for new, hypothetical energetic molecules, among which perspective compounds may be found that surpass the effectiveness of currently known ones.

Acknowledgment

We are grateful to the Krasnoyarsk Region Scientific Foundation for support of this work.

REFERENCES

[1] A. F. McKay, Chem. Rev., 51 (1952) 301–346.

[2] H. A. Hageman, U. S. Patent 3,035,094. 1962.

[3] Y. Guowei, X. Qiwu, W. Daozheng, and Y. Yongzhong, *J. Ind. Explos. Soc. Jap.*, 43 (1982) 2–3.

[4] B. Strauss and S. M. Moy, U. S. Patent 5,325,782. 1994.

[5] A. M. Astachov, I. V. Gelemurzina, A. D. Vasiliev, A. A. Nefedov, L. A. Kruglyakova, and R. S. Stepanov, Energetic Materials – Ignition, Combustion and Detonation. 32st International ICT Conference, July 3–6, 2001, Karlsruhe, Germany, 139/1–139/10.

[6] E. Yu. Orlova, Chemistry and Technology of High Explosives. Leningrad: Khimia, 1973 (In Russian).

[7] R. M. Doherty, and R. L. Simpson, Energetic Materials – Combustion and Detonation. 28st International ICT Conference, June 24–27, 1997, Karlsruhe, Germany, 32/1–32/23.

[8] A. F. McKay, and G. F. Wright, J. Am. Chem. Soc. 70 (1948) 3990–3994.

[9] M. J. Kamlet, Proceedings of the 6th Symposium (International) on Detonation, August 24–27, 1976, San Diego, CA, USA, 312–322.

[10] A. V. Dubovik, Dokl. Acad. Nauk USSR, 286 (1986) 377–380 (In Russian).

[11] G. B. Manelis, G. M. Nazin, Yu. I. Rubtsov, and V. A. Strunin, Thermal Decomposition and Combustion of Explosives and Powders, edited F. I. Dubovitsky, Moscow: Nauka, 1996 (In Russian).

[12] F. Volk, Prop. Explos. Pyrotech., 10 (1985) 139–146.

[13] Y. Oyumi, A. L. Rheingold, and T. B. Brill, Prop. Explos. Pyrotech., 12 (1987) 46–52.

[14] Z. R. Liu, C. Y. Wu, Y. H. Kong, C. M. Yin, and J. J. Xie, Thermochimica Acta, 146 (1989) 115–123.

[15] F. H. Allen, and O. Kennard, Chem. Des. Autom. News, 8 (1993) 31–37.

[16] J. H. Bryden, L. A. Burkardt, and E. W. Hughes, Acta Cryst., 9 (1956) 573–578.

[17] S. Nordenson, and J. Hvoslef, Acta Cryst., B37 (1981) 373–378.

[18] S. Nordenson, Acta Cryst., B37 (1981) 1543–1547.

[19] S. Nordenson, Acta Cryst., B37 (1981) 1774–1776.

[20] C. S. Choi, Acta Cryst., B37 (1981) 1955–1957.

[21] S. Rice, M. Y. Cheng, R. E. Cramer, M. Mandel, H. F. Mower, and K. Seff, J. Am. Chem. Soc., 106 (1984) 239–243.

[22] A. Gao, A. L. Rheingold, and T. B. Brill, Prop. Explos. Pyrotech., 16 (1991) 97–104.

[23] A. D. Vasiliev, A. M. Astachov, A. A. Nefedov, L. A. Kruglyakova, and R. S. Stepanov, Acta Cryst., C57 (2001) 625–626.

[24] A. F. McKay, and G. F. Wright, J. Am. Chem. Soc. 69 (1947) 3028–3030.

[25] R. H. Meen, and G. F. Wright, J. Am. Chem. Soc. 74 (1952) 2077–2079.

[26] F. L. Scott, F. C. Britten, and J. Reilly, J. Org. Chem. 21 (1956) 1519–1522.

[27] C. S. Choi, and E. Prince, Acta Cryst. B28 (1972) 2857–2862.

[28] R. S. Stepanov, A. M. Astachov, and L. A. Kruglyakova, Energetic Materials – Production, Processing and Characterization. 29st International ICT Conference, June 30 – July 3, 1998, Karlsruhe, Germany, 128/1–128/7.

[29] A. M. Astachov, Thermal Decomposition Primary Nitramines in Condensed Phase, Diss., Siberian State Technological University. Krasnoyarsk, 1999. 118 p.

[30] S. R. Harris, J. Am. Chem. Soc., 80 (1958) 2302–2305.

[31] V. G. Avakyan, and O. V. Fateyev, J. Mol. Struct. (THEOCHEM), 262 (1992) 39–53.

[32] V. G. Avakyan, and O. V. Fateyev, Russ. Chem. Bull., 1 (1993) 100–104 (In Russian).

[33] G. T. Afanasiev, and V. K. Bobolev, Initiation of Solid Explosives by Impact, Moscow: Nauka, 1968 (In Russian).

[34] Ch. L. Mader, Numerical Modeling of Detonation, Berkeley-Los Angeles-London. University of California Press, 1979.

[35] M. Finger, E. Lee, F. H. Helm, B. Hayes, H. Hornig, R. McGuire, M. Kahara, and M. Guilry, Proceedings of the 6th Symposium (International) on Detonation, August 24–27, 1976, San Diego, CA, USA, 172–181.

[36] S. A. Gubin, V. V. Odintsov, and V. I. Pepekin, Fiz. Goreniya i Vzryva (Combustion, Explosion and Shock Waves), 23 (1987) 75–84 (In Russian).

[37] L. E. Fried, and P. C. Souers, Prop. Explos. Pyrotech., 21 (1996) 215–223.

[38] M. J. Kamlet, and H. Hurwitz, J. Chem. Phys., 48 (1968) 3685–3692.

[39] V. I. Pepekin, and Yu. A. Lebedev, Dokl. Akad. Nauk. USSR, 234 (1977) 1391–1394 (In Russian).

[40] W. Xiong, J. Energ. Mat., 3 (1985) 263–277.

[41] J. R. Stine, J. Energ. Mat., 8 (1990) 41–73.

[42] V. V. Odintsov, S. A. Gubin, V. I. Pepekin, and L. N. Akimova, Khim. Fiz. (Russ. J. Chem. Phys.), 10 (1991) 687–695.

[43] M. F. Gogulya, and M. A. Brazhnikov, Khim. Fiz. (Russ. J. Chem. Phys.), 13 (1994) 52–63.

STUDY ON THE DESENSITIZATION OF PLASTIC BONDED BIS(β,β,β-TRINITROETHYL-N-NITRO)ETHYLENEDIAMINE

Li Bing-ren and Li xianming

Insitute of Chemical Materilas, China Academy of Engineering Physics,
Mianyang, 621900,Sichuan,China

Abstract:

The crystal form and granularity of Bis(β,β,β-trinitroethyl-N-nitro)ethylenediamine (BTENED), and the type and content of desensitizer have different effects on sensitivity of plastic bonded BTENED (PB-BTENED). TATB-graphite-wax (TATB-G-W) was discovered to be the best desensitizer. Mixing BTENED with HMX , added little TATB-G-W, The sensitivity of PB-BTENED could reach an expectantly low level.

Keyword: *explosive; sensitivity; Bis(β,β,β-trinitroethyl-N-nitro)ethylenediamine, BTENED*

1. INTRODUCTION

Bis(β, β, β-trinitroethyl-N-nitro)ethylenediamine(BTENED), which exhibit a excellent performance, is used as a high explosive.The crystal density of BTENED is 1.870 g/cm^3, and the detonation velocity of BTENED is 8970 m/s when its charge density is 1.842 g/cm^3. BTENED is a zero-oxygen balance high energetic material, whose synthesis materials can be easily got and cost less, and its explosion delay time is short. But the application of BTENED-based plastic bonded explosive (PB-BTENED) is limited because of high mechanical sensitivity, especially of friction sensitivity, which is hard to be desensitized .

Sensitivity of explosive is depend on its instinct physical and chemical characters. Outer condition and additive also have effects on sensitivity of explosive. So desensitization of PB-BTENED has been investigated through changing physical character of explosive granule such as changing crystal form and granule size, through addition of desensitizer and mixture with other explosives.

2. DESENSITIZATION OF PB-BTENED

2.1 Effects of BTENED's granularity on sensitivity of PB-BTENED

Granule size was decreased with a ball grinder. Friction sensitivity of BTENED and PB-BTENED with different granularities was tested. The results indicated that granularity of BTENED has a minor effect on sensitivity of BTENED and PB-BTENED, which are shown in table 1.

Table 1. *Effects of BTENED's granularities on sensitivity*

%

	Original granularity	Grinded for 1h	Grinded for 3h	Grinded for 10h	Pressure /MPa
	20~130μ	76.7%<5μ	87.2%<5μ	91.8%<5μ	
BTENED	24	36	52	60	3.0
PB-BTENED	24	46	57	64	3.5

Notes: □. Formulation of PB-TENDED:BTENED/Binder/Desensitizer=94/3.5/2.5.
□. Under standard test condition (4.0Mpa), friction sensitivity of BTENED and PB-BTENED in table is100%.

2.2 Effects of BTENED's crystal form on sensitivity of PB-BTENED

Crystal form of BTENED is long-stick. Stick crystals interlace with each other, can't move easily, which result in stress concentration and may cause friction sensitivity increasing. Some granular BTENEDS were prepared by recrystallizing with polymer paralyst which restrain axis-growing speed of Stick crystal (figure 1). The tested results for the friction sensitivity of PB-BTENED are shown in table 2. The data in table 2 indicated that the friction sensitivity of PB-BTENED didn't descent sharply after crystal form of BTENED was changed.

Table 2. *Friction sensitivity of PB-BTENED with different crystal form*

%

Granular	Long- stick
20	20, 40

Notes: Formulation of PB-TENDED:BTENED/Binder/Desensitizer=94/3.5/2.5. Test pressure is 3.5Mpa.



a) Original crystal form b) Grinded crystal form c) Recrystallized crystal form

Fig 1. Crystal form of BTENED

2.3 The addition of desensitizer

It is a common desensitization way that desensitizer is added in formulation of explosives. Colloid graphite, 65#wax, 85#wax, liquid wax, boron nitride, molybdenum disulfide, stearic acid, palmitic acid, octadecanol, zinc stearate, silicone grease, silicone oil, organosilicon resin, asphalt, and estane, as single or composite desensitizer, have been

tested, although the results were not satisfactory. The best desensitizers were 65#wax and graphite. The content and addition method of wax and graphite have been tested. The results show that the content of wax and graphite should be less than 3%.

3. APPLICATION OF TATB-G-W COMPOSITE DESENSITIZER

In the experiments mentioned above, PB-BTENED, which was added only with wax or graphite as the desensitizer, has not expectedly high performance. So TATB was added as a desensitizer also, whose tested result are shown in table 3.

Table 3. *Desensitizing effects of wax and graphite on PB-BTENED*

%

The formulation of PB-BTENED				Impact sensitivity	Friction sensitivity
BTENED	Binder	G	W		
97.0	2		1	0	60
97.0	2		1	0	100
96.5	2	0.5	1	0	40

TATB, as a kind of insensitive explosives, can desensitize BTENED. Much TATB is needed in order to get expectantly low friction sensitivity by adding only TATB into PB-BTENED as desensitizer. A small amount of TATB could not desensitize PB-BTENED sharply. Desensitizing effects of TATB on PB-BTENED are shown in table 4.

Table 4. *Desensitizing effects of TATB on PB-BTENED* %

The formulation of PB-BTENED			Impact sensitivity	Friction sensitivity
BTENED	Binder	TATB		
88.0	2	10	72	100
68.0	2	30	12	80
48.0	2	50	12	28

After a lot of experiments, a composite desensitizer consisting of G, W and TATB was discovered to have more obvious desensitizing effects on PB-BTENED than simple desensitizers. The tested results are shown in table 5.

Table 5. *Desensitizing effects of composite desensitizer on PB-BTENED*

%

The formulation of PB-BTENED					Impact sensitivity	Friction sensitivity
BTENED	Binder	TATB	G	W		
86.5	2	10.0	0.5	1	0	20
88.5	2	8.0	0.5	1	4	8
92.0	2	4.5	0.5	1	0	28

The composite desensitizer of TATB-G-W was also iscovered to have obvious desensitizing effects on HMX and RDX . Appear in table 6.

Table 6. *Desensitizing effects of composite desensitizer on PB-HMX and PB-RDX* %

The formulation of PBX						Impact sensitivity	Friction sensitivity
HMX	RDX	Binder	TATB	G	W		
92		2	4.5	0.5	1	/	4
90		5	4	0.5	0.5	0	0
	86	8	5	0.5	0.5	4	8
	89	6.5	4	0.5	1	0	16

4. EFFECTS OF BTENED MIXING WITH HMX ON SENSITIVITY OF PBX

If the main explosive is BTENED, the sensitivity of PB-BTENED is not desensitized obviously when physical character of BTENED such as crystal form and granule size is changed respectvely. So it was considered that BTENED mixing with HMX could change physical character of main explosive system, which may desensitize the friction sensitivity of PB-BTENED.

A lot of experiments show that friction sensitivity is desensitized obviously when the main explosive BTENED is mixed with some HMX, and with TATB-G-W as the desensitizers. See table 7. Friction and impact sensitivity can reach an expectantly low level when the content of HMX ≥6%.

Table 7. *Effects of BTENED mixing with HMX on sensitivity of PBX* %

The formulation of PB-BTENED/HMX						Impact sensitivity	Friction sensitivity
BTENED	HMX	Binder	TATB	G	W		
86	6	2	4.5	0.5	1	0	0
80	12	2	4.5	0.5	1	4	12
70	22	2	4.5	0.5	1	4	0
60	32	2	4.5	0.5	1	4	4
46	46	2	4.5	0.5	1	4	8

5. ROUGH REGULATION OF DESENSITIZATION

5.1 Effects of BTENED and HMX's mixture ratio on sensitivity

The data in table 7 show that friction and impact sensitivity can reach an expectantly low level when the content of HMX is above 6%, if TATB/G/W is 4.5/0.5/1 at fixed ratio.

5.2 Effects of composite desensitizer's compound ratio on sensitivity

In order that the mixture ratio of composite desensitizer has different effects on sensitivity of PBX, many experiments have been done. The tested results are listed in table 8. The data indicates that W and TATB, though have a more obvious effect on sensitivity of PBX, not a single one of the three can be dispensed with.The mixture of BTENED with HMX can't desensitize the mechanical sensitivity of PBX without desensitizer.

Table 8. *Effects of composite desensitizer's compound ratio on PBX* %

The formulation of PB-BTENED/HMX						Impact sensitivity	Friction sensitivity
BTENED	HMX	Binder	TATB	G	W		
70	26.5	2		0.5	1	8	92
48.5	48	2		0.5	1	4	60
60	34.5	2	2	0.5	1	0	16
46.5	46.5	2	4.5	0.5		100	100
80.2	12	2	4.5	0.5	0.8	/	12
60	32.5	2	4.5	0.5	0.5	60	60
50	42.5	2	4.5		1	20	40
83	10	2	4	0.2	0.8	/	72
49	49	2				100	100

To the adding method of desensitize, according to the test. TATB and G must be internal-mixed with main explosives, and W should be coated on the surface of molding powder after granulation, which is the most convenient for water suspension method.

5.3 Effects of PBX containing TNT on sensitivity

The test indicated that TNT could obviously increase the friction sensitivity of PB-BTENED. So TNT, as a kind of plasticizer, can't be added into PB-BTENED or PB-BTENED/HMX.

6. PERFORMANCE OF PB-BTENED/HMX

PB-BTENED/HMX, using TATB-G-W as desensitizer, can reach expectantly low level for mechanical sensitivity.Its performance and formulation are listed in table 9.

Table 9. *Performance of PB-BTENED/HMX containing TATB-G-W*

The formulation of PB-BTENED/HMX %						Impact sensitivity %	Friction sensitivity %	H_{50} cm	D $m.s^{-1}$	P GPa
BTENED	HMX	Binder	TATB	G	W					
70	22	2	4.5	0.5	1	4	0	80	8665	36.24

Notes: Detonation performance was tested under ρ=1.819 g/cm^3.

8. CONCLUSIONS

(1) TATB-G-W composite desensitizer was satisfactory. It desensitized sensitivity of PB-BTENED: impact sensitivity is below 4%, friction sensitivity is below 30%(when the content of TATB is above 4.5%). The composite desensitizer can also desensitize PB-HMX and PB-RDX obviously.

(2) Mixing BTENED with some HMX, and with TATB-G-W as the desensitizere, could further desensitize sensitivity of PB-BTENED/HMX: impact sensitivity is below 4%, friction sensitivity is below 12%.

(3) The mixture ratio of BTENED and HMX, and TATB-G-W composite desensitizer was investigated. Their rough regulation was founded.

(4) The tests indicated that friction sensitivity of PB-BTENED did not descent sharply after crystal form or granularity of BTENED is changed.

(5) The tests indicated that TNT could obviously increase the friction sensitivity of PB-BTENED, and have minor effect on impact sensitivity of PB-BTENED. So TNT, as a kind of plasticizer, can't be added into PB-BTENED.

REFERENCES

[1] DONG HaiSan, ZHOU FenFen. Gao neng zha yao ji xiang guan wu xing neng [M]. Beijing: the Science Publishing House.

THERMOCHEMICAL ANALYSIS OF COMBUSTION PROCESS OF GAS GENERANTS CONTAINING SODIUM AZIDE

Stanisław Cudziło and Waldemar Andrzej Trzciński

Military University of Technology
Kaliskiego 2, 00-908 Warsaw 49, POLAND

Abstract:

Themochemical calculations and calorimetric experiments were performed for gas generating mixtures containing sodium azide and various oxidisers (KNO_3, CuO, MoS_2, S, C_6Cl_6,, polytetrafluoroethylene and chlorinated polyvinyl chloride). An influence of the kind of an oxidiser and its contents in the mixture on the heat of reactions, the adiabatic combustion temperature and the composition of combustion products was determined. Mixtures producing low combustion temperatures as well as effective ways of the temperature minimisation were chosen.

Keywords: *pyrotechnics, thermochemistry of combustion, gas generators.*

1. INTRODUCTION

Gas generating pyrotechnics mixtures are widely used in air bags and belt restraint systems for cars, fast inflatable life rafts, pilot-and-seat ejection devices and automatic fire extinguishers. Most of the gas generants being used today are still based on sodium azide (NaN_3) despite its toxicity and resulting from that problems associated with recycling, disposal and environmental impact [1÷6].

Among the main advantages of sodium azide based formulations, there are short induction period of ignition, high burning rate, generation of practically pure nitrogen with comparatively low temperature, low sensitivity to impact and friction, good thermal stability, good resistance to environmental factors and long life time.

In this study an influence of the kind of an oxidiser and its contents in mixtures with NaN_3 on the fundamental thermochemical characteristics of combustion process, i.e. the composition of combustion products, the adiabatic combustion temperature, the amount of gaseous products and the exothermicity of reactions accompanying combustion, was investigated. These parameters were obtained using the thermochemical code CHEETAH [7]. The calculation correctness was verified by calorimetric measurements of heats of reaction of a range of compositions. Potassium nitrate (KNO_3), copper oxide (CuO), molybdenum disulfide (MoS_2), sulphur (S), heksachlorbenzene (C_6Cl_6), polytetrafluoroethylen (PTFE) and chlorinated polyvinylchloride (SPVC) were used as oxidisers. In each case the initial tested composition of a mixture coincided with the reaction stoichiometry assuring complete binding of sodium released during the decomposition of NaN_3.

2. EXPERIMENTAL

The mixtures tested were prepared by mixing components in a porcelain mortar. All the substances were pure. Before mixing they were sieved through a grading screen and a sieve fraction of below 100 μm was taken to prepare the compositions. The postulated equations of chemical reaction and the composition of the stoichiometric mixtures are listed in Table 1.

Table 1. *Postulated equations of reaction and stoichiometric compositions*

Mixture	Postulated equation of reaction	Composition, [%]	Ref.
$NaN_3/KNO_3/SiO_2$	$10NaN_3 + 2KNO_3 + 5SiO_2 = 5Na_2O{\cdot}K_2O{\cdot}5SiO_2 + 16N_2$	56,0/17,5/26,5	[1, 2]
NaN_3/CuO	$2NaN_3 + CuO = Na_2O + Cu + 3N_2$	62,0/38,0	[2]
NaN_3/MoS_2	$4NaN_3 + MoS_2 = 2Na_2S + Mo + 6N_2$	61,9/38,1	[2]
NaN_3/S	$2NaN_3 + S = Na_2S + 3N_2$	80,2/19,8	[2]
NaN_3/C_6Cl_6	$6NaN_3 + C_6Cl_6 = 6NaCl + 6C + 9N_2$	57,8/42,2	[1]
NaN_3/PTFE	$4NaN_3 + (CF_2\text{-}CF_2) = 4NaF + 2C + 6N_2$	72,2/27,8	[1]
NaN_3/SPCW	$6NaN_3 + 2(C_4H_5Cl_3) = 6NaCl + 7C + 2NH_3 + CH_4 + 8N_2$	55,0/45,0	-

The heats of reaction were measured in a bomb calorimeter. The thermal equivalent of the instrument was determined by burning certified samples of benzoic acid with purified oxygen at a pressure of 2.5 MPa. All tested samples were in the form of a pellet 2-cm in diameter and 10-g in mass pelleted at 50 MPa. A sample was placed in a quartz crucible and ignited by an electrically heated resistance wire. Argon at a pressure of 0.5 MPa was used as an atmosphere in each experiment.

At least two measurements were performed for each mixture and the results obtained did not differ more than 2 % between themselves. Their average values are marked as black points (additionally described as Q_{exp}) in Figs 1÷7 presented in the next section of the paper.

3. THERMOCHEMICAL CALCULATIONS

For the theoretical analysis of the combustion process the code CHEETAH was applied [7]. The calculations were carried out with an assumption of the chemical equilibrium in the combustion products. The thermochemical properties of gaseous products were described by the equation of state for the ideal gas. Before performing the computation, the library of likely combustion products was extended. The necessary thermodynamical functions were taken from Ref. 8.

In order to determine the adiabatic flame temperature, the combustion examined was treated as an adiabatic and isobaric process. After appointing the isobar in an assumed temperature range and after determining the thermochemical equilibrium at some temperatures chosen within the range, a difference between the total enthalpy of the equilibrium state at a temperature of T and the total enthalpy of the mixture at the standard temperature of T_0=298.15 K was calculated. The temperature, for which the difference was close to zero, was found as the adiabatic flame temperature T_a.

$$\sum_{i=1}^{k} n_i \left(I^0_{T_a}\right)_i - \sum_{j=1}^{l} n_j \left(I^0_{T_0}\right)_j = 0 \tag{1}$$

where k and l denote numbers of species of combustion products and ingredients in a mixture, respectively, n_i and n_j are numbers of moles of the i^{th} species of combustion products and the j^{th} ingredient of the mixture, respectively, $\left(I^0_{T_a}\right)_i$ is the total enthalpy of the i^{th} species of combustion products at temperature of T_a, and $\left(I^0_{T_0}\right)_j$ is the total enthalpy of the j^{th} ingredient of the mixture at the standard temperature T_0.

The combustion products can react between themselves when they are cooled from temperature T_a to ambient temperature. As we compared the calculated heats of reaction with the values measured in the bomb calorimeter, it was necessary to take into consideration the composition changes caused by the reactions. We assumed that the final composition of combustion products corresponds to the group of chemical compounds found by CHEETAH after cooling the products to the standard temperature in an isochoric process. Knowing the combustion product composition, the heats of reaction, Q_r, was calculated from the following relation:

$$Q_r = -\left[\sum_{i=1}^{k} n_i \left(\Delta H^0_{fT_0}\right)_i - \sum_{j=1}^{l} n_j \left(\Delta H^0_{fT_0}\right)_j\right] \tag{2}$$

where $\Delta H^0_{fT_0}$ denotes the standard enthalpy of formation of the i^{th} reactant or the j^{th} substrate.

Figs 1÷7 present results of the calculations in the form of dependence of that adiabatic flame temperature T_a, the number of moles of gaseous combustion products at the temperature $n_g(T_a)$ and at the standard temperature $n_g(T_0)$, the number of moles of nitrogen at the standard temperature n_{N2} and the heat of reaction Q_r on the contents of NaN_3 in a mixture. In the Figs, there are also black points (•) described as Q_{exp} that depict the measured heats of reaction.

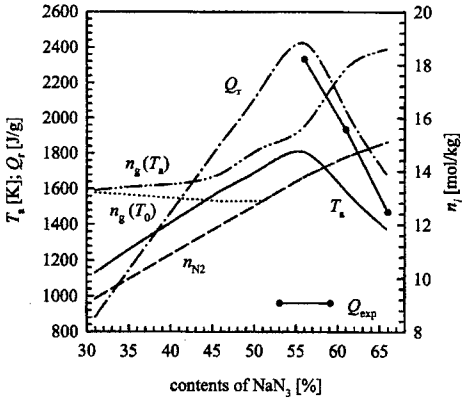


Fig 1. Thermochemical characteristics of combustion of $NaN_3/KNO_3/SiO_2$ mixtures, the mass fraction of SiO_2 was constant (26,5 %)

For the first three compositions the difference between the calculated and measured heats of reaction does not exceed 10 % (Figs 1÷3). Their exothermicity and flame temperature are not as high as for the other formulations. Consequently, the burning rate under atmospheric pressure in charges pressed at 200 MPa is also comparatively low – less than 3.5 mm/s. Moreover in the combustion products of the stoichiometric compositions there was no free sodium. The reasonable agreement between Q_r and Q_{exp} values and the absence of sodium in products removed from the calorimetric bomb suggest that the calculated parameters are a good approximation of their real values.

On the other hand, the comparison of the calculated heats of reaction and that experimental for mixtures containing sulphur, C_6Cl_6, PTFE or SPVC (Figs 4÷7) shows that the theoretical values are substantially higher than the measured ones (by 24÷32 %). This fact and the presence of sodium in combustion products – even for stoichiometric mixtures – indicate that in these cases the assumed chemical equilibrium cannot be justified. In reality only a part of sodium reacts with gaseous decomposition products of the other component in the fast propagating combustion wave – the burning rate at atmospheric pressure ranges from 4 to 6.5 mm/s.

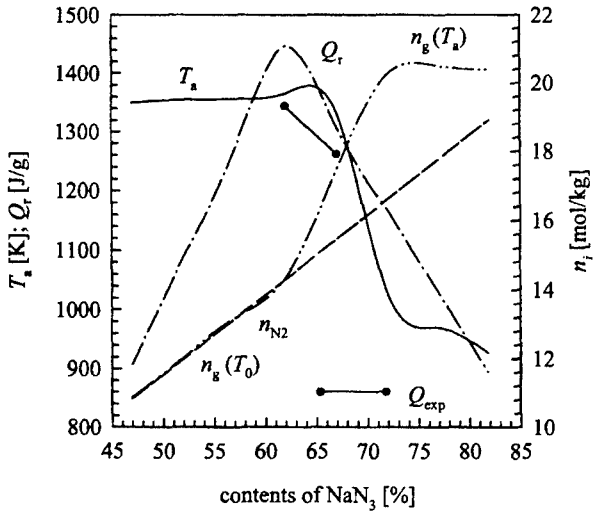


Fig 2. Thermochemical characteristics of combustion of NaN3/CuO mixtures

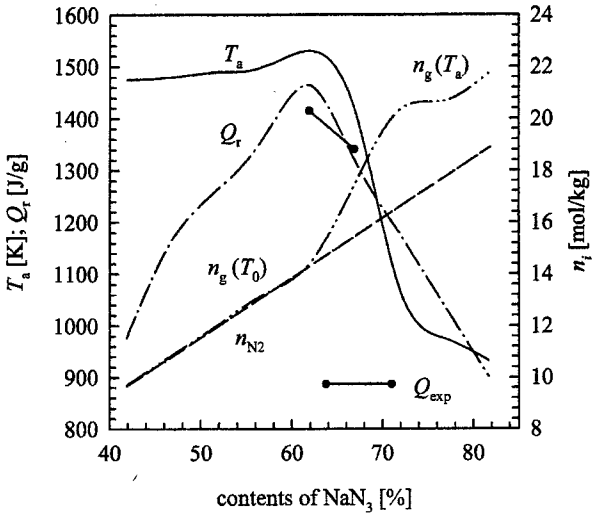


Fig 3. Thermochemical characteristics of combustion of NaN_3/MoS_2 mixtures

Compositions with PTFE have the highest combustion temperatures. The parameters change from of about 2400 K for mixtures poor in NaN_3 to 1500 K for mixtures containing more than 80 % of sodium azide. The lowest temperatures were obtained for NaN_3/CuO and NaN_3/MoS_2 mixtures – they are within a range of 900÷1500 K.

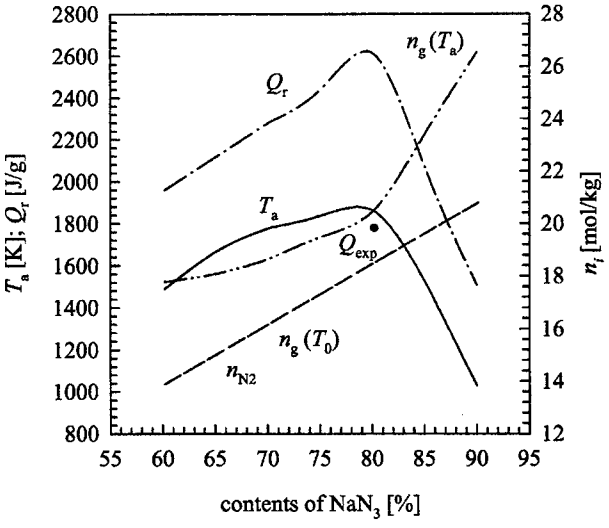


Fig 4. Thermochemical characteristics of combustion of NaN_3/S mixtures

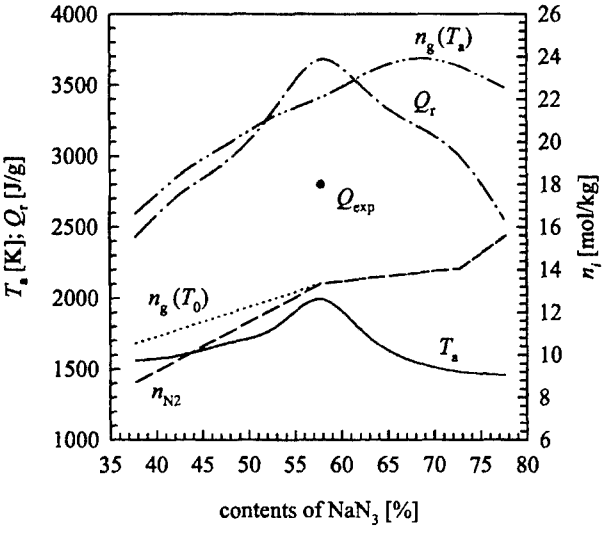


Fig 5. Thermochemical characteristics of combustion of NaN_3/C_6Cl_6 mixtures

The main gaseous combustion product for each formulation is nitrogen. If the contents of NaN_3 exceed the stoichiometric amount, free sodium is present in the combustion products and at the combustion temperature it also appears in the gaseous phase. Therefore in the case of mixtures with relatively low combustion temperature (Figs 1÷4) the numbers of moles of gaseous products at the flame temperature $n_g(T_a)$ increase with increasing contents of NaN_3.

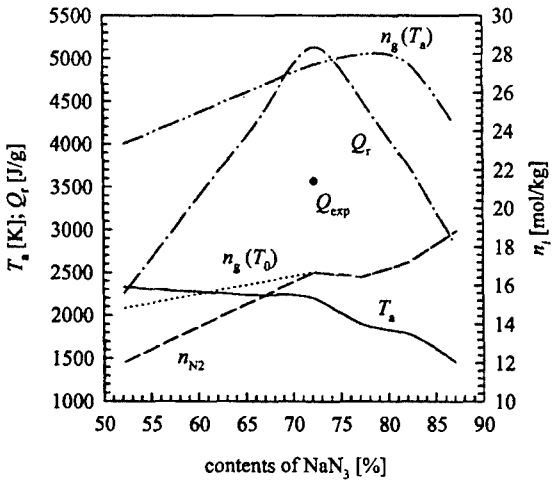


Fig 6. Thermochemical characteristics of combustion of NaN_3/PTFE mixtures

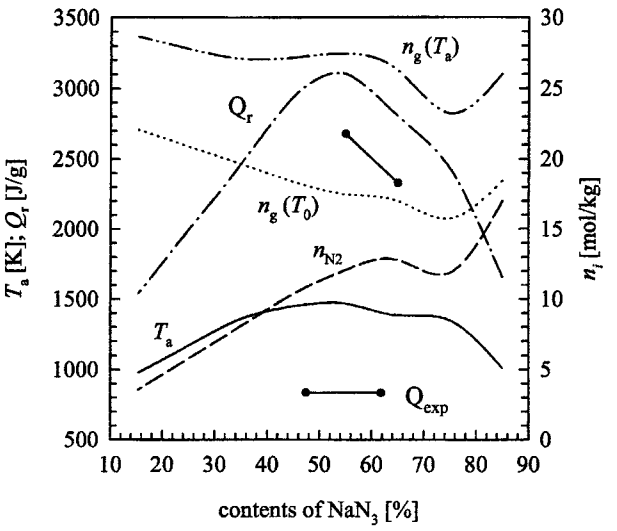


Fig 7. Thermochemical characteristics of combustion of NaN_3/SPVC mixtures

The final combustion products of NaN_3/PTFE mixtures include (besides N_2) carbon, sodium fluoride (NaF), sodium cyanide (NaCN) and tetraflormethane (CF_4). In the combustion products of mixtures containing C_6Cl_6 there are carbon, NaCN and, of course, sodium chloride (NaCl) and a small amount of tetrachloromethane (CCl_4). Combustion of NaN_3/SPVC mixtures leads to formation of carbon, NaCl, NaCN. Methane and ammonia are also present in a quite big amount, especially for compositions poor in NaN_3. The solid combustion products of formulations containing sulphur include sodium sulphide Na_2S. Along with molybdenum, it is also the main component of the residue after combustion of NaN_3/MoS_2 mixtures. Formulations with KNO_3 contained 26,5 % of SiO_2 in order to bind sodium and potassium oxides into chemically inert silicates [1, 2]. For compositions containing less than 56 % of NaN_3, the solid combustion products incorporate sodium and potassium silicates and some amount of their oxides and peroxides. The gaseous products include oxygen and therefore their number of moles does not fall down with decreasing NaN_3 contents. Metallic and gaseous sodium and potassium occur in combustion products when NaN_3/KNO_3/SiO_2 mixtures contain any excess of sodium azide. Reactions in the stoichiometric mixture of NaN_3/CuO mainly lead to formation of sodium oxide and copper. In non-stoichiometric compositions the surplus of CuO does not decompose and the excess of NaN_3 resolves into elements.

4. CONCLUSION

In the case of mixtures with the lowest combustion heats (NaN_3/CuO, NaN_3/MoS_2 NaN_3/KNO_3/SiO_2), the idealised, simple reactions (Table 1) are a fair approximation to the overall thermochemical processes. Therefore it can be assumed that the calculated parameters are close to their real values. Both the coincidence of the maximum

exothermicity with the postulated stoichiometry and the good consistence of the measured and calculated values of the heats of reactions are in favour of the above statements.

For all the mixtures tested, the heat of reaction strongly depends on the contents of NaN_3 so that it can be reduced both by enrichment and depletion of mixtures in sodium azide. Bearing in mind, however, that a decrease in NaN_3 contents leads to a decline in the amount of nitrogen released, this way of modification of the compositions cannot be accepted. Moreover the minimisation of the heat of reaction is usually aimed at reduction of the temperature in the combustion wave, whereas for some of the mixtures examined, e.g. NaN_3/CuO and NaN_3/MoS_2, the adiabatic flame temperature remains practically constant in quite wide range of NaN_3 contents below the stoichiometry.

The use of mixtures that contain more NaN_3 than the stoichiometric ones seems to be a better way of lowering the heat and temperature of combustion. Then the generated amount of nitrogen rises because it is an increasing function of NaN_3 contents. However, for such mixtures the combustion products contain free sodium, and its chemical activity can disqualify them from some applications.

The most interesting properties display mixtures of sodium azide with copper oxide and molybdenum disulfide. Their adiabatic flame temperature does not exceed 1500 K and it can be substantially reduced (even by hundreds of K) by a comparatively small increase in the contents of NaN_3 above the stoichiometry. Such a sharp decrease in the parameter value results from the drop in exothermicity and simultaneous energy losses for evaporation of sodium.

Acknowledgement

This paper was accomplished within the framework of the Project 0 T00A 021 20 financed by the State Committee for Scientific Research

REFERENCES

[1] K. E. Nilsson, S. Zeuner, Airbag-insassenschutz für Automobile Entwicklungsmerkmale und praktische Ausführung des pyrotechnischen Gasgenerators, Proceedings of the 16. Internationale ICT-Jahrestagung (combined with 10th International Pyrotechnics Seminar) Karlsruhe, Germany, July 2-5, 1985.

[2] F. Volk, Utilisation of propellants for inflator and belt restraint systems, Proceedings of the 25th International Pyrotechnics Seminar, Brest, France, Vol. 1, pp. 106-112, June 7-11, 1999.

[3] H. Schmid, N. Eisenreich, A. Baier, J. Neutz, D. Schroter, V. Weiser, Gas generator development for fire protection purpose, Propellants, Explosives, Pyrotechnics, 24, pp. 144-148, 1999.

[4] H. Schmid, N. Eisenreich, Investigation of a two-stage airbag module with azide-free gas generators, Propellants, Explosives, Pyrotechnics, 25, pp. 230-235, 2000.

[5] N. Hirata, N. Matsuda, N. Kubota, Combustion of NaN3 based energetic pyrolants, Propellants, Explosives, Pyrotechnics, 25, pp. 217-219, 2000.

[6] V. Shandakov, V. Puzanov, V. Komarov, V. Borochkin, The method of low temperature generating in solid gas generators, Fizika Goreniya i Vzryva, No 4, pp. 75-78, 1999.

[7] L. E. Fried, CHEETAH 1.39 – User's Manual, Lawrence Livermore National Laboratory 1996.

[8] M. L. Hobbs, M. R. Baer, Nonideal thermoequilibrium calculations using a large product species data base, Shock Waves, No 2, pp. 177-187, 1992.

IRON OXIDE/ALUMINUM FAST THERMITE REACTION DRIVEN PROPAGATION

Luisa Durães*, José Campos and António Portugal***

Laboratory of Energetics and Detonics
*Chem. and **Mech. Eng. Departments - Fac. of Sciences and Technology
University of Coimbra - Polo II - 3030-290 Coimbra - PORTUGAL

Abstract:

Reaction between iron oxide (Fe_2O_3) and aluminum (Al) is the reference of the classic thermite compositions. Ignition of those thermite compositions is recognized to be problematic and the regression rates of its self-sustained reactions are commonly low. Also the efficency of the reaction, for a given initial composition of Fe_2O_3 and Al, is evaluated by the final temperature and by the mass ratio of Al_2O_3 /AlO in products of combustion (in condensed phase).

In order to increase pressure of the products of thermite reaction, the original composition based on Fe_2O_3/Al mixture is mixed, with an original twin screw extruder, with a small percent (< 3%) of propellant binder composed of ammonium or potassium nitrates, mixed with a polyurethane solution. The products of combustion and pyrolysis of this binder, reacting with thermite products, generating high temperature conditions, allow an easier but relatively slow propagation. These experimental thermodynamic conditions are also predicted using THOR thermochemical code. The study also presents DSC and TGA results of components and mixtures, and correlates them to the ignition phenomena and reaction properties. The experimental regression rate of combustion and its final attained temperature, as a function of the pressed thermite composition, are presented and discussed.

In order to generate a fast driven propagation in thermite material, an original configuration is used, driving the reaction with a continuous spark discharge, between an central electrode and the external confinement, from a capacitor discharge. The driven reaction can then be correlated to the original self-sustained reaction, as a function of the composition and of capacitor discharge level. Results show an existing different reaction process, where the energy release, from the capacitor discharge, accelerates and enhances the thermite reaction propagation. Results are presented and the evaluation of additives contribution in this particular case is discussed.

Full paper version wasn't available till the deadline

DETERMINATION OF ADDITIVES FROM EXPLOSIVE MATERIALS WITH GC/MS (EI,NCI)

Eisner A.*, Ventura K.* and Varga R.**

* Univerzity of Pardubice, Faculty of Chemical – Technology,
Department of Analytical Chemistry, Nám. Čs. Legií 565, Pardubice 532 10, CZ

** Univerzity of Pardubice, Faculty of Chemical – Technology,
Department of Theory and Technology of Explosives, Nám. Čs. Legií 565, Pardubice 532 10, CZ

Abstract:

Actual problem of these days is terrorist activities. The identification of explosive materials after terrorist attacks is necessary. The concentration of post-blast residues is very low, therefore is necessarry to use very sensitive detection techniques. In this paper a comparison of two ionisation teechniques for GC/MS is described. This is a electron impact ionisation and negative chemical ionisation.

1. INTRODUCTION:

Very important part of analysis is isolation of post-blast residues from solid matrices.

Actual methods, to isolate the compounds included in the explosives from the soils and other solid matrices, antecedent to the analytical determination, are the Soxhlet extraction and sonication extraction. These methods require relatively high volumes of solvents and are relatively time consuming. In recent years, various attempts have been made for substitution the classical extraction techniques, with the techniques, which would decrease the volume of the extraction solvent, amount of the sample to be analyzed as well as the time of the extraction process. These methods could be a supercritical fluid extraction[1] or a pressurised solvent[2,3] extraction.

The GC/MS and LC/MS are most often[4] used technique for analysis of these extracts. GC/MS with electron impact ionisation may not be enough sensitivite for determination of these concetration levels. In this paper this ionisation technique is compared with negative chemical ionisation. First of all we heve been tested these techniques with using of standard solutions (trinitrotoluene (TNT), 2,4- and 2,6- dinitrotolune (DNT), 1,8-dinitronaphtalene (DNN) and nitroglycerine(NG)).

2. EXPERIMENTAL:

The extracts obtained were analysed by using of the gas chromatograph GC 17A coupled with mass spectrometry detector QP 5050A (EI, NCI, both Shimadzu) and GC/MS solution data system (Shimadzu). The helium (grade 5.0, Linde) was used as carrier gas. Separations were performed on a 30m x 25μm i.d. capillary column coated with a 0,25 μm film of polymethylsiloxane (DB-5 MS). Split injection 1:10 was used. The column oven was isotermally maintained at 180°C. The temperature of injector was 180°C and the temperature

of interface was 230°C. The identification of compounds was based on the comparisoin their mass spectrum with the spectrum in the library (NIST 62, Shimadzu).

3. RESULTS NAD DISCUSION:

We have been prepared solutions of standards (TNT, 2,4- and 2,6- DNT, 1,8-DNN and NG). The concetration level of each compound was about 10 mg/ml in methanol. These solutions have been measured on GC/MS. First with electroimpact ionization. We have been determined a retention time of these analytes from these measurements. Some chromatograms are shown in figure 1. Than we have been measured the same samples with negative chemical ionisation.

Table 1. Comparison of sensitivity of ionisation techniques

compound	area	
	EI	NCI
trinitrotoluene	553908	4616255
2,4-dinitrotoluene	625245	4055854
2,6-dinitrotoluene	1168208	59180757
2,8-dinitronaphtalene	2823291	19501204
nitroglycerine	2164696	183923660

As reaction gas we have been used methane. This method allows to achieve higher sensitivity for this type of samples as shown in table I. The GC/MS with NCI is from six times to eighty times more sensitive than GC/MS EI. Some characteristic chromatogram is shown in figure 2. The negative chemical ionisation was provided charakteristic mass spectrum which mostly include only molecular ion or aduct with reaction gas or another compounds which are included in sample. This is useful thing for obtaining higher sensitivity this ionization method. The aim of this paper is to make library of characteristic mass spectrum with negative chemical ionization of characteristic compounds which are present in explosive materials. This will be used for identification of a post-blast residues.

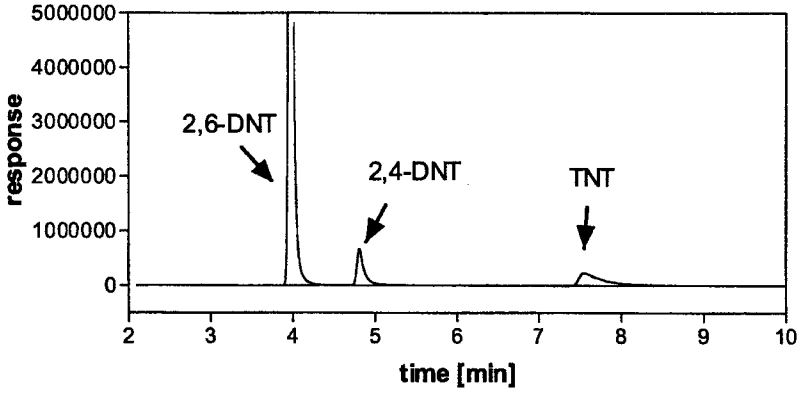


Fig 1. GC/MS-NCI chromatogram of standard mixture of additives

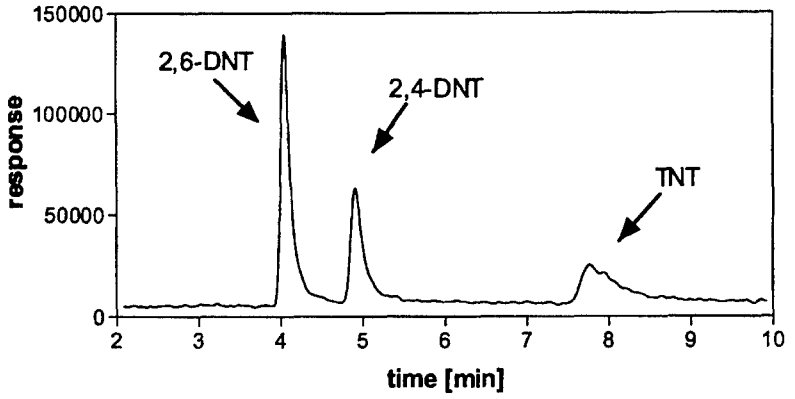


Fig 2. GC/MS-EI chromatogram of standard mixture of additives

4. CONCLUSIONS

Perform experiments have been confirmed the fact, that NCI technique is resulting to the higher sensitivity of determination of additeves included in explosive materials than EI.

Acknowledgements:

Experiments were performed thanks to financial support from the Grant Agency of the Czech Republic (Project 203/02/0023) and from the Ministry of Education, Youth and Sports of the Czech Republic (Project MSM 253100002).

REFERENCES:

[1] Kurečková K., Ventura K., Eisner A., Adam M.: Aplikace fluidních extrakcí při izolaci kontaminantů z půdních vzorků. Chem. Listy, 95, 415-419 (2001).

[2] Ventura K., Adam M., Válková P.: Extrakce olejů ze vzorků krystalického polystyrenu metodou zrychlené extrakce rozpouštědlem. Chem. Listy, 95, 223-226 (2001).

[3] Adam M., Ventura K.: Využití zrychlené extrakce rozpouštědlem pro stanovení esterů kyseliny ftalové a polycyklických aromatických uhlovodíků v půdách a říčních sedimentech. Chem. Listy, 95, 318-318 (2001).

[4] J. Zinon, C. Zitrin: Modern methods and applications in analysis of explosives. ed.: John Wiley & Sons Chichester (1993)

DETERMINATION OF THE DETONATION VELOCITY EMULSIONS EXPLOSIVES IN THE DIFFERENT THERMAL CONDITION

L. Čačić*, Z. Ester and M. Dobrilović****

*Ministry of Interior
Zagreb,Republic of Croatia

**Faculty of Mining, Geology and Petroleum
University of Zagreb,Republic of Croatia

Abstract:

Detonation velocity is the velocity at witch the chemical reaction zone propagates trough a given explosive. It is one of the most important detonation parameters. Bearing in mind the fact that detonation velocities of know high explosives may reach nearly 10 mm/microsecond, the experimental determination of the detonation velocity is not easily achieved. However, when compared to the other detonation parameters, its accomplishment represents the least complicated task. The determination of the detonation velocity is based upon the measurement of the time interval needed for the detonation wave to travel a known distance through the explosive being tested. The measuring equipment used for the determination of the detonation velocity should provide the detection of the arrival of the detonation wave using suitable velocity probes. The measuring of the very short time-intervals (on a microsecond scale) needed for the detonation wave to travel a known distance through the sample between two velocity probes. Velocity of detonation shall be determined at the minimum diameter placed on the market, or the minimum diameter recommended by the manufacturer.

1. THE CHARACTERISTICS OF EMULSIONS EXPLOSIVE

Emulsions in the terminology of explosive is type doesn't have an affair in the oil with the standard structure matrix (nitrate salts 77-83%, the water 15-18%, the fuel to 6% and others to 20%.

The emulsions explosives get the mixing would be concentrated the mixtures of oxidants (usual ammonium the nitrates) on the raised temperature and fuels in the presence of the disperse.

The emulsion matrix becomes mechanical sensitive on the forces produced detonators or boosters the adding senzibilizators (the glass micro balloons which consist of the gas, the injection of gases direct in the emulsion or the adding of chemical substance).

The glass balloons or the bubbles of gas function as local «hot point» and enable the expansions of fronts of detonations. The deposit senzibilizators insures himself «gas pocket» in the explosive. When the detonation wave reaches the gas pocket, contact surface destroys and gas compresses creating the microscopic dot fevers « hot point ».

The hot dots insure the keeping up chemical reaction detonations.

1.1 The structure of emulsions explosive

The components of emulsions explosives include the ingredients like oil (would be continued) the phases, the oxidant as would be scattered (the inner phases) the emulgators, the person making a change densities and fewers of different supplements.

The emulsions explosive system «water in oil» in which is the oxidant the liquor would be scattered in the oil phase. The consideration on the limitations in view of the balances of oxygen and requirement towards the explosion , the contents of oil phase underneath 5% scatters the phases.

The viscosity, the molecular structures of oil phase and her the binding with emulgators is very importantly because of the creation sufficient firm protection wrapping, so that the stops him deformation or shoots the when oxidant, the inorganic salt, like the ammonium nitrate starts crystallize.

The numerous organic substances appropriate for the usage as the oil phases of emulsion explosive. Chose have been connected with the function of oil phase in the explosive. The general every hydrocarbon of suitable consistency can uses (for example waxes, the oils and different polymers).

The consistency of emulsion explosive depends about the choice of material for the oil phase. The regular consistency is very important that stays the sensitive micro bubbles (or the gas preserved firm particle) and so holds the detonation sensitivity in the course of the production and ware housings. If is the consistency short bubbles in the course of the production, the ware housings and usages amass and secrete, what is hazardously in view of the detonation of sensitivities of explosives. If the consistency of too tall emulsions is the favoring ageing, what is inconveniently in view of the stabilities in the course of the ware housings.

The general water mixtures oxidant for the emulsion explosive preparation melts away the ammonium nitrate in the water. The such mixture consists of 70 - 95% the ammonium nitrate and 5 - 35% the waters. The reduction of temperature of fall solubility ammonium nitrate in the water, these he secretes by the shorter temperatures, what is inconveniently for the stability of emulsion explosive.

The emulsion explosive for the purpose of attaining the balances of oxygen and enlargements explosions, add one or upper factors the burnings or the senzibilizators. The oil phase are the hydrocarbons (from the oil, the waxes and polymers) which are and good agents burnings. Monotonous scattered the droplets of oxidant in the intimate contact with the oil wrapping would be continued the phases, which successful encourages and carries the detonation. In the such specific circumstances hydrocarbons function and as senzibilizators.

The persons making a change densities third have been scattered the phases under way creation emulsions. The adjusting of density of emulsion explosive attains introduces the big number micro bubbles. The micro bubbles influence on the density and energy of explosive and important improve the detonation sensitivity of explosive according to the theory «hot points». The Micro bubbles after that the non-stop warming polecat series of warm dots the when temperature in the terse time (10^{-3} do 10^{-5} s) the growths with 400 next to 600 °C activating so the emulsion explosive. The Micro bubbles must what smaller, homogeneous distributed and stable that prevents their accumulation or the going out. The diameter particle moves than about 0,5 to 100 micron, mainly 5 to 50 the micron. The number of active bubble in 1 cm^3 amounts 10^4 do 10^7.

The key component of emulsion explosive is emulgator, the weights represented with 0,5 - 2,0%. Though the smallest according to the contents important influences on the quality of emulsion explosive.

From the other supplements important mentions the following:

- the persons making a change of crystal form (0,1 - 0,3%),
- the emulgator promoters (0,2 - 0,8%),
- the emulsion stabilizers (to 0,5%°).

1.2 Some characteristics of emulsion explosive

a) Detonations velocity

The factors which have influenced in a detonations velocity of emulsion explosive:

- the densities,
- the supplements firm powdery substance,
- the diameter of charge,
- the spacious limitedness,
- the temperatures,
- the contents waters.

The detonations velocity have increased increases the densities if the structure of explosive and conditions make unchanged (fig. 1.).

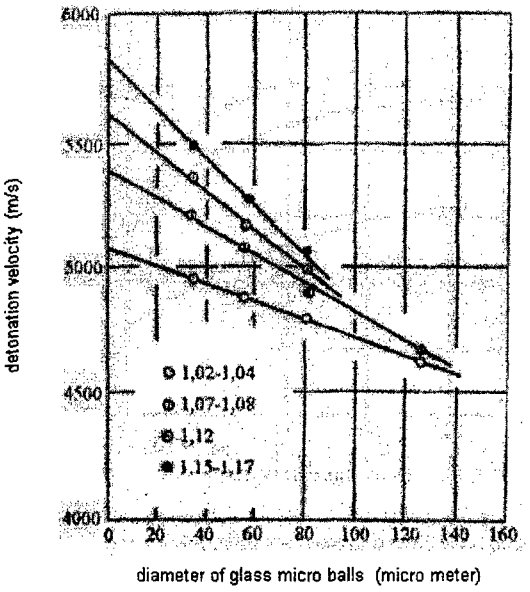


Fig 1. Diameter of glass micro balls and suitable detonation velocity.

The density in the emulsion explosives adapts the adding the micro bubbles in which is consisted of the air. The number, the sizes and form micro bubbles also is influential in a hurry the detonations. In the unlimited patroness, the speeds detonations dependent is about the diameter glass micro bubbles. The speeds detonations increases the decrease measures the micro bubbles (beside the not changed density) and enlargement of number micro bubbles (fig.2.).

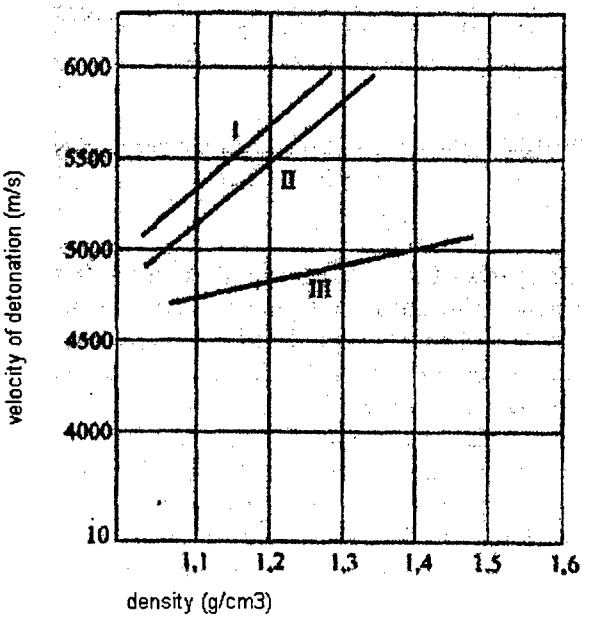


Fig 2. Density of emulsions explosive and suitable detonation velocity.

The velocity of detonations depends, though no important, and about the diameter filling up the respective patronesses.

The velocity of detonations mainly not does change in the temperature area than - 40 to + 40 °C.

The contents water lead significant influences on the stability, the density and sapper characteristics of emulsion explosives. The top speed detonations and brizant attains by the contents guide from 10 to 12%.

b) Brizant of explosives

The sizes brizant for the emulsion explosive big and moves between 16 and 20 mm (the Hesse test, - the pressure test on the lead block).

c) The transfer of detonations

The size of transfer of detonation by the emulsion explosive moves from 25 to 150 mm.

d) Waterproof

Because of the inner physical structures of emulsion explosive of organic particle have protected the continuous oil phase this they possess the good waterproof.

e) The Safety

The safety of emulsion explosive carries off on the mechanical sensitivity, (the blow and rubbing) the sensitivity on the burning, the dot burnings, the getting trough with bullet. The safety of emulsion explosive on the this criterion is very good.

f) The critical diameter of explosive

Critical diameter the emulsion explosive moves between 12 and 37 mm.

2. DETERMINING OF DETONATION VELOCITY OF EMULSIVE EXPLOSIVE "ELMULEX"

The "ELMULEX" is the emulsion explosive of manufacturer ELMECH RAZVOJ d.o.o. Budinšćina, Gotalovec, Republic of Croatia, tested and produced according to the standard HRN.H.D1020.

The "ELMULEX" is brizant explosives the forward pass blasting of middle hard carboniferous rocks (the sheet metal stones and dolomites).

2.1 The basic characteristics of emulsion explosive "ELMULEX" on which is done the testing:

The Density	(kg/l)	1,15
The Gas volume	(l/kg)	925
The Explosion energy	(kJ/kg)	3120
The Explosion temperatures	(°C)	2050
Oxygen balance	(%)	+0,7
Micro balls	(%)	2,3
diameter the cartridge	(mm)	38
length the cartridge	(mm)	550
mass the cartridge (patronesses)	(gram)	700

2.2. Testing of detonation velocity emulsions explosives "ELMULEX"

The patronesses of explosive have left 24 the hour on the temperature -25 °C these after this is done the measurement of detonation velocity.

In the patronesses of explosive are at the distance 300 the mm would be placed two optical cable (fig.3.)

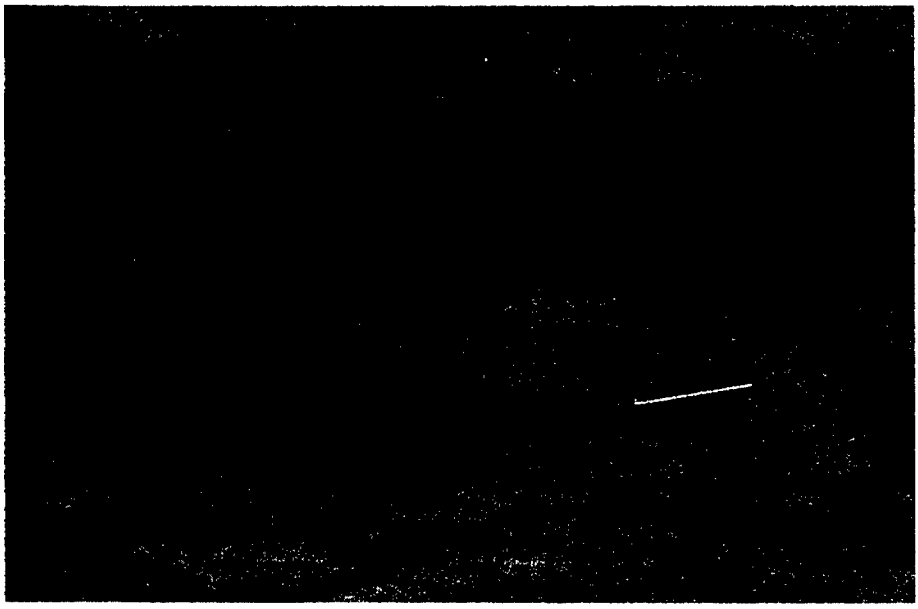


Fig 3. Emulsions explosive ϕ 38 mm with two optical cables and electric detonator (left) and thermometer (right).

The activation of explosives has accomplished with momentary electric the detonator About With Al; 2 x 2 Fe; 0,45 And with ignition machine the Schaffler & the Co type 818 510 W; 100 V; 10 mF.

The measuring method and principle of operation and the Instrumentation

The Timing and detonating velocity meter

The EXPLOMET-FO-MULTIMODE has 5 independent measuring the time intervals between the illumination of 6 optical probes.

One of the probes starts all the timers. Then every triggered probe stops in timer. The result of each timer is displayed in microseconds according to one of 3 following mode:

- Mode 1 (standard: velocity and time) the probes must be illuminated in ascending order, is 1, 2, 3, 4, 5, 6, Time intervals are displayed between two consecutive probes. The Velocity of detonation in meter/second is displayed if the corresponding length, between the probes, was introduced.
- Mode 2 (time only) the probes are illuminated randomly. It displays the measured time in microseconds between the second illuminated probe and the third illuminated probe; and so on: third probe and forth probe until a maximum of 5 measures.
- Mode 3 (time only) the probes are illuminated randomly. It displays the measured time in microseconds between the first illuminated probe and the second illuminated probe, then it displays the measured time between the first illuminated probe and the third illuminated the probe; and so on first probe and forth probe until a maximum of 5 measures.

Easy quality control

Reliability:

advanced microelectronic technology in a robust aluminum the case, the use of fiberglass-optic insure on excellent electrical noise immunity.

Precision:

Time measurement :+/- 0,1 microsecond, Velocity measurement: better than 0,2%.

Safety:

The distances between the EXPLOMET-FO-MULTIMODE and the blasting site: Up to 80 meter.

Easy use:

the usual knowledge for explosive handling is sufficient to operate the EXPLOMET-FO-MULTIMODE, the use of optical fibers permits detonating velocity measurement on very short cartridges, easy and fast set up, as the user only has that to plug the optical probes into the cartridge, each measure destroys only approximately 20 cm of each optical the test probe.

Easy installation:

can be adapted on any existing test sitel (with fixed cables).

Portable:

only 4 kg with all attachments and 100 meter fiberglass optic probes in transport case, allows case transportation on the blasting site.

Operators an batteries:

5 hours autonomy, rechargeable with the AC/DC adapter/charger

Specifications

Dimension:

EXPLOMET-FO-MULTIMODE aluminum case (170 x 130 x 63 the mm), transport case for the EXPLOMET-FO-MULTIMODE (450 x 350 x 150 the mm),

Weight:

The EXPLOMET-FO-MULTIMODE with batteries = 0,5 kg, with attachments in transport case = 4 the kg.

Autonomy:

5 hours of continues operation on rechargeable Ni Cd batteries. The Ac/DC adapter/charger for 220 V/50 Hz or 110 V/60 Hz.Standard batteries charging time 14 - 16 hours.

Operating range:

distances between two optical test probes on the explosives up to 10 meter, detonating velocity up that 10.000 m/s, time interval measurement: 0,1 microsecond up to 10 seconds.

Timers:

5 synchronous timers.

Operating temperatures:

0 - 50 °C.

Accuracy:

+/- 0,1 microsecond.

Fiberglass optic:

plastic fibber optic cable: - core 1 mm diameter, - jacket 2,2 mm diameter.

Optional:

25 the meter of the dual channel armored optical cable extension, 3 mm diameter black the P.V.C. protection the pipe for fibber optic probes.

3. RESULTS

After the done measurements gotten have followed the results:

Table 1. The introduction temperatures and belong be measured the detonations velocity.

Ordinal number	Temp. °C	Speed m/s	Middle speed m/s	Ordinal number	Temp. °C	Speed m/s	Middle speed m/s
1.	-20	4.680 4.920	**4.800**	9.	- 3	4.615 5.000	**4.807**
2.	-15	4.375 4.655	**4.515**	10.	- 2	4.184 4.680 4.608	**4.490**
3.	-13	4.702 4.559 4.237	**4.499**	11.	1	4.838 5.277 4.991	**5.035**
4.	-12	4.636 4.731 4.310	**4.559**	12.	5	5.025 5.120	**5.072**
5.	-10	4.511 4.531	**4.521**	13.	10	4.970 4.608	**4.789**
6.	- 8	4.716 4.680	**4.698**	14.	13	4.739 4.629	**4.684**
7.	- 7	4.761 4.680	**4.720**	15.	20	4.830 4.960	**4.895**
8.	- 5	4.893 5.042	**4.967**				

4. SUMMARY AND CONCLUSIONS

- On the basis of the done measurements of velocities of detonation in different thermal condition is noticed that not has come to the important deviation in the declarer velocity of detonation.
- Consequently the emulsion explosive "ELMULEX " not does change the more significant velocity of detonations in the measured area than -20 to +20 °C.
- The temperature of explosive (-20 to +20 °C.) not does influence in a velocity of detonations.
- From the diagram is unable notice the influence of temperature of explosive in a hurry the detonations, (fig.4) .

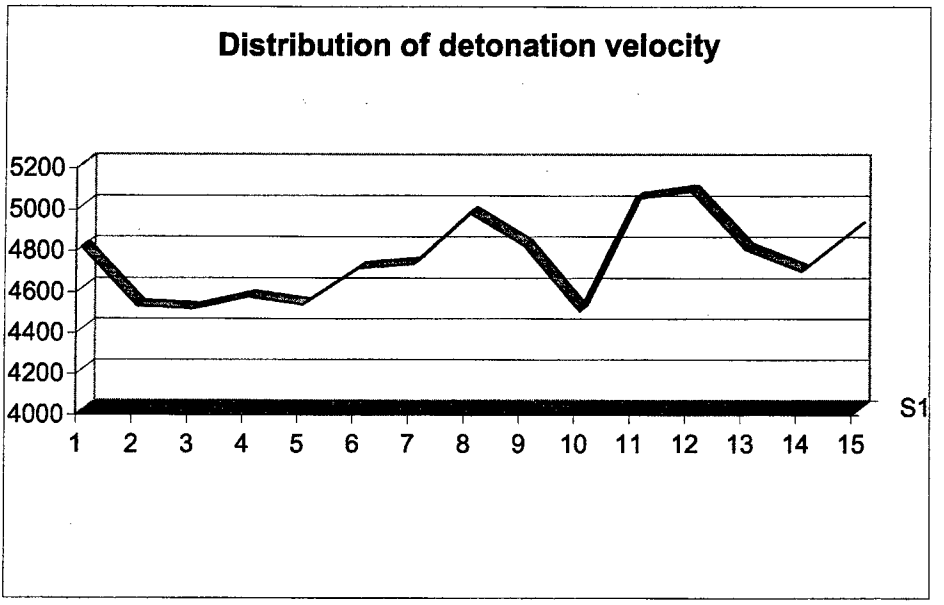


Fig 4. Diagram of the distribution of detonation velocity.

REFERENCES

[1] D.Vrkljan, Utvrđivanje minerskih značajki emulzijskih eksploziva i njihova primjena za miniranje stjena, disertacija, Faculty of mining, geology and petroleum, University of Zagreb, Zagreb,1998.

[2] Nitro Nobel: Product catalog, Magazine, Explosive News, Dyno Explosives Group. Gyttorp. Nora. Sweden.

[3] L.W.Armstrong, N.T.Moxton, Low Shock Energy Emulsion Based Wet Hole Explosives, Fragblast 1990, Brisbane, Australia, pp 45-53.

[4] Characteristics of emulsion explosives ELMULEX, Elmech-razvoj, d.o.o. Budinšćina, Gotalovec, 2000,

[5] EXPLOMET-FO-MULTIMODE, catalog, instructions for use.

THERMOLYSIS OF A PLASTIC BONDED EXPLOSIVE

Gurdip Singh and Prem Felix S

Department of Chemistry, DDU Gorakhpur University, Gorakhpur – 273 009, India

Abstract:

The thermolysis of pure RDX and its plastic bonded explosive (PBX) with hydroxyl terminated polybutadiene (HTPB) has been undertaken using TG-DTG and DTA techniques. Isothermal TG has been done and the data therefrom has been used to evaluate kinetic parameters using a model free isoconversional method. Explosion delay studies have also been undertaken using tube furnace technique. The results of the work done are discussed briefly on a comparative basis by analysing the departure of the thermal behaviour of the PBX from that of RDX.

Keywords: *PBX, thermolysis, RDX, HTPB, isoconversional method*

1. INTRODUCTION

Plastic bonded explosives are a class of composite explosive materials containing a high energetic compound as the filler in a polymer matrix. They are usually less sensitive energetic system, in which good thermal stability and low explosiveness is required. Thermal analysis is an essential part of study of PBXs from the point of view of safety and end use. A detailed knowledge of the thermal behaviour of each component of a PBX as well the PBX itself may also be useful to predict the thermal behaviour of new energetic formulations. Although the studies on the thermal decomposition of pure energetic compounds are known in detail, that of PBXs are rare in open literature.

PBX formulations containing RDX as energetic filler and HTPB as binder is known to be used in rockets for stage separation and other applications. The thermal decomposition of RDX [1,2] and HTPB [3-5] are known in detail and reports are available in numerous papers and monographs. However a systematic attempt to investigate the effect of binder on the thermolysis of energetic fillers is not readily available in literature. However there are some studies on the thermolysis of nitramine propellants [6-8], which are essentially composite energetic materials. We have planned a study concentrating on the thermolysis of PBXs. Thus we have made an attempt to disseminate the effect of HTPB on the thermal behaviour of RDX and the results are reported here

2. EXPERIMENTAL

Materials

The PBX containing 85 % (by weight) RDX and rest IPDI cured HTPB (here after will be named as HTRX-85) and RDX were supplied by High Energy Material Research Laboratory (HEMRL), Pune. RDX was used as received.

TG-DTG studies on RDX and PBX

TG-DTG studies on HTRX-85 and pure RDX (sample mass = 2 mg, heating rate = 10 ^{0}Cmin.$^{-1}$, N_2 atmosphere) have been undertaken at National Institute of Pharmaceutical and Education and Research (NIPER), Chandigarh and the corresponding thermograms are shown in Figure 1 and the phenomenological data is summarized in Table 1.

Non-isothermal TG studies

Non-isothermal TG on RDX and HTRX-85 have been done using an indigenously fabricated TG apparatus [9] in our laboratory (Heating rate = 10 ^{0}Cmin.$^{-1}$, sample mass $\approx$ 25 mg and static air atmosphere). The TG thermograms are shown in Figure 2 and data are summarized in Table 1.

DTA studies

Differential thermal analysis (Universal Thermal Analytical Instruments, Mumbai) has been carried out on RDX and HTRX-85 (Heating rate 10 ^{0}C min.$^{-1}$, sample mass $\approx$ 5 mg, static air atmosphere). The DTA thermograms are shown in Figure 3 and the corresponding data are summarized in Table 1.

Isothermal TG studies

Isothermal TG studies on RDX and HTRX-85 have been undertaken in the previously stated indigenously fabricated TG apparatus (sample mass $\approx$ 25 mg, static air atmosphere) at temperatures 220, 225, 230, 235 & 240 ^{0}C (for RDX) and 195, 200, 205, 210 & 215 ^{0}C (for HTRX-85). The isothermal TG thermograms are shown in Figure 4.

Kinetic Analysis

Kinetic analysis of the isothermal TG data has been performed using a model free isoconversional method [10]. In this method, it is assumed that the reaction model [$g(\alpha)$], in the conventional rate expression is independent of temperature. The equation used in this method is as follows :

$$- \ln t_{\alpha,i} = \ln [A / g(\alpha)] - E_\alpha / RT_i \quad \ldots\ldots\ldots\ldots\ldots(1)$$

where α is the extent of conversion; t, represents time; A is the preexponential (Arrhenius) factor; E_α is the activation energy; R, the gas constant and T is the absolute temperature. $E_{\alpha,i}$ is evaluated from the slope of the plot of $-\ln t_{\alpha,i}$ against $1/T_i$. Thus the values of E_α for RDX and HTRX-85, were evaluated at various α_i. The dependencies of E_α on extent of conversion are given in Figure 5.

Explosion Delay Studies

Explosion delay (D_E) of RDX and HTRX-85 were recorded using tube furnace (TF) technique [11]. The details of the experiment are as reported earlier [11, 12]. The D_E data were found to fit in the following equation [13,14].

$$D_E = Ae^{E^*/RT} \quad \text{.....(2)}$$

where E^* is the activation energy for explosion and T is the absolute temperature. The explosion delay data are summarised in Table 2. The values of E^* (Table 2) were obtained from the slope of the plot of $\ln D_E$ vs 1/T, which is shown in Figure6.

3. RESULTS AND DISCUSSION

TG-DTG thermograms shown in Figure 1 and the phenomenological data summarised in Table 1 show that the thermal decomposition reaction of HTRX-85 is considerably faster than that of pure RDX. The DTG peak temperature has been lowered in the case of HTRX-85. However the initial decomposition temperature (T_i) is same for both RDX and HTRX-85. The non isothermal TG data (Fig. 2 & Table 1) as well as DTA results (Fig. 3 & Table 1) show that atmosphere has not much effect on the thermolysis of RDX and HTRX-85. T_i is almost same in the case of RDX and HTRX-85 in static air atmosphere also. The first endothermic peak in DTA thermogram, at around 200 ^{0}C, is due to the melting of RDX [15]. The exothermic peak temperature for HTRX-85 is at a lower temperature than that for RDX. Thus the thermal studies show that, although the onset temperature for thermolysis for RDX and HTRX-85 remains the same, once the reaction sets in, it occurs at a faster rate in the case of HTRX-85. The fastness in thermolysis may be due to the effect of exothermic decomposition of HTPB and the entrapment of the product gases from the early thermal decomposition of RDX, in the polymer matrix, which undergo secondary reactions in the gas phase. It is reported in the literature [5] that HTPB has a two step exothermic decomposition immediately followed by an endotherm. The IPDI cured HTPB urethanes also undergo two stage decomposition with the DTA curve showing an initial exothermic peak followed by an endothermic peak [3]. Starting decomposition temperature as seen from TG, for HTPB urethane is around 250 ^{0}C. However the exothermic processes during the first stage starts even before this temperature [5]. In the case of HTRX-85, the stage-1 decomposition of HTPB seems to be combined with the thermolysis of RDX. HTPB undergoes further decomposition (Stage 2) in the temperature range approximately 400-500^{0}C which is exothermic in nature followed by an endothermic volatilization of the products of decomposition. In the case of both HTRX-85 the stage 2 decomposition of HTPB also occur to a considerable extent due to the highly exothermic ignition of RDX. Thus it is also possible that the species evolving during the decomposition of HTPB interact chemically with the products of thermolysis of RDX and thus the mechanism of thermolysis may be different for the PBX from that of the pure compounds. But to check whether there is any change in mechanism, further kinetic analysis is required. In order to determine the kinetic parameters of thermolysis for these compounds, isothermal TG thermograms were recorded and this data shows that thermal decomposition reaction occurs at lower temperatures for HTRX-85 in comparison with pure RDX.

The values of activation energy for thermolysis, as shown in Fig. 5, clearly show that the mechanism of thermolysis is different for RDX and HTRX-85, at least in the initial stages of

decomposition. In the case of RDX, initially an activation energy of ~200 $kJmol^{-1}$ has been observed, which gradually changes into ~ 150 $kJmol^{-1}$, at the final stages. Whereas, for HTRX-85, an activation energy of ~ 100 $kJmol^{-1}$, has been observed during the initial stages, which gradually increases upto 150 $kJmol^{-1}$. A detailed study on the thermolysis of RDX and the kinetic parameters for the various reaction channels was reported by Long et al. [16]. Our results for the thermolysis of RDX are similar to that of their results for a closed pan DSC experiment. Thus the initial stages of thermolysis of RDX, is dominated by decomposition in the liquid state whereas gas phase decomposition takes over the final stage. The activation energy of 100 $kJmol^{-1}$, during the initial stages of thermolysis of HTRX-85 may correspond to the heat of vaporization of RDX. However this is not likely the case, as temperatures below the melting point of RDX has also been used for isothermal TG analysis (Fig. 4). The lower value of E, during the initial stages might be corresponding to the complex interreactions of binder decomposition products and RDX and / or its decomposition products. Moreover it may be fairly inferred that the final stages of PBX thermolysis, is dominated by gas phase decomposition of RDX. Thus it can be seen that the higher rate of thermolysis of the PBX, is due to the complex radical chemistry of binder / RDX decomposition which occurs with a lower value of activation energy.

The activation energy of thermal explosion as obtained from the explosion delay measurements is almost same for RDX and HTRX-85. This shows that the mechanism of thermal explosion in the PBX is same as that of pure RDX. However values of D_E (Table 2) at particular temperatures for HTRX-85 is some what lower than that for pure RDX, which shows the lesser thermal stability.

Table 1. TG and DTA data of PBXs

S. No.	Name of the sample	TG data				Peak Temperature (^{0}C)	
		T_i (^{0}C)		T_f (^{0}C)			
		air	N_2	air	N_2	air (DTA)	N_2 (DTG)
1.	RDX	205	214	235*	256	239	239.5
2.	HTRX-85	205	215	214*	226	215	223.4

* Temperature at which the thermal ignition occurs

Table 2. Explosion Delay data on PBXs

S.No.	Compound	D_E (s) at various temperatures (^{O}C)							E ($kJmol^{-1}$)
		275	300	325	350	400	450	500	
1.	RDX	69.67	49.90	42.60	38.95	24.00	22.6	--	20.3
2.	HTRX-85	50.00	38.00	37.50	--	19.63	--	14.23	19.6

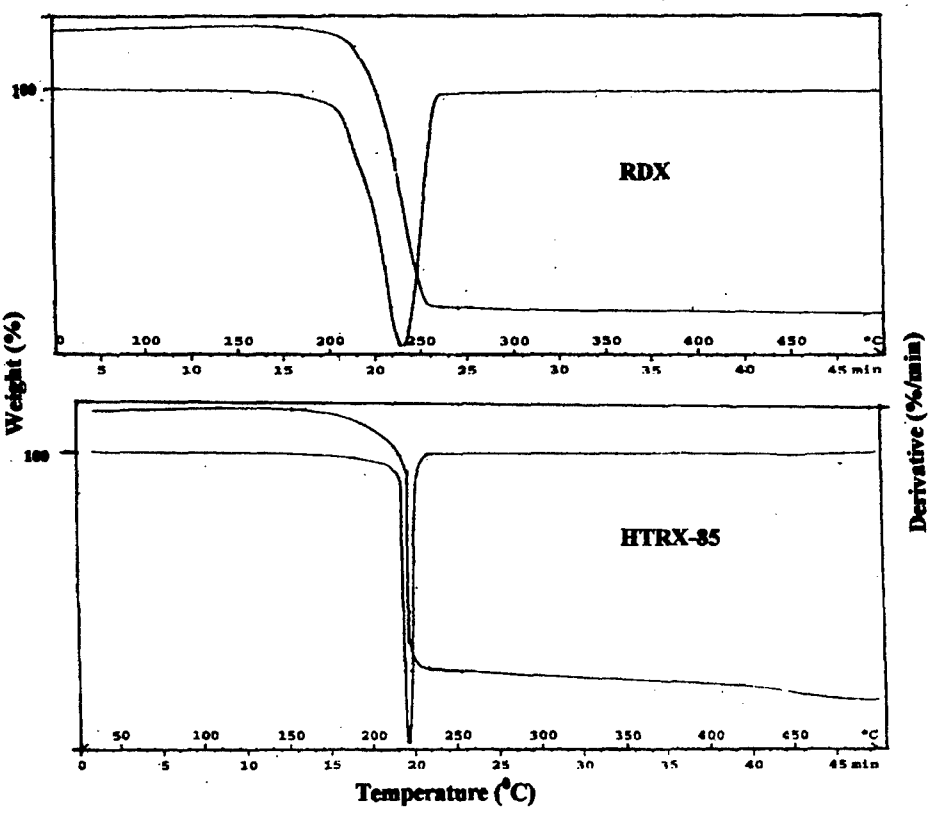


Fig 1. TG-DTG thermograms of RDX and HTRX-85

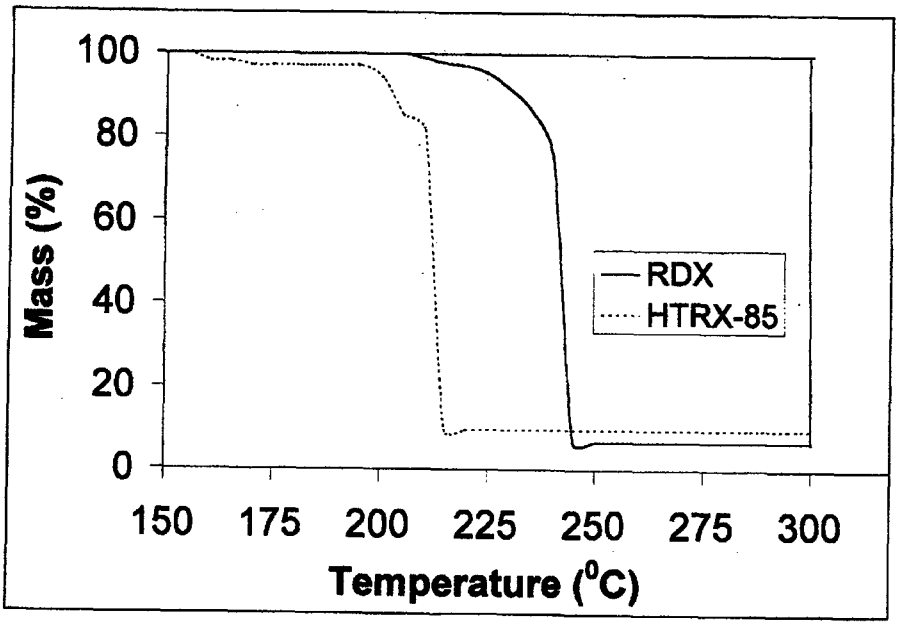


Fig 2. Non isothermal TG thermograms of RDX and HTRX-85 in air atmosphere

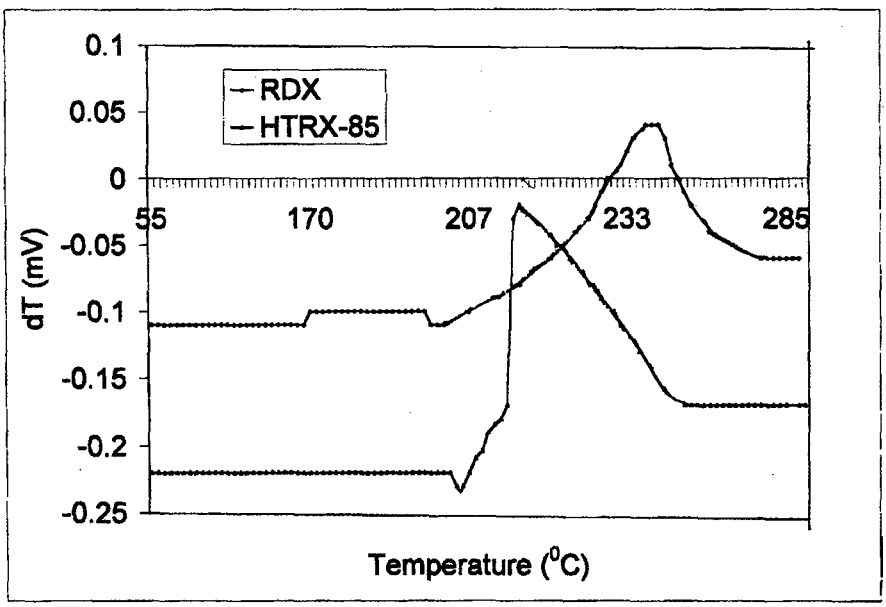


Fig 3. DTA thermograms of RDX and HTRX-85

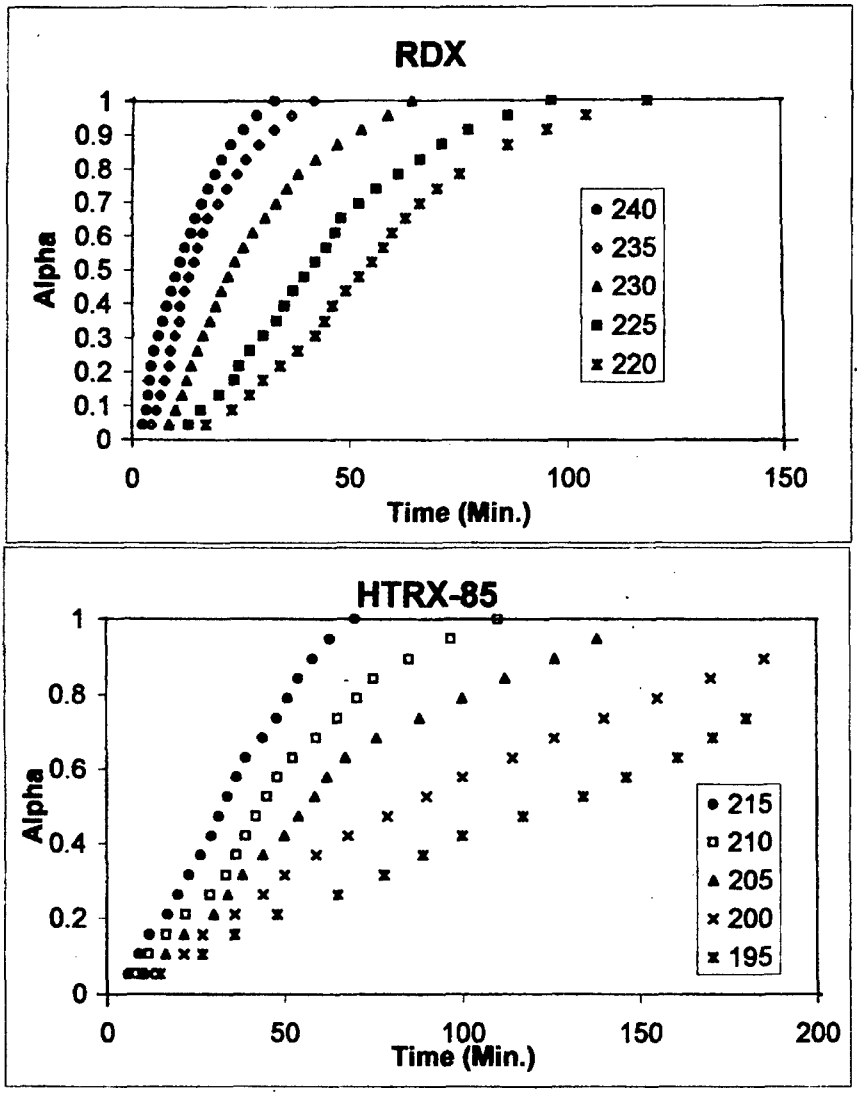


Fig 4. Isothermal TG thermograms of RDX and HTRX-85

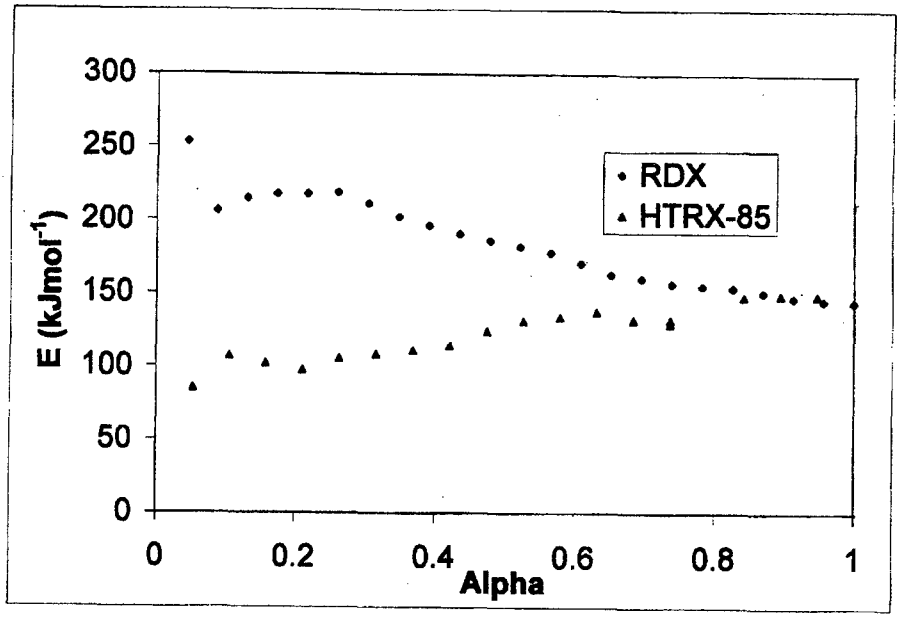


Fig 5. Dependencies of activation energy on extent of conversion for RDX and HTRX-85

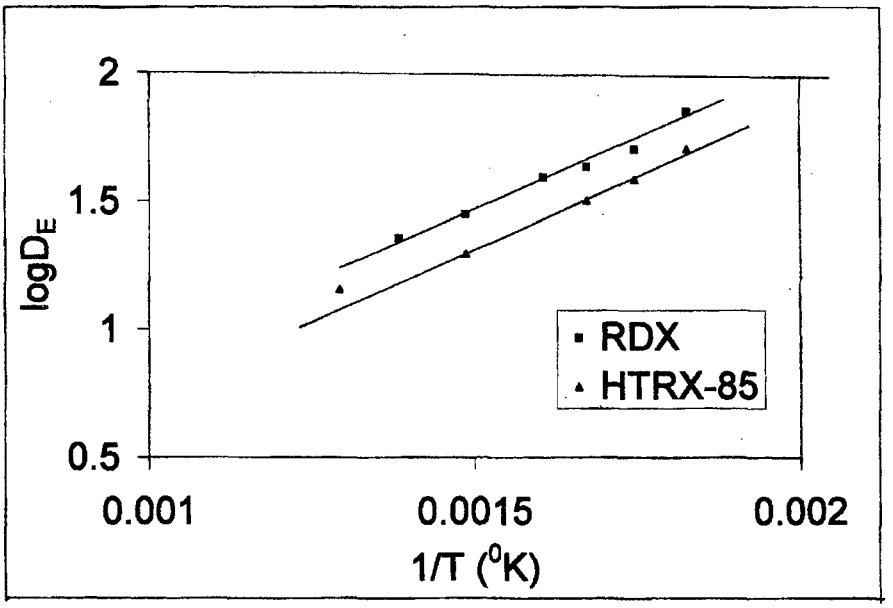


FIG 6. Plot of log D_E versus 1/T for RDX and HTRX-85

4. CONCLUSIONS

The binder ie. HTPB plays a vital role in the thermal decomposition of RDX in HTRX-85. The thermal decomposition of HTRX-85 occurs at a faster rate than that of RDX and the peak temperature in DTA as well as DTG has been considerably lowered in the PBX. Mechanism of thermolysis for RDX and HTRX-85 is different, with differing activation energies. Although the mechanism of thermal explosion for pure RDX and its PBX remains the same, lowering of D_E values are also observed.

REFERENCES

[1] R. N. Rogers and L. C. Smith: Thermochim. Acta, 1, 1, 1990.

[2] Y. Oyumi: Propellants, Explos., Pyrotech., 13, 42, 1988.

[3] K. N. Ninan, K. Krishnan, R. Rajeev and G. Viswanathan: Propellants, Explos., Pyrotech., 21, 199, 1996.

[4] J. K. Chen, T. B. Brill: Combust. Flame, 87, 217, 1991.

[5] D. Tingfa: Thermochim. Acta, 138, 189, 1989.

[6] Y. Oyumi, K. Inokami, K. Yamazaki and K. Matsumoto: Propellants, Explos., Pyrotech., 18, 62, 1993.

[7] M. W. Beckstead: Pure and Applied Chemistry, 65, 297, 1993.

[8] Y. J. Lee, C.J. Tang and T. A. Litsinger: Combust Flame, 117(4), 795, 1999.

[9] G. Singh and R. R. Singh: Res. Ind., 23, 92, 1978.

[10] S. Vyazovkin and C.A.Wight: J. Phys. Chem. A, 101, 8279, 1997

[11] G. Singh, S.K. Vasudeva and I.P.S. Kapoor: Indian J. Chem. Techn., 29, 589, 1989.

[12] G. Singh, I.P.S. Kapoor: J. Phys. Chem., 96, 1215, 1992.

[13] N. Semenov: *Chemical Reactions*, Clarendone Press, Oxford, 1935, Chapter 18.

[14] E.S. Freenman and S. Gorden: J. Phys. Chem. 60, 867, 1956.

[15] R. Meyer: *Explosives*, 3rd Edn., VCH, Weinheim, Germany, 1987.

[16] G. T. Long, S. Vyazovkin, B. A. Breams and C. A. Wight: J. Phys. Chem. B, 104, 2570, 2000.

NEW METHODOLOGIES FOR MILITARY EXPLOSIVE MATERIALS TESTING IN THE CZECH ARMY

Marcel Hanus

Military Institute for Weapon and Ammunition Technology (VTÚVM)
763 21 Slavičín, CZ

Abstract:

This paper summarises results of a transformation of the Czech Army testing system on military explosive materials and presents new testing methodologies implemented into the Czech Army procedures. Qualification of new explosive materials for military service in NATO countries according to STANAG 4170 and Czech Defence Standard 137601 was the first main target in implementation of NATO standards in the armament area. Based on experience gained with implementation of qualification procedures, modernisation of Czech Army surveillance procedures on in-service explosive materials was later managed and standardised by Czech Defence Standard 137603.

Keywords: *military explosive materials, qualification, surveillance*

1. INTRODUCTION

In connection with the entry of the Czech Republic to NATO in 1999, implementation of NATO standards has become one of the main tasks for the Czech Army. In the armament sector, harmonisation of procedures for explosive materials was evaluated as a primary target and a necessary headstone for the following task of ammunition standardisation. There are 36 NATO standards (STANAG, AOP) dealing with military explosive materials and having been prepared by NATO CNAD AC/310 Group on Safety and Suitability for Service of Munitions and Explosives - Subgroup 1 on Explosives. These standards cover two basic topics - definition of quality requirements and test methods on explosives for deliveries from one NATO nation to another and qualification of explosive materials for the military use in NATO countries.

The first topic does not directly affect the Czech Army, as the Army neither owns nor operates its own explosives manufacturing or processing facilities. The standards of the first group however provide national explosives manufacturers instruments how to satisfy themselves with the quality of imported explosive raw materials on one hand and how to ensure quality of their products for export on the other hand. All the STANAGs covering quality requirements on explosive components (Tetryl, RDX, PETN, TNT, Nitrocellulose, HNS, HMX, NH_4ClO_4, aluminium powder, NTO) have already been ratified by the Czech Republic and their implementation in the form of Czech Defence Standard 137602[2] is expected by the end of 2002.

The second topic - qualification of explosive materials before entering service with the Armed Forces is however a very important procedure. The way of its implementation into the Czech Army procedures is described in the next chapter.

2. IMPLEMENTATION OF QUALIFICATION PROCEDURES AND TESTING

STANAG 4170 describes procedure on qualification of a new explosive material for military service, defines what the new explosive is and specifies a list of mandatory tests that the new explosive must undergo. Methodologies on particular tests are specified by 17 separate STANAGs. In this context a new explosive is an explosive which has not yet been qualified (either in this country or abroad), whose composition, nature, manufacturing procedure, manufacturer or manufacturing location have been changed, or which is intended for a role for which it has not been qualified. Existing in-service explosives with unchanged material specification may be regarded as being qualified by sufficient long experience representative for its expected service life and intended use.

List of the mandatory tests is set in such a way allowing to characterise almost all safety properties of the new explosive. The list contains thermal stability tests (DTA, DSC, TGA), chemical stability tests (stabiliser depletion, vacuum stability test), sensitiveness and explosiveness tests when subjected to heat (explosion temperature, slow and fast cook-off), sensitiveness to impact, friction and electrostatic discharge (small scale and large scale tests), sensitivity to shock wave, determination of critical diameter and detonation velocity and determination of mechanical properties (uniaxial compression and tensile test, stress relaxation in tension test, thermomechanical analysis, dynamic mechanical analysis). Attention is also paid to tests of compatibility of a new explosive with construction materials that it contacts in munitions or during processing. Artificial ageing procedures check whether the above-mentioned properties would change during service life of the explosive. A list of the mandatory testing methods as implemented into Czech Defence Standard 137601[1] is presented in Table 1. More detailed description of the methods and procedures applied for qualification was published elsewhere[4,5].

Qualification procedure is conducted by the National Authority for military explosive materials. In the Czech Republic, Military Institute for Weapon and Ammunition Technology is the appointed national authority. Before the start of the qualification procedure, an applicant requesting the assessment of the new explosive identifies some basic characteristics of the explosive and presents results of tests obtained in the development project. The information is evaluated by the National Authority and can be returned for revision if unsatisfactory or incomplete. A producer of the new explosive also has to prove that the explosive can be manufactured and processed in a full production scale and the quality levels required can be met consistently. The National Authority can refuse further qualification testing if it is clear from the preliminary results that the new explosive will not satisfy general requirements for safety and suitability in the intended role.

In case of positive results of the preliminary assessment, the National Authority prepares a list of tests for qualification of the explosive. The tests listed in STANAG 4170 and Czech Defence Standard 137601 are always taken as mandatory. Other tests not included in these standards, but which are suitable to obtain the required information, may also be used in the qualification testing. Results of the optional tests can be taken from the development project of a new explosive.

The National Authority is responsible for the conduct of the qualification tests in its testing laboratories and the subsequent assessment of the new explosives regarding their safety and basic suitability for military purposes. Results of the qualification tests, together with other observations and recommendations are considered by an expert committee of the National Authority, consisted of explosives and ammunition specialists of VTUVM, other Czech military technical institutes, General Staff and Ministry of Defence. The results are evaluated in relation to the results of the same tests carried out on materials of a similar type

and role that have proven history of safety and satisfactory use in service. After completion of the investigation, the National Authority prepares a qualification report in accordance with STANAG 4170 and the qualification certificate with resulting qualification status: (a) qualified, (b) not qualified, (c) qualified with certain restrictions. In case of ammunition system developments requiring the new explosives, these explosives must be qualified before the system design is finalized. The introduction of the explosive for a particular role before conclusion of the qualification procedure and before completion of the technical specification is prohibited in general.

The qualification procedure should ensure that only explosive materials sufficiently characterised and assessed as possessing properties making them safe and suitable for military use are incorporated into service with military forces of NATO nations. Unified and standardised qualification procedure should help with achieving compatibility, interoperability and interchangeability of explosives and munitions among NATO nations. Qualification procedure should prevent from application of explosive materials that may become unstable, not having sufficiently long service-life, being too sensitive to external stimuli and having better substitutes for intended role.

Qualification procedure for new military explosive materials in its complex form as defined by STANAG 4170 has not been established in the Czech Army procedures before 2001. Qualification of new explosives was done on case-by-case basis usually along with the whole ammunition component or system. Results from development phase of an explosive material were usually considered sufficient for qualification. Function reliability and performance were the main goal in the most cases and only little attention was paid for characterisation of ageing behaviour or determination of service life of the new explosives. Problems met during long-term storage of some explosive materials with superior performance however relatively low stability or high sensitiveness showed necessity to change the approach in any case. A requirement to implement STANAG 4170 into the Czech Army procedures was thus very welcome source of complex methodology for qualification of new military explosive materials.

Practical implementation of testing methods required by the new qualification procedure was a very extensive task as only 10 % of methods applied according to Czech or former Warsaw Pact standards in the Czech Army were to some extent compatible with methods defined by NATO standards. For example, thermoanalytical or thermomechanical methods like DSC, TGA, DMA, TMA were completely new in the military explosives testing procedures.

In order to help with implementation of new testing methods required for qualification of explosive materials according to STANAG 4170, a defence research program "Chemical tests of munitions" was initiated. The research program being solved in 1999 - 2001 by VTUVM Slavicin consisted of a deep literature search on the new testing methods, acquisition of STANAG-compatible instrumental equipment and extensive experimental research. The experimental research was focused on artificial ageing of more than 50 in-service military explosive materials and assessment of impact of the ageing on chemical, thermal, physical, mechanical, structural and ballistic stability of these materials and their sensitiveness. Wide range of tests was applied for assessing different types of stability. Chemical stability was tested using stabiliser depletion, vacuum stability test, determination of active metal and decomposition products contents. Thermal stability was analysed by DTA (both small scale and large scale), DSC and TGA. Physical stability was controlled by plasticiser migration. Mechanical stability was checked by uniaxial tensile and compression tests, determination of hardness, DMA and TMA. Structural stability was assessed by visual control, endoscopy and ultrasonic flaw detection. Ballistic stability was evaluated by shots

from ballistic weapons using rounds with aged propellant or using closed vessel test. Sensitiveness testing contained impact, friction and electrostatic discharge tests. Some selected results of the research program were published in earlier proceedings of this seminar[6,7,8].

In its conclusion, the research program ensured acquisition of new STANAG-compatible testing equipment and its practical induction on real samples of military explosives. In addition the program enabled to characterise ageing of a wide spectrum of in-service explosive materials, to establish their service life and to expose critical factors that could affect their safety and suitability for the service. It was possible to select compositions that should be substituted in new munitions by more stable, more reliable or less sensitive materials. The program also helped to collect an extensive database of experimental data on in-service explosives that will be used for comparison with new explosive materials in the qualification process.

At this moment, qualification process for new explosive materials for military use with the Czech Army is fully implemented. VTUVM Slavicin as a national authority for qualification of military explosive materials has established its testing facility for this task that operates equipment compatible with NATO standards. Organisation of the qualification procedure according to STANAG 4170 and particular testing methodologies according to 17 different STANAGs are implemented in Czech Defence Standard 137601 effective from August 2001. Qualification of the first samples of new explosive materials is under preparation now and re-qualification program of all in-service explosives is also proposed.

3. NEW SURVEILLANCE TESTING PROCEDURE

There was also another significant output of the implementation of new testing methods and results of the research program. Extensive literature search and experimental testing of more than 50 in-service military explosive materials using more than 20 different methods enabled to choose suitable methods and evaluative criteria for modernisation of surveillance testing procedures for long term stored explosives and ammunition in the Czech Army. Surveillance program of the Czech Army on explosive materials is responsible for quality and safety of in-service explosives in military munitions for their whole service life which usually represents several dozens years of storage in different climatic conditions.

Modernisation of methods applied for surveillance of in-service explosive materials was evaluated as the second most important task in this field. Most of the methods applied were standardised in 1950s or 1960s and some of them such as Bergmann-Junk test or vacuum stability test for propellants were considered obsolete or not enough representative. Very unsatisfactory situation reigned in surveillance of rocket propellants where only chemical stability was controlled. Need for a significant change of surveillance procedures was also fuelled by long term expeditionary missions of the Czech Army abroad (Desert Storm, UNPROFOR, SFOR, KFOR etc.) where explosives and ammunition are often being stored in very harsh climatic conditions and it is necessary to guarantee their continuing safety and reliability in these conditions.

Results of defence research program "Chemical tests of munitions" were the most important source for modernisation of surveillance testing methods. Analysis of more than 600 publications and of experimental data on ageing characterisation of more than 50 in-service explosives of all types using more than 20 methods testing different forms of stability allowed to choose reliable methods for determination of a critical instability of explosive materials and to establish specific pass/fail criteria. The methods chosen cover the whole spectrum of possible instabilities of explosive materials - physical, chemical, thermal, mechanical, structural and functional instability. Their overview is presented in Table 2.

The surveillance procedure newly contains a principle of artificial ageing that is carried out either by isothermal heating or by temperature shocks. The artificial ageing simulates the expected state of the explosive materials in time of the next periodic control (5-year periods are usually applied). This procedure should guarantee acceptable properties of the explosive material for all the period. Ageing of explosive materials is preferably carried out in original ammunition component (or system) when its size allows. In other cases the explosive charge is sampled and packed to hermetically sealed polymer-aluminum-polymer foil.

Isothermal heating at 60 °C is used for nitrocellulose based propellants, at 70 °C for composite rocket propellants and plastic demolition charges. Time of accelerated ageing is defined both by acceleration coefficients and by ambient storage temperature. Acceleration coefficients were chosen 3,0 per 10 °C for nitrocellulose based propellants and 2,6 per 10 °C for composite rocket propellants and plastic demolition charges. These two coefficients were proven to be conservative enough for all the explosive materials concerned. Ambient storage temperature means 15 °C for ammunition stored in the standard stores in the Czech Republic and 25 °C for ammunition intended to be used in expeditionary missions. For primary explosives and pyrotechnics the isothermal heating procedure has not proven to be representative enough. For these explosive materials, complex temperature cycling program was established based on experience with qualification and surveillance of pyrotechnics-containing ammunition. The program uses several cycles of temperature shocks from -40 to +50 °C (with 95 % relative humidity) with 6 hours duration each, followed by -20 °C to +50 °C (95 % RV) shocks with intermediate steps at a laboratory temperature. Practical experience showed that 4-week duration of the program corresponds to 15 years of natural ageing at ambient storage temperature. For shorter periods in surveillance system, the program is shortened adequately. Temperature shocks are also applied for insulated or case-bonded propellants to check the quality of propellant-insulation or insulation-case bonds.

Primary explosives are not sampled from the ammunition components in surveillance program due to their extreme sensitiveness. They are tested only on safety, reliability and completeness of their function in the original ammunition component according to technical specification of the component. Tests are carried out before and after artificial ageing.

Standard in-service high explosives are not submitted to artificial ageing as no significant change of properties is expected. The only exception represents plastic explosives for demolition charges where mechanical properties of the polymeric binder are subject of ageing. Changes in chemical or thermal stability of high explosives may however be induced by their incompatibility with contact materials in munitions such as lacquers or seals. These changes can reliably be detected by vacuum stability test or by differential thermal analysis. Visual examination (changes in colour, presence of foreign matters, separation of desensitisers from crystalline explosives, exudation of TNT based explosives) and moisture determination are standard surveillance tests carried out before ageing. Mechanical properties of plastic explosives are checked before and after artificial ageing using either tensile tests or plastometers.

Pyrotechnic mixtures are first submitted to visual control (cracking, conglomeration, washing out of oxidisers etc.) and determination of moisture content. Thermal stability of the pyrotechnic mixtures is checked before and after artificial ageing as it may be affected by some decomposition products. The most reliable surveillance test is however a performance test of the pyrotechnics containing ammunition component or system carried out according to technical specification on the ammunition. Safety, function reliability and required performance (time of burning, intensity of light emission, spectral purity of flame colour etc.) are tested before and after artificial ageing.

Gun propellants are first tested by visual examination (migration of nitroglycerine, wash-out of inorganic additives on surface, sticking or cracking of grains etc.) and by determination of moisture and other volatiles. Chemical stability of gun propellants is controlled by determination of remaining effective stabiliser content by liquid chromatography along with analysis of other extractable compounds. As an "insuring" test of chemical stability, 100 °C heat (time-to-fume) test is applied. This classical test has proven to be much more reliable and compatible with depletion of stabilisers than other classic tests e.g. Bergmann-Junk test. Vacuum stability test was evaluated as completely unsatisfactory method for surveillance - some propellants showed even "better" stability with ageing according to this test. Ballistic tests (either with original round using a ballistic gun or in a closed vessel) are the necessary methods for control of ballistic stability of the gun propellants before and after ageing.

Special attention is paid to surveillance of solid rocket propellants (double base and composite). High priority in the testing methods of rocket propellants gained detection of structural defects like cracks, voids, inhomogeneities, insulator-propellant or case-insulator debonding etc. both before and after artificial ageing. These structural defects are checked by visual examination, endoscopy and ultrasonic flaw detection followed by mechanical dissection and machining. Migration of plasticisers inside the propellant grain and to insulation is analysed by liquid chromatography (double base propellants) or gravimetric extractions (composite propellants). Chemical stability of double base rocket propellants is checked by the same methods as of gun propellants - by determination of remaining stabiliser content and by 100 °C heat test. Composite propellants are controlled on their sufficient thermal stability using differential thermal analysis. Live instrumented firings of rocket motors with the respective propellants is generally the most suitable method for confirmation of acceptable structural, mechanical and ballistic stability of the propellants. In surveillance, the live firing should be carried out at application temperature corresponding to the highest mechanical loading of the propellant grain. That is usually the highest application temperature for cartridge-loaded propellants (e.g. +60 °C) and the lowest application temperature for case-bonded propellants (e.g. -60 °C). Where live firings can not be done from practical reasons (e.g. in case of artificial ageing of large rocket motors), propellant strength analysis is applied instead. The propellant strength analysis calculates stress and strain loading of propellant grains as viscoelastic materials in ignition phase of a corresponding rocket motor. Different factors like rate of gas pressure increase, pressure-time and thrust-time data, rocket acceleration, combustion chamber and rocket propellant configurations are included in the analysis. The analytical procedure finally calculates maximum compressive, tensile and shear stresses induced in the propellant grain during the ignition phase. These calculated values are than compared with mechanical properties determined from uniaxial compressive and tensile tests and case-propellant bond shear test shifted on deformation rates corresponding to loading in the rocket motor using time-temperature superposition principle. Dynamic mechanical analysis is used for determination of shift factors of the propellants for time-temperature superposition.

These surveillance methods are standardised in Czech Defence Standard 137603[3] along with definition of organisational background of the surveillance program. Each method has its pass/fail criteria defined. The standard also contains references on optional methods that might be used for finding causes of possible anomalous behaviour of explosive materials and interpretation of disputable results. Surveillance procedures standardised in Czech Defence Standard 137603 were extensively tested for two years in a surveillance program on rocket and missile systems and were proven suitable for this task.

Table 1. Methods used for qualification testing of new explosive materials

Test	Compatible with STANAG	Primary explosives	Booster and main charge high explosives	Gun propellants	Solid rocket propellants	Liquid propellants	Pyrotechnic mixtures
Thermal stability by DTA	4515	+	+	+	+	+	+
Thermal stability by DSC	4515	+	+	+	+	+	+
Thermal stability by TGA	4515	+	+	+	+	+	+
Chemical stability by vacuum stability test	4556		+	+	+		+[5]
Chemical service life determination of stabiliser depletion	4117, 4527, 4541, 4542			+	+[4]		
Chemical compatibility by vacuum stability test	4147		+	+	+		
Chemical compatibility by TGA	4147	+	+	+	+	+	+
Chemical compatibility by DSC	4147	+	+	+	+	+	+
Chemical compatibility by stabiliser depletion	4147			+	+[4]		
Chemical compatibility of azides	4147	+[1]					
Explosion temperature	4491	+	+	+	+	+	+
Slow cook-off test	4491		+	+	+	+	+
Fast cook-off test	4491		+	+	+	+	+
Impact sensitivity	4489	+	+	+	+	+	+
Friction sensitivity	4487	+	+	+	+	+	+
Small scale electrostatic discharge sensitivity test	4490	+	+	+	+		+
Large scale electrostatic discharge sensitivity test	4490		+	+	+		
Shock sensitivity	4488		+	+	+	+	+[6]
Critical diameter	AOP-7 CZ		+	+	+		+[6]
Detonation velocity	AOP-7 CZ		+				
Uniaxial compressive test	4443		+	+[3]	+		+[6]
Uniaxial tensile test	4506		+[2]		+		
Stress relaxation test in tension	4507		+[2]	+[3]	+		
Thermomechanical analysis	4525		+	+[3]	+		+[6]
Dynamic mechanical analysis	4540		+[2]	+[3]	+		+[6]
Ageing characterisation	AOP-7 CZ	+	+	+	+	+	+

Notes:
1 - azide containing explosives only
2 - plastic binder containing explosives only
3 – applicability depends on grain shape
4 - for double base propellants only
5 - in case of content of organic binder
6 - according to decision of national authority

Table 2. Methods used for surveillance testing of in-service explosive materials

Test method	Primary explosives	High explosives	Gun propellants	Double base rocket propellants	Composite rocket propellants	Pyrotechnics
Accelerated ageing by isothermal heating	-	+[1]	+	+	+	-
Accelerated ageing by temperature shocks	+	-	-	+[2]	+[2]	+
Visual control	-	+	+	+	+	+
Endoscopy	-	-	-	+	+	-
Ultrasonic flaw detection	-	-	-	+	+	-
Moisture and volatiles	-	+	+	+	+	+
Stabilisers content	-	-	+	+	-	-
Plasticiser migration	-	-	-	+	+	-
Vacuum stability test	-	+	-	-	-	-
100 °C heat test	-	-	+	+	-	-
Differential thermal analysis	-	+	-	-	+	+
Compressive strength	-	-	-	+	+	-
Tensile strength	-	+[1]	-	+	+	-
Propellant-case bond strength	-	-	-	+[3]	+	-
Dynamic mechanical analysis	-	-	-	+	+	-
Propellant strength analysis	-	-	-	+	+	-
Function tests	+	-	+	+	+	+

Notes:
1 - plastic explosives only
2 - insulated and case-bonded propellants only
3 - case bonded propellants only

4. CONCLUSION

Transformation of the Czech Army testing system on explosive materials is successfully concluded now. New qualification procedure according to STANAG 4170 and 17 other STANAGs was implemented, including acquisition of new equipment, establishment of a testing facility, familiarisation with the new methods, obtaining extensive database of experimental data on the in-service explosives using the new equipment and their standardisation in Czech Defence Standard 137601. Commitments of the Czech Republic in ratification and implementation of STANAGs concerning quality of raw materials for manufacture of military explosives were also accomplished by Czech Defence Standard 137602. Research activities connected with implementation of the methods for qualification of military explosive materials also helped to modernise Army surveillance methods on explosive materials using up-to-date testing equipment and knowledge and later standardised in Czech Defence Standard 137603.

The next step ahead is military ammunition qualification program compatible with AOP-15 and related STANAGs that is of course much more complicated and challenging task than the transformation of the testing system on military explosives was.

Acknowledgment:

This paper presented results of transformation of the Czech Army military explosive materials testing system carried out under a defence research program "Chemical tests of munitions" sponsored by the Czech Ministry of Defence. The author would like to express his thanks University of Pardubice - Dept. of Theory and Technology of Explosives for very close cooperation in this successful task.

5. REFERENCES

[1] CZECH DEFENCE STANDARD 137601: *Organizace a metody schvalování způsobilosti výbušnin pro vojenské účely* (implementing STANAG 4117, 4147, 4170, 4397, 4443, 4487, 4488, 4489, 4490, 4491, 4506, 4507, 4515, 4525, 4527, 4540, 4541, 4556), 2001

[2] CZECH DEFENCE STANDARD 137602: *Technické podmínky pro suroviny dodávané mezi státy NATO k výrobě vojenských výbušnin* (implementing STANAG 4021, 4022, 4023, 4025, 4178, 4230, 4284, 4299, 4300, 4543), draft 2002

[3] CZECH DEFENCE STANDARD 137603: *Provozní zkušebnictví výbušnin v AČR* (implementing STANAG 4021, 4022, 4023, 4025, 4178, 4230, 4284, 4299, 4300, 4543), draft 2002

[4] M. HANUS: *Nový proces schvalování způsobilosti vojenských výbušnin a jeho dopad na výrobce a dovozce munice pro AČR*, Proc. Czech Army Pyrotechnics Conference, Luhačovice, 2000.

[5] M. HANUS: *Nové metody zkoušení vojenských výbušnin v Armádě ČR*, Proc. of 3rd Seminar New Trends in Research of Energetic Materials, 50, Pardubice, 2000.

[6] J.PACHMÁŇ, M. HANUS: *Some aspects of stability evaluation of double based solid rocket propellants*, Proc. of 4th Seminar New Trends in Research of Energetic Materials, 278, Pardubice, 2001.

[7] M. HANUS: *Dynamic mechanical analysis of composite solid rocket propellants*, Proc. of 4th Seminar New Trends in Research of Energetic Materials, 112, Pardubice, 2001.

[8] J.PACHMÁŇ, M. HANUS, J.ŠELEŠOVSKÝ: *Some aspects of service life evaluation of composite rocket propellants*, this proceeding

STABILITY INVESTIGATION OF PLASTIC EXPLOSIVES DURING THEIR AGEING PROCESS.

Martina Chovancová, Peter Očko, Rastislav Ševčík, Ľuboš Čavojský and Jozef Lopúch

Military Technical and Testing Institute Záhorie, Slovak Republic

Abstract:

This elaboration investigates the ageing process influence on the stability and the mechanical properties of plastic explosives.

1. INTRODUCTION

Ageing is a fact of life. We are all sufficient from it. Determination of the ageing influence on explosives properties is an important part of the evaluation process of each explosive. Stability is the main requirement for the military explosives. This requirement is valid for a long-term period of time. Mechanical properties are very important as well. Stability investigation of explosives during their ageing process is very important from the point of view of the safety manipulation keeping, storage, using and combat ability not only very explosives, but even ammunition into which explosives are applied.

Nowadays, there is no unified military procedure of artificial ageing of the explosives tests in service of Slovak army and neither any criteria to be met by the explosives subjected the ageing process. The new explosives had been subjected the ageing tests, before their implementation, according to the developer option or to the co-ordinators developing tasks recommendation.

The ageing has usually been used during the new military explosives tests under the following ageing conditions of 60°C for 60 days, 70°C for 20 days or temperature cycle of 50°C up to +70°C. After the ageing, the explosives samples have been tested relating to the stability, sensitivity and operational tests. The results of these tests, before and after the ageing, have been comparatively evaluated.

Relating to the Slovak Republic mission to NATO, explosives testing has been adapting to NATO standards. STANAG 4170 and related documents AOP-7 and STANAG-s determine the conditions of the explosives ageing, tests and acceptance criteria for a given type of explosive.

2. EXPERIMENTAL

We determined the ageing conditions of 60 °C for 6 months according to AOP-7. Samples are placed in the standardised test-tube (diameter 2,54 cm, length 15,24 cm) according to STANAG 4527. The plastic explosives of A, C, E, F, G, N and H have been subjected to the ageing for a period of 2 months. The explosives of A, C, E, F and G were

made in SR at the end of nineties. Explosives of N (made in 1984) and H (made in 1990) were made in Czech Republic. The explosives of A, C, E, F and G are made on the base of RDX, N on the base of PETN and H on the base of PETN and RDX.

The following parameters have been investigating (before and after the ageing):

- Stability
- Plasticity of the new plastic explosives E and G.

Stability is investigated by means of vacuum thermoanalytic system – The STABIL apparatus, Temperature of ignition apparatus and of Differential thermal analysis – the DTA 500-Ex apparatus. Measurement is carried out in the environment of vacuum and the temperature of thermostat of 140°C for 20 hours for the explosives on the base of RDX and 110 °C for 20 hours for the explosives on the base of PETN. A result is the rate of thermal decomposition – w (ml/g/20).

Differential thermal analysis and determination of the ignition temperature are carried out at constant rate of heating 5 °C/min. When evaluating thermogram, we obtain Tm-temperature as a maximum temperature of the sample exothermic decomposition. The plasticity-modulus of compressibility is determined according to the MIL-STD-650, method 211.2. Plasticity was determined using samples with diameter of 52,5 mm and thickness 19,5 mm. These samples were weighing down by the 5kg weight during period of 20 minutes. Plasticity is given by formula as follows:

Plasticity = (A-B)/1,30, where

A – logarithm of sample thickness in mm at the time "zero"

B – logarithm of sample thickness in mm after 20 min.

The explosive samples were subjected to the ageing in an open pack from the reason of accelerated ageing of the polymer binder.

The following tables present the results obtained by the stability test as follows:

Table 1. Results of the stability tests

Plastic Explosive	Ageing conditions	Vacuum stability test (ml/g/20)	DTA Start (°C)	DTA Maxim. (°C)	Temperature of ignition (°C)
A	Temperature cycle -40°C +70°C	0,1000	-		211
A	Of 70°C for 20 days	0,1000	-		211
F	Temperature cycle -40°C +70°C	0,7800	-		213
F	Of 70°C for 20 days	0,2500	-		212
C	Temperature cycle -50°C +50°C	0,4975	-		-
E	Temperature cycle -50°C +60°C	0,9553	190,2	215,5	-
E	Of +60°C for 60 days	1,0055	189,0	215,3	
G	Temperature cycle +55°C +25°C	0,0964	181,6	210,0	209
G	Of +40°C for 21 days	0,0941	176,9	211,6	209

Table 2. Results of the stability tests

Sample	Vacuum stability test (ml/g/20)	DTA		Temperature of ignition (°C)
		Start (°C)	Maxim. (°C)	
A	0,1244	196,4	226,7	208
A-A	0,0664	193,7	221,2	207
F	0,1452	197,6	222,9	211
F-A	0,0627	195,6	220,2	209
C	0,7931	216,8	223,0	210
C-A	0,3831	190,0	217,8	205
E	0,7509	213,5	221,4	209
E-A	12,9700	210,6	214,8	202
G	0,0979	215	222	205
G-A	0,0872	198,8	219,7	207
H	0,2932	147,5	183,6	183
H-A	0,3999	152,1	187,8	180
N	0,3409	153,4	168,4	182
N-A	0,3877	156,2	186	181

A – ageing

3. DISCUSSION

The data measured resulting in that excepting plastic E-explosive all the others appear to be stable even after ageing. The sample tested is originated from the series made in 1998. The results of the E-explosive tests (1998) are mentioned in table 1. E-explosive is stable as resulting from table1. Decomposition rate was higher than 1,0 ml/g/20, only at sample E after the ageing. This E-sample of the same series was subjected to ageing (65°C, 60days) even in 2001. Figure 1 presents results of the vacuum stability test of E-explosive before and after ageing.

Decomposition rate was 12 times higher than at previous one. The result mentioned shows E-explosive to be unstable. Therefore the compatibility test of the E-explosive individual components was done. The compatibility tests were done with RDX, Al, polymer binder.

Table 3. Results of the stability tests

Sample	Vacuum stability test (ml/g/20)	Sum	Comparison	Evaluation
RDX	0,2692			
Aluminium	0,0810			
Mixture RDX+Al	0,1442	0,3502	0,1442<0,3502	Compatibility
Polymer binder (PB)	0,1651			
Mixture RDX+PB	12,5595	0,4343	12,560>0,4343	Incompatibility
Mixture RDX+PB+Al	14,3066	0,5153	14,307>0,5153	Incompatibility

RDX and polymer binder are incompatible by results mentioned in table 3 and in figures 2, 3.

This incompatibility is a reason for E-explosive instability. Other explosives tested include different type of polymer binder from the E-explosive. For instability and compatibility determination we will have to do test of compatibility of the basic components of polymer binder with RDX, we also have to investigate properties of the polymer binder and its components during ageing and observe the stability changes of other series of the E-plastic explosive during ageing process.

Another observed property of plastic explosives is the plasticity. The plasticity tests were done with samples of E and G. These samples were subjected to ageing for a period of 5 weeks in the open packs for achieving the accelerated ageing. Plasticity testing results are mentioned in tab 4.

Table 4. Plasticity of the E and G explosives before and during ageing.

Time (days)	**0**	**1**	**7**	**14**	**21**	**28**	**35**
Plasticity of E	0,199560	0,093398284	0,071862198	0,051606316	0,050938955	0,03993093	0,199560
Plasticity of G	0,049775	0,011708061	0,009372531	0,008722561	0,008067885	0,00424354	0,049775

The results measured show that plasticity of the E-explosive is expressed by the function of: 0,1494exp(-0,0416x) and G-explosive by the function of 0,0285exp(-0,0551x). The E-explosive plasticity in a sense of valid technical criteria is unacceptable under the given conditions of ageing process after expiration of 26 days and the G-explosive plasticity is unacceptable as early as after 8 days. Such a steep change of the investigated components plasticity was not observed during their ageing process in closed packs.

These results do prove that ageing of explosives is in a large scale accompanied by the changes of consistency and it means even by the mechanical property changes undesirable.

There is need to find out a formula for the accelerated ageing and natural ageing as well.

4. CONCLUSIONS

In conclusion we can say that the plastic explosives ageing appears with the mechanical properties change and partially with decreased stability. Degradation of the used polymer binder is probable reason of aggravated mechanical and stability properties.

Incompatibility of polymer binder and RDX is the reason of instability of the E-explosive. Sorting out this problem continues according to the procedure in part 4 of this elaborate. The case of E-plastic explosive instability and incompatibility its components confirmed that the investigation of the explosive properties, during their ageing process, is very important from the point of view of assessment of their safety and use.

REFERENCES

(1) M.Chovancová: Sledovanie stability plastických trhavín pomocou prístroja STABIL a DTA (An Investigation of Stability the Plastic Explosives by means of STABIL and DTA), License Study Thesis, University of Pardubice, March 2000.

(2) G.B.Manelis: Problemy kinetiki elementarnych chimičeskych reakcij (The Problems of Elementary Chemical Reaction Kinetics). Izdat. Nauka, Moscow **93**, (1973)

(3) STANAG 4170, AOP 7

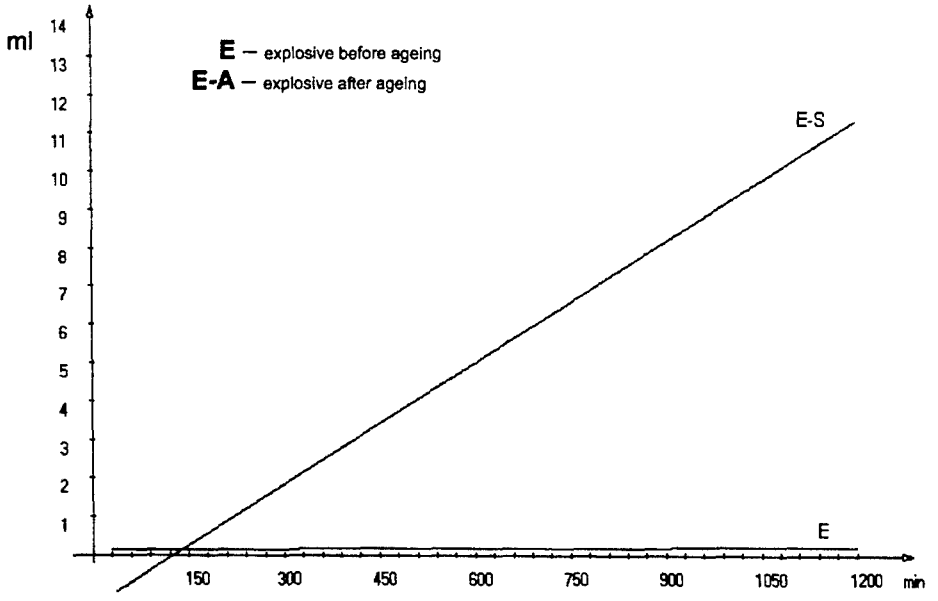


Fig 1. Vacuum stability the E plastic explosive before and after ageing

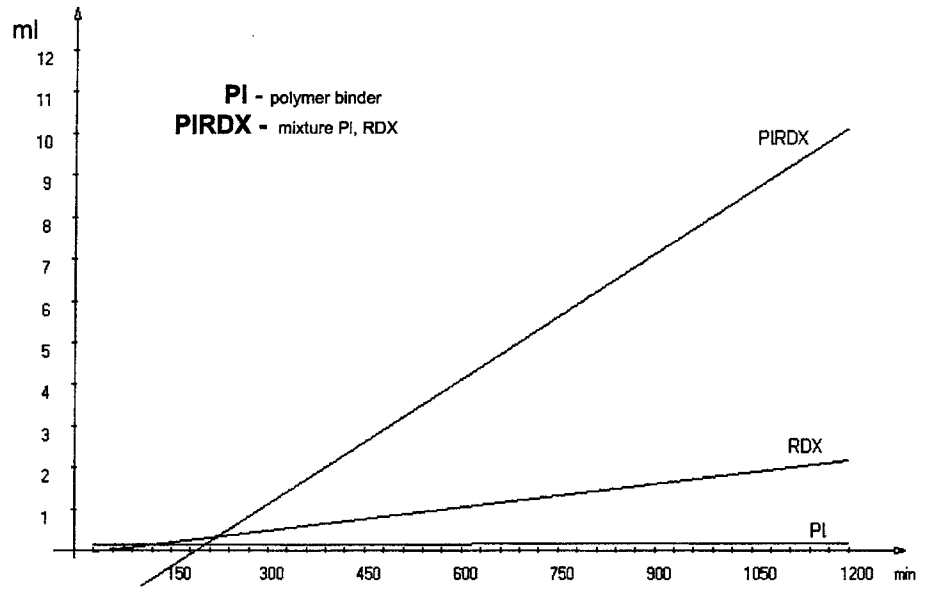


Fig 2. Compatibility RDX and polymer binder

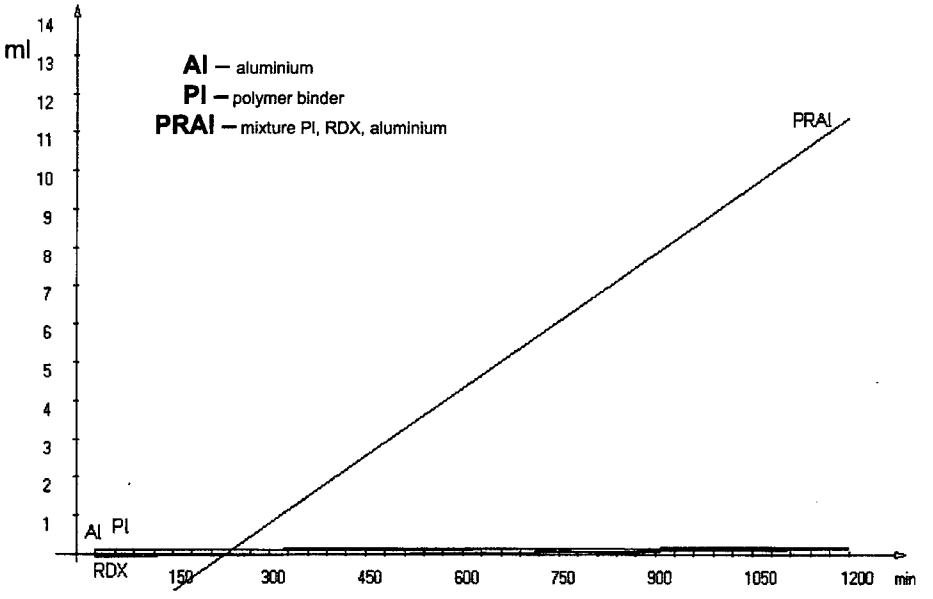


Fig 3. Compatibility of RDX, polymer binder and aluminium

THE INFLUENCE OF REACTION CONDITIONS ON TEX SYNTHESIS

Zdeněk Jalový and Robert Matyáš

University of Pardubice, Department of Theory and Technology of Explosives,
532 10 Pardubice, Czech Republic

Abstract:

4,10-Dinitro-2,6,8,12-tetraoxa-4,10-diazatetracyklo[5.5.0.0^{5,9}0^{3,11}]dodecane (TEX) was prepared by the reaction of 1,4-diformyl-2,3,5,6-tetrahydroxypiperazine (DFTHP) and glyoxal trimer hydrate in nitric acid. The influence of reaction conditions on the yield of product was examinated. The varied reaction conditions were as follows: DFTHP/nitric acid ratio, reaction temperature, reaction time, glyoxal/DFTHP ratio.

Keywords:
4,10-Dinitro-2,6,8,12-tetraoxa-4,10-diazatetracyklo[5.5.0.0^{5,9}0^{3,11}] dodecane, TEX, DFTHP, synthesis

1. INTRODUCTION

There are plenty of substances proposed as Insensitive High Explosives (IHE) in the literature [1,2]. They belongs to various chemical compound groups. 1,3,5-Triamino-2,4,6-trinitrobenzene (TATB) has been used as one of the first substances. Other substance, long time well-known nitroguanidine (NQ), has been used as well. 5-Nitro-1,2,4-triazole-3-one (NTO) is also used at present [3]. The production and processing of IHE is influenced to a great extent by tradition and technological background in various countries. 4,10-Dinitro-2,6,8,12-tetraoxa-4,10-diazatetracyklo[5.5.0.0^{5,9}0^{3,11}]dodecane (TEX) [4-6] and 1,1-diamino-2,2-dinitroethylene (DADNE, FOX-7) [7-9] are in the stage of intensive research now.

2. EXPERIMENTAL

The overall reaction scheme of the procedure used for TEX preparation is shown in Figure 1.

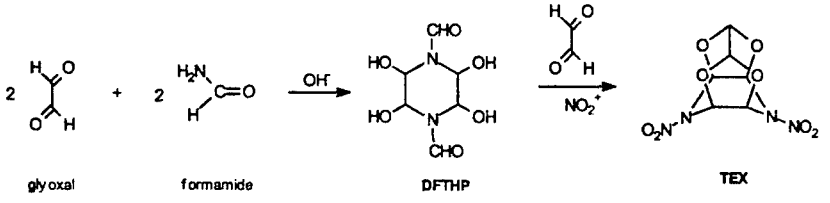


Fig 1. Two Step Synthesis of TEX

Initial DFTHP was prepared by the action of stoichiometric ratios of formamide and glyoxal (40% aqueous solution) under base catalysis by modified procedure of Vail et al [10]. The average yield of DFTHP was about 78% of the theory. DFTHP does not melt; its gradual decomposition occurs at temperatures about 190°C.

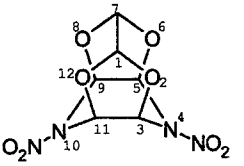
TEX was prepared by the action of DFTHP and glyoxal trimer hydrate in fume (98%) nitric acid, while a small amount of urea was present. The product crystallized directly from the reaction mixture. The following reaction conditions were changed in the procedures:

- DFTHP/nitric acid ratio
- glyoxal/DFTHP ratio
- temperature and reaction time

Results of the processes are summarised in table 1.

Elementary analysis (sample 1.4)

TEX ($C_6H_6N_4O_8$)	**%C**	**%H**	**%N**
calculated	27,48	2,29	21,37
found	27,63	2,32	21,22



NMR (sample 1.5):

^{1}H [δ (ppm)]:
5,96 singlet (2H, H-1, H-7); 6,98 singlet (4H, H-3, H-5, H-9, H-11)

^{13}C [δ (ppm)]: 82,7 (C-3, C-5, C-9,C-11); 102,7 (C-1, C-7)

^{15}N [δ (ppm)], only a signal of nitrogen of nitrogroups was managed to measure, value δ= -33,4; signal of nitrogen N-4, N-10 is probably broadened.
According to minor signals in the spectrum, the sample contained about two percent of unknown impurities.

Table 1. *Preparation of TEX*

Example	Molar ratio DFTHP:glyoxal: HNO_3	Reaction process	Yield (base to DFTHP)
1.1	1:1,1:29,2	4 hrs at 20°C unintended exo. reaction 90°C	1,8 g (24,6%)
1.2	1:1,1:29,2	4 hrs at 20°C unintended exo. reaction 90°C	1,8 g (24,6%)
1.3	1:1,1:29,2	4 hrs at 20°C 1 hrs at 90°C	1,66 g (22,6%)
1.4	1:1,1:29,2	4 hrs at 20°C 30-40 min at 50-60°C	3,05 g (24,0%)
1.5	1:1,3:29,2	4 hrs at 20°C 30-40 min at 50-60°C	1,84 g (25,1%)
1.6	1:1,5:29,2	4 hrs at 20°C 30-40 min at 50-60°C	1,88 g (25,6%)
1.7	1:2,8:29,2	4 hrs at 20°C 1 hrs at 90°C	1,9 g (26,0%)
1.8	1:1,0:29,2	4 hrs at 20°C 30-40 min at 50-60°C	1,79 g (24,4%)
1.9	1:0,5:29,2	4 hrs at 20°C 30-40 min at 50-60°C	1,67 g (22,8%)
1.10	1:0,34:29,2	4 hrs at 20°C 30-40 min at 50-60°C	1,49 g (20,3%)
1.11	1:0,34:29,2	4 hrs at 20°C 30-40 min at 50-60°C	1,55 g (21,1%)
1.12	1:0:29,2	4 hrs at 20°C 30-40 min at 50-60°C	1,27 g (17,3%)
1.13	1:0:29,2	4 hrs at 20°C 30-40 min at 50-60°C	1,15 g (15,7%)
1.14	1:1,1:20,8	4 hrs at 20°C 30-40 min at 50-60°C	1,5 g (20,5%)
1.15	1:1,1:16,7	4 hrs at 20°C 30-40 min at 50-60°C	1,1 g (15,0%)

3. RESULTS and DISCUSION

We came to synthesis of TEX by reaction of DFTHP with solid glyoxal in fume (98%) nitric acid. The stoichiometric excess of nitric acid to DFTHP was in the range of 8,3-14,6. During the reaction, two processes are being run: The formation of the isowurtzitane cage is one of them; secondly, the nitrolysis of tertiary nitrogens accompanied with removing of formyl groups occurred. The sequence of those two processes and detailed mechanism of the reaction have not been published yet. Results of appropriate experiments are summarised in table 1.

It was found that when the reaction mixture is not cooled properly when exothermic reaction started, the violent course of reaction takes place (examples 1.1, 1.2). However, the product is formed in the yield comparable with temperature-controlled processes. It was found that exothermic reaction occurs at the same time as separation of the crystals of the product from reaction mixture. At heating the reaction mixture to about 90°C (example 1.3), the yield of TEX was also comparable to other processes. Further processes (examples 1.14,1.15) with decreased amount of nitric acid offer TEX yields considerably lower. At examples 1.3-1.13, the influence of glyoxal excess on the yield of reaction was tested there. Dependence of TEX yield on glyoxal/DFTHP molar ratio at constant nitric acid/DFTHP molar ratio of 29,2:1 is graphically illustrated in figure 2. It means that TEX yield is not significantly increased at excesses of glyoxal. It was found that TEX is also formed at sub-stoichiometric amounts of glyoxal as well as at full elimination of the glyoxal addition into reaction mixture (examples 1.9-1.13). Yields obtained with elimination of glyoxal fall to values about 15%. This fact indicates the probable decomposition of a part of the initial DFTHP in nitric acid, which yields some amount of glyoxal, which then reacts with remaining DFTHP to produce TEX as also stated in [11], see also figure 3.

Yields of TEX at experimental conditions varied from 15,7 to 25,6% of the theory, calculated on DFTHP. In original process of TEX preparation by nitrolysis DFTHP and glyoxal in nitric acid/ sulphuric acid medium, the yield is 92% (calculated on DFTHP)[12]. Results in presented work correspond rather to yields according to patent [13], where TEX is prepared by nitrolysis DFTHP in sulphuric acid/nitric acid medium and the yields are about 21%.

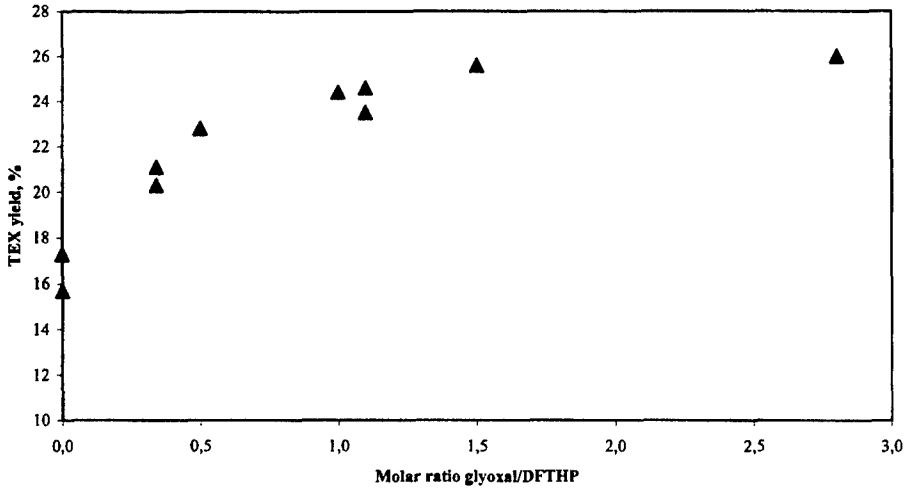


Fig 2. Influence of glyoxal/DFTHP molar ratio to TEX yield at nitric acid/DFTHP constant molar ratio 29,2:1

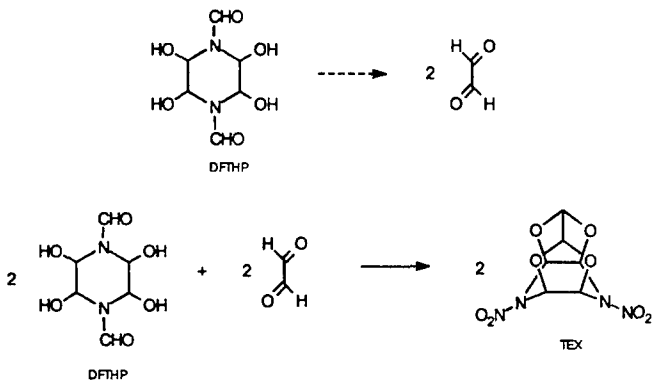


Fig 3. Decomposition of DFTHP in the reaction mixture to produce liberating glyoxal molecule, which reacts with unchanged DFTHP

4. CONCLUSIONS

- TEX was synthesized by the action of 1,4-diformyl-2,3,5,6-tetrahydroxypiperazine and fume nitric with various amounts of glyoxal trimer hydrate.

Under conditions in experimental part:

- The yield of product is only slightly depended on the glyoxal/DFTHP molar ratio.
- TEX may be also formed when glyoxal is not introduced into reaction mixture. It means that a part of DFTHP decomposes to glyoxal during course of reaction. The formed glyoxal can react with DFTHP to TEX.
- Elevated temperatures do not have to significantly decrease TEX yield.
- When appropriate cooling of reaction mixture is not used, rapid exothermic cause of reaction may occur.
- The reaction of DFTHP with glyoxal to form TEX requires high excesses of nitric acid.

Acknowledgment:

The authors would like to thank to Tomáš Weidlich from Department of Organic Chemistry, University of Pardubice for NMR measurements.

REFERENCES

[1] Doherty R.M., Simpson R.L.: "A Comparative Evaluation of Several Insensitive Explosives", 28th Int. Annu. Conf. ICT Proc., Karlsruhe, Germany, 1997, pp. 32.1-32.23

[2] Agrawal J.P.: "Recent Trends in High-Energy Materials", Prog. Energ. Combust. Sci. 24, 1-30 (1998)

[3] Nouguez B., Miermont H., Laudrin Y., Saidenberg N., Freche A.: "High Performance Insensitive Multipurpose Bombs for the French Navy", Insensitive Mun. Energ. Mat. Tech. Symp. Proc., Tampa, USA, 1999, pp. 78-84

[4] Braithwaite P.C., Edwards W.W., Hajik R.M., Highsmith T.K, Lund G.K., Wardle R.B.: "TEX: A Promising New Insensitive High Explosive", 29th Int. Annu. Conf. ICT Proc., Karlsruhe, Germany, 1998, pp. 62.1-62.7

[5] Mareček P., Pokorná J., Vávra P.: "A Study of Some Insensitive Explosives", 29th Int. Ann. Conf. ICT Proc., Karlsruhe, Germany, 1998, pp. 52.1-52.5

[6] Vágenknecht J., Mareček P., Trcinski W.: "Some Characteristics and Detonating Parameters of TEX Explosives", ", accepted for publication in J. Energ. Mat., 2000

[7] Östmark H., Langlet A., Bergman H.,Wingborg N., Wellmar U., Bemm U.: "FOX-7 - a New Explosive with Low Sensitivity and High Performance", 11th Detonat. Symp., Snowmass Village, USA, 1998, pp. 18-23

[8] Latypov N.V., Bergman J., Langlet A., Wellmar U., Bemm U.: "Synthesis and Reactions of 1,1-Diamino-2,2-dinitroethylene", Tetrahedron 54, 1125-1136 (1998)

[9] Jalový Z., Mareček P., Dudek K., Weidlich T.: "Synthesis and Properties of 1,1-Diamino-2,2-dinitro-ethylene", New Trends in Research of Energetic Materials Semin. Proc. IV", Pardubice, Czech, 2001, pp. 151-161

[10] Vail S.L., Moran C.M., Barker R.H.: "The Formation of N,N-Dihydroxyethylene-bisamides from Glyoxal and Selected Amides", J. Org. Chem. 30, 1195-1199 (1965)

[11] Yu Y.Z., Guan X.P., Chen F.B., Duan B.R., Sun J.G.: "Some Aspects on the Synthesis and Properties of Polynitro Cage Compounds", 22nd Int. Pyr. Semin. Proc., Chicago, USA, 1996, pp. 425-432

[12] Ramakrishnan,V.T., Vedachalam M., Boyer J.H.: "4,10-Dinitro-2,6,8,12-tetraoxa-4,10-diaza-tetracyclo [5.5.0.05,903,11]dodecane", Heterocycles 31(3), 479-480 (1991)

[13] Wardle R.B., Hajik R.M., Hinshaw J.C., Highsmith T.K.: "Process for the Large-Scale Synthesis of TEX", WO Patent 00/09509 (2000)

INITIATION STRENGTH OF DETONATORS – AIR GAP TEST METHOD. A SURVEY OF EXPERIMENTAL RESULTS

Marcela Jungová and Jiří Strnad

Department of Theory and Technology of Explosives,
University of Pardubice, Czech Republic

Abstract:

The present paper describes the method of Air Gap Test used for determination of initiation strength of detonators. Factors influencing initiation strength of detonators are stated. Results of the experiments performed at Department of Theory and Technology of Explosives, University of Pardubice are summarized. In general, detonators are used as a source of shock wave to initiate detonations of other explosives, most often low explosives.

1. INTRODUCTION

When assessing the utility value of detonators, one has to evaluate their handling safety, stability, ignition sensitivity, water resistance etc. However, the most significant factor can be seen in their initiation strength (hereinafter I.S.; I.S.D. = initiation strength of detonator), i.e. the ability to bring to detonation a low explosive of certain sensitivity.

The first classification of detonators on the basis of their I.S. is due to Alfred Nobel. He devised a series of 12 classes and ascribed detonators a particular class according to the content of mercury(II) fulminate. This classification has been used till nowadays, other standards being connected to it. The most frequently adopted detonators are those having Nos 3, 6, 8, and 12. Besides the classification by Nobel there exists another series devised by Ahrens: it represents a series of copper initiators having uniform geometric dimensions, the I.S. of individual classes being changed stepwise by the content of potassium chloride in the secondary charge of pentrite (PETN) [1].

1. Activation of the primary charge.
2. Transfer of detonation from the primary charge to the secondary charge of the detonator.
3. Stable detonation of the secondary charge.

When a detonator adjusted in an explosive material detonates, the explosive material is exposed to the action of detonation wave of the secondary charge of detonator, to a compression shock wave of detonation products of the secondary charge, and to that of destruction products of the metal case of detonator. Hence there are three basic initiation mechanisms combined: the initiation by a compression shock wave due to the impact of a fast flying body – the initiation by the shock wave transferred into the explosive being initiated from the detonating secondary charge – the initiation by a detonation wave transferred into the explosive being initiated from detonation of another explosive. The combination of action of these three mechanisms is summarily called "reactive compression shock wave" (R.C.S.W.).

From the point of view of detonator construction the I.S. is affected by the following factors:

a) The detonator case: During the detonation of secondary charge, this case represents a barrier slowing down the spreading of expansion wave. This extends the overpressure cone and improves the detonation conditions. A non-negligible role is played here by the factors of static and dynamic strength of material and wall thickness of the case. The case also represents a significant source of fragments (the detonation is accompanied by tearing up the case and subsequent fragmentation of metal particles), which are accelerated to high velocities and heated to high temperatures. With aluminium cases, the detonation is also accompanied by chemical reactions of the case material with the detonation products (CO_2, H_2O) and their combustion in atmospheric oxygen. These exothermic reactions in the detonation wave produce lower oxides, particularly $Al_2O(g)$ and AlO(s). Then in the expansion zone, the predominant processes include the high-energy reactions of aluminium with the reaction products and air.

b) Effect of the primary charge: The detonation parameters of the primary charge do not significantly affect the I.S. of detonator.

c) Effect of the secondary charge: The I.S. value of a detonator depends strongly on the detonation parameters of the secondary charge adopted and its density. Therefore, highly brisant explosives (Np 10T, RDX) are employed as the secondary charges.

d) While the detonation parameters of these explosives increase with their density, their sensitivity to initiation decreases. That is why the secondary charge is pressed into detonators in two steps (the first layer is pressed by a high pressure and the second by a lower pressure).

e) The contact surface area: The better the initiation of a secondary charge proceeds, the larger its contact surface area is at the interface with the primary charge. Therefore, rough structure is impressed on the surface of the secondary charge, and the primary charge is pressed onto it.

f) Effect of temperature: Temperature has no significant effect of the I.S. value.

g) Effect of orientation of detonator: In this respect, differences are observed between the axial and lateral effects. The result of this effect depends on the explosive used, the construction of detonator, its material, and the case wall thickness.

Practically, the I.S. value is determined on the basis of the deformation and destruction effects produced on a defined type of material. The test methods can be direct or indirect [2].

1. **Direct methods**: The determination of I.S. value by these methods is advantageous from the point of view of practical application of detonators. The chief factor is the ability of detonator to initiate a standard charge of low explosive characterised by various degrees of phlegmatisation. Subsequently, the effects produced are evaluated, such as deformation of Cu or Pb cylinder, magnitude of the hole produced in a Pb cylinder etc. The following methods can be given as examples:

Barrier test (Gap test): The so-called small gap test is based on finding such a wall thickness that results in 50% probability of initiation of an acceptor charge placed in a carbamide capsule. The initiation is proved by a breakdown of the reference steel plate. The method shows good reproducibility but due to the experimental arrangement it is not directly suitable for determination of I.S.D., because the lateral effect of detonator is actually eliminated. The method is used as a standard test for determination of sensitivity to initiation

by shock wave. Without giving experimental details, we can mention other direct method, such as

Test in the large Trauzl cylinder (Pb or Al)

Hess' method

Kast's method

Prior's method [3,4]

Cybulský's pendulum or ballistic mortar

Wenstop's method [5]

Wőhler's method

Zigal's method

SEVRAN method

2. **Indirect methods**: These methods are based on evaluating the effect of detonation of detonator upon the environment, and they are used for evaluation of quality of commercial detonators. However, it must not be forgotten that the individual tests are affected by some properties of detonators only. These methods include:

Breakdown test: This test was standardised in former Czechoslovakia (ČSN 668211), and at present it is described in decree ČBÚ 246/94, Appendix 26. It is used for checking quality and uniformity of industrial production of a given type of detonator.

The test is performed as follows: the detonator tested is placed in the middle of the reference plate (lead, steel), which is supported at the edges. The detonator is made to detonate. The quantity measured is the diameter of hole, the number and character of radii and, as the case may be, the weight of material torn out from the reference plate. This test predominantly measures the axial effect of detonator [17].

Nail test

Sand test

Schafler's test

Ballistic pendulum test (Cybulský's or Straka's pendulum, ballistic mortar)

Test in small Trauzl's cylinder

Besides the methods mentioned, more and more adopted at present are the so-called applied methods, which for evaluation the I.S. value make use of the explosion parameters of a low explosive activated by a detonator tested compared with that activated by the standard detonator.

It is also possible to include among these methods the measurement of detonation parameters of detonators by means of air or water shock wave [6, 7]. Although these measurements do not directly determine the I.S. value, nevertheless, the measurement of overpressure at the front of shock wave and of pressure impulse provides valuable data about the detonation course of the detonator and development of detonation in the secondary charge.

The measurement of air shock wave is carried out in a shock tube, but it can also be performed in open air. The advantage of the former procedure (shock tube) consists in the fact that it allows one to measure (besides the overpressure at the front of shock wave and

overall pressure impulse) also the velocity of shock wave and/or velocity of the particles produced by detonation of the detonator.

This method is relatively precise, reliable, and is not time consuming. Its drawback is in a limited service life of piezo-detectors.

The measurement of water shock wave is carried out by the so-called aquarium test, when the detonator tested is placed in a water container and made to detonate. Suitably located detectors can then monitor the detonation parameters.

This method has an advantage in that it determines two independent components: the energy of shock wave and the energy of detonation products. This possibility comes from the different ways of advance of shock wave in air and in water, which is due to different densities of the two media (because of the higher density of water, the overpressure at the front of shock wave reaches the maximum values immediately). However, the measurements using this method have to take into account the large effect of reflection of shock wave upon the resulting values. With regard to that, the overall geometry of the system is of considerable importance. Another drawback lies in the generation of secondary shock waves by fragments of the detonator case, which is difficult to evaluate.

2. EXPERIMENTAL

Method Used

In practice, the axial and the lateral components of I.S.D. are summed up because the detonator, as an initiator, is inserted in the explosive. In order to quantify the individual components, it is necessary to adopt a method that evaluates them separately and thus enables determination of the dominating factor in I.S.D.

With this aim, a team of DTTE began the I.S.D. measurements by means of Air Gap Test, and this method was (for evaluation of individual factors affecting I.S.D.) complemented by the breakdown test, measurements of detonation velocities of secondary charges, and measurements of parameters of air shock waves.

Air Gap Test

In principle, the Air Gap Test is a modified Gap Test (Barrier Test) described above. This modified arrangement does not use the partition formed by poly(methyl methacrylate) plates (hence the partition is the air only), no primer particles being used either (hence the detonator tested is the donor and the explosive charge is the acceptor). SEMTEX 1 was used as the acceptor explosive: it was located in a plastic tube case of 20 mm inner diameter and 20 mm height. The weight of charge was not constant, ranging from 8.5 g to 9 g. Its density was approximately 1.43 g cm^{-3}. The explosive was taken from a single manufacturing batch, and its sensitivity to initiation by shock wave was verified by means of the Small Gap Test. It was found that the sensitivity slowly drops with time, but within comparable experiments in one time period the relative informative value of measurement results remained unaffected. The results are presented in Table 1 [8, 9, 11].

Table 1. Results of measurements of Small GapTest for Semtex 1A

Year of measurement	1999	2000	2001
Distance of 50% initiation, y_0 [mm]	16.50	17.90	12.45
Standard deviation, s_y [mm]	0.60	1.30	2.65

The measurement proper was carried out on an instrument devised at the DTTE and made by Zbrojovka Vsetín (Fig. 1).

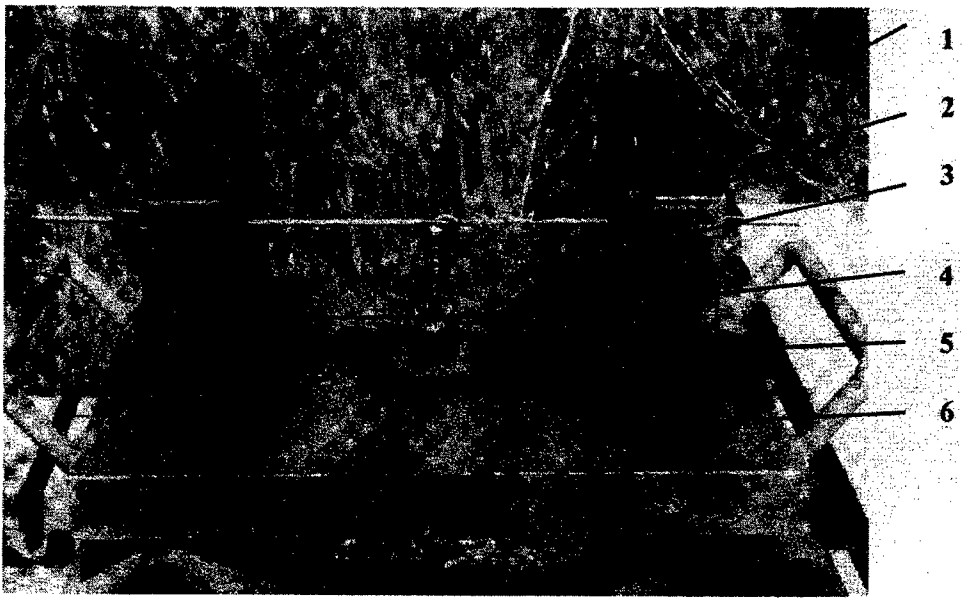


Fig 1. Measurement if I.S.D. – Arrangement for axial effect

Figure description: 1. Fixation wire 2. Adjustment of distance between the detonator tested and acceptor charge 3. Detonator tested 4. Acceptor charge 5. Reference plate 6. Instrument for I.S.D. measurements

In the measurement of axial effect the detonator centre was directed to the centre of acceptor charge while in the measurement of lateral effect the centre of secondary charge was oriented towards the centre of acceptor charge. The quantity measured was the distance between the detonator and acceptor charge. This distance was adjusted with the help of insert gauges.

The values measured were treated by means of a statistical method (RUN DOWN) to give the mean value of $\mathbf{H_{50}}$ [mm] and standard deviation **s** [mm]. The application of this method necessitates that the values followed should exhibit normal distribution.

In this way, both axial and lateral effects of detonators were evaluated.

Breakdown Test

The Breakdown Test is an analogy of the test described in Appendix 26 of Decree ČBÚ 246/1996 except for the thickness of reference plate. In our case the plate thickness was 6 mm and the material was lead of 99.5% purity with hardness H_B (10/100/60˝) = 3.5 to 5.5. The plate dimensions were 40 mm × 40 mm. The test was carried out on the same apparatus as that used for measuring I.S.

The bottom part of detonator is placed immediately on the reference plate, and after firing the diameter of hole (Diameter [mm]) and the amount of material torn out from the reference plate (M [g]) are evaluated. The results are presented in Table 2.

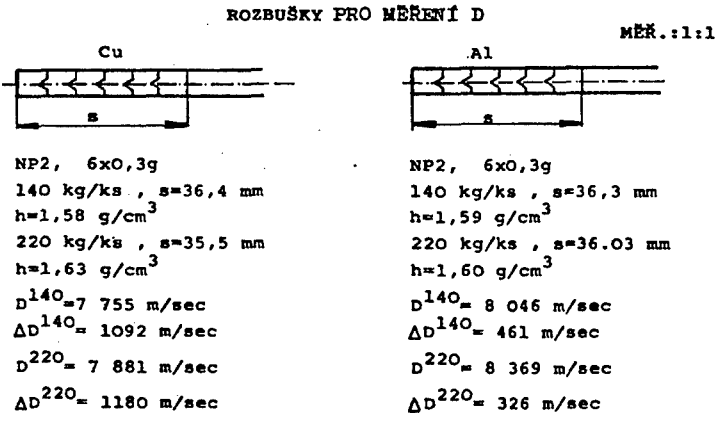
Measurement of Detonation Velocities

The detonation velocities were measured in the same way as that used for measurements of detonation velocities of low explosives (time method [10]). The arrangement only differed in the dependence on the type of detonators measured. The values obtained (D [ms^{-1}]) are given in Table 2

Procedure: The sensors (in this case two 0.3 mm enamel-coated copper wires gently wound together) were placed below the detonator measured (or wound around it). The sensor placed nearer to the initiation served as the start. The second sensor – stop – was placed at a certain, precisely measured distance. When the detonation wave passes the sensor, the latter is short-circuited, which connects the contact start or stop. The time needed for the detonation wave to pass between the two sensors is measured by means of an electronic stopwatch (an adapted chronometer Gold Star FC 2015U, precision of ±0.1 μs).

In order to eliminate the error resulting from the short length of the secondary charge of detonators, we prepared detonators in which six doses of secondary charge were pressed (Fig. 2).

For measuring the detonation velocity of commercially produced detonators the arrangement used was modified. The detonator was fixed in the apparatus for measurement of the Air Gap Test, the start sensor was wound around the detonator several millimetres from the point of beginning secondary charge, the stop sensor was placed on the steel reference plate and the detonator was pressed on it by its bottom.



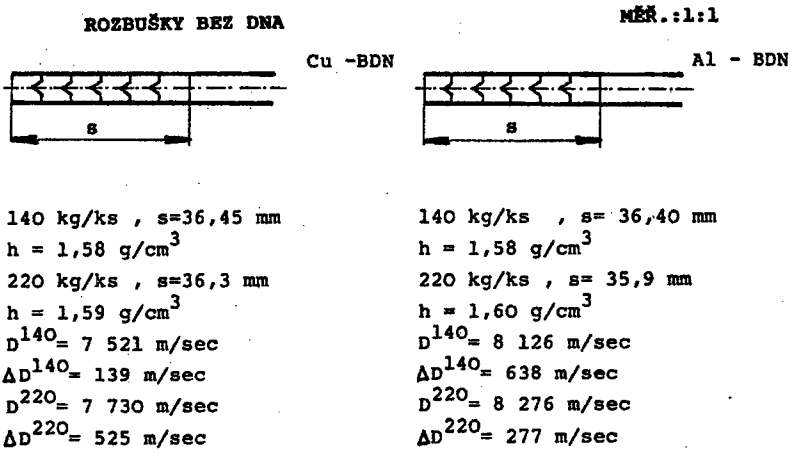


Fig 2. Preparation of column of secondary charge for measuring the detonation velocity. Weighing Np 2, 6x 0.3 g

Measurement of Parameters of Air Shock Waves

The measurement of parameters of air shock waves was performed in a shock tube of 210 mm diameter (in VVÚU Ostrava-Radvanice) and in free air (in the test facilities of the DTTE). In the former case, the detonator tested was placed at the beginning of the shock tube and made to detonate. The distances of sensors (piezoelectric, Kistler) from the beginning of shock tube were 6.25, 8.75, and 11.25 m. The signal from sensors was led *via* an amplifier to oscilloscope, where the data were stored and subsequently treated with the help of a special program. The most distinct record was obtained from the sensor nearest to detonator front (5.25 m).

The measurement in open air was based on the same principle. The sensors (piezoelectric, Kistler) were placed at the distances of 3 m and 5.2 m from the detonating detonator. The sensors and the detonator were located in the same plane. The mean values of the measured quantities $p_{max.}$ [kPa] and I [Pa.s] obtained from the sensors placed at 6.25 m (VVÚU Ostrava) and 3 m (DTTE) from detonator are presented in Table 2.

3. TEST INITIATORS

Whole-case Detonator (WC-Al, WC-Cu)

The aluminium (Al) and copper (Cu) cases, degree 0 of electric initiators (Austin Detonator, Vsetín) were filled with 2 × 0.3 g Np 2 (a low explosive material based on pentrite a phlegmatised with 2% wax), each portion being pressed by means of a hand-operated press at 140 kg/ks (48.2 Mpa) or 220 kg/ks (76 Mpa). The material Np 2 was chosen because of the possibility to press on independent bodies of secondary charge.

The initiation element (a metal cup with lead azide and Np) was pressed on the pre-pressed secondary charge.

Caseless Detonator (CL-Cu)

The bodies of secondary charge were prepared at the same conditions of pressure and weight (the 6.20 mm diameter corresponds to the inner diameter of detonator case). The resulting values were 1.55 and 1.66 g cm^{-3}, respectively (Fig. 3). Subsequently, the initiation elements were stuck on these bodies.

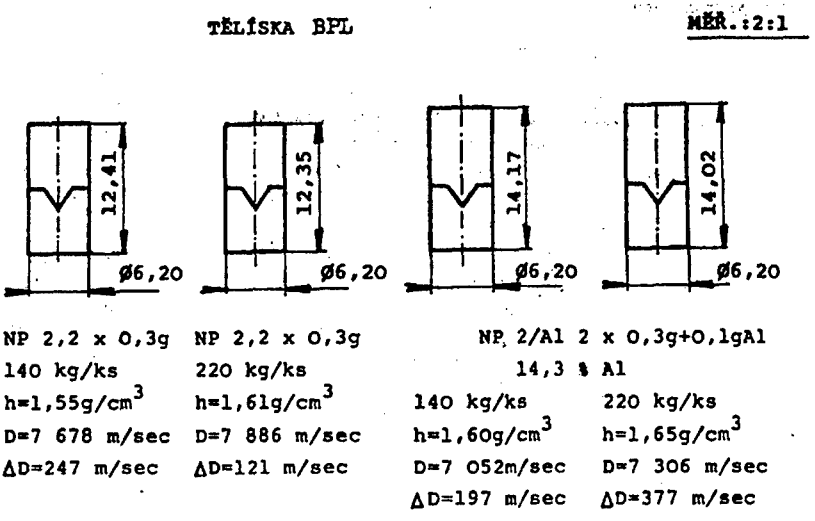


Fig 3. Pressing of bodies of secondary charge for caseless detonator

Caseless Detonator with Aluminium (CL with Al)

Aluminium (14.3 % Al Albo 90) was admixed to Np 2, the next procedure being identical with that used for the caseless detonator.

Bottomless Detonator (BL-Al, BL-Cu)

After cutting off the bottom of case by means of a modified support mandrel, the pressing of charge was identical with that used for whole-case detonator.

Other Detonators Tested

For comparison, the described tests were also applied to standard detonators No 3 and No 8, industrial ignition detonator No 8 Al type II (produced by Sellier & Bellot, a.s., Vlašim), and detonators Nonel Surface 0.2 g Np, No 6, and Nonel Indetshock 0.72 g Np, No 12 (produced by Austin Detonator, a.s., Vsetín).

Table 2. Results of tests with the test initiators mentioned

Detonator tested	Air Gap Test		Brake-down test	Det. velocity	Measuring of air shock waves (mean values)			
	H_{50} [mm], s [mm]		M [g], Diameter [mm]	D [ms^{-1}]	VVÚU Ostrava Sensor 6,25m		DTTE, sensor 3,00m	
	Axial effect	Lateral effect			$P_{max.}$ [kPa]	I^+ [Pas]	$P_{max.}$ [kPa]	I^+ [Pas]
WC-Al (2x 0.3g Np 2.140 kg/ks)	15.8 1.0	32.4 8.24	1.08 5.07	8046	63.0	171.5	2.50	0.62
WC-Al (2x 0.3g Np 2.220 kg/ks)	18.2 2.4	31.2 3.92	1.2 6.77	8369	71.4	164.3	2.26	0.56
WC-Cu (2x 0.3g Np 2.140 kg/ks)	10.2 2.32	25.2 2.99	2.07 10.35	1092	35.2	61.8	2.25	0.43
WC-Cu (2x 0.3g Np 2.220 kg/ks)	10.6 1.50	28.8 5.31	2.58 11.67	1180	35.6	62.3	2.11	0.45
CL-Cu (2x 0.3g Np 2.140 kg/ks)	statistical treatment was not possible		1.48 7.1	7678	52.9	105.2	2.42	0.62
CL-Cu (2x 0.3g Np 2.220 kg/ks)	3.8 1.0	not eva-luated	1.55 7.63	7886	59.6	109.7	2.43	0.48
CL with Al (2x 0.3g Np 2.140 kg/ks)	not evaluated		1.18 5.21	7052	73.1	154.7	2.83	0.74
CL with Al (2x 0.3g Np 2.220 kg/ks)	not evaluated		1.28 5.48	7306	73.3	151.3	2.84	0.68
BL-Al (2x 0.3g Np 2.140 kg/ks)	not eva-luated	35.6 9.76	1.8 8.5	8126	62.5	165.7	2.19	0.62
BL-Al (2x 0.3g Np 2.220 kg/ks)	3.8 0.98	34.4 11.2	2.23 10.35	8276	69.4	163	2.45	0.61
BL-Cu (2x 0.3g Np 2.140 kg/ks)	not eva-luated	28 7.6	2.85 12.97	7521	42.3	72.7	2.23	0.51
BL-Cu (2x 0.3g Np 2.220 kg/ks)	not eva-luated	32 8.76	3.05 12.95	7730	40.2	72.7	2.13	0.50
Standard detonator No 3 (Cu)	3.8 2.72	not eva-luated	0.9 without breakd.	5385	20.8	22	1.42	0.23
Standard detonator No 8 (Cu)	not evaluated		1.4 5.22	5692	41,7	62.2	2.01	-
Ind. ign. detonator No 8, Al type II.	21.1 3.5	15.9 4.52	1.3 4.3	7276	87.1	205.7	2.82	0.64
Nonel Surface 0.2g Np, No 6	7 1.26	3.4 0.8	0.69 1.68	9408	not measured		not measured	
Nonel Indetshock 0.72g Np, No 12	not eva-luated	67.8 2.04	1.62 6.88	9342	not measured		not measured	

4. RESULTS

An initiation of explosive by a detonator that is inserted in it or placed immediately near to it represents a complex process involving effect of shock wave, of expanding products and effect of fragments of the detonator case. With regard to the test methods adopted, the following parameters of a detonator were varied:

Orientation: axial, lateral

Case type: whole case, caseless, copper, aluminium

Pressure used for pressing the secondary charge: 140 and 220 kg/ks

Admixture of Al in the secondary charge body of caseless detonator.

The explosion transformation of secondary charge is finished within 1.5-1.7 μs, and the detonation wave together with the pressure of products cause an increase of case body from initial R_0 to $2R_0$ along the secondary charge. After exceeding the strength limit, the initial velocity of case fragments is proportional to the detonation velocity of the secondary charge and to the ballistic ratio [12]. It can be presumed that the shock wave separates from the reactive wave (from detonation products) at about 10-14 multiple of charge diameter. Before this limit, the measured distances of Air Gap Test describe the action of reactive compression shock wave.

There is no large difference between the temperature coefficients of copper and aluminium ($a^{Cu} = 1.14$ cm^2/s, $a^{Al} = 0.99$ cm^2/s). At the conditions of contact of the case metal with the detonation products (t ~ 2500 °C) it is possible to presume an initial reaction of aluminium with the detonation products and with air oxygen.

The values of $p_{max.}$, I^+ and I^- measured for the caseless detonator with aluminium, as compared with those of the whole-case aluminium detonators, are only slightly higher, which supports the presumption about the exothermal reactions of aluminium predominantly outside the detonation wave. An admixture of 14.3% Al to Np 2 is unable to completely react in the detonation wave and decreases the detonation parameters (the detonation velocity drops by 500-700 ms^{-1}).

The bottomless detonators exhibit an increased lateral effect when I.S.D. is measured by the Air Gap Test, as well as a larger breakdown of lead reference plate in the breakdown test. The markedly lower transfer distance in axial effect of Air Gap Test (comparable with those of caseless detonator) proves a positive effect of particles of the metal bottom of detonator case upon I.S.D.

Still another conclusion can be made from the results of the measurements carried out by the Air Gap Test: The lateral effect of both whole-case and bottomless detonators is always higher than the axial effect. In the lateral effect, the amount of fragments from the part detonator case, what is oriented to the acceptor, is higher and so it can be presumed that the probability of occurrence of fragments with velocities $v > v_{crit}$ will be higher.

The grater I.S. value of aluminium detonators (WC and BL, lateral effect) can be interpreted by a higher velocity of fragments of the aluminium case. This presumption can be supported by calculation. The calculation of velocities of fragments from whole-case aluminium and copper detonators starts from the ballistic ratios $B_{Al} = 0.64$ and $B_{Cu} = 1.49$ and furthermore from the Gurney constant (1) or by introducing the detonation velocity for a particular density (2):

The Gurney constant for Np 2 was calculated with the help of parameter Φ [13], and then from Refs. [14, 15] it follows that $v_g^{Al} = 2508$ ms^{-1} a $v_g^{Cu} = 1897$ ms^{-1}.

According to Ref. [16] for $\rho = 1.58$ g cm^{-3} (which is an average value for the pressures of 140 and 220 kg/ks) it is then $v_g^{Al} = 2259$ ms^{-1} **a** $v_g^{Cu} = 1956$ ms^{-1}.

Hence, from the given facts it follows that the I.S.D. value measured by the Air Gap Test method is substantially affected by the fragmentation effect of decomposition of the metal case of detonator and by the number and velocity of fragments accelerated by the detonation products.

The results obtained with the industrial detonators mentioned in the paragraph Other Initiators and their comparison with standards (the normalised detonators No 3 and No 8, Sellier & Bellot, a.s., Vlašim and detonators Nonel, Austin Detonator, a.s., Vsetín) indicate high quality of the commercially produced detonators.

Workers of the DTTE intend to continue the evaluation of I.S.D. by means of the Air Gap Test and complement the measurements given by further original procedures.

REFERENCES

[1] Ahrens H.: Explosivstoffe Nr. 3, 1972, 20, 132.

[2] Buksa R., Sillinger Fr., Straka A.: Analyses and Tests of Explosives (in Czech), SNTL, Prague, 1954.

[3] Prior J.: Explosivstoffe Nr. 3, 1973, 21, 107.

[4] Prior J.: Methode zur Bestimmung des Zündvermögens von Sprengkapseln und Sprengzündern, Prop. & Expl. 3, 1978, 42-49.

[5] Wenstop K.: Explosivstoffe Nr. 3, 1973, 21, 104.

[6] Feng Ch., Jia Q., Zhen G., Luoy Y.: Direct Methods in Dynamic Measurement of Detonation Output from a Detonator, Eighteen Int. Pyr. Seminar, July 1992.

[7] Svachouček V.: Initiation Strength of Detonators (in Czech), Thesis, VŠCHT Pardubice.

[8] Masař F.: Determination of Axial and Lateral Effect of Detonators No 8, Part II (in Czech), Final-year thesis, University of Pardubice, 1999.

[9] Pavlík D.: Determination of Axial and Lateral Effect of Detonators No 8, Part III (in Czech), Final-year thesis, University of Pardubice, 2000.

[10] Decree ČBÚ 246/1996 Collect. of Law.

[11] Gargela J.: Effect of Detonator Case upon Their Initiation Strength (in Czech), Final-year thesis, University of Pardubice, 2001.

[12] Strnad J.: Means of Blasting Technology. An Expert Manual (in Czech), Pardubice, 1980.

[13] Vávra P.: A Manual to Study Texts on Theory of Explosives (in Czech), University of Pardubice, 1999.

[14] Denkstein J.: Protection of Buildings against Effects of Crash Explosions (in Czech), University of Pardubice, 1995.

[15] Kusák J., Denkstein J.: Protection of Buildings against Effects of Crash Explosions III. (in Czech), University of Pardubice, 1993-5.

[16] Baum F. *et al.*: Physics of Explosion (in Russian), Nauka, Moscow 1975.

[17] Strnad J.: Initiation Properties of High Explosives and Development of Methods of Their Measurements (in Czech), Thesis. VŠCHT Pardubice, 1972.

NOTICES TO DETERMINATION OF THE ELECTRIC SPARK SENSITIVITY OF ENERGETIC MATERIALS

Jiří Kočí, Svatopluk Zeman, Jiří Majzlík and Jiří Strnad

Department of Theory & Technology of Explosives, University of Pardubice
CZ-532 10 Pardubice, Czech Republic

Abstract:

An instrument of a new, relatively simple, construction has been applied to determination of electric spark sensitivity (E_{ES}) of 52 polynitro compounds and 6 inorganic azides. Attention was focused also on the relationship between the E_{ES} values and granulometry of RDX and HMX, and on the dependence of these values upon the content of hard admixtures to RDX (up to 15 % by wt.). Relationships have been found between the resulting E_{ES} values and the values of this sensitivity determined by means of other types of apparatus and in other laboratories. It has been found that these relationships are strongly affected by molecular-structure factors and construction differences between the individual testers. An attempt is presented at specification of the relationship between the E_{ES} of azides and their heats of explosion (Q). The value of $Q = 2.472\ kJ\ g^{-1}$ for mercury(II) azide has been estimated from this relationship.

Keywords: *electric spark, sensitivity, explosives, primers*

1. INTRODUCTION

Recent papers [1-18] published in the field of studies of sensitivity of energetic materials to electric spark have shown that this sensitivity depends not only on the chemical entity of the material given [1,4,6,8,9,12,14], its granulometry [1-3,12] and grain shape [3], its mechanical properties [5,6], temperature [1,13], its moisture content [2,4], its thermal [2,6,7,12,15,17] and impact [7,16,18] reactivities but also on the configuration of electrodes and structure of the circuit [2,4]. Consequently, it has not yet been possible to devise an international standard test specifying this stability [9,10,16]. Irrespective of the above-mentioned spectrum of effects influencing the said sensitivity, however, a linear relationship between the test results obtained with various apparatuses can be found [9,10,11].

Our Department in cooperation with the R&D Department of Austin Detonator Ltd. Vsetín took part in constructing the apparatus for determination of electric spark sensitivity [8-10]. With the help of this apparatus, measurements were carried out on a large set of polynitro compounds of secondary explosive type [8-10,14,17-22]. From the results obtained it was possible to make conclusions in the area of chemical mechanisms of initiation of these compounds [14,17-22]. However, the apparatus mentioned is not suitable for determination of electric spark sensitivity of primers and pyrotechnics. Therefore, with a financial support from Czech Ministry of Industry and Commerce [23], we developed a new apparatus [24] suitable for measurements of energetic materials within the whole scope of technically attractive sensitivities. The present paper gives the first results of measurements realised with this new apparatus. In some cases, these results have been compared with those obtained with other instruments of this type.

2. EXPERIMENTAL

2.1. General principles of the electric spark sensitivity testing

Depending on the prevailing initiation mechanism of the substance tested, the test is carried at one of the two following conditions [24]:

2.1.1. Conditions of undamped discharge [24]

The sensitivity of secondary explosives (i.e. substances with prevailing initiation stimulus by a shock wave) is determined at conditions of undamped discharge of charged condenser into the sample tested. The energy of electric spark, E_{ES}, required for 50 % initiation probability is calculated (up and down method) from the know capacity C (in F) of the circuit and voltage U (in V) at the condenser by means of the well-know relation

$$E_{ES} = 0.5 \,.\, C \,.\, U^2 \qquad (1)$$

Beside the working condenser and test chamber with sample, the series resonance circuit consists of the loss resistor of circuit (whose value varies from 0.27 to 10 Ω) and total parasitic inductance (ranging from 1 to 1.6 μH). In the course of oscillation discharge, the increase in output in the space between the electrodes of testing spark gap reaches the values of $dP/dt \approx 5.10^{18}$ W/s. The time of oscillations (0.5 to 20 μs) as well as the above-mentioned parameters of the apparatus depend considerably on the capacity value (C), testing voltage (U), and the sum of Joule losses in the test substance.

2.1.2. Conditions of damped discharge [24]

The sensitivity of energetic materials initiated predominantly by a relatively long-term heat impulse is determined at the conditions of damped discharge into the sample tested. The damping of discharge is achieved by means of a resistor Rs = 10 kΩ that is inserted in series connection into the circuit (see paragraph 2.1.1). The lower sensitivity limit, E_{min}, is evaluated from the energy that is released between the electrodes where the sample is placed. The E_{min} value is estimated from oscillographic record of time function of current i(t) (in A; s) and voltage u(t) (in V; s) at the spark gap according the formula

$$E_{ES} = \int i(t).u(t).dt \qquad (2)$$

In this modification, the output P_{max} released at the spark gap only attains about 500 W, but the time of thermal load on sample is increased to about 10 ms at the chosen capacity of C = 350 nF.

2.2. Measurement with apparatus of older construction [8-10], code designed as OA

The apparatus, developed in cooperation with Austin Detonator, Ltd. [8], can work only at the conditions described in paragraph 2.1.1. The schemes of its wiring and its spark gap are presented in papers [8-10]. The bottom electrode is a steel base in whose centre there is attached a screw as a leak electrode. Attached to this screw is a plastic cylinder with a cut for fastening a piece of flexible tubing of 5 mm height and 5 mm diameter serving as a container of the sample tested. The top electrode is a steel cylinder of conical shape with attached resistance wire protected by a plastic distance stop, which presses an umafol lid to the flexible tubing. The capacity of the capacitors was chosen so as to allow measurements in the voltage interval from 8 to 14 kV. If the initiation was successful, the next measurement was carried out with a voltage lowered by 0.2 kV; if it was unsuccessful, the voltage was

increased by the same value. We considered an initiation to be successful if the sample disappeared or the flexible tubing was torn. Altogether 25 measurements were carried out with each substance and the results were treated in the sense of eqn. 1 by means of the "up and down method".

2.3. Measurements with new apparatus [24], code designed as NA

The apparatus is designed for a small-scale sensitivity testing of energetic materials. It is able to work at the conditions given in paragraphs 2.1.1 and 2.1.2 above. A high voltage power supply (operating voltage 4-10 kV) and a set of capacitors of overall capacity in the range from 100 pF to 350 nF produces an electrostatic discharge of total energy from 10 mJ to 16 J. A sample of 1 mm height is fitted into an isolation tube mounted on the lower cylindrical metal electrode. The upper electrode is equipped with manual vertically adjustable positioner. The micro container itself is placed in a separate test box with ventilation. The time behaviour of voltage and current at the spark gap is registered with a scope and than evaluated using a microcomputer to give the effective energy transmitted to the sample.

2.4. The energetic materials studied

2.4.1. Individual polynitro compounds

Our attention was focused on polynitro compounds classified as secondary explosives. The substances were synthesised at our Department earlier. Except for several highly insoluble substances, they were purified by crystallization in motion, and often by precipitation crystallization (with good stirring) from organic solvents. The crystallization was carried out in such a way as to obtain the product appearing as individual in thin layer chromatography. However, the granulometry of the substances investigated was not specified. The samples were measured by means of both the instruments (OA and NA). A survey of the substances tested, their codes, and the results of measurements described in the present paper along with those taken from the references specified are given in Table 1.

2.4.2. Technical nitramines RDX and HMX

We had the following samples at our disposal: 1,3,5-trinitro-1,3,5-triazacyclohexane {(RDX); produced by former Chemko Strážske (now Chemza Ltd.) in seven granulometric qualities according to MIL standard R-398C (1977)} and 1,3,5,7-tetranitro-1,3,5,7-tetraazacyclooctane {(HMX); of foreign provenance; in five granulometric qualities according to MIL standard H-45444B (1978)}. The individual classes of these nitamines are characterised in Table 2 by their average grain size (the mean value of limit magnitudes in the given class). This Table also presents the results of measurements.

For evaluation of influence of hot nuclei on the electric spark sensitivity, the lowest-grain RDX was mixed with crushed glass (with grain size below 20 μm). Mixtures containing various amounts of this crushed material were then measured by means of NA apparatus (i.e. according to paragraph 2.3), and the results of measurements along with composition of the mixtures studied are presented in Table 3.

Table 1. Table 1: Survey of the studied polynitro compounds, their code designation and their electric spark sensitivities as our results, LANL results [1] and Roux et. al. results [12].

Polynitro compound			E_{ES} required for 50 % initiation probability				
			Our results		LANL results		Roux results
Data No.	Chemical name	Code design.	OA [J]	NA [mJ]	a [J]	b [J]	[J]
1	1,3-Dinitrobenzene	1,3-DNB	3.15	256.7±14.4			
2	1,4-Dinitrobenzene	1,4-DNB	18.38	403.3±14.4			
3	1,3,5-Trinitrobenzene	TNB	6.31	108.2± 7.8			
4	2,2',4,4',6,6'-Hexanitrobiphenyl	HNB	5.03	286.7±26.7			0.82
5	2,2',2'',4,4',4'',6,6',6''-Nonanitro-m-terphenyl	NONA	16.44	158.2± 7.8			
6	1,8-Dinitronaphthalene	1,8-DNN	13.99	238.2± 9.9			
7	1,5-Dinitronapthalene	1,5-DNN	11.20	180.0±10.9			
8	1,4,5-Trinitronaphthalene	TNN	10.97	210.0±13.3			
9	1,4,5,8-Tetranitronaphthalene	TENN	8.26	95.0± 8.3			
10	1-(2,4,6-Trinitrophenyl)-5,7-dinitrobenzo-triazole	BTX	6.50	135.0± 8.3			
11	2,4,6-tris(2,4,6-Trinitrophenyl)-1,3,5-triazine	TPT	10.61	283.3±27.2			
12	1-Methyl-2,4,6-trinitrobenzene	TNT	6.85	111.8±12.9	0.46	3.75	1.26
13	1,3,5-Trimethyl-2,4,6-trinitrobenzene	TNMs	8.98	292.7±17.0			
14	1-Amino-2,4,6-trinitrobenzene	PAM	6.85	156.7± 7.2			
15	1,3-Diamino-2,4,6-trinitrobenzene	DATB	10.97	175.0 ± 8.3	1.48	10.79	
16	1,3,5-Triamino-2,4,6-trinitrobenzene	TATB	17.75	293.3±14.4	4.25	18.14	
17	1-Hydroxi-2,4,6-trinitrobenzene	PA	9.98	115.5± 6.8			1.22
18	1,3-Dihydroxi-2,4,6-trinitrobenzene	TNR	12.30	230.0±30.0			
19	1-Methoxy-2,4,6-trinitrobenzene	TNA	28.59	436.0±29.6			
20	1-Chloro-2,4,6-trinitrobenzene	CTB	6.71	101.0± 7.7			
21	1,3-Dichloro-2,4,6-trinitrobenzene	DCTB	2.55	31.5± 2.8			
22	2,2',4,4',6,6'-Hexanitroazobenzene	HNAB	8.20	112.0± 8.6			
23	3,3'-Dimethyl-2,2',4,4',6,6'-hexanitro-azobenzene	DMHNAB	13.37	118.2± 7.8			
24	2,2',4,4',6,6'-Hexanitrodiphenylsulfide	DIPS	2.54	125.5± 8.6			
25	3,3'-Dimethyl-2,2',4,4',6,6'-hexanitro-diphenylsulfide	DMDIPS	8.57	112.7± 7.1			
26	2,2',4,4',6,6'-Hexanitrodiphenylsulfone	DIPSO	10.24	186.7± 7.2			
27	2,2',4,4',6,6'-Hexanitrodiphenylamine	DPA	5.02	103.0± 7.6			0.96
28	2,2',4,4',6,6'-Hexanitrodipheny-lmethane	DPM	4.10	136.4 ±7.6			
29	2,2',4,4',6,6'-Hexanitrobibenzyl	DPE	3.89	167.0± 1.5			1.17
30	3,3'-Dimethyl-2,2',4,4',6,6'-hexanitro-biphenyl	BITNT	4.28	206.7± 7.2			
31	2,6-Diamino-3,5-dinitropyridine	DADNP	12.40	358.0±10.8			
32	2,6-bis(2,4,6-Trinitrophenylamino)-3,5-dinitropyridine	PYX	8.90	136.7±10.	1.18	9.00	

Table 1 - continued

Polynitro compound			E_{ES} required for 50 % initiation probability				
			Our results		LANL results		Roux results
Data No.	Chemical name	Code design.	OA [J]	NA [mJ]	a [J]	b [J]	[J]
33	1,3,7,9-Tetranitropheno-thiazine-5-oxide	TNPTM	10.68	195.0± 8.7			
34	1,3,7,9-Tetranitropheno-thiazine-5,5-dioxide	TNPTD	28.93	363.3±14.4			
35	3-Nitro-1,2,4-triazol-5-one	NTO	8.98	220.0± 5.5	0.91	3.40	
36	Pentaerythritol tetranitrate	PETN	1.74	29.3± 5.6	0.19	0.75	
37	N,N'-bis(2-Nitroxyethyl)nitramine	DINA	5.85	169.1± 5.0			
38	1-Methylnitramino-2,4,6-trinitro-benzene	TETRYL	5.49	83.0± 7.6	0.54	3.79	
39	2,5-Dinitro-2,5-diazahexane	DMEDNA	8.24	660.0±51.7			
40	3,5-Dinitro-3,5-diazaheptane	DNDAH	12.49	225.0±11.3			
41	2,4,6-Trinitro-2,4,6-triazaheptane	ORDX	8.08	243.3±14.4			
42	1,9- Diacetoxy-2,4,6,8-Tetranitro-2,4,6,8-tetraazanonane	AcAn	13.93	206.7±14.4			
43	1,3-Dinitro-1,3-diazacyclopentane	CPX	9.68	403.3±14.4			
44	1,4-Dinitro-1,4-diazacyclohexane	DNDC	15.97	190.0± 8.3			
45	1,3,5-Trinitro-1,3,5-triazacyclohexane	RDX	2.49	216.4±15.6	0.21	0.96	
46	1,5-Endomethylene-3,7-dinitro-1,3,5,7-tetraazacyclooctane	DPT	17.42	520.0±20.0			
47	1,3,5,7-Tetranitro-1,3,5,7-tetraaza-cyclooctane	β–HMX	2.89	236.4±10.1	0.23	1.42	
48	trans-1,4,5,8-Tetranitro-1,4,5,8-tetraazadecaline	TNAD	5.43	520.0±53.3			
49	1,1,3-Trinitroazetidine	TNAZ	8.76	78.3± 7.2			
50	2,4,6,8,10,12-Hexanitro-2,4,6,8,10,12-hexaazaisowurtzitane	ε–HNIW	4.70	240.0±41.4			
51	4,10-Dinitro-2,6,8,12-retraoxa-4,10-diazaisowurtzitane	TEX	c	285.5±25.3			
52	Ammonium dinitraminate	ADN	d	386.1±52.4			

Notes to Table 1:

a) the values obtained from the measurements in LANL [1] with samples covered with Pb foils of 3 mils (0.076 mm);
b) the values obtained from the measurements in LANL [1] with samples covered with Pb foils of 10 mils (0.254 mm);
c) the method of measurement (i. e. according to the section 2.2.) fails in this case;
d) it was not measured.

2.4.3. Primers

Azides of barium and heavy metals have been chosen to represent primers in this work. They were synthesised by known methods [25, 26], i.e. conversion of aqueous solution of sodium azide with aqueous solution of the respective heavy metal salt. This conversion was realised with vigorous stirring without any protective colloid. The granulometry of the azides prepared was not specified. A survey of the azides studied, their heats of explosion (taken from refs [26, 27]), and the results of measurements obtained with NA apparatus (i.e. according to paragraph 2.3) are given in Table 4.

Table 2. Electric spark sensitivity of RDX and HMX versus mean values of their grain size

RDX		**HMX**	
Mean value of grain size in μm	E_{ES} in mJ	Mean value of grain size in μm	E_{ES} in mJ
600	1170	1000	875
450	1060	400	495
350	900	150	242
250	535	40	152
150	215	27	87.5
75	137		
30	55		

Table 3. Electric spark sensitivities of the mixtures of RDX with crushed glass.

Crushed glass content in % wt.	E_{ES} in mJ
0	55
5	120
10	180
15	200

Table 4. Electric spark sensitivities and heats of explosion (taken from Ref. [27]) of anorganic azides.

Azide		E_{ES} in mJ	Heat of explosion in kJ g^{-1}
Cation	Ref.		
Pb^{++}	25	0.706	1.535
Cu^{+}	26	0.610	2.326
Cu^{++}	26	0.026	4.055
Ag^{+}	25	1.860	1.891
Ba^{++}	26	3.530	2.358
Hg^{+}	26	0.028	1.113
Hg^{++}	26	5.740	2.472[a]

Note: a) the value predicted in this paper

3. DISCUSSION

2.5. Comparison of results obtained with new (NA) and older (OA) instruments

The analysis of relationship between the EES values obtained by measurements on the two instruments (i.e. OA and NA) revealed that the relationship is not unequivocal. In the sense mentioned, the set of polynitro compounds tested fell into several classes, which is documented by Figs 1-5. This classification is dominated by molecular-structure factors. Thus Fig. 1 presents the relationship mentioned for the data of polynitronaphthalenes having nitro groups at *peri* positions, which is logically obeyed also by the data of 1,4-dinitrobenzene. From the point of view of primary step of their thermolysis (the homolysis of C–NO_2 bond), 1,5-DNN is somewhat deviating: in this derivative the thermal decomposition should start by interaction of oxygen of nitro group with the adjacent *peri*-hydrogen substituent [28]. Figure 2 shows the class of substances whose thermal decomposition begins with homolysis through five- or six-membered transition states. These include e.g. the so-called tritol mechanism of thermal decomposition, which is obeyed by compounds having a hydrogen atom at γ-position with respect to nitro group [29-33], as well as the interaction of oxygen in *ortho*-standing nitro group with bridge heteroatom [28, 33] (e.g. in molecules of DIPS and DMDIPS) or chlorine atom [34]. Figure 3 is an analogy of Fig. 1. Figure 4 documents the effect of –CH_2– linkage on the electric spark sensitivity: whereas in the measurements on the OA instrument the introduction of methyl groups into TNB, HNAB, and DIPS molecules produced an intermediate to distinct phlegmatising effect, this effect was negligible in measurements on the NA instrument. An opposite, i.e. sensitising influence of –CH_2– can be seen in class *A* in Fig. 4, this effect being more distinct in the measurements with NA instrument.

Figure 5 shows the dependence discussed for nitramines. Similar trends in E_{ES} values obtained from the two instruments are exhibited by class *C* of high-energetic cyclic nitramines. On the other hand, class *D* of linear nitramines and particularly class *E* of cyclic nitramines show opposite trends in E_{ES} values. The E_{ES} values obtained for Tetryl and TNAZ by measurements on NA instrument seem to be too low and will have to be experimentally verified.

From the facts given so far it seems to follow that the mechanisms of spark energy transfer into the reaction centre of molecule could be different in the measurements on the

two instruments (OA and NA). The thermal component of discharge in the first instrument may be one of the reasons of this difference. This assumption is also supported by the differences (in order of magnitude) between the E_{ES} values obtained from the individual instruments (see Table 1). Of course, the considerable electric energy losses in the area between the upper electrode and the sample surface in the OA system measurements contribute to the above-mentioned difference between the values.

3.2. Comparison of NA results with those of other laboratories

Linear relationships were described [9, 10] between the results obtained with our OA instrument and the sensitivity measurements in LANL [1] and by Amari *et. al.* [4]. These relationships were unambiguous – the molecular structure of polynitro compounds tested being not projected in the results in any way. A different situation is encountered in the case of NA system results, which is documented in Fig. 6 comparing these results with those of LANL [1]: in this comparison molecular-structure factors dominate like in the dependences shown in Figs 1-5. A similar comparison is given in Fig. 7, this time with the results by Roux *et. al.* [12]: a not much logical relationship is indicated here, but a final conclusion cannot be made due to the small amount of data.

The substantial effect of construction of testing chamber on the output data was verified by testing a series of explosives on both OA and NA instruments, the samples being exposed in standard containers with air gap according to ref. [14]. The E_{ES} data determined in this way were relatively close. The tests of the same substances in the contact chamber according to ref. [24] gave substantially lower E_{ES} values (see Table 1).

3.3. Effect of granulometry on E_{ES} values

This effect was verified by using HMX and RDX. The relationship between HMX granulometry and its sensitivity to electric spark has been dealt with recently by Roux *et. al.* [2, 3]. Our results obtained by measurement on the new apparatus are given in Fig. 8. In contrast to the results obtained by Roux *et. al.* [2, 3], our dependence is roughly linear. However, we suppose that it confirms the statement by Auzanneau *et. al.* [3]: hot spots develop at the thinnest part of the solid, i.e. at intergrain points. The number of these points decreases with increasing grain size, and that increases the corresponding EES values. The grain size effect in dependences shown in Figs 1-6 could have been eliminated to a considerable extent by the fact that the measurements on the two instruments (i.e. OA and NA) were mostly carried out with the same samples of the substances studied.

3.4. Effect of artificially introduced hot nuclei on electric spark sensitivity

Stengach studied the electric spark sensitivity of lead(II) azide and found out that an addition of hard inert admixtures to this azide (up to 10% by wt.) has practically no effect on the electric spark sensitivity [35] (while the impact sensitivity is increased). We have chosen a similar strategy in the measurements on NA instrument at the conditions specified in paragraph 2.1.1. The sample measured was RDX of mean grain size equal to 30 μm with an admixture of crushed glass. The results are given in Fig. 9, and are in accordance with those given by Stengach [35], stating the absence of effect of impact component in the electric discharge used. The trend shown in Fig. 9 can be interpreted by the introduced glass particles separating the RDX grains from each other. Thereby the number of intergrain contact points of RDX grains is decreased, and hence the electric spark sensitivity of the respective mixture is decreased, too. This again stands in accordance with the above-mentioned view by Auzanneau *et. al.* [3].

3.5. Electric spark sensitivity of inorganic azides

The study of relationship between the electric spark sensitivity (OA instrument) and detonation characteristics of individual secondary explosives showed a dependence between the E_{ES} values and square of detonation velocities, D^2, in the following general form [20-22,33]:

$$D^2 = a.E_{ES} + b \qquad (3)$$

Since D^2 can be considered a representative of the heat of explosion Q, dependence (3) is one of the forms of Evans–Polanyi–Semenov equation [33]: this equation correlates the activation energy of e.g. thermolysis and the Q values. It was used in studies of chemical micro-mechanism of initiation of detonation by mechanic and thermal stimuli [33] inclusive of the electric spark initiation [21,22,33].

Using the NA instrument and the measurement conditions as sub 2.1.2, we carried out measurements with barium(II) azide and azides of heavy metals with the aim of verification whether or not there exists a similar dependence between the E_{ES} values thus obtained and the heats of explosion of the azides investigated. The result is shown in Fig. 10. It can be seen that the measurements at the conditions mentioned gave no linear dependence. In tests of primary explosives, the critical condenser value usually is $C \approx 1$ nF, and the time of intensive heating of substance then reaches 50 μs at the most. Therefore, the given time interval can be too short for the heat exchange between the discharge and the sub-surface layers of particles to take place, which can be responsible for this phenomenon. The data for copper azides lie outside the quadratic dependence preliminarily specified for the remaining azides investigated. Using this dependence, we could estimate the value for mercury(II) azide to be $Q = 2.472$ kJ.g^{-1}

4. CONCLUSION

The apparatus developed at our Department [24] for determination of electric spark sensitivity of EM is designed for tests in two different regimes:

- In the modification as sub 2.1.1, the dominating effects are those of jump (impact) increase of transformed energy of discharge. The resulting data correlate well with those obtained with our earlier instrument of this type [8-10]; however, this latter instrument was only suitable for secondary explosives. A distinct correlation of the first data mentioned also exists with the electric spark sensitivity values obtained in Los Alamos Natl. Lab. [1]. These correlations are influenced by construction differences between the individual testers and—very strongly—by molecular-structure factors
- In the modification as sub 2.1.2 (damped discharge), the sample is loaded by a longer thermal impulse; this regime is suitable for tests of primers and pyrotechnics.

The construction of spark gap and container in NA system decreases the electric energy losses. Therefore, the data obtained from NA system for secondary explosives are lower (the difference being in order of magnitude) as compared with those reported from other laboratories. Our preliminary results obtained with this instrument indicate an agreement with the idea by Auzanneau *et. al.* [3] about the mechanism of spark energy transfer into the powdered reactive solid. Hence the described new instrument [24] is relatively simple and still gives results that have physical meaning.

Acknowledgements

The authors express their gratitude to the Ministry of Industry and Commerce of the Czech Republic for support the work within the framework of research project No. FC-M2/05.

REFERENCES

[1] T. E. Larson, P. Dimas and C. E. Hannaford, "Electrostatic Sensitivity Testing of Explosives at Los Alamos", *Inst. Phys. Conf. Ser. No. 118: Section 2 (Electrostatic '91),* IOP Publishing Ltd., 1991, pp. 107-117.

[2] M. Roux, M. Auzanneau and C.Brassy, "Electric Spark and ESD Sensitivity of Reactive Solids. Part. I: Experimental Results and Reflection Factors for Sensitivity Test Optimization", *Propellants, Explos., Pyrotech. 18,* 317-324 (1993).

[3] M. Auzanneau and M. Roux, "Electric Spark and ESD Sensitivity of Reactive Solids. Part. II: Energy Transfer Mechanism And Comprehensive Study on E_{50}", *Propellants, Explos., Pyrotech. 20,* 99-101 (1995).

[4] S. Amari, F.Hosoya, Y. Mizushima and T. Toshida, "Electrostatic Spark Ignitability of Energetic Materials",[Proc.] *21st Int. Pyrotech. Seminar,* Moscow, Sept. 1995, pp. 13-31.

[5] R. Rat, M. Roux and J. P. Chaumat, "Etudes theoriques sur les phenomenes d'initiation des matieres explosibles", in M. Roux (Ed.) [Proc.], *Recueil des communications "Journees d'etudes sur la sensibilité des composants et des substances énergét. á l'electricite statique*, Aussois, Mai 1996, pp. 147-168.

[6] J. P. Chaumat, "L'initiation est elle "thermique"?" in M. Roux (Ed.) {Proc.], *Recueil des communications "Journees d'etudes sur la sensibilité des composants et des substances énergét. á l'electricite statique"*, Aussois, Mai 1996, pp. 173-179.

[7] T. Hasegawa, E. Kawashima, K. Satoh and T. Yoshida, "Correlations Between Screening Test Results of Energetic Materials", [Proc.] *22nd Int. Pyrotech. Seminar*, Fort Collins, Colorado, July 1996, pp. 195-207.

[8] Z. Kamensky, *Electric Spark Sensitivity of Polynitro Compounds,* M.Sc. Thesis, Univ. of Pardubice, June 1995.

[9] S. Zeman, Z. Kamenský, P. Valenta, J. Jakubko, "On the Electrostatic Spark Sensitivity of Some Organic Polynitro Compounds", in M. Roux (Ed.) [Proc.] *Recueil des comunications „Journees d'etudes sur la sensibilité des composants et des substances énergét. á l'electricite statique"*. Aussois, Mai 1996, pp. 197-206.

[10] S. Zeman, P. Valenta, V. Zeman and Z. Kamenský, "Electric Spark Sensitivity of Polynitro Compounds: A Comparison of some Authors' Results", *HanNeng CaiLiao 6,* 118-122 (1998).

[11] T. Matsuzawa, M. Itoh, M. Arai, S. Hatanaka, A. Miyahara and M. Tamura, "Electric Spark Sensitivity for Materials and Compositions of Fireworks", *Kayaku Gakkaishi 55,* 39-45 (1994); *Chem. Abstr. 121*, 13270e.

[12] M. Roux, A. Trevino, M. Auzanneau and C. Brassy, "Sensibilite des substances explosives: Etude de la sensibilite electro-statique d'explosifs polynitres aromatiques", [Proc.] *16th Annual Conf. ICT*, Karlsruhe 1985, pp. 3/1-3/15.

[13] F. Hosoya, K. Shiino and K. Itabashi, "Electric Spark Sensitivity of Heat Resistant Polynitroaromatic Compounds", *Propellants, Explos., Pyrotech, 16,* 119-122 (1991).

[14] S. Zeman, V. Zeman and Z. Kamenský, "Relationship between the Electric Spark Sensitivity and the NMR Chemical Shifts of some Organic Polynitro Compounds", [Proc.] *28th Int. Annual Conf. ICT*, Karlsruhe, 1997, pp. 66/1 - 66/9.

[15] D. Skinner, D. Olson and A. Block-Bolten, "Electrostatic Discharge Ignition of Energetic Materials", *Propellants, Explos., Pyrotech. 23*, 34-42 (1997).

[16] F. Hosoya., Y. Wada, K. Shiino, T. Wainai, K. Itabashi, M. Tamura and T. Yoshida, "Synthesis of Heat-Resistant Nitro Compounds and their Estimation of Explosibility", *Kogyo Kayaku 53,* 14-21 (1992).

[17] J. Kočí and S. Zeman, "Spark Sensitivity of Polynitro Compounds. Part IV. A Relation to Thermal Decomposition Patrameters", *HanNeng CaiLiao 8,* 18-26 (2000).

[18] J. Kočí, V. Zeman and S. Zeman, "Spark Sensitivity of Polynitro Compounds. Part V. A Relationship between Electric Spark and Impact Sensitivities of Energetic Materials", *HanNeng CaiLiao 9,* 60-65 (2001).

[20] V. Zeman and S. Zeman, „Relationship Between the Electric Spark Sensitivity and Detonation Velocities of Some Polynitro Compounds",[Proc.] *28th Int. Annual Conference of ICT*, Karlsrruhe, June 1997, pp. 67/1-67/10.

[21] V. Zeman, J. Kočí and S. Zeman, „Spark Sensitivity of Polynitro Compounds. Part II. A Correlation with Detonation Velocities of some Polynitro Arenes", *HanNeng CaiLiao7*, 127-132 (1999).

[22] V. Zeman, J. Kočí and S. Zeman, „Spark Sensitivity of Polynitro Compounds. Part III. A Correlation with Detonation Velocities of some Nitramines",. *HanNeng CaiLiao 7*: 172-175 (1999).

[23] "Special Scientific and Development Activity in the Field of Energetic Materials", *Project No. FC-M2/05,* Ministry of Industry and Commerce, Prague, 2000-2002, solved by University of Pardubice.

[24] J. Strnad and J. Majzlík, "Determination of Electrostatic Spark Sensitivity of Energetic Materials", [Proc.] *4th Seminar "New Trends in Research of Energetic Materials",* University of Pardubice, April 2001, pp. 303-307.

[25] F. Krejčí, J. Růžička, L. Kacetl and M. Novotný, *„Příručka pro laboratorní cvičení v technologii zvláštních výrob. Část II (A Manual of Laboratory Practice in the Technology of Special Production)"*, Text-book, SNTL Prague, 1959, pp. 101-123.

[26] B. T. Fedoroff, H. A. Aaronson, E. F. Reese, O. S. Shefield and G. O. Cliff, *"Encyclopedia of Explosives and Related Items.",* Vol. 1, PATR 270, Picatinny Arsenal, Dover, N. J., 1960.

[27] S. Zeman, M. Dimun, Š. Truchlik and V. Kabátová, "The Relationship between the Kinetic Data of the Low-Temperature Thermolysis and the Heats of Explosion of Inorganic Azides", *Thermochim. Acta 80,* 137-141 (1984).

[28] S. Zeman and M. Krupka, "Study of the Impact Reactivity of Polynitro Compounds. Part I. Impact Sensitivity as the First Reaction of Polynitro Arenes", [Proc.] *5th Seminar „New Trends in Research of Energetic Materials",* Univ. Pardubice, April 2002, pp.

[29] V. G. Matveev, V. V. Dubikhin and G. M. Nazin, „Soglasovanyi mekhanism razlozheniya aromaticheskikh nitrosoedinii v gazovoy faze (Thermolysis Mechanism of the Aromatic Nitrocompounds in the Gas Phase)", *Izv. Akad. Nauk SSSR, Ser. Khim.* 474-477 (1978).

[30] S. Bulusu, D. I. Weinstein, J. R. Autera, D. A. Anderson and R. W. Velicky, „Deuterium Kinetic Isotope Effec: An Experimental Probe for the Molecular Processes Governing the Initiation of RDX, HMX and TNT", [Proc.] *8th Int. Symp. on Detonation,* Albuquerque, NM, July, 1985.

[31] L. M. Minier and J. C. Oxley, „Thermolysis of Nitroarenes: 2,2',4,4',6,6'-Hexanitrostilbene", *Thermochim. Acta 166,* 241-249 (1990).

[32] J. Wang and H.-Y. Lang, „Mechanistic Study of Polynitro Compounds by XPS: Mechanism of the Thermal Decomposition of Polynitro Phenols", *Science in China, Ser. B 33,* 257-266 (1990).

[33] S. Zeman, "Modified Evans-Polanyi-Semenov Relationshop in the Study of Chemical Micromechanism Governing Detonation Initiation of Individual Energetic Materials", *Thermochim, Acta 384,* 137-154 (2002).

[34] S. Zeman, "Possibilities of Applying the Piloyan Method of Determination of Decomposition Activation Energies in the Differential Thermal Analysis of Polynitroaromatic Compounds and of their Derivatives, Part I. Polymethyl and Polychloro Derivatives of 1,3,5-Trinitrobenzene", *J, Thermal Anal, 17,*19-29 (1979).

[35] V. V. Stengach , „Electric Spark Sensitivity of Lead(II) Azide", *Fyz. Goreniya i Vzryva 6,* 113- 119 (1970).

FIGURES

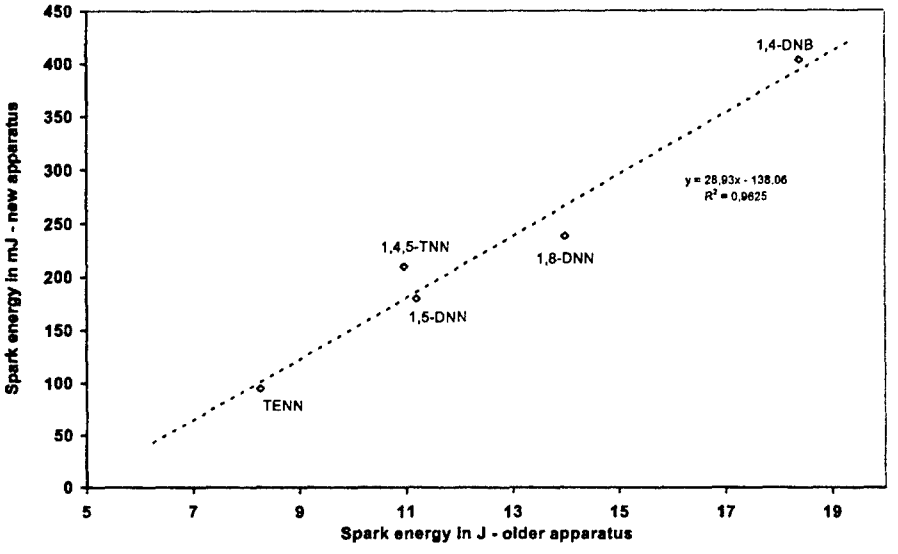


Fig 1. Relationship between the outputs from new and older apparatuses for 1,4-dinitrobenzene a nitroderivatives of naphthalene with nitrogroups in *peri*-positions.

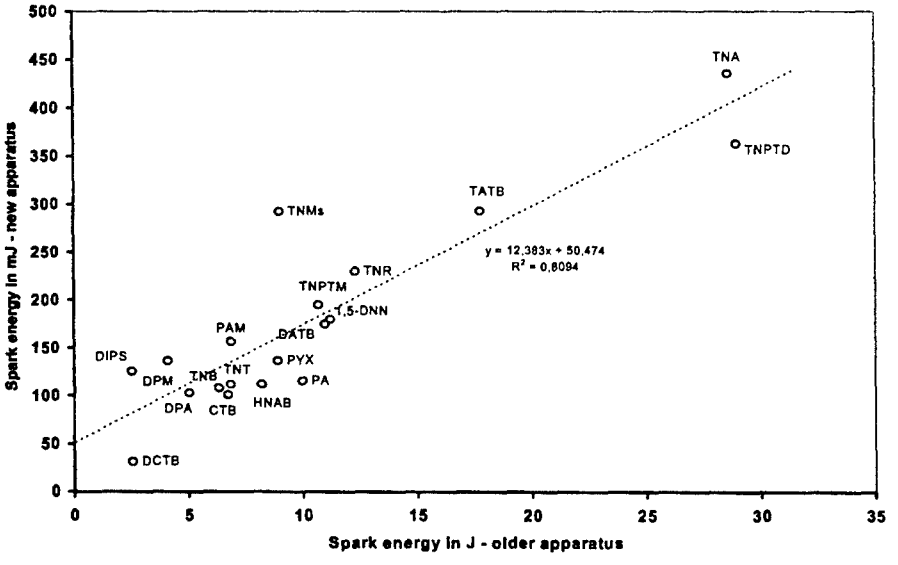


Fig 2. Relationship between the outputs from new and older apparatuses for derivatives of 1,3,5-trinitrobenzene whose primary step of thermolysis lies in homolysis via a five- or six-membered transition state or aci-form.

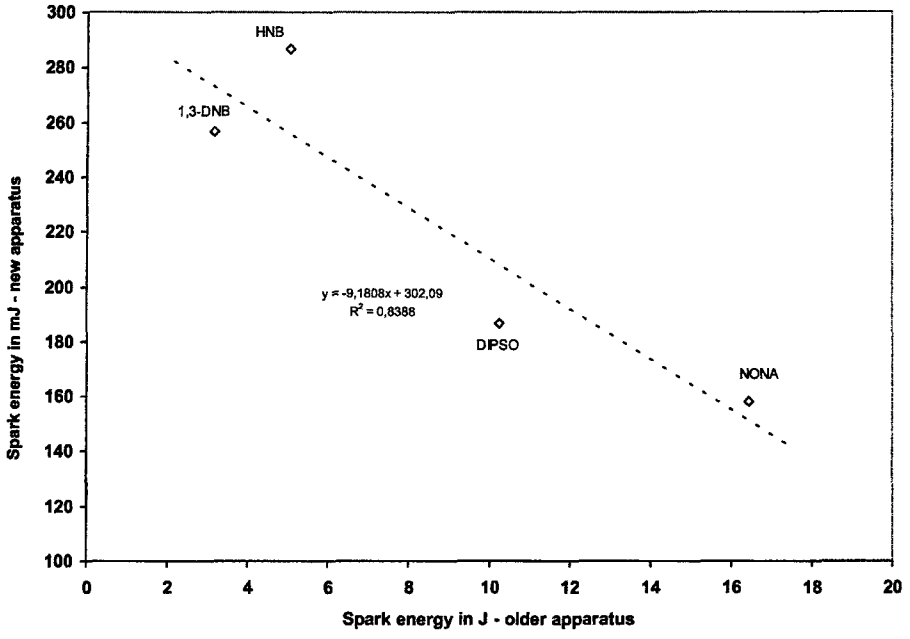


Fig 3. Relationship between the outputs from new and older apparatuses for of 1,3-dinitrobenzene and polypicryl derivatives whose primary step of thermolysis lies in homolysis of C-NO_2 bond.

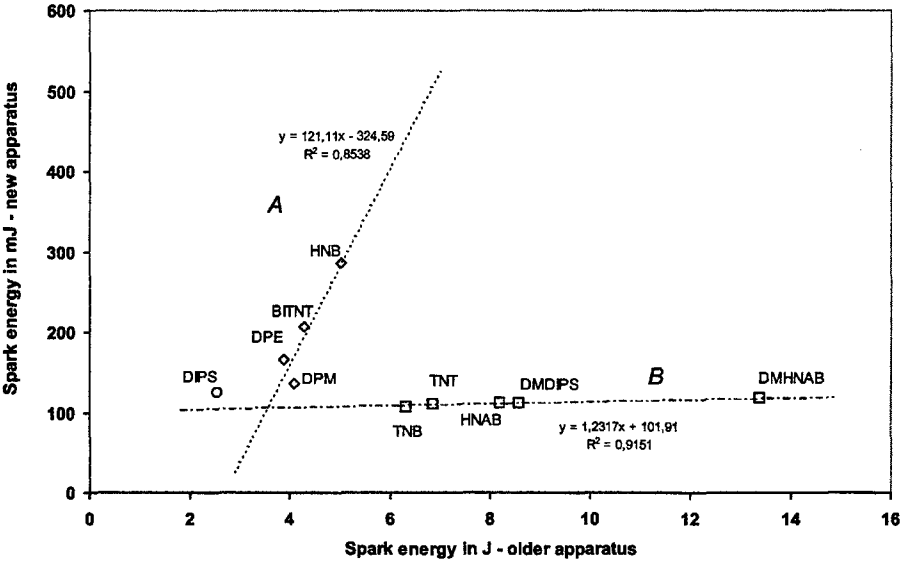


Fig 4. Relationship between the outputs from new and older apparatuses for dipicryl derivatives – an influence of –CH_2- linkage upon a shape of the relationship.

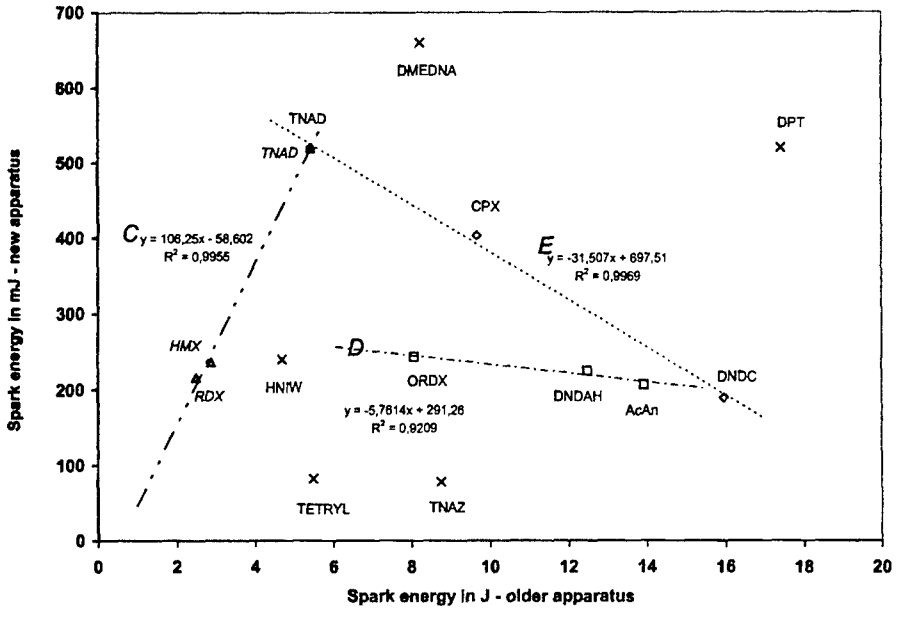


Fig 5. Relationship between the outputs from new and older apparatuses for nitramines.

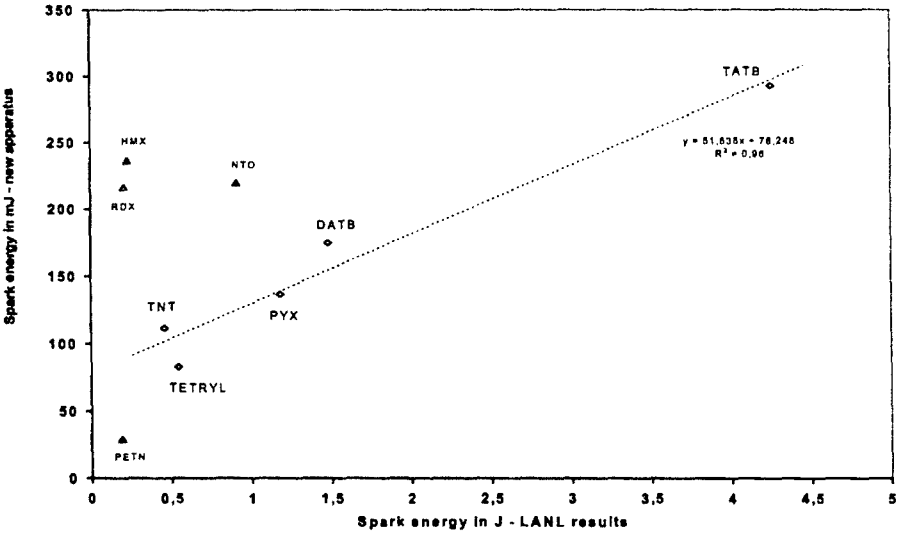


Fig 6. Relationship between results obtained by means of the new apparatus and LANL results from measurements with sample covered Pb foils 0.076 mm (taken from Ref. [1]).

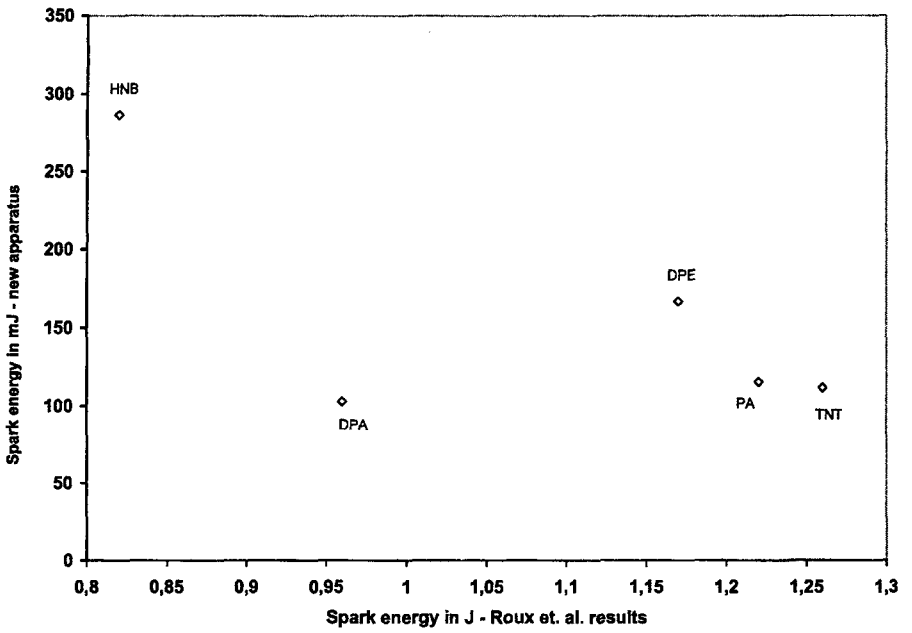


Fig 7. Mutual comparison of the outputs from the new apparatus and results of Roux et. al. [12].

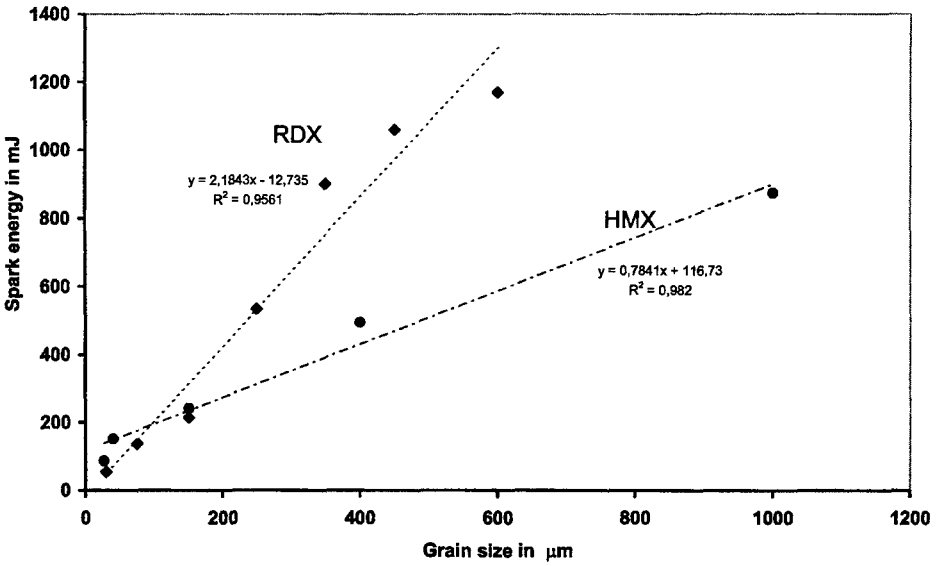


Fig 8. Relationship between the grain size and electric spark sensitivity of RDX and HMX (measured by means of the new apparatus).

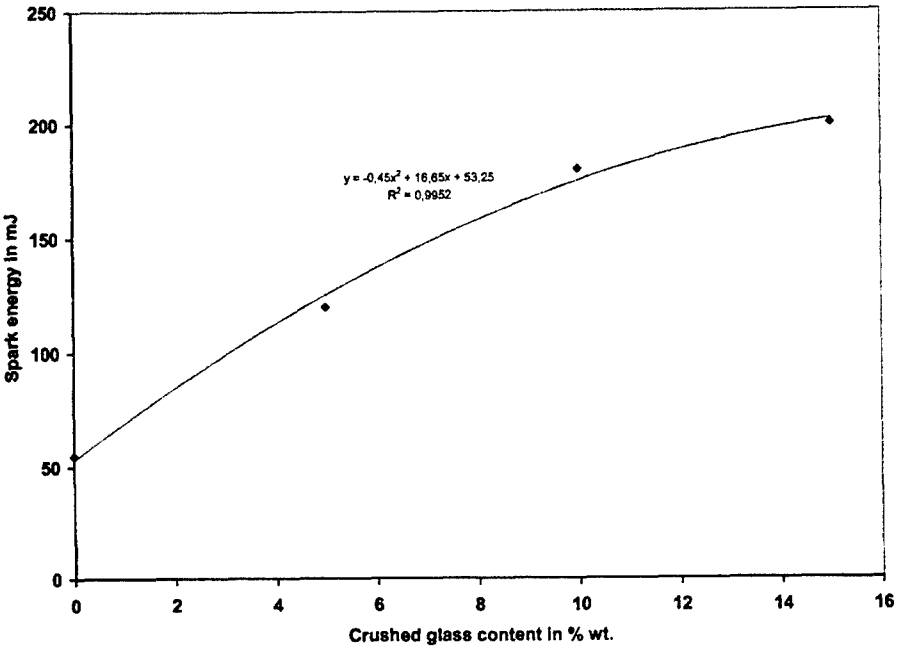


Fig 9. Electric spark sensitivity of the mixture of RDX with crushed glass in relation to the glass content.

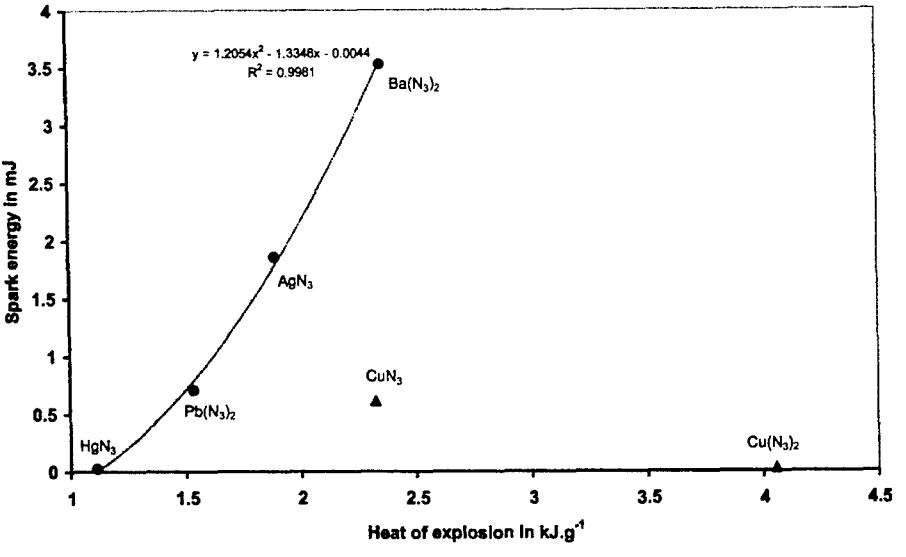


Fig 10. Relationship between the electric spark sensitivity and heat of explosion of azides

STUDY OF THERMAL STABILITY AND COMPATIBILITY OF 2,3-DIMETHYL-2,3-DINITROBUTANE (DMDNB)

Miloslav Krupka and Svatopluk Zeman

Department of Theory & Technology of Explosives, University of Pardubice, CZ-532 10 Pardubice, Czech Republic

Abstract:

The influence of temperature history on stability of 2,3-dimetyl-2,3-dinitrobutan (DMDNB) and its reactivity with high explosives such as RDX and PETN were studied by modified vacuum stability test (MVST-STABIL 16-Ex) at 80, 100 and 120 °C. Samples were analyzed using differential thermal analysis (DTA) after the temperature treatment. Impact, thermal (small scale cook-off tests) and shock sensitivity of DMDNB were further determined.

The samples of pure DMDNB did not exhibit increase in thermal stability in consequence of storage at elevated temperatures. Start of decomposition process can be observed at lower temperatures due to a melting process of mixtures of DMDNB with PETN and RDX respectively.

Keywords:
thermal stability, compatibility, DMDNB, RDX, PETN, explosive, VST, DTA, impact sensitivity, thermal sensitivity, shock sensitivity

1. INTRODUCTION

One of the often used volatile substancies, suggested by ICAO as a detection agent for plastic explosives [1] is 2,3-dimethyl-2,3-dinitrobutane (DMDNB). Some information about thermal decomposition and properties of DMDNB is compiled in literature, especialy by scientist from Canadian Explosives Res. Laboratory in Ottawa (i.e. references [2-9]). However, available literal sources spare the informations about impact and thermal sensitivity of DMDNB, or influence of thermal loading to its stability and reactivity with high explosives like RDX and PETN. The purpose of presented article is to contribute information to fill this gap employing the modernized vacuum stability test STABIL 16-Ex, differential thermal analysis (DTA) and determinate impact, thermal and shock sensitivity.

2. EXPERIMENTAL

Materials

All experiments were carried out using 2,3-dimethyl-2,3-dinitrobutane that is routinely prepared in Research Institute of Industrial Chemistry Pardubice in technical quality and used as a detection agent for plastic explosives. The RDX and PETN samples were purified by recrystallisation.

Vacuum stability test

The experiments were carried out in vacuum environment on modernized VST apparatus STABIL 16-Ex (manufactured by OZM Research), described in detail in article [10]. The amount of sample was 2 g of DMDNB, RDX and PETN, or the mixture of DMDNB and PETN or DMDNB and RDX in 1:1 mass ratio of the same overall mass. Tests were performed for 48 hours at temperatures 80, 100 and 120°C. The dried samples in evacuated glass test tubes were placed into the heating block and tempered to desired temperature. Pressure transducers continuously read off the pressure increase in the glass tubes. The results of these tests are in form of time dependence of gas volume evolved from 1 g of sample and corrected to standard conditions.

Differential thermal analysis

The analysis was performed on DTA 550-Ex apparatus (manufactured by OZM Research) especially developed for measurement of explosives [10]. Its construction allows measurement of forceful decomposition of primary explosives, propellants, pyrotechnics and high explosives. Samples with mass of 50 mg DMDNB, PETN, RDX, or mixtures DMDNB and PETN, DMDNB and RDX were tested in open glass test tubes with linear increase of temperature with 5°C.min^{-1} rate in air atmosphere. The samples before thermal loading, after 24 and 48 hours of thermal loading were examined. The thermal loading was carried out at temperatures 80, 100 and 120°C in glass test tubes with volume of 20 ml. The amount of sample was 1 ml and the test tubes were filled by inert atmosphere of N_2 before testing.

Thermal sensitivity

Procedure for determination of thermal sensitivity (Small scale Cook-off test KTTV) was developed during cooperation with ZŠV Chemko Strážské while working on project of LOVA explosives [11]. This test may be carried out in both miniaturized version (saving the expensive raw material in the development phase) as well as in accordance with standards STANAG or UN standards. The test was conducted in steel pipe with internal diameter 21 mm, length 90 mm and wall thickness 2,5 mm. The pipe was enclosed on both sides by cap nuts with 20 mm long thread. Internal volume of closed pipe was approximately 32 cm^3. The pipe was filled with 18,9 g of poured crystalline DMDNB giving density of 590 kg.m^{-3}. Gas burner was used as a source of heat for fast cook-off. A linear temperature increase of 3,3 °C.min^{-1} for slow cook-off was provided by electric oven with 50 mm internal diameter and 200 mm length.

Shock sensitivity [11]

The sample was enclosed in steel pipe of internal diameter 21 mm, length 200 mm and wall thickness 2,5 mm. Crystalline sample in amount of 59 g was rammed down to give overall density of 827 $kg.m^{-3}$. This pipe charge was initiated with 16 g of Semtex 1A. The start sensors for determination of detonation velocity were located 50 mm and 100 mm from igniting explosive. The span between start and end sensors was 100 mm.

Impact sensitivity

The impact sensitivity was determined on BAM impact machine with 10 kg drop weight in certified testing laboratory num. 1025, VVUÚ in Ostrava. The methodology as well as the used device complied with standard [12].

3. RESULT AND DISCUSION

DMDNB (VST and DTA)

DTA thermogram of a pure DMDNB (fig.1) shows small endo peak with onset temperature 41 °C (DSC 49 °C Fig. 2 [4]). This peak is reported to be a result of an intermolecular transformation, in which rotation around the central C-C bond takes place, resulting in a molecule with NO_2 groups in the trans position. Another endo peak with onset temperature at 110,3 °C (DSC 114 °C [4]) belonging to a phase transformation from triclinic to body centered cube [4] was observed. The melting begins at 205,4 °C (DSC 202 °C [7]) accompanied by evaporation and decomposition process. At the temperature 219,5 °C the exothermal process of decomposition is overshadowed with evaporation of liquid phase when open test tubes are used. The shape of DTA and DSC thermograms of pure DMDNB is identical up to 220 °C where the decomposition begins. Very sharp exothermal peaks are observed when DSC or ARC measurements are conducted in pressure cells (DSC peak at 248 °C [7]). The transformation of DMDNB from solid to liquid phase speeds up the decomposition processes. When closed cells prohibiting evaporization are used pressure builds up causing decrease of melting and decomposition temperatures (DSC 200 °C fig.2 [4], HF 150 °C [9]) compared to measurements at atmospheric pressure.

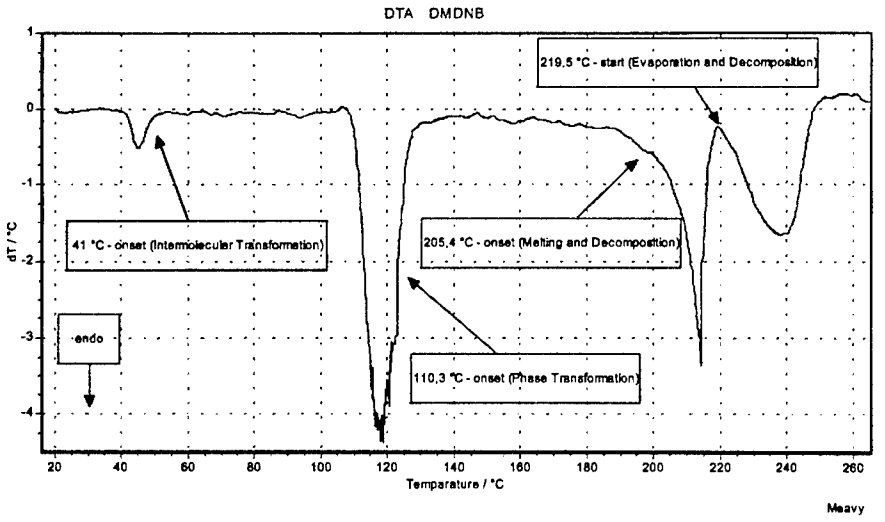


Fig 1. 1 DTA curve for DMDNB (heating rate 5 °C.min^{-1})

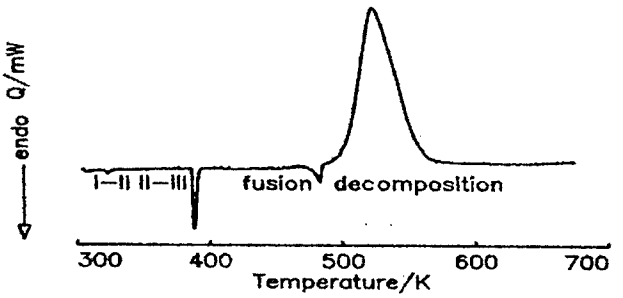


Fig 2. DSC curve for DMDNB (heating rate 5 K.min^{-1})[4]

Thermal decomposition did not occur when DMDNB sample was heated at 120 °C in vacuum for 48 hours. Following DTA measurements of thermally treated samples did not exhibit any changes compared to original ones.

RDX and PETN (VST and DTA)

Decrease of thermal stability of RDX due to a thermal treatment was not observed as predicted. The sample of PETN did not show radical increase of volume of gasseous decomposition products even at 120 °C. The DTA termograms of thermally treated and original samples were the same as those of pure PETN.

DMDNB and RDX mixtures (VST and DTA)

Two endothermal peaks that belong to DMDNB were observed. Distinct endothermal peak believed to be the melting of the RDX with onset temperature 160,1 °C was found for mixture with DMDNB. As mentioned earlier, presence of liquid phase causes decrease of the temperature at which decomposition of DMDNB begins. This is in good agreement with measured shift of start of decomposition temperature of mixture to a 178,6 °C. This temperature is 30 °C lower from pure RDX and 27 °C lower from pure DMDNB. Thermal treatment did not have effect on the shape of thermograms or the results of VST.

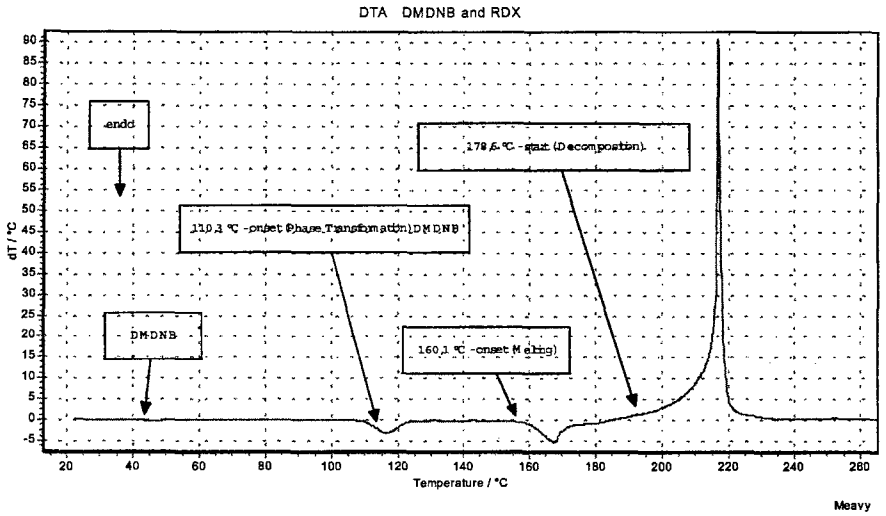


Fig 3. DTA curve for DMDNB and RDX mixtures (heating rate 5 °C.min^{-1})

DMDNB and PETN mixtures (VST and DTA)

DTA curve of sample before thermal treatment (fig.4) shows small endo peak DMDNB with onset temperature at 42 °C. Distinct endothermal change with onset temperature 110,3 °C is melting of the mixture. Further the sample slowly begins to decompose at 142,4 °C. The decomposition temperature is 16 °C lower from PETN and 63 °C lower than DMDNB. DTA curves of samples thermally treated at 80 and 100 °C do not exhibit any differences from the original mixture. Sample treated at 120 °C showed 35 °C decrease of onset temperature of endothermal peak probably due to a presence of decomposition products. Shift of the beginning of decomposition was not observed. Mixtures of DMDNB and PETN exhibit good thermal stability when stored at 80 or 100 °C. At 120 °C instability can be seen accompanied with a rapid gas development.

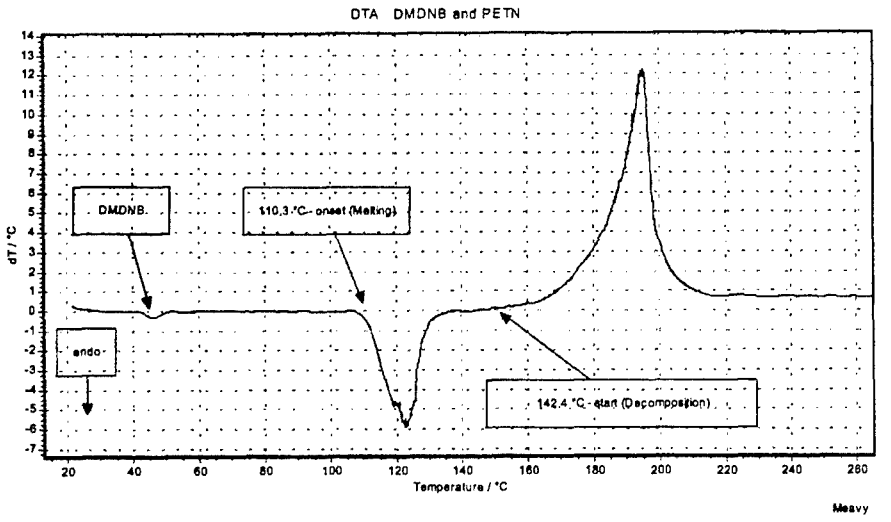


Fig 4. DTA curve for DMDNB and PETN mixtures (heating rate 5 °C.min^{-1})

DMDNB (Thermal sensitivity)

A time to case rupture for fast cook-off test was 55 sec. The cases only opened and fragments were not formed (fig.5). The opened containers did not contain any remains of sample after the test. The slow cook-off ended at 228 °C. Rupture of container occurred and 2 pieces were formed. Fragments were not formed, case just opened and one nut was cut away at the end of thread (Fig.6).



Fig 5. Small scale FCO of DMDNB

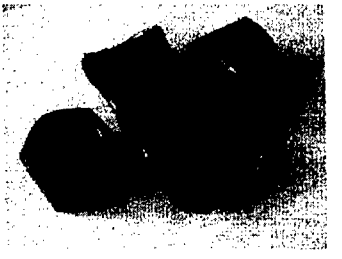


Fig. 6 Small scale SCO of DMDNB

Very high thermal stability of DMDNB can be seen from the results of thermal sensitivity tests. Similar results were obtained in past for plastic explosives. In this case is opening of the container is mainly caused by bulk expansion of the sample. The temperature 228 °C in case of SCO correlates well with thermoanalytical results.

DMDNB (shock and impact sensitivity)

Result of shock sensitivity test was tearing of case approximately to one half of its length. Detonation apparently did not propagate and some traces of unreacted sample were found on the internal surface of the pipe. The damage to the pipe was mainly caused by the initiating charge. Detonation velocity could not be determined, since the detonation extinced before reaching the sensors. The minimum impact energy needed for initiation was found higher tan 50 J [13]. Theoretical calculations using Kamlet-Jacobs equations give for densities in range from 1000 to 1100 $kg.m^{-3}$ detonation velocity over 5000 $m.s^{-1}$. In real conditions it is however expected that the density will not exceed 900 $kg.m^{-3}$ during manipulation and processing. This is a reason to believe that propagating detonation will unlikely occur under real conditions.

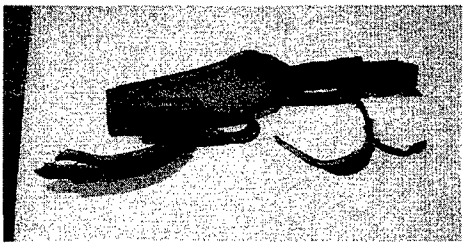


Fig 7. Crushed container after shock sensitivity test

4. CONCLUSION

The presented results and information from literature sources show that thermal treatment of DMDNB at 120 °C does not influence its stability. Starts of decomposition temperature are in the range from 150 to 230 °C depending on pressure and test conditions. The decomposition takes place even in solid phase but is significantly speeded up in presence of liquid phase. DMDNB behaves as mechanically and thermally very insensitive material compared to ordinary explosives.

DMDNB with RDX or PETN form mixtures melting at lower temperatures and as a result of that exhibit decreased thermal stability compared to pure components. The shift of the beginning of exothermal decomposition is apparent from DTA thermograms for both mixtures. As stated above decomposition begins in melt and therefore we can expect it to begin at 160,1 °C for DMDNB/RDX and at 110,3 °C for DMDNB/PETN. This assumption was approved by VST where rapid evolution of gaseous decomposition products at 120 °C was observed for mixture of DMDNB and PETN. DTA measurements were not conducted in pressure cells and therefore additional decrease of decomposition temperature can be anticipated under proper conditions (high pressure and aggravated heat dissipation)

REFERENCES

[1] Doc. 9571 ICAO Convention, International Civil Aviation Organization, Montreal, Canada,1991.

[2] D.E.G. Jones, R.A. Augsten and K.K. Feng: Detection agents for explosives, J. Thermal Anal. 44, 533-546, 1995.

[3] D.E.G. Jones, R.A. Augsten , K.P Murnaghan, Y.P Hanada and C.I. Ratclife: Characterization of DMNB, a detection agent for explosives, by thermal analysis and solid-state NMR, J. Thermal Anal. 44, 547- 561, 1995.

[4] D.E.G. Jones and R.A Augsten: Proc. Thermal studies on DMNB, a detection agent for explosives, 27th Annual. Conf. of ICT, Karlsruhe, , 15/1-14, 1996.

[5] D.E.G Jones and H.T. Feng: A preliminary study of the thermal decomposition of DMNB, an explosive detection agent, using a heat flux calorimeter, Proc. Autumn Seminar on Propellants, Explosives and Pyrotechnics, 46-51, China 1997.

[6] D.E.G Jones, P.D. Lightfoot, R.C. Fouchard and Q.S.M. Kwok: Thermal characterization of DMNB, a detection agent for explosives, Proc. 28th NATAS Annual Conf. on Thermal Anal. and Applications, Orlando, Florida, 412-417, 2000.

[7] D.E.G. Jones, R.A. Augsten and K.K. Feng: Detection agents for explosives, Proc. Int. Pyrotech. Semin 19th, 175-190, 1994.

[8] D.E.G. Jones, R.A. Augsten , K.P Murnaghan: Thermal analysis of DMDNB, an explosive detection agent, Proc. Int. Pyrotech. Semin 19th, 153-174, 1994.

[9] D.E.G Jones, P.D. Lightfoot, R.C. Fouchard and Q.S.M. Kwok: Thermal properties of DMNB, an detection agent for explosives, Proc. Int. Pyrotech. Semin 27th, 599-608, 2000.

[10] M. Krupka: Devices and equipment for testing of energetic materials, New Trends Res. Energ. Mater., Proc. Semin., 4th University of Pardubice, 222-227, 2001.

[11] M. Hanus, M. Krupka, Sv. Zeman, Trhaviny s nízkou zranitelností a metody jejich zkoušení, Výzkumná zpráva KTTV, Dec.1997.

[12] Vyhláška Českého báňského úřadu ze dne 13.8.1996, Sbírka zákonů č.246/1996

[13] Zkušební protokol č. A-00281-01-01: Stanovení citlivosti k nárazu vzorku 2,3-dimethyl-2,3-dinitrobutanu (DMDNB), VVUÚ, a. s., Ostrava-Radvanice, 14.09. 2001.

THERMODYNAMIC PROPERTIES OF BINARY SYSTEM NITROCELLULOSE+ 2,4,6 – TRINITROTOLUENE

A. Książczak[*] and T. Wolszakiewicz[**]

*Department of Chemistry, Warsaw University of Technology, Noakowskiego 3, 00 – 664 Warsaw, Poland [*]

[**]Institute of Organic Industrial Chemistry, Annopol 6 03 – 236 Warsaw, Poland [**]

Abstract:

Enthalpy of melting and mixing of system 2,4,6 – trinitrotoluene and nitrocelulose was determined by DSC method. The enthalphy of mixing of components was calculated. Maximum of mixing enthalpy in melting point is H^{M}_{max} *= -3.29 kJ mol*$^{-1}$ *for molar fraction* $x_{w2,4,6\text{-}TNT}$ *= 0.503. The Flory-Huggins interaction parameter was determined using calculated enthalpy of mixing. Temperature of glass transition (*T_g*) was determined using the sequential cycle of measurements. It was predicted by Lu-Weiss model which takes into consideration the Flory-Huggins interaction parameter The second measurement on the same sample was performed after the few day storage of samples in the room temperature. The interpretation of melting peaks leads to the conclusion that the melting process of 2,4,6-TNT undregoes in the limited space of microfibre and unlimited space, outside the fibre.*

1. INTRODUCTION

TNT is cheap, stable, low sensitivity explosive [1]. It's low melting point enables to form stable mixtures, without the possibility of degradation by partial decomposition and decreasing stability. Even the trace amounts of decomposition products can act as catalyst for further degradation. It can have the influence of term of warranty of ready-to-use product. The application of TNT as softener for nitrocellulose could raise the energy of combustion and could modify advantageously the launching parameters.

2. EXPERIMENTAL

The wooden NC produced in ZTS „Pronit" in Pionki, with nitrogen content 13.2% and average molecular mass $M_n = 54 \cdot 10^3$ [g/mol] was used for experiments. Before experiments NC was rinsed by distilled water during 24 h to remove the impurities. Exactly purified and dried NC was stored in dessicator under P_2O_5.

2,4,6-DNT was crystallised from acetone to improve purity. After crystallisation purity was determined by cryometry and it was 99.7 %, and melting enthalpy was $\Delta H_m = 99.45$ J g^{-1}

Mixtures of NC with 2,4,6-TNT was prepared by exact mixing the components and pressing them for the shape of sample pan under pressure 1 GPa during 1 minute. The sample was closed in alumina pans under reduced pressure about 1.3 kPa. Experiments were performed in using the differential scanning calorimeter by Perkin Elmer model Pyris - 1. The melting process was carried out with heating rate $\beta = 2$ K/min, and glass transition with heating rate $\beta = 20$ K/min.

3. RESULTS AND DISCUSSION

The lattice model is one of the models, allows which to for predict the properties of polymer solutions. This theory was elaborated for athermal solutions, when polymer is mixed with low molecular weight solvent. In this model, for every concentration is examined the amount of ways to place a solution in links of lattice. Flory and Huggins [2 - 4] proposed the expression for mixing enthalpy for one mol of lattice:

$$\Delta H_m = RT\phi_0\phi_1\chi \qquad (1)$$

where: R –gas constant, T – temperature, $\phi_{0,1}$ – volume fractions, χ – parameter of interaction. Parameter of interaction determines the interactions between polimer and solvent. Expression of free enthalpy of two-component polymer solution is given by equation known as a Flory – Huggins equation:

$$\Delta G_m = RT(\phi_0 \ln\phi_0 + \phi_1 m^{-1} \ln\phi_1 + \phi_0\phi_1\chi) \qquad (2)$$

Taking into consideration that measured enthalpy is connected with interaction between particles, it is possible to calculate interaction according to equation:

$$\chi = \frac{H^M}{RT\phi_1\phi_2\left(x_1 + x_2\frac{v_2}{v_1}\right)} + \chi_S \qquad (3)$$

where: ϕ_1 ϕ_2 are respectively volume fractions of component 1 and 2 respectively , V_1 and V_2 are molar volumes of component 1 and 2; R is gas constant, T temperature of measurement, x_1 and x_2 are molar fractions expressed for one polymer unit (2) analogously as for calculations H^M; χ_s is enthropy contribution, for the calculation purposes agreed that it is constant value 0.34 [2 - 4].

The enthalpy of mixing, calculated from the first measurement was placed in the Table 1. The minimum was obtained for the weight fraction $x_{wTNT} = 0.503$ and has the value $H^M = -3.97$ kJ/mol. According to analysis of parameter χ values large changes for low and high content of TNT should be attributed by relatively high experimental errors. The values with errors were eliminated from calculation of correlations between parameter χ, and weight fraction of TNT. This relation could be described by equation:

$$\chi = -2.37x_{wTNT} - 1.31 \qquad (4)$$

The correlation coefficient is r = 0.362. The relation of this function and weight fraction of TNT is presented in Figure 1.

Table 1. Enthalpy of mixing (H^M) and Flory -Huggins parameter of interaction (χ)

$x_{w2,4,6\text{-TNT}}$	H^M[kJ/mol]	χ
0.024	-0.09	-0.67
0.035	-0.26	-1.75
0.060	-0.26	-1.07
0.128	-1.04	-2.34
0.258	-1.59	-2.16
0.450	-1.29	-1.34
0.503	-3.29	-3.97
0.600	-2.25	-2.83
0.652	-1.20	-1.48
0.744	-2.14	-3.65
0.878	-2.16	-7.14
0.937	0.22	0.03
0.971	0.40	4.33

Equation 4 was used for prediction of liquid-solid equilibrium for consideration that components have full miscibility in liquid phase and no miscibility in solid phase Assuming that components have full miscibility in liquid phase and have no miscibility in solid phase forming crystalline phase, for prediction of equilibrium liquid-solid the Flory-Huggins theory of solutions and parameter of interaction estimated by mixing enthalpy were used. The solubility curve of nitrocelulose was estimated according to equation [5]:

$$\Delta T_{m2} = -\frac{RTT_{m2}}{\Delta H_{f2}}[\ln\Phi_2 + (1-\Phi_2)(1-m) + \chi m(1-\Phi_2)^2] \tag{5}$$

$$\Delta T_{m2} = T_{m2} - T \tag{6}$$

where: T is temperature of liquid-solid equilibrium, T_{m2} is the temperature of melting of component 2, m is volume ratio of components, ΔH_{m2} is a melting enthalpy of component 2.

Figure 1 presents the solubility curves of components, plotted by thin lines. The calculated eutectic temperature was T_e = 335.9 K for weight fraction x_{wTNT} = 0.550. This result led to the conclusion that examined mixtures, when stored in the beginning temperature should be in solid phases as pure components. Glass transition temperature was estimated by Lu–Weiss model using interaction parameter χ. The results of calculation were plotted in Fig 1 as thick line. The results of calculations of components solubility and glass transition temperature are collected in Table 2. The curve of glass transition temperature intersects the curve of TNT solubility at the temperature of T_{gm1} = 323.4 K for weight fraction x_{wTNT} = 0.450. This point lays beneath the NC solubility curve and it is impossible for experimental practice due to NC properties. It is not possible to obtain the state of overcooled liquid. The curve T_{gm} intersects the NC solubility curve in temperature T_{gm2} = 282.1 K and weight fraction x_{wTNT} = 0.650.

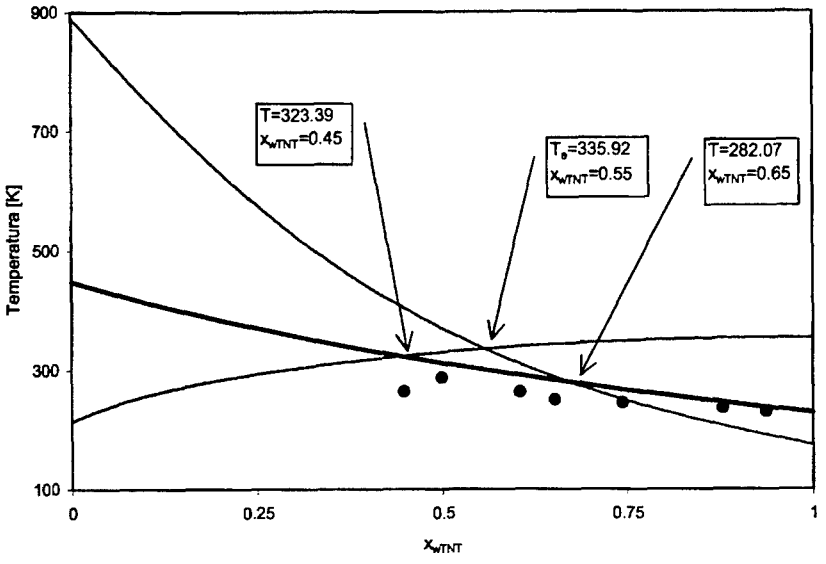


Fig 1. The liquid-solid equilibrium (thin lines) and temperatures of glass transition (thick line) calculated from Flory –Huggins theory and Lu –Weiss model.

Table 2. The glass transition temperatures (T_{gm}) and jump of heat capacity (ΔC_p) established in second heating.

x_{wTNT}	T_{gm} [K]	ΔC_p
0.449	264.2	0.022
0.500	287.5	0.014
0.605	263.3	0.239
0.652	251.1	0.265
0.744	245.5	0.300
0.878	237.3	0.428
0.937	230.6	0.003
1	228.2	0.021

During several days of storage, mixtures underwent the complete crystallisation of liquid phase and the jump of baseline, typical for glass state was not observed. Only in the case of second heating in measuring cycle this type of jump was observed. In this case the pure liquid appeared as a result of melting of TNT crystals, desolving NC and forming liquid solution, kept in temperature 383 K during 1 minute and subsequently cooling with the of rate β = 20°C/min. to 173 K, where again was kept 1 min. and with the same rate was heated. The short periods between measurements (about 11 min) allowed for converting liquid phase into solid. The full vitrification of liquid phase was observed in the range of 0.878 - 0.600 weight fraction of TNT. In this cases the exothermal peaks of crystallisation in the cooling curve were not observed.

Typical shape of curves DSC: cooling and second heating was presented in Fig.2 for mixture $x_{wTNT} = 0.744$ for TNT. For the weight fractions 0.449, 0.500 i 0.937 only partially vitrification was observed, because the small change of heat capacity was accompanied. It was not observed the glass transition for extreme weight of fraction as an exothermic peak of cooling curve.

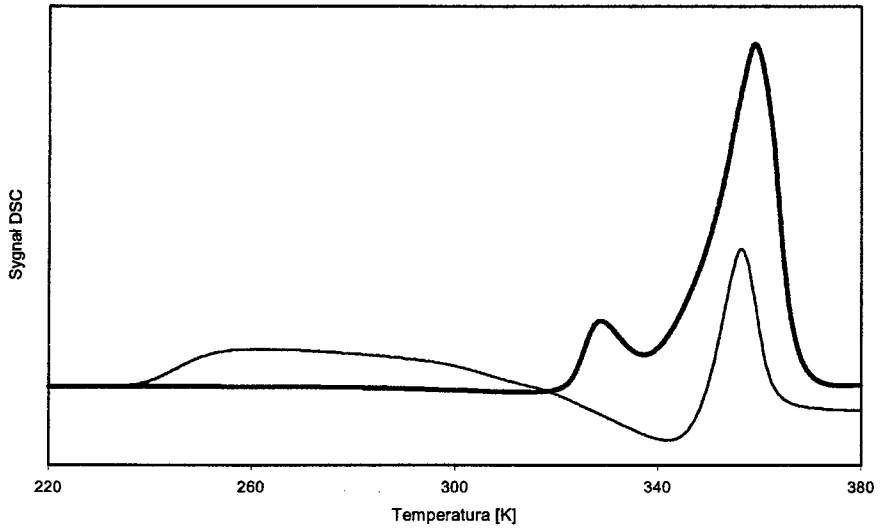


Fig 2. Typical curves DSC of first heating (thick line) and second (thin line) for mixture $x_{wTNT} = 0.744$ for the same measurement.

Fig. 3 presents the augmented part of the DSC curve before main melting peak of TNT for first heating for $x_{wTNT} = 0.971$ after 212 days. The flat peak before exothermal peak is connected with β relaxation [6] and superimposes the beginning of melting process connected with the main peak. The crystallisation process in the unlimited space, connected with gel degradation also superimposes on mentioned effects. The gel structure in this case is exceptionally stable and do not undergo degradation during long storage. In the second heating of the same cycle, the β relaxation is not observed, which it is normal and it means the lack of reconstruction of primal structure.

For the better comparison of results, Fig. 4 presents the augmented fragments of curves in first (thick line) and second (thin line) heating for the same measurement cycle. To compare both curves it is possible to see that articulative differences in curves begin in temperature 253 K and increases with growth of temperature. The deflection of DSC curve in the first heating towards endothermal effects shows for interaction between NC and TNT, and crystallisation of TNT as an effect of degradation structures formed previously.

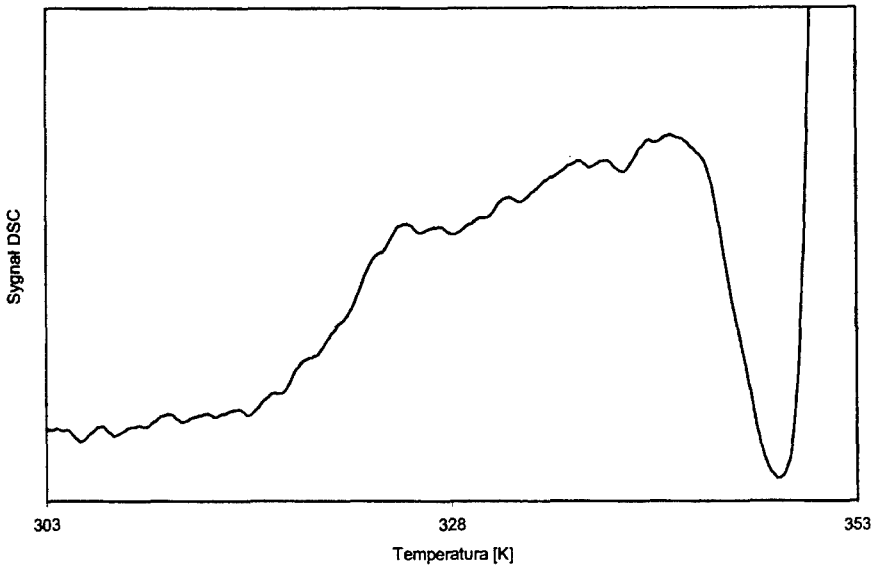


Fig 3. The augmented part of the DSC curve before the TNT main melting peak TNT for the first heating for mixtures $x_{wTNT} = 0.971$after 212 days.

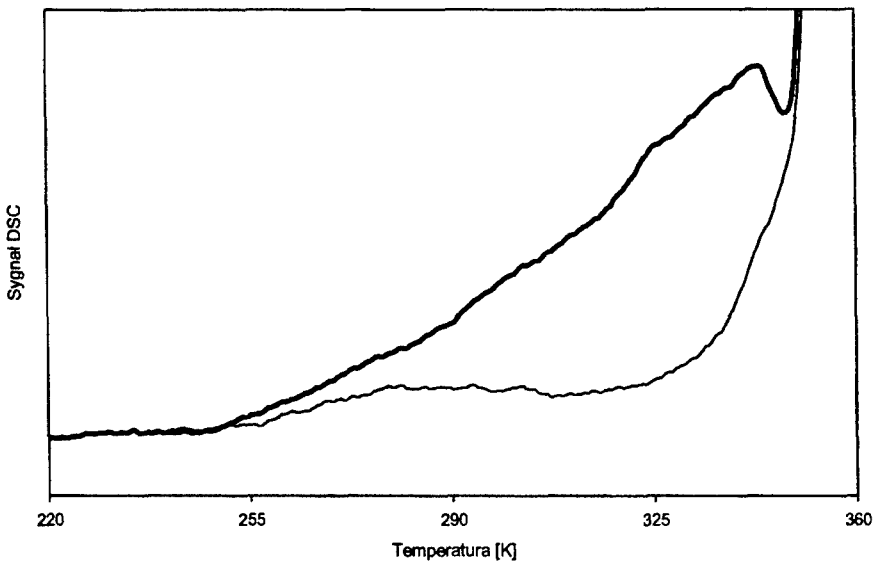


Fig 4. Fig.4. The augmented parts of DSC curves of mixtures $x_{wTNT} = 0.971$ after 212 days. First (thick line) and second measurement (thin line) for the same measurement cycle.

For the mixtures x_{wTNT} = 0.937 after 191 days the exothermal effects in the first and second process of heating for the same cycle of measurement were obtained. Thermal effects for this process are in agreement, so for this composition reconstruction of output structure takes place. The augmented parts of curves in the first (thick line) and second (thin line) heating of the same measurement cycle for the same mixtures are presented in Fig. 5. The same sample was examined after 587 days of storage from the previous measurement. The exothermal effects were iteratively lover. In the first measurement was ΔH_{kr} = -0.42 J/g, and in a second ΔH_{kr} = -0.84 J/g. The change of crystallisation enthalpy in this measurement cycle could be attributed of superimposing endothermal effect of β relaxation present only in the first heating on the exothermal crystallisation effect. β relaxation moves towards the higher temperature range with increasing time of storage.

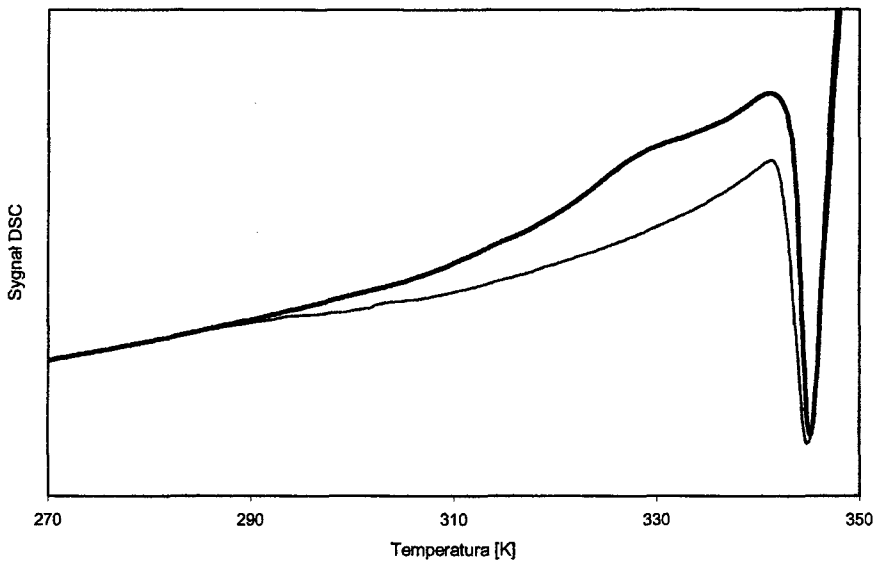


Fig 5. The augmented parts of DSC curves in the first (thick line) and second (thin line) heating the same measurement cycle for mixtures x_{wTNT} = 0.937 after 191 days.

It should be adopted that the thermal effect in a second measurement is weighed lower uncertainty. Thermal effect of crystallisation was diminished after 587 days 3.2 times which means that gel structures are unstable and durnig the sufficiently long time they can disappear.

For the mixtures containing x_{wTNT} = 0.878 after 212 days of storage, DSC curves had no exothermal peaks, it indicates that structures appearing in mixtures described above disappear. The DSC curves for first (thick line) and second (thin line) heating in the same measurement cycle are presented in Fig. 6. In the first process of heating peak β relaxation and melting peak appears and in the second heating of the same cycle glass transition is observed and subsequently the peak of cold crystallisation and melting peak. It is suprising that for mixtures containing higher amount of TNT the effect of full glass transition was not

obtained. It is supposed that growth of surfaces results in TNT particles and promotes the cooling of liquid phase and vitrification. It could be observed in second process of heating in the beginning of melting peak small jump which could be attributed to melting in limited space. The DSC obtained from the same sample performed after 588 days are in agreement general in main transitions. In this case, the disputed jump on the curves was present in the first and second heating.

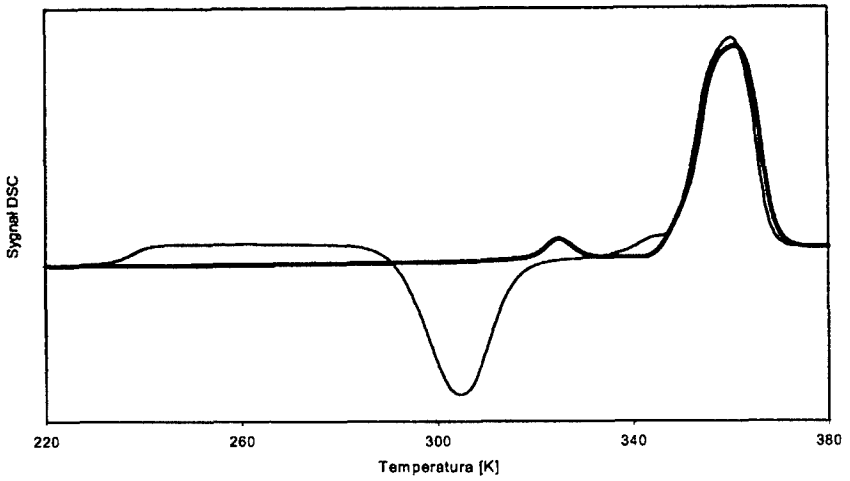


Fig 6. The DSC curve of first (thick line) and second (thin line) heating in the same measurement cycle for mixtures $x_{wTNT} = 0.878$ after 212 days of storage.

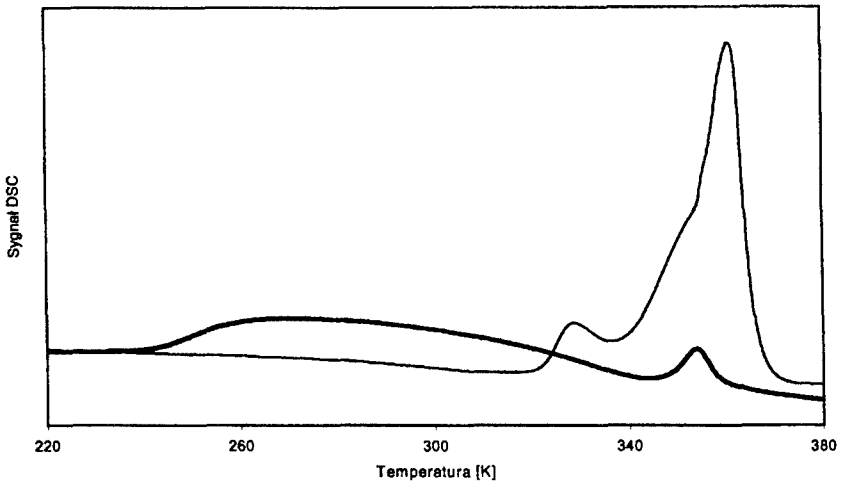


Fig 7. The DSC curves of mixtures $x_{wTNT} = 0.652$ after 555 days of storage in the beginning temperature. First measurement (thin line) and second (thick line).

In the mixture containing $x_{wTNT} = 0.503$ (Fig. 8), the process of glass transition in second heating was not observed which means that TNT particles are stable bonded to NC chains and after sufficiently long time, of storage the disclaiming from polymer matrix into large spaces appears, because the position of peak maxima is in agreement with maximum of melting peak of pure substance. It is no always observed in the DSC curve in the first heating and period of storage of 187 days not contain the peak of β relaxation. But in the next measurement performed after 588 days, same peak of β relaxation was good formed.

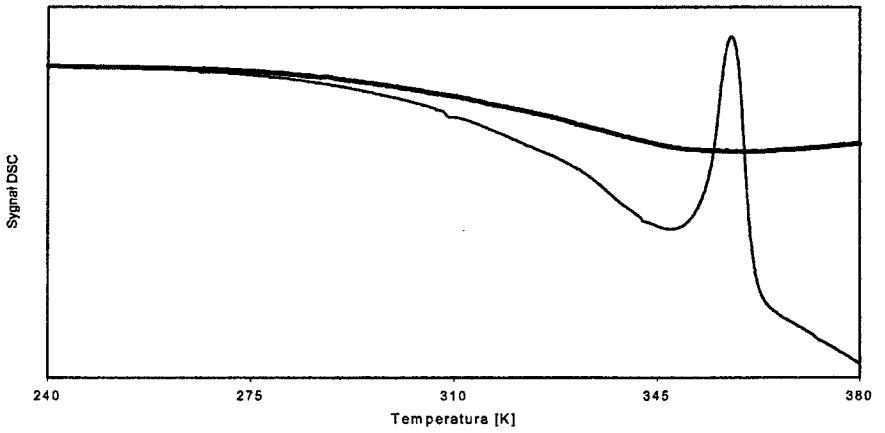


Fig 8. DSC curves of mixtures $x_{wTNT} = 0.503$ after 187 days of storage in the beginning temperature. First measurement (thin line) and second (thick line).

The DSC curve in Fig.9 shows plot for the composition of lowest weight fraction $x_{wTNT} = 0.024$, after 218 days from the first measurement. Thick line presents the curve of first heating and thin line curve of second heating. Both curves are covered each other in the area of experimental error from 173 K to 303 K. The growing effect can of melting in the limited space and melting peak in unlimited space. The curve of first heating is laying over the curve of second heating and it means that heat capacity of sample in first heating is higher than in second heating. It should be underlined that in, second process of heating all particles are bonded to NC chains.

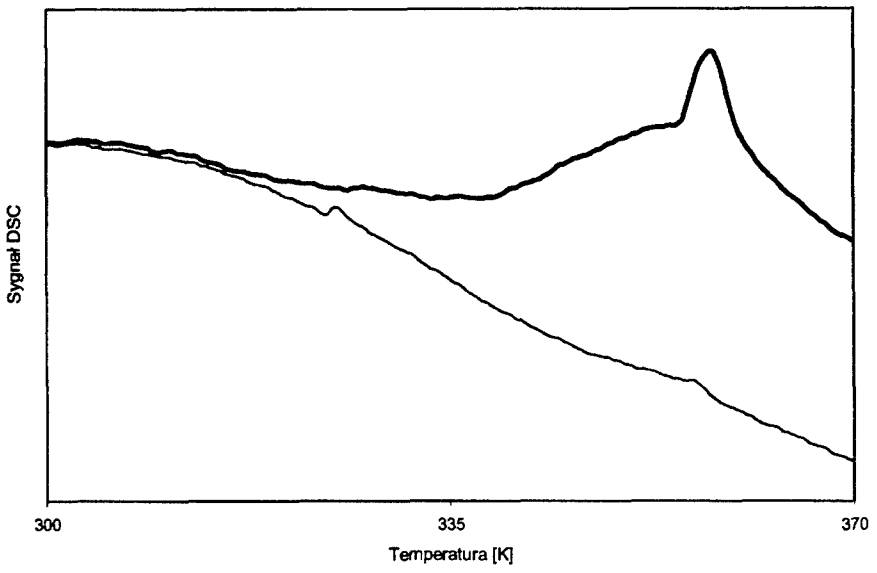


Fig 9. The DSC curves for mixtures x_{wTNT}=0.024 after 218 days from the first measurement. The curve after first heating (thick line) and curve after second heating (thin line)

4. CONCLUSION

The negative values of mixing enthalpy in whole concentration range led to the conclusion about strong interactions between NC chains and 2,4,6-TNT particles. The maximum value of enthalpy of mixing is H^M_{max} = -3.29 kJ mol^{-1} for molar fraction $x_{w2,4,6\text{-}TNT}$ = 0.503. In previous work [7] using the same procedure the enthalpy of mixing for NC + s–diethylodiphenylourea system (C1)> The maximum enthalpy of mixing was H^M_{max} = -4.59 kJ mol^{-1} for x_{C1} = 0.555. This results proves that C1 is the better solvent for NC.

REFERENCES

[1] R. S. Farinato, P. L. Dubin, Colloid-Polimer Interactions, From Fundamentals to Practice, A Wiley-Interscience Publikation, str. 51 –56, (1999)

[2] P. J. Flory; Principles of Polymer Chemistry, Cornel University Press, N.Y., (1966)

[3] P. J. Flory, Principles of polymer chemistry. Ithaca, N.Y: Cornel University Press, (1953)

[4] M. L. Huggins., J. Am. Chem. Soc. 64, p.1712, (1942)

[5] A. Turi, Thermal characterization of polymeric materials, Second Edition, str.420, (1997)

[6] F. S. Baker, M. Jones, T. J. Lewis, G. Privett, D. J. Crofton, R. A. Pethrick; Polymer, Vol. 25, 815 (1984)

[7] Książczak A., Książczak T., Journal of Thermal Analysis, 54, 323 (1998)

ANALYSIS OF POSSIBILITY OF WASTE ENERGETIC MATERIAL APPLICATION IN MINING BLASTING AGENTS

Andrzej Maranda*, Katarzyna Lipińska and Marek Lipiński****

*Military University of Technology, 2 Kaliskiego str. 00-908 Warsaw, Poland

**Institute of Industrial Organic Chemistry 6 Annopol str. 03-236 Warsaw Poland

Abstract:

Some problems connected with the application of waste energetic materials (smokeless powder propellants, composite propellants, high explosives) as raw materials for the production of various products useful in civilian applications was presented. The mining industry is a basic consumer of commercial explosives and one of the ways of waste energetic material recycling is to use them as ingredients of mining blasting agents. Some examples of commercial products were showed.

1. INTRODUCTION

Thousands of kilograms of waste energetic materials such as powders, rocket motor propellants and explosives are generated every year. Usually these materials are desensitized and than disposed of through incineration, open burning or open detonation. Disposal through open burning or open detonation is less attractive today due to environmental cost and safety concerns. Some of energetic material disposal is by landfills but it leaves an unwanted legacy for future generations with the risk that chlorine and other constituents may leach into the surrounding soil and pollute groundwater. But none of above-mentioned methods takes advantage of the energy content of these materials. They can be recycled. Many research workers examined the use of them as raw materials for the production of various products useful in civilian and military applications. One of the ways of waste energetic materials recycling is to use them as ingredients of mining blasting agents, as the mining industry is a basic consumer of commercial explosives.

2. RESEARCH WORK PROCEDURE

Commercial explosives must have an oxygen balance close to zero in order to reduce to the minimum the amount of toxic gases, particularly carbon monoxide, and nitrous gases, which are evolved in the fumes. Military explosives have high negative oxygen balance. Besides military explosives contain components being more sensible than commercial explosives. That is why the direct use of waste energetic explosives for blasting works in the industry cannot be recommended mainly because of safety problems.

If waste military explosives and propellants are to be used in blasting agents some initial work have to be done. Initial work is done using a theoretical performance code to determine the effect of energetic material type and percentage on key explosive parameters: oxygen

balance, detonation velocity and pressure, major detonation products and initial explosive density. Afterwards some compatibility tests such as differential scanning calorimetery, differential thermal analysis, accelerated rate calorimetery, are conducted to assure the various ingredients used in blasting agents and these energetic materials will be stable when mix together. Next safety properties are established. Series of small mixes are made in order to determine basic safety properties. The tests include sensibility to impact and friction, responses to electrostatic discharge and determining an auto-ignition temperature. The bigger mixes are made to determine such processing properties as rheology and working life and performance properties – detonation velocity, critical diameter and minimum booster. The mixtures also need to demonstrate good stability on aging during accelerated aging tests.

Recycling of waste energetic materials in mining blasting agents

Smokeless powder propellants

Smokeless powder propellants have been used as sensitizing ingredients in commercial explosive formulations for many years. One of such explosives was Permonex BP, a mixture of smokeless small-grained powder and ammonium nitrate for compensation of oxygen balance.

Smokeless powder propellants can be used as sensitizer ingredients in watergel slurry explosives or water-in-oil emulsion explosives. They usually contain 25 – 35% either single base or double base smokeless powder propellants. Because of the mixing and pumping requirements of their production, the small particles are needed. It was also found that smaller propellant grains or particles usually produced a significantly more sensitive blasting agent, with a smaller critical diameter.

As examples of commercial explosives containing smokeless propellants some products can be given [1]. One of them is Gianite™ by ICI Explosives, a glass bubble sensitized water-in-oil emulsion packaged explosive, which contains about 35% single base smokeless powder propellant as an energetic ingredient. The emulsion-based product usually contains whole propellant grains. The other one is Dynogel™ by DynoNobel – smokeless powder sensitized watergel slurry packaged blasting agent. A water-wet granular double base by-product propellant resulted as a waste from Olin's ball powder sporting ammunition production was used as a sensitizer in ammonium nitrate/sodium nitrate based watergel slurry matrix. This explosive is promoted as high density, high velocity, high shock energy and "deadpress" resistant blasting agent, suitable for use in extreme blasting conditions. The last example, Slurran 430 developed for Slurry Explosive Corporation by Universal Tech Corporation, can be descriped as a smokeless powder sensitized watergel slurry packaged blasting agent. This explosive differs from the above-mentioned packaged explosives in that it contains a significantly higher percentage of propellant – 60% whole grain triple base smokeless powder propellant. This blasting agent contains smokeless powder propellant as its only sensitizer and that is why it is promoted as "deadpress" resistant explosive.

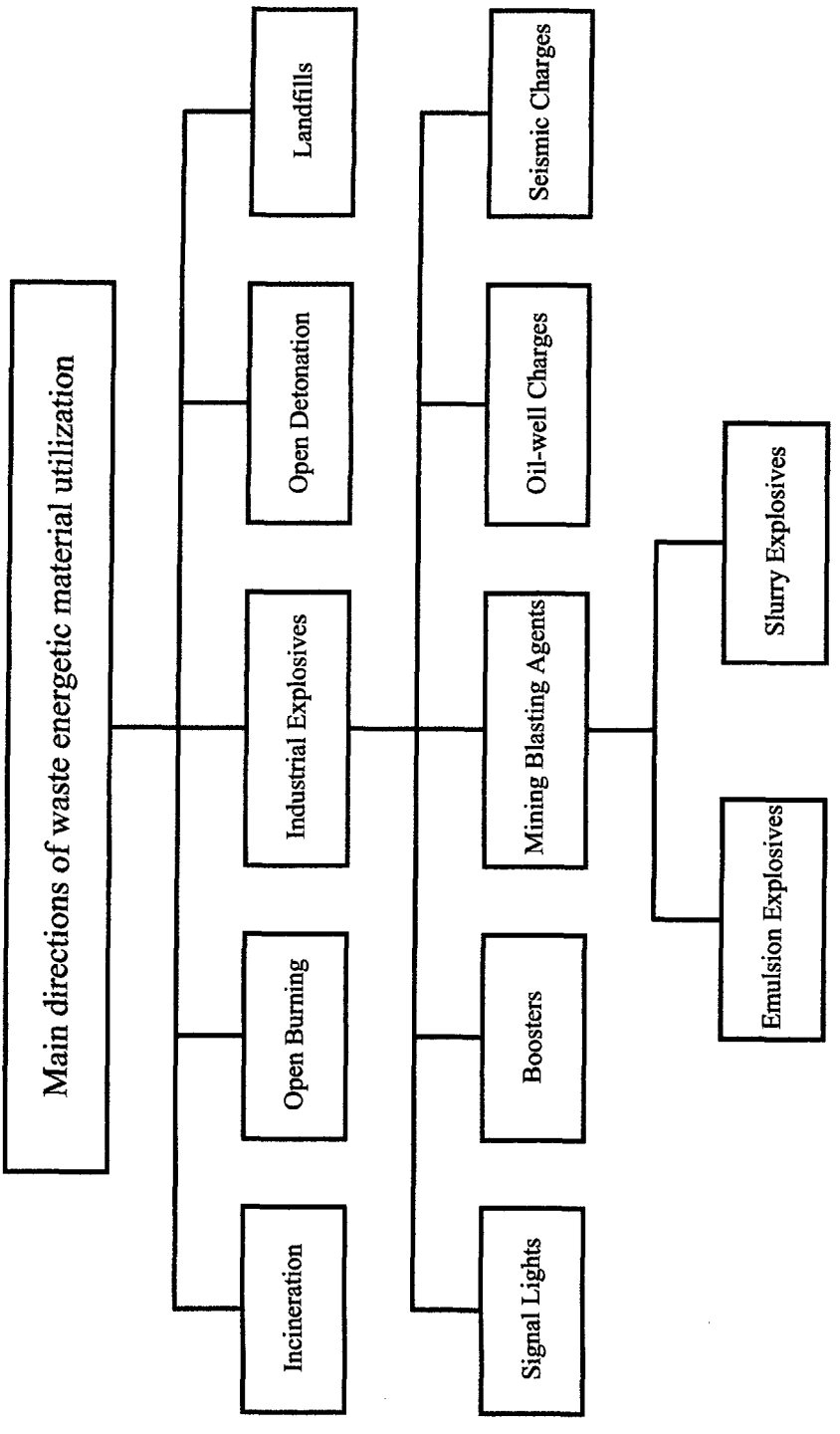


Fig. 1. Scheme of energetic material utilization

Composite propellants

The more complicated problem is the composite propellant utilization. The common ingredient in solid rocket propellants is ammonium perchlorate and its amount is up to 70%. This may cause some environmental problems if it is incorporated into a commercial explosive due to that hydrogen chloride is one of the products of ammonium perchlorate decomposition. Including a stoichiometric amount of sodium or calcium nitrate in the mixture can solve this problem and then virtually no hydrogen chloride is formed. Propellants also typically contain burn rate modifiers, which may be lead-based or contain other heavy metals. Although the concentrations of such components are small, consideration should be given to their potential environmental impact.

The use of composite propellants as energy enhancing additives in commercial watergel and emulsion explosives was investigated, for example packaged commercial explosive product containing shredded composite propellant was developed [2,3]. The most promising formulations were based on hexamine/ammonium nitrate watergel slurry matrix.

The conversion of propellants and pyrotechnics in conjunction with CHO compounds such as glycerin, lactose and starch to develop insensitive heterogeneous explosive compositions for blast applications was proposed [4]. These explosive compositions are capable of detonation directly if sufficiently small pyrotechnics particle sizes are used, bringing the oxidizer and fuel into closer contact.

Explosive components

Explosive components such as TNT or RDX added to commercial explosives increase the sensitivity of the explosive and the total energy of the composition. Such compositions can provide much more effective blast performance for specific applications.

Explosive components can sensitize slurry and emulsion explosives. The packaged mining commercial emulsion explosives sensitized by high explosives can be used for blasting in mines with severe conditions and as boosters and borehole charges of 60 – 90 mm diameter in blasting operations on the surface. [5] These commercial explosives contain 15 – 30% high explosives.

Size reduction

One of the most important problems of waste energetic materials, especially propellants, incorporating is their downsizing into useful dimensions. The special size reduction equipment is needed. Size reduction can be achieved by mills, grinders or shredders. For safety reasons this process should be conducted under a liquid and should be conducted remotely.

An interesting and environmentally friendly processing method is crocycling technology [6]. In the cryocycling process propellants are repeatedly subjected to cycles of rapid freezing in liquid nitrogen followed by rewarming to near ambient temperatures. After three to four cryocycles most bulk propellants are reduced to particles in the size range 5 – 20 mm (suitable for application in commercial explosives) without any cutting or generating a secondary waste stream.

3. CONCLUSIONS

The reuse of demilitarized explosives in commercial explosive compositions is the good solution of waste energetic material disposal problem. Commercial blasting agents on the base of these explosives, powders and propellants could not be less technological and environmental safety in comparison with wide used commercial explosives. It is necessary to stress that technological processes should be adapted if possible to existing productions in order to reduce economic problems.

REFERENCES

[1] Eck G., Machacek O., Tallent K. "The Use of Surplus Smokeless Powder Propellants As Ingredients In Commercial Explosive Products in the United States" p. 119, in Application of Demilitarized Gun and Rocket Propellants in Commercial Explosives, Kluwer Academic Publishers, Dordrecht 2000

[2] US Patent 5,536,897 (1996)

[3] US Patent 5,612,507 (1997)

[4] Tulis A. J. "Powerful Insensitive Hybrid Explosives using Inorganic Propellants/Pyrotechnics in Conjunction with Organic CHO Compounds for Tailorable Blast Applications" p. 215, in Application of Demilitarized Gun and Rocket Propellants in Commercial Explosives, Kluwer Academic Publishers, Dordrecht 2000

[5] Rabotinsky N. I., Sosnin V. A., Vorozhtsov A. B. "The Application of Reclaimed Explosives in Commercial Emulsion Explosives" p. 193, in Application of Demilitarized Gun and Rocket Propellants in Commercial Explosives, Kluwer Academic Publishers, Dordrecht 2000

[6] Lipkin J., Baxter L. L., Whinnery L. R., Griffiths S., Nilson R., Kaminska J., Mower G., Munson W., McNair J., Elliott J. "Application of Cryocycling to Rocket Motor Propellant Size Reduction" p. 35, in Application of Demilitarized Gun and Rocket Propellants in Commercial Explosives, Kluwer Academic Publishers, Dordrecht 2000

MECHANICAL DESTRUCTION OF ENERGETIC POLYMERIC COMPOSITES (EPC)

V.A. Malchevsky, N.A. Zarytovskaya and T.A. Mikhailikova

D.I. Mendeleev Russian Chemical Technological University,
Miusskaya pl. 9, Moscow, 125047

Abstract:

The research relates to the area that deals with one of the most important issues of the physical-chemical mechanics of polymeric materials - the problem of "kinetic" and "critical" alternatives for the evaluation of mechanical destruction of polymeric composites. It sets a practical goal of developing a method for the calculation of kinetic parameters of the mechanical destruction process on the grounds of tests with the use of standard tearing machines at constant straining velocities (ε = const.), i.e. trials based on the understandings about mechanical destruction as a critical phenomenon. The research resulted in a number of interrelated dependences that facilitated calculations of the EPC destruction kinetics on the basis the strength- temperature function $\sigma=f(T)$ and the strength-loading velocity (V_σ) or strength-tension (ε) dependence. The results of the analysis of EPC strength characteristics attained on the basis of tests at uniaxial stretching and σ=const or ε=const show that they do not contradict and are complementary.

1. INTRODUCTION

The evaluation of damaging of energetic polymeric composites in stress at long-term storage, transportation and propulsion system operation bases on the research of their destruction and deformation kinetics [1,2]. Studies on temperature-force dependences of EPC strength are conducted under the conditions of static uniaxial tension or dynamic loads at **σ-const** [3.4]. When necessary, influence of the following accompanying factors is taken into account: humidity, various kinds of radiation, aggressive media, etc

This work focuses on opportunities to calculate the EPC destruction kinetics from temperature dependences of their strength determined with the use of standard tearing machines at constant velocity of deformation **(ε-const)**. This problem is a significant component of general physical mechanics of energetic composites and material studies [6-10].

2. THEORY

General calculation principles were developed on the grounds of a few different approaches.

1 If we write the generic equation for the kinetics of solids destruction as

$$\sigma=U_0/\gamma - 2{,}3RT(\lg\tau-\lg\tau_0)/\gamma, \qquad (1)$$

then Equation {1} will express a straight line, provided **τ-const** and well-known kinetic parameters of mechanical destruction U_o, γ, $\lg\tau_o$ do not vary in the studied temperature range. At $\sigma = 0$, the equation transforms to Equation (2) for calculating initial energy of process actuation:

$$U_0=2{,}3RT_0\Delta\lg\tau, \qquad (2)$$

where $\Delta\lg\tau=\lg\tau-\lg\tau_0$, $\lg\tau\approx\lg\tau_3$ - durability equivalent to the selected test mode, and T_0 - temperature that corresponds to linear extrapolation of σ (T) to $\sigma=0$. If we assume in (1) that $T=0$ it will be possible to attain an expression for determining a structure-sensitivity factor γ (3):

$$\gamma=U_0/\sigma_0, \qquad (3)$$

where σ_0 is the extrapolation value of strength when $T=0$. To solve Equations (2) and (3) we need to know a value of equivalent durability (τ_e) that would conform with destruction conditions at **ε-const** when the load on the specimen is growing in the ongoing experiment. One of the calculation alternatives for τ may base on the use of Equation (4), i.e. on the principle of damage summing. In the case of a linearly increasing load, the specimen break occurs when stretching is σ, to which durability τ corresponds that is $\alpha\sigma$-fold less than the loading period [6]. Then

$$\tau_3=t/(\alpha\sigma), \qquad (4)$$

where **t** - time of the specimen loading until breaking, α - coefficient depending on the parameters of strength time dependence (5) [11]:

$$\lg\tau=\lg A - 0{,}43\alpha\sigma. \qquad (5)$$

The value **lgA** can be obtained from Equation (1):

$$\lg A=\lg\tau_0+0{,}43U_0/RT. \qquad (6)$$

While solving jointly (5), (6), (2) and (4), it becomes clear that the equation for calculating τ_3 will be expressed as follows: $\tau_3 \lg(\tau_e/\tau_0) = 0{,}43Tt/(T_0-T)$.

When τ varies over 0,001-1000 sec, i.e. by 6 orders of magnitude, the multiplier $\lg(\tau_e/\tau_0)$ changes by no more than ± 20 %. With consideration of the U_0-τ logarithmic dependence it is possible to neglect this alteration and, for computational convenience, to replace this equation for (7):

$$\tau_e = 3.7\ 10^2\ t\ T/(T_0 - T)\ . \qquad (7)$$

Equation (7) shows that even when destruction occurs at **t-const**, τ_3 depends on the temperature range under study.

Actually, while testing in a broad range of deformation temperatures and velocities pre-destruction time cannot be a constant value. A source of errors in evaluation of τ_3 may also be related with non-linearity of the load build-up in the specimen under real loading conditions.

All the above testifies to the fact that the dependence $\sigma=f(T)$ may be, strictly speaking, non-linear that is why the errors in measuring kinetic parameters of the process, which may emerge due to variability of τ_e, require experimental assessment.

It is known that the kinetics of the EPC mechanical destruction process is complicated by such effects as the deviation from linear dependences $\lg\tau=f(\sigma,T)$ in the region of positive temperatures and low values of strength as well as by "pole shift" effects $1/T_P$ [1,2]. In such cases Equation (1) acquires the expression of Equation (1a)

$$\sigma=U_0/\gamma - 4.63(\lg\tau-\lg\tau_0)/(1/T-1/T_0)\gamma \qquad (1a)$$

and the calculation of the process kinetic parameters can be carried out by Equations (8) and (9):

$$U_0=4.63(\lg\tau_e-\lg\tau_0)/(1/T-1/T_P) \qquad (8)$$

$$\gamma=U_0/\sigma_0. \qquad (9)$$

It however gets dramatically more complicated as it is not always possible to justify the choice of values $1/T_p$.

2. Another alternative of calculating linear sections of dependences $\lg\tau=f(\sigma,T)$ is achievable on the basis of a principle of accumulated damage additivity [6]:

$$\int_0^t dt/\tau(\sigma)=1, \qquad (10)$$

where $\tau(\sigma)$ is a functional dependence of composite durability from the acting load, **dt** - an infinitely small period of time, during which σ that affects the composite may be assumed as constant. As a $\tau(\sigma)$ dependence, the most generic and effective approach to solving the problem is Equation (11) [3]:

$$\tau=C[\ln(\sigma_K/\sigma)]^\beta, \qquad (11)$$

where **C** and $\beta>>1$ - empiric coefficients, and σ_K - limit tensile strength. This alternative excludes obligatory knowledge of constants $1/T_P$ and τ_e and thereby notably simplifies the calculation of $\tau(\sigma,T)$ dependences and makes the calculation results more credible. It is possible to show that Equation (11) transforms to Equation (12) in the low-tension region:

$$\tau=B\sigma^{-m}, \qquad (12)$$

where **B** and **m** – empiric coefficients, and simultaneously

$$B=C(\ln\sigma_K)^\beta,\ m=\beta/\ln\sigma_K. \qquad (12a,b)$$

While decomposing Equation (11), after logarithm taking, to Tailor's series in the vicinity of a point that corresponds to tension $\sigma'=\sigma_K/e$, it is possible to demonstrate that in the tension region $|\sigma-\sigma_K/e|<\sigma_K/e$, where **e** is a natural logarithm base, Equation (11) transforms to the known time-strength dependence Equation (5), where

$$A=C\exp\beta.\ \alpha=\beta e/\sigma_K. \qquad (12c,d)$$

If we express the tension value as $\sigma=V_\sigma t$ at the loading velocity V_σ, then, solving simultaneously (5) and (10), it is possible to reveal a relation between strength and loading velocity through coefficients **A** and α:

$$\sigma=(2,3/\alpha)\lg(A\alpha)+(2,3/\alpha)\lg V_\sigma. \qquad (13)$$

The equation is apparently a linear function that allows to calculate coefficients **A** and α, i.e. linear sections of dependences $\lg\tau=f(\sigma,T)$. Load velocities V_σ under test conditions at ε-**const** can be constant, if dependences $\sigma=f(\varepsilon)$ are linear or close to linear, and variable, if these dependences are non-linear. In the latter instant, knowing σ_b and time before the break, V_σ can be determined as a generic or averaged loading velocity.

3. The most important and challenging issue for practice is to necessarily forecast long-term strength in the small-load region, i.e. non-linear sections of these dependences. This problem is solvable on the grounds of a joint use of dependences (12) and (10). After relevant transformations it is easy to obtain Equation (14):

$$\lg\sigma=[1/(m+1)]\lg[B(m+1)]+[1/(m+1)]\lg V_\sigma, \qquad (14)$$

which evidently is a linear function that links material strength with its loading velocity through coefficients **B** and **m**. Knowing **B** and **m**, it is possible to calculate non-linear sections of dependences $\tau(\sigma,T)$. The calculation of the parameters **B** and **m**, **C** and β is also feasible on the basis of Equations (12a,b) and (12c,d) for interrelations between coefficients **A**, α, **B**, **m**, **C** and β.

Therefore the use of Equation (11) allows to substantiate a feasibility of the complex approach to solving the problem of the EPC destruction kinetics originating from experimental evaluations of their strength over a broad temperature and loading velocity range. Note that in so doing no knowledge of τ_e and $1/T_P$ parameters is needed. Experiment proves well the above theory.

3. EXPERIMENT

Experimental researches were carried out for a great number of EPC formulations of different nature and for pilot formulations. Main experiment and calculation results are given below. They are basically discussed on the example of a high-charge composite with an elastomeric matrix. Results for double-base polymeric energetic composites were detailed earlier in [13].

Fig. 1 shows a temperature dependence of triple-base composite strength in the range of true deformation velocities $\varepsilon\sim 2.66*10^{-4}\div 2.66*10^{-1}c^{-1}$ and in a temperature range $+50\div -30^0C$. This dependence is typical for all EPCs we examined. As seen from the plot, it is rectilinear over the entire deformation velocity and temperature range under study. Pre-destruction time (t) varied from 190 sec to 400 sec. It remained actually constant at the same temperature and loading velocity. Our researches and analysis of the testing results derived from various literature sources show that correlation coefficients of such dependences **R>0.935** for a great number of double-base propellants. Linearity of dependences $\sigma=f(T)$ is one of the conditions that governs the correct use of this approach. Research results shown in Fig. 1 indicate that dependences $\sigma=f(T)$ obtained at different deformation velocities, when extrapolated to the region $\sigma\rightarrow O$, intersect at one point at $T_0=390^0K$. At $T = 0$ they have different values of σ_0 **(1 - 26.0, 2 - 30.8, 3 - 36.5 4 - 42.9 kg-f/cm^2).** It means that activation energy of the process U_0 stays unchanged in the studied modes, meanwhile the structure-sensitivity factor γ results from deformation velocity. This is in line with the physical fundamentals of destruction of polymeric composites of this type. In this case it is possible to calculate the destruction kinetic parameters (U_0 and γ) and linear sections of the dependence $\tau=f(\sigma,T)$ through Equations (8) and (9) if we know parameters $1/T_p$ and τ_3. It makes sense to determine these parameters quantitatively only for double-base composites since it is possible to approximate only their destruction kinetics using Equation (1a). Linear sections of dependences $\tau=f(\sigma,T)$ of such formulations are in the region of loads that are practicable for identifying their shelf life and serviceability. The researches show that the value $1/T_p$ for double-base formulations can be considered as the material constant equal to $\sim 1.85*10^{-3},{}^0K^{-1}$. The value of $\lg\tau_3$ in the studied deformation velocity and temperature interval amounts to $\lg\tau_3 \sim 0 \div 0.5$.

The destruction kinetics of triple-base high-charge formulations is normally described with the help of Equations (11) and (12). In this instant, it is necessary to calculate the temperature-time dependence parameters (**B** and **m**) by Equation (14) from dependences $\mathbf{lg\sigma = f(lgV_\sigma)}$. These dependences are given in Fig. 2. As we expected, they are linear. The Figures show the temperature-time dependences of the studied composite strength plotted basing on the calculation results and verified using direct measurements at **σ-const**. It is apparent that the calculation results are rather close to the experiment. Table 1 shows calculation results for the parameters **B** and **m**, their correlation with certified technical specifications and error values.

Table 1. Experimental values and certified technical specifications of the destruction kinetic parameters for the examined formulation

T, °K	Technical specifications		Experiment		ΔlgB, %	Δm, %
	lgB	m	lgB	m		
323	15.38	16.33	14.98	17.67	-2.6	8.2
293	16.55	16.84	15.28	15.50	-7.7	-8.0
262	-	-	15.70	14.60	-	-
243	-	-	17.8	15.3	-	-
223	19.26	16.26	-	-	-	-

As seen, the errors in determining **lgB** and **m**, which were calculated by Equation (1), are within the limiting error for the determination of formulation long-term strength.

4. CONCLUSION

This research has resulted in the development of the proposed method that allows to forecast the EPC destruction kinetics on the basis of tests on standard tearing machines at **ε=const** without direct experiments at **σ=const** and to solve inverse problems. The outputs of the analysis on EPC strength characteristics obtained on the basis of "kinetic" and "critical" understandings of the mechanical destruction process prove that these understandings are not in conflict.

REFERENCES

[1] Falkovsky M.G., Malchevsky V.A., Zheleznov V.I. Time and temperature-time dependence of polymer strength in the small-load region. // Proceedings of USSR Science and Engineering Symposium on Polymeric Materials and Constructions. Rostov-on-Don, 1971, 97-103.

[2] Malchevsky V.A., Regel V.P, Falkovsky M.G. Influence of NC plastisizers on the value of activation energy of its destruction. // Mech. Pol., 1973, 62, - p. 355-358.

[3] Goikhman B.D. On one equation for the time dependence of polymer strength. // High Mol.Comp. Ser. B,1969, 11, 244-245.

[4] Savitsky A.V., Malchevsky V.A., Demicheva V.P. A device for tensile testing of fine threads over a broad temperature range. // Zav. Lab., 1973, 4, 476-477.

[5] Zheleznov V.I., Malchevsky V.A., Falkovsky M.G. A device for investigating physical-mechanical properties of materials under uniaxial stretching. // Zav. Lab., 1973, 4, 476-477.

[6] Regel V.P., Slutsker A.I., Tomashevsky E.Ye. Kinetic Nature of Solids Strength. // M.:Nauka, 1974, 560.

[7] Kazale A., Porter R. Polymer Stress Reactions. // Akad. Press. N. Y.,San Fran.,London. 1978-79, 441.

[8] Kaush G. Polymer Fracture . // Spring. – Verlag, Berlin, Heidelberg, N. Y.,1978, 440.

[9] Emanuel N.M., Buchachenko A.L. Chemical Physics of Polymers Molecular Destruction and Stabilization. // M.:Nauka, 1988, 367.

[10] Ratner S.B., Yartsev V.P. Physical Mechanics of Plastics. // M.:Khimia, 1992, 320.

[11] Savitsky A.V., Malchevsky V.A., Sanfirova T.P., Zosin L.P. Temperature dependence of polymer strength. // High Mol. Comp., Ser. A, 1974, v. 16, 2130-2135.

[12] Regel V.P., Vershinina M.P., Leksovsky A.M., Malchevsky V.A. Forecast of mechanical durability of polymeric materials under different operational conditions. // Proceedings of USSR Science and Engineering Symposium on Engineering Assessment of Polymeric Materials and Constructions. // Rostov-on-Don, 1971, 107-113.

[13] Malchevsky V.A., Zarytovskaya N.A. To the problem of kinetic and critical evaluations of mechanical destruction of energetic polymeric composites (EPC) // Theory and Practice of Energetic Materials. V.IV. China Science and Technology Press. Beijing, 2001, 472-480.

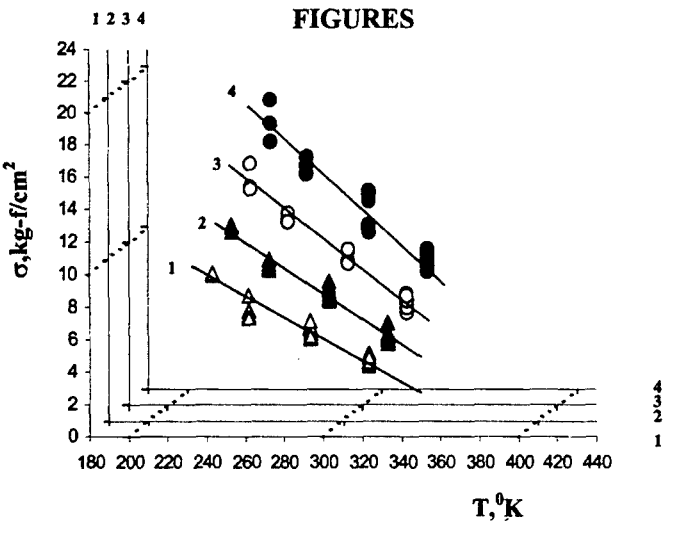


Fig 1. Temperature dependence of strength for the triple-base high-charge EPC. 1-$\varepsilon = 2.66*10^{-4}c^{-1}$, 2-$\varepsilon = 2.66*10^{-3}c^{-1}$, 3-$\varepsilon = 2.66*10^{-2}c^{-1}$, 4-$\varepsilon = 2.66*10^{-1}c^{-1}$

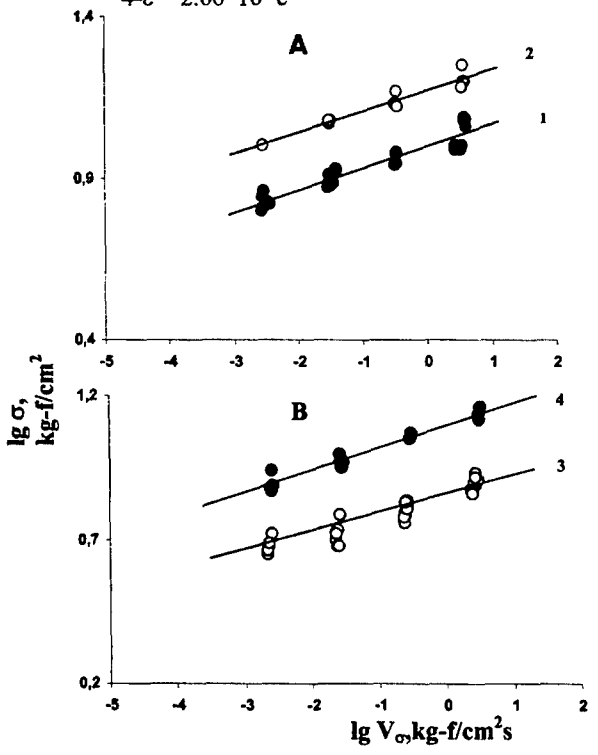


Fig 2. Dependence of formulation strength from loading velocity. A: 1 - 20⁰C, 2 - -30⁰C, 3 - 50⁰C, 4 - -11⁰C.

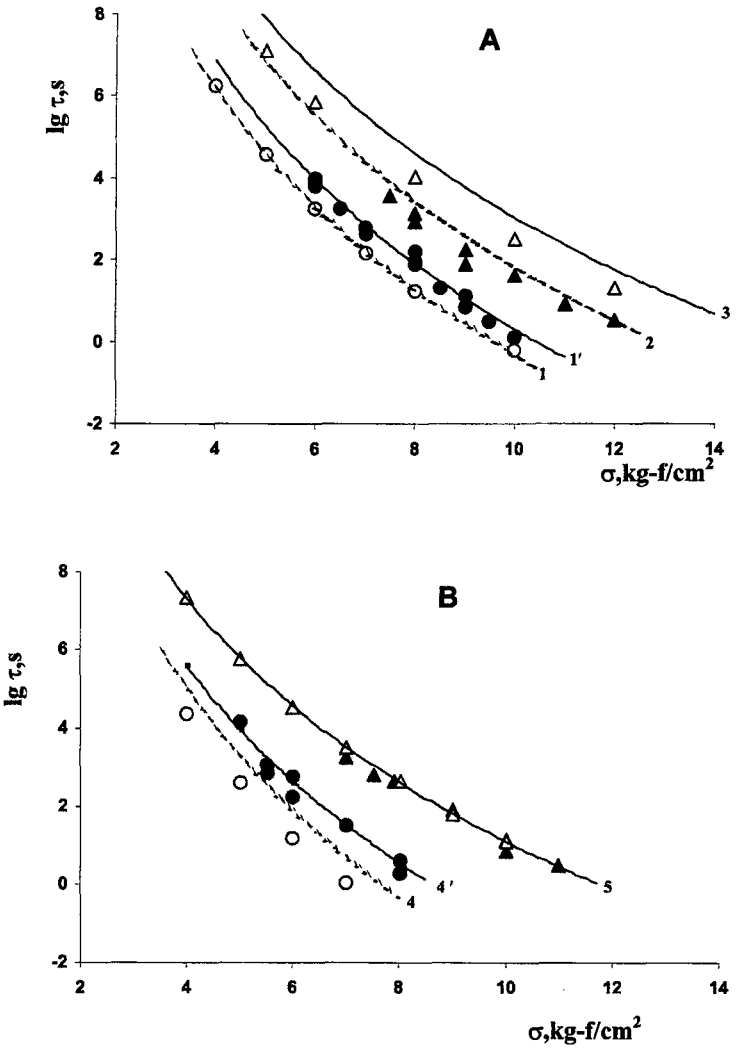


Fig 3. Temperature-time dependence of the formulation stength.
A: 1 - 20°C, 2 - -30°C, 3 - -50°C; B: 4 – 50°C, 5 - -11°C.
○, Δ - calculation by dependence lg σ = *f*(lgV$_\sigma$),
•, ▲ - experiment at σ = const,
1′, 3, 4′ - calculation by technical specifications.

DETONATION AND APPLICATION CHARACTERISTICS OF THE LATEST GENERATION OF EMULSION EXPLOSIVES

Andrzej Maranda*, Barbara Gołąbek and Johann Kasperski****

*Military University of Technology, Warsaw, POLAND

**BLASTEXPOL, Duninów, POLAND

Abstract:

Emulsion explosives have been very important blasting agents since some years. That results from their unquestionable advantages and introduction of new emulsion explosive generations into the market. The range of application of individual emulsion explosives in Polish and western countries mining are presented. Compositions, detonation parameters and properties of some types of emulsion explosives offered by "Blastexpol" are also presented and their ecological advantages are showed.

1. INTRODUCTION

The 20th century was a period of very fast science and technology development. On the basis of the results of experiments and theoretical estimations, which were conducted using numerical techniques, some modern technologies were worked out. They allowed getting materials and systems of increased parameters, which were used in various devices. Technological revolution ensued. But that progress did not concern all fields of technology. New types of explosives arose slower than new types of cars, TV sets or computers. But mining explosives evolved, too. In the second half of 19th century and at the beginning of 20th century as a result of A. Nobel's invention – dynamite, the main component of mining explosives was nitroglycerin, but from the beginning of the thirties of past century ammonium nitrate became an important component of these explosives. Research works were carried out to get modified ammonium nitrate, which could guarantee high detonation parameters and optimal application properties. On the basis of the results of experiments, using physical and chemical properties of ammonium nitrate (high solubility in water, crystallographic forms), ANFO explosives containing porous ammonium nitrate, slurry and emulsion explosives were developed.

The range of application of individual emulsion explosives in Polish and western countries surface mining are presented. Some trends of emulsion explosives development on the basis of analysis of compositions and detonation parameters of blasting agents offered by "Blastexpol" are also showed.

2. THE RANGE OF APPLICATION OF INDIVIDUAL EMULSION EXPLOSIVES

The supply of blasting agents has a decisive influence on blasting standard. But the amount of permitted by *Central Mining Institute* in Katowice explosives is not such important as their quality. Even though for example in 1996 the amount of explosives offered by producers was over 70 [1], mainly packaged or loose explosives, manually loaded to blast holes, were used for getting rock masses in domestic mining. The structure of explosive consumption in Poland at that time is presented in Fig. 1.

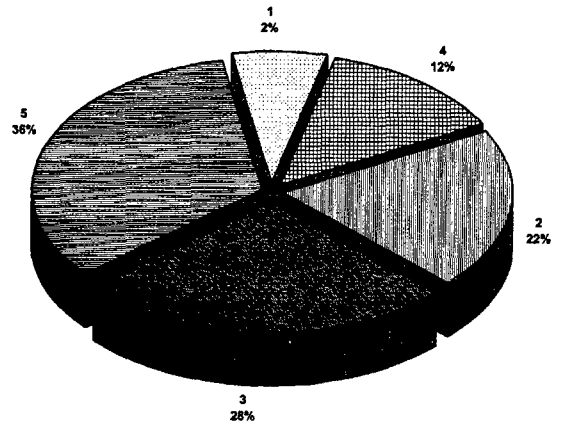


Fig 1. The structure of explosives consumption in Poland in 1996:
1 – loose in bulk, 2 - packaged, 3 – granular, 4 – TNT, 5 – plastic packaged [1]

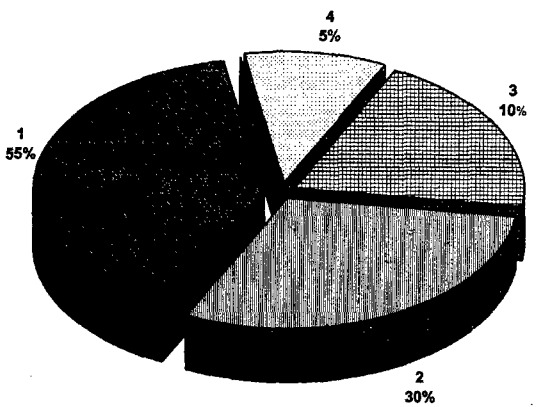


Fig 2. The structure of explosives consumption in Western Europe in 1996:
1 – ANFO, 2 – emulsion explosives, 3 – dynamites, 4 – other [2]

In 1996 the structure of mining explosive consumption in Western Europe was different (Fig. 2). Such explosives like ANFO and emulsion explosives dominated and their consumption was suitably 55 % and 30 %.

During last years some fundamental changes in consumption of individual explosives occurred in Western Europe (Fig. 3, Table 1).

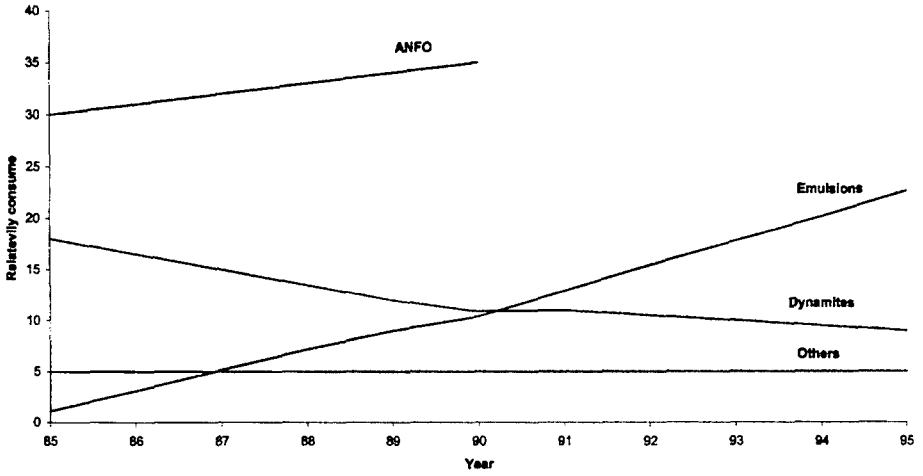


Fig 3. The change of explosives consumption in Western Europe [2]

Table 1. *Explosive consumption in German mines [3]*

Explosives	Year			
	1978 – West Germany		1998- All Germany	
	[Mg]	[%]	[Mg]	[%]
ANFO	11 000	40,7	13 000	32,5
Powder explosives	3 000	11,1	1 000	2,5
Dynamites	10 000	37,0	11 000	27,5
Slurries	3 000	11,1	-	-
Emulsions	-	-	15 000	37,5
Total	27 000	100	40 000	100

Data in Fig. 3 and Table 1 follow that emulsion explosives are becoming one of the most popular blasting agents used in mining in developed countries. It is very characteristic that slurry explosives are not used in German mining. Domestic extractive industry also started to show more interest in emulsion explosives in the nineties and it manifested itself in some opinions by *Experimental Mine "Barbara"* in Mikołów until 1997. More positive opinions concerning emulsion explosives and their permissions by *Central Mining Institute* in Katowice were given in next years.

3. TRENDS OF EMULSION EXPLOSIVE DEVELOPMENT

Intensive experimental works were conducted on compositions, technologies of preparations and detonation mechanism of slurry explosives in sixties. The most important producers of blasting agents continued works on technologies of commercial scale of slurry explosive production, which seemed to be the most promising explosives. That is why the first patent by F. Bluhm (Atlas Chemical Industries) [4], concerning emulsion explosives including W/O emulsion, remained inconspicuous. High explosive additives, plastic micoballoons and mechanical aeration sensitized them. They detonated with booster. An important step in emulsion explosives evolution was then in 1978 Ch. G. Wade from Atlas Powder Company evolved emulsion explosives, which could detonate from blasting cap no 6. They were sensitized by glass microspheres with low bulk density (0,1 ÷ 0,4 g/cm^3). Since then glass microspheres became the dominant component used as emulsion sensitizer.

Compositions and detonation properties of emulsion explosives, like other mining explosives, continually evolved after 1978. Fundamental differences between emulsion explosives types resulted from different methods of sensitization, occurrence of loose substances or their lack, water content. Researches were conducted to minimize water content and they resulted in Low Water Compositions (LWC). Emulsion explosives can be divided into eight following generations [5]:

1. Emulsion + microspheres,
2. Emulsion + microspheres + loose substances,
3. Emulsion + gas admission,
4. Emulsion + gas admission + loose substances
5. Emulsion LWC + microspheres
6. Emulsion LWC + microspheres + loose substances
7. Emulsion LWC + gas admission
8. Emulsion LWC + gas admission + loose substances

„Blastexpol" in Duninów, before Westspreng GmbH Germany, produces emulsion explosives of the latest generation. Basic detonation parameters of some emulsion explosives are presented in Table 2.

Table 2. *Composition and parameters of emulsions produced by "Blastexpol"*

Composition/ Parameters	Explosives		
	Emulgit LWC	Emulgit LWC-AL	Emulgit LWC-ALAN1
Ingredients [%]			
- mixtures AN i SN	89,3	86,5	88,5
- water	4,7	4,5	4,0
- Al	-	3,0	2,0
- other	6,0	6,0	5,5
- Density [g/cm^3]	1,12	1,10 ÷ 1,20	1,10 ÷ 1,20
- Lead block test [cm^3]	291	382	366
- Detonation velocity [m/s]	3930	3868	4048

Most of presented in Table 2 emulsion explosives possess relatively high detonation parameters (detonation velocity, available work potential). Application of some Emulgits LWC (especially ALAN-1, ALAN-2 and ALAN-3) in copper ore mines showed that in spite of lower than dynamites (14G5, 10G5H, 16G5H) detonation velocities, emulsion explosive consumption is lower per ground tone. It follows that the value of detonation velocity does not determine mining capacity of explosives. LWC Emulgits ALAN, beside classic emulsion W/O type, contain big amounts of solid phase – ammonium nitrate grains and aluminum dust.

Like other explosives containing components of diverse detonation, physical and chemical properties, they undergo so-called selective detonation. In chemical reaction zone of detonation wave the smallest constituents of fuel - oxidizer system transform that means an emulsion in emulsion explosives. However remaining components react in expansion wave, generating additional amount of energy. That is why in order to characterize precisely non-homogeneous explosives it is necessary to estimate their thermochemical parameters and carry out supplementary experiments. They should include among other things ideal detonation velocity, brisance and available work potential determined by modern research methods for instance cylindrical test or measurement of shock wave (burst wave) intensity in air.

Measurements of noxious gas product contents were also made. The results of experiments for some types of emulsion explosives in comparison with dynamites are presented in Table 3.

Table 3: Noxious gas product content [6]

Explosives	NO_x		CO	
	[m^3/Mg]	[%]	[m^3/Mg]	[%]
Dynamites	35 ÷ 40	100	160 ÷ 240	100
ANFO	30	75	51	21
Emulsions	1 ÷ 2	5	11 ÷ 46	19
Emulsions LWC	0,6	1,5	27	11

The other emulsion explosives produced by "Blastexpol" in Duninów also have small noxious gas content in detonation products.

The additional advantage of emulsion explosives is a possibility of detonation parameter control depending on deposit properties. That is why as a result of correct shooting it is obtained low intensity seismic burst waves. It is shown by measurements of seismic vibrations after first in Poland 20 tones mining shooting in Rock Material Mine in Zaręba in 14th November 2000. Maximal intensity of seismic vibration was 1,88 mm/s (permissible 3,50 mm/s) and overpressure of burst wave was 2,0 ÷ 3,8 Pa (permissible 120 Pa).

4. SUMMARY

Since some time there have been a not very precisely defined idea of *ecological explosives* in science publications. Some producers of explosives take advantage of this expression and advertise their products as ecological. But certainly this expression can be used with reference to modern generations of emulsion explosives. High water resistance of emulsion explosives protects against a penetration of their components into environment that is typical for other ammonium nitrate based explosives, especially sensitized by nitroesters. It should also be emphasized that organic phase components of modern emulsion explosives (oils, paraffin, waxes, emulsifying agents) are used in cosmetic industry (they are harmless) and in case of a penetration into environment they are decayed. The application of explosives in bulk, loaded mechanically, reduces the amount of wastes, which are wrapping papers or foils. That is why it is obvious that emulsion explosives should become dominant blasting agents, which should be used with modern and non-electric initiation systems.

LITERATURE

[1] R.Biessikirski, R.Morawa, *Zastosowanie emulsyjnych materiałów wybuchowych ładowanych mechanicznie w warunkach polskich kopalń odkrywkowych.* Materiały Konferencji Technika Strzelnicza w Górnictwie. Problemy Urabiania Skał. Jaszowiec 1998. 107-118.

[2] R.Morawa, *Mechanizacja załadunku materiałów wybuchowych przy robotach strzałowych.* ibd. 95-106.

[3] W.Thum, *Blasting techniques in the German quarry industry,* Proceedings 1st World Conference on Explosives Blasting Technique, Munich, September 2000, 389-398.

[4] H.F.Bluhm, pat. USA 3 447 978 (1969).

[5] A.Maranda, B.Gołąbek, J.Kasperski, *Materiały wybuchowe ekologiczne nowej generacji* [w:] Jakość Środowiska. Techniki i Technologie, Biblioteka KOMEKO, Wyd. Komdrug-Komag, Gliwice 2001, 249-260.

[6] B.Gołąbek, J.Kasperski, *Prezentacja firmy „Blastexpol". Wprowadzenie nowej generacji MW w KGHM „Polska Miedź" S.A.,* Suplement Międzynarodowej Konferencji Naukowo-Technicznej. Nowe Technologie w Górnictwie i Przeróbce Mechanicznej Rud, Lubin 2001, 30-35.

CAST TNAZ MIXTURES

Pavel MAREČEK and Kamil DUDEK

ALIACHEM a.s., Division SYNTHESIA, Research Institute of Industrial Chemistry (VÚPCH), 532 17 Pardubice - Semtín, Czech Republic

Abstract

Preliminary testing of TNAZ mixtures with active components (HMX, RDX) has been performed in laboratory scale.
The parameters evaluated were compatibility, sensitivity to impact, sensitivity to friction, thermal stability, shock sensitivity and detonation velocity. The results especially with regard to utilization of TNAZ as a component of explosive charge, are discussed.

1. INTRODUCTION

1,3,3-Trinitroazetidine (TNAZ) is a relatively new explosive, which was first synthesised by two chemists of Naval Research Laboratory USA, T. G. Archibald and K. Baum, in 1984[1].

Chemically this is a cyclic nitramine containing geminal nitro groups. Owing to its effectiveness and sensitivity parameters (which are comparable with those of RDX), low melting temperature, and stability in liquid phase within a broad temperature interval, TNAZ has been suggested for use as an explosive suitable for casting either alone or as a casting matrix for other explosives.

2. EXPERIMENTAL

TNAZ was prepared in our laboratory by modified Coburn[2] method. The RDX used was from DYNO company (Class A), HMX from SNPE (Class 1). TNAZ mixtures of a given composition were cast into the prepared matrixes. Casting temperature varied within 105 - 110^{0}C . For compatibility, sensitivity to impact, sensitivity to friction and thermal stability measurements the castings were crushed and fractions of given size were sucked.

Compatibility test

TNAZ compatibility with HMX, RDX in mixtures has been tested by means of vacuum test at 110 °C for 20 hours.

Table 1. Vacuum test of TNAZ mixtures at 110 °C for 20 hours.

	RDX/TNT 60/40	RDX/TNAZ 60/40	HMX/TNAZ 60/40	TNAZ	TNT	RDX	HMX
Density ($g.cm^{-3}$)	1.72	1.78	1.85	1.84	1.65	1.80	1.90
Volume of gas (cm^3)	0.13	0.10	0.04	0.01	0.01	0.03	0.06

Sensitivity to impact

Table 2. Sensitivity to impact of TNAZ mixtures.

	RDX/TNT 60/40	RDX/TNAZ 60/40	HMX/TNAZ 60/40	TNAZ	TNT	RDX	HMX
h_{50} (cm) (kg hammer)	71,8 (5)	55,7 (5)	52,1 (5)	26,0 (2)	60,0 (5)	35,0 (2)	30,0 (2)
(E_{d50}) [J]	36,0	28,0	26,0	5,2	30,0	7,0	6,0

Sensitivity to friction

Table 3. Sensitivity to friction of TNAZ mixtures

	RDX/TNT 60/40	RDX/TNAZ 60/40	HMX/TNAZ 60/40	TNAZ	TNT	RDX	HMX
Load [N]	360	100	110	110	>360	80	110

Thermal stability

Thermal stability has been determined by DTA method.

Table 4. Thermal stability of TNAZ mixtures

	RDX/TNT 60/40	RDX/TNAZ 60/40	HMX/TNAZ 60/40	TNAZ	TNT	RDX	HMX
Beginning of 1st endo [°C]	78	94	95	94	77		187
Beginning of 2nd endo [°C]			187				
Beginning of exotherm [°C]	188	183	190	191	224	203	272

Sensitivity to shock wave

Sensitivity to shock wave has been determined by means of the so called „small„ GAP-Test (Ø 21 mm). The results are given in Table 5.

Table 5. GAP-Test of TNAZ mixtures

	Density ($g.cm^{-3}$)	TMD (%)	p_i^* (GPa)
RDX/TNT 60/40	1.70	98.0	2.70
RDX/TNAZ 60/40	1.78	98.0	1.00
HMX/TNAZ 60/40	1.85	98.7	1.10
PETN[3] 5% wax	1.60	94.4	1.10

$^*p_i$ -initiation pressure

Detonation velocity

Detonation velocities of cast TNAZ mixtures (∅ 21 mm) are given in Table 6.

Table 6. Detonation velocities of TNAZ mixtures

	Density ($g.cm^{-3}$)	TMD (%)	$D_{measured}$ ($m.s^{-1}$)	$D_{calculated}$ ($m.s^{-1}$)
RDX/TNT[4] 60/40	1.720	99.0	7890	8000
RDX/TNAZ 60/40	1.780	98.0	8720	8730
HMX/TNAZ 60/40	1.851	98.7	8980	8970

3. DISCUSSION

The data from vacuum test confirmed good TNAZ compatibility with both two nitramines (RDX, HMX).

Both TNAZ mixtures are more sensitive to impact and also to friction, which is given by a high sensitivity of TNAZ as such. Thermal stability is practically identical at all of the three mixtures observed. At mixture RDX/TNT, the beginning of decomposition is caused by RDX decomposition, while at TNAZ mixtures it is caused by TNAZ decomposition.

Sensitivity to shock wave of cast TNAZ mixture is somewhat higher in comparison with RDX/TNT. Sensitivity to shock wave of TNAZ cast charges with nitramines are on the same level as of phlegmatized PETN. We suppose that sensitivity of these mixtures would by lowered using vacuum casting and for practical purposes it would probably be necessary to use desensitizing additives.

The measured values of detonation velocities of cast TNAZ mixtures exceed detonation velocity of RDX/TNT. In case of RDX/TNAZ mixture by 800 $m.s^{-1}$. Measuring of detonation velocity of cast TNAZ mixture confirmed compliance between experimental and calculated values.

4. CONCLUSION

In compliance with the assumptions, the results showed TNAZ to be a substance with high performance parameters, applicable for preparation of castable mixtures. At present, high price, higher sensitivity (compared to TNT) and vapour tension cause that this substance cannot be utilized more widely. Future works should be aimed at removal of these drawbacks of TNAZ with high performance parameters being retained.

REFERENCES

[1] Archibald T.G., Baum K.: „Synthesis and X-ray Crystal Structure of 1,3,3-trinitroazetidine,,, J. Org. Chem. **55**, 2920-2924 (1990).

[2] Coburn D., Hiskey M.A.: „Synthesis and Spectra of some ^{2}H-, ^{13}C-, and ^{15}N-Labelled Isomers of 1,3,3 - trinitroazetidine and 3,3 - dinitroazetidinium nitrate,,, J. Energet. Mat. **16**, 73-99(1998).

[3] Brebera S.,: „Military explosives and technology of explosive charges", University of Pardubice, 2001, pgs.39-48

[4] Majzlík J., Dusík V.,: DETPAR - The Catalogue of Detonation Parameters, Synthesia, Research Institute of Industrial Chemistry, Pardubice - Semtín, 1998.

DETERMINATION OF PHYSICAL CHARACTERISTICS OF DETONATION PRODUCTS

František Masař, Pavel Vávra and Jiří Vágenknecht

University of Pardubice, KTTV, 530 12 Pardubice, CZ

Abstract:

Physical characteristics of detonation products such as velocity, conductivity and length of conductive zone were measured. Influence of potassium nitrate addition into the explosive was consequently determined.

Keywords: *conductivity, velocity of detonation products, explosives*

1. INTRODUCTION

The results summarized in this article are part of introductory research of explosive with high conductivity of detonation products. Hollow charges were used in our measurements to direct the products of detonation into the measuring channel. Fast moving flow of conductive gaseous products was obtained and its physical properties were studied.

2. EXPERIMENTAL

Explosives

The SEMTEX A1 and later SEMTEX A1 doped with potassium nitrate was used for determination of physical properties of cumulative flow of detonation products. Based on the results of pre-tests it was decided to use following configuration of experiment:

- 8 g of explosive was introduced into a plastic tube and hollow space was created on the bottom of the charge

- central ignition from the top of the charge by detonator was used

Used expolosives:

- Semtex 1A

- Semtex 1A + 2 % KNO_3

- Semtex 1A + 6 % KNO_3

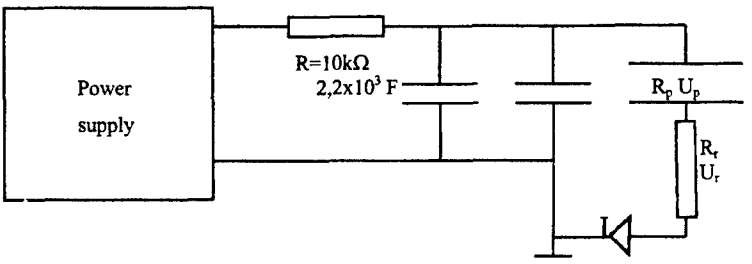


Fig 1. Electric circuitry

Measuring canal

Single-shot canals of the same construction were prepared from construction plastic. Cross-section of the canal was 10 x 10 mm square. The conductivity measurements were done by three pairs of cooper (burnished) electrodes with dimensions of 20 x 10 mm each. The distance between individual electrode pairs was 100 mm.

3. RESULTS

As a result of hollow charge detonation a fast moving flow of detonation products is formed. This flow was directed on to the canal and following properties were determined different types of explosives.

- velocity of cumulative flow
- resistivity of cumulative flow
- length of conductive zone

Velocity of cumulative flow

Three values of velocity were measured for each test (first from a distance of charge from electrode, second and third from a distance between the electrodes). Time was measured with oscilloscope Tektonix TDS 3012. Addition of potassium nitrate practically did not affect velocity of cumulative flow.

Table 1. Velocity of cumulative flow of detonation products

Distance form charge [mm]	50	170	290
Velocity [m/s]	7739	7680	6522

Resistivity of cumulative flow

The following formulas were used to calculate resistivity of cumulative flow from known values of U_0, R_r and measured value of R_p

1. $i_v = \frac{U_{max}}{R_r}$ [A]
2. $R_p = \frac{U_0 - U_p}{i_v}$ [Ω]
3. $\rho = \frac{R_p \times S}{l}$ [Ωcm^2/cm]

Table 2. Resistivity values

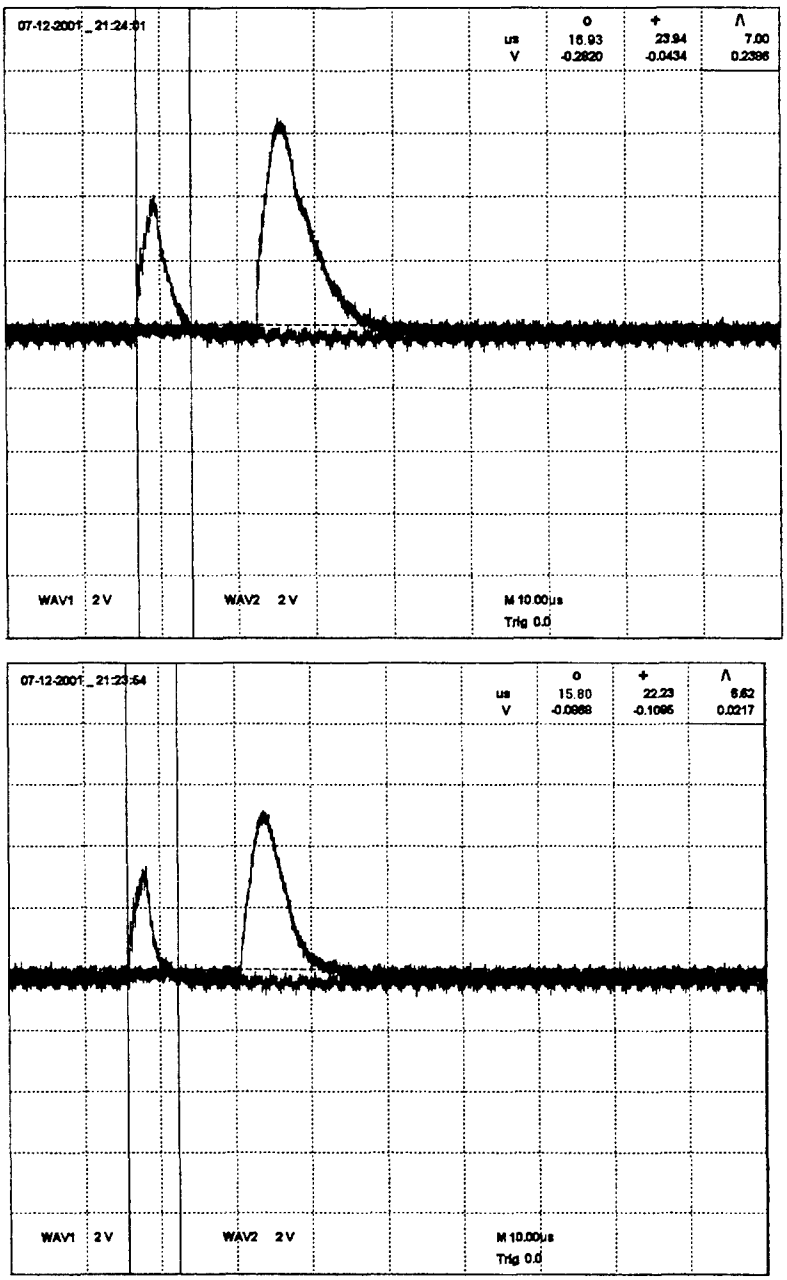
Distance from charge 50 mm	amount of KNO_3 in explosive [%] 0	2	6
Resistivity [Ωcm^2/cm]	2,832	2,298	2,092
Distance from charge 170 mm	amount of KNO_3 in explosive [%] 0	2	6
Resistivity [Ωcm^2/cm]	1,822	1,581	1,143

Length of conductive zone

From the distance between the electrodes and measured time of the pulse we were able to calculate length of the conductive zone as it passed through the canal.

Table 3. Length of conductive zone [mm]:

Distance from charge [mm]	amount of KNO_3 in explosive [%] 0	2	6
50	20,6	30,3	30,9
170	44,0	66,6	75,0
290	64,8		97,4



Graph 1. Sample of acquired data

4. DISCUSSION

Velocity

The maximal measured initial velocity of cumulative flow did not exceed detonation velocity of used explosive. As can be seen from acquired results, drop of detonation products flow initial velocity did not exceed 16% on the length of the canal.

Resistivity of cumulative flow

The measured values of resistivity are 10^5 higher compared to conductors and 10^9 lower compared to isolating materials. The presence of K^+ ion approved increase conductivity.

Length of conductive zone

Determined values of length of conductive zone indirectly indicate that additional reactions take place in the cumulative flow of detonation products. With an increasing amount of K^+ ions in the explosive elongation of conductive zone was observed. Reactions taking place in this zone further stretch the zone. As a result of this phenomenon rapid drop of conductivity may take place at the end of the canal.

5. CONCLUSION

This article presented part of the results measured during the first part of our research. Further investigation of this problem is now being done and literature survey is being completed.

Acknowledgment

Authors would like to thank Mr. Jiří Majzlík for help provided during all of the measurements.

SYNTHESIS OF NEW HETEROCYCLIC AZIDONITRAMINES

Alevtina S. Medvedeva*, Luybov P. Safronova, Maria M. Demina, Galina S. Lyashenko, Vladimir V. Novokshonov, Andrei V. Afonin and Galina I. Sarapulova

A. E. Favorsky Irkutsk Institute of Chemistry,
Siberian Branch of the Russian Academy of Sciences, 664033 Irkutsk, Russian Federation

Abstract:

Syntheses of new six- and seven-membered heterocyclic azidonitramines are presented. These nitramines are: 3-azidoethyl-1,5-dinitro-1,3,5-triazacycloheptane, 5-azido-1,3-dinitro-1,3-diazacyclohexane and 5,5'-diazido-1,1',3,3'-tetranitro-1,1',3,3'-tetraaza-2,2'-dicyclohexane. The molecular structures of them are confirmed by IR and ^{13}C NMR spectroscopies.

Cyclic azidonitramines are of specific interest as a potentially stable high energetic compounds. The literature data about synthesis of cyclic azidopolynitramines are very bounded [1,2]. We have synthesized some new six- and seven-membered heterocyclic azidonitramines: 3-azidoethyl-1,5-dinitro-1,3,5-triazacycloheptane (**3**), 5-azido-1,3-dinitro-1,3-diazacyclohexane and 5,5'-diazido-1,1',3,3'-tetranitro-1,1',3,3'-tetraaza-2,2'-dicyclohexane.

Synthesis of 3-azidoethyl-1,5-dinitro-1,3,5-triazacycloheptane (**3**) includes Mannich condensation of ethylenedinitramine with formaldehyde and monoethanolamine to give 3-ethanol-1,5-dinitro-1,3,5-triazacycloheptane (**1**) in 71% yield; the displacement of hydroxyl by tosyl group to give 3-p-toluenesulfonylethyl-1,5-dinitro-1,3,5-triazacycloheptane,3-diamino-2-propanol (**2**) in 73% yield and nucleophilic displacement of tosyl group in (**2**) with azide ion in DMF to form (**3**) in 54% yield (Scheme 1).

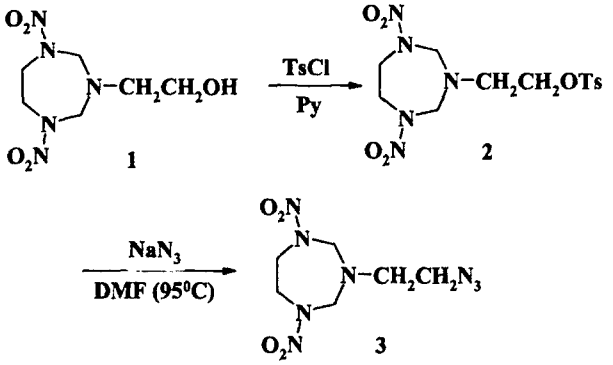


Fig 1. Scheme 1.

Synthesis of 5-azido-1,3-dinitro-1,3-diazacyclohexane (**6**) was realized by consequent reactions of glyoxal with 1,3-diamino-2-propanol, nitrozation *in situ* generated 5,5′-dihydroxy-1,1′,3,3′-tetraaza-2,2′-dicyclohexane into 5-nitroso-1,3-dinitro-1,3-diazacyclohexane (**4**) and followed by nitration with 100% HNO_3 to form 5-nitroxy-1,3-dinitro-1,3-diazacyclohexane (**5**). Displacement of nitroxy groups in the latter compound by azido groups leads to target compound (**6**) (Scheme 2).

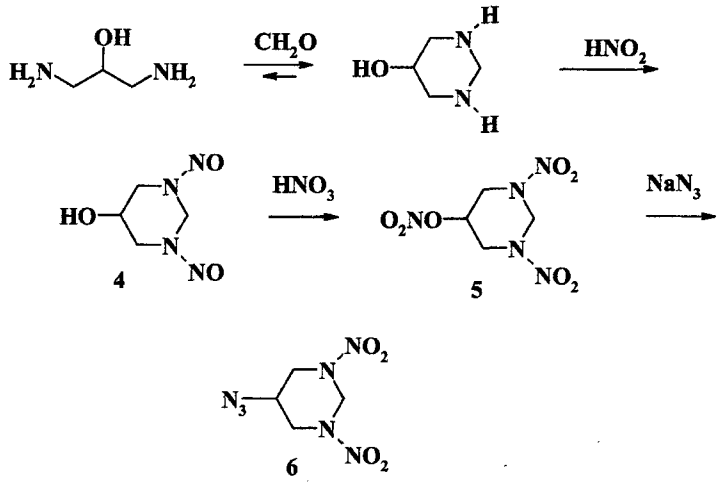


Fig 2. Scheme 2

Analogous strategy of synthesis was used for the preparation of 5,5′-diazido-1,1′,3,3′-tetranitro-1,1′,3,3′-tetraaza-2,2′-dicyclohexane (**9**).

Mannich condensation of 1,3-diamine-2-propanol with 40% glyoxal solution at 80-90 °C followed by nitrosation with nitrous acid gave the 5,5′-dihydroxy-1,1′,3,3′-tetranitroso-1,1′,3,3′-tetraaza-2,2′-dicyclohexane (**7**) (mp 180-185 °C) in 35% yield. Hindered rotation of the nitrosamine group leads to the existence of some rotational isomers of compound (**4**) and (**7**). The assignments of signals in ^1H NMR Spectra of (**7**) were made on the basis of comparison of ^1H NMR Spectra of 1,3-dinitroso-1,3-diaza-5-hydroxycyclohexane (**4**) and (**7**) by two dimentional ^1H-^1H NMR Spectroscopy (COSY) method.

5,5′-Dinitroxy-1,1′,3,3′-tetranitro-1,1′,3,3′-tetraaza-2,2′-dicyclohexane (**8**) was prepared by reaction of tetranitroso-derivative (**7**) with 100 % nitric acid in 51% yield. The structure of this compound confirmed by ^1H and ^{13}C NMR Spectroscopy ^1H NMR Spectra. IR Spectra (nujol) indicates the asymmetric stretching band 1530 (ν_{as} NO_2) of N-NO_2 fragment and 1625 (ν_{as} NO_2), 1280 (ν_s NO_2) cm^{-1}.

The synthesis of 5,5′-diazido-1,1′,3,3′-tetranitro-1,1′,3,3′-tetraaza-2,2′-dicyclohexane (**8**) was carried out by reaction of 5,5′-dinitroxy-1,1′,3,3′-tetranitro-1,1′,3,3′-tetraaza-2,2′-dicyclohexane (**7**) with sodium azide in dry dimethyl sulfoxide at the temperature 70-75°C for 23 h in satisfactory yield (Scheme 3). This compound (white crystals) is decomposed at the temperature more than 200 °C without melting. The structure of (**8**) was confirmed by IR, ^1H, ^{13}C NMR spectroscopy. IR spectral method is very convenient to control the dynamic of this reaction in DMSO: the lowering of intensity of strong absorption band at

1625 (ν_{as} NO_2) of ONO_2 group in (7) and increasing of peak intensity at 2100 (ν_{as} N≡N) cm^{-1} in (**8**), characterize the dynamic of process of azido formation.

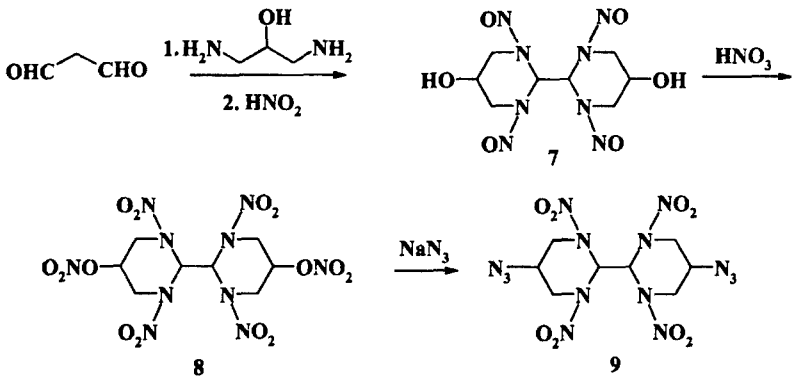


Fig 3. Scheme 3

^{1}H NMR Spectra (δ, CD_3CN) is characterized with synglet of protons of 2-N-CH-N-, 2'-N-CH-N- groups at 8.302, synglet of -$CH-N_3$ protons at 4.153 and two doublets of 4,6, 4',6'-CH_2 –protons at 4.894 and 3.840 (J= 15.8 Hz) ppm. IR Spectra (nujol) of this compound is characterized by the strong asymmetric stretching band 1530 (ν_{as} NO_2) of N-NO_2 fragment and 1330 (ν_s NO_2), 1350 (ν_s N_3), and absorption band at 2100 (ν_{as} N≡N) cm^{-1}. ^{13}C NMR Spectra (δ, CD_3CN) contains the signals at 64.767 (N-C-N), 63.746 (C-N_3), 49.563 (4,6, 4',6'-CH_2) ppm. The assignements of signals in ^{13}C NMR Spectra of (**9**) were made on the basis of two dimentional ^{1}H, ^{13}C NMR Spectroscopy (CHCORR) method.

Acknowlegment. This research was supported by EOARD grants No. B338295 and No. SPC 99-4080

REFERENCES

[1] Frankel M.B., Woolery D. O. // J. Org. Chem. 1983. Vol. 48. P. 611.

[2] Flanagan J.E., Frankel M.B., Woolery D.O. // AFOSR/AFRPL rocket Propulsion research Meeting, Lancaster, CA, Feb 1983, Air Force Office of Scientific Research: Washington, DC, 1983.

DEVELOPMENT OF THE DIVERGENT DETONATION WAVE IN PBX BASED ON RDX

R. Mendes, J. Campos, I. Plaksin and J. Ribeiro

LEDAP - Lab. of Energetics and Detonics, Mech. Eng. Dept., Fac. of Sciences and Technology, Polo II, University of Coimbra, 3030-201 Coimbra, Portugal

Abstract

To characterize the initial phase of the divergent detonation wave in PBX, a hemispheric explosive sample was initiated by a long cylindrical charge with the same explosive composition. The tested PBX is formed by 85 % (in mass) of RDX (bimodal particle distribution - 75 % of d_{50} = 96μm and 25 % of d_{50} = 22μm) and 15 % of HTPB binder, presenting an effective density of 1.574 g/cm^3 (> 99 % TMD) and detonation velocity of 7.90 mm/μs. An optical method based on 64 optical fibbers ribbon (250μm of diameter each fibber) connected to a fast electronic streak camera, allows the measurement of the detonation velocity inside the PBX sample, as a function of the run distances, for several angles with the axis of initiation channel. The results, presented as a radius-time and velocity-radius diagrams, show the evolution of a divergent detonation wave in its run, up to the radius of 33 – 34 mm (6.6 – 6.8 times the diameter of the cylindrical initiation channel). The obtained real shape of the divergent detonation wave is significantly different from those predicted with an ideal propagation model. Measurements of the pressure in the induced shock wave in an inert standard barrier were performed, from the divergent detonation wave generated by the long cylindrical PBX charge. It presents an initial divergent detonation wave of positive constant curvature with relatively significant amplitudes in velocity and pressure values.

Keywords: *Initiation; Divergent Detonation wave; PBX-RDX.*

1. INTRODUCTION

When an explosive bulk is initiated directly by a long cylindrical charge, a spherical divergent detonation wave (DW) is formed in the bulk explosive. The observed detonation parameters, namely detonation velocity[1,2,3,4] and detonation pressure[4,5,6] are different from those observed in the normal detonation propagation in the long cylindrical charges.

When a semi sphere explosive sample is initiated in the central zone, it can be observed an divergent DW arriving early at the periphery surface zone, that locates under the angle θ with the axis [7,8]. The value of the angle θ is a function of the explosive density[9] and it decreases when the density increases. It was also observed, for the PBX based on RDX and HMX, that the divergent complex detonation wave presents a non-monotonic propagation at different zones, generated from a existing delay of propagation, in the axis and its normal directions, relatively to the intermediated zones [9,10,11,12]. Corner turning experiments, with Cu and PMMA confinements, show the first 5 mm radius the divergent detonation front presenting an irregular profile with preferential acceleration directions[11,12]. These results were obtained and verified in the registrations of DW propagation using a high-resolution optical method[13], based on 64 optical fibers with 250 μm diameter each one.

The present work concerns the studied phenomena of the divergent DW propagation in PBX, based on RDX, during the transient zone, showing the scale of difference between pressure amplitude in the observed divergent DW and in a constant front curvature DW.

2. EXPERIMENTS AND RESULTS

The tested PBX is composed by 85 % (in mass) of RDX (bimodal particle distribution, d_{50} = 96μm and d_{50} = 22μm) and 15 % of HTPB binder, presenting an effective density of 1.574 g/cm^3 (> 99 % TMD), and a detonation velocity, Dn (measured in long cylindrical PBX charges), equal to 7.90 mm/μs.

The hemispherical charges of PBX were initiated by long cylindrical charges, formed by the same explosive material, with 5 mm of diameter. The diameter of the initiator charge exceeds 1.3 times the critical diameter of PBX, but is less than the limit diameter for the nominal detonation velocity. The values of critical and limit diameters, for the studied PBX, are equal respectively to 3.75 mm and 10 – 15 mm [11].

The profile and the velocity of the divergent DW have been measured using the experimental set-up presented in **Chyba! Nenalezen zdroj odkazů.**. The experimental set-up has eleven sets of 5-6 optical fibers each one. The splited optical fibers sets are placed between two non-transparent films, and oriented to the point that is coincident to the axis, at the end of initiator charge. The set of the windows were opened, in the non-transparent film, for fixed radial distances. When the Detonation Front (DF) is intersecting the window, the irradiated light, transmitted through the optical multi-fiber strip, can be recorded by an electronic streak camera.

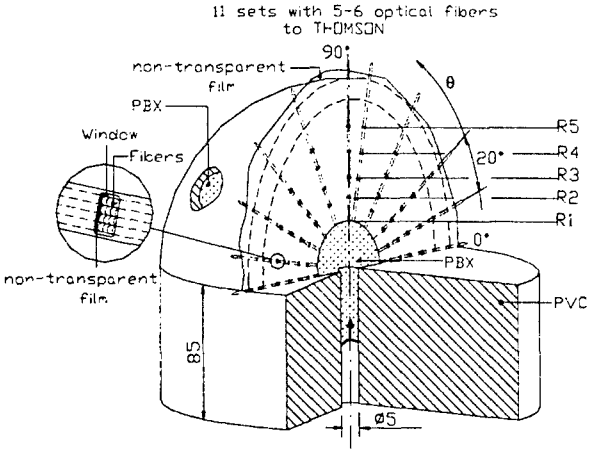


Fig 1. Experimental set-up for the recording of the profile and detonation velocity of the divergent DW.

The typical streak record of the divergent DW propagation, inside the PBX, is presented in Figure 2. It shows the DW front arriving first, for a same radius distance, at the angle directions equal to 40°-50° relatively to the charge axis.

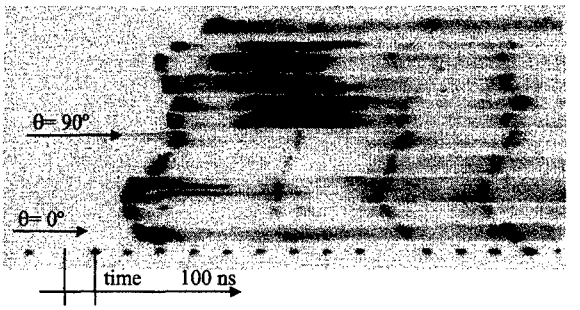


Fig 2. Typical streak camera record obtained with the experimental set-up presented in Figure 1.

These experimental results allow to evaluate the profiles of the divergent DW, for a set of time intervals, i.e. the DF isochrones. The real isochrones, obtained experimentally, and the isochrones obtained by an ideal propagation model of the divergent DW, are shown in **Chyba! Nenalezen zdroj odkazů.**. The presented results show a great deviation of real divergent DW isochrones, from the ideal propagation model. In the equatorial zone, they attained up to 30% of deviation. Consequently an ideal propagation model is not acceptable to describe precisely the divergent DW in PBX, in the initial phase of its propagation (for R less than 10 – 20 mm).

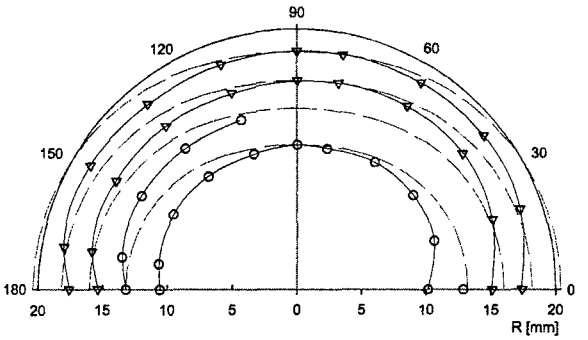


Fig 3. Real isochrones of the divergent DF (solid lines) and isochrones obtained with an ideal propagation model (dotted lines).

The measured profile of the DW front has a quasi-spherical geometry, but with the virtual center of initiation located inside the bulk charge. It presents also some peculiarities on the equatorial zone. These results are in agreement with the earlier published work[8].

The detonation velocity, Dd, at different DF zones and along the predefined directions (line of windows), can be evaluated correlating the distance between the windows and the measured the time intervals. The Dd values can be compared with the value of Dn = 7.90 mm/μs, for a long charge detonation. The diagram of the ratio between velocities values, Dd/Dn, as a function of the ratio R/ri (R is taken from the axial terminal point of initiator), for the directions of 0°, 40° and 90°, is presented in **Chyba! Nenalezen zdroj odkazů.**.

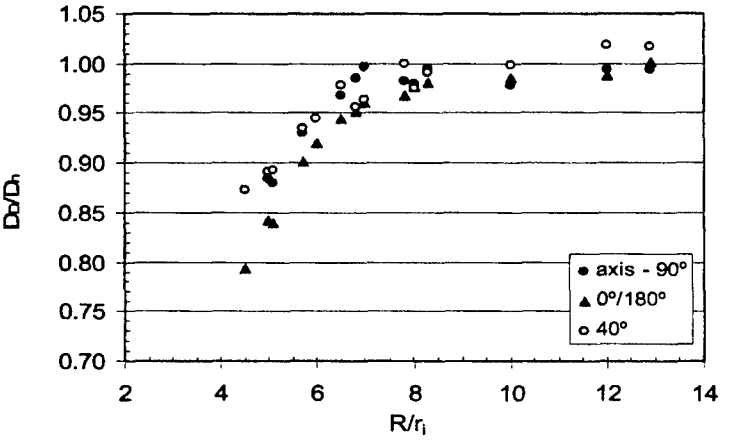


Fig 4. Dd/Dn ratio of the divergent detonation wave, as a function of R/ri, for several θ angles.

The results show the non-monotonous increase of DF velocity along the directions of registration, and their relative differences, for fixed radius. The growing of the divergent DW inside the bulk part of PBX, when it is initiated directly by long cylindrical charges of relatively small diameter, is attended by the successive phases of acceleration and slowing down.

Previous published works show the non-monotonous behavior of the divergent DW in PBX, at a different radius of its propagation, R=0-6mm[12] and R=0-15mm[15], recorded by a continuous method. The presented results confirm previous measurements [10], present at **Chyba! Nenalezen zdroj odkazů.**, confirming the non-monotonous (pulsing) growing of the DW velocity, in two fixed directions.

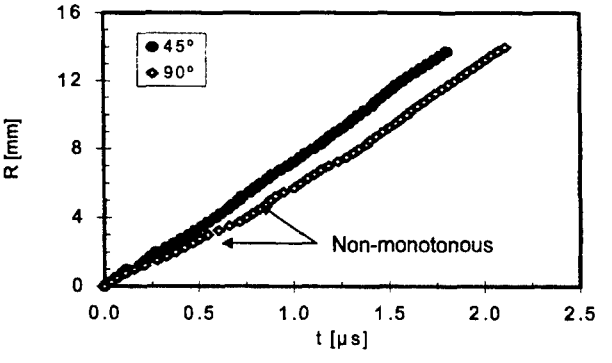


Fig 5. Non-monotonous grow of the divergent DF in PBX, based on RDX, for 45° and 90° angles [10].

Induced shock wave (SW) pressure from DW, in a standard inert barrier, and its process of attenuation (inside the barrier), were measured in the central zone of the DF (θ=90°), using the set-up with two different geometric configurations: PBX hemispheric charge set-up, for the

diverging DW, and long cylindrical charge set-up, of 25 mm diameter, where the positive DF curvature is assumed constant.

To evaluate the pressure, induced by the divergent DW, it was used the method of closing gaps in a multi-layer barrier, presented in **Chyba! Nenalezen zdroj odkazů.**. This barrier is formed by several "kapton" layers, with 125 μm each one. When the DW pass through the inert layer, it closes the micro gap existing between each to pair of layers, producing a light pulses that can be recorded in a electronic streak camera. The typical photo-chronogram is presented in **Chyba! Nenalezen zdroj odkazů.**.

The **Chyba! Nenalezen zdroj odkazů.** presents the attenuation processes of the SW pressure, inside the barrier, that were initially induced by the divergent detonation, in the two described experiments - the hemispherical PBX charges, of radiuses equal respectively to R=15mm and 20mm, and the long cylindrical charge of diameter of 10 mm. The results show, in the case of divergent DW, the induced pressures are locally increasing with increasing radius of PBX hemispherical sample. However, in despite of the radius of the hemispherical charges, they are 1,9 - 2.8 times less those measured in the cylindrical configuration.

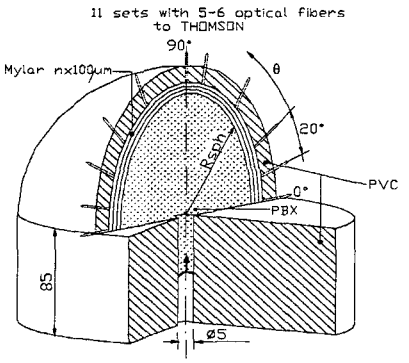


Fig 6. Experimental set-up to measure the induced pressure on a multi-layer inert barrier.

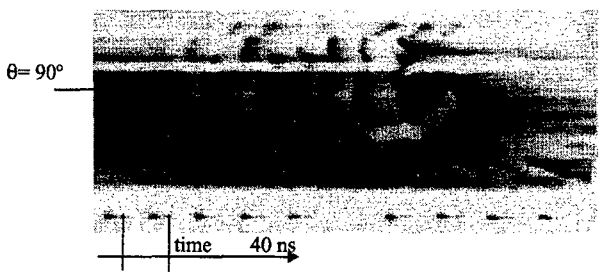


Fig 7. Induced shock wave attenuation, by the divergent DW, inside the inert multi-layer barrier.

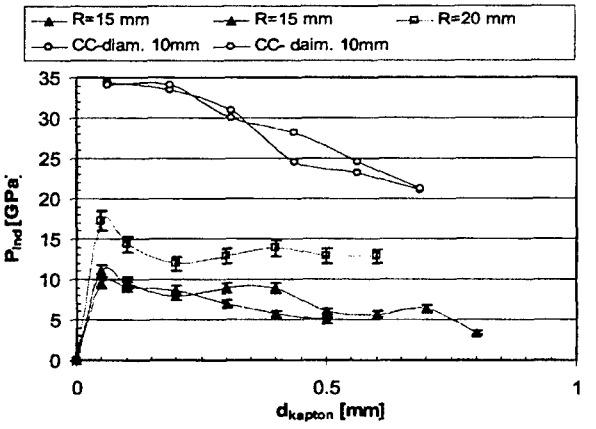


Fig 8. Induced pressure on a barrier, by a divergent DW and by a DW front propagation in a cylindrical charge

The most significant results of these measurements comes from the fact that the difference between the values of DW velocities, for the considered two different DW geometries, are very small (4.5% for R_{sph}= 15mm and 1.5% for R_{sph}= 20mm), and the values of the induced pressure are important: 65% for R_{sph}= 15mm and 45 % for R_{sph}= 20mm.

This scale of differences, in detonation velocity and induced pressure, between constant positive curvature and divergent DW, in PBX, agree with preceding published results [4].

3. CONCLUSIONS

The transient process of the development of the divergent DW, initiated in PBX hemi-spherical charges, by long cylindrical charges of low diameter, has been studied, using the high resolution optical method based on the 64-optical fiber strip. The obtained results show significant deviation from an ideal propagation model. The divergent DW presents a delay of propagation in the direction of the axis of the initiation charge and in its normal direction, relatively to intermediate directions.

The results confirm the non-monotonous growing of the divergent DW in PBX, under the applied conditions of initiation. The difference in the values of PBX detonation velocity, in the axial direction of its initiation channel, between the long charge detonation and the divergent detonation, during the first 20 mm of its run, reaches not more than 1.5% – 4.5%, but the scale of difference in amplitudes of pressure in SW, induced in the standard inert barrier, is significantly (1.9 – 2.8 times) more important.

REFERENCES

[1] CHERET, R. and VERDES, G., 1970, "Divergent Spherical Detonation Waves in a solid Explosive", *Proceedings of the 5th Symposium (International) on Detonation*, ONR, ACR 184, Office of Naval Research, Passadena, USA, pp. 31-39.

[2] BONTHOUX, F., DENEUVILLE, P. e LONGUEVILLE, Y., 1981, "Diverging detonations in RDX and PETN based cast-cured PBX", *Proceedings of the 7th Symposium (International) on Detonation*, NSWC MP 82-334, Naval Surface Wapons Center, Annapolis, USA, pp.408-415.

[3] MADER, C.L., 1979, *"Numerical modelling of Detonation"*, ed. by University of California Press, Berkley, 1st Ed.

[4] GERASIMOV, V. M., GUBACHEV, V. A., VAKIN, V. A., PLAKSIN. I. E. e SHUTOV, V. I., *Sov. J. Chem. Phys.*, 1994, **12**(5), 1091-1097.

[5] TARVER, C. and URTIEV, P. A., *Progr. In Astronautic and Aeronaut.*, 1984, V94, pp. 369.

[6] TITOV, M. V., KARAKHANOV, S. A., e BORDZILOVSKY, S. A., 1985, "Pressure variation upon initiation of a cast RDX/TNT 50/50 charge by diverging shock wave", *Proceedings of the 8th Symposium (International) on Detonation*, NSWC MP 86-194, Naval Surface Wapons Center, Albuquerque, USA, pp. 143-150.

[7] COX, M. e CAMPBELL, A. W., 1981, "Corner turning in TATB", *Proceedings of the 7th Symposium (International) on Detonation*, NSWC MP 82-334, Naval Surface Wapons Center, Annapolis, USA, pp. 624-633.

[8] HELD, M., "Influence of the Initiation Intensity on the Radial Detonation Breakthrough", *Propellants, Explosives and Pyrotechnics*, 1995, 20, pp. 245-251.

[9] HILL, L.G., SEITZ, C.A., FOREST, C.A., AND HARRY H.H., 1997, "High Explosive Corner Turning Performance and the LANL Mushroom Test", *Shock Compression of Condensed Matter*, ed. by S. C. Schmidt *et al.*, AIP Conference Proceedings 429, NY, 1998, pp. 751-754.

[10] MENDES, R., PLAKSIN, I., and CAMPOS, J., 1997, "Single and Two Initiation Points of PBX", *Shock Compression of Condensed Matter-*, ed. by S. C. Schmidt *et al.*, AIP Conference Proceedings 429, NY, 1998, pp. 715-718.

[11] PLAKSIN, I., CAMPOS, J., MENDES, R., MENDONÇA, M. and GOIS, J., *"Interaction of Double Corner turning Effect in PBX", American Physics Institute, Shock Waves in Compressed Matter*, Amherst, MA, USA, 27-31 Julho, 1997. Edited by S. C. Schmidt et al., AIP Conference Proceedings 429, NY, 1998, pp. 755-758.

[12] PLAKSIN, I., CAMPOS, J., MENDES, R., RIBEIRO, J. e GÓIS, J., 1998, "Pulsing behaviour and corner turning effect in PBX" *Proceedings of the 11th Symposium (International) on Detonation*, OCNR 33300-5, Office of Naval Research, Snowmass, USA, pp. 679-685.

[13] MENDONÇA, M., PLAKSIN, I, CAMPOS, J., e GOIS, J., 1996, "Emulsion explosives with TNT", Shock Waves in Condensed Matter, St. Petersburg, Russia; *Chem. Phys. Reports*, 1998, Vol 17 (1-2), pp. 137-150.

EFFECT OF DISCONTINUOUS PHASE OF EMULSION ON THE STABILITY OF EMULSION SLURRY EXPLOSIVES

Milka Matejic Grguric

Tehnicki opitni centar, Vojvode Stepe br. 445, 11000 Belgrade, Serbia, Yugoslavia

Abstract:

Emulsion slurry explosives (ESE) are modern blasting agents. It investigated the effect of the discontinuous phase of emulsion on the stability high emulsion type water-in-oil. Discontinuous phase of emulsion is saturated water solution some inorganic salts of nitric acid (ammonia nitrate, sodium nitrate, calcium nitrate). Stability of emulsion is changed by composite and pH value of discontinuous of emulsion in course of time. Changes of stability of emulsion were measured by changes of detonation velocity and waterproof of emulsion after 1, 2, 3, 6, 12 and 18 months. It was considered that discontinuous phase had influence on stability of emulsion. With increased content of ammonium nitrate, water and pH solution salts was increased stability of emulsion.

Keywords: *explosives, commercial explosives, emulsion, heavy ANFO*

1. INTRODUCTION

Emulsion slurry explosives are high emulsion type water-in-oil with high ratio discontinuous and continuous phases. Emulsion is consisted by discontinuous phase from 80 to 95 %. Droplet of discontinuous phase is not spherical, but it is deformed. The size of droplet is in range of diameters [1]. The surface strength is great. For good stability in emulsion is added surfactants – emulsifying agents. The molecules of surfactant are arranged on interfaces and they are reduced interfacial tension with stabilization honeycomb structure of emulsion. Emulation is depended by composition of phases, ratio of discontinuous and continuous phases, type of surfactants, time and rate of mixing. This parameters effect to characteristics of emulsion slurry explosives. Density effects to characteristics of emulsion slurry explosives. In paper done effect composition of discontinuous phase on stability of emulsion slurry explosive.

2. EXPERIMENTAL

In consideration influence discontinuous phase on stability of emulsion slurry explosive is used one emulsifying agent to avoid other effect on stability of emulsion. Continuous phase is organic fuel. Fuel is mixture of hydrocarbons with more than 12-carbon atom in molecules, product of refinement naphtha like fuel, waxes and oil. In this paper continuous phase does not change to avoid other effect on stability of emulsion. Time, temperature and rate of mixing does not change because of same reason. Also density of emulsion slurry explosive does not change [2].

Discontinuous phase of emulsion is water solution some inorganic salts of nitric acid. Inorganic salts in using are ammonia nitrate, calcium nitrate and potassium nitrate. Calcium nitrate is product of reaction nitric acid on calcium carbonate. Different effect on stability

has content of water solution and ratio of two salts in composition of solution. With increase content of water, ESE is more stabile than lower content of water. It was measured conductivity water over the emulsion to detect stability of ESE. Conductivity of water was resulted dissolved inorganic salts from emulsion. It was measured also detonation velocity of ESE sensibilised with prilled ammonium nitrate.

Composition of water solution salts effects on stability and detonation characteristics modern blasting explosives – especially on emulsion explosives. In production modern emulsion explosives the most delicate operation is emulation process. Small disorder in content (composition) of water solution salts make impossible emulation. In case production emulsion explosive from commercial salts is easy made the best composition of water solution salts. It is measured ordered quantity of salts and dissolved in water. Solutions are saturated and temperature of dissolvation is high. In case production emulsion explosive from salts, product's chemical reactions nitroacid on calcium oxide or calcium carbonate, is necessary controlled content of salts in water before emulation. In products chemical reactions nitroacid on calcium oxide and calcium carbonate are calcium nitrate and ammonia nitrate and water (to 40 %) It is usually changed determined composition of water solution salts addition second salts to made desired composition water solution two salts [3]. Characteristics of using inorganic salts and water are determined in table T-1 [2].

Table 1. Physical - chemical characteristics salts and water

Numb	Characteristic	Calcium nitrate	potassium nitrate	Ammonium nitrate	Water
1.	Density, kg/m^3	1100	950	900	995
2.	Mechanical impurity, %	0,8	0,005	0,2	0
3.	Content of calcium nitrate, %	70,0	0	0	1,4
4.	Content of ammonium nitrate, %	6,0	0	99,5	
5.	Silicate and alumosilicate, %	in trace	in trace	in trace	in trace
6.	Content of iron (Fe), mg/l	2	-	-	1
7.	Content of chloride, mg/l	-	-	-	50
8.	Total rigidity, mg CaO/l	-	-	-	120
9.	Content of water, %	24,0	1,0	0,5	98,5

Emulsion is made stirring (propeller mixers) water solution salts with fuel on + 60° C. Rate of emulsification is 1000 1/min. Mixing time is 5 s. For consideration effect of content water solution salts on stability of emulsion without other influence composition of emulsion was constant. It was used same emulsifying agents, fuels, salts and water. Content of discontinuous phase was changed in two steps. First steps was changing of content of water in solution from 10 to 22 %. Second step was changing of salts. Expected change stability emulsion is attended by microscope, measuring waterproof and detonation velocity.

3. RESULTS AND DISCUSSION

To seeing structure of emulsion continual phase is colored by red paint. Emulsion is attended by microscope and cough no sight of measurable change of emulsion. Watching emulsion was not done successful photographs – all photographs are similar.

Change of emulsion stability is attended by change of waterproof of emulsion. It is measured conductivity of water over the emulsion in range from 1 day to time breaking emulsion. In Table 2 is done change of conductivity of emulsion. Emulsion was sensitized by prilled ammonium nitrate and was packed in patron diameter 65 mm. It was measured detonation velocity by Dautriche method [3].

Table 2. Effect of content of water

content of water %	detonation velocity m/s	waterproof, days			
		250Ω	200Ω	150Ω	100Ω
10	1420	-	-	12	55
14	4110	28	52	83	130
16	4085	45	53	68	90
18	4150	60	64	72	83
20	4287	107	140	178	220
22	4156	72	78	82	92

Detonation velocity does not change for range of content of water from 14 to 22 %. Lower detonation velocity show low stability of emulsion. Stability is measured by conductometric method. Conductivity of water over the emulsion depends of solubility salts from emulsion. In table 2 done waterproof for days when it is measured change from 250Ω to100Ω. Second value 100Ω was minimum for ESE with calcium nitrate and ammonium nitrate [3]. Stability of emulsion grow if content of water grow.

Effect of diferent salts in solution on caracteristics ESE done for emulsion with calcium nitrate (KN1, KN2 and KN3) and with potasium nitrate (NN1 and NN2). In Table 3 is done characteristic of ESE with different salts.

Table 3. Effect of content of different salts

Caracteristic	KN1	KN2	KN3	NN1	NN2
Content of AN,%	55	57	61	57	65
Content of KN,%	24	22	18	-	-
Content of NN,%	-	-	-	22	14
Detonantion velocity in 40 mm, m/s	4370	4100 (40 mm)	5000	4200	4580
Stability, months	3	5	6	6	18
Detonantion velocity, after temperature cycling, m/s	-	3860	4720	4100	4370

Caracteristic of ESE, like stability, are beter if content of second salt is lower until 14 %. ESE with potasium nitrate is beter than ESE with calcium nitrate [5]. It is considered that emulsion which pH value is in range from 5,5 to 7 has good stability – over the year. In Table 4 is done results of measuring waterproof of emulsion. The best stability is for pH value 6. In table 5 is done results of measuring detonation velocity and the best stability is for pH 6, to.

Table 4. Waterproof of emulsion , ohm

Time, month	pH value of emulsion							
	4,5	5	5,5	6	6,5	7	7,5	8
1 day	200	235	310	335	260	310	275	250
1	180	235	310	330	270	310	260	210
2	105	227	-	-	254	290	251	182
3	48	-	283	297	225	270	-	167
6		120	250	264	168	174	160	56
9		39	180	203	105	135	62	0
12		0	120	185	42	70	0	
18			62	105	0	0		
24			0	31				

* - 0 breaking emulsion

Table 5. Detonation velocity emulsion explosives

Time, month	pH value of emulsion							
	4,5	5	5,5	6	6,5	7	7,5	8
1 day	4155	4122	4225	4145	4201	4171	4053	4201
1	4095	-	4259	4128	-	4259	-	4182
2	3617	3992	4275	4275	4008	-	4117	4036
3	det	-	4073	4328	-	4307	4594	3997
6		4166	4307	4594	4095	4073	4032	det
9		3370	4201	4328	3611	3756	3370	
12		det	4085	4166	2780	2954	det	
18			3259	3977	det	det		
24			det	2954				

det is detonation velocity lower than 2000 m/s

4. CONCLUSION

Discontinuous phase is 90% of ESE and its characteristics effect to characteristic of ESE. If content of water in discontinuous phase grow, stability of ESE grow until 22% of water . If content of second salt in discontinuous phase is lower, stability of ESE grow until 14% of second salt. ESE with potasium nitrate is beter than ESE with calcium nitrate. It is considered that emulsion which pH value is in range from 5,5 to 7 has good stability.

REFERENCES

[1] K.Lissant: "EMULSIONS AND EMULSION TECHNOLOGY" I, MARCEL DEKKER,INC, New York, 1974

[2] M.Matejić: "Prilog proučavanju karakteristika ANFO-t eksploziva, njegovih konstituenata i mogućnosti primene u savremenoj eksploataciji u rudnicima", magistarski rad, TMF, Beograd, 1995

[3] M.Hristovski: "Eksplozivne materije rečnik", NIU Vojska, Beograd, 1994

[4] M.Matejić:"Određivanje kritičnog prečnika punjenja savremenih privrednih sredstava za miniranje", NTP, Beograd, 1996

[5] M.Matejić: "Karakteristike emulzionih slari eksploziva sa staklenim mikrobalonima", Tehnika, Beograd, 1999,

A CONTACT COMPATIBILITY INVESTIGATIONS BETWEEN SMOKELESS POWDERS AND EPOXIDE PAINT BY MEANS OF TGA, DSC THERMAL ANALYSIS AND ISOTHERMAL HEATING AT 75°C

Maciej MISZCZAK, Eugeniusz MILEWSKI, Jan SZYMANOWSKI, Jacek BORKOWSKI, Andrzej MARCZUK and Beata ŚMIGIELSKA

Research Department of Combat Means, Military Institute of Armament Technology, Wyszyńskiego 7, Str., 05-220 Zielonka, POLAND

Abstract:

In this paper there are presented investigations on contact compatibility between three types of nitrocellulose propellants and epoxide paint. Tested on contact compatibility material set up – smokeless powder / paint exists in packages used during transportation and storage of throwing materials. The tests on compatibility were done by means of differential thermogravimetry analysis (TGA) and differential scanning microcalorimetry (DSC) – both in dynamic option according to STANAG 4147 [1] and by isothermal heating at 75°C for 48 hrs due to UN method [2].

1. INTRODUCTION

In order to save high physico-chemical quality of smokeless powders, which have directly influence on keeping of combat parameters, in these – ballistic ones for ammunition in which they are applied as throwing materials and in order to ensure their safe usage ie. during transportation and storage in appropriate packages, tests on contact compatibility of above mentioned high-energetic materials with package material directly contacting with high-energetic material should be conducted. One of the basical packages, in which smokeless powders are stored, are containers covered inside by epoxide paint. So, taking into consideration above requirements, contact compatibility between smokeless nitrocellulose propellants and epoxide paint was tested. To tests on compatibility of smokeless powders with epoxide paint, three types o nitrocellulose powders were selected – two types of artillery propellants ie. 4/1 and 9/7 propellants and one fine-grain, chemically modified small arms propellant marked in the text as PMCH propellant. Compatibility of the smokeless propellants with the paint was investigated by means of TGA and DSC techniques – both in dynamic mode according to STANAG 4147 [1] and by isothermal UN method at 75°C [2,3].

2. EXPERIMENTAL RESEARCH

Description of principles of measurements and criteria on contact compatibility by means of TGA, DSC methods – both used in dynamic option and by isothermal UN method at 75°C

Compatibility testing by TGA technique is based on determination of difference expressed in mass percentage between measured mass loss of materials forming mixture, mixed at mass ratio of ca. (1/1) and calculated sum of measured mass losses separately heated materials taking into consideration their real mass parts in admixture composition. If this difference is negative or positive but less than 4% (m/m), tested materials are compatible in contact sense. If this difference is greater than 4% (m/m) and less than 20% (m/m), contact compatibility of these materials should be additionally tested by another method, advisably in kinetic option. If above mentioned difference is greater than 20% (m/m), tested materials are treated as incompatible.

Compatibility testing by DSC method is based on determination of difference between temperature corresponding to maximum of DSC peak of decomposition reaction of mixture of materials mixed in mass ratio of ca. (1/1) and temperature corresponding to DSC peak of decomposition reaction of separately heated material samples, especially high-energetic material. If this difference is positive, tested materials are compatible. If this difference (shift of DSC peaks) is negative and it is less or it equals 4°C, tested materials show also contact compatibility. If this difference is negative and it is between 4°C and 20°C, compatibility between tested materials should be additionally checked with usage of another method, advisably by kinetic one in this case it is advised DSC or dTGA method in kinetic option. The dTGA and DSC tests on compatibility in kinetic option rely on determination of kinetic parameters of the tested mixture and its components, such as activation energy (E), Arrhenius frequency factor (A) and decomposition rate constant (k) on the basis of course of TGA (dTGA) and DSC curves describing thermal decomposition (three courses of DSC and TGA (dTGA) curves for each sample) at three different rates of linear increase of heating temperature taken from the range <0,2°C/min.; 2,0°C/min.>. Advised rates of heating are 0,5°C/min., 1,0°C/min. and 2,0°C/min. For calculations of above kinetic parameters, Kissinger method is used [4].

Initial temperature of heating should equal temperature of environment or should be less at least 50°C than the temperature of appearance of an exothermal peak. If a given ingredient of an admixture causes decrease of activation energy (E) of decomposition reaction of an admixture and simultaneously causes increase of Arrhenius frequency factor (A) and decomposition rate constant (k), these ingredients are incompatible. After determination of (E) and (A) factors, decomposition rate constant (k) can be calculated from the following expression:

$$\ln k = \ln A - (E/RT)$$

where: (T) is determined constant measured temperature

(R) is universal gas constant.

Above mentioned calculations are realised under assumption that with the changes of temperature of heating, mechanism of decomposition reaction does not change. If value of decomposition rate constant (k) for admixture is significantly higher than for separately

heated its ingredients (for example 10^3 times greater), it exists high probability that tested materials are not compatible at room temperature.

- Procedure of kinetic analysis on compatibility of tested materials by TGA (dTGA) and DSC is as follows:
- Determine temperatures of maximum values for dTGA and DSC peaks for tested admixture and its ingredients at three different rates of heating – T_{1max}, T_{2max}, T_{3max}.
- Plot curve (linear course) describing dependence of $\ln(B/T^2)$ as a function of (1/T), where (B) is rate of heating expressed in K/min., (T) represents T_{1max}, T_{2max} and T_{3max} temperatures.
- Calculate activation energy (E) from slope (S) of the above linear function from the following equation:

$$E = -SR$$

- Calculate Arrhenius frequency factor (A) [min-1] according to expression:

$$A = \frac{BEe^{(E/RT)}}{RT^2}$$

- using (B) as a middle value taken from three values of heating rates.
- Calculate decomposition rate constant (k) as follows:

$$k = Ae^{(-E/RT)}$$

- Compare determined decomposition rate constants (k), Arrhenius frequency factors (A) and activation energies (E) for the tested admixture and its ingredients.

If activation energies (E) are less and Arrhenius frequency factors (A) are larger for admixture than for its high-energetic ingredient, the tested materials are incompatible.

If small differences between above compared (E) and (A) factors exist for tested admixture and for its ingredients, but decomposition rate constant (k) for admixture is greater than for its high-energetic ingredient at room temperature, tested materials are incompatible, as well.

If there are small differences between decomposition rate constants (k) and simultaneously decomposition rate constants (k) are less or equal 10, tested materials are compatible.

Compatibility test due to UN isothermal method at 75°C relies on determination of difference (R) (called "mass reactivity factor") between mass loss of tested admixture of ingredients mixed at mass ratio (1/1) and sum of mass losses of separately, isothermally heated ingredients at 75°C for 48 hrs.

Tested high-energetic materials (in this case single-base propellants) are treated as compatible with contact material (here – epoxide paint) if mass loss of admixture is less or equals 0,5% in comparison with sum of mass losses for separately thermostated ingredients.

Preparation of samples to tests on compatibility

Samples of 9/7 and 4/1 smokeless powder were grinded to from of small pieces of thickness 0,1 mm.

Samples of smokeless powder PMCH were not disintegrated.

Epoxide paint samples were prepared in from of dry powder.

Masses of individual samples of materials (ingredients) and their admixtures used to TGA and DSC analyses were in the range from 1 mg to 3 mg. In UN method at 75°C mass of each ingredient was 25 g and mass of admixture of these ingredients (1/1) [m/m] was 50 g.

Before tests on compatibility, all samples were initially dried at 50°C for 48 hrs in order to remove from them an excess quantities of volatile substances.

Apparatus

To TGA and DSC analyses, apparatus TGA-50 and DSC-50 (SHIMADZU firm – Japan) were used respectively. These thermal analysers ensure linear growth of heating at 2°C/min. in the range of temperature <20°C; 500°C>.

For samples thermostating at 75°C, VC-0020 heating chamber (HERAUS firm – Germany) was applied which is enable to keep temperature 75°C ± 1°C.

Investigations results and their discussion

Test results of contact compatibility of investigated materials by means of TGA, DSC and UN method at 75°C are presented in Tables 1 – 4 and by characteristic TGA and DSC Thermograms (Fig. 1 – 4).

Results gathered in Tables 1 – 3 and the Thermograms 1 – 6 show that nitrocellulose propellants 9/7, 4/1 and PMCH are compatible with epoxide paint due to compatibility criteria (STANAG 4147 [1]) because measured mass loss of mixture – propellant / paint is less than sum of mass losses of separately heated samples (Table 2) taking into consideration mass percentage of each ingredient in the admixture (Table 1) in the case of smokeless powders 4/1 and PMCH and in the case of 9/7 propellant mass loss of admixture propellant / paint is larger than sum of mass losses of separately heated propellant and paint samples but this sum is only larger by 0,8% (m/m) (Table 2).

Table 1. Test results on contact compatibility of nitrocellulose propellants – 4/1, PMCH and 9/7 with epoxide paint obtained by TGA in dynamic option according to STANAG 4147

Sample	Temperature of dTGA peak corresponding to the fastest mass changes of the tested sample [°C]	Mass loss of the tested sample [%(m/m)]	Temperature range of sample heating [°C]	Mass of sample or ratio of ingredients masses in the mixture sample [mg/mg]
Propellant 4/1	204,1	36,4	30,6 – 204,0	1,63
Propellant 4/1 / paint	199,5	18,2	30,3 – 199,7	1,56/1,46
Propellant PMCH	202,6	27,4	30,3 – 202,5	1,5
Propellant PMCH / paint	198,1	13,2	29,9 – 198,3	1,48/1,51
Propellant 9/7	202,5	34,1	30,0 – 202,7	1,41
Propellant 9/7 / paint	200,3	19,3	30,9 – 202,6	1,57/1,40
Paint	–	1,0	30,2 – 204,0	2,1

Table 2. Calculated (due to STANAG 4147) and measured by TGA technique in dynamic option mass losses of tested separately nitrocellulose propellants and mass losses of their mixtures with epoxide paint of compositions given in Table 1

Propellant	Calculated mass loss of propellant samples heated separately [%(m/m)]	Measured mass loss of propellant mixture with epoxide paint [%(m/m)]
Propellant 4/1	19,6	18,2
Propellant PMCH	14,1	13,2
Propellant 9/7	18,5	19,3

Table 3. Table 3. Results on contact compatibility of nitrocellulose propellants – 4/1, 9/7 and PMCH with epoxide paint, obtained by DSC technique in dynamic option according to STANAG 4147

Sample	Temperature of DSC peak of thermal decomposition [°C]	Sample mass [mg] or ratio of ingredients masses in the mixture sample [mg/mg]
Propellant 4/1	191,3	1,47
Propellant PMCH	191,1	1,50
Propellant 9/7	189,9	1,44
Propellant 4/1 / paint	191,3	1,44/1,40
Propellant PMCH / paint	190,1	1,52/1,51
Propellant 9/7 / paint	190,3	1,48/1,36

Table 4. Table 4. Tests on compatibility of nitrocellulose propellants with epoxide paint on the basis of their thermostating at 75°C for 48 hrs.

Sample name	An average mass loss of tested sample after its thermostating in relation to initial mass of the sample (ie. before its heating) [%(m/m)]	Mass reactivity factor (R) (determined in part 2.1. of this paper) [%(m/m)]
Propellant 9/7	0,81	R=0,07
Epoxide paint	0,10	
Propellant 9/7 / epoxide paint (1/1) [m/m]	0,98	
Propellant 4/1	0,77	R=0,36
Epoxide paint	0,10	
Propellant 4/1 / epoxide paint (1/1) [m/m]	1,23	
Propellant PMCH	0,79	R=0,06
Epoxide paint	0,10	
Propellant PMCH / epoxide paint (1/1) [m/m]	0,95	

According to compatibility measured by DSC, all propellant samples meet contact compatibility criteria with the paint (STANAG 4147 [1]) because: exothermal DSC peak for mixture containing 9/7 propellant is shifted to higher temperature in comparison to DSC exothermal peak for this propellant itself, DSC peak for mixture containing 4/1 propellant is not shifted in relation to DSC peak for 4/1 propellant itself and DSC peak for mixture containing PMCH propellant is shifted 1°C to lower temperatures in comparison with DSC peak of PMCH propellant (Table 3)

From results which comprises Table 4 it appears that mass reactivity factor (R) for tested materials creating binary mixtures, is distinctly less than 0,5% (m/m). So, it should be assessed that above tested materials are compatible according to UN method at 75°C.

3. CONCLUSION

Tested single-base Polish propellants – 9/7, 4/1, PMCH and epoxide paint are compatible in commercial packages used during storage and transportation.

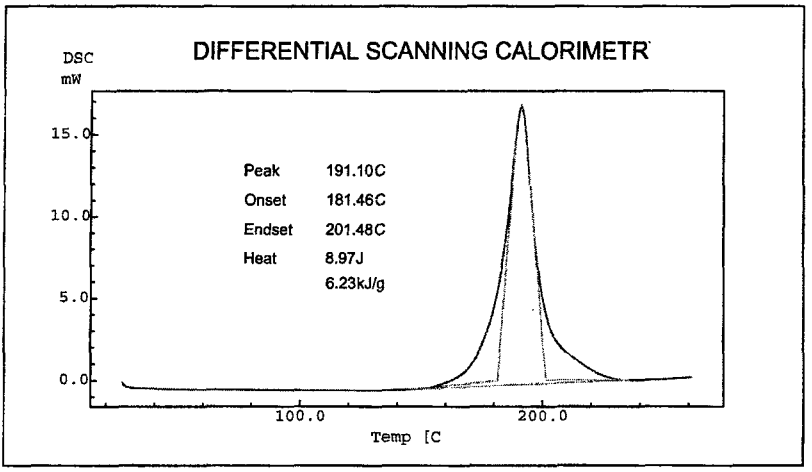
REFERENCES

[1] The NATO Standardisation Agreement (STANAG 4147), Chemical Compatibility of Ammunition Components with Explosives and Propellants (Nonnuclear Applications); draft edition 2, 1996;

[2] Norma Europejska EN 268:1991 pt. „Materiały wybuchowe do amunicji handlowej. Wymagania i metody badań";

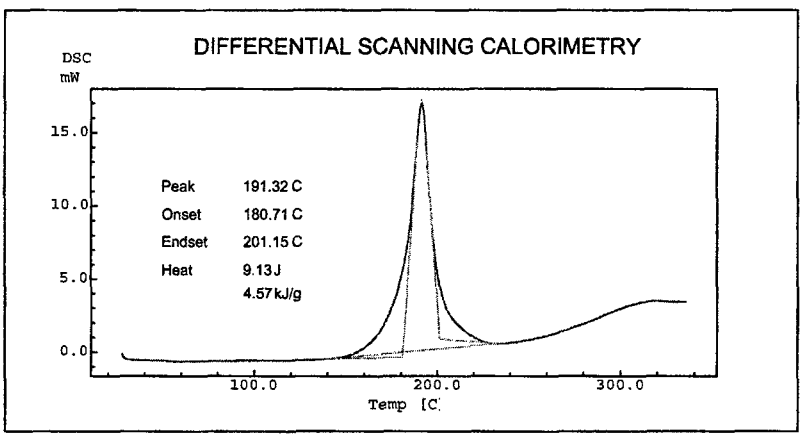
[3] Polska Norma PN-V-04011-22 pt. „Kruszące materiały wybuchowe o przeznaczeniu wojskowym. Metody badań. Oznaczanie reaktywności (zgodności kontaktowej)";

[4] H. E. Kissinger, Analytical Chem. 29, 1702 (1957).



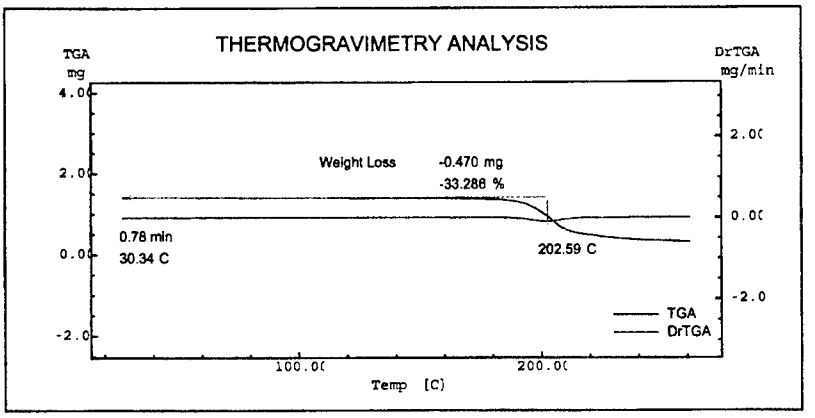
		[Temp Program]		
Detector:	DSC50	Temp Rate	Hold Temp	Hold Time
Sample Name:	055P3 PROCH NC 9-7	[C/min]	[C]	[min]
Sample Weight:	1.440[mg]	2.00	500.0	240
Cell:	Aluminum Seal			
Atmosphere:	Air			

Fig 1. DSC Thermogram in dynamic option of thermal decomposition of propellant 9/7



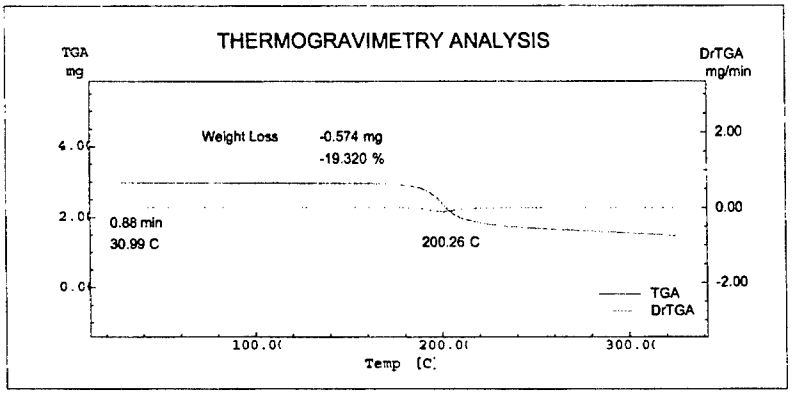
		[Temp Program]		
Detector:	DSC50	Temp Rate	Hold Temp	Hold Time
Sample Name:	055P3-P6 PROCH9-7-FARBA	[C/min]	[C]	[min]
Sample Weight:	2.000[mg]	2.00	500.0	240
Cell:	Aluminum Seal			
Atmosphere:	Air			
Annotation:	P3-P6 1,48-1,36			

Fig 2. DSC Thermogram in dynamic option of thermal decomposition of propellant 9/7 with epoxide paint



Detector:	DTG50	[Temp Program]		
Sample Name:	055P3 PROCH NC 9-7	Temp Rate	Hold Temp	Hold Time
Sample Weight:	1.412[mg]	[C/min]	[C]	[min]
Cell:	Aluminum	2.00	500.0	120
Atmosphere:	Air			

Fig 3. TGA/DTG Thermogram in dynamic option of thermal decomposition of propellant 9/7



Detector:	DTG50	[Temp Program]		
Sample Name:	055P3-P6 PROCH9-7-FARBA	Temp Rate	Hold Temp	Hold Time
Sample Weight:	2.971[mg]	[C/min]	[C]	[min]
Cell:	Aluminum	2.00	500.0	120
Atmosphere:	Air			
Annotation:	P3-P6 1,57-1,40			

Fig 4. TGA/DTG Thermogram in dynamic option of thermal decomposition of propellant 9/7 with epoxide paint

CONTACT COMPATIBILITY INVESTIGATIONS OF HIGH-ENERGETIC MATERIALS USED IN MORTAR AUGMENTING PROPELLING CHARGES

Maciej MISZCZAK, Jacek BORKOWSKI, Eugeniusz MILEWSKI, Jan SZYMANOWSKI, Andrzej MARCZUK and Beata ŚMIGIELSKA

Research Department of Combat Means, Military Institute of Armament Technology, Wyszyńskiego 7, Str., 05-220 Zielonka, POLAND

Abstract:

In this paper, investigations on contact compatibility between burning containers (made on the basis of nitrocellulose (NC)) and extruded – impregnated propellants (EI propellants) manufactured on the basis of NC and nitroglycerine (NG) forming high-energetic materials set-up in mortar augmenting charges are presented. The investigations were done for these high-energetic materials unaged and aged at 75°C for 30 days (RH ca.=50%). Compatibility measurements were done by means of Thermogravimetry Analysis (TGA), Differential Scanning Calorimetry according to STANAG 4147 and by thermostating at 75°C for 48 hrs due to UN test.

1. INTRODUCTION

During last several years problem of incompatibility of mortar propulsion systems have appeared especially for augmenting throwing charges. Mortar augmenting charges are very sensitive to changes of environmental (weather) conditions, particularly to humidity and temperature. Homogeneous throwing materials (smokeless propellants) are usually used in mortar augmenting charges i.e. double-base propellants (nitroglycerine propellants) containing ca. 40% (m/m) of nitroglycerine (NG). These propellants are most often inserted in cotton, silk, aluminum, celluloid or nitrlocellulose containers. Such propellants systems (throwing charges) have several disadvantages because under the influence of humidity, the containers become destroyed. In these high-energetic materials set-up, diffusion process of NG goes on [1]. NG migrates outside the propellant into the container. Parallel plasticizer e.g. camphor being in container escapes from it to the propellant grains. Too high content (concentration) of NG in the container causes its cracking (hightened brittleness of container material) at low temperatures, otherwise in elevated temperatures this material becomes too plastic. As a consequence, these phenomena cause decrease of ballistic parameters and simultaneously cause increase of danger of accidents appearance during usage of mortar ammunition.

Because of relatively many accidents connected with usage of mortar ammunition, above mentioned propulsion mortar system is classified as dangerous one which does not meet NATO requirements described in STANAG 4225 [2] concerning safety usage of mortar ammunition. From these reasons, works on new mortar propulsion charges (systems) were developed. These works based on change of type of propellant and container material. Replacement of nitroglycerine propellant by nitrocellulose one caused elimination of NG diffusion. Such propellant charge burns easily even at low temperature, but on the other hand

some serious disadvantages appear. Container plasticizer usually (camphor) migrates easily to nitrocellulose propellant changing distinctly its energetic and in consequence ballistic characteristics. Very often single-base propellant has too low energy to ensure complete burning of the container. Only partly burning of the container material often causes closure of mortar muzzle which can lead to muzzle destroying while firing next round. Moreover nitrocellulose propellant is very hygroscopic. This propellant absorbing humidity too strong decreases its ballistic and energetic parameters. From above observations it results that propellants characterized by high content of NG or without it do not meet usage requirements related to mortar throwing charges. To avoid above mentioned disadvantages caused first of all by too high level of masses exchange between the propellant and the container in mortar augmenting propulsive charge, various barriers in form of layer isolating propellant from container were applied, for example polymeric ones [3]. Other research works were undertaken to manufacture new type of propellant combined itself advantages of nitroglycerine propellants and nitrocellulose ones, characterized by diminished NG diffusion outside the propellant grain. This way, technology of manufacturing of EI-propellants was carried out. Such type of propellant has diminished content of NG.

In order to save high physico-chemical quality of EI-propellants and burning containers which have directly influence on keeping of combat parameters, in these – ballistic ones for mortar ammunition in which they are applied as throwing materials forming propulsive augmenting charges and in order to ensure their safe usage i.e. during transportation and storage, tests on contact compatibility of above mentioned high-energetic materials should be conducted.

Compatibility investigations were done for high-energetic materials unaged and aged at 75°C for 30 days (RH ca.=50%). Compatibility measurements were done according to STANAG 4147 [4] by means of Thermogravimetry Analysis (TGA), Differential Scanning Calorimetry and according to UN method by thermostating at 75°C for 48 hrs [5,6].

2. EXPERIMENTAL RESEARCH

2.1. Description of principles of measurements and criteria on contact compatibility by means of TGA, DSC methods – both used in dynamic option and by isothermal UN method at 75°C

Compatibility testing by TGA technique is based on determination of difference expressed in mass percentage between measured mass loss of materials forming mixture, mixed at mass ratio of ca. (1/1) and calculated sum of measured mass losses separately heated materials taking into consideration their real mass parts in admixture composition. If this difference is negative or positive but less than 4% (m/m), tested materials are compatible in contact sense. If this difference is greater than 4% (m/m) and less than 20% (m/m), contact compatibility of these materials should be additionally tested by another method, advisably in kinetic option. If above mentioned difference is greater than 20% (m/m), tested materials are treated as incompatible.

Compatibility testing by DSC method is based on determination of difference between temperature corresponding to maximum of DSC peak of decomposition reaction of mixture of materials mixed in mass ratio of ca. (1/1) and temperature corresponding to DSC peak of decomposition reaction of separately heated material samples. If this difference is positive, tested materials are compatible. If this difference (shift of DSC peaks) is negative and it is less or it equals 4°C, tested materials show also contact compatibility. If this difference is

negative and it is between 4°C and 20°C, compatibility between tested materials should be additionally checked with usage of another method, advisably by kinetic one in this case it is advised DSC or TGA method in kinetic option.

Compatibility test due to UN isothermal method at 75°C relies on determination of difference (R) (called "mass reactivity factor") between mass loss of tested admixture of ingredients mixed at mass ratio (1/1) and sum of mass losses of separately, isothermally heated ingredients at 75°C for 48 hrs.

Tested high-energetic materials are treated as compatible if mass loss of admixture is less or equals 0.5% in comparison with sum of mass losses for separately thermostated ingredients.

2.2. Samples of high-energetic materials

There were selected three types of EI-propellants and one type of burning container. These three types of EI-propellants originate from different concentration of NG in them. They are marked as EI-7, EI-12 and EI-16 because of NG mass concentration which was in them 7.60%, 12.60% and 16.45% respectively. Burning container was made of nitrocellulose (NC) and cellulose-acrylic fibers felted by polymeric binder – polyvinyl acetate. Application of varied NG concentration in EI-propellants came from a need to investigate influence of NG content on physico-chemical properties of propulsive charges type EI-propellant/burning container. Modules of mortar augmenting charges were consisted of ca. 10 g of EI-propellant which was inserted into the burning container of mass ca. 2 g.

2.3. Samples preparation

EI-propellants were not grinded, but burning containers were disintegrated to form of small pieces of size ca. 0.1 mm.

Masses of individual samples of materials (ingredients) and their admixtures of mass ratio ca. (1/1) used to TGA and DSC analyses according to STANAG 4147 [4] were in the range from 1 mg to 3 mg. In UN method at 75°C [5,6] mass of each ingredient was 25 g and mass of admixture of these ingredients (1/1) [m/m] was 50 g.

Before tests on compatibility, all samples were initially dried at 50°C for 48 hrs in order to remove from them an excess quantities of volatile substances.

2.4. Apparatus

To TGA and DSC analyses, apparatus TGA-50 and DSC-50 (SHIMADZU firm – Japan) were used respectively. These thermal analyzers ensure linear growth of heating at 2°C/min in the range of temperature <20°C; 500°C>.

For samples thermostating at 75°C, VC-0020 heating chamber (HERAUS firm – Germany) was applied which is enable to keep temperature of 75°C ± 1°C.

2.5. Investigations results and their discussion

Test results of contact compatibility of investigated materials by means of TGA, DSC and UN method at 75°C are presented in Tables 1 – 4.

Results gathered Tables 1 – 4 show that EI-propellants are compatible with burning containers due to compatibility criteria of STANAG 4147 [4] and UN test method at 75°C [5,6] because: determined by TGA technique reactivity factors (STANAG 4147) for unaged and aged EI-propellants and burning containers were negative (Table 2), determined by DSC technique temperature shifts of DSC peaks of mixtures type EI-propellant/burning container in relation to EI-propellants were positive (Table 3) and calculated reactivity factors for UN test were negative (Table 4).

Above mentioned reactivity factors, their signs (positive or negative) show that unaged and aged mixtures type EI-propellant/burning container are more stable than unaged and aged EI-propellants. From comparisons of temperatures of thermal decompositions abtained by DSC (Table 3) it results that burning container plays role as stabilizing agent in relation to EI-propellant and otherwise NG of EI-propellant is destabilizing substance in tested samples. Aged burning containers showed a little bit less thermal stability and aged EI-propellants showed more stability in comparison with their unaged samples respectively (opposite shifts of DSC peaks for EI-propellants and burning containers). A reason of mutually opposite changes (tendencies) in stability of burning containers and EI-propellants during their ageing comes from migration of NG from EI-propellant to burning container and thermal decomposition of NG.

Table 1. Measured and calculated due to STANAG 4147 [4] by means of TGA technique in dynamic option i.e. at the rate of heating increase of 2°C/min and in the range of heating temperatures from 30°C to temperature corresponding to extremum of derivative curve, mass losses of individual and mixed (1/1)[m/m] unaged and aged at 75°C for 30 days EI-propellants, burning containers and their mixtures

Sample	An average mass depletion of unaged samples [%(m/m)]	An average mass depletion of aged samples [%(m/m)]
EI-7 propellant	37.1	36.1
EI-12 propellant	32.5	33.3
EI-16 propellant	39.1	37.6
Burning container	27.2	27.7
EI-7 propellant/burning container	31.2	30.6
EI-12 propellant/burning container	29.5	27.7
EI-16 propellant/burning container	31.8	30.0

Table 2. Reactivity factor determined according to STANAG 4147 [4] by means of TGA techniques in dynamic option i.e. at the rate of heating increase of 2°C/min and in the range of heating temperatures from 30°C to temperature corresponding to extremum of derivative curve, on the basis of results from Table 1, expressing compatibility of EI-propellants with burning containers and which equals difference between mass depletion of mixture and a sum of mass depletions of individual (separately heated) ingredients taking into consideration their content in the mixture

Set-up of materials	Reactivity factor for compatibility between EI-propellants and burning containers [%(m/m)]
Unaged EI-7 propellant/unaged burning container	-0.95
Unaged EI-12 propellant/unaged burning container	-0.35
Unaged EI-16 propellant/unaged burning container	-1.35
Aged EI-7 propellant/aged burning container	-1.30
Aged EI-12 propellant/aged burning container	-2.80
Aged EI-16 propellant/aged burning container	-2.65

Table 3. Results on contact compatibility for unaged and aged EI-propellants, burning containers and their mixtures due to DSC test in dynamic option i.e. at the heating rate of 2°C/min, based on measured temperatures of decomposition reaction corresponding to DSC peak maximum

Sample	An average temperature of DSC peak of decomposition reaction for unaged samples [°C]	An average temperature of DSC peak of decomposition reaction for aged samples [°C]	An average shift of temperatures of DSC peaks of decomposition of mixtures in relation to temperature of DSC peaks of decomposition of EI-propellants [°C]	
			Unaged samples	Aged samples
EI-7 propellant	179.4	187.4	–	–
EI-12 propellant	182.8	186.3	–	–
EI-16 propellant	183.6	185.5	–	–
Burning container	190.4	189.8	–	–
EI-7 propellant/burning container	189.0	187.5	9.6	0.1
EI-12 propellant/burning container	186.3	187.8	3.5	1.5
EI-16 propellant/burning container	190.7	192.1	7.1	6.6

Table 4. Results on compatibility of unaged and aged at 75°C for 30 days EI-propellants, burning containers and their mixtures according to UN test based on thermostating of the samples at 75°C for 48 hrs [5,6]

Sample	An average mass depletion of unaged sample after its thermostating at 75°C for 48 hrs in relation to initial mass of the sample (i.e. before its thermostating) [%(m/m)]	An average mass depletion of aged sample after its thermostating at 75°C for 48 hrs in relation to initial mass of the sample (i.e. before its thermostating) [%(m/m)]	Reactivity factor between material of EI-propellant and burning container material determined as a result of subtraction of mass loss of EI-propellant/burning container admixture and sum of mass losses of its ingredients during their separate heating under UN test conditions [%(m/m)]	
			Unaged samples	Aged samples
EI-7 propellant	0.85	0.53	–	–
EI-12 propellant	0.99	0.62	–	–
EI-16 propellant	1.19	0.80	–	–
Burning container	0.09	0.15	–	–
EI-7 propellant/burning container	0.37	0.25	-0.57	-0.43
EI-12 propellant/burning container	0.45	0.32	-0.63	-0.45
EI-16 propellant/burning container	0.53	0.41	-0.75	-0.54

3. CONCLUSIONS

Tested unaged and aged EI-propellants and burning containers creating mortar augmenting propulsive charges show high compatibility. NG of EI-propellant diminishes thermal stability of set-up type EI-propellant/burning container. In contrary burning container plays role as stabilizing material (construction material) of this set-up.

REFERENCES

[1] B. BrÖnnimann et.al., Symp. Chem. Probl. Connected Stab. Explos. (Proc.) 1992, 9 th, 215;

[2] The NATO Standarization Agreement (STANAG No. 4225). "The Safety Evaluation of Mortar Bombs";

[3] H. Schalkwyk, I. M. Venter, C. F. van Vuren, NIXT Int. Workshop on Research and Development in the Explosives Industry (Proc.) Pretoria, RSA, 1996, 21;

[4] The NATO Standardisation Agreement (STANAG 4147), Chemical Compatibility of Ammunition Components with Explosives and Propellants (Nonnuclear Applications); draft edition 2, 1996;

[5] Norma Europejska EN 268:1991 pt. „Materiały wybuchowe do amunicji handlowej. Wymagania i metody badań";

[6] Polska Norma PN-V-04011-22 pt. „Kruszące materiały wybuchowe o przeznaczeniu wojskowym. Metody badań. Oznaczanie reaktywności (zgodności kontaktowej)";

IRON OXIDE/ALUMINUM FAST THERMITE REACTION USING NITRATE ADITIVES

Joel Morgado*, Luisa Durães, José Campos* and António Portugal****

Laboratory of Energetics and Detonics
* Mech. and Chem.** Eng. Departments - Fac. of Sciences and Technology
University of Coimbra - Polo II – 3030 Coimbra - PORTUGAL

Abstract

Reaction between iron oxide (Fe_2O_3) and aluminum (Al) is the reference of the classic thermite compositions. Ignition of those thermite compositions is recognized to be problematic and the regression rates are commonly low. The selection of an additive binder, based in ammonium or potassium nitrates, in small concentrations, generate a different global ignition phase, because the reaction between these additives and part of the existing aluminium generates enough energy that helps ignition and further reaction propagation between iron oxide and aluminium.
These experimental thermodynamic conditions are also predicted using THOR thermochemical code. THOR code assumes the thermodynamic equilibria of all possible products, for the minimum Gibbs free energy, using H_L EoS. The code allows the possibility of estimating pyrolysis decomposition of additives, as a function of absorbed energy or as a function of final temperature in adiabatic conditions. The global reaction, predicted for isobar adiabatic conditions can then be correlated to the preceding decomposition results. The presented predictions prove not only the contribution of additives in global reaction but also the significant influence of transition phase from gas to solid of formed Al_2O_3.
The experimental study was performed mixing the original composition, based on Fe_2O_3/Al mixture, with a small percent (< 10 %) of propellant binder composed of ammonium and sodium nitrates (AN/SN), mixed with Paraffin. The reaction velocity is evaluated by the adimensional regression rate as a function of the adimensional time. When the ignition of AN/SN additives occurs, Tb decreases significantly - this effect with the expansion of combustion products gases show 5% to be the best AN/SN additives concentration with the most stable tested combustion.

1. INTRODUCTION

Exothermic reactions between a metal and a metal oxide (thermite) and reactions of combustion of metals (metal oxidation reactions) are known sources of energy production and high temperature generators. Many compositions are proposed and calculated in bibliography (1). Ignition of those thermite compositions is recognized to be problematic and the regression rates of its self-sustained reactions are commonly low. The ignition can be performed using a thermal impulse from explosion, hot wire, exploding bridge wire or any semiconductor bridge igniter, or even laser or shock initiation. The influence of final state of products, being solid (condensed) or gas, or the energetic contribution from its transition, during the end of combustion, releasing energy to the local environmental products, is very important to understand the real mechanism of reaction (2).

Reaction between iron oxide (Fe_2O_3) and aluminum (Al) is the reference of the classic thermite compositions. The products are, for a stoechiometric composition with an ideal

reaction, alumina (Al_2O_3) and iron. Also the efficiency of the reaction, for a given initial composition of Fe_2O_3 and Al, is evaluated by the achieved final temperature and by the mass ratio of Al_2O_3 /AlO in combustion products. The selection of an additive, like ammonium or potassium nitrates, in small concentrations, can contribute for this combustion process. The products of combustion and pyrolysis of this additive, reacting with thermite combustible reactant and products, generating high temperature conditions, allow an easier ignition and faster propagation (3). The advantages of using ammonium nitrate come from its stable behaviour, no toxicity, and production of water included in the products of combustion. The advantage of using potassium nitrate comes also from its thermal stability, its oxidiser capability and continuous thermal decomposition.

Consequently our base composition is formed of stoechiometric aluminium/iron oxide, or an over aluminised composition, with ammonium and potassium nitrates as main additives.

2. THEORETICAL PREDICTIONS

The existing reactions in pyrolysis or combustion, generating intermediary chemical species and compounds, are very hard to follow by experiments, because these processes are very fast or proceed with increasing pressure and temperature. The studies concerning theoretical prediction of the probable pathways of pyrolisis or thermal decomposition of energetic materials are not numerous.

The method of predicting final composition of combustion products, as a function of temperature and pressure, uses a thermochemical computer code, named THOR. This predicting code is based on theoretical work of Heuzé et al. (4), (5), later modified by Durães et al. (6), (7). The final composition is estimated for all the possible compounds, as a function of temperature and pressure, for the minimum Gibbs free energy at thermodynamic equilibrium. In THOR code, several equations of state may be used, namely Perfect Gas, Boltzmann, BKW, H_9, H_{12} and H_L. The validation of these EoS has been presented in previous works (Durães et al. (6), (7)). H_9 and H_{12} EoS are the natural development of a Boltzmann EoS type, with similar results to the BKW, KHT and JCZ3 EoS (Tanaka (8), Chaiken (9), Heuzé (5) and Campos (10)). H_L EoS (Durães et al., (6), (7)) is supported by a Boltzmann EoS ($PV/RT=\sigma(V,T,X_i)$, being $\sigma=1+x+0.625x^2+0.287x^3-0.093x^4+0.014x^5$ with $x(V,T,X_i)=\Omega/VT^{3/\alpha}$ and $\Omega=\Sigma(X_i\omega_i)$), but based now on physical intermolecular potential of gas components instead of correlations from final experimental results. This EoS takes $\alpha=13.5$ to the exponent of the intermolecular potential and $\theta=1.4$ to the adimensional temperature. Obtained results prove the importance of calculated products composition and the influence of $\Gamma=dH/dU)_S$ value (Brown (11)). The chemical equilibrium equations and validation have also been presented in previous works (Durães et al. (12), (13)). The energetic equation of state is related to the internal energy $E=\Sigma(x_i e_i(T)+\Delta e)$, $e_i(T)$ being calculated from JANAF Thermochemical Tables (14) and polynomial expressions of Gordon and McBride (15).

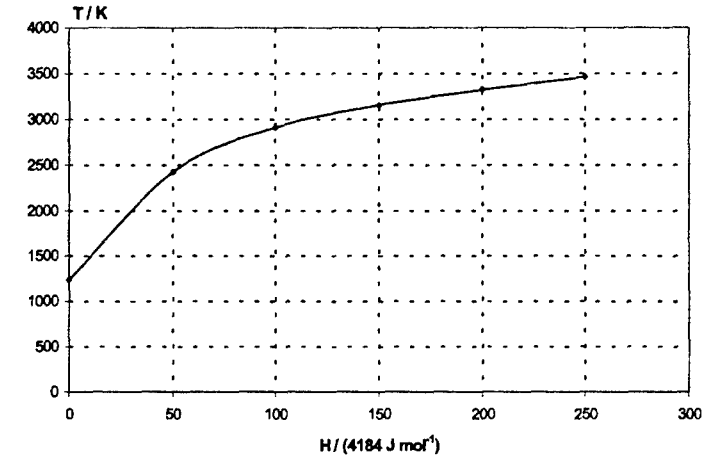
The Gordon-McBride's coefficients for the considered products, including solid or condensed materials, were obtained from the coefficients presented in a more recent form of Gordon-McBride's polynomials (16) by the following method: assuming $\frac{C_p}{R}=\frac{b_1}{T^2}+\frac{b_2}{T}+b_3+b_4\cdot T+b_5\cdot T^2+b_6\cdot T^3+b_7\cdot T^4=I(T)$ (recent form of Gordon-McBride's polynomials (16) with known coefficients), and

$\frac{C_p}{R} = a_1 + a_2 \cdot T + a_3 \cdot T^2 + a_4 \cdot T^3 + a_5 \cdot T^4 = F(T)$ (original form (15) of Gordon-McBride's polynomials with unknown coefficients), it is possible to calculate the a_i coefficients from the b_i coefficients, calculating the function $G(a_1, a_2, a_3, a_4, a_5) = \int_{i_1}^{i_2} [\delta(T)]^2 dT$, assuming $\delta(T) = F(T) - I(T)$, and $[i_1, i_2]$ as the interval where the approximation is needed (to measure the distance between these two polynomials). When the function $G(a_i)$ is minimised, allowing the calculation of a_i, the condition $\frac{\partial G}{\partial a_i} = 0$ is verified. The used Gordon-McBride's coefficients are only valid in the 1000-6000 K range temperature.

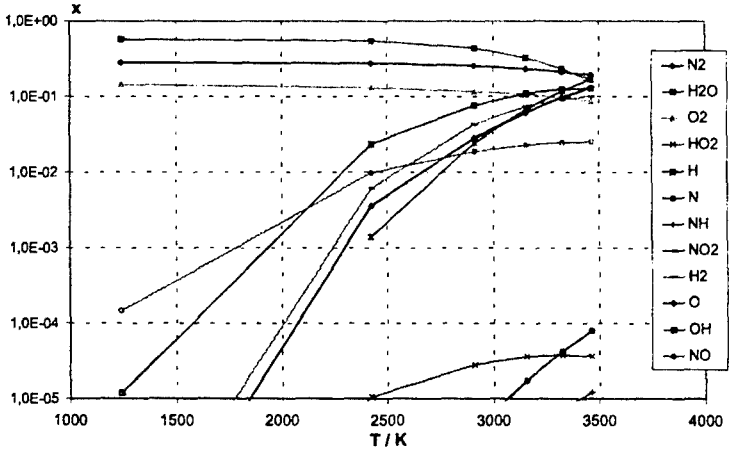
The decomposition or reaction regimes of energetic materials are assumed as global adiabatic processes (Durães (12), (13)) - the isobar adiabatic combustion verifies equal initial and final total enthalpy $H_b^{Tb} = H_O^{To}$. The reaction path has been explained (17), starting from one initial reactive composition A to the final products composition C. If this reactive initial composition A decomposes in an intermediary composition B, and this composition B decomposes in final products composition C, the reactions can be presented in a simple way like: $A \rightarrow C$, being $A \rightarrow B$ and $B \rightarrow C$. At isobar combustion regime, the total enthalpy released by any reaction is converted to increase the temperature of the products of reactions. Assuming the preceding reaction scheme, from the initial temperature T_0, to the final temperatures T_b, T_b', T_b'', respectively, it can be written, for the total enthalpy: $H_A^{T0} = H_C^{Tb}$; $H_A^{T0} = H_B^{Tb'}$ and $H_B^{T0} = H_C^{Tb''}$. The preceding equations are equivalent to $H_A^{T0} - H_C^{T0} = -\Delta H_{A-C}^{T0} = H_C^{Tb} - H_C^{T0}$, $H_A^{T0} - H_B^{T0} = -\Delta H_{A-B}^{T0} = H_B^{Tb'} - H_B^{T0}$ and $H_B^{T0} - H_C^{T0} = -\Delta H_{B-C}^{T0} = H_C^{Tb''} - H_C^{T0}$. So, $\Delta H_{A-B}^{T0} + \Delta H_{B-C}^{T0} = H_C^{T0} - H_A^{T0} = \Delta H_{A-C}^{T0}$. Then, if the reaction is incomplete, the intermediary final products are B, and $\Delta H_{A-B}^{T0} = \Delta H_{A-C}^{T0} - \Delta H_{B-C}^{T0} = H_C^{Tb''} - H_C^{Tb}$. Obtaining the theoretical results of reactions A-C and B-C, the necessary data to calculate ΔH_{A-B}^{T0} is then obtained.

In a similar way the decomposition of an energetic material can be predicted adding a ΔH to its enthalpy of formation, and verifying the calculated value of isobar adiabatic temperature.

The application of preceding scheme allows to predict the thermal decomposition of ammonium and sodium nitrates (Figures 1 and 2), where it can be seen the influence of temperature and absorbed energy on the composition of pyrolysis products.

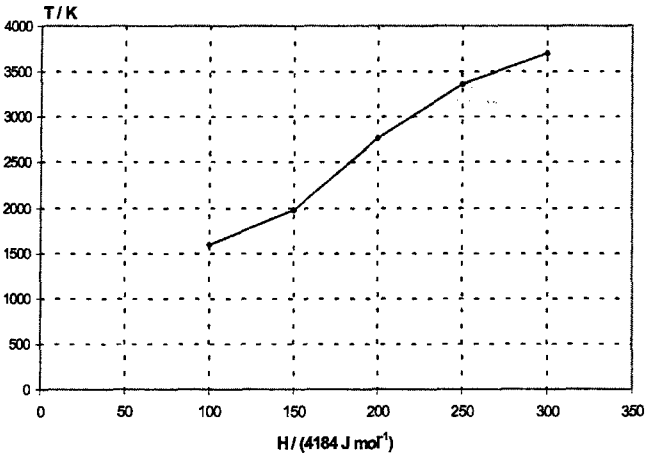


(a)

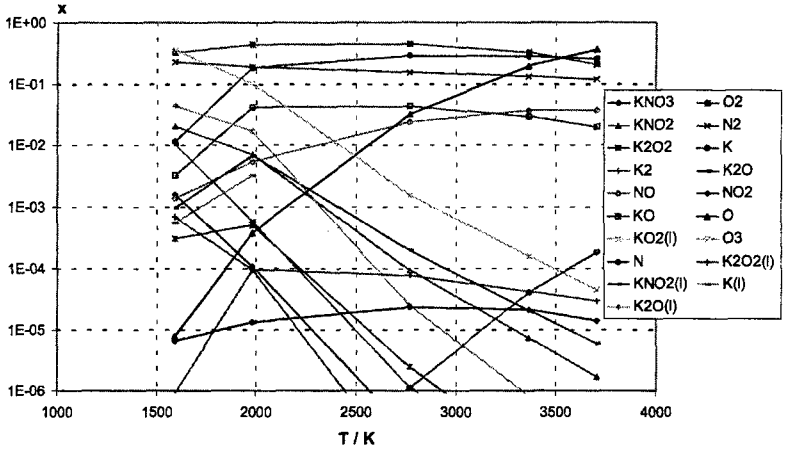


(b)

Fig 1. Theoretical prediction of (a) temperature and (b) products composition of the thermal decomposition of Ammonium Nitrate.



(a)



(b)

Fig 2. Theoretical prediction of (a) temperature and (b) products composition of the thermal decomposition of Potassium Nitrate.

Products composition and attained temperatures of isobar adiabatic combustion of selected additives and aluminium (Figures 3 to 4) show clearly the influence o concentration of aluminium and the influence of thermal decomposition products of additives on the reaction.

The global combustion of aluminium and iron oxide can be predicted for stoechiometric concentrations of Al e Fe_2O_3, corresponding to a mass ratio of 25/75 %, or for over-aluminised compositions, corresponding to ratio of 30/70 %.

Consequently it can be added 0, 2.5 and 5 % (in mass) of additives to the Al/ Fe_2O_3 reference compositions.

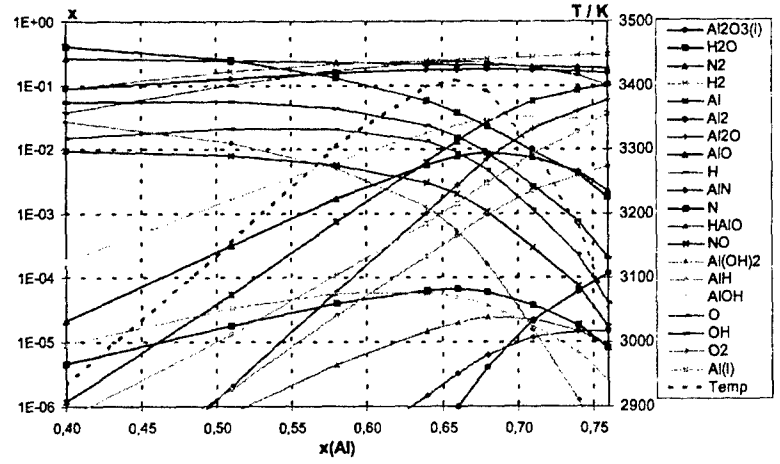


Fig 3. Theoretical prediction of combustion products temperature and composition of Ammonium Nitrate / Aluminum.

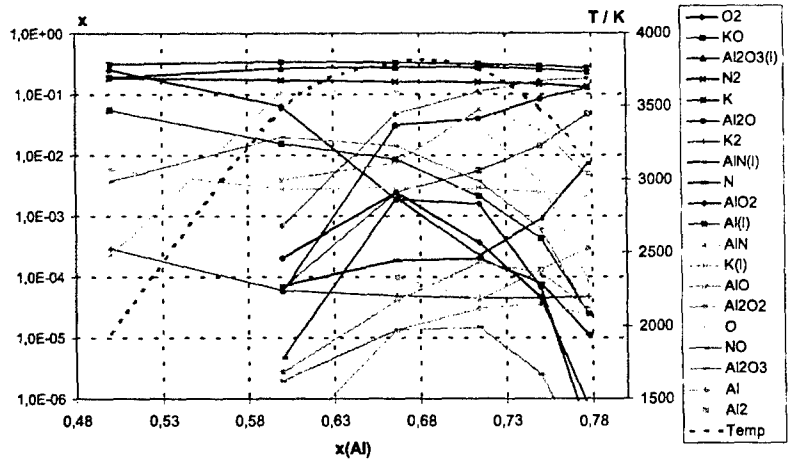


Fig 4. Theoretical prediction of combustion products temperature and composition of Potassium Nitrate / Aluminum.

The presented results in Figures 5 to 8 show clearly the influence of the two kinds of additives. The theoretical prediction, assuming only gas products corresponds to the local combustion reaction. However, the prediction assuming only gas products do not can generate enough energy to progress the reaction (the adiabatic combustion temperature is very low). Consequently in these reactions it is very important the contribution of gas/solid transition of formed Al_2O_3 on energy released to fresh materials, allowing a more effective and stable progression of reaction.

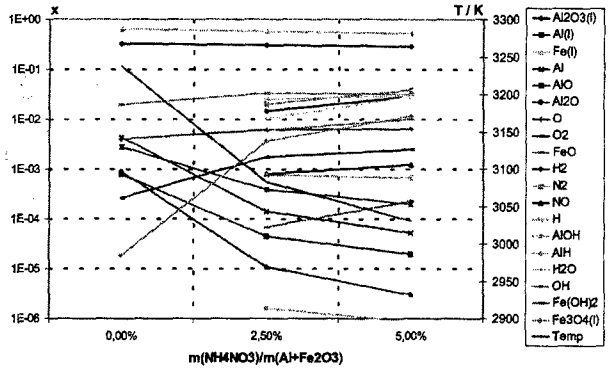


Fig 5. Theoretical prediction of combustion products temperature and composition of Fe_2O_3 / Al (75/25 % w/w) with NH_4NO_3 additive.

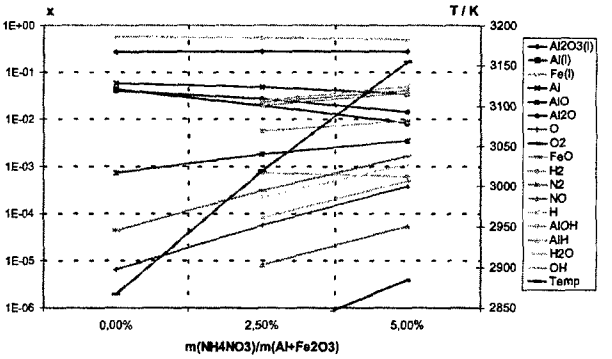


Fig 6. Theoretical prediction of combustion products temperature and composition of Fe_2O_3 / Al (70/30 % w/w) with NH_4NO_3 additive.

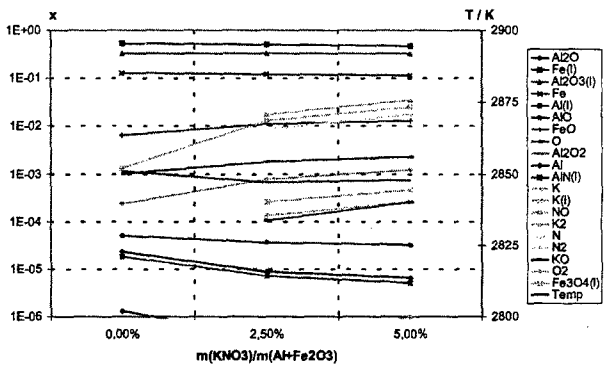


Fig 7. Theoretical prediction of combustion products temperature and composition of Fe_2O_3 / Al (75/25 %w/w) with KNO_3 additive.

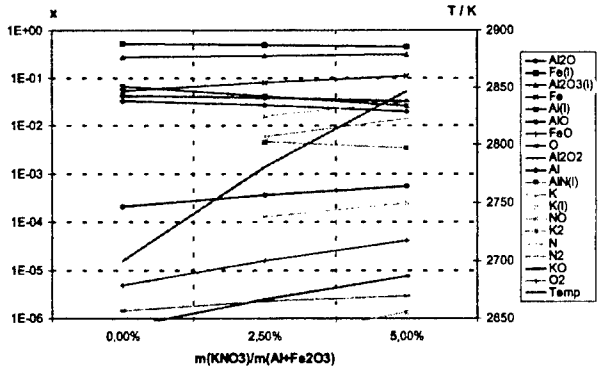


Fig 8. Theoretical prediction of combustion products temperature and composition of Fe_2O_3 / Al (70/30 % w/w) with KNO_3 additive.

3. EXPERIMENTAL STUDY

Components caracterization

Table 1 presents the physical main properties of the main reactants Fe_2O_3 and Al. The evaluation of particle sizes, densities and surface areas was done using Laser Diffraction Spectrometry (Coulter LS 130), Helium Pycnometry (Accupyc 1330) and Nitrogen Gas Adsorption (ASAP 2000), respectively. Additionally, Figures 9 and 10 show reactants size distributions.

Purity data was based on fabricant reports. Mössbauer Spectroscopy studies revealed that the only phase present in Fe_2O_3 is Hematite (α-Fe_2O_3). The aluminium particles melting point was measured as 660°C by Differential Scanning Calorimetry, the same value as for pure aluminium. These facts may indicate purity levels better than those indicated in the table below.

Table 1. Reactants physical properties.

	Particle size, d_{50} and d_{90}-d_{10} (μm)	Density, ρ (kg m^{-3})	BET surface area, A_s (m^2 kg^{-1})	Purity (%)
Fe_2O_3 (Bayer Bayferrox 180)	1.6 3.4 – 0.9	5.06 x 10^3	3149	96-97
Al (Carob - Al black)	19.5 80.1 – 3.2	2.70 x 10^3	4475	89.3

The selected additives, NH_4NO_3 (Hydro - Nitrate d'Amonnium Poreux AG) and KNO_3 (Carob – Nitrato Potásico Origen Tarragona), were triturated during 5 minutes, to reduce particles sizes. Their purities are >99.5% and >93.4% respectively.

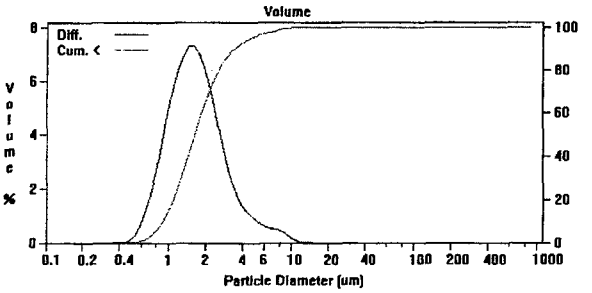


Fig 9. Fe_2O_3 (Bayer Bayferrox 180) size distributions obtained by Laser Diffraction Spectrometry.

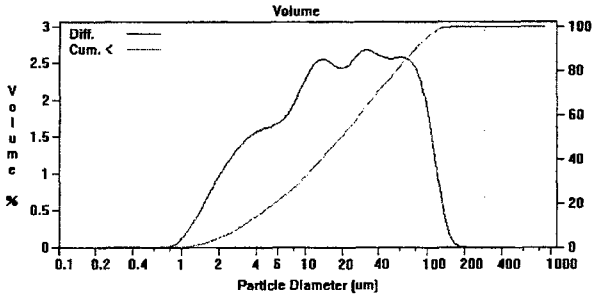


Fig 10. Aluminium (Carob) size distributions obtained by Laser Diffraction Spectrometry.

The Ammonium Nitrate_is a crystalline white solid, colourless, very hygroscope and highly water-soluble. It is usually used as prills due to his strong water affinity. This component shows five different physical solid sate phases in the temperature range –18°C to +125°C. The AN used in this work was tested by DCS/TGA techniques, presented in previous works, proving that we are in presence of a phase stabilized ammonium nitrate (PSAN). In order to stabilise the mixtures using Ammonium Nitrate (AN) as additive, in the tested experimental compositions it was added to AN 10 % (in mass) of Sodium Nitrate. It is a crystalline white solid, colourless, very hygroscope and highly water-soluble. SN produces a characteristic yellow flame due to the presence of Na chemical element. This salt melts at 306.8 °C and decomposes at 380 °C, releasing oxygen and converting into nitrite. SN is also usually used as prills due to his strong water affinity. Prills of AN and SN were mixed in the constant ratio of 86% AN to 14% SN (as it was explained before). Then, they were reduced together to a fine powder, which can be seen in the picture b) - Figure 11.

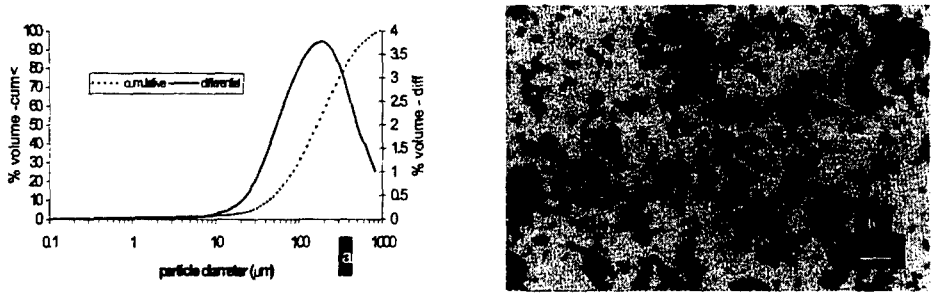


Fig 11. Granulometric curves (a) and optic microscope picture (b) from the AN/SN crystal mixture.

In order to optimise particle size distribution of AN and to promote these salts diffusion into the main particles it was used, in mixtures preparation, the N,N-dimethyl-formamide (DMFA) as solvent. Solubility tests were made previously with DMFA and other solvent candidates, such as ethanol and methanol. DMFA presented better solubility results for both AN and SN: 63g AN / 100g DMFA and 15.8 g SN /100g DMFA at 60°C. It was observed an interesting result from these solubility tests, which was the re-crystallization of AN and SN (when the DMFA solutions cool to the room temperature). In fact, the new crystals have the needle appearance, that can be seen in Figure 12, and no morphology changes were then observed, even during months, to light exposure.

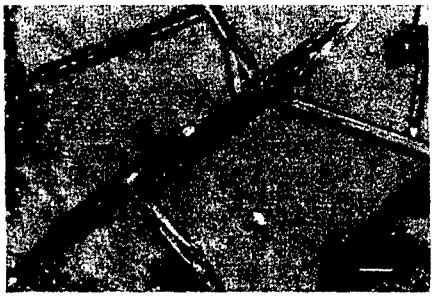


Fig 12. AN crystals from re-crystallization of AN/DMFA solution, obtained by temperature reduction from 60°C to room temperature.

The final additive binder composition was completed mixing the nitrate particles with paraffin.

Experimental compositions.

The main reactants thermophysical properties of components of mixtures and its experimental compositions are presented in Tables 2 and 3.

Table 2. Reactants thermophysical properties.

Reactant	Formula	ρ^o (kg m^{-3})	ΔH^o_f (kcal mol^{-1})	Cp^o (kcal mol^{-1} K^{-1})
Iron (III) Oxide	Fe_2O_3	5240	-197.3	24.8
Aluminum	Al	2702	0	5.8
Ammonium Nitrate	NH_4NO_3	1720	-87.3	32.9
Sodium Nitrate	$NaNO_3$	2261	-111.8	21.8
Paraffin	$C_{18}H_{38}$	777	135.9	135.1

Note: The superscript (o) refers to the reference state, 298.15 K and 101325 Pa.

Table 3. Reactant mixtures compositions and densities.

Reactant mixtures	Mass compositions (% w/w) Fe_2O_3, Al, $C_{18}H_{38}$, NH_4NO_3, $NaNO_3$	ρ(TMD) (kg m^{-3})	Air added (% w/w)	ρ(exp) (kg m^{-3})
TA1/TA2	75 + 23.5 + 1.5 + 0 + 0	4009	0.03	1957
TA3/TA4	71.25 + 22.325 + 1.425 + 4.5 + 0.5	3769		1864
TA5/TA6	67.5 + 21.15 + 1.35 + 9 + 1	3556		1900
TB1/TB2	70 + 28.2 + 1.8 + 0 + 0	3829	0.03	1902
TB3/TB4	66.5 + 26.79 + 1.71 + 4.5 + 0.5	3618		1851
TB5/TB6	63 + 25.38 + 1.62 + 9 + 1	3427		1785

Experimental set-up and results.

The used experimental apparatus (Figure 13) allows the:

- *Temperature recording and thermal determination of regression velocities.* It was used two Cr/Al thermocouples (Thermocoax TKI 10/10/NN), shown in Figure 13, connected to a digital signal analyser (Tektronix TDS 320);
- *Mass loss recording, as a function of time (gravimetric analysis).* It was used a digital 0.001g precision balance (Mettler), connected to a data acquisition system;
- *Video-crono-photography.* It was used a video camera of 50 fps and second time resolution, recording directing the flame front from a reflecting mirror, in order to get the upper plan of the flame combustion with the minimum optical deformation.



Fig 13. Experimental apparatus and sample.

The ignition procedure was performed by flame transmission from a igniting mixture formed by black powder and used thermite, with mass proportions of of 44/56 % . It was verified that the ignition by flame transmission is more difficult for thermite with 0% of AN/SN additives.The thermocouple and mass regression records, performed as a function of time, (Figure 14) allows the evaluation of velocity of reaction from the velocity of mass regression (Vfm) and from the mean velocity (Vft) obtained from thermocouples signals.

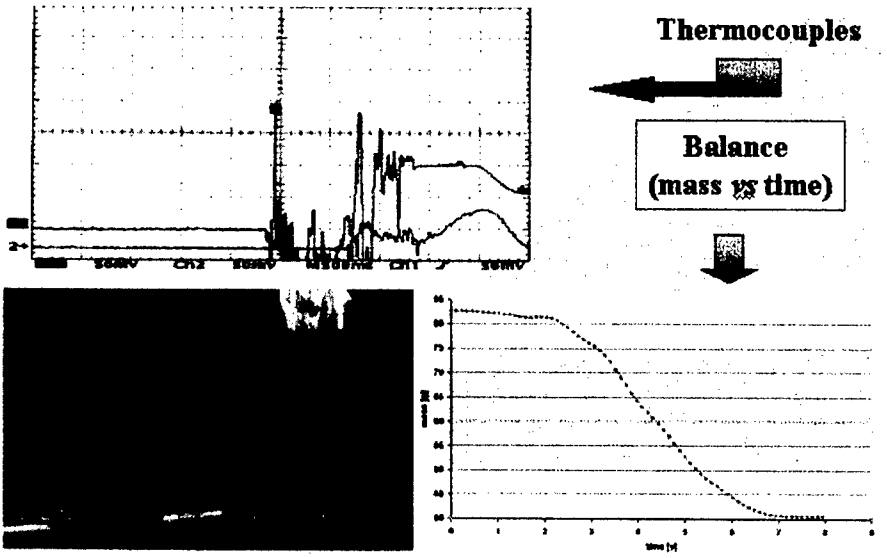


Fig 14. The thermocouple and mass regression direct records.

The obtained results, presented in Figure 15, allow by the expression [$(m_0-m) /(m_0-m_{final})$ *vs* $(t_{final}- t) /(t_{final} - t_0)$] the calculation of the adimensional regression rate, as a function of the adimensional time, presented in Figure 16 for the tested compositions.

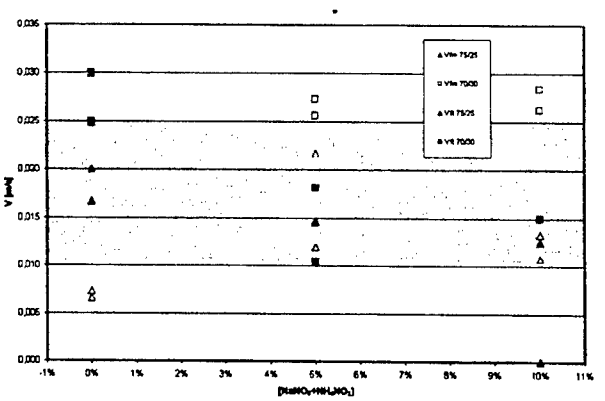


Fig 15. Velocity of mass regression (Vfm) and mean velocity (Vft) from thermocouples signals, as a function of additives concentration.

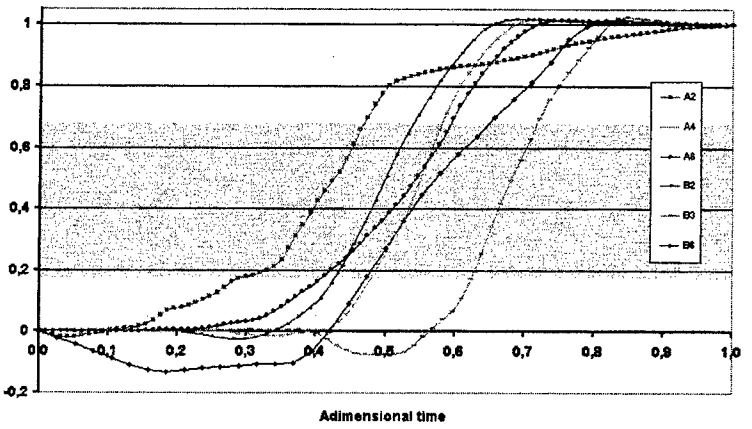


Fig 16. Adimensional regression rate, as a function of the adimensional time for tested compositions.

It was tested compositions with 10% of additives, i. e. the double concentration of the maximum predicted using THOR Code. It was verified that when the ignition of the 10% of AN/SN additives occurs, Tb decreases significantly and sometimes, by the expansion of combustion products gases, thermite reaction (between Fe_2O_3 and Al) is not completely achieved. This effect of the expansion of combustion products gases show 5% to be the best AN/SN additives concentration with the most stable combustion.

It was also experimentally verified that low density of samples generates many gas products. However the combustion presents many significant flame oscillations and fluctuations, increased when the additives concentration is increased.

Frolov combustion model (2) seems to be observed:

- the final measured temperature is very high and many used thermocouples were fused at the end of experiments;
- -the combustion scheme seems to be Fe2O3(s) + Al (s) ==» Fe (s) + Al(g) + AlO (g) + Al2O (g) ==» Fe (s) + Al2O3 (s)
- final transition phase from gas to solid of Al2O3 seems to be important to an effective reaction.

Future experiments will be performed using potassium nitrate as additive material.

4. CONCLUSIONS

Iron oxide – aluminum (thermite reactants) and nitrates as additives prove to be an excellent composition for high temperature fast gas generators. Thor predictions are in a very good agreement with observed combustion scheme. The code allows the possibility of estimating pyrolysis decomposition of additives, as a function of absorbed energy or as a function of final temperature in adiabatic conditions. The global reaction, predicted for isobar adiabatic conditions can then be correlated to the preceding decomposition results.

The presented predictions prove not only the contribution of additives in global reaction but also the significant influence of transition phase from gas to solid of formed Al_2O_3.

The experimental study was performed mixing the original composition, based on Fe_2O_3/Al mixture, with a small percent (< 10 %) of propellant binder composed of ammonium and sodium nitrates, mixed with a paraffin solution. The effect of the expansion of combustion products gases show 5% to be the best AN/SN additives concentration with the most stable tested combustion.

REFERENCES

[1] Fisher, S. H. and Grublelich, M. C., "Theoretical energy release of thermites, intermetallics and combustible metals", *Procedings of the 24th International Pyrotechnics Seminar*, IPS – USA, pp. 231-286, 1998.

[2] Frolov, Yu., "Some phenomenological aspects of heterogeneous condensed systems combustion", *Procedings of the 24th International Pyrotechnics Seminar*, IPS – USA, pp. 287-300, 1998.

[3] Foote, J. P., et al., "*Combustion of aluminium with steam for underwater propulsion*", in "*Advances in chemical propulsion*", edited by Roy, G., CRC Press, Washington, pp. 133-146, 2002,

[4] Heuzé, O. et al., "The Equations of State of Detonation Products and Their Incorporation into the Quatuor Code", *Proc. of the 8th Symposium (International.) on Detonation*, Albuquerque, New Mexico, pp. 762-769, (1985).

[5] Heuzé O., *Cálculo Numérico das Propriedades das Misturas Gasosas em Equilíbrio Termodinâmico*, Universidade de Coimbra, Portugal, (1989).

[6] Durães, L. et al., "New Equation of State for the Detonation Products of Explosives." *Proc. of 1995 APS Topical Conference on Shock Compression of Condensed Matter,* Seattle, WA, USA, pp. 385-388, (1995).

[7] Durães, L. et al., "Deflagration and Detonation Predictions Using a New Equation of State", *Proc. of the 26th International Annual Conference of ICT*, pp. 67.1-13, (1995).

[8] Tanaka, K., "Detonation Properties of Condensed Explosives Computed Using the Kihara-Hikita-Tanaka Equation of State", *Report from National Chemical Laboratory for Industry*, Ibaraki, Japan, (1983).

[9] Chaiken, R. et al., "Toxic Fumes From Explosives: Ammonium Nitrate - Fuel Oil Mixtures", *Report of Investigation n° 7867 - Pittsburgh Mining and Safety Research Center*, Pittsburgh, PA, U.S.A., (1974).

[10] Campos, J., "Thermodynamic Calculation of Solid and Gas Combustion Pollutants Using Different Equations of State", P*roc. of 1st International Conference on Combustion Technologies for a Clean Environment,* Vilamoura, Algarve, Portugal, pp. 30.4-1-30.4-11, (1991).

[11] Brown, W. B., "Sensitivities of Adiabatic and Gruneisen Gammas to Errors in Molecular Properties of Detonation Products, *Proc. of the 9th Symposium (International) on Detonation*, Portland, Oregon, pp. 513-524, (1989).

[12] Durães, L. et al., "Thermal Decomposition of Energetic Materials Using THOR Code", *Proc. of the Twenty Second International Pyrotechnics Seminar*, Fort Collins, Colorado, pp. 497-508, (1996).

[13] Durães, L. et al., "Combustion and Detonation Modeling Using THOR Code", *Proc. of the 28th International Annual Conference of ICT*, pp. 89.1-89.10, (1997).

[14] Janaf, *Thermochemical Tables*, 2nd Edition, National Bureau of Standards, Washington DC., (1971).

[15] Gordon, S., McBride, B.J., "Computer Program for Calculation of Complex Chemical Equilibrium Compositions, Rocket Performance Incident and Reflected Shocks and Chapman-Jouguet Detonations", *Report NASA SP 273*, NASA Lewis Research Center, (1971).

[16] Gordon, S., McBride, B.J., "Computer Program for Calculation of Complex Chemical Equilibrium Compositions and Aplications",I and II, *Report NASA SP 1311*, NASA Lewis Research Center, (1984).

[17] Durães, L. et al., "Thermodynamical Prediction of Combustion and detonation properties using modified thor code", to be published in *Proc. of 2000 APS Topical Conference on Shock Compression of Condensed Matter,* Grand Junction, USA.

INFLUENCE OF TESTING CONDITIONS ON RESULTS OF DYNAMIC MECHANICAL ANALYSIS OF DOUBLE BASE ROCKET PROPELLANTS

Sanja Matečić Mušanić, Muhamed Sućeska and Bakija Sanko

Brodarski institut – Marine Research & Special Technologies
Av. V. Holjevca 20, 10020 Zagreb, Croatia

Abstract:

Dynamic mechanical analysis (DMA) is a powerful technique for determination of mechanical properties of rocket propellants. This technique enables determination of the storage and loss modulus of a propellant against time, temperature or frequency of an oscillation load, while the temperature of the sample in a specified atmosphere is programmed.

However, like many other thermal methods DMA gives results that may depend greatly on the conditions used during the experiment. Thus, it is very important to use such experimental parameters that will minimise the error caused by the dynamic nature of the experiment, sample dimensions, etc.

In this work we have studied influence of heating rate, frequency, and length to thickness ratio on results of dynamic mechanical analysis. The results obtained have shown that the experimental parameters may have significant influence on values of the viscoelastic function for double base propellant.

1. INTRODUCTION

According to their chemical composition double base rocket propellants are mixtures of nitrocellulose, liquid organic nitrates, nitroaromates, other plasticisers, stabilisers, inorganic catalyst, and other compounds. By their structural characteristics they belong to the group of viscoelastic polymeric materials.

A complete characterisation of any energetic material aimed for military use requires knowing the material behaviour in the temperature range of possible operational use. Chemical reactions and physical processes that may take place during the storage of propellant may cause significant changes of a number of propellants properties, including their mechanical properties. The instability is caused mainly by the decomposition of organic nitrates to nitrogen oxides. Significant changes of mechanical properties of double base rocket propellants also can rise as a result of light up condition (stress and strain caused by fast increase of pressure, rocket fly, acceleration, rotation), condition of storage (temperature, moisture) or preparation condition (chemical stress caused by the polymerisation). All these changes in the propellant properties may affect ballistic performances of a rocket motor in such extent that an accidental explosion may occur at the ignition phase [1].

The dynamic mechanical analysis (DMA) is a very powerful technique, which allows determination of mechanical properties (modulus end damping), detection of molecular motions (transitions), and evaluation of morphology relationships (crystallinity, molecular weight, crosslinking, etc) [2,3]. In this experimental technique the storage and loss modulus of the sample, under oscillating load, can be monitored against time, temperature or frequency of oscillation while the temperature of the sample in a specified atmosphere is programmed [2,3].

However, like other thermal methods DMA gives results that may depend significantly on the conditions used during the experiment: heating rate, sample dimension, surrounding atmosphere, frequency of deformation, etc [2,4,5]. Influence of individual experimental parameters generally is known – e.g. higher heating rates causes greater thermal lags, surrounding gas having higher thermal conductivity enables higher heat transfer to the sample, etc [2]. In order to measure the dynamic mechanical properties of rocket propellants more precisely, the influence of individual experimental parameters should be known, i.e. experimentally determined very accurately. Also, it is essential, whenever DMA experiment is reported, that the precise conditions used are included in the report. A comparison of results should only be made when they are obtained under the same experimental conditions.

In this paper we have studied influence of heating rate, frequency, and length to thickness ratio on the results of dynamic mechanical analysis – the storage modulus, loss modulus, damping (tan δ), glass transition temperature, etc.

2. EXPERIMENTAL

The experiments are curried out using double base rocket propellant having the following chemical composition: 58,82 % nitrocellulose (12,62 % of nitrogen), 36,54 % of diglykoldinitrate, 2,34 % of centralite I, and 3.14 % of other additives. Testing samples used in the study, being of rectangular shape (40 x 10 x 3 mm), were cut from the propellant block.

All dynamic mechanical measurements were carried out on *TA Instruments* DMA, Model 983. Measuring conditions were:

- heating rate: 1, 2, 5 and 10°C/min
- frequency of an oscillatory load: 0.5, 1, 5, 7 and 10 Hz
- length to thickness ratio: from 10 to 35
- temperature range: -120°C to +80°C
- amplitude of deformation: ± 0.2 mm

3. RESULTS AND DISCUSSION

DMA parameters of tested double base propellant, obtained with 2 °C/min heating rate, 0.2 mm oscillation amplitude, and 1 Hz frequency, are shown in Figure 1. The result is typical for double base propellant – the storage modulus is almost constant till about -70 °C, when a slow drop take place with temperature as a consequence of the glass transition. Another distinct change in the storage modulus slope is visible at about 30 °C, corresponding to the propellant sample softening.

The maximum of the loss modulus at –53.22 °C is taken to be the glass transition temperature. The tan δ also increases at the glass transition region, as well as at the softening region.

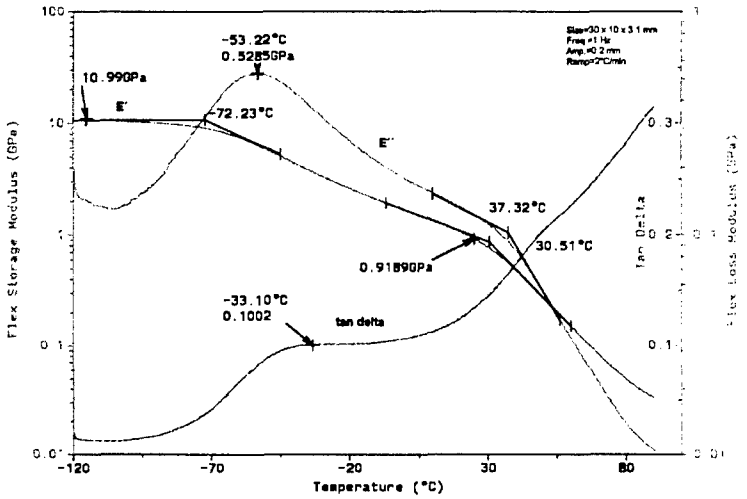


Fig 1. Storage modulus, loss modulus, and tan δ profiles for double base rocket propellant

The reproducibility of determination of the viscoelastic properties of double base rocket propellants by DMA analyser was tested at the room temperature using rectangular samples having dimensions: 30 x 10 x 3 mm. The results of five measurements are given in Table 1.

Table 1. Reproducibility in determination of some viscoelastic functions of double base rocket propellants

Number of measurement	Storage modulus (E'), MPa	Loss modulus (E''), MPa	tan δ
1	735.8	113.6	0.1543
2	720.9	110.0	0.1526
3	720.4	110.2	0.1529
4	687.8	111.5	0.1622
5	704.6	109.2	0.1550
Mean value	**713.9 ± 2.56 %**	**110.9 ± 1.55 %**	**0.1554 ± 2.51 %**

It follows from Table 1 that the viscoelastic functions of double base rocket propellants can be measured by DMA 983 instrument by the error less than 2.5 %.

3.1. Influence of length to thickness ratio

The clamping arrangement of DMA 983 imposes a cantilever-like deformation of the samples. This deformation can be described as consisting of two components: a flexural contribution and a shear deformation contribution. Normally, DMA 983 operates either with long thin samples in a (almost pure) flexural bending deformation, or with short thin samples in a (almost pure) shear deformation. The equations used to calculate the complex modulus are based on the fundamental theoretical relationships in the DMA module, which are combining the results of equations that describe the physical instrument with parameters derived from viscoelestic beam-bending theory. These equations were derived to account for the contribution of instrument calibration constants to sample modulus. However, the calculations are complicated by the fact that the instrument correction terms are dependent on modulus of the sample tested.

The general equations handle deformation modes ranging from pure flexural bending to pure shear, and all combinations between. Typical geometry for measuring the properties of relatively stiff materials is long thin sample. Length to thickness ratio (L/T) typically is greater than ten, and often reaches fifty or more for very stiff materials. At a commonly used L/T ratio of ten the error in determining the flexural storage modulus is less than 5%. The error drops to 1% at $L/T = 20$ where deformation mode is virtually pure flexural [3].

On the contrary, DMA can be used to perform pure shear experiment on soft rubbery materials by using a short thick sample. The error in measuring the shear storage modulus is less than 1% at $L/T < 0.2$.

Because of that, it is of great importance to determine, for each individual double base propellants, the correction term which takes into account variations in L/T ratio. In this paper we have performed experiments using rectangular propellant samples having 9.4 mm in width, 2.5 mm thickness, and 15 to 30 mm in length. That means that the L/T ratio is varied from 6 to 12. The experiments were performed at the room temperature applying fixed frequency of 1 Hz. The results obtained are given in Figures 2, 3 and 4.

It is visible from Figure 2 that the storage modulus varies from 645.7 to 620.7 MPa (about 20 MPa, or ~ 4%) if L/T varies from 5.9 to 12. The extrapolated value of the storage modulus at $L/T = 20$ (almost pure flexural deformation) equals 589.7 MPa, while the extrapolated value of the storage modulus at $L/T = 0.2$ (almost shear deformation) equals 669.6 MPa. It means that the storage modulus value at $L/T = 10$ includes almost 50 % of shear, and 50 % of flexural deformation contribution.

Similarly, at L/T in the range 5.8 – 12 the tan δ varies for about 4%, while the loss modulus varies about 2%. The above stated results confirm the great influence of sample dimensions on the results obtained. Thus, in it necessary to find out the correction term which takes into account various L/T ratios for each individual propellant.

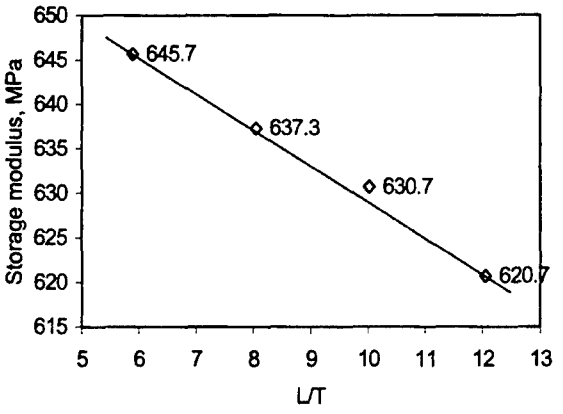


Fig 2. Storage modulus *vs.* length to thickness ratio at frequency 1 Hz and room temperature

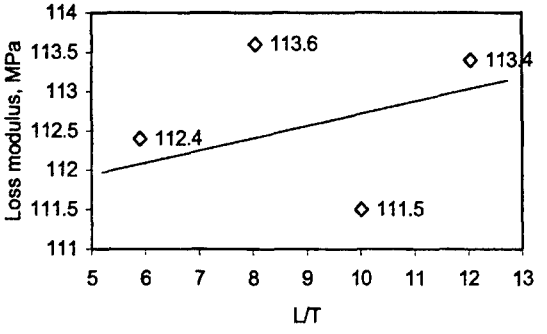


Fig 3. Loss modulus *vs.* length to thickness ratio at frequency 1 Hz and room temperature

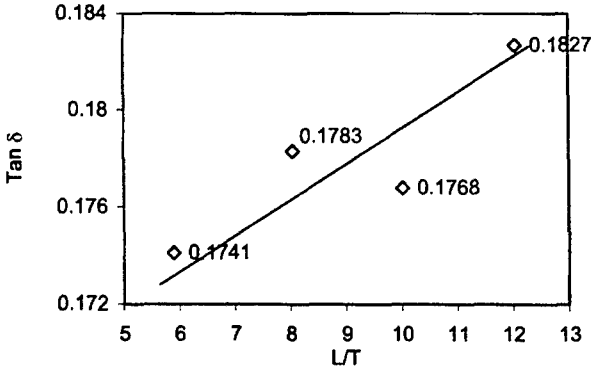


Fig 4. Tan δ *vs.* length to thickness ratio at frequency 1 Hz and room temperature

3.2. Influence of heating rate

The influence of heating rate on results of thermal methods is well known. The heat transfer from the furnace to the sample is not instantaneous, but depend on the conduction, convection and radiation that can occur within the DMA instrument. There is bound to be a thermal lag between different parts of the instrument, and the higher the rate of heating, the greater this lag is likely to be.

To test influence of heating rate on results of DMA analysis of selected double base propellant we have performed several experiments at different heating rates (1, 2, 5 and 10°C/min) using propellant samples being of rectangular bar shape (30 x 10x 3 mm). The experiments are run under flexural deformation at a fixed frequency of 1 Hz.

The results obtained are given in Table 2 and Figures 5, 6 and 7.

Table 2. The glass transition temperature, onset temperature, flexural storage and loss modulus, and tan δ at heating rates 1, 2, 5 and 10°C/min.

	Heating rate (β), °C/min			
	1	2	5	10
Glass transition temp., °C	-56.97	-53.22	-45.19	-41.41
Onset temperature, °C	-74.56	-72.23	-63.43	-60.09
E' at -115 °C, GPa	9.949	10.99	8.763	8.707
E' at 25 °C, GPa	0.7562	0.9189	1.078	1.161
E" at glass transition temp., GP	0.4720	0.5285	0.4461	0.4098
Tan δ at max.	0.10	0.10	0.10	0.10

From Figures 5, 6 and 7 it is visible that $E' - T$, $E'' - T$ and $tan\ \delta - T$ curves shift to higher temperatures with the increase in heating rate. The values of individual viscoelastic functions at the glass transition region do not change significantly with heating rate change (Table 2), while the shift of the curves to higher temperatures causes significant changes of some properties. For example, the glass transition temperature changes from –56.97 °C at the heating rate of 1 °C/min to –41.41 °C at the heating rate of 10 °C/min; i.e. for about 15 °C (Figures 6 and 8).

Also, Figure 8 shows that there is an linear relationship between $\ln(\beta)$-$1/T_g$ in the range 1–10 °C/min heating rates.

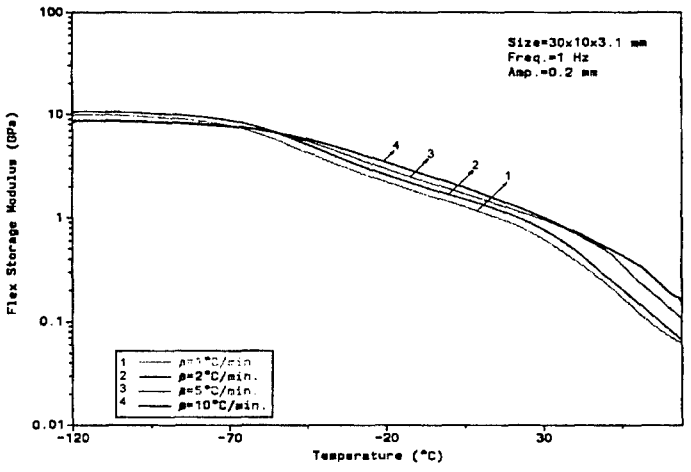


Fig 5. Flexural storage modulus *vs.* temperature at 1, 2, 5 and 10°C/min heating rates

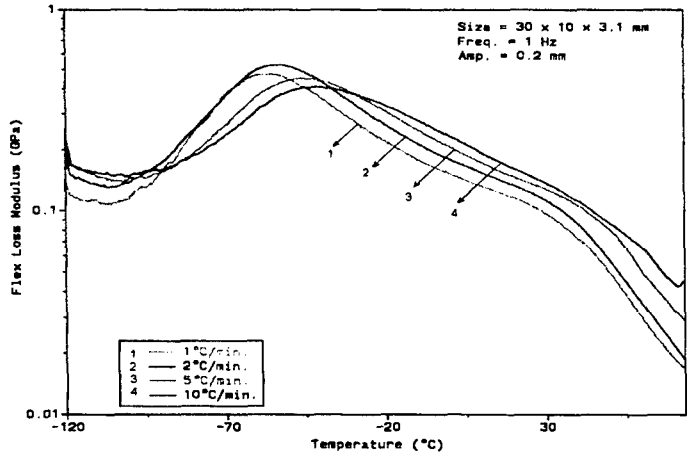


Fig 6. Flexural loss modulus *vs.* temperature at 1, 2, 5 and 10°C/min heating rates

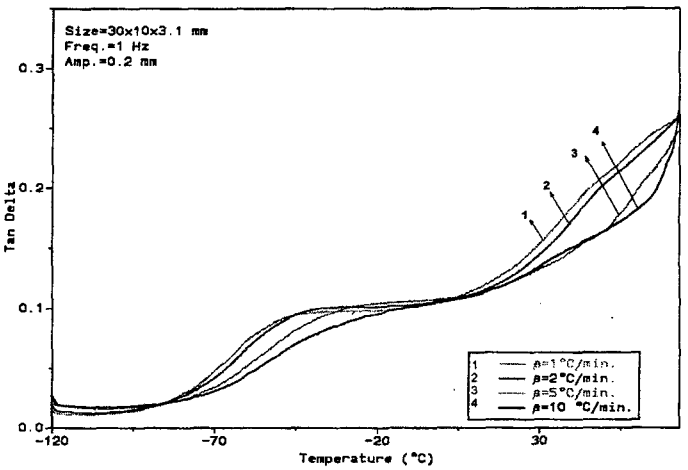


Fig 7. Tan δ *vs.* temperature at 1, 2, 5 and 10°C/min heating rates

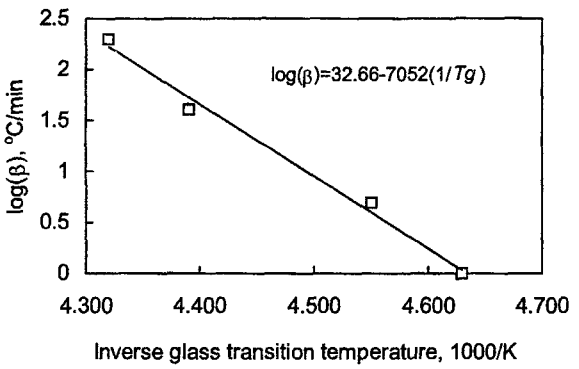


Fig 8. Glass transition temperature–heating rate relationship

3.3. Influence of frequency

The influence of frequency on DMA results is analysed under flexural deformation at a fixed frequency of 0.5, 1, 5, 7 and 10 Hz, and a heating rate of 5°C/min. The propellant samples were in form of rectangular bars 30 x 10x 3 mm. The influence of frequency on storage modulus, loss modulus, and tan δ, is illustrated in Figures 9, 10 and 11, and Table 3.

The influence of frequency on results of DMA analysis manifests mostly in shifting DMA curves to higher temperatures with increase of frequency (i.e. the rate) of deformations. According to the time-temperature superposition principle (equivalency) an increase in frequency has the same effect on the measured viscoelastic property as an decrease in temperature or decrease in time. It should be noted that such experiments might be used for the evaluation of the shift factor by applying the time-temperature superposition principle.

Table 3. Glass transition temperature, onset temperature, storage modulus, and tan δ for frequency 0.5, 1, 5, 7 and 10 Hz.

	Frequency, Hz				
	0.5	1	5	7	10
Glass transition temp., °C	-47.47	-45.19	-40.75	-39.94	-39.24
Onset temperature, °C	-62.57	-63.43	-59.45	-57.22	-60.03
E' at -115 °C, GPa	9.014	8.763	9.279	8.894	9.045
E' at 25 °C, GPa	1.144	1.078	1.237	1.186	1.181
E'' at glass transition temp., GP	0.4720	0.4461	0.4720	0.4654	0.4278
Tan δ at maximum	0.10	0.10	0.10	0.10	0.11

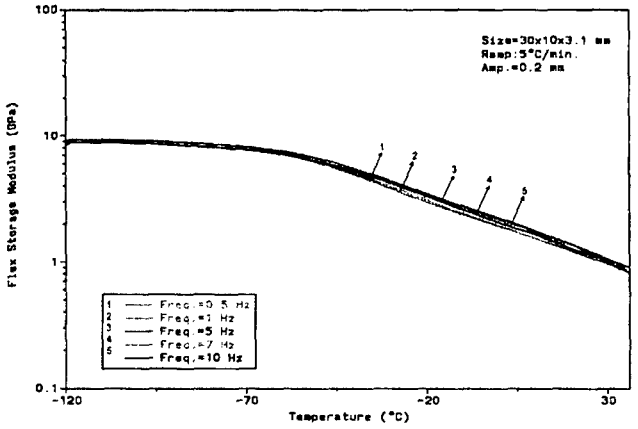


Fig 9. Storage modulus *vs.* temperature at 0.5, 1, 5, 7 and 10 Hz frequencies

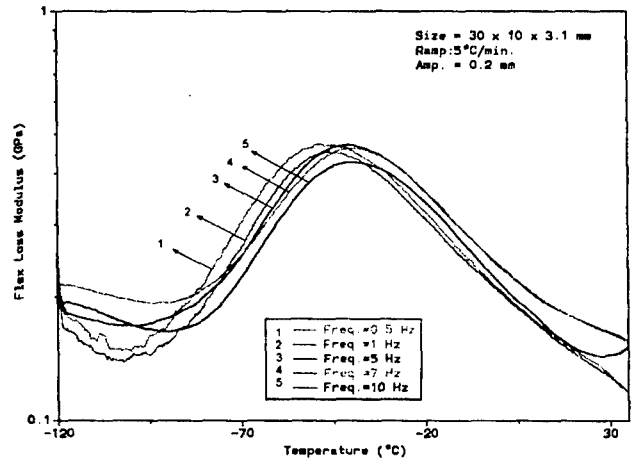


Fig 10. Loss modulus *vs.* temperature at 0.5, 1, 5, 7 and 10 Hz frequencies

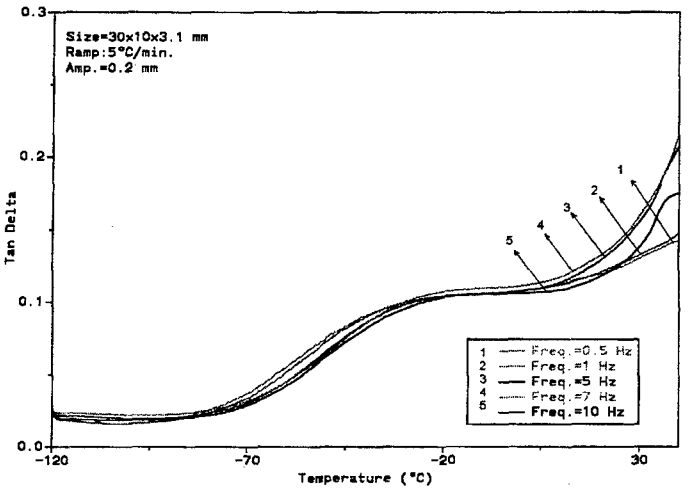


Fig 11. Tangent δ *vs.* temperature at 0.5, 1, 5, 7 and 10 Hz frequencies

T. Murayama [6] has stated that the dissipation factor (tan δ) and loss modulus (E'') go through a maximum at a temperature that increases with frequency. This behaviour can be illustrated by a model having single relaxation time. According to this model the following relationship between glass transition temperature and frequency may be deduced [6]:

$$\ln(f) = \frac{E}{R}\frac{1}{T_g} \tag{1}$$

where: f – frequency, E – activation energy, T_g – glass transition temperature, and R – gas constant. This equation suggests that the shift in the glass transition temperature is dependent on the activation energy.

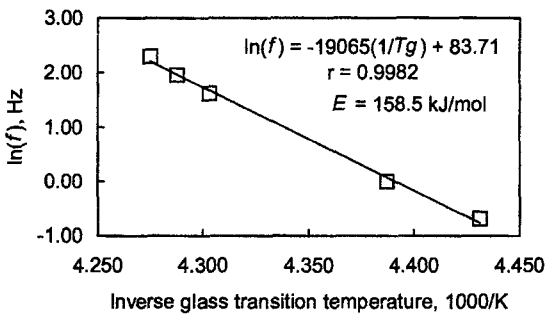


Fig 12. Glass transition temperature–frequency relationship

It follows from Figure 12 and Eq. 1 that an increase in frequency for factor of 10 causes increase in the glass transition temperature for factor of 6.2 °C. For most polymers the glass transition temperature increases about 7 °C for tenfold increase in frequency.

4. CONCLUSIONS

The results presented in this work have confirmed that experimental parameters, such as sample dimensions (length to thickness ratio), frequency of deformation, heating rate, may have significant influence on DMA results.

It is shown that, under identical experimental conditions, the storage modulus, loss modulus, and tan δ may be determined with the error less than 2.5 %.

Sample dimensions, i.e. length to thickness ratio has significant influence on the DMA results – in the range $5.8 < L/T < 12$ value of the storage modulus may vary for about 4 %. Thus, it is necessary to take into account correction term for the L/T ratio variations.

The temperature corresponding to the loss modulus maximum commonly is taken to be the glass transition temperature. For tested double base propellant it may vary from –56,97 °C to –39.24 °C, depending on the heating rate and frequency of oscillatory deformations.

An increase in heating rate or in frequency shifts DMA curves to higher temperatures. The shift causes significant changes of DMA properties in the viscoelastic region (at temperatures close to the room temperature).

The above stated confirms that when DMA results are reported, the precise conditions used should be indicated in the report. A comparison of results should only be made when they are obtained under the same experimental conditions.

REFERENCES

[1] M. Hanus, Dynamic Mechanical Analysis of Composite Solid Rocket Propellants, Proc. of the IV. Seminar " New Trends in Research of Energetic Materials", 2001, pp. 112-121.

[2] P. J. Haines, Thermal Methods of Analysis-Principles: Applications and Problems, Bleckie Academic & Professional, London, 1992, pp. 139-154.

[3] Quantitative Calculations and Theoretical Principles of the 983 Dynamic Mechanical Analyzer, TA Instruments, TA-032.

[4] D. A. Tod, Dynamic Mechanical Analysis of Propellants, Proc. of 18th Int. Conference of ICT, Karlsruhe, 1987, pp. 44/1-44/14.

[5] A. Gõcmez, M. Y. Özen, B. Veral, F. Pekel, S. Özkar, Comparison of Two HTPB Based Composite Propellants by Dynamic Mechanical Analysis, Proc.of 30th Int. Conference of ICT, Karlsruhe, 1999, pp. 29/1-29/12.

[6] T. Murayama, Dynamic Mechanical Analysis of Polymeric mMaterials, Elsevier Scientific Publishing Company, Amsterdam, 1978, pp. 19-22.

STUDY OF BIODEGRADATION OF SELECTED EXPLOSIVES BY PLANTS - ALTERNATIVE WAY OF SOIL AND WATER DECONTAMINATION

Aleš Nepovím*, Radka Podlipná*, Hartmuth Thomas, Andre Gerth**, Zdeněk Jalový***, Svatopluk Zeman*** and Tomáš Vaněk***

*Dept. of Plant Tissue Cultures, Institute of Organic Chemistry and Biochemistry, AS CR, Flemingovo nám. 2, 166 10 Praha 6, Czech Republic.

**Bioplanta GmbH, Delitzsch, Germany

*** Dept. of Theory and Technology of Explosives, University of Pardubice, 532 10 Pardubice, Czech Republic

Phytoremediation is a bioremediation technique used for cleaning contaminated sites by plants. The phytoremediation of trinitrotoluene (TNT), pentaerythritol tetranitrate (PETN), and glyceroltrinitrate (GTN) was studied. The plants were cultivated as a cell suspension culture and hydroponically cultivated plants under sterile conditions and thus were used as model system for description of metabolic processes. The metabolites of degradation were analysed by HPLC and identified by comparing retention times and UV spectra of standards of known or expected metabolites. Our results indicated that plants effectively degraded TNT, PETN, and GTN. All studied compounds were removed from the cultivation medium and transformed to the metabolites, which were partially excreted back into cultivation medium and rest bound to the cell structures.

1. INTRODUCTION

Phytoremediation allows using plants *in situ* for contaminated soil or constructed wetlands for contaminated water. The effectiveness of phytoremediation is depending on plant species, depth of root system on the one hand and on the other hand on type, concentration, and availability of contaminant (1). Root uptake and translocation within plant are governed by the lipophilic properties of the organic compound, which is usually expressed as the octanol-water partition coefficient, K_{ow}. For moderately hydrophobic compounds (log K_{ow} ~ 0.5-3.0) the removal mechanism is at its most efficient (2, 3) Contamination of soils and water by explosives such as 2,4,6-trinitrotoluene (TNT), glyceroltrinitrate (GTN) generated as a waste from the munitions and defence industries, is a significant worldwide environmental problem. All of them exhibit high toxicity for living organisms. Only limited numbers of publications concern toxicity of degradation products. The phytotoxicity of TNT was determined on white mustard seeds by measurement of length of primary root in five-days experiment. The concentration 40,6 mg/l inhibited the growth in 50%.

TNT, GTN and PETN represent suitable substrates, which were removed from the medium and most of the degradation products were fixed by bond into the cell structures (TNT) (4) and/or used as carbon source. Especially in case of GTN and PETN the final fate of glycerol and pentaerythritol should be verified by labelled compounds ([^{14}C]GTN, [^{14}C]PETN).

2. EXPERIMENTAL

Plant material

Rhubarb (*Rheum palmatum*) - suspension culture was cultivated in a liquid medium MS (5) supplemented with phytohormone NAA (10 mg/l) under day light, at 25°C (6).

Soapwort (*Saponaria officinalis*) - suspension culture was cultivated in a liquid medium MS supplemented with 10 mg/l 2,4D and 1 mg/l BAP and 1 mg/l Kin under dark at 25°C.

Flax (*Linum utitatisimum*) – suspension culture was cultivated in a liquid medium MS supplemented with phytohormone 0,225 mg/l 2,4D and 0,215 mg/l Kin under dark, at 25°C.

Poplar (*Populus nigra*) and aspen (*Populus tremula x tremuloides*) – hole plants were cultivated hydroponically in the hormone-free medium MS under day light, at 25°C

Chemicals

Samples of explosives as well as their degradation products were prepared at the Department of Explosives, University of Pardubice, (Pardubice, Czech Republic).

HPLC analysis

The analysis was performed on binary high pressure pumps (DeltaChrom SDS 020 and SDS 030) with a mixer (SunChrom GmbH). an injection valve Rheodyne 7725 (Rheodyne, USA), and PDA detector MD-1510 (Jasco, Japan). Stainless steel column (250 x 4 mm) was packed by reverse phase Si-C18, Biospher, 7 μm size (Labio Ltd. Czech Republic) and linear gradient of mobile phases: t_0=0 min, 10% MeOH; t=40 min, 100%B. Data were processed by Borwin PDA program and the concentration of TNT and its degradation products were calculated from peak area at wavelength 230 nm, whereas concentration of GTN and PETN were calculated from peak areas at wavelength nm.

3. RESULTS and DISCUSION

We have studied degradation of trinitrotoluene (TNT), glyceroltrinitrate (GTN) and pentaerythritoltetranitrate (PETN) in suspension culture of rhubarb (*Rheum palmatum*) and flax (*Linum utitatisimum*) and in hydroponics of poplar (*populus nigra*) and aspen (*Populus tremula x tremuloides*).

TNT was removed from the cultivation medium of rhubarb and flax suspension cultures in six and from 80% in 8 hours, respectively. Major degradation products such as aminodinitrotoluenes and minor degradation products such as trinitrobenzene (TNB) were identified in all cultures according to the scheme in figure 1. Only some of minor degradation products such as hydroxyaminodinitrotoluene (HADNT) were detected in suspension culture of rhubarb (7, 8). GTN and PETN were degraded by sequential denitration to glycerol (see figure 2a) and pentaerythrytol (see figure 2b), respectively. All PETN degradation products – pentaerythritol trinitrate, -dinitrate, mononitrate and pentaerythritol were identified from suspension culture of rhubarb. The GTN was degraded in 10 days only from 37% and only one degradation product, glycerolmononitrate (at 11% of GTN initial concentration) was detected (9).

The main difference between suspension culture and hydroponics is in the time of uptake of parent compound. We have determined difference in TNT treated cultures when the suspension culture degraded TNT in a few hours whereas in hydroponics it took for a few days.

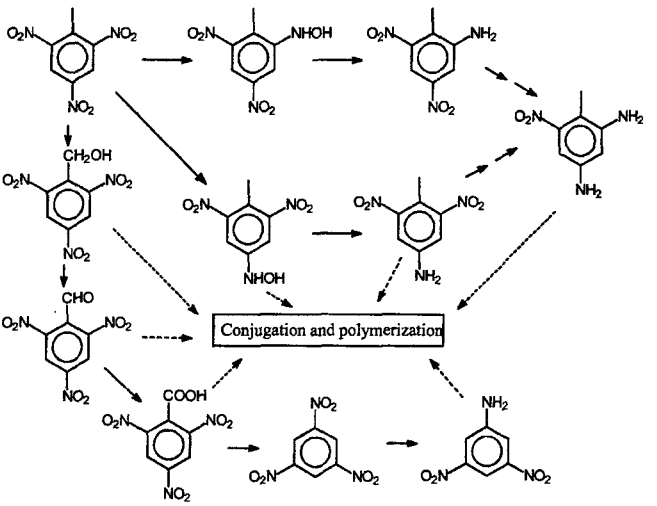


Fig 1. Proposed degradation pathway of TNT in suspension culture of rhubarb (*Rheum palmatum*)

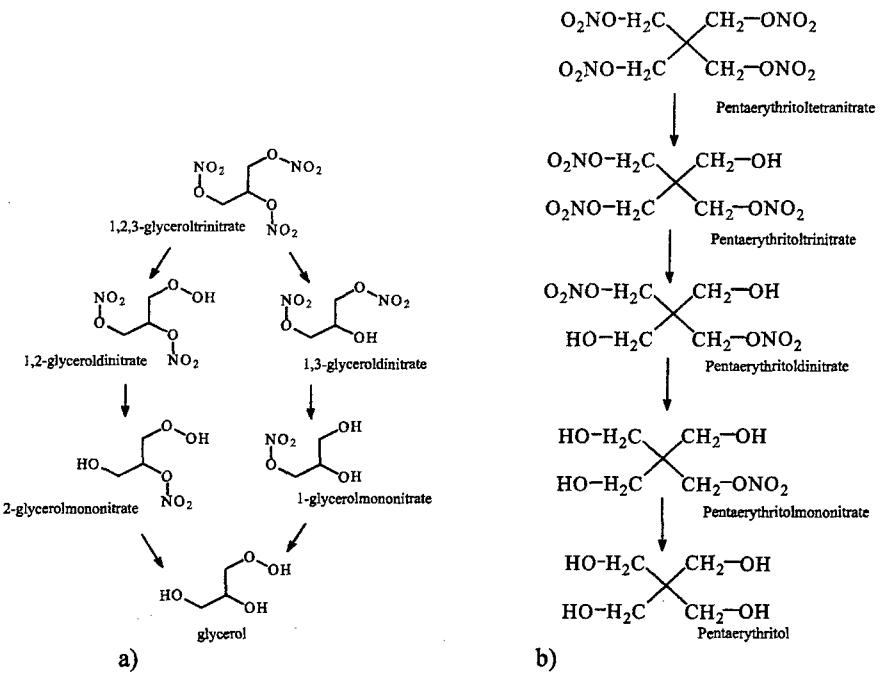


Fig 2. Degradation pathway of GTN (a) and PETN (b) in suspension culture of rhubarb (*Rheum palmatum*)

Characterization and identification of the degradation products was the first step of our research and the following step is a study of enzymes, which participates the metabolism. Understanding the metabolic pathways may allow find responsible enzymes and using biological-molecular tools allow us affection of the expression of crucial or particular enzyme.

4. CONCLUSION

We have given an overview of results concerning the phytoremediation of selected explosives. We have shown that plants have good potential to degrade explosives such as TNT, GTN and PETN to give appropriate degradation products. Both models of plant cultures, suspension and hydroponics, gave the same degradation products in case of TNT degradation. These results have given good background for field application of phytoremediation and for further experiments in contaminated sites, which started last year in Germany.

Acknowledgment:

This work was supported by GAČR projects: 206/99/1252, 206/02/P065, MŠMT project no CZE 01/024

REFERENCES:

[1] Z. SNELLINX, A. NEPOVÍM, S. TAGHAVI, J. VANGRONSVELD, T. VANĚK and D. VAN DER LELIE: *Biological remediation of explosives and related nitroaromatic compounds*, Environ. Sci. Poll. Res. **9**, 48-61, 2002. J.L. SCHNOOR, L.A. LICHT, S.C. MCCUTCHEON, N.L. WOLFE and L.H. CARREIRA: *Phytoremediation of organic and nutrient contaminations.* Environ. Sci. Technol. **29**, 318-323, 1995.

[3] J.G. BURKEN and J.L SCHNOOR: *Predictive relationship for uptake of organic contaminants by hybrid poplar trees.* Environ. Sci. Technol. **32**, 3379-3385, 1998.

[4] C. SENS, P. SCHEIDEMANN and D. WERNER,: *The distribution of ^{14}C TNT in different biochemical compartments of the monocotyledonous Triticum aestivum.* Environ. Pollution **104**, 113-119, 1999.

[5] T. MURASHIGE and F. SKOOG: A revised medium for rapid growth and bio assays with tobacco tissue cultures. Physiol. Plant. **15**, 473-497,1962.R. DUC., P. SOUDEK. T. VANĚK and J.P. SWITZGUÉBEL: *Accumulation and transformation of sulfonated aromatic compounds by rhubarb cells (Rheum palmatum)*, Int. J. Phytoremed. **1**, 255-271, 1999.

[7] T. VANĚK, A. NEPOVÍM and S. ZEMAN: *Phytoremediation of selected Explosives in a model system of plant tissue cultures,* Korean J. Plant Tissue Culture **27**, 379-385, 2000.

[8] A. NEPOVÍM, M. HUBÁLEK, S. ZEMAN and T. VANĚK: *In vitro degradation of 2,4,6-trinitrotoluene by plant tissue culture of Solanum aviculare and Rheum palmatum.* Acta Biotechnologica, accepted, 2002

[9] T. VANĚK, A. NEPOVÍM, PODLIPNÁ, R., S. ZEMAN and M. VÁGNER: *Phytoremediation of selected explosives*, Water, Air, & Soil Pollution, accepted, 2002

RESEARCH OF PHYSICOCHEMICAL PROPERTIES OF PLASTIC EXPLOSIVE

Andrzej Orzechowski*, Witold Pągowski* and Andrzej Maranda**

[1]Institute of Industrial Organic Chemistry

[2]Military Academy of Technology

Abstract:

The users would like to receive plastic explosive of the appropriate plasticity, chemical and physical stability and appropriate explosive properties in range of temperatures - 40^{0}C to +70^{0}C. Plasticity is one of the most important parameters and determine of the application. The influence of the polymer and its content, modifying agents and the content of explosive on plasticity was examinated. Plastic explosive (PE) was produced in Poland, but this material did not have right chemical and physical stability. Liquid component exudation from plastic explosive results in the deterioration of its chemical and physical stability. The influence of the explosive and polymer content on the exudation of liquid component was investigated.

1. INTRODUCTION

PE ought to be characterized by right plasticity, physical and chemical stability, good explosive properties in the range of temperatures from –40^0 C to +70^0 C. The type and explosive content have the main influence on explosive properties of PE. Actually produced PE contain hexogen, pentryt or octogene. Detonation parameters can be regulated by the change explosive content. The type of binder influence physical and chemical properties of PE. That is why we investigated the influence of binder component on PE properties.

The methods of PE production were patented in Poland [1,5]. It was characterized the explosive was mixed with before prepared binder (rubber or some other polymer was dissolved in a solvent or in a plasticizer). Because of technological problems all of these methods were not introduced. PMW-10M (plastic explosive produced in Poland) is made by mixing of plastifed nitrocellulose with hexogen. But there are some problems with keeping physical and chemical stability and plasticity stability during storage [6]. Good physical and chemical properties posses C-4 (PE produced in the United States) that contains polyisobutylene [7]. Fluoro-polymers also have good properties and high temperature resistance [8-10].

The application of PE imposes their composition and that follows their rheological and explosive properties. The best solution is manufacturing a few types of PE but it is uneconomical. We researched influence composition of plastic explosive on physicochemical properties.

2. BINDER SELECTION AND PREPARATION OF SAMPLES.

Taking into consideration physical and chemical properties and accessibility we choose three polymers for our researches: polyisobutylene, butadiene – styrene copolymer and fluoro-polymers.

Polyisobutylene was dissolved in ADO and subsequently mixed with HX.

Butadiene – styrene copolymer in the form of water suspension was added to HX and then dehydrated.

Fluoro-polymer in the form of water suspension was added to hexogene and dried. Next dioctyl phthalate (FDB) and fluoro-elastomer dissolved in acetone were added, mixed and the solvent was evaporated.

3. DETERMINATION OF PLASTICITY.

Plasticity is one of the most important parameters of PE in consideration of their application and technological conditions. Measurements of plasticity were done according to PN-79/C-04133. We determined depth of standard cone penetration in the sample for predetermined conditions: weight, time and temperature.

We chose this method because it enables to define rheology properties versus temperature.

4. RESEARCH RESULTS.

4.1. The influence of used polymer on plasticity.

Polymer is the most important component. Polymer affects physical and chemical properties of PE. A high elasticity and a low vitrification temperature should characterize chosen polymer as it is shown in Fig. 1.

The samples of PE kept the plasticity in temperatures from -40^0 C to $+70^0$ C and they had small gradient increases of plasticity versus temperature. The samples contained 88% HX.

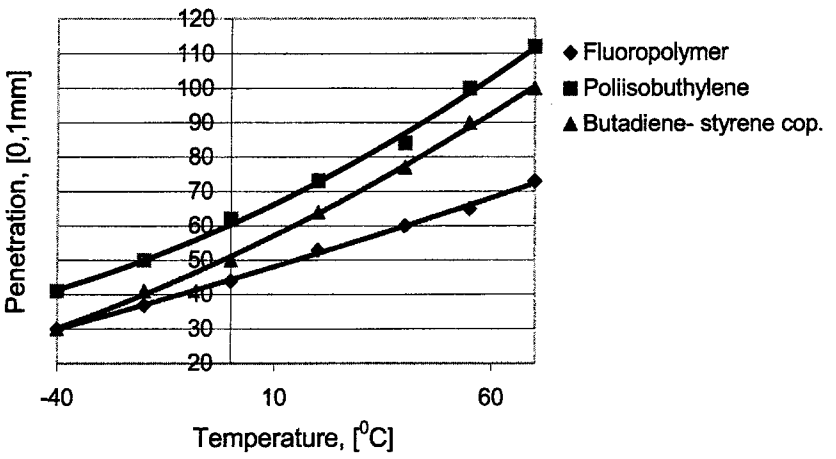


Fig 1. Relationship between penetration and temperature for different polymers.

4.2. The influence of polymer content on plasticity

We investigated two different binders (butadiene – styrene copolymer and fluoro-polymers). The content of polymer was changed. Compositions of PE samples are presented in Table 1.

Table 1. Compositions of plastic explosive.

Polymer	Content			**Plasticizer**
	Polymer [%]	HX [%]	Plasticizer [%]	
Butadiene – styrene copolymer	2	84	14	ADO
	3	84	13	ADO
	4	84	12	ADO
	5	84	11	ADO
Fluoro-polymers	2,8	92,5	4,7	FDB
	3,4	90,8	5,8	FDB
	4,1	88,4	7,5	FDB

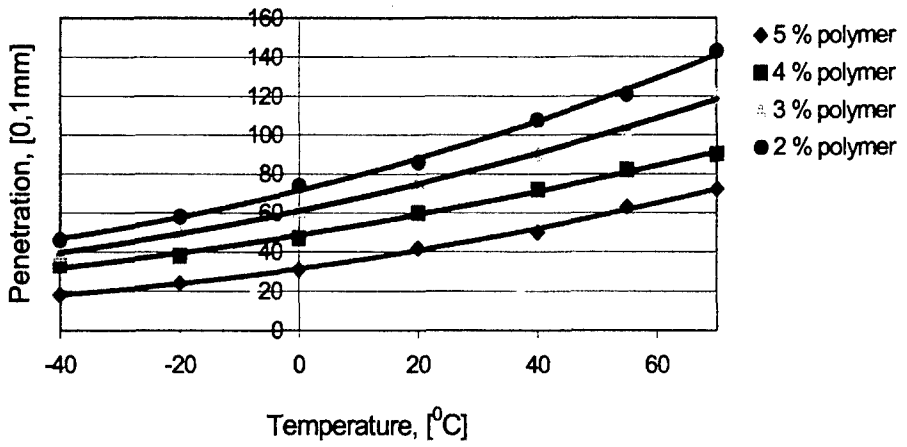


Fig 2. Relationship between penetration and temperature for different polymer content.

The results presented above (Fig. 2) show that PE plasticity is inversely proportional to polymer content. The samples with fluoro-polymers are presented in Fig. 3. When polymer content decreases plasticity increases, just like in the case of butadiene – styrene copolymer.

During researches we noticed the content of polymer has the bigger influence onto plasticity than the content of high explosive. That is why we can reach required plasticity by changing polymer content without other content changes (for instant high explosive content).

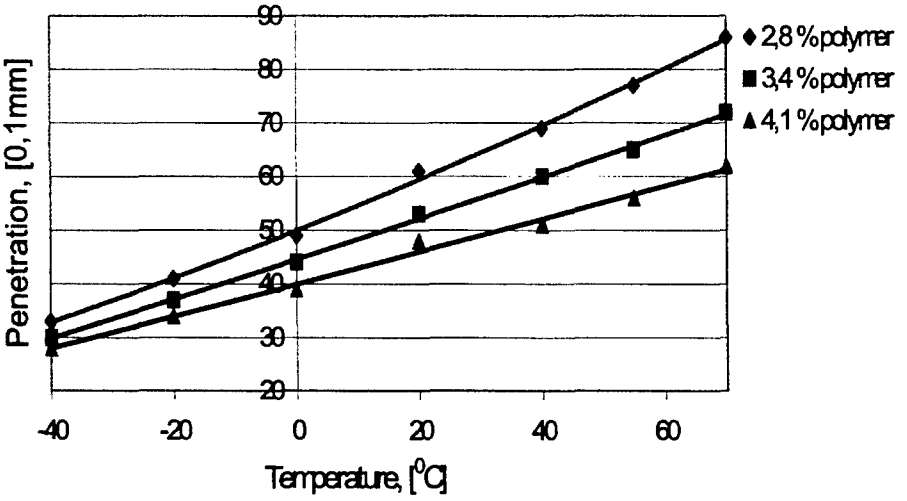


Fig 3. Relationship between penetration and temperature for different fluoro-polymers content.

4.3. Influence of plastic explosive content on plasticity.

PE samples contained butadiene – styrene copolymer and dioctyl adipate (as plasticizer). We prepared three samples of PE. The samples contained: 84%, 86% and 88% HX. We did not change the content of binder. The results are presented in Fig. 4.

We have found that with increasing of explosive content the plasticity of PE decreased. Above certain explosive content PE lost coherence.

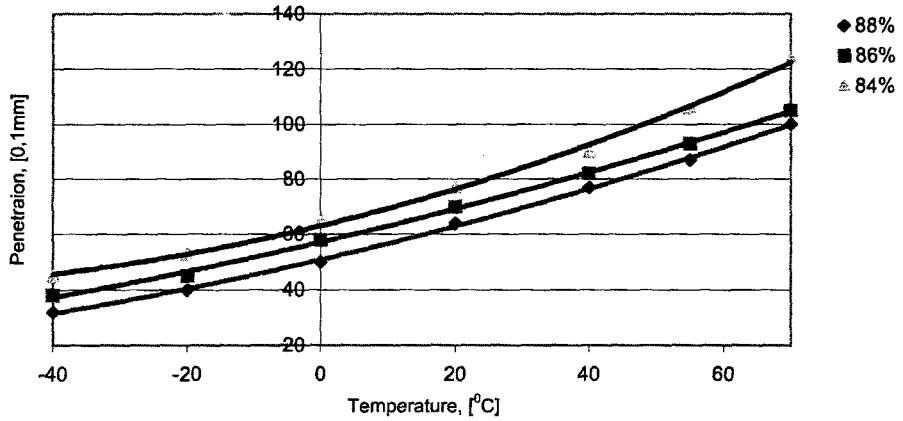


Fig 4. Relationship between penetration and temperature for different HX content.

4.4. The influence of modifying substance on plasticity.

We investigated three samples of PE (84% HX). Compositions are presented in Tab. 2. Research results are presented in Fig. 5. Glycerin stearate had major influence on plasticity. But gradient increased too much within the range of high temperatures.

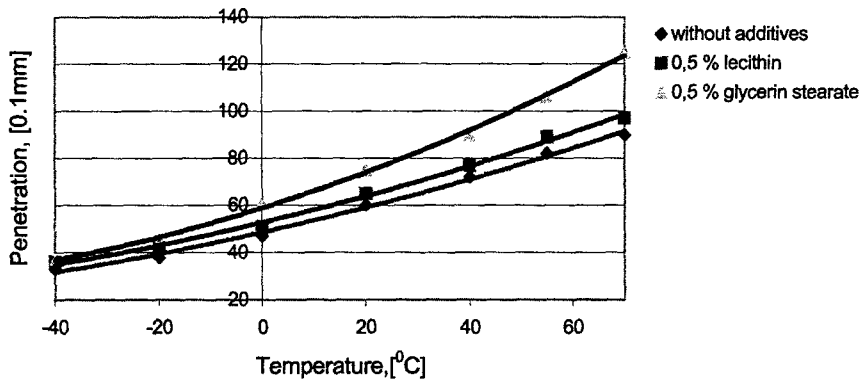


Fig 5. Relationship between penetration and temperature for different additives.

Due to precaution and safety which must be kept during technological operation we applied modifying additives.

The increasing of plasticity reduces PE warming up during mixing, plasticizing, extruding.

Table 2. Modifying additives.

Sample	Additive	Contents	
		Additives [%]	Polymer [%]
1	-	-	4
2	Lecithin	0,5 – in proportion to all mass	4
3	Glycerin stearate	0,5 – in proportion to all mass	4

4.5. The influence of plastic explosive component content on exudation

The ability of permanent fixation of all PE components influences on their physical and chemical stability, explosive parameters and application properties.

The most important is PE ability for keeping liquid components. When exudation is too big it means the wrong plasticizer was chose or there were unprofitable changes of physical and chemical properties of polymer.

The excessive amount of plasticizer is good for plasticity reasons. But in this case we noticed some troubles in application and PE storage. They ought to be stored in special packages, because their exudation can provoke the changes of PE properties.

We researched exudation in weighed bottles (diameter about 8 cm). On the bottom of the bottle was a filter – paper ring (a ring diameter was fit to the diameter of the bottle). We dried all for approx. 2 hours in 75^0 C.

Subsequently, we weighted the bottles and PE samples (formulated as ring: diameter 7mm, thickness approx. 5mm) on the analytical balance and warmed everything up in 75^0 C for 24 hours. Next we cooled the bottles with sample in exsiccator.

The samples of PE were taken out from the bottles and we weighted bottles with paper rings only. We defined the increment of weigh - it was the leakage from PE.

4.5.1. The influence of polymer content on exudation.

We researched PE samples with different polymer content (2% - 3% polymer). The amount of HX was steady 84%. The results are presented in Fig. 6.

When polymer content increases, the amount of liquid component exudation decreases. We noticed that one of PE composition had optimal polymer content.

The reduction of optimal polymer content provokes a substantial increase of PE exudation.

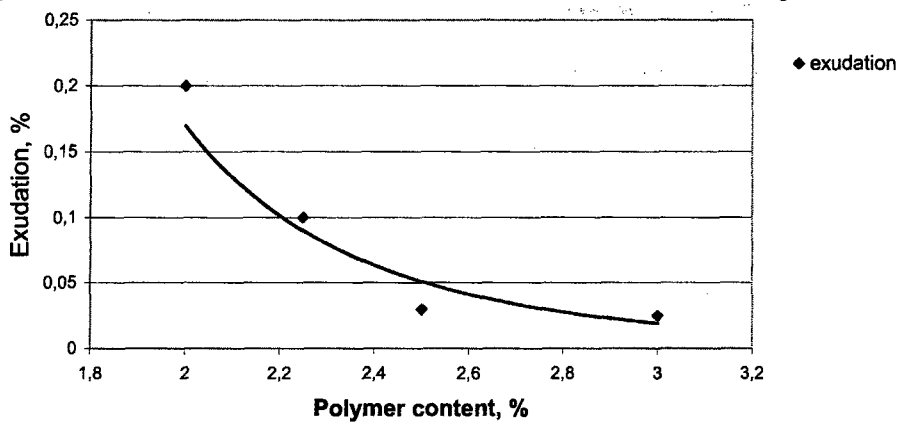


Fig 6. Relationship between exudation and polymer content.

4.5.2. Influence of HX content on exudation

We researched two samples of PE with 2% and 3% of polymer content. The amount of HX was changed. The results are presented in Fig. 7.

The decrease of HX content (below optimal limit for each PE composition) provokes a substantial change of exudation. This is connected with the optimal surface of explosive crystal.

The increase of polymer content profitable moves the limit of the substantial change of exudation, it depends on bonding between plastificator and polymer.

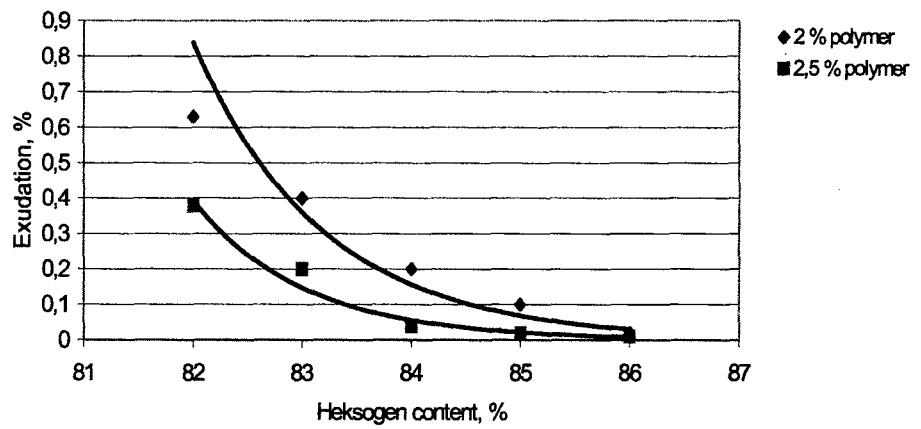


Fig 7. Influence of explosive content on exudation.

4.5.3. Influence of granulometric explosive component on exudation

Table 3. Hexogen (HX) parameters.

		HEXOGEN	
Producer		A[1]	B[2]
Bulk density		0,76 g/cm^3,	0,64 g/cm^3
Shaked bulk density		0,96 g/cm^3,	0,80 g/cm^3
Sieve analysis:	0,125	5,9	0,1
Residue	0,09	9,2	0,6
Sieve mesh	0,045	60	43,2
[mm]	below	24,9	56,1

1- Z.Ch. „Organika-Sarzyna" S.A.; 2 - Z.Ch.„Nitro – Chem" S.A.

We investigated PE exudation. The samples were different in the kind of polymer (component was steady).

Characteristics of HX grain size influence on the exudation and plasticity of PE. Low refinement influences on the reduction of the exudation but it is unprofitable because of worse plasticity. It is connected with the surfaces of crystals .Test results are presented in Tab. 5.

Table 4. Test results.

Sample	Producer	Contents		Exudation, %	Plasticity in 20 C^0, mm
		HX	polymer		
1	B	84	2	0,015	60
2	A	84	2	0,16	100
2	B	84	2,5	0,012	55
3	A	84	2,5	0,05	95
4	B 50 % A 50 %	84	2	0,05	81
5	B 50 % A 50 %	84	2,5	0,03	75

5. CONCLUSIONS.

Applied research method enables to determine PE plasticity in the large range of temperatures.

The type and polymer content influence on PE plasticity to a largest extent. It can be regulated by the changes of the type and content of binder.

Exudation depends on polymer content, explosive content and explosive grain size.

These researches give the possibility of PE plasticity and exudation fitting into technological and application requirements and enables the influence on other PE properties.

LITERATURE

[1] Patent polski, 113750 (1982).
[2] Patent polski, 116272 (1983).
[3] Patent polski, 119635 (1983).
[4] Patent polski, 143972 (1988).
[5] Patent polski, 161471 (1989).
[6] A. Sikorska, W. Pągowski, A. Bednarski, B. Zygmunt, A. Orzechowski, „ Nowy plastyczny materiał wybuchowy" Materiały z VI konferencji „Problemy Techniki Uzbrojenia i Radiolokacji" , Rynia 1997.
[7] Patent USA, 3.321.341 (1967).
[8] W. Szlezyngier „Tworzywa sztuczne " WNT, Warszawa 1981.
[9] J.A. Panszin „Tworzywa Fluorowe " WNT, Warszawa 1982.
[10] W.W. Korszak „Technologia tworzyw sztucznych" Oficyna wydawnicza Politechniki Rzeszowskiej – Kaszów 1996.

SYNTHESIS AND CRYSTAL STRUCTURE OF TETRAACETYLDICHLOROACETYLHAXAAZAISOWURTZITANE TRIHYDRATE

Ou Yuxiang, Liu Lihua, Chen Boren and Lijin

School of Chemical Engineering & Material Science,
Beijing Institute of Technology,Beijing 100 081, China

Abstract

A novel hexasubstituted hexaazaisowurtzitane – tetraacetyldichlorohexaaza isowurtzitane (TADCIW) was synthesized, and the colorless and transparent single crystal of TADCIW•3H_2O was prepared by evaporating solvent slowly. The crystal belongs to monoclinic system and space group Cc with parameters a = 1.0469(2) nm, b = 1.5347(3) nm, c = 1.5364(4) nm; $\beta = 95.00°$; Z = 4; V = 2.4591(9) nm^3; D_c = 1.468 $g.cm^{-3}$; R = 0.0487, W_R = 0.1168.

Key words: *tetraacetyldichloroacetylhexaazaisowurtzitane, crystal structure, synthesis*

1. INTRODUCTION

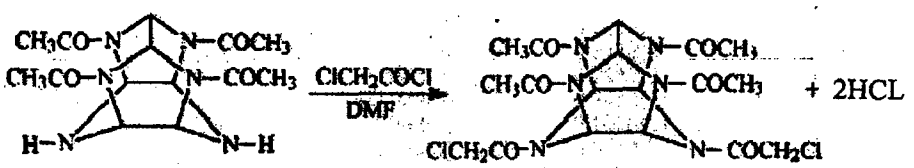
Hexabenzylhexaazaisowurtzitane (HBIW) is the first example of hexasubstituted hexaazaisowurtzitane. The synthesis of HBIW and its derivatives with substituted benzyl group were reported by A. T. Nielsen in 1990 [1]. Since then, the study of hexaazaisowurtzitane derivatives has been focused on the high energy density compound – hexanitrohexaazaisowurtzitane (HNIW, CL-20) and a number of related compounds have been synthesized [2-4]. The authors have been successful on synthesizing firstly the title compound which should be the intermediate of some energetic compounds, such as tetranitrodiazidoacetylhexaazaisowurtzitane and tetranitrodinitroacetylhexaaza-isowurtzitane etc. Besides, TADCIW•3H_2O crystal structure was measured by X-ray diffraction technique.

2. EXPERIMENTAL

2.1 Synthesis of TADCIW and preparation of single crystal of TADCIW•3H_2O

20.4 g of tetraacetylhexaazaisowurtzitane which was prepared based on literature [3] and 100 ml of DMF were added in a flask. Heat the contents of the flask to 45 °C and add 25 ml of chloroacetyl chloride with vigorous stirring. Close the reaction flask and vacuum the released HCl. Let reaction proceed at 45 °C for 2 hours. Remove the unreacted chloroacetyl chloride and a part of DMF by distillation under reduced pressure. Pour the contents of flask into 300 ml of cold water and obtain 26.0 g of the colorless solid (m. p. 265~266 °C) by filtration and washing with cold water and acetone. The yield of TADCIW reached about 90 %. Elementary analysis: calculated for $C_{18}H_{22}Cl_{12}N_6O_6$ (%): C, 44.17; H, 4.50; N, 17.18; Cl, 14.52; found (%): C, 44.10; H, 4.64; N, 17.12; Cl, 14.47. IR (KBr, cm^{-1}): 3045, 2993, 2942, w; 1685, 1655, s; 1413, 1362, 1337, 1293, 1264, 1162, s; 1060,979, 942, 868, m. MS (Cl)

m/z: 519 $(M+2+C_2H_5-H)^+$, 517 $(M+C_2H_5-H)^+$, 490 $(M+H)^+$, 488 $(M-H)^+$, 455 $(M-Cl+H)^+$. ^1H NMR (DMSO-d_6, ppm): δ 6.89~6.31 (m, 6H(CH)), δ 4.93~4.71 (4H(CH_2)), δ 2.06~1.97 (m, 12H (CH_3)).



Dissolve the dry product in a acetone-water mixture and evaporate slowly the solvent to certain extent in a vacuum desicator to obtain a colorless and transparent single crystals of TADCIW•3H_2O (0.4x0.4x0.4 mm) for X-ray diffraction analysis.

2.2 Diffraction data collection and structure solution refinement of TADCIW•3H_2O

Single crystal.

The diffraction analysis was carried out on Siemens P4 diffractmeter and the highly oriented graphic crystal monochrometer with radiation Moka (λ = 0.071073 nm) was used. The related data are given below: scan type 2θ-ω, θ = 2.36°~30.00°, collected reflection 4422, reflections for structure solution refinement 4134 {1>2σ(I)}. All strength data were corrected by Lp factors. The chemical formula and relative molecular mass of the compound are $C_{18}H_{28}Cl_{12}N_6O_9$ and 543.36 respectively. The single crystal belongs to monoclinic system, space group Cc with parameters a = 1.0469(2) nm, b = 1.5347(3) nm, c = 1.5364(4) nm; β = 95.00°; Z = 4; V = 2.4591(9) nm^3; D_c = 1.468 $g.cm^{-3}$; F(000) = 1136; μ = 0.324 mm^{-1}. The crystal structure was solved by direct method. Atomic coordinates and equivalent isotropic thermal parameters of all nonhydrogen atoms were refined by full matrix least-squares method. Within the range of I>2σ(I), R = 0.0467, W_R = 0.1168. Parameters of least-squares method for refinement amount to 321. $\Delta\rho_{max}$ = 328 e/nm^3, $\Delta\rho_{min}$ = 256 e/nm^3.

3. RESULTS AND DISCUSSION

Atomic coordinates and equivalent isotropic parameters of nonhydrogen atoms are listed in Table 1. The bond lengths and bond angles of nonhydrogen atoms and hydrogen bonds are listed in Table 2. Fig.1 and Fig. 2 show the molecular configuration and cell packing of TADCIW•3H_2O single crystal respectively.

Crystal structure shows that TADCIW•3H_2O is caged polycyclic molecule composed two five-membered rings and one six-membered ring. The six membered ring exists in boat conformation. None of the two five-membered rings lies in a plane. The angle and the distance between the plane of C(17)C(18)N(6)N(5) and the plane of C(13)C(14)N(4)N(3) are 5.80° and 0.2605 respectively. The single bond length of C(15) and C(16) which connect two five-membered rings is 0.1587 nm. The distance between C(15) and the plane of C(13)C(14)N(4)N(3) is 0.0547 nm, while that between C(16) and the plane C(17)C(18)N(6)N(5) is 0.0541 nm. This means that the TADCIW•3H_2O molecule possesses high strain energy.

Table 1. Atomic coordinates and equivalent isotropic thermal parameters (nm^2, $x10^5$) of nohydrogen atoms.

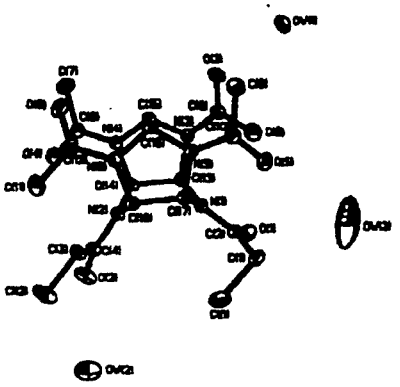
atom	x	y	z	U_{eq}
Cl(1)	0.4768(1)	0.2310(1)	0.3460(1)	63(1)
Cl(2)	0.9999(1)	0.4347(1)	0.3603(1)	87(1)
O(1)	0.3584(3)	0.4457(2)	0.3823(2)	55(1)
O(2)	0.8115(3)	0.3291(2)	0.2605(2)	60(1)
O(3)	0.2432(3)	0.6277(2)	0.0931(2)	64(1)
O(4)	0.8030(3)	0.6073(2)	0.1422(2)	66(1)
O(5)	0.2000(3)	0.3385(2)	0.1382(2)	63(1)
O(6)	0.6539(3)	0.4451(2)	-0.0616(2)	62(1)
N(1)	0.4359(2)	0.4208(2)	0.2521(2)	33(1)
N(2)	0.6685(2)	0.4321(2)	0.2136(2)	34(1)
N(3)	0.3991(3)	0.5512(2)	0.1649(2)	36(1)
N(4)	0.6017(3)	0.5595(2)	0.1308(2)	37(1)
N(5)	0.3812(3)	0.3952(2)	0.0989(2)	36(1)
N(6)	0.5834(2)	0.4036(2)	0.0654(2)	37(1)
C(1)	0.3417(4)	0.3008(2)	0.3331(2)	51(1)
C(2)	0.3801(3)	0.3953(2)	0.3252(2)	36(1)
C(3)	0.8546(3)	0.4752(3)	0.3112(2)	47(1)
C(4)	0.7777(3)	0.4043(2)	0.2610(2)	38(1)
C(5)	0.2219(5)	0.6020(3)	0.2454(3)	63(1)
C(6)	0.2870(3)	0.5962(2)	0.1626(2)	43(1)
C(7)	0.6703(4)	0.6502(3)	0.0134(3)	64(1)
C(8)	0.6982(3)	0.6048(2)	0.0996(6)	45(1)
C(9)	0.1870(4)	0.4160(3)	0.0025(3)	62(1)
C(10)	0.2529(3)	0.3803(2)	0.0846(2)	42(1)
C(11)	0.7957(5)	0.3566(3)	0.0329(3)	68(1)
C(12)	0.6733(3)	0.4051(3)	0.0066(2)	45(1)
C(13)	0.4714(3)	0.5122(2)	0.2405(2)	35(1)
C(14)	0.6128(3)	0.5185(2)	0.2165(2)	33(1)
C(15)	0.4730(3)	0.5448(2)	0.0899(2)	36(1)
C(16)	0.4618(3)	0.4495(2)	0.0498(2)	36(1)
C(17)	0.4549(3)	0.3647(2)	0.1781(2)	33(1)
C(18)	0.5964(3)	0.3711(2)	0.1553(2)	34(1)
OW1	0.0001(3)	0.6986(2)	0.0687(2)	56(1)
OW2	0.9173(5)	0.2159(3)	0.4086(2)	94(1)
OW3	0.0593(8)	0.2159(4)	0.2460(7)	218(5)

The length of C-Cl bonds, C=O bonds and C-H bonds are basically in the normal ranges in TADCIW•$3H_2O$ molecule. The sp^3C-sp^3N bond length from 0.1444 to 0.1466 nm, and the sp^3C-sp^3N length from 0. 1349 to 0.1369 nm are also normal. There exist some differences among the six sp^3C-sp^3C bonds and they are within the range of 0.1488-0.1522 nm. This might result from the difference of the groups to which the acetyl groups attach and their orientation with respect to the five- and six-membered rings. The lengths of sp^3C-sp^3C bonds in TADCIW•$3H_2O$ are slightly longer than the normal value of the single sp^3C-sp^3C bond which is 0.154 nm. For example, thelength is 0.1559 nm for C(13)-C(14) bond, 0.1587 nm for C(15)-C(16) bond, and 0.1554 nm for C(17)-C18) bond, 1.2 %, 3.1 %, and 0.9 % longer than that sp^3C-sp^3C bond respectively. But this deviation is not as large as that of HNIW because of the smaller electron withdrawing effects of N-acetyl comparing to N-nitro group positioned on both sides of sp^3C-sp^3C bonds. In TADCIW•$3H_2O$, there are intramolecular hydrogen bonds not only between H(16) on the cage or H(i) of acetyl from one molecule and O(1) of chloroacetyl from another molecule, but also between H(3) chloroacetyl from one molecule O(6) of acetyl from another molecule.

Table 2. Bond lengths (0.1 nm) and bond angles (°) of nonhydrogen atoms and hydrogen bonds.

Cl(1)-C(1)	1.772(4)	N(4)-C(15)	1.454(4)
Cl(2)-C(3)	1.752(4)	N(4)-C(14)	1.455(4)
O(1)-C(2)	1.206(4)	N(5)-C(10)	1.361(4)
O(2)-C(4)	1.208(4)	N(5)-C(16)	1.444(4)
O(3)-C(6)	1.224(4)	N(5)-C(17)	1.460(4)
O(4)-C(8)	1.229(5)	N(6)-C(12)	1.361(4)
O(5)-C(10)	1.216(4)	N(6)-C(16)	1.456(4)
O(6)-C(12)	1.217(5)	N(6)-C(18)	1.464(4)
N(1)-C(2)	1.368(4)	C(1)-C(2)	1.511(5)
N(1)-C(17)	1.455(4)	C(3)-C(4)	1.522(5)
N(1)-C(13)	1.466(4)	C(5)-C(6)	1.498(5)
N(2)-C(4)	1.369(4)	C(7)-C(8)	1.502(5)
N(2)-C(14)	1.450(4)	C(9)-C(10)	1.488(5)
N(2)-C(18)	1.460(4)	C(11)-C(12)	1.506(6)
N(3)-C(6)	1.359(4)	C(13)-C(14)	1.559(4)
N(3)-C(15)	1.446(4)	C(15)-C(16)	1.587(5)
N(3)-C(13)	1.459(4)	C(17)-C(18)	1.554(4)
N(4)-C(8)	1.349(4)		
C(2)-N(1)-C(17)	124.7(3)	N(3)--C(6)-C(5)	117.7(3)
C(2)-N(1)-C(13)	120.4(3)	O(4)-C(8)-N(4)	119.2(3)
C(17)-N(1)-C(13)	114.7(2)	O(4)-C(8)-C(7)	123.5(3)
C(4)-N(2)-C(14)	126.0(3)	N(4)-C(8)-C(7)	117.3(7)
C(4)-N(2)-C(18)	119.3(3)	O(5)-C(10)--N(5)	118.7(3)
C(14)-N(2)-C(18)	114.6(2)	O(5)-C(10)-C(9)	124.3(3)
C(6)-N(3)-C(15)	122.3(3)	N(5)-C(10)-C(9)	117.0(3)
C(6)-N(3)-C(13)	128.0(3)	O(6)-C(12)-N(6)	120.5(3)
C(15)-N(3)-C(13)	109.3(2)	O(6)-C(12)-C(11)	123.7(3)
C(8)-N(4)-C(15)	128.4(3)	N(6)-C(12)-C(11)	115.8(3)
C(8)-N(4)-C(14)	122.8(3)	N(3)-C(13)-N(1)	111.7(2)
C(15)-N(4)-C(14)	108.8(2)	N(3)-C(13)-C(14)	102.9(2)
C(10)-N(5)-C(16)	128.7(3)	N(1)-C(13)-C(14)	110.1(3)
C(10)-N(5)-C(17)	121.6(3)	N(2)-C(14)-N(4)	111.6(2)
C(16)-N(5)-C(17)	109.2(2)	N(2)-C(14)-C(13)	110.1(3)
C(12)-N(6)-C(16)	121.9(3)	N(4)-C(14)-C(13)	103.8(2)
C(12)-N(6)-C(18)	128.3(3)	N(3)-C(15)-N(4)	100.6(2)
C(16)-N(6)-C(18)	109.1(2)	N(3)-C(15)-C(16)	110.2(2)
C(2)-C(1)-Cl(1)	112.0(3)	N(4)-C(15)-C(16)	110.2(3)
O(1)-C(2)-N(1)	122.3(3)	N(5)-C(16)-N(6)	100.2(2)
O(1)-C(2)-C(1)	119.2(3)	N(5)-C(16)-C(15)	110.9(2)
N(1)-C(2)-C(1)	118.5(3)	N(6)-C(16)-C(15)	110.4(2)
C(4)-C(3)-Cl(2)	111.5(3)	N(1)-C(17)-N(5)	111.3(3)
O(2)-C(4)-N(2)	121.7(3)	N(1)-C(17)-C(18)	109.6(2)
O(2)-C(4)-C(3)	123.0(3)	N(5)-C(17)-C(18)	103.7(2)
N(2)-C(4)-C(3)	115.3(3)	N(2)-C(18)-N(6)	111.2(2)
O(3)-C(6)-N(3)	118.6(3)	N(6)-C(18)-C(17)	110.8(2)
O(3)-C(6)-C(5)	123.7(3)	N(6)-C(18)-C(17)	102.8(2)
H(16)···O(1)	2.350(4)	C(16)···O(1)	3.146(4)
H(3A)···O(6)	2.276(5)	C(3)···O(6)	3.232(5)
H(9A)···O(1)	2.487(5)	C(9)···O(1)	3.422(5)
C(16)-H(16)···O(1)	137.82(10)	C(9)-H(9A)···O(1)	164.65(13)
C(3)-H(3A)···O(6)	168.26(11)		

1.



2.

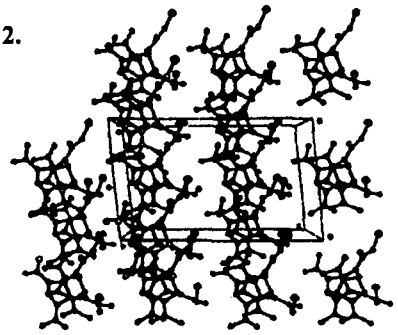


Fig 1. Molecular configuration of TADCIW.$3H_2O$

Fig 2. Cell packing of TADCIW.$3H_2O$

REFERENCES

[1] Nielsen A. T., Nissan A. R., Vanderah J. D. et. al, "Polyazapolyciclics by Condensation of Aldehydes with Amines. Formation of 2,4,6,8,10,12-Hexabenzyl-2,4,6,8,10,12-hexaazatetracyclo[5.5.0.$0^{5.9}$.$0^{3.11}$]dodecanes from Glyoxal and Benzylamines". J. Org. Chem. 55, 1459~1406 (1990).

[2] Bellamy A. J., "Reductive Debenzylation of Hexabenzylhexaazaisowurtzitane", Tetrahedron 51, 4711`4722 (1995).

[3] Kodama T., Tojo M., Ikeda M, World Patent WO 9623,792 (1996).

[4] Nielsen A. T., Chafin A. P., Christian S. L., et. al., "Synthesis of Polyazapolycyclic Caged Polynitramines", Tetrahedron 54, 11973~11912 (1998).

SOME ASPECTS OF SERVICE LIFE EVALUATION OF COMPOSITE ROCKET PROPELLANTS

Jiří Pachmáň*, Marcel Hanus and Jakub Šelešovský***

*University of Pardubice, Dept. Theory and Technology of Explosives, 532 10 Pardubice, CZ

**Military Institute for Weapon and Ammunition Technology (VTÚVM), 763 21 Slavičín, CZ

Abstract:

This paper summarizes and comments experimental results of aging characterization of ten different in-service composite solid rocket propellants. The aim of this work was to determine and to evaluate changes in chemical composition (sol/gel content), thermal stability (TGA, DTA), mechanical properties (uniaxial tensile and compression tests, hardness), thermomechanical properties (DMA, TMA), sensitiveness to impact, friction and electric spark induced by aging.

Keywords: *rocket propellants, aging, thermal stability, thermomechanical properties, sensitiveness*

1. INTRODUCTION

Characterization of explosives aging is an important part of ongoing cooperative research between the University of Pardubice (UPa) and Military Institute for Weapon and Ammunition Technology (VTÚVM). Purpose of this program is to characterize aging of in-service military explosive materials, to provide comparison data for qualification of new explosives and to develop reliable methodologies for service life controls of ammunition systems incorporating these explosives [1,2,3]. Some of the results concerning composite solid rocket propellants are summarized in this article.

Composite solid rocket propellants are made of relatively vast volume of solid particles (ammonium perchlorate or other oxidizers, aluminium or other fuels) dispersed in soft matrix material (usually plasticized elastomers). It is apparent that the composition does not have to preserve only its energy but also has to retain its mechanical properties for many dozens of years during its service life. In opposite case cracks or other flaws may propagate through the grain and cause malfunction or even catastrophic failure due to an increase of burning surface. Composite propellants are in principle specific types of oxidizer - fuel pyrotechnic mixtures. As with pyrotechnics, there is also a concern whether decomposition induced by aging may affect thermal stability of the propellants or their sensitiveness to external stimuli.

In this article part of the results gained during studies of some composite solid rocket propellants in service with the Czech Army will be presented. These propellants were imported and there are no baseline data available from their manufacture. As there is still a need for extension of their service life, the necessary task was to characterize aging behavior of these propellants i.e. what properties are expected to change during aging and what trend the changes follow.

Aging of composite solid rocket propellants is evidently caused by degradation of the binder of the propellant as an effect of temperature, humidity and air oxygen. An isothermal accelerated aging at elevated temperatures is a method that influences properties of the propellant grain to a greatest extent. Beside this method it is suitable to realise a program of artificial aging with temperature shocks, which allow better detection of possible imperfect connection of propellant and insulation.

The process of aging of composite solid rocket propellants may be into a certain level observed by methods of chemical analysis. The degradation of binder matrix is often monitored by FTIR [4] or GPC [5] (determination of low-molecular fragments of polymers). The same property can be monitored indirectly by determination of the content of sol and gel [6,7,8], microcalorimetry [9] (especially for the determination of reactivity of individual components of the composition and their compatibility with the contact materials) eventually HPLC can be used for determination of remaining antioxidant content. However none of these chemical methods itself allows determination of the pass/fail criterion for service life prediction. The results of these methods always need to be correlated with results of mechanical tests.

Determination of plasticizer migration in the propellant grain is a very important method for the evaluation of its quality [10,11]. The increased migration of the plasticizer (especially into the insulation) can produce internal stresses in the propellant grain and affect the bond strength between the propellant and the insulation.

The composite solid rocket propellants are unique types of pyrotechnical mixtures, when considering their chemical composition, hence their thermal analysis exhibits similar characteristics as observed during thermal analysis of pyrotechnic mixtures. The effect of various additives on the reactivity of the composition [12,13], or compatibility with the constructive materials [14] can be easily determined by methods of thermal analysis. Changes of the thermal stability [15] during the artificial aging are less probable. The DTA, TGA and DSC are popular methods for testing of composite solid propellants.

The crucial problem with composite solid propellants is the determination of structural stability and integrity of the grain [16]. The failure of structural stability and integrity, caused by formation of cracks in the grain, separation of the insulation from the grain or the motor case can lead to critical conditions of rocket motors. The prediction and modeling of these changes is extremely complicated and requires use of finite element method (FEM), viscoelastic analysis and determination of cumulative damage. The flaw detection methods including X-ray, laser or optical [17,18] or ultrasonic [19] are the most usable methods for characterization of the structural integrity. The micromechanical changes like dewetting on the matrix-filler interface [20] influence results of mechanical properties such as tensile or compressive strength. The tensile strength tests are used also for determination of the bond strength on the grain/bondline interface [21].

Aging of composite solid propellants reflects to a deterioration of mechanical properties [22,23,24,25]. Usually decrease in deformation capacity on one hand and increases of hardness and toughness on the other is observed in the case of HTPB based solid propellants. DMA appears to be a very good method for complex characterisation of mechanical properties of solid propellants in the wide range of temperatures and frequencies [26,27]. However, the DMA does not allow the definition of single value failure criterions for solid propellants. Therefore it should be followed by determination of tensile [28,29] or compressive [30] strength and stress relaxation. Data acquired from these tests can provide necessary input parameters for structural analysis. Other methods providing additional

information on material behavior like the determination of hardness [31] or impact toughness [32] are also able to detect some changes in material properties of solid rocket propellants.

Determination of the interior ballistic properties of solid propellants (the time curves of pressure and thrust in the rocket motor) also necessary for determination of a stress-strain conditions of solid propellant in the rocket motor and fulfilment of performance characteristics.

2. EXPERIMENTAL

Ten in-service composite rocket propellants with different chemical compositions were selected for aging characterization. The propellants were mostly based on ammonium perchlorate (64 - 84 %) as oxidizer. In one case, ammonium nitrate (60 %) was used. Aluminium (10 - 18 %) was mostly applied as metal fuel. Different burning catalysts (lead salts, ZrO_2, NH_4VO_3, ferrocene) were incorporated. Variety of polymer binders was also applied, e.g. HTPB polyurethane, PBAN copolymer or epoxy resins, plasticized by phtalates, sebacates, aliphatic or naphtenic oils etc. Eight of the propellants were in configuration of cartridge-loaded grains; two of them were case-bonded propellants. Natural age of the propellants under the test ranged between 15 and 23 years (all beyond their guaranteed service life).

Block of propellants of about 1 kg weight were wrapped into aluminum foil and sealed. These samples were aged at 70 °C in a heating box for 28, 57 and 113 days. Acceleration coefficient (increase in decomposition rate with temperature) of composite propellants is usually considered between 2,3 and 2,6 per 10 °C of temperature. Aging at 70 °C for 113 days thus corresponds to about 30 or 60 years of natural age at 15 °C (average storage temperature in the Czech Republic), respectively. This natural age is much longer than expected actual service life of rocket and missile systems incorporating these propellants. This mode of aging characterization was thus considered representative enough to reveal changes that might occur in the propellants during service life of corresponding systems.

After each period of aging the blocks were taken out of climatic boxes and machined into a desired shape (samples for mechanical and thermomechanical tests), remaining chips were used for chemical analysis and thermal stability. Before and during machining, all samples underwent a visual inspection to see whether cracks, changes in color, layer separation or other visible changes occurred.

Aging characterization of composite rocket propellants consisted of chemical analysis (sol content), thermal analysis (DTA, TGA), mechanical properties determination (uniaxial tensile and compression tests, hardness), thermomechanical analysis (DMA, TMA) and sensitiveness tests (impact, friction, electric spark).

Chemical analysis for determination of sol (plasticizers and polymer fractions with low molecular weights) content was conducted in line with STANAG 4581 by repeated (4 times) extraction of 2 grams of shredded sample with 100 ml of toluene over 24 hours.

Differential thermal analysis (DTA) was carried out using L.E.X. DTA-550Ex with 50 mg sample in glass micro test tubes. A linear heating rate of 5 °C.min^{-1} in range from 20 °C to 500 °C and static air atmosphere were used. Thermogravimetric analysis (TGA) was conducted in accordance with STANAG 4515 on SHIMADZU DTG-60 with 10 mg of sample in open ceramic crucibles. Linear heating rate of 10 °C.min^{-1} in range from 20 to 1000 °C and dynamic nitrogen atmosphere 50 ml.min^{-1} were used.

Thermomechanical stability of the propellant samples was assessed using dynamic mechanical analysis (DMA). DMA analyses were carried out on a R.M.I. DMA DX-04T in accordance with STANAG 4540. The samples were prepared in form of rectangular blocks 40 x 10 x 5 mm by die cutting of plates milled from the propellant grain. The measurements were done at the temperature range from –100 °C to +100 °C and scan rate of 3 °C.min^{-1} with sinusoidal force at frequency of 1 Hz. A deformation amplitude ±0,05 mm was applied to the sample mounted as a single cantilever. Temperature dependence of coefficient of thermal expansion α was measured in temperature range from -100 °C to +100 °C on TMA CX-04R. Linear heating rate 3 °C.min^{-1} and cylinder samples (8 mm length x 5 mm radius) were used to comply with STANAG 4525.

Uniaxial tension (STANAG 4506) and compression (STANAG 4443) tests were carried out on INSTRON TT-CM tester at three temperatures - 40 °C, +20 °C and +50 °C with constant crosshead speed of 10 mm.min^{-1}. The compression tests were carried out with rectangular samples 5 x 5 x 10 mm and tension tests with 40% reduced STANAG 4506 dog bones.

The BAM impact machine was used to determine impact sensitivity of tested propellants. The sample size was 40 mm^3 and out of the available weights, 1 kg drop weight was used. Methodology and test device were in agreement with STANAG 4489. The BAM friction apparatus was employed for the evaluation of friction sensitivity in accordance with STANAG 4487. The samples of 20 mg were used and maximum force applied was 360 N. The sensitivity to electrostatic discharge was determined on small-scale tester in line with STANAG 4490. The samples were prepared in form of cylinders with diameter 2,5 mm and length 1 mm by die cutting from chips. All samples were stored in dessiccator for at least 1 hour prior to the test. It was not expected to find any stable trends in sensitiveness and therefore only original and most aged (113 days) samples were measured.

3. RESULTS AND DISCUSSION

Visual examination

Visual inspection is one of the most common tests used to determine appearance of cracks in propellant grains, debonding of insulation or changes in color due to a chemical or physical changes in polymer matrix. It is very simple but requires dissection of tested grain making ballistic tests of this grain impossible. However in case of studied propellants dissection did not present a problem.

Cracks or other critical flaws were not observed in neither of the tested propellants. Propellants containing dye stuff exhibited changes in color. Sweating of dye followed by its oxidation probably caused this phenomenon, which is not critical itself.

Chemical analysis

Increased temperature during period of accelerated aging may speed up changes taking place within polymer matrix. For example HTPB propellants may undergo additional cross-linking, epoxy resins may depolymerize and plasticizers can evaporate or change in gradient within the grain.

Determination of extractable portions as an indirect method of determination of polymer degradation was chosen for our tests. Increase of extractable portions was most apparent in case of insulated propellants containing epoxy resin as a binder. Insulation

played significant role, since practically identical propellant only without isolation exhibited decrease of extractable portions. This phenomenon is probably caused by joint effect of depolymerization of propellant matrix and evaporation of plasticizer. Depolymerization takes place in both cases, but is overwhelmed by evaporation of plasticizer when insulation is present. No significant general trends were observed. Results of different propellants are summarized in Fig.1.

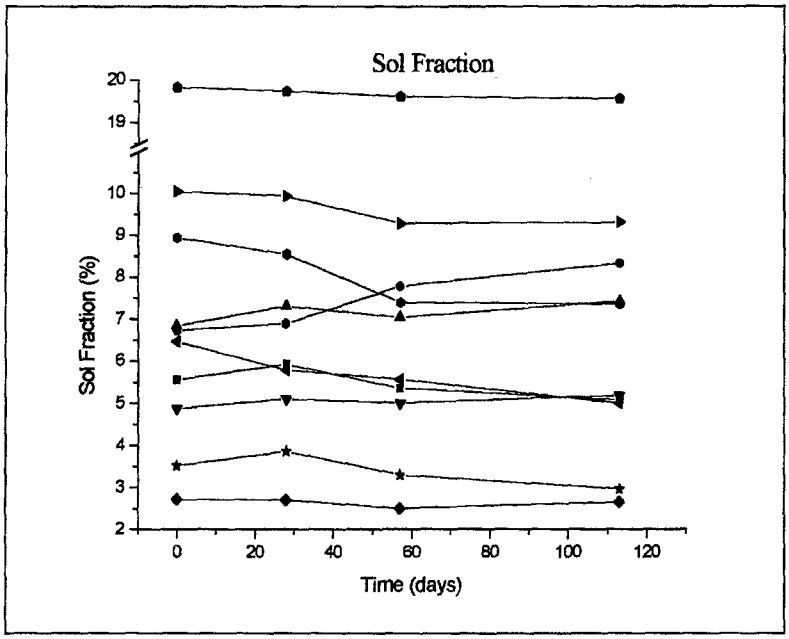


Fig 1. Amount of sol fraction as a function of time of accelerated aging

Thermal stability

Termogravimetric analysis (TGA)

Starts, onsets and maxima of decomposition were evaluated from thermogravimetric curve. No significant changes in thermal stability of samples were observed outside of the usual range of inaccuracy caused either by inhomogeneity of tested material or subjective determination of the beginning of decomposition. It is apparent from results that the thermal stability of AP based samples is rather high and there is no reason to believe that they could present self-ignition danger even if stored in hot climate. Thermal stability of AN propellant is lower in absolute values when compared with samples containing AP.

Differential thermal analysis (DTA)

Starts and maxima of decomposition were evaluated from DTA curve. DTA did not provide results that could be easily evaluated without certain level of experience. The beginning of decomposition is sharper when compared to pyrotechnic mixtures unlike the

maximum of decomposition that has a character of multiple step process depending into a great extent on a form of the sample, its position in the test tube and other effects (the differences between two results of the same sample were sometimes as high as 20 °C). Slight decrease in beginning of decomposition was observed in case of AP/epoxy resin composition. Accelerated aging did not influence stability of other samples.

Mechanical properties

Uniaxial Compression and Tension

Maximum stress σ, deformation at maximum stress ε and modulus E were determined from σ-ε dependence at compression and tension for three temperatures. Samples were compressed in all three possible directions to determine whether the properties change with respect to a direction in the grain. Unlike in case of double base propellants, no anisotropy was observed as assumed. Changes in mechanical behavior determined by uniaxial loading were only very small. This indicates that isothermal aging of tested propellants was not sufficient to damage them enough to cause decrease in mechanical capacity.

Some results of maximum stress as a function of accelerated aging time are presented for compression and tension loading in figure 2 and 3 respectively.

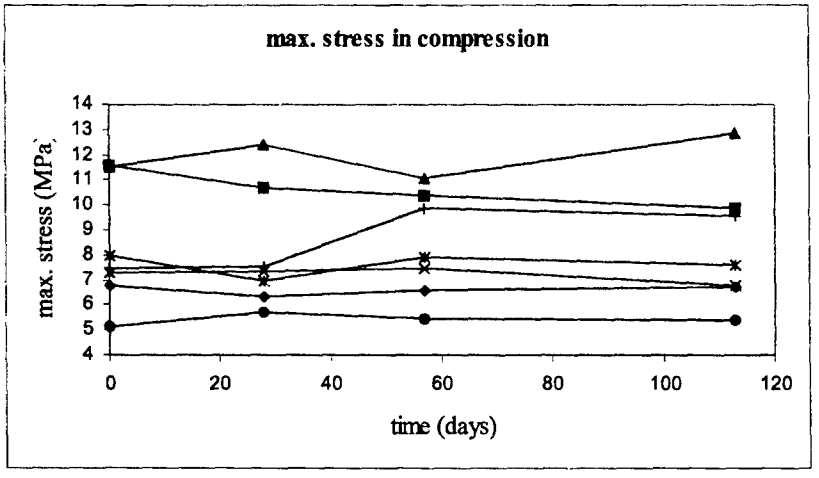


Fig 2. Maximum stress in compression at 20°C and rate 1 $cm.min^{-1}$

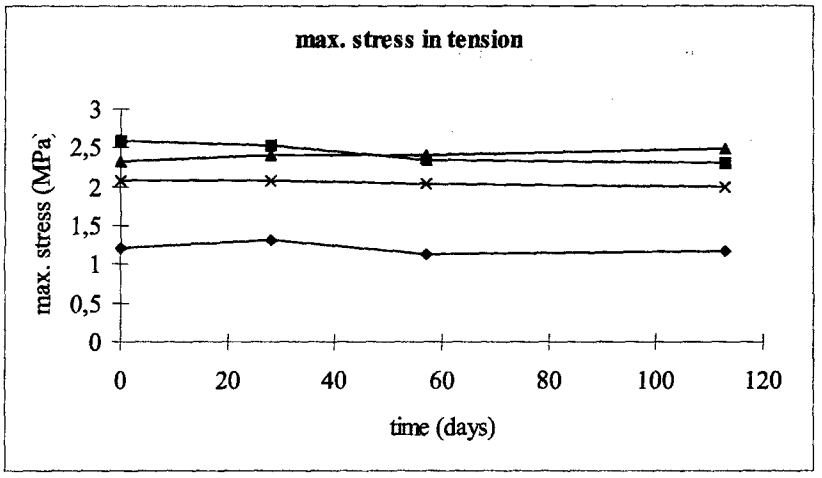


Fig 3. Maximum stress in tension at 20°C and rate 1 cm.min^{-1}

Thermomechanical properties

Dynamic mechanical analysis (DMA)

The entire curves were compared to evaluate changes in real (E′) and imaginary (E′′) part of the modulus as well as changes in loss tangent (tan δ) as a result of accelerated aging. Glass temperatures were determined from the maximum of tan δ. Another parameter determined was complex modulus (E).

Two basic trends in mechanical behaviour were observed during artificial ageing of tested propellants. Some propellants showed a stable decreasing trend in storage modulus. This "softening" process of these propellants can probably be attributed to dewetting of crystalline fillers from binder matrix rather than depolymerization of the binder. Other samples showed the opposite (increasing) trend in dynamic storage modulus after artificial ageing. This "hardening" process can be attributed to additional crosslinking reactions inside the three-dimensional polymer net typical for HTPB based propellants. At last some propellants were not affected by ageing even after 113 days at 70 °C (fig.4). Practically no influence of artificial ageing on values of glass transition temperatures of any propellant sample was detected.

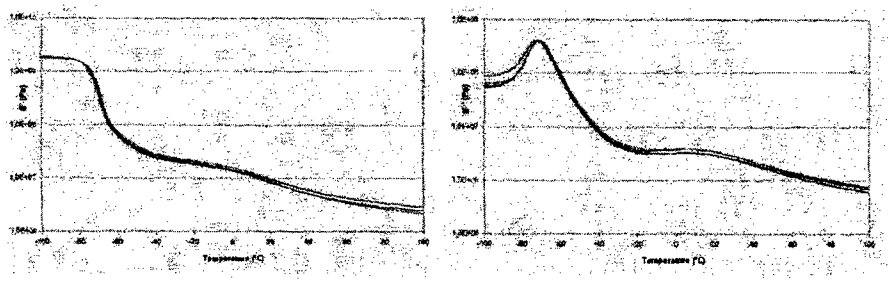


Fig 4. Dynamic mechanical behaviour

Thermomechanical analysis (TMA)

Temperature dependencies of coefficients of thermal expansion were measured. From comparison of original and artificially aged samples can be conducted that in most cases the dependence of coefficient of thermal expansion does not change. In case of two samples slight changes in the coefficient were observed - decrease for one and increase for the other.

Sensitiveness

Impact sensitivity

As can be seen from the results in figure 5 significant increase of sensitivity was observed only in case of one propellant. This sample contained AP and an epoxy resin. In case of two samples neither decrease nor increase in E_{50} value was observed. The rest of tested propellants became slightly less sensitive to impact as an effect of accelerated aging.

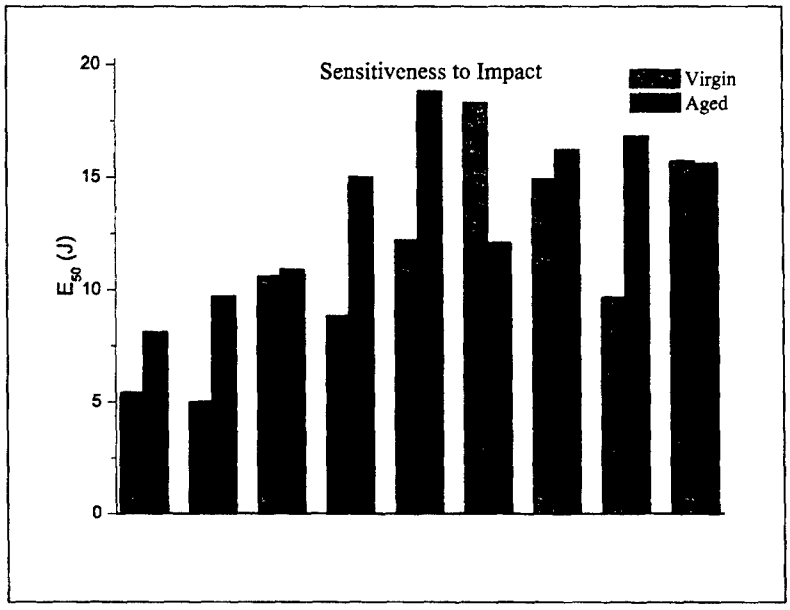


Fig 5. Sensitiveness to impact

Even it is not the primary goal of this article it is interesting to compare absolute values of sensitivities of measured propellants with sensitivities of some common explosives. Two most sensitive samples exhibited sensitivities of crystalline PETN. Other samples were less sensitive and could be fitted into interval with crystalline RDX on one end and PETN/TNT mixture on the other. Sample containing AN was found to be relatively insensitive to impact. In general it is important to consider AP composite rocket propellants to be very sensitive to impact!

Friction sensitivity

Decrease of friction sensitivity was observed for all but three samples as shown in figure 6.

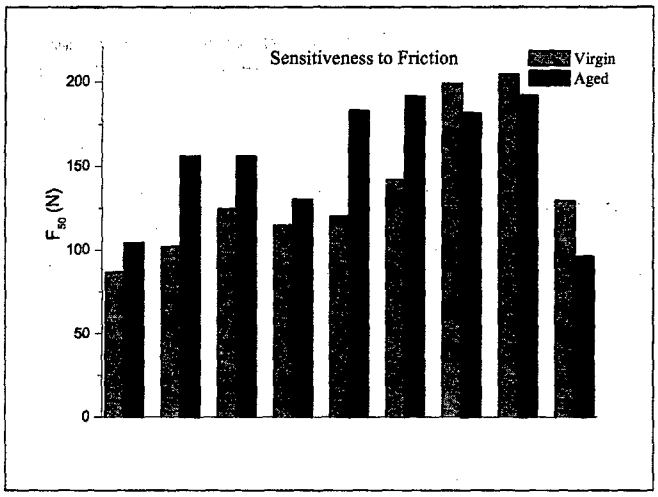


Fig 6. Sensitiveness to friction

Electric spark sensitivity

Trend common to all AP propellants was not observed. Some samples exhibited increase while other decrease in sensitivity to electric spark (figure 7). It can be stated that tested propellants were not too sensitive neither prior to nor after the artificial aging. The biggest decrease in sensitivity was observed with AN propellant where the minimum activation energy almost tripled.

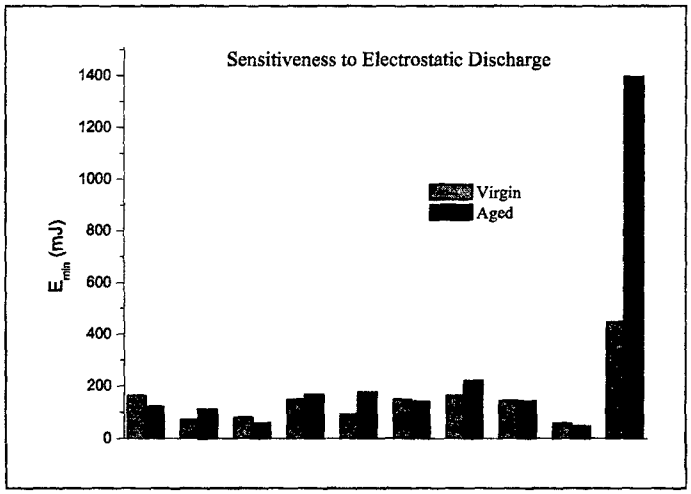


Fig 7. Sensitiveness to electrostatic discharge

4. CONCLUSION

Ten in-service composite solid rocket propellants were submitted to artificial aging for evaluation of changes in their properties, stability and sensitivity that are expected to occur in next several dozens of years of natural aging. Results of these tests were necessary for selecting appropriate methods for surveillance procedures of the propellants.

Prior to this work it was expected based on information in literature that deterioration of composite propellants properties would follow some typical trends like the one proposed by Layton for mechanical properties or the well-known Arrhenius dependence for thermo-mechanical properties. It was however found that the properties stay more or less constant and are not influenced by relatively short-term isothermal accelerated aging into an important enough extent. No significant changes were detected in thermal stability of the propellants induced by artificial aging. Composite solid rocket propellants showed relatively high sensitiveness to external stimuli. The sensitiveness characteristics were increased by aging only in a very few cases.

It is apparent that conducted tests are not sufficient to determine safety and guarantee performance of tested propellants. It would be necessary to perform complete stress analysis including computer modeling, complete failure analysis including multidimensional testing and ballistic tests for data acquisition and confirmation of predicted results. However based on the results presented above we believe that no significant changes compared to the present state will take place within the propellants under the tests in at least next twenty years if controlled storage environment (15 °C, hermetical sealing) is provided.

Acknowledgement

This paper presented selected results from a defence research program „Chemical tests of munitions" sponsored by the Czech Ministry of Defence under contract No.0/50/1/7/3/316. Authors would like to thank Ms. Šárka Ochmanová for providing some of the analytical results.

REFERENCES

[1] M. HANUS: Proc. 4th Seminar New Trends in Research of Energetic Materials, Pardubice, 112 (2001).

[2] M. HANUS: Proc. Czech Army Pyrotechnics Conference, Luhačovice, (2000).

[3] J.PACHMÁŇ, M. HANUS: Proc. of 4th Seminar New Trends in Research of Energetic Materials, Pardubice, 278 (2001).

[4] Torry, Simon; Cunliffe, Anthony: Int. Annu. Conf. ICT, Karlsruhe, **31**, 25 (2000).

[5] Chevalier S., Perut C., Billon L. et al.: Int.Annu.Conf.ICT, Karlsruhe, **25,** 12(1994).

[6] Amer A.A., Moeen M.H., Ameen H.H.: Int.Annu.Conf.ICT, Karlsruhe, **25**, 103 (1994).

[7] Layton L.H.: Report AD-A010731,185 (1975).

[8] Layton L.H.: Report AD-759564 (1973).

[9] Chin A., Ellison D. S.: Proc. Int. Pyrotech. Sem. **20**, 203 (1994).

[10] Gottlieb L.: Int.Annu.Conf.ICT, Karlsruhe, **25**, 90 (1994).

[11] Keizers H.L.J.: Proc.Int.Symp.Energ.Mater.Technol.,200 (1995).

[12] Shen S., Chen S., Wu B.: Thermochim Acta **223**, 135 (1993).

[13] Lokander, M.; Stenberg, B.; Sanden, R.: Propellants, Explos., Pyrotech. **23** (5), 272 (1998).

[14] Cheng C. S., Hwu W. H., Huang C. C.: Proc. Int. Anu. Conf. ICT, Karlsruhe, **24**, 80 (1993).

[15] Oyumi Y., Kimura E., Nagayama K.: Propellants, Explos., Pyrotech. **22**, 263 (1997).

[16] Geiler, E.; Eisenreich, N.; Geiler, A.; Hubner, C.: Int. Annu. Conf. ICT, Karlsruhe, **31**, 149 (2000).

[17] Samsonov V.P.: Int.Annu.Conf.ICT, Karlsruhe, 27 118 (1996).

[18] Lohrmann M., Huebner Ch.: Int.Annu.Conf.ICT, Karlsruhe, **27**, 140 (1996).

[19] Agrawal J.P., Singh H.: Propellants, Explos., Pyrotech. **18**,106 (1993).

[20] Hubner C., Geissler E., Elsner P. et al.: Propellants, Explos., Pyrotech. **24**, 119 (1999).

[21] Haska S.B., Pekel F.: Int.Annu.Conf.ICT, Karlsruhe, **26**, 49 (1995).

[22] Zee, F.W.M.: Int.Annu.Conf.ICT **14**, 337 (1983).

[23] Scedlbauer F.: Int.Annu.Conf.ICT, Karlsruhe, 275 (1971).

[24] Miedema J.R., Zee F.W.M., Meulenbrugge J.J.: Int.Annu.Conf.ICT, Karlsruhe, **20**, 13 (1989).

[25] Sbriccoli E., Saltarelli R., Martiucci S.: Proc. Int. Anu. Conf. ICT, Karlsruhe, **20**, 15 (1989).

[26] Tod D. A.: Proc. Int. Anu. Conf. ICT, Karlsruhe, **20**, 19 (1989).

[27] Ho S.Y., Tod D.A.: Int.Annu.Conf.ICT, Karlsruhe, **21**, 30 (1990).

[28] Liu Z., Hao Z., Xie J. et al.: Theory Pract.Energ.Mater.(Proc.Int.Autumn Semin. Propellants, Explos., Pyrotech.), 194 (1996).

[29] Amer A. A., Moeen M., Ameen H. H.: Proc. Int. Anu. Conf. ICT, Karlsruhe, **25**, 103 (1994).

[30] Cruz E., Guillermo J.: Proc. Int. Anu. Conf. ICT, Karlsruhe, **30**, 80 (1999).

[31] Gaudin C., Meyen M.: Int.Annu.Conf.ICT, Karlsruhe, **13**, 301 (1982).

[32] Marom G., Harel H., Rosner J.: J.Appl.Polym.Sci. **21**, 1629 (1977).

CHARACTERISATION OF EXPLOSIVE MATERIALS USING MOLECULAR DYNAMICS SIMULATIONS

Miroslav Pospíšil*, Pavla Čapková*,
Pavel Vávra and Svatopluk Zeman****

* Department of Chemical Physics and Optics, Faculty of Mathematics and Physics, Charles University Prague, Ke Karlovu 3, 12116 Prague 2, Czech Republic.

** Department of Theory and Technology of Explosives, University of Pardubice, 53210 Pardubice, Czech Republic.

Abstract:

Classical molecular dynamics simulations of the unimolecular decomposition have been performed for selected molecules exhibiting different impact sensitivity and different detonation energy: (1) $(CH_2NNO_2)_3$, more commonly known as RDX, (2) $(CH_2NNO_2)_4$, known as HMX, (3) $(NH_2)_2CC(NO_2)_2$, known as DADNE and (4) $(NH_2)_2CNNO_2$, known as NQ (see figures 1-4a). A potential energy was described using empirical force field cvff_950. Molecular dynamics simulations were carried out in Cerius² modelling environment. The analysis of dynamic trajectories enabled us to reveal step by step the mechanism of decomposition and to characterize the impact sensitivity and explosives performance (detonation energy) of these energetic materials. The characteristic parameters determined from the dynamics trajectory simulations are in agreement with the experimentally measured sensitivity and detonation energy.

Keywords: *energetic molecules, molecular decomposition, explosives, molecular dynamics simulations.*

1. INTRODUCTION

The work presented here is a continuation of studies focused to unravelling of molecular decomposition process in explosive materials [1- 7]. We use the classical molecular dynamics in *Cerius²* modelling environment for the simulation of molecular decomposition. The aim of the present work is to reveal step by step the mechanism of explosion and to find the way of reliable characterisation of high explosive materials using molecular dynamics simulations of the decomposition process. The characteristics describing the sensitivity and performance of explosives found by computational studies can reduce the cost and risk to personnel by experimental work.

Two similar molecules have been chosen for the present study: cyclotrimethylene-trinitramine, known as RDX and β-cyclotetramethylene-tetranitramine, known as HMX. These compounds belong to the most important energetic materials. HMX exists in four polymorphic modifications known as α, β, γ and δ form. The β form is stable at room temperature and is used in the general applications. The structure of molecules is in the figure 1a,b. The crystal structure is reported in [8] for RDX and [9] for β-HMX.

The impact sensitivities of the RDX and β-HMX were studied using the drop weight apparatus and were reported together with the detonation energy in [10]. Two decomposition pathways have been reported in the previous studies [1,5] (see the next paragraphs).

2. STRATEGY OF MOLECULAR DYNAMICS SIMULATIONS

A natural starting point for a theoretical study is to investigate the chemical decomposition at the molecular scale. Classical molecular dynamics simulations in *Cerius*^{2} modelling environment [11] were carried out to calculate dynamics trajectory for one isolated molecule. Searching for the optimum strategy we have found the following conditions for dynamics simulations:

- We used the "*Impulse dynamics*", that means at the beginning the system get the initial impulse, corresponding approximately to double of the chosen temperature to assign the initial velocities to the atoms.
- The calculations were performed in *microcanonical ensemble* (NVE). Newtons equations of motion were integrated by using Verlet integrator. Although the temperature is not controlled during NVE dynamics, *Cerius*^{2} allows us to hold the temperature within specified tolerances by periodic scaling of the velocities.
- Dynamics trajectories were calculated under following conditions: force field *cvff_950* [12] has been used, dynamics time step 0.001ps. The length of the dynamic trajectory in *ps*, the initial temperature and consequently the initial energy impulse were dependent on the sensitivity of the molecule investigated. Atomic charges in *Cerius*^{2} are calculated using the charge equilibration method [13].
- In all initial models the crystallographic conformation was used as a starting geometry.

The dynamic trajectories include the data such as the model structure, temperature and energies in dependence on the time (in *ps*). The animation of the dynamic trajectories enables us to visualise the time dependence of the unimolecular decomposition process, starting from the first bond scission to the release of the nitro-groups NO_2. The course of dynamic trajectories, i.e. the time dependence of temperature, kinetic, potential and total energy allows us to estimate the parameters characterising the explosives as to the sensitivity and performance.

3. RESULTS AND DISCUSSION

Dynamics trajectories revealed the mechanism of the molecular decomposition for selected molecules: RDX, β–HMX, DADNE and NQ (see figure 1a-d). As one can see in the figure 1, selected molecules can be divided into two groups with the similar structure: (1) RDX and β–HMX and (2) DADNE and NQ. The analysis of dynamic trajectories showed that there is also the similarity in the decomposition process and similarity in course of the time dependence of temperature, kinetic, potential and total energy during the decomposition process for RDX and β–HMX. Similarity of decomposition characteristics has been found also for DADNE and NQ molecules.

In the case of RDX two decomposition processes are suggested on the base of experiment (B.M. Rice et al. [5] and Shalashilin & Thompson [1]):

$$RDX \rightarrow C_2H_4N_3O_4 + NO_2 \qquad (R1)$$

$$RDX \rightarrow 3CH_2NNO_2 \qquad (R2)$$

In the reaction R1 the rupture of the first C-N bond is followed immediately by the rupture of the first N-NO_2 bond (release of the nitrogroup), as one can see in the figure 2a. Then the rest of the molecule is gradually totally decomposed. Reaction R2 starts with the rupture of three C-N bonds and subsequent break up of the molecule into three CH_2NNO_2 fragments (see figure 2b). Afterwards the NO_2 groups are released from the fragments. Both processes R1 and R2 were observed in our dynamic trajectories calculated for RDX and β–HMX, as it is illustrated in the figure 2a,b for RDX. β–HMX exhibits the same decomposition behaviour as RDX as to the reaction pathways R1 and R2. Analysis of about 40 dynamic trajectories calculated for RDX and β–HMX showed that both processes occur with the same probability at low and high temperature. The dynamic analysis also showed that the most probable process of decomposition is the combination of both reactions R1 and R2. Two examples of the dynamic trajectories for the molecule RDX are presented in the figure 3a,b, where the figure 3a illustrates the reaction pathway R1 and the figure 3b shows the trajectory for the reaction R2. Figure 4 shows the example of trajectory for β–HMX, where the decomposition process is the combination of R1 and R2 reactions. Decomposition of the molecules DADNE and NQ starts by the scission of the H-N bonds, with a subsequent rupture of C-N bonds and afterwards the NO_2 groups are released. In this case the bond scission is accompanied with the large fluctuations of temperature and kinetic energy, as one can see in the figures 5,6.

Figures 3-6 show the course of temperature along the dynamic trajectory of the system for the molecules RDX, β–HMX, DADNE and NQ. Comparing the dynamic trajectories for all investigated molecules, one can see the similar character of $T \sim time$ dependence for the molecules of the first group (RDX and β–HMX) and similarity in $T \sim time$ dependence for the molecules of the second group (DADNE and NQ). Analysis of dynamic trajectories enabled us to determine two parameters, characterising reliably the decomposition process:

- $T(NO_2)$ - is the instantaneous value of temperature corresponding to the rupture of C(N) - NO_2 bond and release of the first NO_2 group
- ΔT_{50} - is the temperature increment per 50 fs after the release of the first NO_2 group, i.e. in the time interval $t(NO_2)$ - $t(NO_2)+50fs$. This parameter characterises the slope of the $T \sim time$ dependence after the release of the first nitro-group. In case of DADNE and NQ the ΔT_{50} was calculated after the time averaging of the dynamic trajectory from the smoothed $T \sim time$ curve.

These calculated parameters were compared with the experimentally determined characteristics of the explosives like impact sensitivity h (the critical value of the fall height of the drop weight) and detonation energy E_D (see table 1), where the h and E_D values are overtaken from the work [10]. The comparison of calculated and experimental characteristics is in the table 1 for all investigated molecules. As one can see in the table 1, the $T(NO_2)$ values exhibit the same trend as the h values in dependence on the molecule type. On the other hand, the course of the parameter ΔT_{50} agrees with the course of the detonation energy E_D in dependence on the molecule type. Both parameters $T(NO_2)$ and ΔT_{50} obtained from the classical molecular dynamics simulations agree with the experimental characteristics, that means: $T(NO_2)$ can be used to characterise the impact sensitivity and ΔT_{50} characterises the detonation energy.

Table 1. *Comparison of experimental (h, E_D) and calculated (T (NO_2) , ΔT_{50}) characteristics of the explosive materials; h - the impact sensitivity, E_D - detonation energy, T (NO_2) - temperature corresponding to the release of the first nitro-group, ΔT_{50} - temperature increment per 50fs after the release of the first nitro-group*

Molecule:	h (cm)	T (NO_2) (K)	E_D (kJ/cm^3)	ΔT_{50} (K)
RDX	24	6240	8.321	45500
β–HMX	26	8300	8.858	70500
DADNE	100	834100	7.889	34700
NQ	177	1718100	6.650	23200

4. CONCLUSIONS

Present results showed that classical molecular dynamics simulations represent very useful and reliable tool for the characterisation of the explosive materials. Dynamic trajectories revealed in details the mechanism of the molecular decomposition for four selected molecules: RDX, β–HMX, DADNE and NQ. Parameters obtained from dynamic trajectories agree with the experimental values of characteristics describing the impact sensitivity and detonation energy in case of investigated molecules. This investigation should be extended to a larger group of explosive materials to confirm the validity of present conclusions. Anyway, present results offered us a good chance to characterise the explosive materials by a reliable way using molecular dynamics simulations.

Acknowledgements:

The authors express their gratitude to Grant Agency of the Czech Republic for support of an access to the crystallography database in Cambridge (within the framework of the project No. 203/02/0436) and gratefully acknowledge grant-in-aid from the Ministry of Industry and Commerce of the Czech Republic (project No. FC-M2/05).

REFERENCES:

[1] D. V. Shalashilin and D. L. Thompson: Monte Carlo Variational Transition-State Theory Study of the Unimolecular Dissociation of RDX, J. Phys. Chem. A, **101**, 961-966, 1997.

[2] Y. Kohno, K. Ueda and A. Imamura: Molecular Dynamics Simulations of Initial Decomposition Process on the Unique N-N Bond in Nitramines in the Crystalline State, J. Phys. Chem, **100**, 4701-4712, 1996.

[3] P. Vávra: Electronic Density of Molecule and Some Properties of High Explosives, Proc. 4th Seminar "New Trends in Research of Energetic Materials" Univ. of Pardubice, CR, p. 3-5, April 2001.

[4] S. Zeman, R. Huczala and Z. Friedl: The study of Chemical Micromechanism Governing Detonation Initiation of Some m-Dinitrobenzopolyazaarenes, J. Energet. Mater. **20**, in press, 2002.

[5] B. M. Rice, G. F. Adams, M. Page and D. L. Thompson: Classical Dynamics Simulations of Unimolecular Decomposition of CH_2NNO_2: HONO Elimination vs N-N Bond Scission, J. Phys. Chem. **99**, 5016-5028, 1995.

[6] Ch. J. Wu and L. E. Fried: First-Principles Study of High Explosive Decomposition Energetics, Proc. 11th International Symposium on Detonation, Colorado, 490-497, 1998.

[7] H. Dorsett: Computational Studies of FOX-7, a New Insensitive Explosive, DSTO Aeronautical and Maritime Research Laboratory, Salisbury South Australia, 2000.

[8] C. S. Choi and E. Prince: The Crystal Structure of Cyclotrimethylene-Trinitramine, Acta Cryst., **B 28**, 2857-2862, 1972.

[9] C. S. Choi and H. P. Boutin: A Study of the Crystal Structure of β-Cyclotetramethylene Tetranitramine by Neutron Diffraction, Acta Cryst., **B 26**, 1235-1240, 1970.

[10] P. Vávra: Studie o energii trhavin, Proc. 3rd Seminar "New Trends in Research of Energetic Materials" Univ. of Pardubice, CR, p. 223-227, April 2001.

[11] *Cerius*^{2} documentation, June 2000, San Diego: Molecular Simulations Inc, 2000.

[12] A. T. Hagler, E. Huler and S. Lifson: Energy Functions for Pepetides and Proteins. I. Derivation of a Consistent Force Field Including the Hydrogen Bond from the Amide Crystals, J. Am. Chem. Soc, **96**, 5319-5327, 1974.

[13] A. K. Rappé and W. A. Goddard III: *Charge Equilibration for Molecular Dynamics Simulations*, J. Phys. Chem., **95**, 3358-3363, 1991

Figures description:

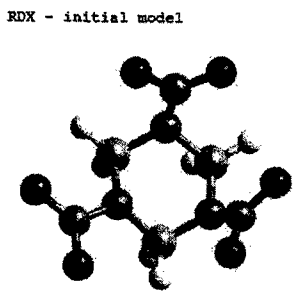


Fig 1a RDX molecule

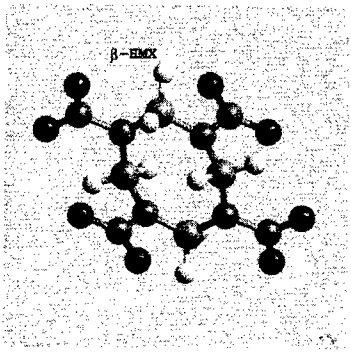


Fig 1b β-HMX molecule

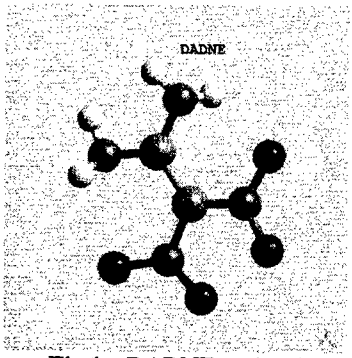


Fig 1c DADNE molecule

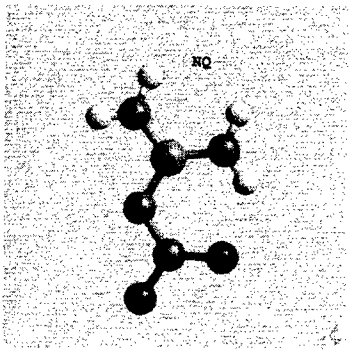


Fig 1d NQ molecule

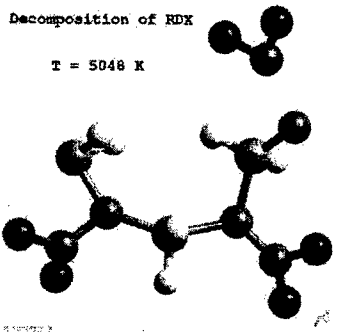


Fig 2a Decomposition of RDX molecule – reaction R1

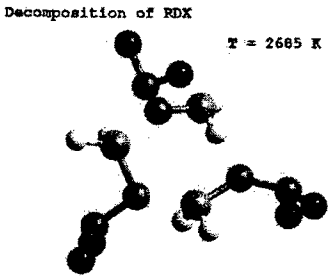


Fig 2b Decomposition of RDX molecule – reaction R2

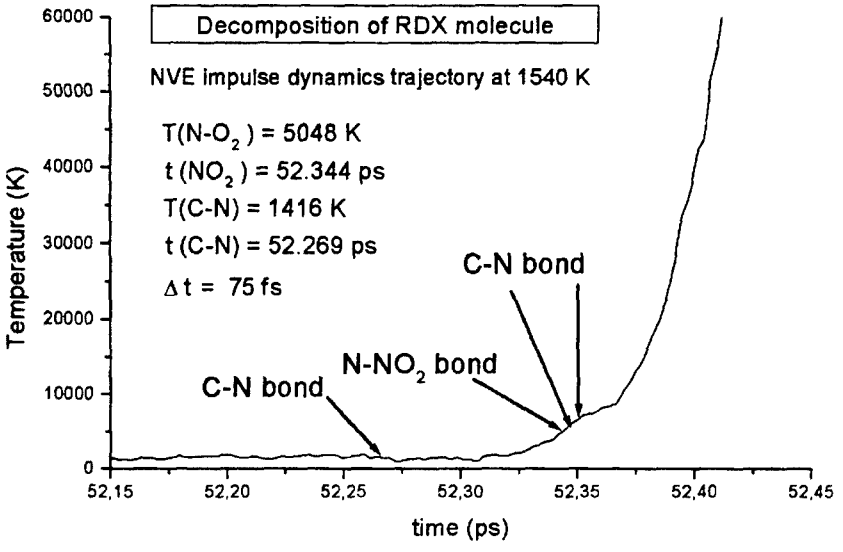


Fig 3a Dynamics trajectory for RDX molecule - reaction R1.

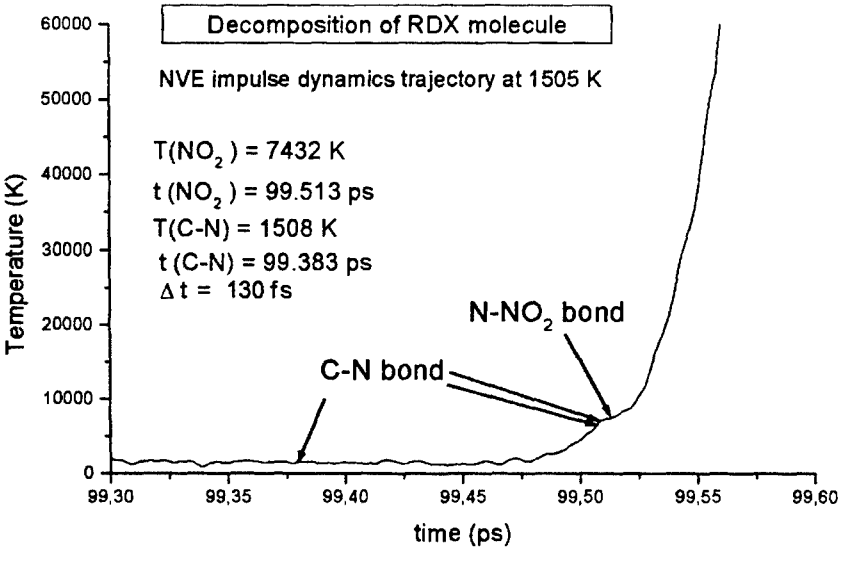


Fig 3b Dynamic trajectory for RDX molecule - reaction R2

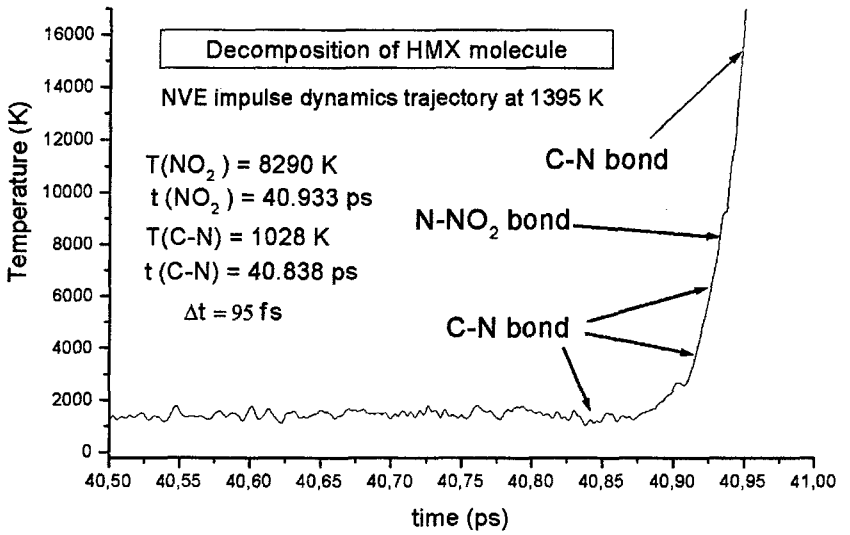


Fig 4 Dynamics trajectory for HMX molecule

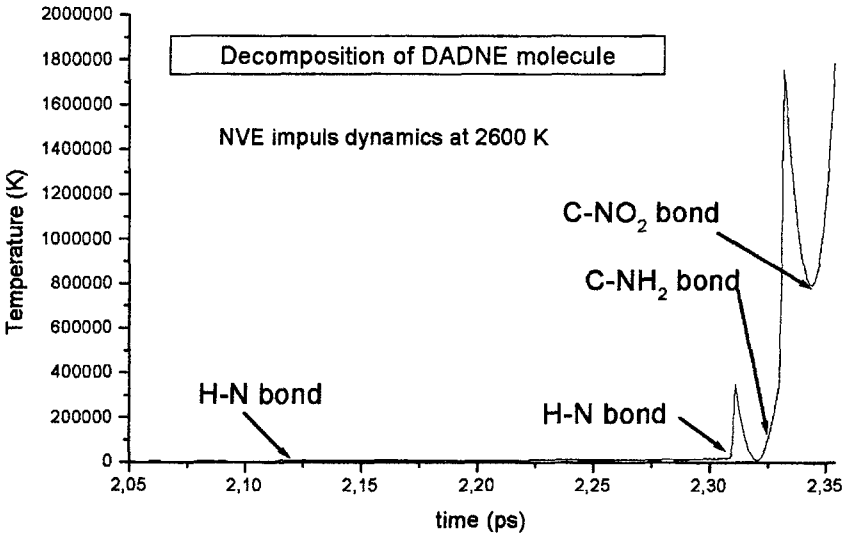


Fig 5 Dynamic trajectory for DADNE molecule

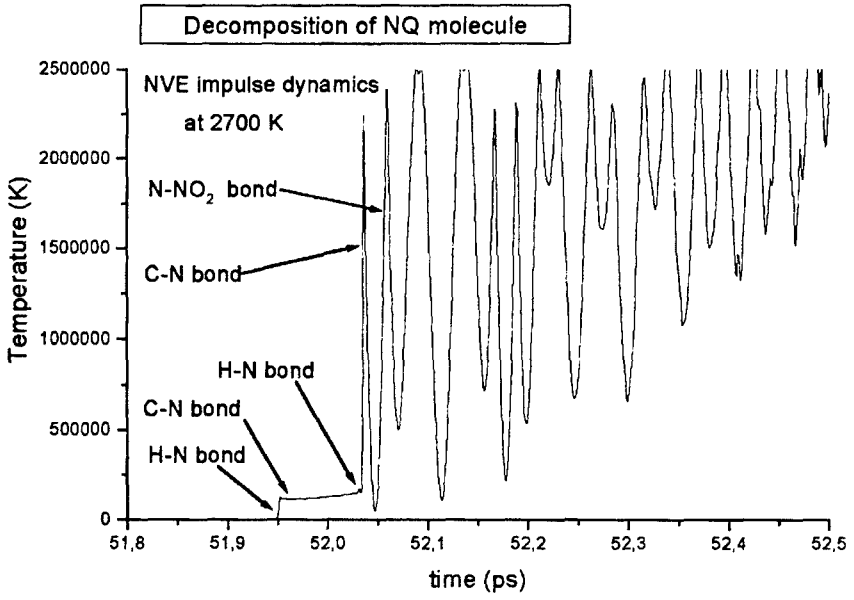


Fig 6 Dynamic trajectory for NQ molecule

THERMAL PROPERTIES OF A NITROCELLULOSE PROPELLANT UNDER ACCELERATED AGEING CONDITION

Maša Rajić and Muhamed Sućeska

Brodarski institut - Marine Research & Special Technology
Av. V. Holjevca 20, 10000 Zagreb, Croatia

Abstract:

The stabiliser content, sample mass, thermal and kinetic properties of a nitrocellulose propellant were followed during the accelerated ageing at 100 °C.

The differential scanning calorimetry (DSC) and thermogravimetric analysis (TGA) were used for determination of the thermal and kinetic properties, while stabiliser content has been determined by UV-VIS spectrophotometer.
It was found out that, at selected ageing temperature, the stabiliser consumes almost completely after four-five days, while at the same time some thermal properties do not change so significantly (e.g. onset, endset, and peak maximum temperature on DSC thermogram). The kinetic and thermal parameters decrease with the ageing, however this decrease is not monotonous along the investigated ageing period.

1. INTRODUCTION

Because of the wide use and practical importance of nitrocellulose, its degradation mechanism and kinetics have been the subject of numerous investigations[1,2,3,4,5,6,7,8,9,10,11,12].

The thermal decomposition reactions in nitrocellulose, which is the basic component of all homogeneous propellants, limit the safe use and safe storage time of propellants. Under certain conditions the decomposition many lead to the well-know phenomenon of self-ignitions.

The ageing of propellants is not only a safety problem. It also causes the decreases of a number of important properties of the propellants. Therefore, it is necessary to quantify the ageing by measuring both the changes of these relevant properties and the hazard potential figures-of-merit of the propellant, as a function of the time and temperature.

Apart from ageing due to the chemical reaction, there is also ageing due to physical and physical-chemistry processes. Both chemical and physical ageing results in changes of a number propellant properties, such as decrease of nitrocellulose molar mass, decrease of stabiliser content, decrease in mass, changes of mechanical and ballistic properties, etc.

The aim of this work was to identify and to study changes of some thermal properties, as well as kinetic properties, of a nitrocellulose propellant under accelerated ageing at 100 °C.

2. EXPERIMENTAL

In order to follow the changes of stabiliser content, thermal, and kinetic properties of a nitrocellulose propellant during the accelerated ageing, the propellant samples weighing 10 g were subjected to the accelerated ageing in the close vessels at 100 °C temperature.

The thermal measurements were carried out by using differential scanning calorimeter (*TA Instruments,* DSC Model 2910), and thermogravimetric analyser (*TA Instruments*, SDT Model 2960). The measurements are performed using aluminium sample pans.

The non-isothermal DSC curves were obtained using ~ 0.5 mg samples placed in a perforated aluminium sample pans, with heating rate of 3 °C min^{-1}, and under nitrogen atmosphere (purity above 99.996%) with flow rate of 50 ml min^{-1}. The DSC cell was calibrated by indium.

The isothermal TGA curves were obtained at several temperatures in the temperature range 130-160 °C, in the following way. The apparatus furnace was preheated to the temperature of interest, and then heated isothermally about ten minutes before the sample was introduced. After that, when the temperature gets equilibrated, the pan with the sample was placed on the sample platform.

The amount of diphenylamine (DPA) as a stabiliser, was determined using an UV-VIS spectrophotometer (*Varian*), at wavelength of 560 nm. The DPA derivatives were extracted by methyl chloride. Concentration of active DPA was determined by adding ethanol and Fe(III)-chloride, which give blue colour with DPA.

3. RESULTS AND DISCUSSION

Ageing of propellant

The selected single base propellant was aged for 9 days at 100 °C. These are conditions that correspond to 20 – 30 years of storage at the room temperature. During predetermined time of accelerated ageing propellant sample was weighed in order to follow changes in the sample mass. The results obtained in this way are presented in Figure 1.

After 60 minutes of heating at 100 °C sample mass loss was 0.49 %. This mass loss, which is due to water and residual solvent evaporation, is not shown in Figure 1. It was found that the sample mass loss during the first five days of ageing may be described the best by the power law kinetic model given by the following equation:

$$\frac{d\alpha}{dt} = m \cdot k \cdot \alpha^{\left(\frac{m-1}{m}\right)}, \qquad (1)$$

where k is the temperature-dependent reaction rate constant, t is time, α is conversion, $d\alpha/dt$ is rate of conversion, and m is constant, or in integral form:

$$\alpha^{\frac{1}{m}} = kt \qquad (2)$$

By the non-linear curve fitting of the experimentally obtained data it was found that constant m in Eq. 1 and 2 has value close to 0.5, which means that the reaction is diffusion

controlled (since one-dimensional diffusion-controlled reaction may be described by the equation: $\alpha^2 = kt$).

The sample mass loss during the first five days of ageing corresponds probably to low molecular mass decomposition product of NC with no autocatalysis, while the sample mass loss after that period is due to NO_x autocatalytic action. The red-brown fumes observed after eight days of ageing confirm beginning of intensive autocatalytic reactions. It is indicated in the Figure 1 by dashed lines.

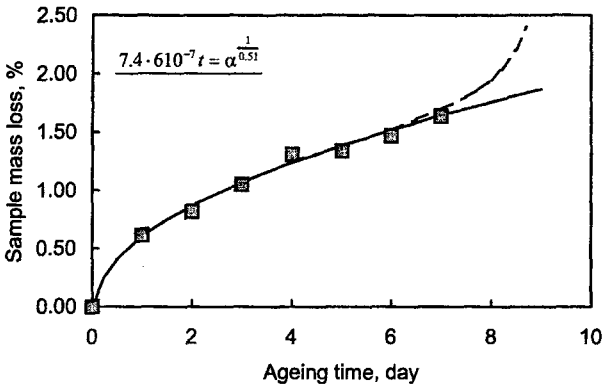


Fig 1. Sample mass loss during ageing at 100 °C

On the other hand, results given in Figure 2, and results given in Figure 1, are in accord – the autacatalytic reactions begin after the consumption of almost all DPA, i.e. after 4-5 days of the ageing.

Consumption of stabiliser

Different analytical methods have been used in order to follow quantitatively amount of stabiliser during the ageing of propellants. The kinetics of stabiliser consumption during the ageing of propellants has been successfully modelled by the first order kinetics with respect to the amount of stabiliser consumed. It has been suggested that an ageing experiments combined with the kinetic analysis could be used to determine quantitatively the useful lifetime of the propellant.

In this work the amount of DPA as stabiliser was determined by the use an UV-VIS spectrophotometer. The results are presented in Figure 2, where DPA content (expressed in percents) as a function of ageing time at 100 °C temperature is given.

It was proved that the first order kinetic model may describe well the experimentally obtained data. According to this model the amount of stabiliser at any time ($S(t)$) is given by equation:

$$S(t) = S(0)e^{-kt} , \qquad (3)$$

where $S(0)$ is initial amount of stabiliser, or in differential form,

$$\ln[S(0)] - \ln[S(t)] = kt \tag{4}$$

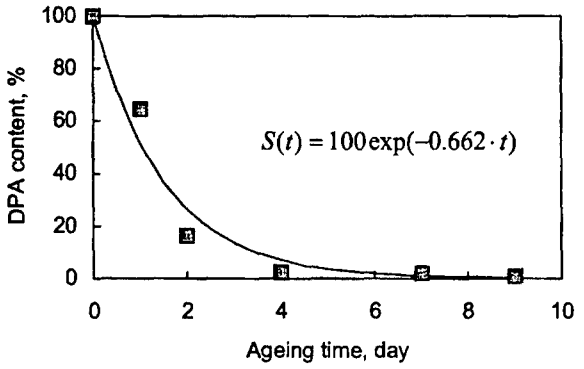


Fig 2. Consumption of DPA during the ageing at 100 °C

Thermal characterisation

The DSC curves of aged and non-aged propellants are shown in Figure 3. DSC measurements were performed on samples of about 05 mg in mass, using perforated aluminium sample pan, and with heating rate of 3 °C min^{-1}, and under nitrogen atmosphere.

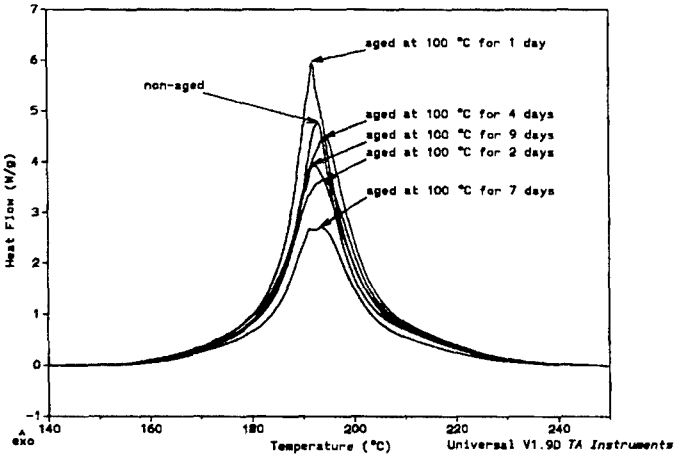


Fig 3. DSC curves of non-aged and aged propellants

The heats of decomposition and characteristic points on DSC curves given in Figure 3 are summarised in Table 1.

Table 1. Summarised DSC results of non-aged and aged propellant

Sample	*Heat of decomposition, kJ/kg	Onset of decomposition, °C	Endset of decomposition, °C	**DSC peak maximum temperature, °C
non-aged	1516	166.98	226.12	192.68
aged at 100 °C for 1 day	1784	167.43	225.61	192.09
aged at 100 °C for 2 days	1669	166.85	225.44	139.60
aged at 100 °C for 4 days	1619	166.41	225.56	193.48
aged at 100 °C for 7 days	1586	165.19	225.39	193.03
aged at 100 °C for 9 days	1521	166.99	225.95	192.58

From data given in Table 1 it seems that the onset temperature, endset temperature, and peak maximum temperature do not change significantly during the ageing. On the other hand, the shape of DSC peak changes slightly, which results in change of the peak area with the ageing, and consequently in change of the heat of decomposition (Figure 4).

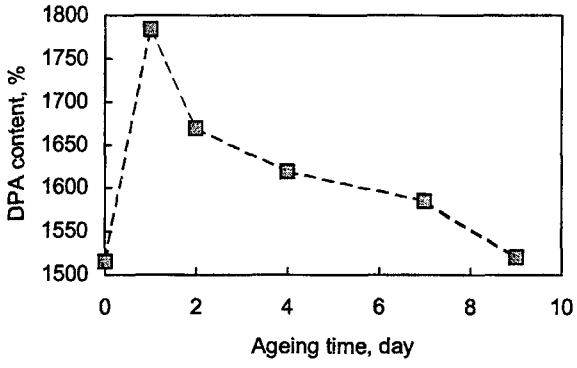


Fig 4. Heat of decomposition versus ageing time

It follows from Figure 4 that the heat of decomposition increases for about 15 % after the first day of ageing, and then decreases gradually with the ageing. Such (unexpected) results show that much more work has to be done in order to find out precisely early stage of ageing of propellants.

* mean values from two measurements
** determined as onset

Isothermal kinetics

The isothermal thermogravimetry measurements carried out at temparatures 130, 140, 150 and 160 °C for non-aged sample, and samples aged at 100 °C for 2 and 9 days, are given in Figure 5.

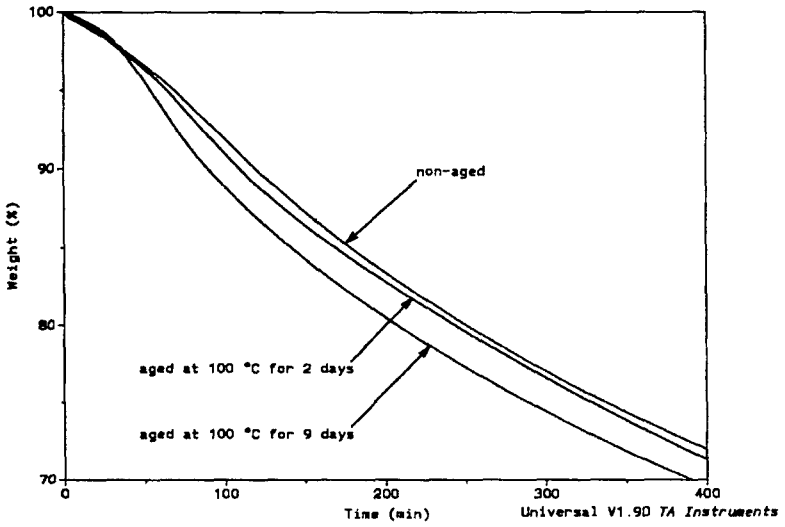


Fig 5. Isothermal TGA curves of non-aged sample and samples aged at 100 for 2 and 9 days, obtained at 150 °C

The isothermal TGA curves given in Figure 5 show that the aged propellants decompose with higher rates at the early stage. Also, one can note that the curves are of sigmoid shape, characteristic for autocatalytic reactions. In odder to derive kinetic data the experimentally obtained thermogravimetric curves are treated in the following way. The sample mass loss as a function of time is converted into the degree of conversion as a function of time, according to the following equation:

$$\alpha = \frac{m_i - m_t}{m_i - m_f} \tag{5}$$

where m_i is the initial sample mass, m_f is the final sample mass, and m_t the sample mass at particular time.

The kinetic parameters are derived for the acceleratory stage of decomposition, i.e. for decomposition up to the inflexion point on $m - t$ (or $\alpha - t$) curve. This point, which corresponds to the maximum decomposition rate, attains at about 6-10 % of decomposition.

The t-α data required for the further kinetic treatment in accordance with Eq. 6 are presented in Figure 6.

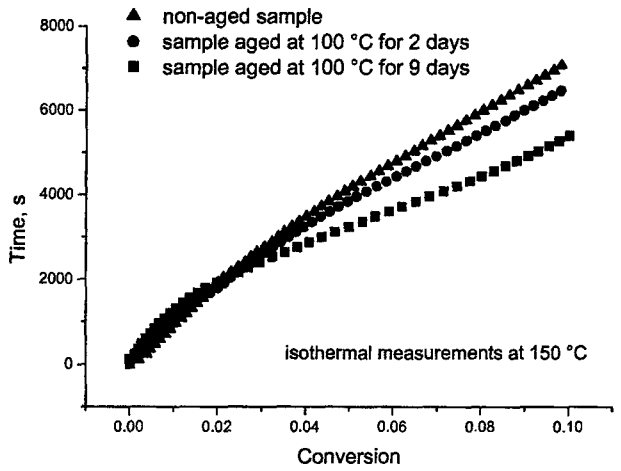


Fig 6. Time vs. conversion of non-aged sample and samples aged at 100 ° for 2 and 9 days, obtained at 150 °C

By the non-linear curve fitting procedure of data given in Figure 6 in accordance with the power law kinetic model (Eqs. 1 and 2):

$$\alpha^{\frac{1}{m}} = kt \ ,$$

$$\frac{d\alpha}{dt} = k \cdot m \cdot \alpha^{\frac{m-1}{m}} \ ,$$

the rate constants (k) are determined for each temperature. Then, the activation energy and pre-exponential factor are calculated from the rate constant-temperature dependence, in accordance with the Arrhenius equation (Figure 7).

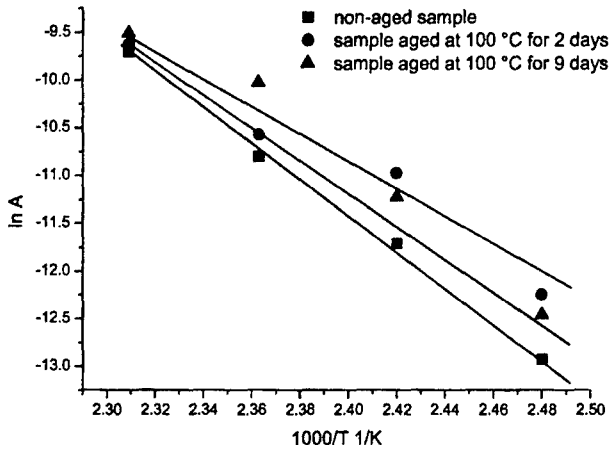


Fig 7. Arrhenius plots for non-aged sample and samples aged at 100 °C for 2 and 9 days

Table 2. Kinetic results for non-aged and aged propellant

Sample	Activation energy, kJ/mol	ln *A*
non-aged	154,26	33,12
aged at 100 °C for 2 days	120,84	23,93
aged at 100 °C for 9 days	146,96	31,49

The results obtained show that there is (in general) a decrease of the activation energy with the ageing. However, this decrease is not monotonous within the ageing range studied.

Bohn and Eisenreich[10] have shown that various low nitrated DPA derivatives exist, showing their maximum concentration at different ageing stages. We suppose that the increase in the activation energy and in the heat of decomposition after a few days of ageing may be connected with the existence of various DPA derivates in the investigated ageing range, and with their different stabilising effects. In other words, we suppose that the change of the thermal and kinetic properties versus ageing time should follow (in some way) the concentration of DPA and its consequent nitrated derivatives.

4. CONCLUSIONS

The results presented show that kinetic and thermal properties of nitrocellulose propellant change significantly during the accelerated ageing, e.g. stabiliser content, heat of decomposition, and kinetic parameters.

The ageing does not have significant influence on DSC peak onset, endset and maximum temperature.

Presence of various low nitrated DPA deviates in the investigated ageing range and change of their concentration at different ageing stages, their different stabilising effect, nonmonotonic change of heat of decomposition and kinetic parameters (which are probably connected with the concentration of various DPA derivatives), etc., suggest that much more work has to be done in order to learn in details the early stage of propellants ageing.

REFERENCE

[1] J. Isler, D. Kayser *6th Symp. Chem. Probl. Connected Stab. Explos*, Kungalav, Sweden, (1982), pp. 217-237

[2] J. Isler *Propell. Explos. Pyrotechn.* **11** (1986) 40-44

[3] F. Volk, M. A. Bohn, G. Wunsch *Propell. Explos. Pyrotech.* 1986, **12** 81-87

[4] J. Kimura *Propell. Explos. Pyrotech.* 1988, **13** 8-12

[5] A. Bergens, B. Nygard *Proccedings of the Ninth Symposium on Chemical Problems Connected with Stability of Explosives*, Margretetorp, Sweden, 1992

[6] M. A. Bohn, F. Volk *Propell. Explos. Pyrotech.* 1992, **17** 171-178

[7] A. Miszezak, J. Bladek *Proccedings of the Ninth Symposium on Chemical Problems Connected with Stability of Explosives*, Margretetorp, Sweden, 1992

[8] M. A. Bohn *Propell. Explos. Pyrotech.* 1994, **19** 266-269

[9] M. A. Bohn *Proc. of the 4th Life Cycles of Energetic materials Conference*, March 29 – April 1, Fullerton, USA, 1998

[10] M. A. Bohn, N. Eisenreich *Propell. Explos. Pyrotech.* 1997, **22** 125-136

[11] M. Rajić, M. Sućeska *High Temperatures-High Pressures* 2000, **32** 171-178

ENGINEERING CALCULATIONS OF GAS EXPLOSION PARAMETERS IN CLOSED AND VENTED VESSELS

Tadeusz J. Rychter and Andrzej Teodorczyk

Warsaw University of Technology, ITC, Nowowiejska 25, 00-665 Warszawa, Poland

Abstract

A simple mathematical model for the prediction of the pressure and temperature changes during a totally confined or vented gaseous explosion is presented. The model is based on solutions of conservation equations of mass, momentum and energy supplemented with equilibrium calculations of the physical and chemical properties of combustion products. The influence of turbulence on combustion is included by the use of empirical relations taken from literature.
A computer program VEX, written to solve the mathematical model is presented in details for potential users. The program computes typical explosion problem in few seconds on PC computer. The program has graphical pre- and postprocessor enabling convenient input of data and output of results. A mixture of 6 fuels (H_2, CH_4, C_2H_2, C_2H_4, C_2H_6, C_3H_8) with air or oxygen can be used in calculations. Spherical, cylindrical and cuboidal geometry of the vessel with arbitrary axial ignition location and arbitrary location and size of the vent can be used. The predictions from the model have been validated against experimental results obtained from the literature and from author's studies.
The program has also the separate option for calculations of equilibrium combustion products composition and temperature at constant pressure or constant volume.

1. INTRODUCTION

The ability to predict of pressure development during a totally confined or a vented explosion is of prime importance in hazard assessment, design of explosion relief and evacuation analyses of industrial vessels and process plants.

Models of differing complexity, which are empirical in nature, exist in the literature [1-7]. However, the applicability of empirical formulas used in these models is usually restricted to a prescribed range of vessel sizes and geometry.

The most sophisticated and useful models published so far are full numerical solutions of full equations describing three zones of burnt, unburnt and vented gases [8-10].

This paper presents a relatively simple mathematical model which has been developed for spherical, cylindrical or cuboidal geometry of the vessel is presented in this paper when the ignition takes place in arbitrary location along the vessel axis of symmetry and a vent is placed at fully arbitrary location. Some predictions obtained from the model have been validated against experimental results obtained from literature and from studies carried out in test chambers by the authors.

The model includes temperature dependence of specific heats, accommodates flame shape resulting from non-central ignition, as well as venting of the burnt or unburnt gas. Empirical relations for laminar and turbulent burning velocity, as well as for heat transfer are incorporated into the model.

2. MATHEMATICAL MODEL

2.1. Assumptions

The model equations are based on the following assumptions:

1. A premixed, quiescent and uniform combustible mixture of ideal gases is ignited by the point source of negligible energy and volume;
2. Burnt gas behaves as ideal gas;
3. A spherical flame infinitely thin propagates outward from the point of ignition;
4. Two-zone, quasi-dimensional model of burning is used (Fig.1);
5. The flame speed is low relative to sound speed, thus the pressure is uniform in the vessel;
6. Compression and expansion processes of venting unburnt and burnt gases are isentropic;
7. The properties of burnt and unburnt gases are spatially uniform;
8. Burnt gas mixture is always at chemical equilibrium.

2.2. Governing Equations

Mass conservation equation has the form:

$$\frac{dx_u}{dt}+\frac{dx_b}{dt}+\left(\frac{dx_{vu}}{dt}+\frac{dx_{vb}}{dt}\right)=0 \qquad (1)$$

where: $x_u = (m_u/m_i)$ – unburnt mass fraction in the vessel, $x_b = (m_b/m_i)$ – burnt mass fraction in the vessel, $x_{vu} = (m_{vu}/m_i)$ – unburnt vented mass fraction (outflowing from the vessel), $x_{vb} = (m_{vb}/m_i)$ – burnt gas vented mass fraction; t – time; i, u, b and v stand for initial, unburnt, burnt and vented respectively.

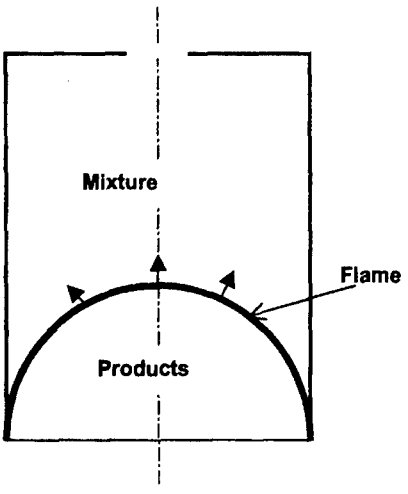


Fig 1. Schematic of two zone model

Mass fraction in equation (1) may be expressed as follows:

$$x_u = \frac{m_u}{m_i} = \left(\frac{\rho_u V_u}{\rho_i V_i} \right) \tag{2}$$

where: ρ - density, V - volume. Using isentropic relation:

$$\frac{P}{(\rho)^{\kappa_u}} = const \tag{3}$$

where P means pressure and κ_u specific heat ratio for combustible mixture, equation (2) transforms to:

$$x_u = \frac{m_u}{m_i} = \sigma^{1/\kappa_u} (1 - f_b) \tag{4}$$

where: σ - ratio of pressure (P) at given time t to initial pressure (P_i), $f_b = (V_b/V_i)$ – ratio of volume occupied by products to initial volume.

Similarly we can get:

$$f_b = -x_u \frac{1}{\sigma^{1/\kappa_u}} + 1 \tag{4a}$$

The term describing outflow from the vessel by the vent opening may be expressed with the use of orifice discharge realtion:

For the chocked condition, $P_d/P \leq (P_d/P)_{crit}$:

$$\frac{dx_v}{dt} = C_d \frac{A_v}{m_i} \left[\kappa P \rho \left(\frac{2}{\kappa + 1} \right)^{\frac{\kappa+1}{\kappa-1}} \right]^{1/2} \tag{5}$$

For subsonic condition, $P_d/P < (P_d/P)_{crit}$:

$$\frac{dx_v}{dt} = C_d \frac{A_v}{m_i}\left[\frac{2\kappa P\rho}{\kappa - 1}\left(\frac{P_a}{P}\right)^{2/\kappa}\left[1-\left(\frac{P_a}{P}\right)^{(\kappa-1)/\kappa}\right]\right]^{1/2} \tag{6}$$

where: C_d – coefficient of discharge (assumed constant and equal to 0.6), P_a – exit pressure, A_v – vent area, ρ and κ - density and specific heat ratio of upstream of the vent. The values of ρ_b and κ_b are used if burnt gas is vented, and ρ_u and κ_u are used if unburnt gas is vented. The critical pressure ratio is given by:

$$\left(\frac{P_a}{P}\right)_{kryt} = \left[\frac{2}{(\kappa+1)}\right]^{\frac{\kappa}{\kappa-1}} \tag{7}$$

Energy conservation equation for the case of unburnt gas venting has the form:

$$\frac{d}{dt}(x_u U_u) + \frac{d}{dt}(x_b U_b) + \left(U_{vu}\frac{dx_{vu}}{dt} + U_{vb}\frac{dx_{vb}}{dt}\right) + \frac{dq}{dt} = 0 \tag{8}$$

where:

$$U = u_o + \Delta u, \tag{9}$$

$$\Delta u = u(T) - u(To), \tag{10}$$

u_o – internal energy of formation at T_o and p_o, $u(T)$ – specific internal energy at temperature T, q – heat exchanges with the walls.

Substituting equations (9 and 10) and assuming time invariant composition of burnt and unburnt gases, we get:

$$\frac{d}{dt}(x_u \Delta u_u) + \frac{d}{dt}(x_b \Delta u_b) + \left(\Delta u_u \frac{dx_{vu}}{dt} + \Delta u_b \frac{dx_{vb}}{dt}\right) = -u_{ou}\left[\frac{dx_u}{dt} + \frac{dx_{vu}}{dt}\right] - u_{ob}\left(\frac{dx_b}{dt} + \frac{dx_{vb}}{dt}\right) - \frac{dq}{dt} \tag{11}$$

By substituting of equation (1) the right hand side of above can be simplified to:

$$(u_{ou} - u_{ob})\left(\frac{dx_b}{dt} - \frac{dx_{vb}}{dt}\right) - \frac{dq}{dt} \tag{12}$$

Using the ideal gas equations:

$$\Delta u = c_v(T - T_o) \tag{13}$$

where c_v is the average specific heat of the mixture, and assuming that c_v is constant, equation (11) has the form:

$$\begin{aligned} &c_{vu}\frac{d}{dt}(x_u T_u) + c_{vb}\frac{d}{dt}(x_b T_b) + c_{vu}T_u\frac{dx_{vu}}{dt} + c_{vb}T_b\frac{dx_{vb}}{dt} = \\ &= (u_{ou} - u_{ob})\left(\frac{dx_b}{dt} - \frac{dx_{vb}}{dt}\right) + T_o c_{vu}\left(\frac{dx_u}{dt} + \frac{dx_{vu}}{dt}\right) + T_o c_{vb}\left(\frac{dx_b}{dt} + \frac{dx_{vb}}{dt}\right) - \frac{dq}{dt} \end{aligned} \tag{14}$$

Substituting (1) to (14) the right hand side of (14) simplifies to:

$$\{u_{uo} - u_{bo} + T_o[c_{vb} - c_{vu}]\}\left(\frac{dx_b}{dt} + \frac{dx_{vb}}{dt}\right) - \frac{dq}{dt} \tag{15}$$

By dividing both sides of (14) by $c_{vu}T_i$ and using relations for ideal gas:

$$PV = mRT \tag{16}$$

$$R = c_v\,(\kappa - 1) \tag{17}$$

we get:

$$\frac{d}{dt}\left[\sigma\left(1-f_b\right)\right]+k\frac{d}{dt}\left(\sigma\, f_b\right)=K\frac{dx_b}{dt}-\sigma^{\left(1-1/\kappa_u\right)}\frac{dx_{vu}}{dt}+\left(K-k\sigma\, f_b\frac{1}{x_b}\right)\frac{dx_{vb}}{dt}-\frac{dq}{dt}\frac{1}{c_{vu}} \tag{18}$$

where constants k and K are given by:

$$k=\frac{\kappa_u-1}{\kappa_b-1} \tag{19}$$

$$K=\frac{u_{ou}-u_{ob}+T_o\left(c_{vb}-c_{vu}\right)}{c_{vu}T_i} \tag{20}$$

For closed, adiabatic, unvented vessel, equation (18) has the form:

$$\frac{d}{dt}\left[\sigma\left(1-f_b\right)\right]+k\frac{d}{dt}\left(\sigma\, f_b\right)-K\frac{dx_b}{dt}=0 \tag{21}$$

By differentiation of above equation we get:

$$\sigma\left(1-f_b\right)+k\sigma\, f_b-Kx_b=const \tag{22}$$

For the initial conditions: $\sigma = 1, f_b = 0, x_b = 0,$ the constant $const = 0.$

At the end of combustion: $\sigma = \sigma_f, f_b = 1, x_b = 1.$ Thus:

$$K=k\sigma_f-1 \tag{23}$$

Dissociation changes properties of burnt gases (κ_b, σ_f). Dissociation of such products as H_2O, O_2, N_2 and CO_2 occurs at the temperatures above 1300 K and increases with temperature. Dissociation is endothermic process, so it decreases the burnt gas temperature and the final pressure in the vessel. The calculation of quantities σ_f and κ_b are made with the use of equilibrium subroutine. The quantity κ_u is calculated as mean value of initial and final value of specific heat ratio of unburnt mixture.

By using equation (4a) and transforming equation (18) one can get relations describing the pressure variation $d\sigma/dt$ as well as burnt gas volume fraction variation df_b/dt:

$$\frac{d\sigma}{dt}=\frac{B+\left[-\frac{dx_b}{dt}-\left(\frac{dx_{vu}}{dt}+\frac{dx_{vb}}{dt}\right)\right]\frac{1}{\sigma^{1/\kappa_u}}\left[\sigma\left(k-1\right)\right]}{\left[1+f_b\left(k-1\right)\right]+\left(1-f_b\right)\frac{1}{\kappa_u}\left(k-1\right)} \tag{24}$$

$$\frac{df_b}{dt}=\frac{-\left[-\frac{dx_b}{dt}-\left(\frac{dx_{vu}}{dt}+\frac{dx_{vb}}{dt}\right)\right]\left[1+f_b\left(k-1\right)\right]+B\left[\left(1-y_b\right)\frac{1}{\kappa_u}\sigma^{\left(1/\kappa_u-1\right)}\right]}{\left[\left(1-f_b\right)\frac{1}{\kappa_u}\sigma^{\left(1/\kappa_u-1\right)}\right]\sigma\left(k-1\right)-\left(-\sigma^{\frac{1}{\kappa_u}}\right)\left[1+f_b\left(k-1\right)\right]} \tag{25}$$

where:

$$B = K\frac{dx_b}{dt} - \sigma^{\left(1-1/\kappa_u\right)}\frac{dx_{vu}}{dt} + \left(K - k\frac{\sigma f_b}{x_b}\right)\frac{dx_{vb}}{dt} - \frac{dq}{dt}\frac{1}{C_{vu}} \tag{26}$$

Equations (1) and (8) together with additional relations (5) and (6) as well as relation between A_f/V_i in equation (9) and f_b constitute closed set of equations for three non-dimensional variables σ, f_b and x_b. Time is an independent variable.

2.3 Burning Rate

The rate of combustion products formation, expressed as the mass fraction of initial mass, is given by:

$$\frac{dx_b}{dt} = \frac{1}{m_i}\rho_u S A_f - \frac{dx_v}{dt} \tag{27}$$

where: A_f – flame surface, S – burning velocity (function of pressure, temperature, mixture composition and turbulence). By substituting $m_i = \rho_i V_i$ and using isentropic relation one can get:

$$\frac{dx_b}{dt} = \frac{A_f}{V_i}\sigma^{1/\kappa_u} S - \frac{dx_v}{dt} \tag{28}$$

where: V_i – initial volume of the vessel.

The functional dependency between A_f/V_i and f_b is defined by flame shape in the given volume. This relation is one of input data to the model.

2.4. Laminar burning velocity

Detailed values of burning velocity are key problem in the model. Laminar burning velocity is the function of pressure, temperature and mixture composition.

Laminar burning velocity for fuel-air and fuel-oxygen mixture as a function of equivalence ration is calculated in the model from the following relation:

$$S_{u0} = a + b\Phi + c\Phi^2 + d\Phi^3 + e\Phi^4 \tag{29}$$

The polynomial coefficients *a, b, c, d, e* were obtained by interpolation of experimental data.

The dependence of laminar burning velocity on pressure and temperature is given by:

$$S_u = S_{uo}\left(\frac{T_u}{T_o}\right)^{\alpha}\left(\frac{P_o}{P}\right)^{\beta}(\chi + \Omega) \tag{30}$$

where: S_{uo} – laminar burning velocity at initial temperature T_o and pressure P_o, T_u – temperature of combustible mixture, P – pressure, α and β - empirical coefficients, for example for methane-air and ethylene-air: $\alpha = 2$ and $\beta = 0.25$; while for propane-air $\alpha = 2.13$ and $\beta = 0.17$; Ω - empirical coefficient taking into account initial turbulence of combustible

mixture, for motionless mixture $\Omega = 0$; χ - coefficient taking into account the influence of turbulence generated by vent, $\chi = 1$ for closed vessel.

Coefficient χ is calculated from the formula [9, 12]:

$$\chi = \beta_1 \left(\frac{\mathrm{Re}_v}{10^6} \right)^{\delta} \tag{31}$$

where

$$\mathrm{Re}_v = \frac{\rho_v u_v r_v}{\mu_v} \tag{32}$$

$$u_v = \frac{dm_v}{dt} \frac{1}{\rho_v A_v} \tag{33}$$

$$\delta = \beta_2 \frac{1}{S_u} y_b \tag{34}$$

where: ρ_v – density of vented gas, r_v – radius of the vent, u_v – gas velocity by the vent, μ_v – kinematic viscosity of vented gas, , A_v – surface area of the vent, V_f – volume of combustion products, V_z – volume of the vessel, $\beta_1 = 1.23$ – empirical constant, $\beta_2 = 4.87\ 10^{-2}$ m/s – empirical constant.

3.2 Turbulent burning velocity

Turbulence greatly increases burning velocity. Determination of the influence of turbulence on combustion is one of the most difficult task in this area. In the engineering practice the empirical formulas describing influence of various flow parameters and geometry on turbulence and burning velocity are used. In this model the simple method was applied [6]:

$$S = S_u \cdot \eta \tag{35}$$

where: S_u – laminar burning velocity, η – coefficient of proportionality taking into account the influence of flame area increase by folds and eddies:

$$\eta = \left(\frac{\mathrm{Re}_f}{\mathrm{Re}_c} \right)^{\Theta} \tag{36}$$

where: Re_f – flame Reynolds number

$$\mathrm{Re}_f = \frac{\rho_u S_u r_f}{\mu_u} \tag{37}$$

and Re_c – critical Reynolds number

$$\mathrm{Re}_c = 155555 \frac{\rho_b}{\rho_u} - Z_c \tag{38}$$

in the above equations: Θ - turbulence intensification coefficient (assumed by model user); r_f – flame sphere radius; $Z_c = 16667$ – empirical constant [6]. For $Re_f < Re_c$ $\eta = 1$, but for $Re_f \geq Re_c$ the above given formula is valid.

2.5. Heat transfer to walls

The heat transfer between gas and the vessel walls occurs only by convection. The heat transferred to the walls is given by [13]:

$$q = \frac{1}{m}\left[\int_0^t \alpha_{cb} A_{wb} (T_b - T_w)dt + \int_0^t \alpha_{cu} A_{wu} (T_u - T_w)dt\right] \tag{39}$$

where: m – actual mass of gas in the vessel, t – time, A_{wb} – surface area of the vessel walls in contact with burnt gas, A_{wu} – surface area of the vessel walls in contact with unburnt gas, A_f – flame surface area, T_b – temperature of combustion products, T_w – temperature of vessel walls, T_u – temperature of unburnt mixture, α_{cb} – convective heat transfer coefficient for burnt gas, α_{cu} – convective heat transfer coefficient for unburnt gas.

The heat flux to vessel walls is given by:

$$\frac{dq}{dt} = \frac{1}{m}\left[A_{wb}\alpha_{cb}\left(\sigma f_b \frac{1}{x_b} - 1\right) + A_{wu}\alpha_{cu}\sigma^{\left(1-1/\kappa_u\right)}\right] \tag{40}$$

The method developed by Olikara and Borman [14] was applied to calculate the equilibrium composition of the combustion products.

3. COMPUTER CODE

3.1. General introduction

Computer code called VEX (Vented Explosions) is a very compact piece of programming (only 504 kB) designed for execution in PC computers equipped with the DOS or Windows operational system. Code includes all the necessary libraries and it communicates with the user by windowing screens independent of the operation system windows; it makes operation easy for everybody.

The computer code is written in C++ programming language. It is also equipped in built-in graphical procedures which make it possible for immediate graphical presentation of the results of calculations in a variety of forms. It is also possible to mark the experimental points on the plots presenting results of calculations.

3.2. Brief description of program options

The VEX computer code is composed of four major blocks:

- **Normal Run**. It is used for calculations of the explosions in closed or vented vessels. It allows for setting a variety of input data: vessel geometry expressed by a number of parameters, mixture composition and its dynamic state (turbulence level);
- **Equilibrium calculations**. It is an independent block which allows for calculations of equilibrium parameters of combustion products at constant pressure or constant volume, for the assumed initial state of the mixture. The correctness of the results of calculations has been entirely validated by their thorough comparison with the results

obtained from well documented methods offered by the STANJAN [15] and NASA [16]. VEX code offers the same accuracy of calculations and the use of this option seems to be easier.

- **Configuration Setup**. This block allows for easy adjusting all the program options according to the user personal preferences.
- **Experimental Data**. This block allows to create files which contain sets of experimental data provided by the user. The experimental data can be later used for graphical comparison with the results of the calculations.

3.3. Experimental validation

Experimental validation of the results of calculations is a very difficult task, primarily because of the lack of the reliable experimental data for a wide variety of vessel geometries and initial conditions. The lack of such data is especially noticeable for the large vented vessels. Despite the fact that authors tried to verify the results of the calculations against the experiments (it was basically impossible for a large variety of the vessel dimensions and initial conditions) the obtained results have to be treated with the great caution regarding the quantitative agreement with experimental data. It has been checked that the VEX computer code makes it possible to present the true tendency of the change of the combustion parameters and by that – to deliver qualitative information on the character of the combustion processes. In the range of the small closed vessels the results of the calculations were thoroughly validated in a number of cases where the reliable experimental data (or data obtained from the experiments performed by the authors) have been available in the literature (Fig.2). It is possible for the user to change several coefficients used in the computer model (heat exchange coefficient, coefficients which determine the turbulence level etc.) in order to match the results of calculations with experimental results. This option makes VEX computer code very flexible and easy to adjust for any particular case.

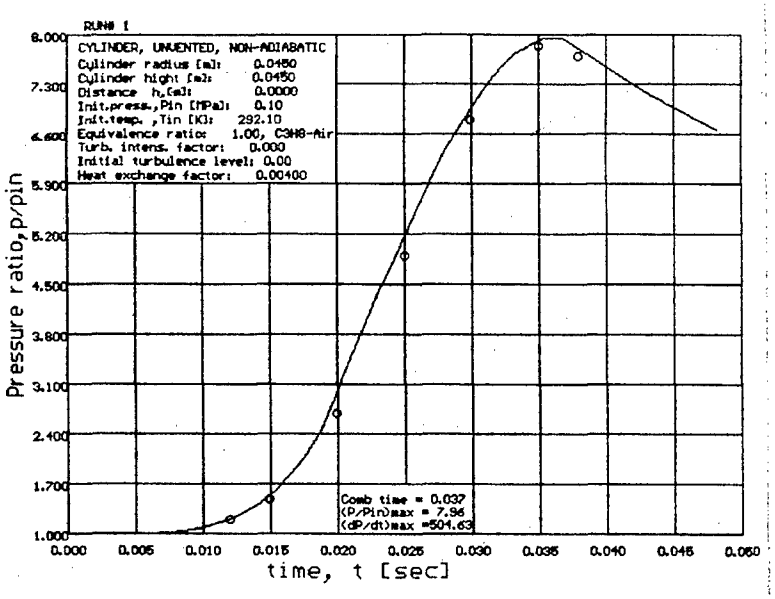


Fig 2. Pressure ratio versus time in unvented cylindrical vessel – comparison with experimental results (circles)

4. EXAMPLE OF CALCUATIONS

A good demonstration of the analysis performed with the use of the VEX computer code is the following example. The explosion of the stechiometric methane-air mixture takes place in the low cylindrical vessel. The vessel is equipped in the vent which opens at the 1.8 bar. The ignition point is located in the middle of the cylinder. The changes of the pressure, burnt gas fraction and the burning velocity with time are presented in figure 3. The location of the vent close to the ignition point is a cause that from the beginning of the process the combustion gases are vented and because of that the sudden pressure drop is observed. Than the pressure start to built up because of the combustion acceleration.

Interesting are the reactions of the combustion system on the changing of the position of the vent with respect to the ignition point. (Fig.4). At each different vent location the character of the pressure traces change. When the vent is located far away of the cylinder axis the vent opening remains almost not noticed although the magnitude of the pick pressure is significantly decreased. It can also be noticed that sometimes only small displacement of the vent position (between 3 and 4) is causing the remarkable change in the character of the combustion process.

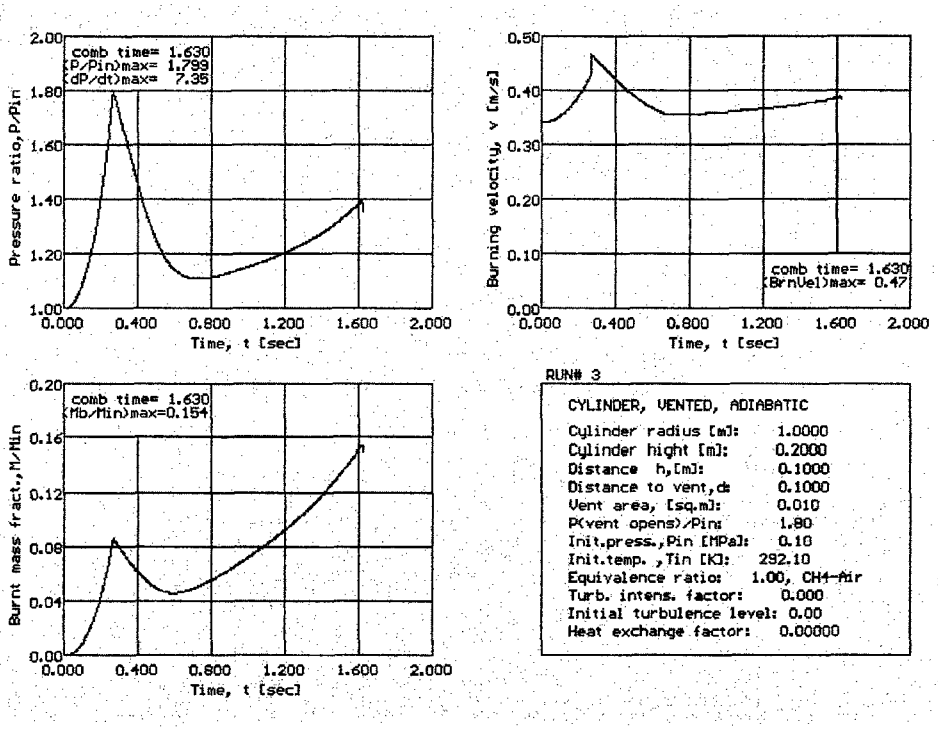


Fig 3. Changes of pressure, burnt gas mass fraction and the burning velocity with time for explosion in vented cylindrical vessel

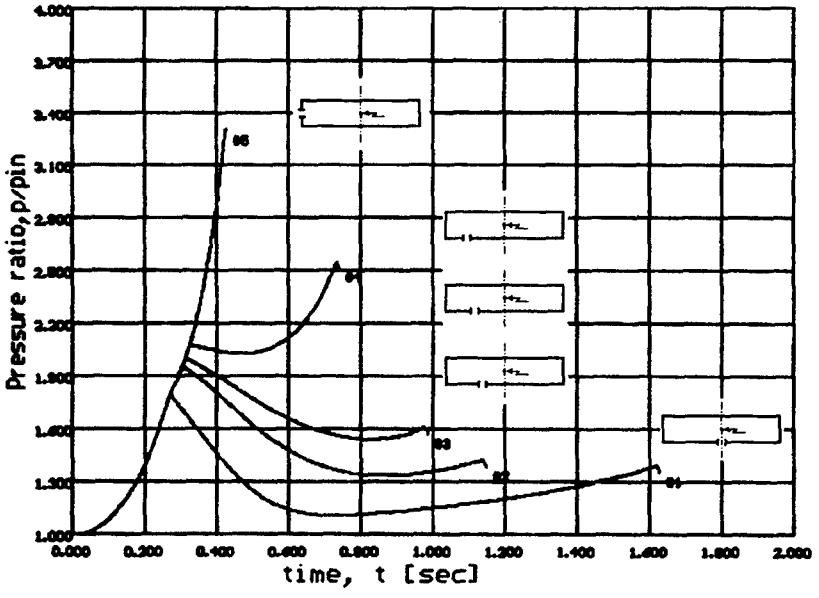


Fig 4. Pressure ratio versus time for different positions of the vent with respect to the ignition point

REFERENCES

[1] Bradley D., Mitcheson A.: *Mathematical Solutions for Explosions in Spherical Vessels*, Comb. and Flame 26(1976), pp. 201-217

[2] Bradley D. Mitcheson A.: The Venting of Gaseous Explosions in Spherical Vessels (Part I and II), Comb. and Flame 32(1978), pp.221-236

[3] Mulpuru S.R., Wilkin G.B.: A Model for Vented Deflagration of Hydrogen in a Volume, Atomic Energy of Canada Limited, AECL-6826, 1982

[4] Munday G.: Institution of Chemical Engineers Symposium Series No.15, London, 1966, p.46

[5] Palmer K.N.: J.Inst.Fuel 29 (1956), p.293

[6] Maisey H.R.: Chem.Proc.Eng., October (1965), p.527

[7] Anthony E.J.: J.Haz.Mat. 2(1977/1978), p.23

[8] Fairweather M., Vasey M.W.: 19th Symp. (Int.) on Combustion, The Combustion Institute 1982

[9] Chippet S.: *Modeling of Vented Deflagrations*, Comb. and Flame 55(1984), p.127

[10] Catlin C.A., Mahos A., Tite J.P.: Trans.IChemE B 71 (1993), p.89

[11] Wu Y., Siddall R.G.: Trans.IChemE B 74 (1996), p.31

[12] Canu P., Rota R., Carra S., Morbidelli M.: Vented Gas Deflagrations. A Detailed Mathematical Model Tuned on a Large Set of Experimental Data, Comb. and Flame 80(1990), p.49

[13] Tanaka Y.: Three-Dimensional Flame Development in a Closed Vessel; Comparison between Measured and Theoretical Results. Bulletin of JSME, Vol.29, No.258, Dec.1986

[14] Olikara C., Borman G.L.: A Computer Program for Calculating Properties of Equilibrium Combustion Products with Some Applications to IC Engines" SAE Paper 750468, 1975

[15] Reynolds C.W.: The Element Potential Method for Chemical Equilibrium Analysis: Implementation in the Interactive Program STANJAN, Department of mechanical Engineering, Stanford University, 1986

[16] Gordon S., McBride B.: Computer Program for Calculation of Complex Chemical Equilibrium Composition, Rocket performance, Incident and Reflected Shocks, and Chapman-Jouget Detonations, NASA SP-273, 1971

ACID-BASE CHARACTERISTICS OF FOX-7 AND ITS MONOHYDRAZO ANALOGUE

Camilla Sandberg*, Nikolaj Latypov*, Patrick Goede*, Rolf Tryman* and Anthony J. Bellamy**

* FOI, Swedish Defence Research Agency, Department of Energetic Materials, S-147 25 Tumba, Sweden.

** Department of Environmental and Ordnance Systems, Cranfield University, Royal Military College of Science, Shrivenham, Swindon, Wilts SN6 8LA, England.

Abstract:

1,1-diamino-2,2-dinitroethylene, FOX-7 (1) is a novel explosive with high performance and low sensitivity[1,2]. In addition 1-amino-1-hydrazino-2,2-dinitroethene (Hydrazo FOX-7, HDF) (2) has recently been prepared by reaction of FOX-7 with hydrazine. Several studies of FOX-7 have been performed and complementary studies with acid-base characterization of both FOX-7 and HDF are presented in this paper. The effect of varying pH on both FOX-7 and HDF and the formation of their respective salts are discussed along with the basic hydrolysis of FOX-7 to dinitromethane.

1. INTRODUCTION

1,1-diamino-2,2-dinitroethylene, FOX-7 (**1**) was first synthesized by N. Latypov *et.al*[1]. Subsequent studies by U. Bemm and H. Östmark[3] indicated that the structure of this molecule allows one to expect its zwitterionic character and, according to our quantum mechanical calculations, some trans-amination reactions[4,5]. This was successfully shown to be the case with aliphatic amines[6]. In this paper we report reactions of FOX-7 with hydrazine, resulting in substitution of one amino-group and formation of 1-amino-1-hydrazino-2,2-dinitroethene, HDF (**2**). Further attempts to get the analogous di – substituted derivative failed. This paper describes the chemical behaviour of both compounds in pH region (1-13), with determination of their pK_a values as well as the properties of the products formed.

2. RESULTS

2.1 Reactions of FOX-7

In an attempt to prepare a more energetic compound, FOX-7 (**1**) was reacted with hydrazine in water at various temperatures, from room temperature to approximately 90° C. The product formed under these conditions was the novel monosubstituted compound HDF (**2**). A preliminary investigation of the properties of HDF has been completed and the results are presented in this report. HDF was also reacted with hydrazine in order to produce the disubstituted compound. However, at room temperature reaction of HDF with one equivalent of hydrazine produced a complex between HDF and hydrazine (1:1), which was later shown

to be the hydrazinium salt of HDF (**3**). The salt proved to be unstable and decomposed back to HDF with loss of hydrazine after a period of 3-4 days at room temperature in an open vessel. Attempts to produce the disubstituted product by reacting the hydrazinium salt of HDF with an excess of hydrazine under more vigorous conditions (approx. 90° C) proved unsuccessful and led to tarry products.

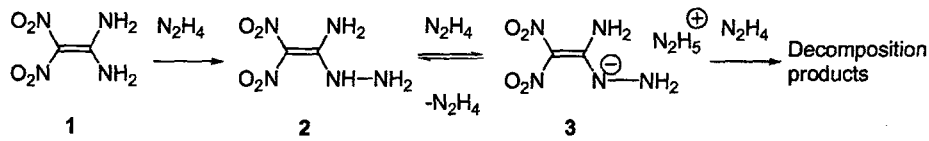


Fig 1. Scheme 1

2.2 Acid-base behaviour of FOX-7 and HDF

It was observed during our work on FOX-7 and HDF that their solubility increased significantly in basic media, therefore suggesting some possible interactions. Using UV spectroscopy we have shown that both FOX-7 and HDF behave as typical acids of different strength. The effect of varying pH on the structure of FOX-7 is illustrated in Figure 2.

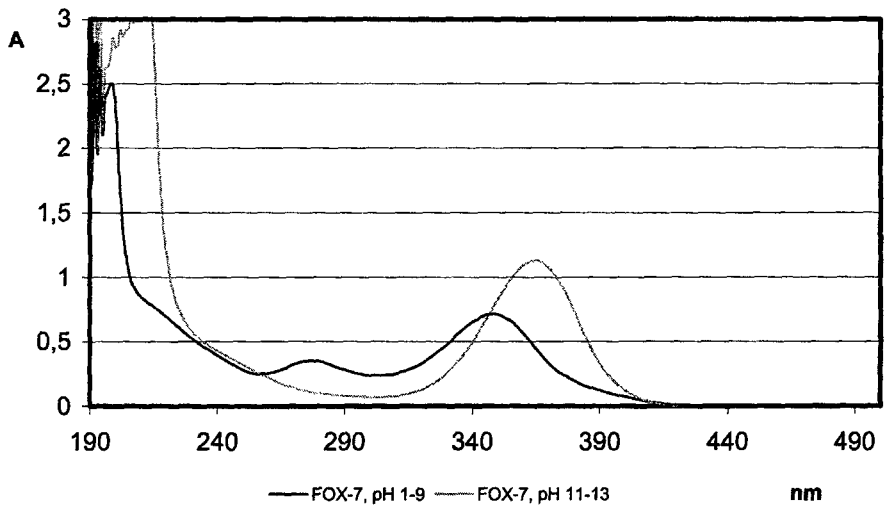


Fig 2. UV analysis of FOX-7 at varying pHs

According to the UV analysis two possible different structures of FOX-7 are present within the pH scale, Scheme 2.

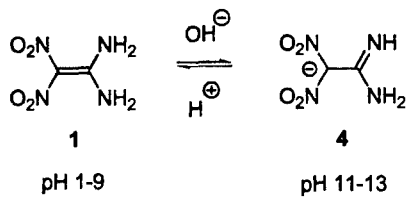


Fig 3. Scheme 2

The pK_a value of FOX-7 was determined to be approximately 10.6[7]. The formation of the FOX-7 anion (**4**) was also confirmed by elemental analysis of its potassium salt (see experimental section). The different states of FOX-7 were supported by NMR studies. The ^{13}C absorptions for FOX-7 in a neutral solution (DMSO-d_6) were 128.0 and 157.7 ppm. In basic solution (D_2O and NaOD) the absorptions shifted to 135.0 and 160.9 ppm.

It was also shown that under more vigorous reaction conditions (t > 70° C), FOX-7 (**1**) dissolved in aqueous KOH and was easily hydrolysed to potassium dinitromethane (**5**) in a 75 % yield, Scheme 3. Melting point and UV analysis of the product were consistent with those reported previously[8,9].

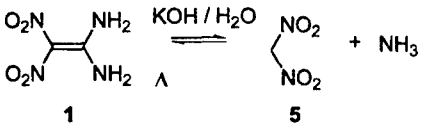


Fig 4. Scheme 3

The effect of varying pH on the structure of HDF is illustrated in Figure 5.

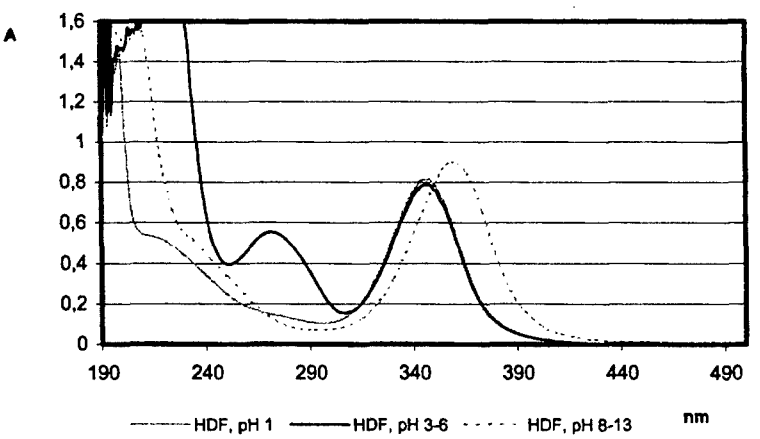


Fig 5. UV analysis of HDF at varying pHs

From Figure 5 we conclude that there are three different structures of HDF, which therefore must correspond to more than one pK_a value. A scheme for the various possible structures of HDF at varying pHs is given below.

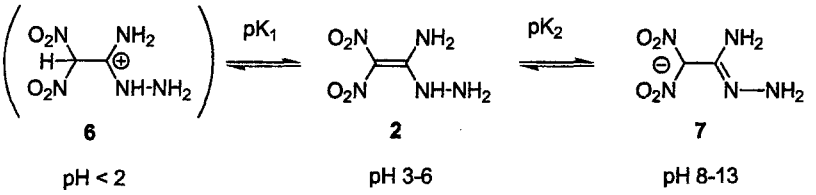


Fig 6. Scheme 4

pK_2 for HDF was determined to be approximately 6.7[7]. pK_1 has not yet been determined. ^{13}C NMR of HDF in pH 3-6 (DMSO-d_6) shows absorptions at 126.3 and 157.6 ppm. In more basic solutions (**7**) (D_2O and NaOD) the absorptions shift to 131.6 and 144.6 ppm. The formation of the anion was confirmed by elemental analysis of two different salts of HDF (see experimental section).

2.3 Proton exchange

It was also shown that under basic conditions in aqueous solutions both FOX-7 (**1**) and HDF (**2**) show rapid proton exchange. FOX-7 and HDF were dissolved in NaOD and D_2O and analysed using NMR. The NMR spectra show that when FOX-7 and HDF are dissolved in NaOD and D_2O only the proton signal of water is present. The disappearance of the NH_2 proton signals indicates complete proton exchange. To confirm the NMR results, FOX-7 was dissolved in NaOD and D_2O to induce proton exchange. The fully deuterated FOX-7 (**9**) was precipitated out of solution with acetic acid-d_1 or sulphuric acid-d_2 and analysed using mass spectrometry.

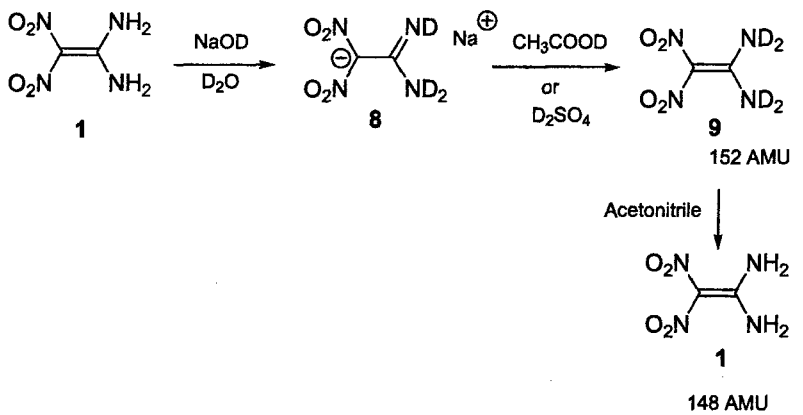
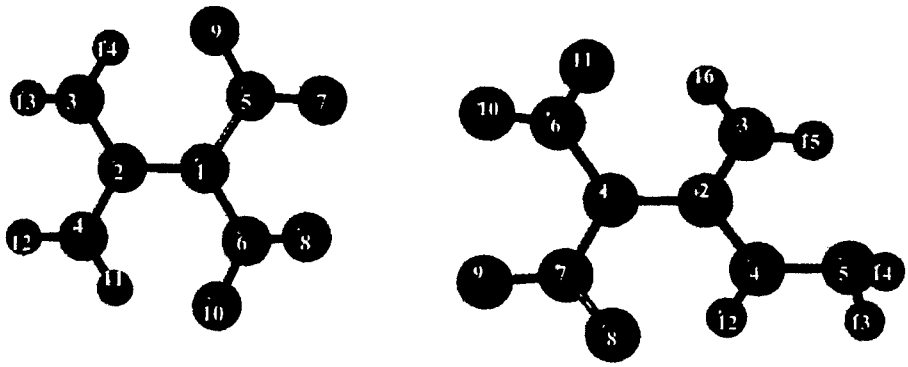


Fig 7. Scheme 5

When undried acetonitrile was used as a solvent (Scheme 5) the product showed a molecular ion at 148 AMU corresponding to a fully protonated FOX-7 (1), thus indicating proton exchange with the solvent. For this reason, MeOD was used as a solvent with the resulting mass spectrum showing a molecular ion at 152 AMU, which means that FOX-7 has been fully deuterated (9). The deuterated FOX-7 was also analysed using IR spectroscopy. Two peaks corresponding to ND_2 were found at 2565 and 2406 cm^{-1}, respectively.

2.4 Quantum mechanical calculations

Quantum mechanical calculations of the charge distribution in both FOX-7 and HDF were performed and the results are given in Table 1 and 2[10]. The calculations indicated that the 2 (C) carbons on FOX-7 and HDF are the most electropositive ones and therefore the nucleophilic attack should take place at those carbons. This was later confirmed by the reaction of FOX-7 with hydrazine, Scheme 1. When HDF was treated with hydrazine a salt was formed. No nucleophilic substitution at 2 (C) was observed, Scheme 1.



1a **1b**

Fig 8. Representation of 3-d structure and charge distribution in **1a. FOX-7** and **1b. HDF**

Table 1. Quantum mechanical calculations of the charge distribution of FOX-7

1 (C)	2 (C)	3 (N)	4 (N)	5 (N)	6 (N)	7 (O)
0,38	0,587	-0,777	-0,782	0,364	0,364	-0,366
8 (O)	9 (O)	10 (O)	11 (H)	12 (H)	13 (H)	14 (H)
-0,358	-0,455	-0,459	0,404	0,348	0,344	0,406

Table 2. Quantum mechanical calculations of the charge distribution of HDF

1 (C)	2 (C)	3 (N)	4 (N)	5 (N)	6 (N)	7 (N)	8 (O)
0,382	0,656	-0,794	-0,563	-0,584	0,355	0,357	-0,472
9 (O)	10 (O)	11 (O)	12 (H)	13 (H)	14 (H)	15 (H)	16 (H)
-0,372	-0,362	-0,463	0,395	0,35	0,341	0,375	0,401

3. CONCLUSIONS

Reaction of FOX-7 with hydrazine led to the monosubstituted product, HDF. Reactions of HDF with one equivalent of hydrazine produced the unstable hydrazinium salt, which subsequently decomposed after a period of 3-4 days. Attempts to produce the disubstituted compound proved unsuccessful, possibly due to low thermal stability and predicted high acidity. According to quantum mechanical calculations, reactions of FOX-7 and HDF with nucleophiles should lead to nucleophilic attack at the most electropositive carbon atom. However, experimental observations indicate that proton abstraction as well as nucleophilic attack occurs. UV and NMR studies showed that both FOX-7 and HDF behave as weak acids, having pK values of 10.6 and 6.7 respectively. Further studies are however necessary to completely understand the acid-base behaviour of FOX-7 and HDF.

4. EXPERIMENTAL SECTION

Caution: The compounds described in this paper are powerful and sensitive explosives and should be handled with appropriate precautions. Employ all standard energetic materials safety procedures in experiments involving such substances. NMR spectra were obtained using a Bruker AV 400 spectrometer. UV spectra were recorded with a Perkin-Elmers UV/Vis-spectrometer, Lambda-20/40. Decomposition temperatures were determined with a Mettler DSC 30. Mass spectra were recorded with a Bruker esquire 3000. Elemental analyses were carried out by H Kolbe Mikroanalytisches Laboratorium, Mülheim an der Ruhr, Germany.

4.1 Potassium salt of FOX-7 (K-FOX-7)

FOX-7 (1) (1.48 g; 10 mmol) was suspended in 8 ml of water and to it a solution of KOH (1.2 g in 2.0 ml of water) was added dropwise. The solution formed was diluted with 30 ml methanol. The resulting suspension was filtered off, washed with methanol (2×5ml) and dried at 40° C. 1.25 g of $C_2H_3N_4O_4K$ was obtained (as a hemi-hydrate). Dec.temp. 225° C. KFOX-7: ^{13}C NMR (DMSO-d_6): δ 133.6, 154.5. $C_2H_3N_4O_4K$ * 0.5 H_2O requires: C, 12.31; H, 2.05; N, 28.72; K, 20.07. Found: C, 12.62; H, 1.24; N, 28.89; K, 20.00.

4.2 Hydrolysis of FOX-7

FOX-7 (1) (2.96 g, 20 mmol) was dissolved in a solution of 5.9 g KOH in 50 ml of water; the resulting solution was warmed up to 85-90° C and was kept at this temperature three hours until evolution of ammonia ceased. After that the solution was cooled to room temperature and the pale yellow product formed was collected by filtration, washed with water and dried. All spectral and thermal characteristics of the product were identical with those of potassium dinitromethane (5)[8,9]. Yield 2.1g (73 %).

4.3 Synthesis of HDF (2) from FOX-7 (1).

FOX-7 (0.75 g 5.07 mmol) was suspended in 6 ml water and to this mixture 0.43 g (7.6 mmol) of hydrazine-hydrate was added; the mixture was warmed up to 85-90° C and was kept at this temperature until the solid dissolved. After this 50 ml ethanol was slowly added to the solution and cooled to room temperature. A pale yellow solid precipitated. The

product was filtered, washed with ethanol (2 × 5 ml) and dried at 40° C. The product decomposed violently at 120° C. HDF: ^{1}H NMR (DMSO-d_6): δ 5.4, 9.0, 10.8; ^{13}C-NMR (DMSO-d_6): δ 126.3, 157.6; ^{13}C-NMR (D_2O and NaOD): δ 131.6, 144.6. ^{15}N NMR (rel. NH_3), 64.0, 106.4, 138.7 and 355.4 ppm (NO_2). $C_2H_5N_5O_4$ requires: C, 14.72; H, 3.07; N, 42.94. Found: C, 14.71; H, 3.84; N, 42.72. In comparison with FOX-7: ^{13}C-NMR (DMSO-d_6): δ 128.0, 157.7. ^{13}C-NMR (D_2O and NaOD): δ 135.0, 160.9. ^{15}N NMR (rel. NH_3), 107.8 (NH_2), 355.7 ppm (NO_2).

4,4 Hydrazinium salt of HDF (H-HDF) (3)

HDF (2), 1.0 g (6 mmol) was suspended in 5 ml of water and 1.5-2.0 ml of hydrazine-hydrate were added until the solid dissolved completely; to this solution 12-15 ml of ethanol were added to precipitate the salt, which was filtered off, washed with 5 ml ethanol and dried at 40° C. Yield 0.63 g (53 %). Dec.temp. 140° C. $C_2H_9N_7O_4$ requires: C, 12.31; H, 4.62; N, 50.26. Found: C, 12.54; H, 4.38; N, 49.15.

4.5 Potassium salt of HDF (K-HDF)

HDF 0.68 g (4.17 mmol) was suspended in 5 ml of water and to it a solution of 0.27 g (4.5 mmol) KOH in 1 ml of water was added drop wise at 25-30° C whereupon the solution became homogeneous. The reaction mixture was slowly diluted with 15 ml of ethanol and cooled to 5-10° C. The precipitate formed was filtered off, washed with ethanol and dried at 40° C. 0.59 g (70 %) of K-HDF was obtained. Dec.temp.180°C. KHDF: ^{1}H NMR (DMSO-d_6): δ 4.60, 5.15; ^{13}C NMR (DMSO-d_6): 132.8, 142.1. $C_2H_4N_5O_4K$ requires: C, 11.94; H, 1.99; N, 34.83; K, 19.4 Found: C, 12.01; H, 1.96; N, 34.88; K, 19.48.

4.6 Synthesis of deuterated FOX-7 (9)

0.1 g FOX-7 (1) was dissolved in 5 % NaOD solution to induce proton exchange. FOX-7 was then precipitated out of the solution with 96 % acetic acid-d_1. The product was then removed by filtration and dried at 40° C. 0.1 mg of the deuterated FOX-7 was then dissolved in 1 ml methanol-d_4 and analysed using electrospray (ES) mass spectrometry analysis. MS m/z 150 $(M\text{-}D)^-$, 175 (MNa^+). c.f. FOX-7 exhibits m/z 147 $(M\text{-}H)^-$, IR (KBr) 2565.2, 2406,5 (ND_2) cm^{-1}. c.f. FOX-7 (KBr) 3417, 3315, 3200 (NH_2) cm^{-1}.

4.7 UV analysis of FOX-7 and HDF

The pKa constants were determined using the method presented in "The Determination of Ionization Constants"[7]. Acetonitrile and buffer solutions were used as solvents.

4.8 Theoretic calculation of the charge distribution of FOX-7 and HDF

For theoretical estimates of the optimal geometry and charge distribution of FOX-7 and HDF the quantum chemical program Gaussian 98 has been used[10]. The level of theory used is B3LYP/6-31G(d), which gives good accuracy for molecules with 15 to 25 atoms.

REFERENCES

[1] Latypov, N. V.; Bergman, J.; Langlet, A.; Wellmar, U.; Bemm, U. *Tetrahedron* **1998**, *54*, 11525-11536.

[2] Östmark, H.; Langlet, A.; Bergman, H.; Wingborg, N.; Wellmar, U.; Bemm, U. In *11Th Symposium (international) on Detonations* Snow Mass Co, **1998**.

[3] Bemm, U.; Östmark, H. *Acta Cryst* **1998**, *C54*, 1997-1999.

[4] Rajappa, S. *Tetrahedron* **1981**, *37*, 1453-1480; section 4.3.

[5] Fetell, A. I.; Feuer, H. *J. Org. Chem* **1978**, *43*, 1238.

[6] Bellamy, A. and Latypov N. To be published, *Journal of Chem. Res.* .

[7] Adrien, A.; E.P, S. *The Determination of Ionization Constants*; 2 ed.; Chapman and Hall Ltd:, **1977**.

[8] Fedorov, Y. A.; Odokienko, S. S.; Selivanov, V. F. *Journal of Applied Chemistry of the USSR* **1979**, *52*, 2201-2202.

[9] Grakauskas, V.; Guest, A. M. *Journal of Organic Chemistry* **1978**, *43*, 3485-3488.

[10] Frisch, M. J.; G. W. Trucks, H. B. S., G. E. Scuseria, M. A. Robb, ; J. R. Cheeseman, V. G. Z., J. A. Montgomery, Jr., ; R. E. Stratmann, J. C. B., S. Dapprich, J. M. Millam, A. D. Daniels,; K. N. Kudin, M. C. S., O. Farkas, J. Tomasi, V. Barone, M. Cossi, R. Cammi,; B. Mennucci, C. P., C. Adamo, S. Clifford, J. Ochterski, G. A. Petersson,; P. Y. Ayala, Q. C., K. Morokuma, D. K. Malick, A. D. Rabuck, K. Raghavachari, ; J. B. Foresman, J. C., J. V. Ortiz, B. B. Stefanov, G. Liu, A. Liashenko,; P. Piskorz, I. K., R. Gomperts, R. L. Martin, D. J. Fox, T. Keith,; M. A. Al-Laham, C. Y. P., A. Nanayakkara, C. Gonzalez, M. Challacombe,; P. M. W. Gill, B. J., W. Chen, M. W. Wong, J. L. Andres, C. Gonzalez,; M. Head-Gordon, E. S. R., and J. A. Pople ; Gaussian, Inc.: Pittsburgh PA, **1998**.

KINETICS AND MECHANISM OF TRIAMINOGUANIDINE NITRATE THERMAL DECOMPOSITION

Sergey Smirnov and Boris Lurie

Mendeleev University of Chemical Technology,
Miusskaya sq. 9, Moscow, 125047, Russia

Abstract:

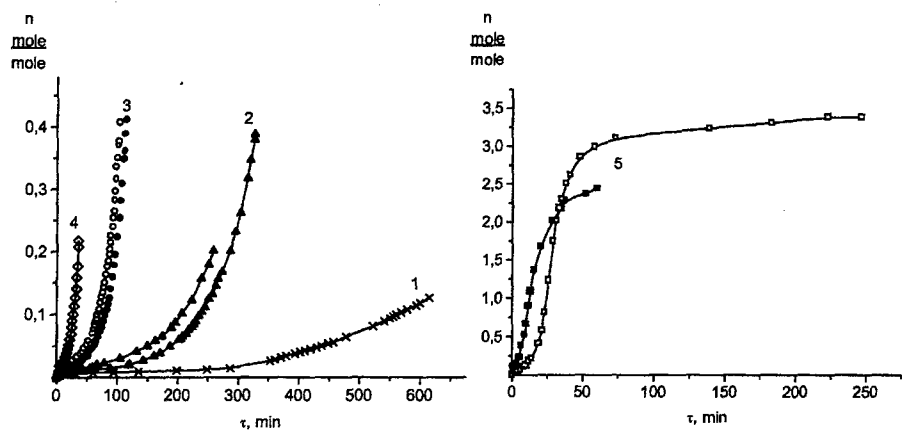
Kinetics of Triaminoguanidine nitrate (TAGN) thermal decomposition have been studied in both solid and liquid (in solution of Ammonium nitrate and also of aromatic nitrocompounds)) states. Decomposition of the solid substance goes with strong acceleration. Its formal kinetic characteristics have been determined. The main cause of the acceleration is progressive melting of the solid substance during its chemical transformation. TAGN decomposition in solution goes with decreasing rate. This rate is in ten time higher than in the solid state. The main gaseous products of decomposition are N_2, N_2O and H_2O. Chemistry of the thermal decomposition process is discussed.

1. INTRODUCTION

Triaminoguanidine nitrate (TAGN) is considered as a perspective oxydizer for some specific propellant compositions whose combustion products are rich of nitrogen [1,2]. It has a high melting point (~215°C) that is significantly more than for Ammonium nitrate (AN) (~170°C). There is a little information on kinetics of TAGN thermal decomposition. But some information about chemical characteristics of a high temperature transformation is available [1]. In present work, the main parameters of TAGN thermal decomposition are compared with the known data on decomposition of other salts of HNO_3 and amines: NH_3 [3-5], NH_2-NH_2 [3], NH_2OH [3,6], for which one of primary decomposition reactions is dissociation of the salt to the corresponding base and acid [3].

2. EXPERIMENTS

Kinetics of TAGN thermal decomposition has been studied by gas evolution under isothermal condition in glass manometers of Burdon type [7]. Gaseous products noncondensing after cooling to room temperature were analysed on a gas chromatograph [8]. Two samples of the powdery TAGN have been investigated: one was synthesized in our laboratory of Mendeleev University in Moscow (Russia) and the other – in Institute of Chemical Technology in Pfinztal-Berghausen (Germany). The first sample was presented by Dr. Valery Serushkin and the second one – by Dr. Manfred Bohn.



(a) (b)

Fig 1. Kinetics of gas evolution in the solid TAGN thermal decomposition at different temperatures: (a) 1 – 160, 2 – 170, 3 – 180, 4 – 190 °C, (b) 5 – 200°C; sample 1 – solid dot, sample 2 – open dot

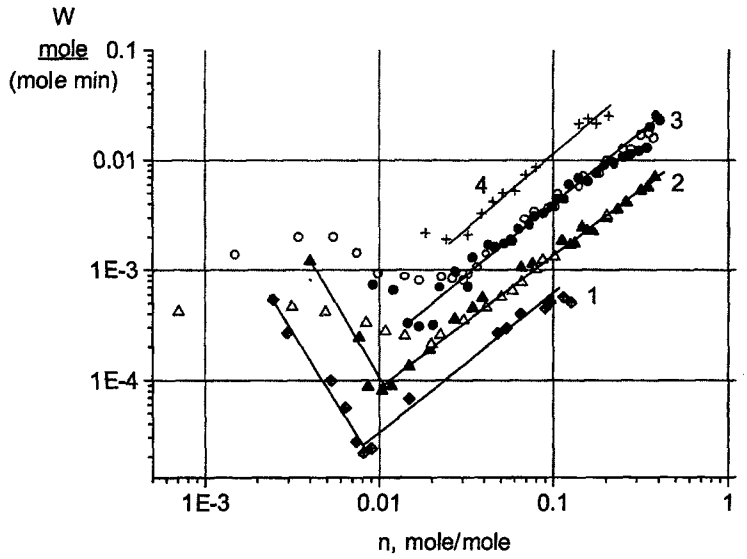


Fig 2. Change of the decomposition rate of solid TAGN during transformation at different temperatures: 1 – 160, 2- 170, 3 – 180, 4 – 190 C.

3. RESULTS

Decomposition of the solid substance has been investigated at 160-200°C at a filling density of the vessel by the substance (m/v – ratio of weight to free volume of vessel) ~ 0.04 g/cm^3. It is characterised by a gradual strong acceleration of the process (Fig. 1,2). The complete decomposition was carried out at significantly lesser m/v < 0.001 g/cm^3. Maximum rates are higher than initial ones almost 30 times. They are observed at the extent of transformation ~ 25-30 %. The growth of rate on the main part of transformation is described in logarithmic co-ordinates lg W = f (lg n) (Fig. 2) by straight lines with equal tangents of their slope angle ~ 1.7 independently from temperature.

On thermal decomposition of the both samples, there is a short initial stage characterized by some decreasing of the gas evolution rate (Fig. 2). The cause of this phenomenon may be either action of a chemical active admixture (at the surface of the solid substance) or a topochemistry specific change of a crystal defectiveness. This stage is more expressed at lower temperatures when the process goes comparatively slowly. With the temperature growth, it quickly transforms in the next stage where decomposition rate increases.

The temperature coefficient of TAGN decomposition rate in the solid state does not practically change during the process. Being estimated at equal extent of transformation the activation energy of decomposition is ~ 170 kJ/mole. If the activation energy is calculated formally from the minimum rate on the initial stage of process (believing that just here the process is not complicated by secondary occurrences), its magnitude will be somewhat higher ~ 230 kJ/mole. The reason of this phenomenon may be displacement of the minimal rates to the area with some higher extents of transformation during temperature grows.

The rate constant of TAGN decomposition was calculated as $k = W_{init}/V_{end}$. Magnitude of V_{end} equal to 3 mole/mole is the final amount of gaseous products after complete decomposition of substance. If W_{init} values at the extent of transformation corresponding to evolution ~ 10^{-2} mole of gases per mole of the initial substance when the change of rate constant with temperature for solid TAGN is described (Fig. 3) by the following Arrhenius-type expression:

$$\lg k = 14.67 - 173000/RT, [s^{-1}], \quad (E - \text{in Joule/mole})$$

Ammonium nitrate (AN) was tested as an inert solvent for TAGN. Experiments were carried out at 160 - 180°C and the ratio of TAGN to AN was ~ 1: 3 by weight and m/v values (for TAGN) ~ 0.005 g/cm^3. In this case rate of decomposition of liquid TAGN reduce with time (Fig. 4). Decrease in the rate is not described by a simple kinetic dependence of the first order. On initial state of transformation decrease of rate is more intensive then after that. Rate constants of the liquid TAGN decomposition were calculated formally the same as for solid substance. The value of rate for TAGN in liquid state is 30 times higher than one in crystalline state. The temperature dependence for liquid TAGN is described by expression:

$$\lg k = 15{,}87 - 172500/RT, [s^{-1}]$$

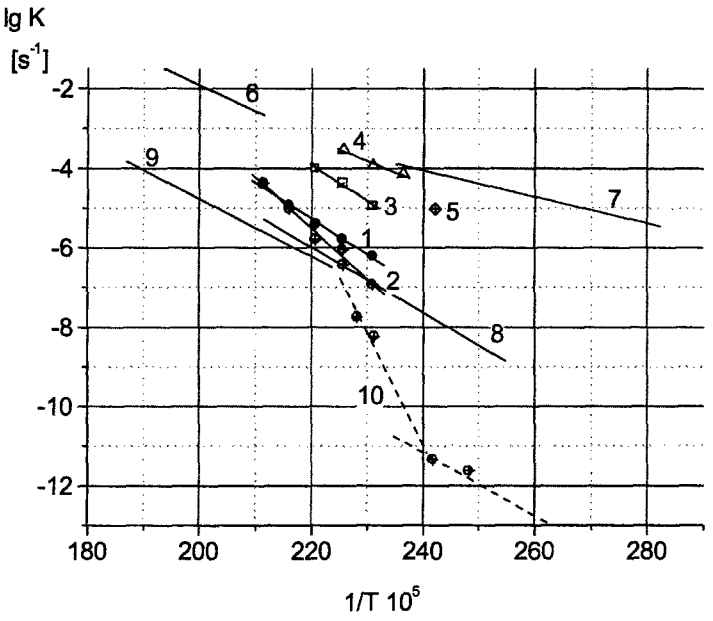


Fig 3. Arrhenius plot for the rate constant of thermal decomposition of crystalline (1,2) and liquid TAGN in AN (3), DNB+TNB (4) and TNT (5) solution in comparison with liquid (melt) (9) and solid (10) AN, with liquid NH_2OH HNO_3 (6) [2], (7) [5] and $N_2H_5NO_3$ (8) [4]. 1 – rate constant was calculated by means of W_{min}.

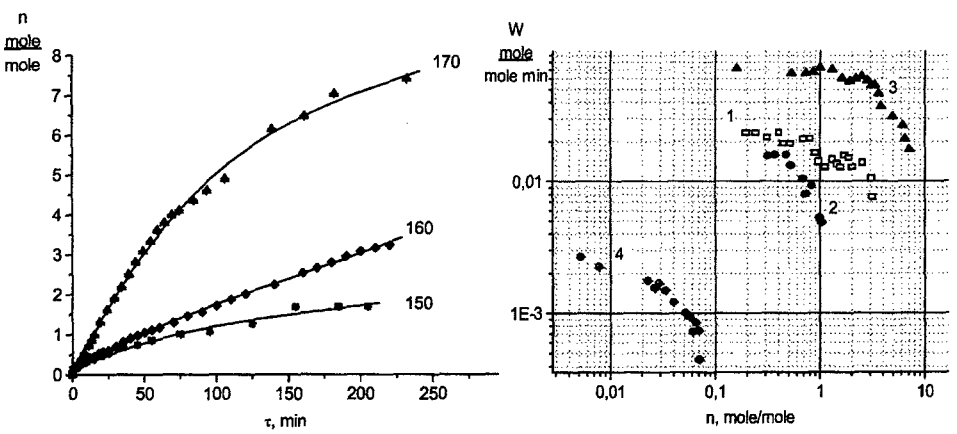


Fig 4. Kinetics of the gas evolution in TAGN thermal decomposition in the liquid state (in solution of Ammonium nitrate): 1 – 160, 2 – 170, 3 – 180°C.

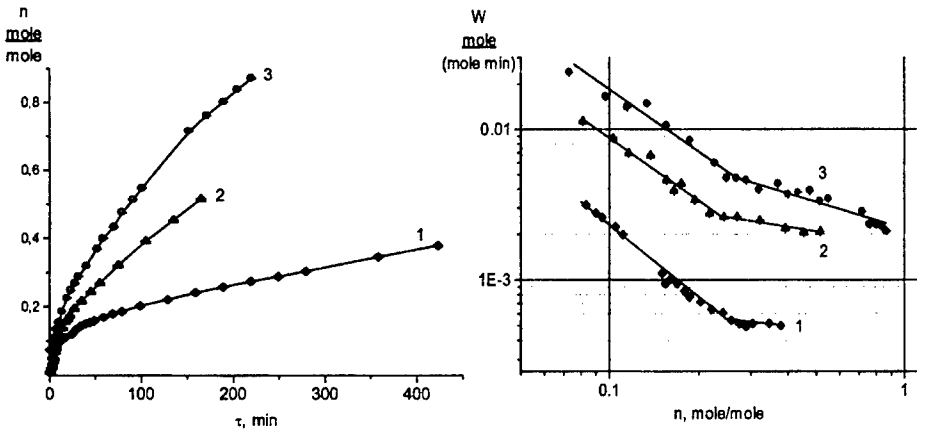


Fig 5. Change of TAGN decomposition rate with time at the different temperatures into DNB+TNB solution: 1 – 150, 2 – 160, 3 – 170°C.

TAGN decomposition has been also studied in a mixture solution of Dinitrobenzene (DNB) with Trinitrobenzene (TNB) (~ 1:3) at TAGN content ~ 8% weight (m/v for TAGN ~ 0.0006 g/cm^3) at the temperature interval 150-170°C. One of experiment was made with mixture of TAGN and Trinitrotoluene (TNT) at 140°C (C_{TAGN} = 21% weight, m/v for TAGN = 0.016 g/cm^3). In this case a complete dissolving of the investigated substance was not observed. These nitroaromatic compounds are very thermal stable [3] and often have been used as inert solvents for thermal decomposition of other nitrocompounds (nitroesters [9-11] and nitramines [12]). They do not practically decompose in individual form at such temperatures. A qualitative kinetic picture of TAGN decomposition in solution of nitroaromatic substances is the same as in AN solution (Fig. 5). But initial rates are almost one order of magnitude higher (Fig. 3) and value of activation energy is less:

$$\lg k = 9.27 - 108700/RT, \ [s^{-1}]$$

A must be given to the fact that solution colour is strong change and much more (almost 2 times) of gaseous products are formed during complete decomposition at 180°C. This indicates that nitroaromatic compounds are not inert during TAGN thermal decomposition. Perhaps they decay under action of the different amine reducer [13] appeared in the course of TAGN chemical transformation.

The gaseous products of TAGN thermal decomposition are mainly N_2, H_2O, and N_2O. Nitrous oxide appears only at later stages of process. After complete decomposition, the yield of N_2 is equal to 1,5, H_2O – 1 and N_2O – 0,5 mole/mole. CO_2 is present in trace amounts, whereas CO is absent. In this case, a white film of a crystalline substance, probably NH_4NO_3, is observed on the inside walls of the reaction vessel.

4. DISCUSSION

The rate constants of solid TAGN decomposition prove to comparable with decomposition rate of ammonium [3-5] and hydrazine (HN) [3] nitrates in the molten state (Fig. 3). Being in the same aggregate state, TAGN is considerably less stable (almost 3 orders of magnitude). Decomposition rates of liquid TAGN are close to those of hydroxyl amine nitrates (NHA) [6].

The main reason for solid TAGN decomposition acceleration is its progressive melting in the reaction centers (nucleuses), i.e. a gradual transformation of the solid substance into liquid state in which the decomposition rate is considerably higher. Liquation arises from decreasing in the melting point of the main substance under influence of appearing decomposition products. A mechanism of this process and its kinetic description was considered by G.B.Manelis [14,15] many years ago. Y.Y.Maksimov [16] showed an important role of the progressive melting phenomenon for a specific temperature dependence of the decomposition rate of solid substances near their melting points, where temperature coefficient of the rate became very high. Similar phenomena were observed for substances of different chemical nature: nitroesters (PETN [9] and MHN [10]), cyclic nitramines (Tetryl [14], RDX [12]). and for TAGN (Fig. 3).

The material balance by elements after complete decomposition of TAGN gives summary composition of the gaseous products as $H_2O_{1.5}N_4$. Then, the brutto composition of the condensed remainder will be $CN_3H_7O_{1.5}$. Its consideration will be more simple if a possible formation of included in NH_4NO_3 is proposed as one of the products of TAGN transformation. If all oxygen of the nonanalysed condensed remainder is NH_4NO_3, its maximum quantity will be ~ 0.5 mole/mole. In this case, the final residue has a summary formula CN_2H_5, ahd the general scheme of TAGN chemical transformation can be written as:

$$C(NHNH_2)_3NO_3 \rightarrow 1.5\ N_2 + H_2O + 0.5\ N_2O + 0.5\ NH_4NO_3 + CN_2H_5 \qquad (1)$$

The thermal decomposition of AN and NHA mainly proceeds with formation of N_2O mainly, whereas HN transformation results in AN and the main gaseuse products N_2, NH_3 and N_2O. It is assumed that the leading stage of HN decomposition is a destruction of the complex hydrazine ion with its cation with formation of NH_3 and N_2 [3]. TAGN decomposition does not result in NH_3 under our experimental conditions.

Until now mechanism of TAGN thermal decomposition is not clear for us completely. Formally, they are two ways of the primary chemical transformation that may be considered for compounds of such type [3]. The first way is dissociation into base and acid

$$C(NH\text{-}NH_2)_3NO_3 \leftrightarrow HNO_3 + NH_2\text{-}N{=}C(NH\text{-}NH_2)_2 \qquad (2)$$

and the second one is decomposition of the cation, which may have two variants of the beginning, correspondingly connected with rupture of either N-N or C-N bond:

$$C(NH\text{-}NH_2)_3NO_3 \nearrow {}^{\bullet}NH_2 + {}^{\bullet}N{=}C(NH\text{-}NH_2)_2 + HNO_3 \qquad (3)$$

$$C(NH\text{-}NH_2)_3NO_3 \searrow NH_2\text{-}{}^{\bullet}NH + NH_2\text{-}NH\text{-}{}^{\bullet}C{=}N\text{-}NH_2 + HNO_3 \qquad (4)$$

For any initial act, reactions of HNO_3 reduction may play an important role in the stages of the transformation. From the balance expression of TAGN decomposition (1), it follows that only a half of the initial nitrate is reduced, because the other 0.5 mole goes to form NH_4NO_3. Since oxygen-containing products, in particular N_2O, can not be formed without anion destruction, it may be logically assumed that the other half of nitrate is used in this direction. This may be realize through a primary reduction of HNO_3 to HNO_2 and the following nitrosation of amine. The classic source of N_2O is the nitrosation reaction of hydroxylamine with nitrouse acid [17]:

$$NH_2OH + HNO_2 \rightarrow N_2O + 2H_2O \qquad (5)$$

Thus, the material balance shows that the main quantity of N_2 is formed by the way of cation decomposition by means of secondary red-ox reactions with participation of amine radicals. Probably, this is a main direction of the TAGN chemical transformation.

There are several sources of NH_3 to form AN and NH_2OH to form N_2O. It may be the decay of cation to give radical $^{\bullet}NH_2$, or hydrolysis of triaminoguanidine, which is a similar to hydrolysis of guanidine [18]:

$$NH_2\text{-}N{=}C(NH\text{-}NH_2)_2 + H_2O \rightarrow O{=}C(NH\text{-}NH_2)_2 + NH_2OH + NH_3 \qquad (6)$$

Probably, the absence of C- and O-containing substances as well as CO_2 in the products is indicative of the radical nature of mechanism of NH_3 and NH_2OH formation which is the same as in the case of thermal decomposition of hydrazine nitrate [3].

REFERENCES

[1] Oyumi Y., Brill T.B. Solid-phase transitions and the decomposition of 1,2,3,-Triaminoguanidinium Nitrate. // J.Phys.Chem. 1985. v. 89, p. 4325.

[2] Kubota N., Hirata N., Sakamato S. Decomposition chemistry of TAGN. // Propel.Expl.Pyrot. 1988, v. 13, p. 65.

[3] Manelis G.B., Nazin G.M., Rubtsov Yu.I., Strunin V.A.. Thermal decomposition and combustion of explosives and propellants. Moscow, Nayka. 1996.

[4] Bespalov G.N..Filatova L.B, Shidlovskii A.A.. Termal decomposition of ammonium nitate. // Zh.Fiz.Khim. (USSR). 1968. v. 42, N 10, p. 2623.

[5] Lurie B.A., Chang Lianshen. Kinetics and mechanism of thermal decomposition of Ammonium Nitrate under action of carbon black. // Comb. Eplos. Shock Waves. 2000. v. 36, N 5, p. 607.

[6] Schoppeirei J.W., Brill T. Kinetics of aqueous $[NH_3OH]NO_3$ at 463-523 K and 27.5 Mpa by infrared spectroscopy. // J.Phys.Chem. (A). 1997. v. 101, N 46, p. 8593.

[7] Golbinder A.I. Laboratory works on a course in the theory of explosives. Rosvuzizdat, Moscow. USSR. 1963.

[8] Lurie B.A., Mikhno A.V. Interaction of NO_2 with Soot. // Kinet. and catal. 1997. v. 38, N 4, p. 490.

[9] Andreev K.K., Kaidymov B.I. Thermal decomposition of Nitroesters. 3. Pentaeritrit Tetranirate. // Zh.Phiz.Khim. (USSR). 1961.v. 35, N 12, p. 2676

[10] Lurie B.A, Svetlov B.S. Thermal decomposition of Mannit hexanitrate. // Proc. Mendeleev Chem. Techn. Inst., Moscow. USSR. 1967. v. 53, p. 51.

[11] Lurie B.A., Svetlov B.S. The kinetic parameters of the primary stage of thermal decomposition of organic nitrates. // Kinetics and catalysis. 1994. V. 35, N 2. P. 145.

[12] Maksimov Y.Y. Thermal decomposition of HMX and RDX. // Proc. Mendeleev MCTI. Moscow. (USSR). 1967. v. 53, p. 73.

[13] Zbarski V.L., Zhilin V.F. Toluene and its Nitro derivatives. Moscow. 2000.

[14] Manelis G.B., Dubovitskii P.I. Thermal decomposition of explosives below of melting point. // Doklad Akad. Nauk.(USSR). 1959. v. 126. p 813.

[15] Manelis G.B. Some characteristics of reactions mechanism in solid phase. // The kinetic problems of elementary chemical reaction. Moscow, Nauka, 1973. p. 93.

[16] Maksimov Y.Y. Anomaly temperature dependence of the explosives decomposition rate below their melting point. // J.Phys.Chem. (USSR). 1967. v. 41, N 5, p. 1193.

[17] Huges M.N., Stedman G. Kinetics and mechanism of the decomposition of Hyponitrous acid. // J.Chem.Soc. 1964, p. 163.

[18] Karrer P.. Lehrbuch der Organischen Chemie. Stuttgart. Oeoro Thieme Verlag. 1959.

INFLUENCE OF THERMAL DECOMPOSITION KINETIC MODEL ON RESULTS OF PROPELLANTS SELF-IGNITION NUMERICAL MODELING

Muhamed Sućeska

Brodarski institut – Marine Research & Special Technologies,
Av. V. Holjevca 20, 10000 Zagreb, Croatia

Abstract

Thermal decomposition of nitrocellulose propellants is accompanied by generation of heat, and under certain conditions can lead to the well-known phenomenon of the self-ignition. Therefore, it is of great concern to predict whether or not a propellant specimen will ignite under given conditions (specimen mass and shape, surrounding temperature, etc.).

An own computer program, named THERMEX, based on the thermal explosion theory and the finite difference method, was developed in order to describe the reactive heat conduction phenomena in infinite slab, cylindrical, and spherical geometry of an explosive material. Up to now the program is tested by the comparison of the calculated times to ignition with the times to ignition experimentally obtained or calculated by other authors. A good agreement was found under identical computational conditions.

However, it was noticed that, along with some input data (e.g. space and time increments), thermal decomposition kinetic model used in calculations have a large influence on the calculation results. The influence of three kinetic models, commonly used to describe thermal decomposition of propellants, on the results of calculation is analysed in this paper. It was found out that the power law kinetic model gives the best agreement between the experimentally obtained and the calculated values of times to ignition.

1. INTRODUCTION

If specimen of a propellant is heated, and if it decomposes with the rate given by the equation [1]:

$$\frac{d\alpha}{dt} = k_T f(\alpha) = A e^{(-E/RT)} f(\alpha) \qquad (1)$$

where α – conversion; t – time; $d\alpha/dt$ – rate of conversion; k_T – temperature dependent rate constant, $f(\alpha)$ – function which represents the hypothetical model of the reaction mechanism (so-called reaction model); E – activation energy; A – pre-exponential factor, and R – universal gas constant, than the specimen heat balance can be described by the following equation [1,2]:

$$\rho c \frac{\partial T}{\partial t} = \lambda \nabla^2 T + \rho Q A e^{(-E/RT)} f(\alpha), \qquad (2)$$

where T is temperature; c – specific heat capacity; ρ – density; λ – thermal conductivity; ∇^2 – Laplacian operator; Q – heat of decomposition.

The left-hand side of Eq.2 gives the rate of the heat build-up in the propellant specimen; the first term in the right-hand side is the rate of heat loss into the surroundings; while the last right-hand term is the rate of heat generation due to exothermic reactions obeying the zero-order kinetic law.

Thermal ignition of explosive components in ammunition is always a problem of concern. This is the reason why the explosive community is permanently searching for an efficient method for solving reactive heat conduction problem in propellants and explosives. An analytical solutions to the heat conduction problems in the absence of chemical reactions, the so-called non-reactive heat conduction, is relatively easy to deduce, however, an analytical solution of the heat conduction equation with chemical reaction, the so-called reactive heat conduction, is out of question. Thus, the approximate techniques and numerical methods are most frequently the subjects of investigation in this field.

Different simplifications to the Eq.2 have been proposed in order to calculate the critical conditions of self-ignition. N. N. Semenov, for example, allowed the temperature to be uniform through a sample, and reaction to follow the zero-order kinetic law. He was than able to compare the heat generation and the heat loss rates, and to derive the critical conditions of self-ignition [cited in 1,3]. D. A. Frank-Kamanetskii tried to find steady state solution of Eq.2 in the case of the zero-order kinetic law, but without assuming the temperature to be spatially uniform through a specimen [cited in 1,3].

To obtain time-dependent solution of the heat of equation different numerical techniques were proposed. J. Zinn and C. Mader used numerical method based on a Fourier series spatial representation of solutions to obtain the ignition times for slabs, cylinders, and spheres of explosive material [2,4]. A. Merzhanov and co-workers were the first that applied the finite difference method to solve the heat conduction equation with the zero-order kinetic reaction model. C.A. Anderson developed the finite difference code for one-dimensional heat conduction, based on zero-order kinetic model and the Crank-Nicolson method. This code treats the problems of layered media in slabs, cylindrical, or spherical geometry, and incorporates temperature dependent thermal properties and phase transitions [5].

Since thermal decomposition model plays a crucial role in each numerical method, some authors have tried to incorporate more complex kinetic model into computer codes based on the finite difference method. For example, J. Isler used the power law kinetic model to describe thermal ignition of a nitrocellulose propellant [1,6]. R. McGuire and C. Tarver used 2-3 steps chemical decomposition models, deduced from available kinetic data for some explosives, and incorporated them to a thermal conduction code based on the finite difference method, obtaining good agreement with experimental results [7].

The above stated facts have motivated me to try in this paper to incorporate into the own computer code based on the finite difference method, named THERMEX, three different kinetic models commonly used to describe the thermal decomposition of nitrocellulose propellants: zero-order, power law, and autocatalytic model, and to analyse the applicability of the individual models.

1.1. Numerical technique applied in computer code

In the special case of infinite long cylinders, infinite slabs, and sphere, the Laplacian operator (∇^2) in the general heat conduction equation (Eq. 2) reduces in one dimension [4]:

$$\nabla^2 = \lambda\left(\frac{\partial^2}{\partial r^2} + \frac{m}{r}\frac{\partial}{\partial r}\right), \tag{3}$$

where r is radius of cylinder (or sphere). The integer m has a value 0 for slabs, 1 for cylinders, and 2 for spheres). In the case of an infinite slab r is replaced by slab thickness (x). Thus, for example, Eq. 2 for an infinitely long cylinder will have the form:

$$\rho c\frac{\partial T}{\partial t} = \lambda\left(\frac{\partial^2 T}{\partial r^2} + \frac{1}{r}\frac{\partial T}{\partial r}\right) + \rho Q A e^{(-E/RT)} f(\alpha) \tag{4}$$

Time dependent solution of Eq. 4 can be obtained by applying the finite difference method, i.e. by approximating partial derivatives with finite differences. The finite difference scheme of an infinitely long cylinder whose time-dependent temperature field we wish to compute from an initial temperature distribution, surrounding temperature, and boundary conditions may be represented by Figure 1.

The radius of an infinitely long cylinder (r_c) is divided into k cells, thickness of which is Δr ($\Delta r = r_c / k$). The initial temperature (at $t = 0$, i.e. $j = 0$, where j is time index) is specified at individual mesh points ($T_{0,i}^{j=0}$, $i = 0$ to k-1, where i is space index), while the temperature at the cylinder surface (T_r^j) is specified by the boundary conditions (Eqs. 12 and 13).

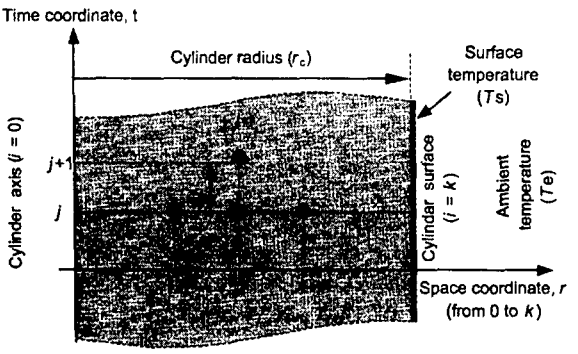


Fig 1. Finite difference scheme of an infinitely long cylinder

For the case of an infinitely long cylinder the space derivatives in Eq. 4, in a time j, may be approximated by the following finite differences [5]:

$$\left(\frac{\partial^2 T}{\partial r^2} + \frac{1}{r}\frac{\partial T}{\partial r}\right) = \left(\frac{T_{i+1}^j + T_{i-1}^j - 2T_i^j}{(\Delta r^2)} + \frac{1}{r}\frac{T_{i+1}^j - T_i^j}{\Delta r}\right) \tag{5}$$

For the case of spheres and infinite slabs the space derivatives will be [5]:

$$\left(\frac{\partial^2 T}{\partial r^2}+\frac{2}{r}\frac{\partial T}{\partial r}\right)=\left(\frac{T_{i+1}^j+T_{i-1}^j-2T_i^j}{(\Delta r^2)}+\frac{2}{r}\frac{T_{i+1}^j-T_i^j}{\Delta r}\right), \tag{6}$$

$$\left(\frac{\partial^2 T}{\partial x^2}\right)=\left(\frac{T_{i+1}^j+T_{i-1}^j-2T_i^j}{(\Delta x^2)}\right). \tag{7}$$

The time derivative in Eq. 4 may be replaced by its simplest finite difference approximation [5]:

$$\left(\frac{\partial T}{\partial t}\right)=\frac{T_i^{j+1}-T_i^j}{\Delta t}, \tag{8}$$

where Δt is time increment.

By replacing the space and time derivatives in Eq. 4 by the finite differences (Eqs. 5–8), the equation for the calculation of temperature distribution along a space co-ordinate, at time t^{j+1}, can be derived. For example, in the case of a cylinder this equation will be:

$$T_i^{j+1}=T_i^j+\frac{\lambda(\Delta t)}{c\rho}\left(\frac{T_{i+1}^j+T_{i-1}^j-2T_i^j}{(\Delta r^2)}+\frac{1}{r}\frac{T_{i+1}^j-T_i^j}{\Delta r}\right)+\frac{(\Delta t)}{c}QAe^{(-E/RT)}f(\alpha) \tag{9}$$

It follows from the above equation that the temperature distribution along a cylinder radius at time t^{j+1} is evaluated from temperature distribution at earlier time (t^j), where:

$$t^{j+1}=t^j+\Delta t. \tag{10}$$

By an analogous way the equations for the calculation of temperature distribution along a sphere radius or a slab thickness can be obtained from Eqs. 6, 7,8, and 4.

In additions to the finite difference approximation to the reactive heat conduction equation, the approximations to the initial and boundary conditions should be included in order to calculate time-temperature distribution along a specimen space co-ordinate.

The initial conditions give an initial temperature distribution (at $t = 0$) along a specimen radius. In the most usual way the initial conditions are given in the form:

$$T_i^{j=0}=T_{0,i}^{j=0} \text{ where } i = 0, 1, 2, 3 \ldots k\text{-}1 \tag{11}$$

The boundary conditions give the temperature at a specimen surface at any time (T_s^j). The simplest case is when the specimen surface temperature remains constant during the whole process. In this case the boundary conditions can be written in the form:

$$T_s^j=T_e=const. \tag{12}$$

where T_e is surrounding temperature. However, in the case of convective heat transfer from an ambient fluid to a specimen surface, the boundary conditions are given by the following equation [5, 6]:

$$\varepsilon(T_s - T_e) = -\lambda\left(\frac{\partial T}{\partial r}\right)_s, \quad \text{i.e.}$$
$$\varepsilon(T_s - T_e) = -\lambda\frac{T_s - T_{k-1}}{\Delta r} \tag{13}$$

where ε is the heat transfer coefficient ($W/m^2 K$).

2. RESULTS AND DISCUSSION

2.1. Accuracy of the method

Since an explicate finite difference solution to differential equations is often conditionally stable, and since correct choice of space and time increments is of crucial importance to obtain accurate solutions, the influence of time and space increments on the results of calculations was studied in detail in previous paper [9]. As a test model hexogen (RDX) spheres 25.4 mm in diameter were used in the study.

The values of the kinetic and thermal parameters of RDX used in the calculations were: ρ = 1.8 g/cm^3; Q = 2093 J/g ; E = 199 kJ/mol; A = 3.16 10^{18} 1/s; c = 2.093 J/Kg, and λ = 0.293 W/m K [2,4,8].

The times to thermal ignition at given surrounding temperature were calculated for different space and time increments applying the boundary conditions given by Eq. 12. As an example, the results of calculations for the surrounding temperature of 240 °C are given in Figure 2.

It is evident from Figure 2 that the times to ignition depend strongly on values of space and time increments. For small values of time increments the time to ignition-time increment relationships is practically linear. The slopes and the intersections of individual time to ignition-time increment curves with Y axis depend on space increment.

By the linear extrapolation of the time to ignition-time increment data given in Figure 2, the values of the time to ignition corresponding to $\Delta t \to 0$ were derived for individual space increments. In this way the dependence of time to ignition at $\Delta t \to 0$ ($t_{s\ \Delta t \to 0}$) on space increment was obtained (Figure 3).

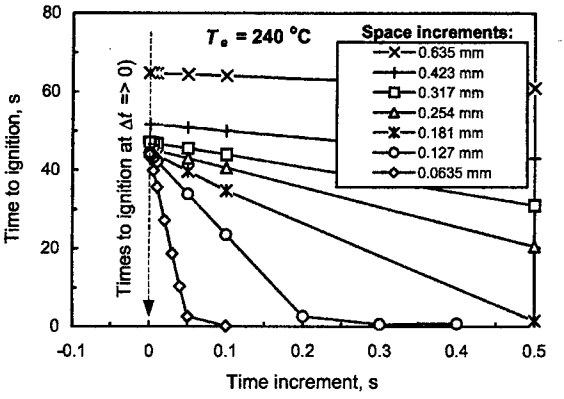


Fig 2. Dependence of calculated times to ignition of RDX sphere on time increment for different space increments at surrounding temperature of 240 °C.

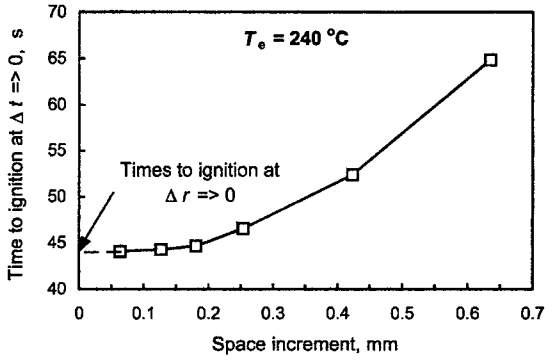


Fig 3. Dependence of calculated times to ignition of RDX sphere on space increment at surrounding temperature of 240 °C.

By the extrapolation of a non-linear dependence the times to ignition-space increment, given in Figue 3, the times to ignition at $\Delta r \to 0$ ($t_{s\ \Delta t \to 0,\ \Delta r \to 0}$) for specified surrounding temperature is obtained. The values of times to ignition obtained in this way are the true calculated ignition times for a given surrounding temperature.

A further analysis has shown that the time increment that enables the times to ignition to be calculated with a small error may be chosen on the basis of the stability criterion given by the equation [5]:

$$\frac{\lambda}{\rho c} \cdot \frac{\Delta t}{(\Delta r)^2} < f_s \qquad (14)$$

According to R.D. Richtmyer results (cited in Ref. 5) the finite difference methods is stable if $f_s < 0.5$. The results of our work have shown that in order to obtain the ignition times which differ less than 1% in respect to the ignition times obtained by the extrapolation to $\Delta t \to 0$, the value of f_s should be less than 0.01 (Figure 4). Almost the same value of f_s was obtained for all surrounding temperatures in the range 180–260 °C.

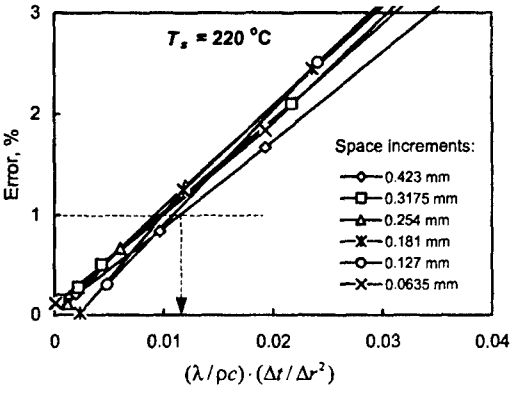


Fig 4. Error in values of calculated ignition times *vs.* value of $(\lambda/\rho c)\cdot(\Delta t/\Delta r^2)$

2.2. Kinetics and self-ignition study of NC propellant

In order to test influence of kinetic model used on results of the self-ignition calculations by the computer program THERMEX, based on the finite difference method, the thermal decomposition and the self-ignition data obtained experimentally by J. Isler and D. Kayser are used in the paper [1]. The authors have carried out the thermal decomposition experiments in air by both manual (130–150 °C) and by thermogravimetry technique (150–170 °C), using NC propellant samples being ~5 mg in mass.

The self-ignitions experiments the authors have realised with cylindrical samples of NC propellant having 7 mm in diameter, 26 mm in length, and 1.3 g in mass. The central temperature of samples was measured by 0.5 mm wide thermocouple inserted into a hole made along the cylinder axis.

On the basis of the thermal decomposition experiments they have obtained degree of conversion –time dependency given in Figure 5. It is evident from Figure 5 that all α–t curves are of sigmoid shape, with the inflexion at about 0.25 conversion (25 % decomposition). That means that the rate of conversion (Figure 6), and consequently the rate of heat generation, increase up to this point, and decreases gradually above it. The rate of conversion–conversion dependency shown in Figure 6 is typical for autocatalytic reactions and may by described mathematically by the equation:

$$\frac{d\alpha}{dt} = k_T \alpha^n (1-\alpha)^m, \tag{15}$$

which means that the reaction model, i.e. function $f(\alpha)$ in Eq. 1,2,4 and 9, has the form:

$$f(\alpha) = \alpha^n (1-\alpha)^m \tag{16}$$

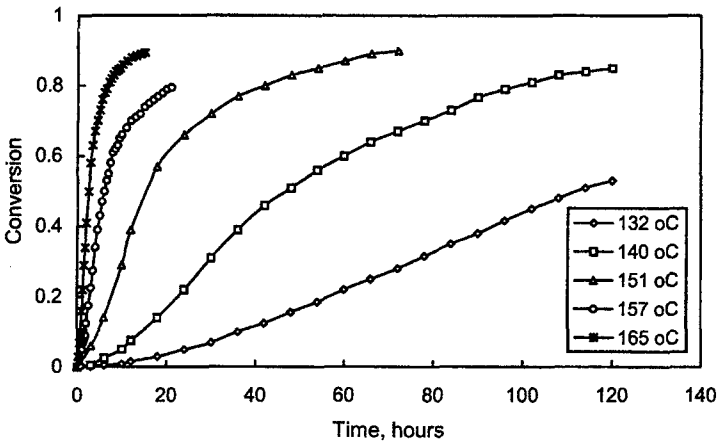


Fig 5. NC propellant conversion as a function of time at different environmental temperature

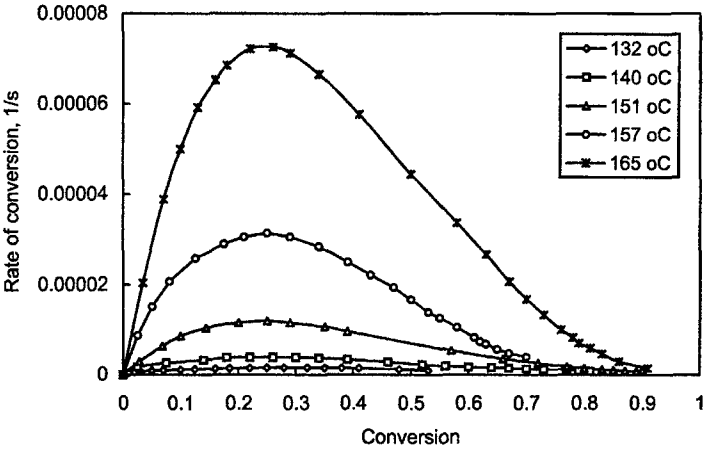


Fig 6. Dependence of rate of NC propellant conversion on degree of conversion for several different environmental temperatures

By the non-linear curve fitting procedure of experimentally obtained data given in Figure 6, constants m, n, and rate constant k_T in Eq. 15 are evaluated for each temperature. The activation energy and the pre-exponential factor are then obtained from $\ln k_T - 1/T$ linear dependency, according to the Arrhenius equation. The following values of kinetic parameters are obtained in this way:

$E = 170.60$ kJ/mol $A = 7.57 \cdot 10^{16}$ 1/s
$n = 0.67$ $m = 2.27$

Since the rate of heat generation decreases above 0.25 conversions it is reasonable to suppose that the self-ignition of NC propellant studied may occur only below that conversion. This means that, in order to study the self-ignition phenomena, we may limit our kinetic study to the early stage of NC propellant decomposition: $0 < \alpha < 0.25$. By the non-linear curve fitting procedure it was found out that for conversions lying between 0 and 0.25, the power law kinetic model given by the equation:

$$\frac{d\alpha}{dt} = k_T \alpha^n , \tag{17}$$

describes the best $d\alpha/dt$–α experimentally obtained dependency shown in Figure 6. In the case of the power law kinetic model the function $f(\alpha)$ in Eq. 1,2,4 and 9, has the form:

$$f(\alpha) = \alpha^n \tag{18}$$

In the way described above the following values of kinetic parameters are obtained:

$E = 182.20$ kJ/mol $A = 4.20 \cdot 10^{17}$ 1/s
$n = 0.29$

From the curves given in Figure 5 one may note that α–t dependency is almost linear in the range $0 < \alpha < 0.25$ conversions. Accordingly, the zero-order kinetic model may be used to describe (roughly) early stage of NC propellant decomposition. Another reason while the zero-order kinetic model is often used to describe the thermal decomposition of energetic materials is in its simplicity (Eq. 19):

$$\alpha = k_T \alpha , \text{ or in differential form : } \frac{d\alpha}{dt} = k_T . \tag{19}$$

In the case of the zero-order kinetic model the function $f(\alpha)$ in Eq. 1,2,4 and 9, will be:

$$f(\alpha) = 1 \tag{20}$$

The zero-order kinetic model applied for early stage of decomposition ($0 < \alpha < 0.1$) gave the following values of kinetic parameters:

$E = 189.14$ kJ/mol $A = 1.40 \cdot 10^{18}$ 1/s

From the results given above it follows that the activation energies values obtained applying different kinetic models vary between 170 and 189 kJ/mol, while pre-exponential factors vary between $7.57 \cdot 10^{16}$ and $1.40 \cdot 10^{18}$ 1/s.

Using the above mentioned kinetic models and the values of kinetic parameters obtained, the self-ignition calculations for cylindrical NC propellant specimen 7 mm in diameter was carried out using computer program THERMEX. The following values of thermokinetic parameters of NC propellant are used in the calculations:

- specific heat capacity (c) = 1.254 J/gK
- heat of decomposition (Q) = 3970 kJ/kg
- thermal conductivity (λ) = 0.16 W/m K
- heat transfer coefficient (ε) = 0.22 W/m^2 K
- density (ρ) = 1.6 g/cm^3

Other parameters used in calculations were:

- space increment (Δr) = 0.1 mm
- time increment (Δt) = 0.01 seconds
- initial specimen temperature = 20 °C
- boundary conditions given by Eq. 13
- ignition temperature = 200 °C

It is important to note that the conversion at a given time was calculated by the numerical integration of the rate of conversion equation used. For example, when the autocatalytic kinetic model (Eq. 15) was used than the conversion is calculated according to the equation:

$$a(t) = k_T \int_0^t a^n (1-\alpha)^m dt \tag{20}$$

The conversion at $t = 0$ was taken in the calculations to be 10^{-10}.

As an example the times to ignition of tested NC propellant at 156 °C environmental temperature, computed using different kinetic models (Eq. 15, 17 and 19) are given in Figure 7. The results presented in Figure 7 show very large influence of kinetic model on the calculated values of times to ignition. At the same time the results show that power law kinetic model gives the best agreement between experimentally obtained and calculated times to ignitions.

It is convenient to plot logarithms of the calculated time to ignition *vs.* the reciprocal of the ambient temperature in order to determine the critical temperature of a specimen of a given size, shape and composition [4]. These plots are linear over quite a large region but bend upward sharply near the critical temperature. At the critical temperature the plot becomes vertical, indicating an infinitely long induction period. Such plot for 7 mm in diameter NC propellant cylinder is given in Figure 8.

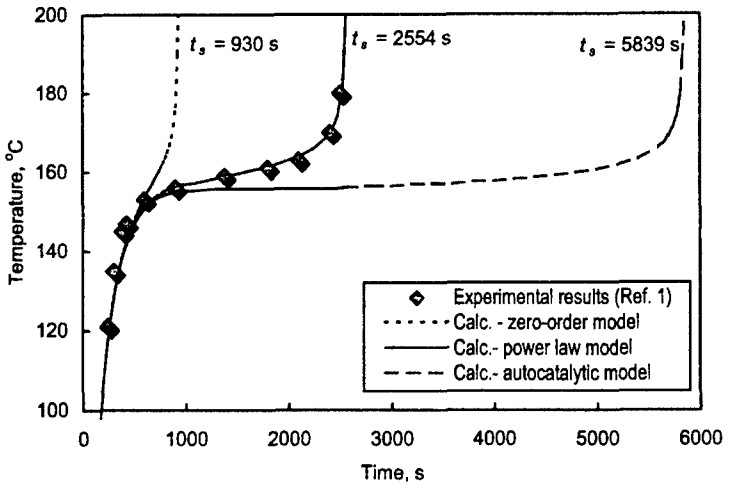


Fig 7. Times to ignition of cylindrical NC propellant specimen 7 mm in diameter at 156 °C environmental temperature calculated using different kinetic models

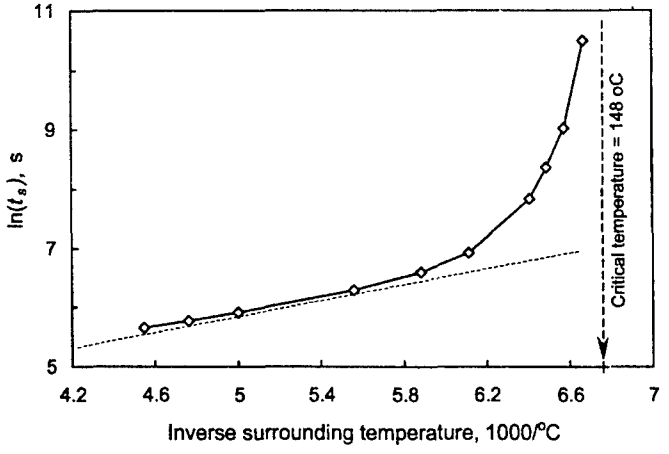


Fig 8. Determination of critical temperature for cylindrical NC propellant specimen being 7 mm in diameter (calculations are carried out using power law kinetic model)

It was found from Figure 8 that the critical temperature for 7 mm diameter NC propellant cylinder equals ~148 °C. J. Isler and D. Kayser have found that the critical equals 146 °C.

An interesting conclusion follows from the curves given in Figure 9 showing calculated values of conversions at the moment of the self-ignition.

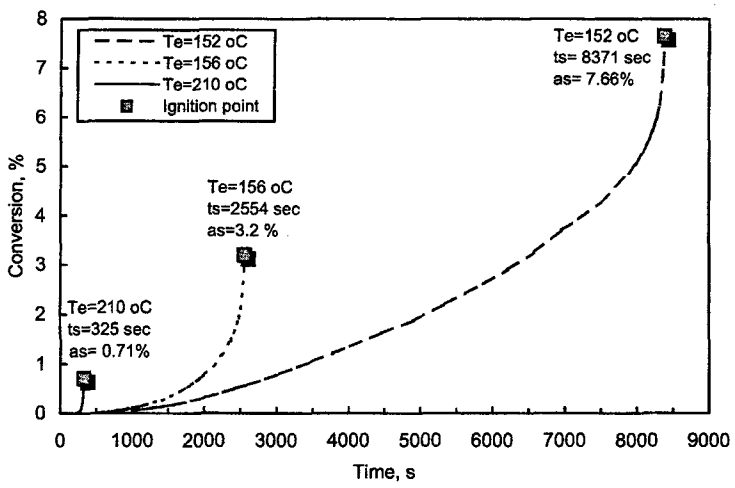


Fig 9. Calculated values of conversions at ignition temperatures for several surrounding temperatures

It follows from Figure 9 that for higher surrounding temperatures the self-ignition occurs at very early decomposition stage. For example, at 210 °C surrounding temperature the self-ignition occurs at the NC propellant cylinder surface after 0.71 % of decomposition. At lower surrounding temperatures the ignition, which occurs at the NC propellant cylinder centre, occurs at higher conversion. At temperatures close to the critical temperature (148 °C) the self-ignition occurs at conversion at which maximal decomposition rate attains (0.25 conversion, Figure 6). The above stated is clearly visible from Figure 10.

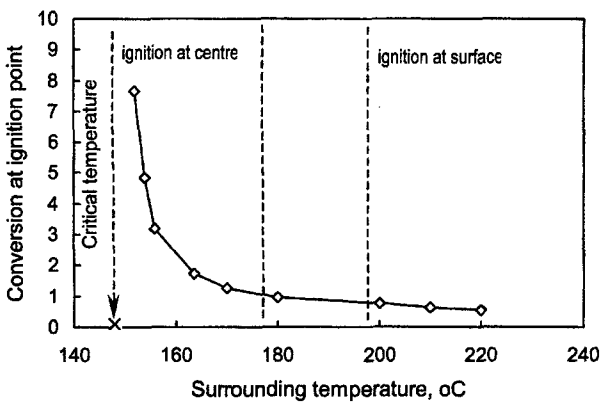


Fig 10. Dependence of conversion at the ignition point on the surrounding temperature

Such results confirm supposition that the self-ignition may only occur at conversions at which the rate of conversion, i.e. heat generation rate, increases – this is range from 0 and 0.25 conversion (Figure 6). Also, it means that the kinetic parameters needed for the self-ignition calculations should be evaluated for conversions between 0 and 0.25.

2.3. Space- and time-temperature profiles

Although the time to ignition and the critical temperature are essential parameters for the prediction of self-ignition possibility of a propellant specimen, we are usually interested to have details of the heat flow, i.e. to have temperature-time profile at a given position within a specimen, and temperature-radius profiles at a given time.

It is known that the time to ignition decreases with the surrounding temperature (see Figure 9), as well as that the ignition of the specimen occurs at a position closer to the specimen surface with the increase of the surrounding temperature. The last is visible from Figure 11, which shows the spatial distribution of temperature for NC propellant cylinder subjected to several different surrounding temperatures.

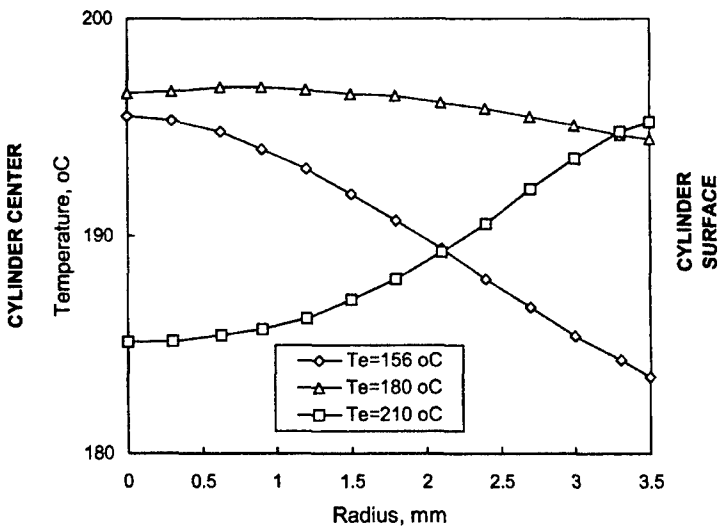


Fig 11. Calculated temperature-radius profiles for times near the end of induction period ($t = t_s \cdot 0.99$) for NC cylinder 7 mm in diameter being initially at 20 °C

For example, at 210 °C surrounding temperature the ignition occurs at the cylinder surface, while at the same time temperature at the cylinder centre is for about 15 °C lower. For lower surrounding temperatures, e.g. 156 °C, the ignition occurs at the cylinder centre, while at the same time temperature at the cylinder surface remains for about 15 °C lower. For medium surrounding temperatures, e.g. 180 °C, the ignition occurs at the position somewhere between cylinder centre and surface ($r_c \approx 1$ mm for $T_e = 180$ °C). The above mentioned is also visible from Figure 12, showing the time-temperature distribution at two location within NC propellant cylinder subjected to 156 °C surrounding temperature. It is visible that at the position near the cylinder surface the temperature increases relatively

quickly, while at the cylinder centre the temperature reaches the same value at later times due to the heat conduction phenomena. A quicker rise of the temperature at the cylinder centre at the end of the induction period is due to the heat liberated in exothermic decomposition of NC propellant sample.

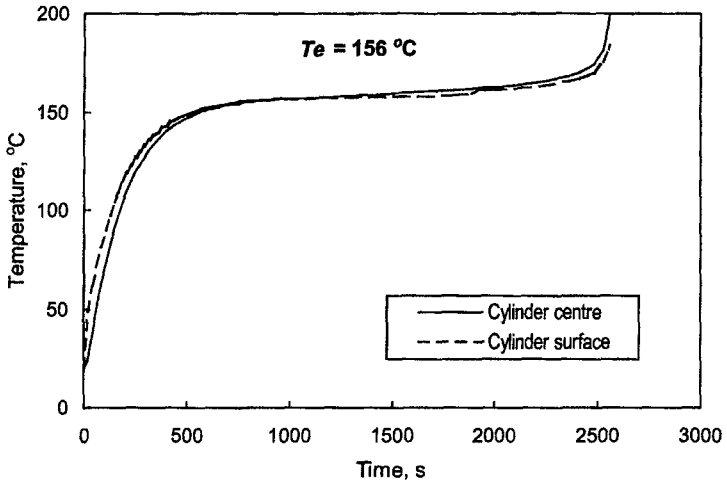


Fig 12. Calculated temperature-time profiles at two locations inside 7 mm NC propellant cylinder specimen subjected to 156 °C surrounding temperature

3. CONCLUSIONS

The presented numerical model for the studying initiation phenomena of explosives, based on the finite difference method, can be used to predict the time to ignition, the critical temperature, as well as to obtain temperature-time, and temperature-space co-ordinate profiles of an explosive material specimen.

The accuracy of solution is greatly affected by the values of space and time increments, as well as by the kinetic model used in the calculations.

It was shown that the power law kinetic model gives the best agreement between the calculated and experimentally obtained ignition times. Also, it is shown that the self-ignition occurs at the early stage of decomposition (bellow 25 %), which depends on the surrounding temperature.

4. References

[1] J. Isler, D. Kayser, Correlation Between Kinetic Properties and Self-Ignition of Nitrocellulose, 6th Symp. Chem. Probl. Connected Stab. Explos, Kungalav, Sveden, (1982), pp. 217-237.

[2] J. Zinn, C. L. Mader, Thermal Initiation of Explosives, J. Appl. Phys. 31(2) (1960) 323.

[3] A. G. Merzhanov, V. G. Abramov, Thermal Explosion of Explosives and Propellants. A Review, Propellants and Explosives 6 (1981) 130.

[4] C. L. Mader, Numerical Modeling of Explosives and Propellants, CRC Press, Boca Raton, 1998, pp. 136-187.

[5] C. A. Anderson, TEPLO – A Heat Conduction Code for Studying Thermal Explosion in Laminar Composites, Report LA-4511, Los Alamos Scientific Laboratory, Los Alamos, 1970.

[6] J. Isler, Auto-inflammation de poudres a simple base, Propellants, Explos. Pyrotechn. 11 (1986) 40.

[7] R. R. McGuire, C. M. Tarver, Chemical Decomposition Models for Thermal Explosion of Confined HMX, RDX, and TNT Explosives, Report UCRL-84986, Lawrence Livermore Laboratory, Livermore, 1981.

[8] J. F. Baytos, Specific Heat and Thermal Conductivity of Explosives, Mixtures, and Plastic-Bonded Explosives Determined Experimentally, Report LA-8034-MS, Los Alamos Scientific Laboratory, Los Alamos, 1979.

[9] M. Sućeska, A Computer Program Based on Finite Difference Method for Studying Thermal Initiation of Explosives, J. Thermal Analysis and Calorimetry (in press).

AN ANALYSIS OF LARGE SCALE ETHYLENE RELEASE AND EXPLOSION

Andrzej Teodorczyk

Warsaw University of Technology,
ITC, Nowowiejska 25, 00-665 Warszawa, Poland

Abstract

In the paper an engineering analysis is presented of ethylene release from the ruptured reactor in the polyethylene installation of petrochemical plant in Poland. Gas release was also analysed by computer simulation using KIVA3V CFD code. Approximately 100 kg of ethylene was released during pressure decrease in the reactor from 243 MPa to 110 MPa.

Time of release of 100 kg of ethylene calculated from the simple model was equal to about 3.1 s. This was is close to the time of pressure drop in the reactor from 243 MPa do 110 MPa, recorded by measuring equipment (about 4 s).

In addition, simple analysis of the TNT equivalent of gas explosion was calculated, based on mass released and recorded damages.

1. INTRODUCTION

In August 1999 an accident occurred at polyethylene installation in petrochemical plant in Poland. Failure of installation occurred due to the fatigue fracture of lens ring with thermocouple socket on one of the reactor pipes. After short period of time of ethylene outflow from the pipe (4s according to the readings of instruments) an explosion occurred followed by the fire inside reactor bunker. An explosion has caused damages to the bunker walls and to the reactor itself. There were also serious damages outside bunker: broken windows,doors, side walls of coolers, etc. over the distance of 1 km. Clear evidences of gas jet erosion on the wall and flour were consistent with the position and orientation of the fractured ring.

This paper presents an engineering analysis of ethylene release from the ruptured reactor, supplemented by computer simulation of gas outflow, as well as simple analysis of the TNT equivalent of gas explosion.

2. ETHYLENE RELEASE FROM DAMAGED REACTOR

2.1. Initial state

The reactor consists of 81 pipes of the length of 10 m and of internal diameter of 46 mm, which gives total volume of $V = 1.345\ m^3$. The thermodynamic parameters of ethylene in the reactor are: pressure $p_0 = 243$ MPa, temperature $T_0 = 518$ K and density $\rho_o = 500\ kg/m^3$. At such conditions the behaviour of ethylene considerably differs from ideal gas. For example the value of compressibility factor at above conditions is:

$$Z = \frac{p_0}{\rho_0 R T_0} = 3.17$$

where: R = 296 J/(kg K) - gas constant of ethylene.

After isentropic ethylene expansion to the pressure of 110 MPa, its temperature equals to 463 K, density equals to 425.5 kg/m^3 and compressibility factor is Z = 1.88. The departure of ethylene behaviour from ideal gas decreases with the decrease of pressure, however in the model of ethylene release the ideal gas assumption can not be used.

The initial mass of ethylene in the reactor at the pressure equals:

$$m_0 = V \cdot \rho_0 = 1.345 \cdot 500 = 672.5 \text{ kg}$$

The mass of ethylene in the reactor at the pressure of 110 MPa equals to 1.345 m^3 ·425.5 kg/m^3 = 572.3 kg. This means that about 100 kg of ethylene was released from reactor during pressure decrease from 243 MPa to 110MPa.

2.2. Critical parameters at the exit from the crack

Detailed inspection of the reactor after accident has revealed that the ethylene release occurred probably by the crack in metal gasket which was also used as thermocouple socket.

Exit parameters of the ethylene from the crack in gasket can be estimated with the assumption of sonic and isentropic flow. At the beginning of outflow (t = 0) the pressure, temperature, density and sound speed at the exit cross section are equal to, respectively:

$$p^* = p_0 \left(\frac{2}{k+1} \right)^{\frac{k}{k-1}} = 135 \text{ MPa}$$

$$T^* = T \left(\frac{2}{k+1} \right) = 463 \text{ K}$$

$$\rho^* = \rho_0 \left(\frac{2}{k+1} \right)^{\frac{1}{k-1}} = 0{,}623 \rho_0 = 311 \text{ kg/m}^3$$

$$c = V^* = \sqrt{\frac{k p^*}{\rho^*}} = 733 \text{ m/s}$$

where: k = 1.237 - ethylene specific heat ratio.

2.3. Ethylene release from the reactor

The mass flow rate is given by:

$$\frac{dm}{dt} = \rho^* A^* c$$

where: ρ^* and A^* are critical density and cross section area, c is the sound speed.

From detailed inspection and measurements of cracked gasket it was concluded that the minimum cross section area of the crack was rectangular with the sides equal to 4 mm and 60 mm, thus the minimum critical cross section can be assumed as:

$$A^* = 4 \cdot 60 = 240\ mm^2 = 2.4 \cdot 10^{-4}\ m^2$$

The density and velocity of outflowing ethylene change with the decrease of pressure in the reactor. Assuming that pressure and density of ethylene in the reactor vary linearly in time during release, the relations for critical pressure, critical density and critical outflow velocity take the form:

$$p^* = 0.56 \cdot (-35.75 \cdot t + 243) \cdot 10^6 \quad [\text{Pa}]$$

$$\rho^* = 0.623 \cdot (-18.625 \cdot t + 500) \quad [\text{kg/m}^3]$$

$$c = 0.7 \cdot \sqrt{\frac{1.237 \cdot 0.56 \cdot (-35.75 \cdot t + 243) \cdot 10^6}{0.623 \cdot (-18.625 \cdot t + 500)}} \quad [\text{m/s}]$$

The coefficient 0.7 in the formula for critical velocity is used due to flow viscous losses in the crack (in reality the flow rate is always smaller than it follows from the sound speed).

Table 1 shows the values of p^*, ρ^* and c for release times from 0 to 4 s.

Table 1. *Values of p^*, ρ^* and c for release times from 0 to 4 s*

t [s]	p* [MPa]	ρ* [kg/m^3]	c [m/s]
0	136.1	311.5	588.1
1	116.3	299.9	554.2
2	96.6	288.3	515.1
3	76.9	276.7	468.9
4	57.1	265.1	413.1

Substituting above relations to the equation for flow rate one will get:

$$\dot{m}(t) = \frac{101959216213}{48346123} \frac{\sqrt{-141t + 972}}{\sqrt{-298t + 8000}} 0.7 \cdot 0.00024 \cdot 623(-18.625t + 500)$$

which is graphically presented in Fig.1.

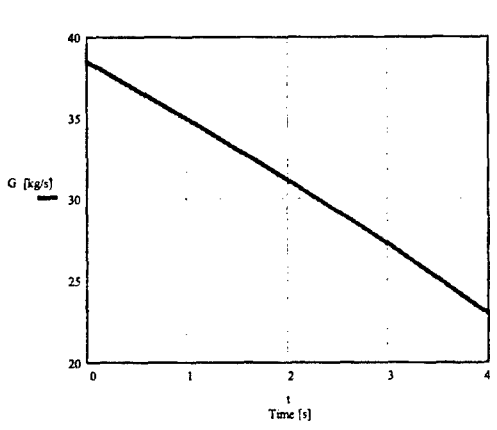


Fig 1. Mass flow rate of ethylene release

The plot shows that mass flow rate changes approximately linearly in time, which can be written in the form:

$$\frac{dm}{dt} = -4 \cdot t + 39 \qquad [\text{kg/s}]$$

The integration of this equation in time limits from 0 to 4 s gives mass of ethylene equal to 124 kg. The mass of 100 kg releases during the time of 3.1 s.

3. CONCLUSIONS

1. Approximately 100 kg of ethylene was released during pressure decrease in the reactor from 243 MPa to 110 MPa.
2. Time of release of 100 kg of ethylene calculated from the simple model given above equal to about 3.1 s, is close to the time of pressure drop in the reactor from 243 MPa do 110 MPa recorded by measuring equipment (about 4 s).
3. Analysis of ethylene explosion

3.1. Ethylene combustion and detonation parameters

Ethylene (C_2H_4) has the boiling temperature of 169.3 K. It is colourless in gaseous state. The flammability limits of ethylene in the mixture with air are equal in volumetric %: lower – 2.7 %; upper – 36 %. Minimum temperature of self-ignition in air is equal to 763 K. The laminar burning velocity is 74.5 cm/s. Minimum ignition energy in air is equal to 0.07 mJ. In comparison the minimum ignition energy for ethane is equal to 0.26 mJ, and for acetylene – 0.017 mJ. The stoichiometric volume of ethylene in air is equal to 6.54 %. Heat of combustion of ethylene is equal to 49.586 MJ/kg.

Detonation limits for ethylene in air are by volume: 3.3 % and 14.7 %. Detonation velocity for stoichiometric mixture of ethylene with air equals to 1825 m/s, pressure rise in detonation wave is 1.836 MPa, and temperature is 2926 K (for the initial parameters of combustible mixture: 0.1 MPa and 293 K).

3.2. Formation of explosive gas cloud

Ethylene, which was released from the reactor has formed the gas cloud partially mixed with air. Detailed estimation of the size of the cloud and the level of its mixing with air is impossible due to the fact of physical and geometrical complexity of the problem. Ethylene has released with large velocity from the crack in the reactor. Ethylene is slightly lighter than air so it moves upward mixing with air. Large quantity of pipes inside the reactor bunker intensified the mixing process.

Figure 2 presents the results of two-dimensional computer simulation of dynamics of ethylene release from the crack in the reactor and mixing with air in the horizontal cross section of the bunker. The simulation, which shows the growth of combustible ethylene-air cloud in the bunker, was made with the use of KIVA-3V code on SGI-Octane workstation. The time period of simulation was limited to initial stage of ethylene release (50 ms) due to limitation in computer time. The full simulation could be made only on powerful supercomputer. Nevertheless the results of simulation confirm very fast mixing of ethylene with air and the hypothesis that only small part of bunker volume is occupied by the mixture inside the flammability limits. The real mixing process was probably much faster due to the presence of pipes and other obstacles in the reactor bunker.

3.3. Strength of explosion

The ignition of ethylene-air mixture could occur from many sources: static electricity, electric spark or shock wave formed at the exit from cracked gasket. The mechanism of ignition from the shock wave was studied and explained by Wolański and Wójcicki [1]. After ignition there was probably rapid acceleration of the flame caused by internal obstructions which resulted in the formation of shock wave. The transition to detonation was also possible.

It is very well known that in the explosions of gas clouds only small fraction of the released fuel exists within flammability limits and takes part in the explosion. Usually this is from 2 to 10% of the total amount of the released fuel.

For example, during the Flixborough accident in 1974 about 60 tons of cyclohexan was released to the atmosphere. The large gas cloud has formed which after explosion destroyed the whole plant and killed 29 people. The blast wave was later estimated as equivalent to 15 tons of TNT which is equal to about 5% of heat of combustion of the whole released fuel.

On 3rd of June 1989 the rupture of LPG pipeline occured near Ufa in Siberia. The pipeline of 720 mm in diameter contained LPG under the pressure of 3.5 MPa. The released fuel vaporized, formed gas cloud and exploded after mixing with air. There were two trains with 1284 people on board in the region of explosion. Most of the passengers died. The explosion has destroyed about 350 m of railway track, 3 km of track and telephone line and destroyed trees in the forest on the area of 2.5 km^2. The glass in windows was broken within the radius of 15 km from the center of explosion. The strength of explosion was estimated by the damage to be about 200-300 tons of TNT, while the amount of LPG released to the atmosphere was about 1200 tons.

The explosion of ethylene and isobutane occurred also in 1989 Philips Petroleum plant near Houston in USA killing 24 people.

The following damage indications were taken into account in the estimation of explosion strength at accident in poliethylene plant:

- The metal sheets were broken from the walls of coolers distant about 200 m from the explosion;
- Broken windows, light walls and doors in the building distant about 150 m;
- Broken glass windows within the range of 2 km;
- Broken and bended steel door in the bunker;
- Fractured and pushed out reinforced concrete bunker walls.

By assuming that 100 kg of ethylene was released from the reactor, the equivalent energetically mass of TNT equals to:

$$M_{TNT} = \frac{M_{eth} H_{eth}}{H_{TNT}} = \frac{100\,kg \cdot 49.586 \cdot 10^6\,J/kg}{4.618 \cdot 10^6\,J/kg} = 1074 \quad kg$$

where: H_{eth} – ethylene heat of combustion; H_{TNT} – TNT heat of combustion

The 10 % of total TNT mass equals to:

$$(M_{TNT})_{10\%} = 107 \quad kg$$

The 2 % of total TNT mass equals to:

$$(M_{TNT})_{2\%} = 21 \quad kg$$

Thus, it can be concluded from the amount of released ethylene that the explosion strength could be approximately within the range of 21 to 107 kg of TNT.

In practice the strength of explosion, expressed in the mass of TNT, is usually estimated on the basis of damages with the use of diagrams of ovepressure versus scaled distance, made on the basis of data taken from other explosions [2]. The use of such diagram gives the strength of explosion of the order of 100 kg TNT.

REFERENCES

1. Wolański P., Wójcicki S.: *Mechanizm powstawania wybuchu przy nadkrytycznym wypływie paliwa gazowego do atmosfery*, Archiwum procesów spalania, Vol.2 (1971), Nr 3, str. 141-155
2. Strehlow R.A., Baker W.A.: *The characterisation and evaluation of accidental explosions*, NASA, CR 134779, June 1975

Fig. 2. Numerical simulation of ethylene outflow from broken pipe in 8.5m per 10.7m
2D geometry.

There are solid walls on bottom and both sides, open pressure boundary on top.
Initial pressure - 1 bar; Initial temperature - 297 K; Outflow velocity - 472 m/s;(2500 bar in the pipe);

Opening diameter - 10 mm
blue - pure air; red - pure ethylene.
Time interval between frames – 10 ms

ANALYSIS OF THE MOTION OF METAL PLATES IN MODEL REACTIVE ARMOURS

Waldemar Andrzej Trzciński, Radosław Trębiński and Stanisław Cudziło

Military University of Technology, Kaliskiego 2, 00-908 Warsaw, POLAND

Abstract:

An analysis of the process of driving metal plates of model reactive armours by the gaseous products of the detonation was studied in experimental and theoretical ways. The detonation in confined layer of explosive was initiated by the fuse or by the jet at various incidence angles. The X-ray impulse photography was applied to record the motion of plates. The theoretical analysis was performed by the use of a simple model, in which the plate deformation and finite time of its acceleration were taken into account. The time-space characteristics of motion of model reactive armour elements obtained from experiments and numerical modelling can be applied for designing cumulative heads destined for destroying armours protected by reactive armour.

1. INTRODUCTION

Knowledge of the space-time characteristics of the process of interaction of a jet with a cassette of explosive reactive armour (ERA) is necessary for designing two-stage (tandem) shaped charges (Ref. [1]) destined for destroying armours protected by ERA. The ERA cassette consists of a layer of explosive, which is confined two-sided by metal plates [Refs. 2-3] The attack of the jet produced by the first charge of the tandem initiates detonation of the explosive [Ref. 4]. The interaction of the jet with the detonation products and the plates accelerated by the explosion weakens the ability of jet penetration into the main armour [Refs. 2,5]. However, after some period of time, the disturbing action of the reactive armour decays due to the expansion of the detonation products and the displacement of the plates out of the axis of the jet. To ensure the proper performance of the second charge, it must be located at the distance, at which the explosion of the ERA cassette does not influence the process of formation of the second jet. Thus, the selection of the time delay for initiation of the second stage of tandem warhead and the distance between both charges inside the warhead depends on the space-time characteristics of the process launched by the impact of jet, produced by the first stage, on ERA container.

In the present work, the behaviour of plates of model reactive armours after detonation of the explosive layer was investigated. The detonation was initiated by the fuse or by the jet at various incidence angles. The placements and shapes of plates at different time delays were recorded by the use of X-ray flash photography. The results of recording were compared with those obtained from numerical modelling and, in this way, the used theoretical model was verified.

2. EXPERIMENTAL

Schemes of the tested systems are shown in Fig. 2.1 and 2.2. Two metal rectangular plates P1 and P2 were separated by a layer of plastic explosive (E). In the first case, the plates were made of duraluminium (DAl) and the explosive was composed of 90 % RDX, 6.5 % dybutilsebacat and 3.5 % Viton A. The mean density of the explosive was ρ_0 = 1390 kg/m^3. An electrical fuse (F) was inserted into the explosive charge by the manner shown in Fig. 2.1. In the second system (Fig. 2.2), two steel plates were separated by the explosive, which was composed of 80 % RDX and 20 % binder. The mean density of the explosive was ρ_0 = 1610 kg/m^3. The shaped charge C was placed above the upper steel plate. The distance and angle α between the charge and the plate were established by a vinyle tube T. In each test, the distance between the charge centre and steel plate was 80 mm. Shaped charges of 37 mm diameter were used with sintered copper liners of about 35 g mass, 1.37 mm thickness and cone shape with 42° angle. The shaped charges were positioned in such a way, that their axes passed through the centre of the explosive layer.

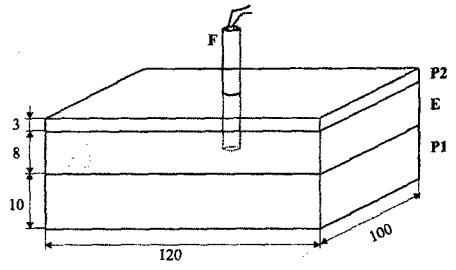


Fig. 2.1 Diagram of the first system tested

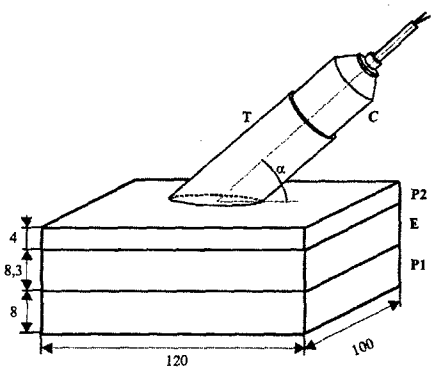


Fig. 2.2 Diagram of the second system tested

The driving process was monitored by the use of a SCANDIFLASH X-ray set. The system tested was placed between the X-ray source and a film cassette. The longer side of plates was perpendicular to the line connecting the X-ray apparatus and the cassette. The radiograph was taken twice before and after detonation of the explosive. The radiographs taken before the detonation were used in a scaling procedure. For the first system, the X-ray pulse was triggered after a chosen delay τ from the moment when an explosion wave had reached the end of the fuse, what approximately means, when the detonation had been initiated at the centre of explosive layer. Chosen radiographs are shown in Figs. 2.3÷2.5. For the second system, the X-ray source was released after a chosen delay τ from the moment when detonation had been initiated in the shaped charge. Selected results of recording are shown in Figs. 2.6÷2.9.

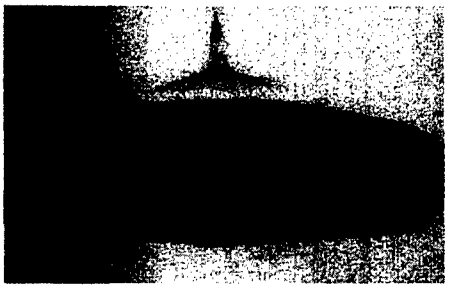


Fig. 2.3 X-ray picture of DAl plates for $\tau = 10$ μs



Fig. 2.4 X-ray picture of DAl plates for $\tau = 30$ μs

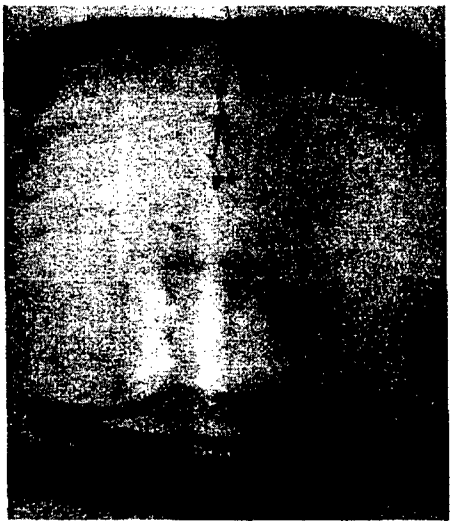


Fig. 2.5 X-ray picture of DAl plates for $\tau = 50$ μs

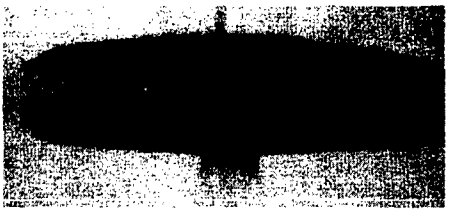


Fig. 2.6 X-ray picture of steel plates for $\tau = 35$ μs (α=90°)



Fig. 2.7 X-ray picture of steel plates for $\tau = 55$ μs (α=90°)

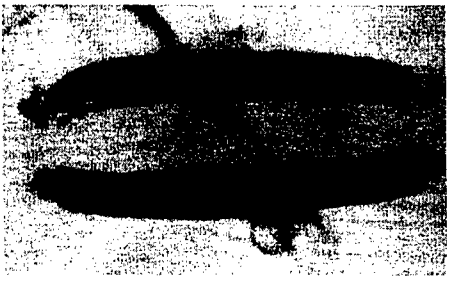


Fig. 2.8 X-ray picture of steel plates for $\tau = 46$ μs (α=60°)

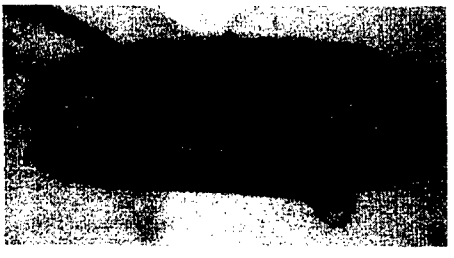


Fig. 2.9 X-ray picture of steel plates for $\tau = 50$ μs (α=30°)

From Figs. 2.3÷2.9 it follows, that the driven plates are generally continuous for tested period of time. However, the splinters are visible at the side boundaries of plates. They are produced when a shock wave reaches the plate edge and strong rarefaction waves are generated in the material of plate. On the other hand, the rarefaction waves propagating in the detonation products from the free surface of the charge result in curving the plates at their ends. The small splinters are also observed in the places of interaction of the jet with steel plates.

3. THEORETICAL ANALYSIS

For numerical analysis of the process of launching metal plates by the products of detonation grazing along their surfaces, the theoretical model described fully in Ref. [6] was applied. It is assumed in this model that a cylindrical detonation wave is initiated in a layer of explosive of thickness δ_0 at the line being perpendicular to this layer ($r = 0$). The wave travels at a velocity D in the radial direction (Fig. 3.1). At the moment, when the detonation wave reaches the lateral surface of the charge, rarefaction waves are generated and they propagate inside the expanding detonation products. The motion of these waves into the centre of the system is relatively slow, since they propagate in the medium moving in the opposite direction and the medium velocity is close to a local velocity of sound. This fact enables us to assume that the influence of lateral rarefaction waves on the motion of the central part of plates is small. Thus, we assume that at the moment, when these waves reach successive elements of plates, the process of acceleration is practically finished and the velocity of each element is close to the maximal one. This assumption enables us to adopt some approximations in the theoretical model. The negligence of influence of lateral rarefaction waves means that the motion of the plates can be treated as the motion of circular plates of a radius R. We assume that the maximal velocities of particular elements of a rectangular plate are close to those of a circular plate located at the same distance r from the system centre. Using estimated values of these velocities, the second phase of driving plates can be modelled by an inert motion of particular elements with constant velocities. Verification of this method of estimation of space-time characteristics of motion of plates in the system considered was done in Ref [6].

To describe the expansion of the detonation products, the equations of unsteady axially symmetric gas dynamic flow were used. The physical properties of the detonation products were described by the polytropic gas model. The motion of the material of plates was modelled by the use of the hydrodynamic approximation. Material compressibility was described by the Gruneisen equation of state obtained from an expansion of the internal energy about an empirical shock adiabate $D_s = a + b\,u_s$, in which D_s and u_s denote the speed of a shock wave in a medium and the mass velocity, respectively. The solution of the problem of acceleration of plates by the detonation products was constructed by means of the Godunov's scheme [Ref. 7] for unsteady two-dimensional gas-dynamic flow.

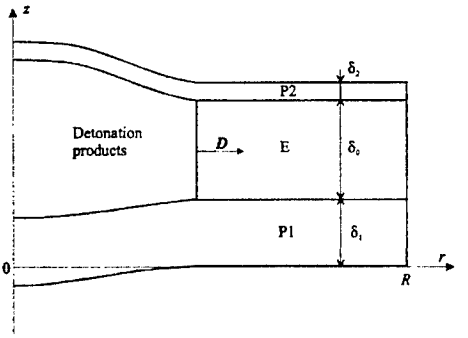


Fig. 3.1. Diagram of the system investigated

The process of driving metal plates by the products of detonation grazing along their surfaces was modelled for the data corresponding to the explosive armour systems tested in Sect. 2. The parameters characterizing the plates and the explosive charges were assumed as follows. For the first system, the dimensions of the duralumin plates were $\delta_1 = 10$ mm, $\delta_2 = 3$ mm, $R = 60$ mm, the density $\rho_{0P1} = \rho_{0P2} = 2700$ kg/m^3, the coefficients in the equation of state $a = 5328$ m/s, $b = 1.338$, the Gruneisen coefficient $\gamma_0 = 2.0$ – Ref. [8]. The detonation characteristics of the plastic explosives were estimated by the use of the CHEETAH code – Ref. [9]. For the first explosive of the density $\rho_{0E} = 1390$ kg/m^3, the following parameters were obtained: $D = 7240$ m/s, $k = 2.7$. The thickness of the explosive layer was $\delta_0 = 8$ mm. For the second system, the dimensions of the steel plates were $\delta_1 = 8$ mm, $\delta_2 = 4$ mm, $R = 60$ mm, the density $\rho_{0P1} = \rho_{0P2} = 7800$ kg/m^3, the constants $a = 3800$ m/s, $b = 1.58$, $\gamma_0 = 1.69$ – Ref. [8]. Calculated detonation parameters of the used plastic explosive of the density $\rho_{0E} = 1610$ kg/m^3 were: $D = 7530$ m/s, $k = 3.0$. The thickness of the explosive layer was $\delta_0 = 8.3$ mm.

The computer simulation of the process of driving plates was conducted up to the time $t = 10$ μs after initiation of the detonation at $r = 0$. At that moment, the shapes of plates were determined and the distributions of a mean mass velocity of the plates in the axial (z) and the radial (r) directions were calculated. The velocity was averaged across the thickness of the plates. Values of mean velocity were assumed constant in time and they were used for estimation of the displacement of plates in further stages of the motion. Estimated in this way placements of the external surfaces of duraluminium plates are compared with the profiles obtained from X-ray radiographs for $\tau = t = 10$, 20, 30, 40, and 50 μs (Fig. 3.2). There is a good quantitative agreement between the experimental and theoretical data.

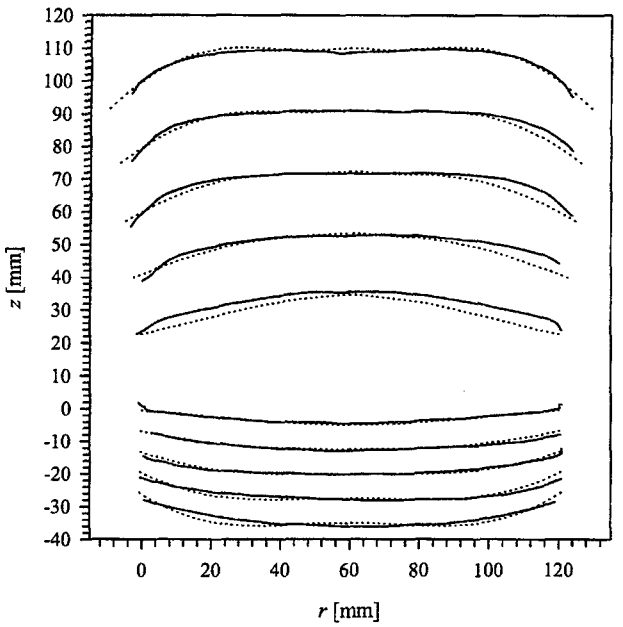


Fig. 3.2. Comparison of experimental (dotted lines) and theoretical (solid lines) profiles of duraluminium plates for time $\tau = t = 10, 20, 30, 40$ and 50 μs

Estimated in similar way placements of the external surfaces of steel plates are shown in Fig. 3.3÷3.5 by dotted lines for the time $t = 5, 10, ..., 35$ μs.

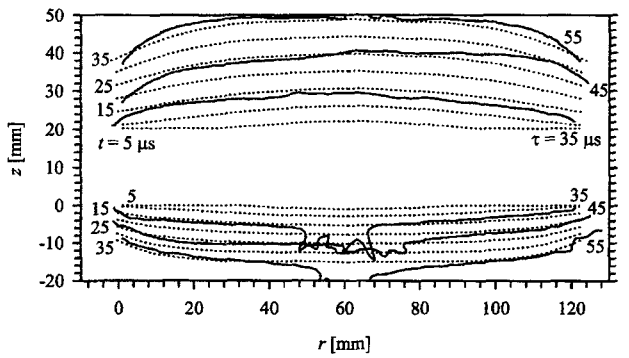


Fig.3.3. Experimental (solid lines) and theoretical (dotted lines) shapes of external surfaces of steel plates for $\alpha = 90^{\circ}$

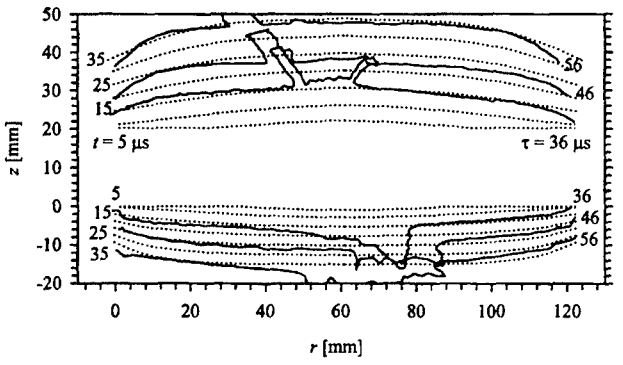


Fig.3.4. Experimental (solid lines) and theoretical (dotted lines) shapes of external surfaces of steel plates for $\alpha = 60°$

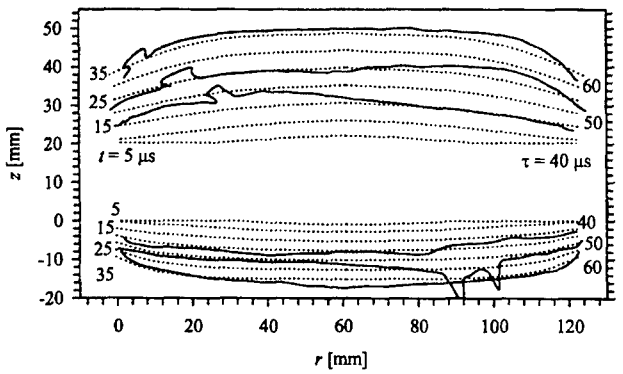


Fig.3.5 Experimental (solid lines) and theoretical (dotted lines) shapes of external surfaces of steel plates for $\alpha = 30°$

The experimental profiles are also presented in Figs. 3.3÷3.5 (solid lines). The symbol τ denotes the time, which went on after the initiation of shaped charge explosion. To compare the experimental and calculated profiles, the time-period (τ_p) passing from the initiation of shaped charge to the attack of the jet on the central part of the explosive layer was estimated. The time of propagation of the jet and its penetration of the upper steel plate and explosive layer was taken into considerations. Estimated values of τ_p were 20.8, 21.1 and 22.7 μs for the angle $\alpha = 90$, 60 and 30°, respectively. Thus, the experimental profile recorded for given value of τ should be compared with that obtained from numerical modelling for $t = \tau - \tau_p$.

The analysis of the profiles presented in Figs. 3.3÷3.5 indicates that there is a good agreement between the experimental and theoretical positions of plates. To appraise this agreement, the fact must be taken into account that, in the case of the oblique attack of a jet, the symmetry of the detonation wave initiated in the explosive layer significantly differs from the cylindrical one assumed in the model. That is why there are notable differences between the experimental and calculated profiles for small values of time. However, this discrepancy becomes smaller for further stages of the motion of plates and the satisfying

agreement between predicted and experimental data is obtained. The discrepancies between the estimated time of displacement of a plate to a given position in space and the similar time obtained from the experimental results do not exceed 5 μs. On the other hand, delay times for initiation of the second charge of tandems are of order of 100÷1000 μs. Thus, the error of 5 μs in estimation of time is insignificant from the point of view of the selection of delay times in tandems.

4. SUMMARY

The proposed method of modelling the process of acceleration of metal plates by the detonation products can be applied to predict, with satisfactory precision, the time-space placement of elements of reactive explosive armours after jet attack. It can be used for designing of tandem charges to estimate a time delay for the second stage and a distance between two charges.

Acknowledgements

This paper was accomplished within the framework of the Project 0 T00A 035 19 financed by the State Committee for Scientific Research.

REFERENCES

[1] Persson, A theoretical analysis of the mechanics of tandem shaped charges and their interaction with different targets, Proc. of the 7th Intern. Symp. on Ballistics, Hague, Netherlands, 1983, 251-256.

[2] M. Held, M. Mayseless, E. Rototaev, Explosive reactive armour, Proc. of the 17th Intern. Symp. on Ballistics, Midrand, South Africa, 1998, Vol.1, 33-46.

[3] Wiśniewski, Armours. Construction, designing, testing (in Polish), WNT, Warsaw 2001.

[4] J. Brown, D. Finch, The shaped charge jet attack of confined and unconfined sheet explosive at normal incidence, Proc. of the 11th Intern. Symp. on Ballistics, Brussels, Belgium, 1989, Vol.II, 211-232.

[5] M. Held, The importance of jet tip velocity for the performance of shaped charges against explosive reactive armor, Propellants, Explosives, Pyrotechnics, 19, 15-18 (1994).

[6] S. Cudziło, R. Trębiński, W. A. Trzciński, Analysis of the process of acceleration of plates of a model reactive armour, Journal of Technical Physics (to be published).

[7] S. K. Godunov, Numerical solution of multi-dimensional problems of gas dynamics (in Russian), Nauka, Moscow 1976.

[8] M. A. Mayers, L. E. Murr, Shock waves and high-strain-rate phenomena in metals, Plenum Press, New York, 1981.

[9] L. E. Fried, CHEETAH 1.39 – User's manual, Report UCRL-MA-117541 (1996), Lawrence Livermore National Laboratory, Los Alamos, USA.

FTIR SPECTROSCOPIC STUDY OF THE PROTONATION OF CONDUCTING POLYMER WITH ENERGETIC COMPOUND

Miroslava Trchová*, Irina Sapurina and Jaroslav Stejskal*****

* Charles University Prague, Faculty of Mathematics and Physics, 180 00 Prague 8, CZ
** Institute of Macromolecular Compounds RAS, St. Petersburg 199004, RUS
*** Institute of Macromolecular Chemistry AS CR, 162 06 Prague 6, CZ

Abstract:

The preparation of materials combining the features of conducting polymers and energetic compounds is demonstrated. The FTIR spectra are used to discuss changes in the molecular structure of product of protonation reaction between two non-conducting compounds, polyaniline (PANI) base and 3-nitro-1,2,4-triazol-5-one (NTO). Three ways of preparation have been tested: the interaction of PANI base with NTO dissolved in water, the polymerization of aniline in the aqueous medium containing NTO, and solid-state blending of both components. The progress of protonation of PANI with NTO was assessed by the changes in conductivity.

Keywords: *FTIR spectroscopy, energetic compounds, conducting polymer, 3-nitro-1,2,4-triazol-5-one, NTO, polyaniline, protonation*

1. INTRODUCTION

Protonation of polyaniline (PANI) base with acids is of fundamental importance in exploiting the electrical properties of this polymer.[1] In such a process, a conductivity of PANI base, 10^{-10}–10^{-9} S cm^{-1}, increases by several orders of magnitude to the level of 10^{-1}–10^{0} S cm^{-1}. Besides the preparation of polymer materials of defined conductivity, the response in the conductivity and color to the change in protonation has been proposed for the sensing of ammonia[2,3] and in the detection of free halogens.[4]

Various types of acids have been used in the protonation of PANI. These are introduced directly during the polymerization of aniline or they react with *a priori* prepared PANI base. Inorganic acids are the most common ones, hydrochloric and sulfuric acids being typical examples. Organic acids have often been used to improve the processibility of PANI. Sulfonic acids, especially camphorsulfonic[5-7] and dodecylbenzenesulfonic acids,[8,9] have been most frequently used, while carboxylic acids, e.g. formic,[10] maleic,[11] or tartaric[12] acids, have been used in a limited number of studies. Lewis acids have also been demonstrated to yield conducting PANI after interaction with PANI base.[13,14]

Besides typical acids mentioned above, there are other organic compounds that can provide a proton and thus participate in the protonation of PANI. Picric acid[15] (2,4,6-trinitrophenol) and *m*-cresol[16] that both contain a sufficiently acidic hydrogen in hydroxyl group may serve as examples. Picric acid has been demonstrated react with PANI base even in the solid state to yield a conducting PANI picrate.[15,17] The films cast from PANI picrate solution in *m*-cresol were reported[18] to have a conductivity of 150 S cm^{-1}. Similarly, the films of PANI camphorsulfonate cast from the same solvent had a conductivity[19] exceeding 100 S cm^{-1}. The solid-state protonation of poly(*o*-toluidine) with picric acid was used to prepare conducting composites with ABS rubber.[20]

Vibration spectroscopy is extremely sensitive to the electronic-structure changes in polyaniline. By using the IR spectroscopy it is possible – besides the characterisation of polyaniline – to study the changes of bonds and the mechanism of doping during the protonation and oxidation processes.[21] In this paper, the protonation with an insensitive explosive,[22-26] 2-nitro-1,2,4-triazol-5-one (NTO), has been studied by FTIR spectroscopy. It is demonstrated that NTO is able to protonate PANI in a controlled manner and can be thus used for the preparation of PANI of varying conductivity. This is a new type of material that combines the electric properties of conducting polymer with energetic character of an organic compound. In the systems comprising such material, the ignition could possibly be achieved by the Joule heat evolved by passing electric current.

2. EXPERIMENTAL

PANI base

Aniline hydrochloride (0.20 mol, 25.9 g; Fluka, purum) was dissolved in water to 500 ml of solution, similarly like ammonium peroxydisulfate (0.25 mol, 57.1 g; APS; Fluka, purum). Both solutions were mixed at room temperature and left to polymerize. Next day, the precipitated PANI hydrochloride was collected on a filter and washed copiously with 1 M ammonium hydroxide. The resulting PANI base was dried at 60°C *in vacuo.*

Protonation of PANI base

Protonation of PANI base with NTO. NTO was provided by the University of Pardubice. PANI base (20 mmol, 362 mg) was suspended in 100 ml of an aqueous solution containing various concentration of NTO (up to 3 mmol, 390 mg). The concentration of NTO and its decrease in the supernatant liquid after the reaction with PANI base were assessed by the reduction of optical absorption at wavelength of 320 nm with a UV-Vis spectrophotometer Lambda 20 (Perkin Elmer, UK). The degree of protonation was calculated from the amount of consumed NTO. The partly protonated PANI was collected on a filter and dried in vacuo at 60 °C.

Preparation of PANI in the presence of NTO. Aniline (20 mmol) was oxidized in the presence of NTO (20 mmol) with APS (25 mmol) in 100 mL of aqueous medium. The collected precipitate was washed with a saturated aqueous solution of NTO, with acetone, and dried as above.

Solid-state protonation. In another approach, the protonation of PANI in the solid state was used.[15] PANI base was mechanically blended with an equimolar amount of NTO for 15 min in a mortar.

Infrared spectra

Fourier-transform infrared (FTIR) spectroscopic measurements were performed with a Nicolet IMPACT 400 FTIR spectrometer in a water-purged environment. All spectra in the range 400 – 4000 cm^{-1} with 2 cm^{-1} spectral resolution were obtained from compressed KBr pellets in which the PANI.NTO powders were evenly dispersed. Two hundred scans were recorded for each FTIR spectrum. The spectra were corrected for the presence of the moisture and carbon dioxide in the optical path.

3. RESULTS AND DISCUSSION

Handling of dangerous materials

NTO (Scheme 1) is an energetic compound. Even though NTO is an insensitive explosive, the appropriate safety regulations should be obeyed. The careful laboratory handling of gram quantities has never caused any problems. The metallic salt of NTO, however, may be highly explosive.



Scheme 1. Keto–enol forms of 3-nitro-1,2,4-triazol-5-one (NTO).

Spectral features of individual compounds

PANI base. Absorption spectrum of PANI base (Figure 1) is in a good agreement with previously reported results.[27-29] The main peaks at 1590 cm^{-1} and 1500 cm^{-1} correspond to stretching deformations of quinone and benzene rings, respectively (Scheme 2). The band at 1374 cm^{-1} is attributed to C–N stretching in the neighborhood of a quinoid ring. The 1308 cm^{-1} band is assigned to C–N stretch in a secondary aromatic amine whereas, in the 1010–1170 cm^{-1} region, the aromatic C–H in-plain bending modes are observed. In the region of 800–880 cm^{-1}, the out-of-plane deformations of C–H in 1,4-disubstituted benzene ring are located.

Protonated PANI. The spectrum of PANI sulfate (Figure 1) exhibits a broad absorption band at wavenumbers higher than 2000 cm^{-1} (only a part of this band is shown). It is characteristic of the conducting form of PANI[30] the metallic polaron energy band being responsible for the broad absorption.[31] The main peaks (observed at 1590 cm^{-1} and 1500 cm^{-1} in the spectrum of PANI base) are red-shifted to 1570 cm^{-1} and 1480 cm^{-1}. The band at 1374 cm^{-1} (C–N stretching in the neighborhood of a quinonoid ring, usually observed at the spectrum of PANI base) is absent in the spectrum of PANI sulfate. The absorption band at 1308 cm^{-1} (C–N stretching of secondary aromatic amine) is strengthened during the protonation. Because of various configurations of polymer chains, the C–N bonds have different chemical environment[32] and, consequently, different frequencies of the C–N stretching vibration band. The band characteristic of the conducting protonated form is observed at about 1240 cm^{-1}. It has been interpreted as $C–N^{+\bullet}$ stretching vibration in the polaron structure.[29] The 1140 cm^{-1} band can be assigned to a vibration mode of $–NH^{+}=$ structure, which is formed by protonation (Scheme 2). This indicates the presence of positive charges on the chain and the distribution of the dihedral angle between the quinone and benzenoid rings. The band increases with the degree of protonation of the PANI backbone.[33] The band at about 1610 cm^{-1} is attributed to the stretching of imine N=ring bond. The region 900–700 cm^{-1} corresponds to aromatic out-of-plane C–H deformation vibrations. Their

frequencies are mainly determined by the number of adjacent hydrogen atoms in the ring but are not very much affected by the nature of substituents[34].

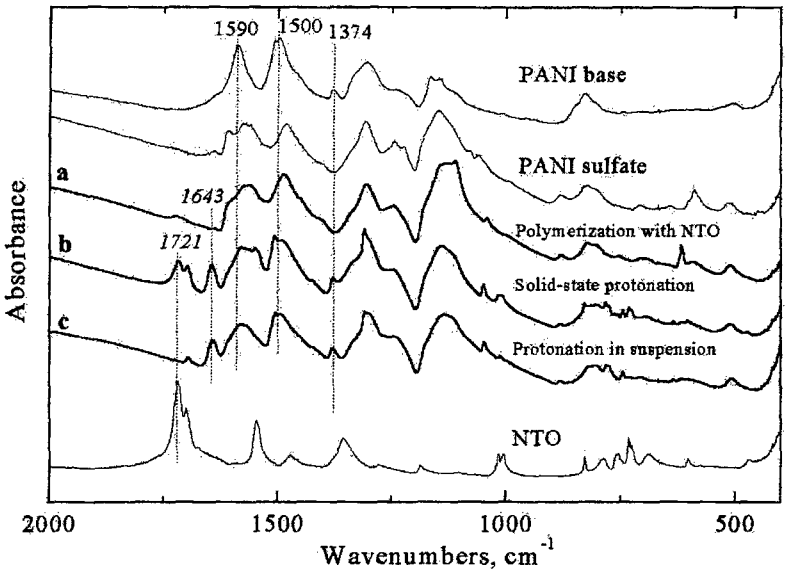


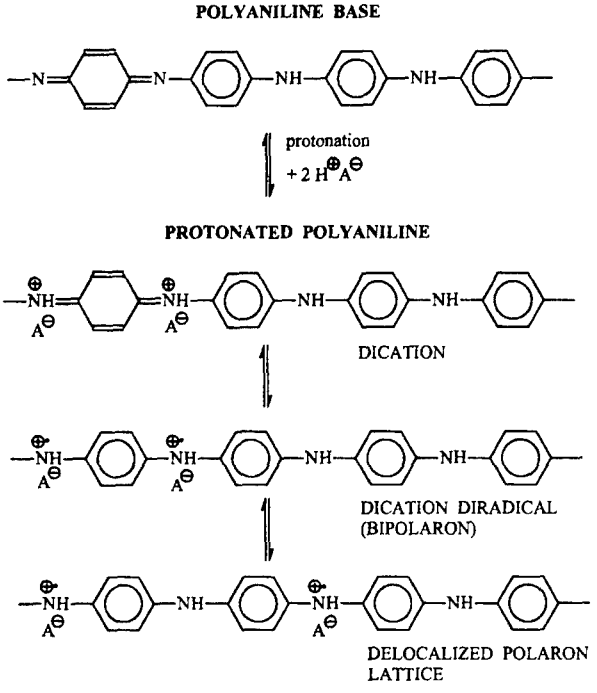
Fig 1. FTIR spectra of PANI base, PANI sulfate, PANI prepared in the presence of NTO (a), the product of solid-state protonation with NTO (b), and PANI protonated with NTO in suspension, $(n_{NTO}/n_{PANI})_0 = 1.5$, (c). The spectrum of NTO is included for comparison.

NTO. The spectrum of polycrystalline NTO dispersed in KBr pellets (Figure 1) is close to the spectrum of thin NTO film presented by Sorescu *et al.*[22] The peaks at 3478 cm^{-1}, 3248 and 3210 cm^{-1} correspond to the N–H stretching vibrations (cf. Scheme 1). The peak at 1721 cm^{-1} in the spectrum of NTO has been interpreted as carbonyl C=O stretching vibration,[22] with a secondary peak at 1698 cm^{-1} corresponding probably to the N–O asymmetric stretching mode. The absorptions at 1548 and 1476 cm^{-1} belong to the N–H bending vibrations. The broad band at about 1356 cm^{-1} is related to the C–NO_2 stretching vibrations. The bands at about 1010 cm^{-1} can be assigned to the in-plane vibrations of the ring and the region from 900 to 600 cm^{-1} corresponds to the out-of-plane torsion ring vibrations.

Protonation of PANI base in aqueous suspension

The keto–enol tautomeric forms of NTO (Scheme 1) reveal the presence of hydrogen in the hydroxyl group of enol form. This group is sufficiently acidic to react with the bases. The salts of NTO comprising an inorganic cation are well known and exploited as explosives.[35] It was thus expected that NTO will form a "salt" also with a PANI base. The reaction of non-conducting blue PANI base with an acid generally leads to a conducting green

protonated PANI (Scheme 2). The rearrangement of electrons in PANI produces cation radicals that act as charge carriers and are responsible for the electrical conduction. The extent of conductivity is dependent on the balance of the individual PANI forms (Scheme 2).



Scheme 2. Non-conducting PANI base reacts with an acid (HA) to a conducting protonated PANI. The resulting "salt" may have a dication structure that is partly transformed by redistribution of electrons to dication diradicals and delocalized cation radicals. Unpaired electrons are responsible for the conduction in protonated PANI.

PANI base was suspended in the aqueous solutions of NTO. The use of various ratios of NTO moles per 1 mole of PANI base (calculated per 2 aniline units), $(n_{NTO}/n_{PANI})_0 = 0 - 1.5$, allowed for the control of the degree of protonation in the polymer, expressed similarly as n_{NTO}/n_{PANI}. The formula of the hypothetical PANI, fully protonated with NTO, $n_{NTO}/n_{PANI} = 1$, is depicted in Scheme 3. The consumption of NTO by PANI base from the supernatant liquid proved that the protonation indeed takes place. The degree of protonation increases with increasing content of NTO used for the protonation (Figure 2). The maximum degree of protonation which was achieved in this way was $n_{NTO}/n_{PANI} \sim 0.3$.

FTIR spectra. When the PANI base reacts with NTO, the appearance of a broad band at wavenumbers higher than 2000 cm^{-1}, characteristic of the conducting form of PANI,[30] is the most significant feature (Figure 3). The horizontal dashed lines in Figure 3 are placed at a level of absorption at 1590 cm^{-1}. The intersection of these lines with an absorption tail at wavenumbers >2000 cm^{-1} clearly moves to the lower wavenumbers as the protonation degree increases.

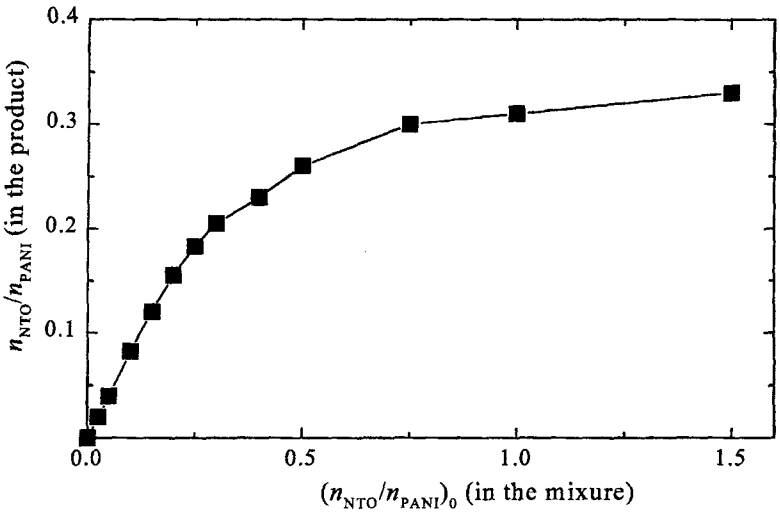


Fig 2. Degree of PANI protonation, n_{NTO}/n_{PANI}, in dependence on the molar ratio of NTO and PANI base in the protonating medium, $(n_{NTO}/n_{PANI})_0$.

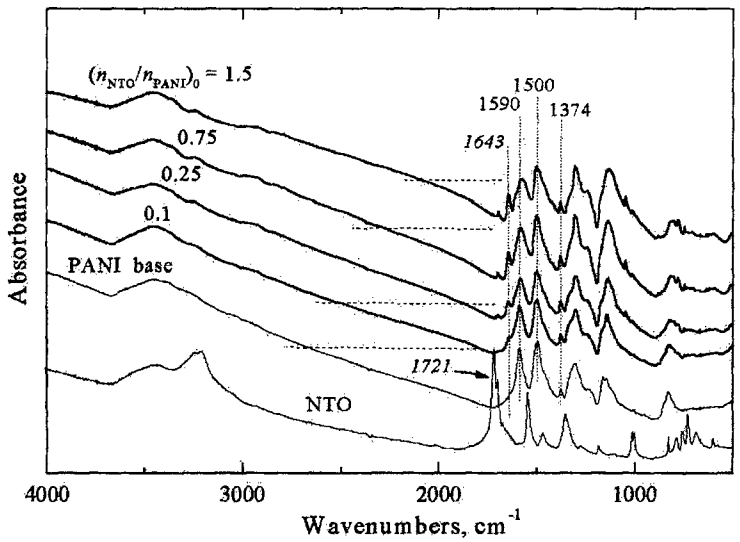
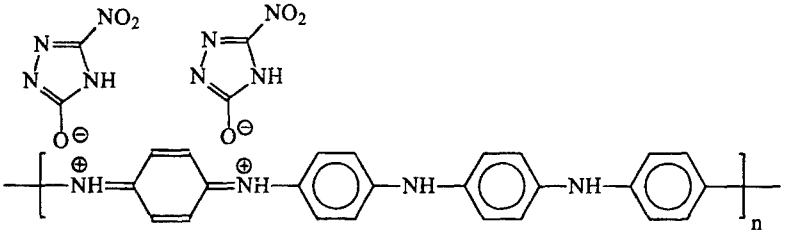


Fig 3. The FTIR spectra of PANI base protonated with various proportions of NTO, $(n_{NTO}/n_{PANI})_0$ (shown at the individual spectra). The spectrum of pristine NTO is shown for comparison.

The band at about 1590 cm^{-1} in the spectrum of PANI base is red-shifted to 1581 cm^{-1} as NTO content increases and a shoulder at about 1608 cm^{-1} corresponding to protonated form of PANI[30] appears. The absorption band at 1308 cm^{-1} is strengthened during the protonation[32] and the band characteristic of the conducting protonated form at about 1240 cm^{-1} increased. A band at about 1116 cm^{-1} appears, indicating the presence of positive charges on the chain[33] (Scheme 3). All these features give evidence of the progressing protonation of PANI. On the other hand, the peak at 1374 cm^{-1}, typical of PANI base, is observed in all spectra (Figure 3). This indicates that the protonation, although well documented, has not been complete.

Even more straightforward evidence is obtained from NTO spectra. The band at 1721 cm^{-1} corresponding to the carbonyl C=O stretching vibration disappeared after an interaction of NTO with PANI base (Figure 3) and a new band at 1643 cm^{-1} corresponding to the OH deformation vibration has been found instead. This is consistent with the fact that NTO interacts with PANI in enol form (Scheme 3). The additional peaks of pristine NTO at 3248 and 3210 cm^{-1}, at 1019 and 1008 cm^{-1} and the peaks in the region of 830–600 cm^{-1} (Figure 3) are shifted, which also indicates a more intimate interaction between the PANI and NTO.



Scheme 3. PANI protonated with NTO.

Conductivity. The protonation is well documented by the conductivity measurements. The conductivity of PANI base, 3.5×10^{-9} S cm^{-1}, increased after *ca* 30 % protonation to 3.4×10^{-3} S cm^{-1}, i.e. by 6 orders of magnitude (Figure 4). This is a level of conductivity which may be of practical interest.

Polymerization of aniline in the presence of NTO

PANI is produced by the oxidation of aniline in aqueous acidic medium. In combining the conducting polymer with energetic compounds, it is logical to propose the introduction of NTO directly in the reaction mixture. If instead of, e.g., aniline hydrochloride we oxidize the equimolar mixture of aniline and NTO with ammonium peroxydisulfate, the conductivity of PANI produced in this way is 0.21 S cm^{-1}, only a slightly lower than of PANI hydrochloride, 4.4 S cm^{-1}. This optimistic result, however, should be subjected to a critical assessment. During the oxidation of aniline, ammonium peroxydisulfate is decomposed to ammonium sulfate and at the same time protons are released. The produced sulfuric acid thus may compete with NTO in the protonation of PANI. The same conclusion is reached on the basis of FTIR spectra (Figure 1, spectrum a), where the peak at 1643 cm^{-1} corresponding to NTO is completely missing. The shifts of 1500 and 1590 cm^{-1} peak to lower wavenumbers, however, clearly prove that we are dealing with the protonated form of PANI. The incorporation of NTO into PANI during the preparation of the polymer is thus ineffective and the observed protonation is afforded by sulfuric acid rather than with NTO.

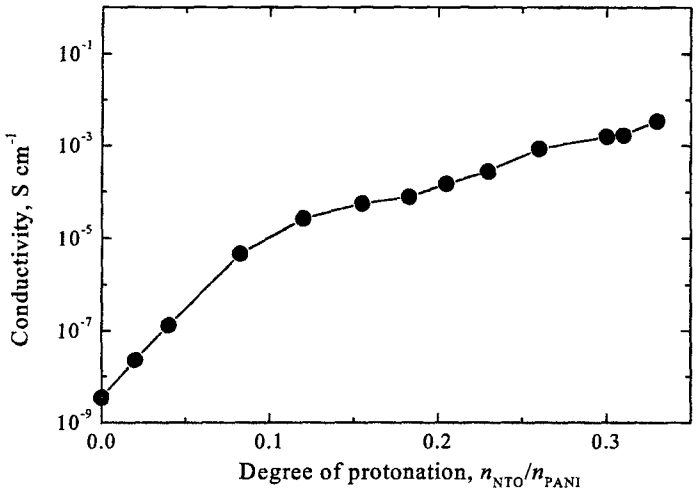


Fig. 4. Conductivity dependence on the degree of protonation, n_{NTO}/n_{PANI}.

Solid-state protonation

It has been earlier reported that PANI base can be protonated by a mechanical blending with an acid in the solid state.[15,18] If the PANI base (conductivity of 3.5×10^{-9} S cm^{-1}) is treated in a mortar with NTO (conductivity of 7.6×10^{-15} S cm^{-1}) in equimolar proportion (Scheme 3), the product with the conductivity of 1.93×10^{-3} S cm^{-1} is obtained. This demonstrates that the protonation depicted in Scheme 2 takes place. The solid-state blending thus offers an alternative to the treatment of PANI base with the solutions of NTO in producing the materials that might be of potential use in the modification of energetic compounds.

The FTIR spectra again support this conclusion and the spectrum of PANI (Figure 1, spectrum b) corresponds to the conducting form of PANI. As expected, the protonation reaction between PANI base and NTO is not complete. A presence of residual NTO (keto form, 1721 cm^{-1}) is confirmed by spectra along with the NTO incorporated into PANI (enol form, 1643 cm^{-1}). The peak 1374 cm^{-1}, typical of PANI base, also suggests the incomplete interaction between PANI base and NTO. Both reactions in the solid-state (Figure 1, spectrum b) and in the suspension (Figure 1, spectrum c) thus lead to a partial protonation of PANI with NTO. In a suspension process, the residual NTO remains in the liquid phase and the product after drying thus does not contain any free NTO (Figure 1, spectrum c, the absorption at 1721 cm^{-1} is missing).

4. CONCLUSIONS

The FTIR spectroscopy has been used to study the protonation of the non-conducting PANI base with NTO, which yields a new type of material combining the electrical properties of conducting polymers and energetic character of protonating compound. Three different ways of preparation have been tested. The FTIR spectra prove that NTO is incorporated into PANI in enol form in the reaction of PANI base suspended in aqueous solutions of NTO. The product achieves up to ~30 % degree of protonation and the conductivity increases during protonation by six orders of magnitude. In case of the solid-state protonation the FTIR spectra revealed that the protonation reaction is not complete and a part of free NTO remains in the product. On the contrary, the polymerization of aniline in the presence of NTO yields PANI sulfate, a conducting product that does not contain any significant amount of NTO.

Acknowledgment:

The authors thank Professor S. Zeman from the University of Pardubice for research sample of NTO and to Dr J. Prokeš from Charles University Prague for the determination of electrical conductivity. This work was supported by the Grant Agency of the Czech Republic (202/02/0698) and by the Ministry of Education, Youths, and Sports of the Czech Republic (VZ 113 2000 01).

5. REFERENCES

[1] D.C. TRIVEDI: *Handbook of Conductive Molecules and Polymers, H.S. Nalwa, Ed.,* Vol. 2, Chap. 12, Wiley: Chichester, UK, 1997

[2] Z. JIN, Y. SU: *Sens. Actuators B* **72**, 75, 2001

[3] M.E. NICHO, M. TREJO, A. GARCIA-VALENZUELA, J.M. SANIGER, J. PALACIOS, H. HU: *Sens. Actuators B* **76**, 18, 2001

[4] J. STEJSKAL, M. TRCHOVÁ, J. PROKEŠ, I. SAPURINA: *Chem. Mater.* **13**, 4083, 2001

[5] V. ABOUTANOS, L.A.P. KANE-MAGUIRE, G.G. WALLACE: *Synth. Met.* **114**, 313, 2000

[6] S.-J. SU, N. KURAMOTO: *Macromolecules* **34**, 7249, 2001

[7] P.A. MCCARTHY, J. HUANG, S.-C. YANG, H.-L. WANG: *Langmuir* **18**, 259, 2002

[8] M.G. HAN, S.K. CHO, S.G. OH, S.S. IM: *Synth. Met.* **126**, 53, 2002

[9] S.G. KIM, J.W. KIM, M.S. CHO, H.J. CHOI, M.S. JHON: *J. Appl. Polym. Sci.* **79**, 108, 2001

[10] D.W. HATCHETT, M. JOSOWICZ, J. JANATA: *J. Phys. Chem. B* **103**, 10992, 1999

[11] A.B. SAMUI, A.S. PATANKAR, R.S. SATPUTE, P.C. DEB: *Synth. Met.* **125**, 423, 2002

[12] S. PALANIAPPAN: *Eur. Polym. J.* **37**, 975, 2001

[13] F. GENOUD, I. KULSZEWICZ-BAJER, B. DUFOUR, P. RANNOU, A. PRON: *Synth. Met.* **119**, 415, 2001

[14] B. DUFOUR, P. RANNOU, P. FEDORKO, D. DJURADO, J.-P. TRAVERS, A. PRON: *Chem. Mater.* **13**, 4032, 2001

[15] J. STEJSKAL, I. SAPURINA, M. TRCHOVÁ, J. PROKEŠ, I. KŘIVKA, E. TOBOLKOVÁ: *Macromolecules* **31**, 2218, 1998

[16] M. TRZNADEL, P. RANNOU: *Synth. Met.* **101**, 842, 1999

[17] W.M. SAYED, T.A. SALEM: *J. Appl. Polym. Sci.* **77**, 1658, 2000

[18] S.M. AHMED: *Eur. Polym. J.*, 2002, in press

[19] Y. CAO, J.J. QIU, P. SMITH: *Synth. Met.* **69**, 187, 1995

[20] S.M. AHMED, R.C. PATIL, M. NAKAYAMA, K. OGURA: *Synth. Met.* **114**, 155, 2000

[21] Z. PING, G.E. NAUER, H. NEUGEBAUER, J. THEINER and A. NECKEI: *Electrochim. Acta* **24**, 1693, 1997

[22] D.C. SORESCU, T.R.L.SUTTON, D.L. THOMPSON, D. BEARDALL, C.A. WIGHT: *J. Mol. Struct.* **384**, 87, 1996

[23] T.S. SUMRALL: *Propell. Explos. Pyrot.* **24**, 61, 1999

[24] G. SINGH, I.P.S. KAPOOR, S.K. TIWARI, P.S. FELIX: *Hazardous Mater.* **81**, 67, 2001

[25] W.L. YIM, Z.F. LIU: *J. Am. Chem. Soc.* **123**, 2243, 2001

[26] E.A. ZHUROVA, A.A. PINKERTON: *Acta Crystallogr. B* **57**, 359, 2001

[27] X.-R. ZENG, T.-M. KO: *J. Polym. Sci. B: Polym. Phys.* **35**, 1993, 1997

[28] R.P. MCCALL, M.G. ROE, J.M. GINDER, T. KUSUMOTO, A.J. EPSTEIN, G.E. ASTRURIAS, E.M. SCHERR, A.G. MACDIARMID: *Synth. Met.* **29**, E433, 1989

[29] S. QUILLARD, G. LOUARN, J.P. BUISSON, M. BOYER, M. LAPKOWSKI, A. PRON, S. LEFRANT: *Synth. Met.* **84**, 805, 1997

[30] Z. PING: *J. Chem. Soc., Faraday Trans.* **92**, 3063, 1996

[31] A.J. EPSTEIN, J.M. GINDER, F. ZUO, R.W. BIGELOW, H.S. WOO, D.B. TANNER, A.F. RICHTER, W.S. HUANG, A.G. MACDIARMID: *Synth. Met.* **16**, 303, 1986

[32] J. TANG, X. JING, B. WANG, F. WANG: *Synth. Met.* **24**, 231, 1988

[33] J.C. CHIANG, A.G. MACDIARMID: *Synth. Met.* **13**, 193, 1986

[34] G. SOCRATES: *Infrared Characteristic Group Frequencies*, Wiley: Chichester, 1980.

[35] G. SINGH, S.P. FELIX: *J. Hazardous Mater.* **90**, 1, 2002

MEASUREMENT OF DETONATION VELOCITIES OF FORMED LINEAR CHARGES

Jiří Vágenknecht*, Zbyněk Akštein and Pavel Vávra***

* University of Pardubice, Department of Theory and Technology of Explosives, 530 12 Pardubice, CZ

** Research Institute of Industrial Chemistry (RIICH), 532 17 Pardubice - Semtin, CZ

Abstract:

By measurement of detonation velocity in formed linear charge (FLC) of plastic explosive with parallel use of continuous and discontinuous method there was performed an experiment to study the influence of forming the charge on character of propagation of the detonation wave in profile of the charge.

***Keywords**: linear charge (LC), formed linear charge (FLC), measurement of velocity of the detonation (VOD), continuous VOD*

1. INTRODUCTION

Linear charges (LC), i. e. the charges with one size (usually the length), which distinctively exceeds the other ones, are very interesting phenomenons with a large spectrum of practical use regarding their specific geometry. Although in common use there distinctively predominate "extensive" applications of linear charges, when first of all their general performance effect is discussed (excavation of trench, transfer of detonation, breaking of constructional elements etc.) they are getting at present inconsiderable meaning and also applications of relatively small sizes. Example of modern and effective use of concentrated energy of explosion at this kind of charges can be the linear shaped charges (LSC). LSC offer a number of possibilities of their setting in many specialized applications, especially at linear destructions of various constructional elements - at so-called cuttings by "cumulative cutter".

Although there already exist several kinds, which were mentioned above (also commercial available), of "cutting applications", that are popular first of all in a formable version (see e. g. [1]), there were not presented any works so far, that would sufficiently document and/or explain the influence of formation of similar charges on their function.

Description of basic factors and their combinations, which influence total performance of linear shaped charges, is very complicated and for the present there were not published any works, that would this problems generally solve in a needed extension. Not many available information mostly deal with empirical matters of specific arrangement. Nobody was successful in finding even references on any work, that would consider at least a partial analysis of the influences of fundamental marginal conditions, what is e.g. a propagation of the front of detonation wave at least in a primitively deformed linear charge.

Therefore there were proposed basic experiments, which would, according to acquired data, this event enable to qualify and subsequently according to its results and possibilities also further analyse.

2. EXPERIMENTAL

2.1. Estimate and project of the experiment

Basic deformation, which it is possible to presuppose at linear charges, is their curve. At curve at plastic charges (it doesn't matter whether it is cross or linear) there occur two possible effects on form and mass of the charge. As it is evident from the illustrative picture No. 1 (for a good illustration there was created a dimensionally extreme model with a semicircular bend), there occur among other changes of the length of the wall of the charge on inner and outer side of the curve. This can be related with indicated density changes (different size of the elements in profile - smaller element = bigger density) in profile of the charge. Such changes must be evidently demonstrated to a certain extent on the way of diffusion of detonation wave of the charges. What kind and how significant the changes will be, should be cleared by realisation of the proposed experiments.

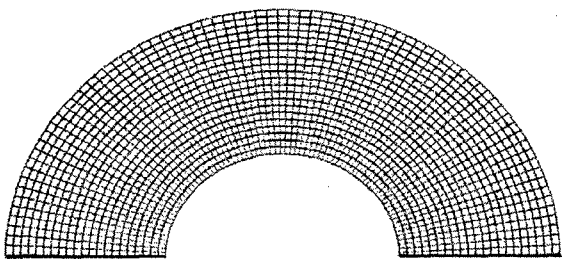


Fig. 1 Mesh model of curved LC

2.2. Testing charges

For experiments at RIICH there were made linear plastic charges of circular cross-section for these tests. Charges were made from the explosive Pl SE M. This explosive is realized on basis of crystal RDX (hexogen - brisant component) and synthetic rubber (binder) with 88 % filling. Density of the charges ρ_0 was cca 1,50 g. cm^{-3}, weight 360g, length 350 mm and diameter 29 mm.



Charges for the tests were carefully curved, so that there could not occur their other undesirable deformations. They were curved over the wall of circular profile of outer radius 223 mm (fig. 2).

Fig. 2. Curved linear charge of a plastic explosive



Evident changes of the length of inner and outer side of the curved charge were possible to measure by a flexible linear measuring instrument. By the help of device for measurement of length differences there was at least orientationally determined the dimensional deformation of the curved charge – its flattening – ovality (fig. 3)

Fig. 3. Measurement of the ovality of charge's section

Expected density changes of the charge in its profile were measured throughout its length in sections (outside, centre, inside) by double weighing method (determination of the volume of the element from difference of its weight on air and in water) – see fig. 4

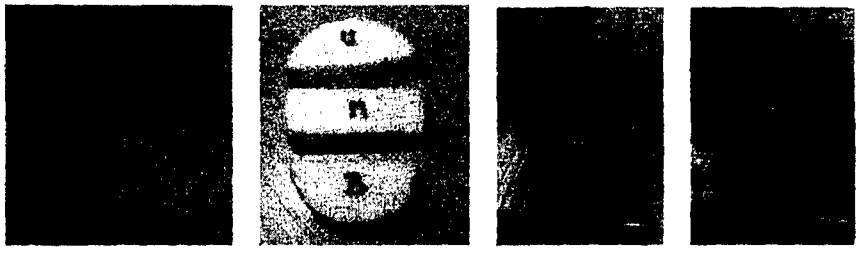


Fig. 4. Measurement of density of the explosive in profile of the charge

Influence of both variables (density and geometry) on the mode of propagation of the detonation wave should be according to all hypotheses synergetic. Distinction of the influences of particular factors should at least partly help to use the parallel application of time and continuous method at measurement of detonation velocity.

2.3. VOD measurement - a time method

At present the dominant method for measuring detonation velocities is a time method with use of various ionisation sensors. This method is based on registration of moving the detonation wave by a given linear section of the charge. Moving detonation wave short-circuits suitable sensors (wire, tubular etc.), which is recorded by a data-recorder - oscilloscope, electronic stopwatch etc. This method is generally well managed, relatively not difficult and in dependence on used techniques also reliable and accurate. Even there exists a possibility how to measure the detonation velocity at relatively short sections, as a serious disadvantage here remain problems connected with accurate localisation of the sensors and first of all the impossibility to involve accurately the possible discrepancy of the values of detonation velocity in places between the sensors.

Time method in this experiment was not treated only as a referential method. But with use of combined oscilloscopic two-channel record of the short-circuiting of ionisation sensors on four bases it was used also for accurate determination of the time process of the detonation wave's front at opposite locations in different places of the whole charge. (see Fig. 6)

2.4. VOD measurement - continuous method

First of all the escalating development of measure and record techniques enabled the development of requested and perspective methods of measurement of moving of the detonation wave of the charges by the help of resistive probes in so-called continuous regime until the realisation of current commercial available and user's highly comfortable measure devices. One of the dominant companies in the market with these devices is a Canadian firm MREL[2]. Its 10-bit data-recorder working with a source of constant voltage of 1 MHz frequency was used at continuous scanning of the progreess of detonation wave on the sides of the charge by the help of the special resistive sensor - proberod (fig. 5)

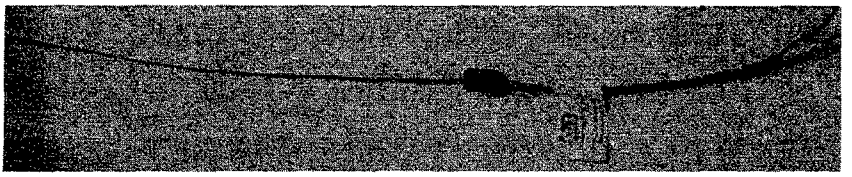


Fig. 5. Sensor for continuous measurement of detonation velocity - proberod

It was supposed, that by the help of continuous measurement it will be possible to involve the eventual change of diffusion velocity of detonation wave on the sides of the charge. It would be proved by the change of the gradient on record of change in resistance (length) of proberod on time

2.5. Arrangement of the experiment

As it was already said, in suggested experiment there was used a combination of continuous and time method at test of determination of the mode, how the detonation wave is passing in the FLC of the plastic explosive.

Particular arrangement of the experiment is illustrated on the block scheme at fig. 6 disposition of the charge. Disposition of the charge for experiments is evident in fig. 7 (letters A - F indicate an idealized localization of ionizating probes for the time method).

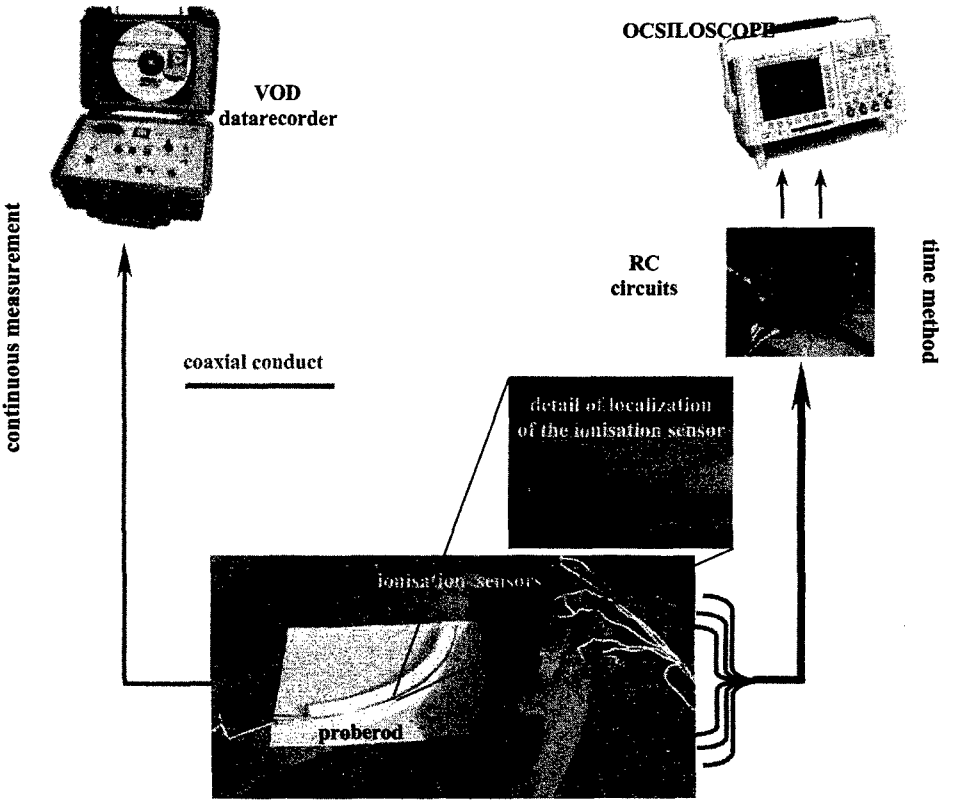


Fig. 6. Scheme of arrangement of the experiment

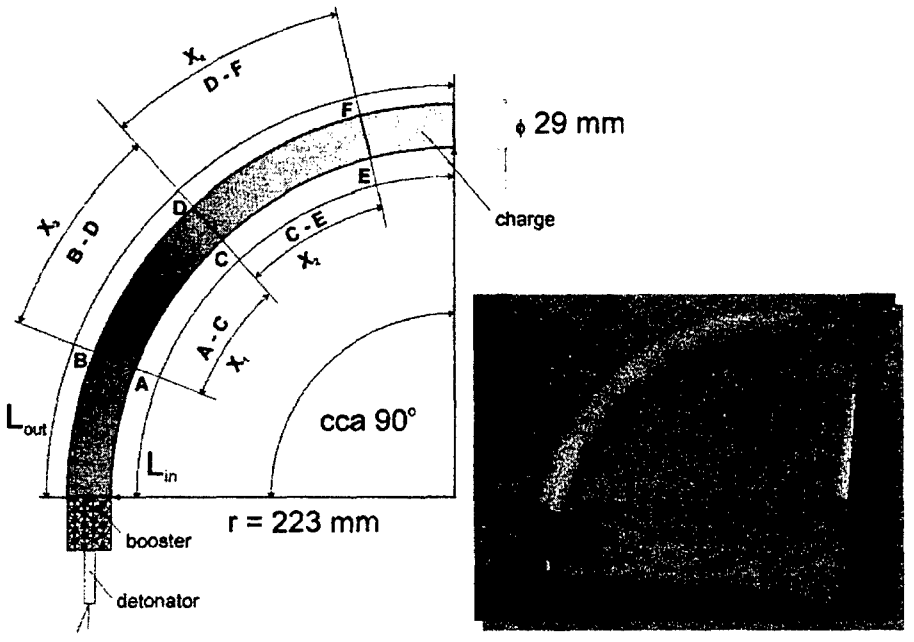


Fig. 7. Arrangement of the charge

3. RESULTS

With respect to limited capacity possibilities there were successfully tested on the whole only 4 testing sets - two were with continuous sensor enclosed to outer circumference, two were with sensor on inner circumference.

3.1. Characteristics of the charge at mechanical bending stress

At curving of the charge there occurs a nearly negligible length contraction on inner side of the charge and a corresponding equivalent change of the length on its outer circumference. Inner and outer dimensions of the charges correspond only with slight variations to theoretical sizes of quarter-circle segment i. e. Lin = 350 mm, Lout = 396 mm.

In comparison with previous hypotheses there was not prove almost any influence of forming charges on their density profiles. Experimentally determined values of the densities oscillated within the limits 1,497 - 1,506 $g.cm^{-3}$, what more or less responds to previous common oscillation of the densities in profile of the charge. It wasn't possible to presuppose the significant influence of density gradients in the charge on the mode of propagation of detonation in the charge.

Changes of the geometry of cross-section of the charge were more evident at curving. Especially in central part of the charge there occurs a crosswise extension of the charge to the contrary of its height (in curve direction). Oval form of the charge in these places was evident very well. Regarding plastic character of mass of the charge and related specific irregularity already in cross-section of the previous charge there was managed to measure the character of ovality of the charge only approximately. Maximum differences between height and width of the charge in exposed places were however bigger than 2 mm on behalf of its width. It presents in volume of the displaced mass definitely a significant quantity (more than 10% - 15%!).

3.2. VOD measurement -time method

Acquired oscilloscopic records from discontinuous method (typical record see fig. 4) were evaluated and the acquired results were processed into table 1 by a computer.

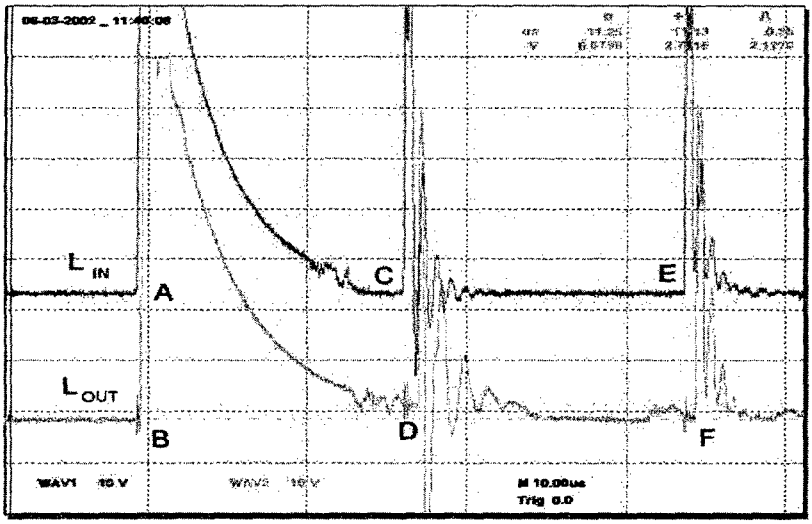


Fig. 8. Typical oscilloscopic record of measurement of the detonation velocity on two channels by a multi-point time method.

Table 1. Basic data of discontinuous VOD measurement

	DISTANCE [mm]				TIME [μs]						
position	X_1	X_2	X_3	X_4	A-B	C-D	E-F	A-C	C-E	B-D	D-F
	104	117	142	160	0,47	0,9	0,83	13,55	18,56	14,00	18,54
	127	143	133	150	0,26	0,97	0,69	16,71	17,62	17,39	17,39
	129	146	145	164	-0,05	0,81	0,64	16,64	19,20	17,56	19,01
	111	125	127	143	0,404	0,69	0,64	14,70	16,57	14,97	16,53

Values of detonation velocity are summarised in table 2. (They are calculated from results in table 1.)

Table 2. VOD values - discontinuous measurement

position	X_1	X_2	X_3	X_4
VOD [m.s^{-1}]	7675,3	8357,1	7650,9	8630,0
	7600,2	8223,1	7548,2	8625,6
	7752,4	8314,4	7552,1	8627,0
	7551,0	8347,8	7664,5	8650,9
average VOD	7551,0	8347,8	7664,5	8650,9

3.3. Continuous method

By parallel VOD measurement by continuous method (typical evaluated records are in fig. 9) were found out values of detonation velocities presented in table 3:

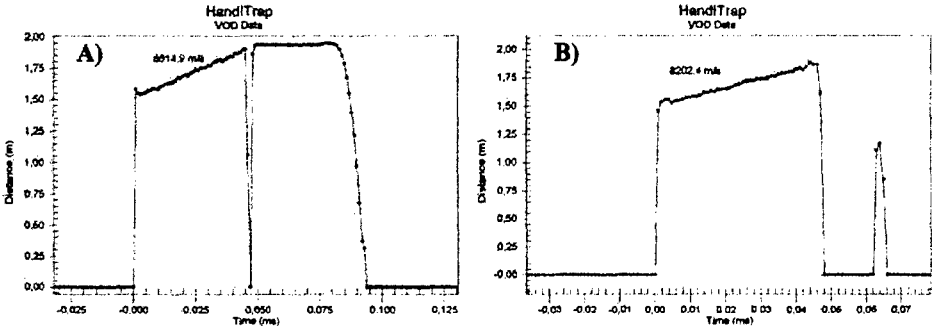


Fig. 9. Records of continuous VOD measurement for outer (A) and inner (B) side

Table 3. VOD values - discontinuous measurement

	position	
	in	out
Cont. VOD [m.s^{-1}]	8159,8	8614,9
	8202,4	8658,2
average cont. VOD	8181,1	8665,7

4. DISCUSSION

Combination of time and continuous method of measurement of the detonation velocity at realised experiments provided many interesting and very useful information. The tests documented and explained several basic aspects of functioning of the FLC. But acquired results at the same time evoked a need at least to preformulate possible causes of some surprising discoveries.

Results of discontinuous and also continuous measurements of progression of the detonation wave through curved charge definitely proved the fact, that detonation wave passes through the charge more or less vertically on axis of this charge. Absolute values of measured velocities of progress of the detonation wave through the charge over inner and outer side of the curved charge were relatively surprising. Rather questionable was the exact explanation of the difference between numerical values of velocity of propagation of the detonation wave over inner circumference of the charge, where the continuous method provides distinctively higher velocity in comparison with the time method.

Regarding construction of used resistive sensors and possible mechanism of their short-circuiting; it is necessary to state that values of detonation velocities found out by continuous measurement on inner side of the charges are evidently not relevant. In a given arrangement to a great extent there can be applied functional switching at their mechanical deflection (this

is proved by adequate results at mechanical preferable arrangement and functioning of the probe at its localisation on outer side of the FLC).

This negative finding is indeed very important for other practical application of resistive probes at future measurements. Now we have to appreciate that unsuitable arranging of the experiment can easily harm the result, by a badly identifiable systematic mistake.

It was not successful to find out expected changes of this velocity during the measurement by analysis of the record of continuous VOD measurement. This was indicated e.g. by the time method. It seems that sensitivity of this method (or sensors) is insufficient for stated tests. Nevertheless the found absolute values of VOD at suitable localisation of the sensors are in absolute correspondence with values found by another method. So that this measurement helped at least as a valuable comparative test.

So, as it is evident from the results of measurements by both methods, propagation of detonation wave on its outer circumference seems to be much faster in comparison with propagation on inner side. This discovery was one the most interesting things in the whole experimental part. Exact explanation of this event would obviously need more extended simulation and also real experiments, which would intercept most of the marginal influences, that can be projected to the whole situation by a different extent. But primary moment of the whole solution is evidently a simple geometry of the experiment. Mentioned geometry shows a causal connection with the known event of detonation of layer of the slow explosive, which is in contact with the layer of detonating fast explosive – explosive with lower detonation velocity is systematically initiated by the faster explosive and it seems as it is detonating by a velocity, which is not its own. It is perhaps similar also in this case. Explosive on inner circumference is detonating by a common – nominal velocity and initiating impulse is then propagating by this velocity (with necessary shift phase) also on outer (longer) side of the curved charge (explosive). That then detonates during the time, which is corresponding to propagation of the detonation on shorter side of the charge, though it must propagate over a longer distance. This hypothesis is proved also by primitive calculation, when the time corresponding with the propagation of detonation of nominal velocity on shorter (inner) side of the charge related to longer side gives in this idealized case values round 8595 m.s-1, which corresponds with discovered results very well. Certain question so far remains the discovered rising of the velocity on outer circumference ($8300 \rightarrow 8600$ $m.s^{-1}$). Here is expected suggestion of other experiments, which should explain this. It is very probable, that this event is somehow related with expected deformation of front of the detonation wave. This thesis is supported first of all by evident time difference between short-circuiting of the opposite points (see times A vs. B, C vs. D and E vs. F in table No. 1). It is evident, that here occurs a certain variable retardation of progress of front of the detonation wave.

It is possible to suppose, that very interesting indicia, which lead to better orientation in monitored problems, could provide at least basic simulation of the studied problem by some of the modern computational-simulation programmes. As a perspective method is first of all the use of Finite Element Method, e.g. in ANSYS – LS DYNA3D system[3]. Regarding complications of the creation, harmonizing and final processing of the functional model, which is necessary to perform in co-operation with external workplaces (at our department there are not these possibilities available). It is possible to expect the realization of this alternative only in a long-term time horizon.

5. CONCLUSION

It was checked by the realized measurement, that propagation of the detonation wave in deformed - curved linear charge is in principle vertical on axis of this charge. Outer demonstration of this way of propagation of the detonation wave is a proportional change of velocity of propagation of the detonation wave on outer circumference of curved charge in comparison with inner circumference. At the same time there surely occurs deformation of front of the detonation wave, which is so far not very accurately specified. This deformation is in dependence on character of deformation of the linear charge. It was found out, that effects mentioned above are not related to density changes in profile of the charge. It does not considerably change, first of all the changes of charge geometry are determinant.

Acknowledgment:

Here we would like to thank to of Research Institut of the Industrial Chemistry workers - first of all to Ladislav Říha, MSc. and Miroslav Štancl, MSc. for useful help at material and organizational guarantee of the experiments.

Special thanks come to Mr. Jiří Majzlik from Department of Theory and Technology of Explosives University of Pardubice for his professional guarantee of experimental instrumentation.

REFERENCES

[1] BLADE – The Cuting Edge, publicity matter, British Aerospace – Royal Ordnance

[2] www.mrel.com - Company Web Presentation
http://www.mrel.com/Portable_VOD-Data_Recorders/index.html – products pages

[3] ANSYS: (1996) Ansys/LS-Dyna3D, theoretical manual

EFFECT OF INTERMOLECULAR FORCES ON SOME PROPERTIES OF EXPLOSIVES

Pavel Vávra*, Miroslav Pospíšil and Jarmila Repáková****

* Department of Theory and Technology of Explosives
Faculty of Chemical Technology, University of Pardubice
53210 Pardubice, Czech Republic

** Department of Chemical Physics and Optics,
Faculty of Mathematics and Physics, Charles University
12116 Prague, Czech Republic

Abstract:

Values of total sublimation energy and its van der Waals, Coulomb, and hydrogen-bond energy contributions have been calculated for a selected set of explosives on the basis of their structural data, and their non-negligible effect on sensitivity parameters, densities and melting temperatures has been established. These parameters are significantly affected by hydrogen bonds and total magnitude of intermolecular forces. Also other factors affecting these parameters are discussed.

Keywords:
intermolecular forces, calculations, high explosives, HE, properties of molecules

1. INTRODUCTION

A previous paper[1] reported the relationship between the magnitude of volume detonation energy, E_D, and the impact sensitivity expressed by the fall height, h, which was derived for a set of 34 explosives. The E_D value was calculated by means of Eqs (1) and (2),

$$E_D = P/(2(\gamma - 1)) \quad (1)$$

$$\gamma = (\rho D^2)/P - 1 \quad (2)$$

where E_D means the volume detonation energy in $kJ.cm^{-3}$, D is detonation velocity in $km.s^{-1}$, P is detonation pressure in GPa, ρ is the theoretical maximum density (TMD) in $g.cm^{-3}$, and γ is adiabatic coefficient.

Comparison of the E_D and h values has divided the set of explosives into a class of compounds with higher volume detonation energies and higher sensitivities, and a class with lower sensitivities and lower values of detonation energy. However, in both classes there were exceptions that did not obey this rule. Such exceptions involved the distinctly less sensitive 1,1-diamino-2,2-dinitroethylene (DADNE) in the first class, and in the second *N*-methyl-2,4,6,*N*-tetranitroaniline (TE, tetryl), which is currently classified as a more sensitive explosive.

A presumption was made that the lower sensitivity of DADNE was due to the presence of hydrogen bonds, while on the other hand such bonds do not play any substantial role in tetryl. However, verification of this presumption necessitated the knowledge of non-bond energy values of structures in the set of individual explosives with different configuration.

2. CALCULATIONS

For determination of values of non-bond energies of intermolecular forces such substances were selected for which X-ray analyses were available[2]. In this set, the values of detonation velocity and pressure were calculated with the help of equations by Kamlet and Jacobs[3], and besides that the volume detonation energy (Eq. (1)). The results are given in Table 1 along with the values of fall height h, and their order is in principle determined by the magnitude of E_D value. The differentiation between the less and more sensitive explosives on the basis of the detonation energy values is shown in Fig. 1.

The calculations of non-bond energies of these explosives were carried out in the *Cerius*[2] modelling environment[4]. The individual structures were built in *Crystal Builder* module on the basis of published X-ray data. The non-bond energy was calculated in *Crystal Packer* module. The charges of atoms were calculated by the charge equilibration method[5].

The *Crystal Packer* module contains the Universal force field[6], the Dreiding II force field[7], and the Tripos 5.2 force field[8] for van der Waals parameters. The individual structure models are initialised in *Crystal Packer* module. That means the rigid units and the dimensionality of the model are assigned and the hydrogen bonds are calculated. The force field is selected to describe the van der Waals parameters. Then the total sublimation energy and its contributing van der Waals, Coulomb, and hydrogen-bond energies are calculated. The structure models of explosives have not been minimised.

The results are presented in Table 2. The calculated and experimental densities are included.

Further parameters were calculated for the investigated set of explosives with general formula $C_aH_bN_cO_d$:

- oxygen balance OB from the equation
  $$OB = ((d - 2a - 0.5b)*1600)/\text{mol. mass} \quad (3)$$
- ratio of sum of masses of the nitrogen (cN) and oxygen (dO) atoms present in the molecule to molecular mass M expressed in %
  $$(N + O)/M*100$$
- furthermore, the ratio of inter-forces per one molecule
  $$TOTAL/Z$$
  where Z is number of molecules in crystal lattice
- similarly, the value of inter-hydrogen bond HB per one molecule
  $$HB/Z$$
  expressed in kcal.mol^{-1} and the proportion of HB per one molecule expressed in %
  $$HB/TOTAL*100$$

The results are given in Table 3 along with the density values and melting points.

3. DISCUSSION

The investigated set of explosives includes nitro compounds having nitro group attached to carbon atom (aliphatic and aromatic nitro compounds), nitrogen atom (secondary nitramines), oxygen atom (nitrate esters), or the molecule contains their combination. Besides that also included are some cyclic as well as cage-structure compounds.

First we followed the effect of hydrogen bond energies on the sensitivity of the compounds. The comparison of data on oxygen balance and the share of hydrogen bond energy in the total sublimation energy (Fig. 2) shows that compounds with a share of hydrogen bond energy (written in *underlined italics* in all the pictures) belong to the class of less sensitive explosives. The negligible difference observed with BTNEU was not considered. Three further less sensitive compounds – TNB, HNS, and TNT – possess a very negative oxygen balance and, at the same time, the lowest detonation energy (See Table 1 and Fig. 1).

The relationship of total sublimation energy (per one molecule, TOTAL/Z) to relative number of nitrogen and oxygen atoms in molecule is presented in Fig. 3. At the left-hand side (< 70% (N + O)/M), tetryl (TE) is the only more sensitive substance of all; the above-mentioned triad (TNB, HNS, TNT) has the lowest relative share of N and O, and the other compounds have hydrogen bonds. On the other hand, at the right-hand side of the picture – substances with larger content of nitrogen and oxygen, i.e. nitro groups – there are more sensitive substances except for those containing hydrogen bonds (2,4-DNI, NQ, and DADNE). With these three compounds, the magnitude of total sublimation energy does not attain high values – e.g. DADNE exhibits the lowest value in the whole set.

The effect of total sublimation energy on the density value is not distinct – on the other hand, as it can be seen from Fig. 4 – higher nitrogen and oxygen content together with hydrogen bonds very likely contribute to the higher density of a number of members of the set. It must be pointed out that the crystal density is considered in the case of NG.

The situation is opposite with the melting points (Fig. 5). The effect of higher value of total sublimation energy and hydrogen bonds on the higher melting (or decomposition) temperature is observable, on the other hand the share of nitrogen and oxygen in molecule obviously does not affect this parameter in any substantial way.

When evaluating the effect of energy of intermolecular forces on some properties (sensitivity, density, melting temperature) in a selected set of explosives we considered its total magnitude, i.e. the sum of van der Waals, Coulombic, and hydrogen-bond energies, and the effect of hydrogen bonds was evaluated separately. As in the case of hydrogen bonds, we separately evaluated the van der Waals and Coulombic forces, but in this case we have not found any marked effect on the properties followed.

4. CONCLUSION

On the basis of calculated values of total sublimation energy for a set of explosives with experimentally determined molecular structure (X-ray analysis), we have found that in a significant number of cases the intermolecular interactions – especially hydrogen bonds - contribute to sensitivity decrease, melting temperature increase, and density increase. Although other factors affect the properties mentioned, too, in many explosives a distinct role can be played by intermolecular interactions – in particular hydrogen bonds.

Acknowledgements:

The authors acknowledge the Czech MPO (Project FC – M2/05) and GA ČR (Project 203/02/0436 – CSD) for financial support.

REFERENCES:

[1] Vávra P.: Study about energy of explosives, Proc. III. Seminar „New trends in research of EM", University of Pardubice, p. 223, Pardubice 2000,CR

[2] Vávra P.: Electronic density of molecule and some properties of high explosives, Proc. IV.Seminar „New trends in research of EM", University of Pardubice, p. 345, Pardubice 2001, CR and lit. cited there

[3] Kamlet M.J., Jacobs S.J.: J. Phys. Chem. **48**, 23,1968

[4] Cerius^2 documentation, June 2000, San Diego: Molecular Simulations Inc, 2000

[5] Rappé A K., Goddard III W.A.: Charge Equilibration for Molecular Dynamics Simulations, J. Phys. Chem. **95**, 3358-3363, 1991

[6] Rappé A.K., Casewit C.J., Colwell K.S., Goddard III W.A. and Skiff W.M.:UFF, a Full Periodic Table Force Field for Molecular Mechanics and Molecular Dynamics Simulations, J. Amer. Chem. Soc. **114**, 10024 – 10035, 1992.

[7] Mayo S.L., Olafson B.D. and Goddard III W.A.: DREIDING: A Generic Force Field for Molecular Simulations, J. Phys. Chem. **94**, 8897 – 8909, 1990

[8] Clark M., Cramer III R.D. and Opdenbosh N. Van: Validation of the General Purpose Tripos 5.2 Force Field, J. Comp. Chem. **10**, 982 – 1012, 1989

TABLES

Table 1. *Properties of selected high explosives*

No.	Name	ρ [g.cm^{-3}]	H_f [kcal.mol^{-1}]	P [GPa]	D [km.s^{-1}]	E_d [kJ.cm^{-3}]	h [cm]
1	**HNIW**	2,03	99,2	43,99	9,620	9,684	23
2	**HNB**	2,00	47,0	42,000	9,437	9,372	12
3	**HMX**	1,90	17,8	38,080	9,119	8,858	26
4	**BTNEN**	1,96	-175,9	39,080	9,157	8,861	5
5	**BTNEU**	1,86	-71,7	36,570	8,993	8,657	17
6	**TNAZ**	1,84	3,0	36,080	8,960	8,614	21
7	**RDX**	1,80	14,7	34,240	8,786	8,321	24
8	**PETN**	1,77	-129,0	33,130	8,686	8,157	12
9	**DADNE**	1,88	-32,0	33,600	8,591	7,889	120
10	**DINA**	1,67	-74,0	28,540	8,208	7,348	23
11	**BDNPN**	1,73	-65,3	29,300	8,226	7,343	29
12	**NG**	1,59	-118,7	27,070	8,121	7,224	10
13	**ADNBF**	1,90	36,8	30,420	8,152	7,074	160
14	**2,4-DNI**	1,76	4,9	27,500	7,926	6,806	100
15	**TATB**	1,94	-33,3	29,340	7,958	6,710	320
16	**NQ**	1,77	-22,0	27,010	7,843	6,650	177
17	**TE**	1,73	8,0	26,290	7,792	6,590	32
18	**DATB**	1,84	-23,6	26,780	7,719	6,394	320
19	**TNA**	1,77	-18,0	24,900	7,530	6,131	177
20	**PA**	1,76	-57,3	24,700	7,513	6,108	87
21	**HNS**	1,74	16,1	22,970	7,270	5,731	54
22	**TNB**	1,68	-24,6	21,970	7,189	5,631	100
23	**TNT**	1,65	-18,0	20,540	6,991	5,336	160

Abbreviations:

HNIW – 2,4,6,8,10,12 – hexanitro – 2,4,6,8,10,12 – hexaazatetracyclo [5.5.0.0^{5,9}.0^{3,11}] dodecane
HNB – hexanitrobenzene
HMX – 1,3,5,7 – tetranitro – 1,3,5,7 – tetraazacyclooctane
BTNEN – di (2,2,2 – trinitroethyl) nitramine
BTNEU – di (2,2,2 – trinitroethyl) urea
TNAZ – 1,3,3 – trinitroazetidine
RDX – 1,3,5 – trinitro – 1,3,5 – triazacyclohexane
PETN – pentaerythritol tetranitrate
DADNE – 1,1 – diamino – 2,2 – dinitroethylene
DINA – di (2 – nitratoethyl) nitramine
BDNPN – di (2,2 – dinitropropyl) nitramine
NG – glycerine trinitrate
ADNBF – 7 – amino – 4,6 – dinitrobenzofuroxane
2,4 – DNI – 2,4 – dinitroimidazole
TATB – 1,3,5 – triamino – 2,4,6 – trinitrobenzene
NQ – nitroguanidine
TE – N – methyl – 2,4,6,N – tetranitroaniline
DATB – 1,3 – diamino – 2,4,6 – trinitrobenzene
TNA – 1 – amino – 2,4,6 – trinitrobenzene
PA – 1 – hydroxy – 2,4,6 - trinitrobenzene
HNS – 2,2′,4,4′,6,6′- hexanitrostilbene
TNB – 1,3,5 – trinitrobenzene
TNT – 2,4,6 – trinitrotoluene

Table 2. *Calculated intermolecular forces of selected high explosives*

No.	Name	TRIPOS				UNIVERSAL				DREIDING				Z	DENSITY	
		VdW	Coul	HB	Total	VdW	Coul	HB	Total	VdW	Coul	HB	Total		calc.	exp.
		[kcal.mol^{-1}]				[kcal.mol^{-1}]				[kcal.mol^{-1}]					[g.cm^{-3}]	
1	HNIW	-93,14	-80,72	0	-173,9	-92,48	-80,72	0	-173,2	-107,8	-80,72	0	-188,6	4	1,988	2,03
2	HNB	-68,97	-40,86	0	-109,8	-46,71	-40,86	0	-87,58	-65,79	-40,86	0	-106,7	4	1,988	2,00
3	HMX	-36,94	-77,47	0	-114,4	-32,5	-77,47	0	-110	-32,16	-77,47	0	-109,6	2	1,893	1,90
4	BTNEN	-63,82	-38,56	0	-102,4	-37,02	-38,56	0	-75,58	-50,75	-38,56	0	-89,31	4	1,918	1,96
5	BTNEU	42,3	-55,41	-0,29	-98	-42,33	-55,41	-0,29	-98,03	-50,81	-55,41	-0,29	-106,5	2	1,861	1,86
6	TNAZ	-120,1	-110,6	0	-230,7	-108,5	110,46	0	-219,1	-120,4	-110,6	0	-231	8	1,860	1,84
7	RDX	-129,3	-206	0	-335,3	-122,6	-206		-328,5	-128,1	-206	0	-334,1	8	1,805	1,80
8	PETN	-36,75	-55,28	0	-92,04	-32,73	-55,28	0	-88,02	-35,84	-55,28	0	-91,13	2	1,781	1,77
9	DADNE	-37,65	-5,12	-20,69	-63,47	-34,04	-5,12	-20,69	-59,85	-42,87	-5,12	-20,69	-68,68	4	1,905	1,88
10	DINA	-65,67	-143,8	0	-209,5	-61,05	-143,8	0	-204,9	-59,08	-143,8	0	202,92	4	1,665	1,67
11	BDNPN	-43,03	-75,94	0	-119	-45,23	-75,94	0	121,16	-45,84	-75,94	0	-121,8	2	1,745	1,73
12	NG	-68,33	-71,16	0	-139,5	-59,93	-71,16	0	-131,1	-68,85	-71,16	0	-140	4	1,841	1,59
13	ADNBF	-73,93	-59,96	-14,47	-148,4	-78,71	-59,96	-14,47	-153,1	-92,45	-59,96	-14,47	-166,9	4	2,013	1,90
14	2,4-DNI	-62,19	-180,3	-26,8	-269,3	-29,56	-180,3	-26,8	-236,6	-37,97	-180,3	-26,8	-245	8	1,770	1,76
15	TATB	-34,4	42,11	-2,62	-79,12	-37,86	-42,11	-2,62	-82,58	-44,22	-42,11	-2,62	-88,94	2	1,937	1,94
16	NQ	-92,76	-241,9	-125,9	-460,6	-79,59	-241,9	-125,9	-447,4	-98,5	-241,9	-125,9	466,31	16	1,755	1,77
17	TE	-70,15	-113,9	0	-184,1	-73,14	-113,9	0	-187	-78,38	113,91	0	-192,3	4	1,731	1,73
18	DATB	-33,17	-45,65	-4,62	-83,44	-36,89	-45,65	-4,62	-87,16	-39,2	-45,65	-4,62	-89,47	2	1,838	1,84
19	TNA	-61,39	-72,63	-10,87	-144,9	-67,85	-72,63	-10,87	-151,4	-76,52	-72,63	-10,87	-160	4	1,773	1,77
20	PA	-122,4	-147,5	-4,1	-274	-132,5	-147,5	-4,1	-284,1	-151,5	-147,5	-4,1	-303	8	1,767	1,76
21	HNS	-99,32	-173,2	0	-272,5	-102,4	-173,2	0	-275,6	-109,3	-173,2	0	-282,5	4	1,745	1,74
22	TNB	-222,2	-244,2	0	-466,4	-237	-244,2	0	-481,2	-257,3	-244,2	0	-501,5	16	1,676	1,68
23	TNT	-139,1	-164,7	0	-303,9	-153,1	-164,7	0	-317,8	-159,8	-164,7	0	-324,5	8	1,654	1,65

Table 3. *Some properties of selected high explosives*

No.	Name	M	OB	(N+O)/M	TOTAL	HB	Z	ρ	b.t.	TOTAL/Z	HB/Z	HB/Z
		[g.mol^{-1}]	[%]	[%]	[kcal.mol^{-1}]	[kcal.mol^{-1}]		[g.cm^{-3}]	[°C]	[kcal.mol^{-1}]	[kcal.mol^{-1}]	[%]
1	HNIW	438	-10,96	82,19	-173,86	0	4	2,03	212	-43,46	0	0
2	HNB	348	0	79,31	-109,83	0	4	2,00	258	-27,46	0	0
3	HMX	296	-21,62	81,08	-114,40	0	2	1,90	265	-57,20	0	0
4	BTNEN	388	16,7	86,59	-102,38	0	4	1,96	95	-25,60	0	0
5	BTNEU	386	0	82,90	-98,00	-0,29	2	1,86	101	-49,00	-0,15	0,30
6	TNAZ	192	-16,66	79,16	-230,71	0	8	1,84	100	-28,84	0	0
7	RDX	222	-21,62	81,08	-335,33	0	8	1,80	204	-41,92	0	0
8	PETN	316	-10,13	78,48	-92,04	0	2	1,77	141	-46,02	0	0
9	DADNE	148	-21,62	81,08	-63,47	-20,69	4	1,88	215	-15,87	-5,17	32,60
10	DINA	240	-26,66	76,66	-209,51	0	4	1,67	51	-52,38	0	0
11	BDNPN	326	-34,35	74,84	-118,97	0	2	1,73	187	-59,49	0	0
12	NG	227	3,52	81,93	-139,49	0	4	1,84	13	-34,87	0	0
13	ADNBF	241	-49,80	68,87	-148,37	-14,47	4	1,90	267	-37,09	-3,62	9,75
14	2,4-DNI	158	-30,40	75,94	-269,26	-26,80	8	1,76	274	-33,66	-3,35	9,95
15	TATB	258	-55,81	69,76	-79,12	-2,62	2	1,94	350	-39,56	-1,31	3,31
16	NQ	104	-30,77	84,61	-460,57	-125,91	16	1,77	246	-28,79	-7,87	27,34
17	TE	287	-47,38	68,98	-184,05	0	4	1,73	131	-46,01	0	0
18	DATB	243	-55,96	68,31	-83,44	-4,62	2	1,84	286	-41,72	-2,31	5,54
19	TNA	228	-56,14	66,66	-144,89	-10,87	4	1,77	188	-36,22	-2,72	7,50
20	PA	229	-45,41	67,24	-273,99	-4,10	8	1,76	122	-34,25	-0,51	1,50
21	HNS	450	-67,55	61,33	-272,54	0	4	1,74	316	-68,14	0	0
22	TNB	213	-56,34	64,78	-466,35	0	16	1,68	123	-29,15	0	0
23	TNT	227	-74,00	60,79	-303,86	0	8	1,65	80	-37,98	0	0

FIGURES

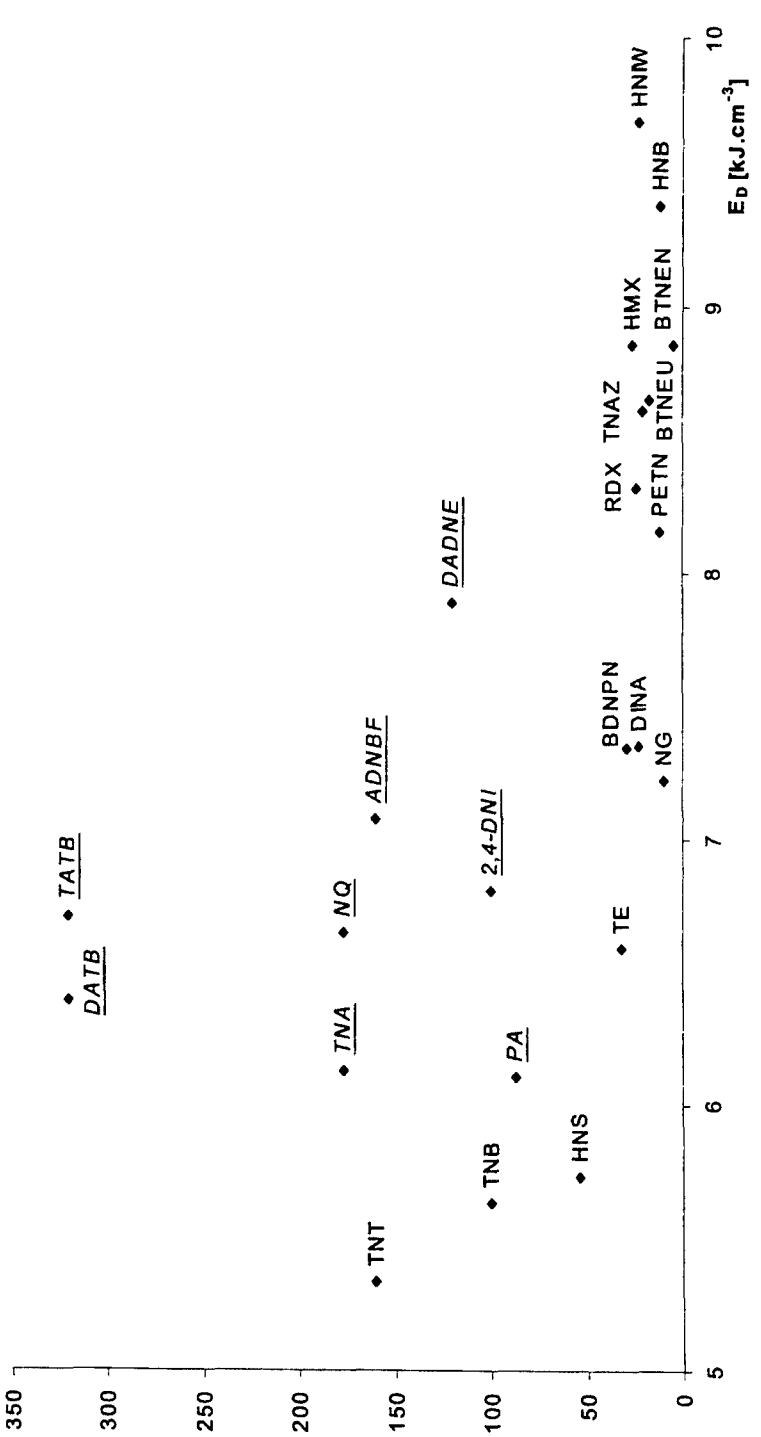


Fig 1. *Relationship impact sensitivity - energy of detonation*

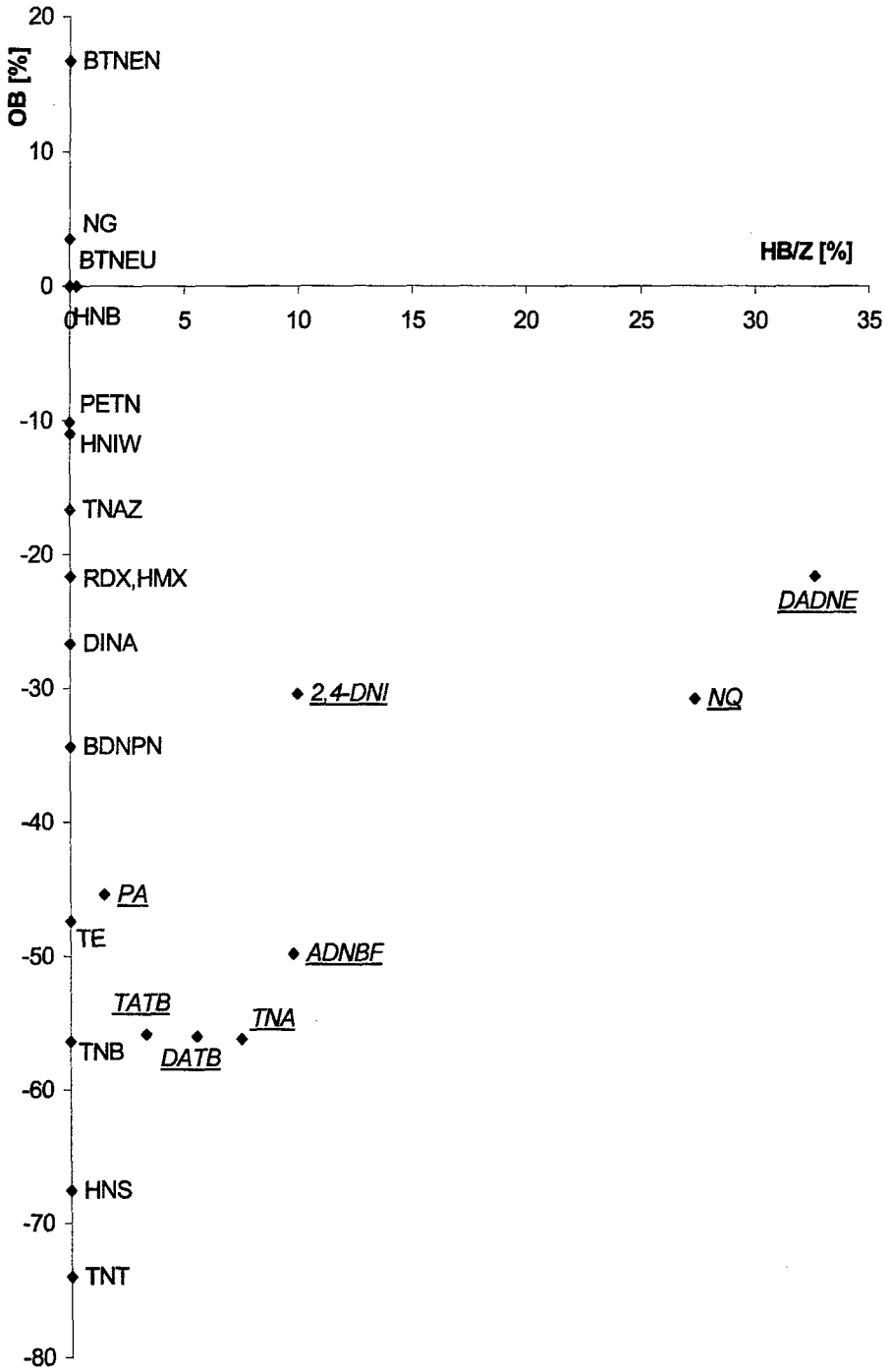


Fig 2. *Relationship balance of oxygen - hydrogen bond*

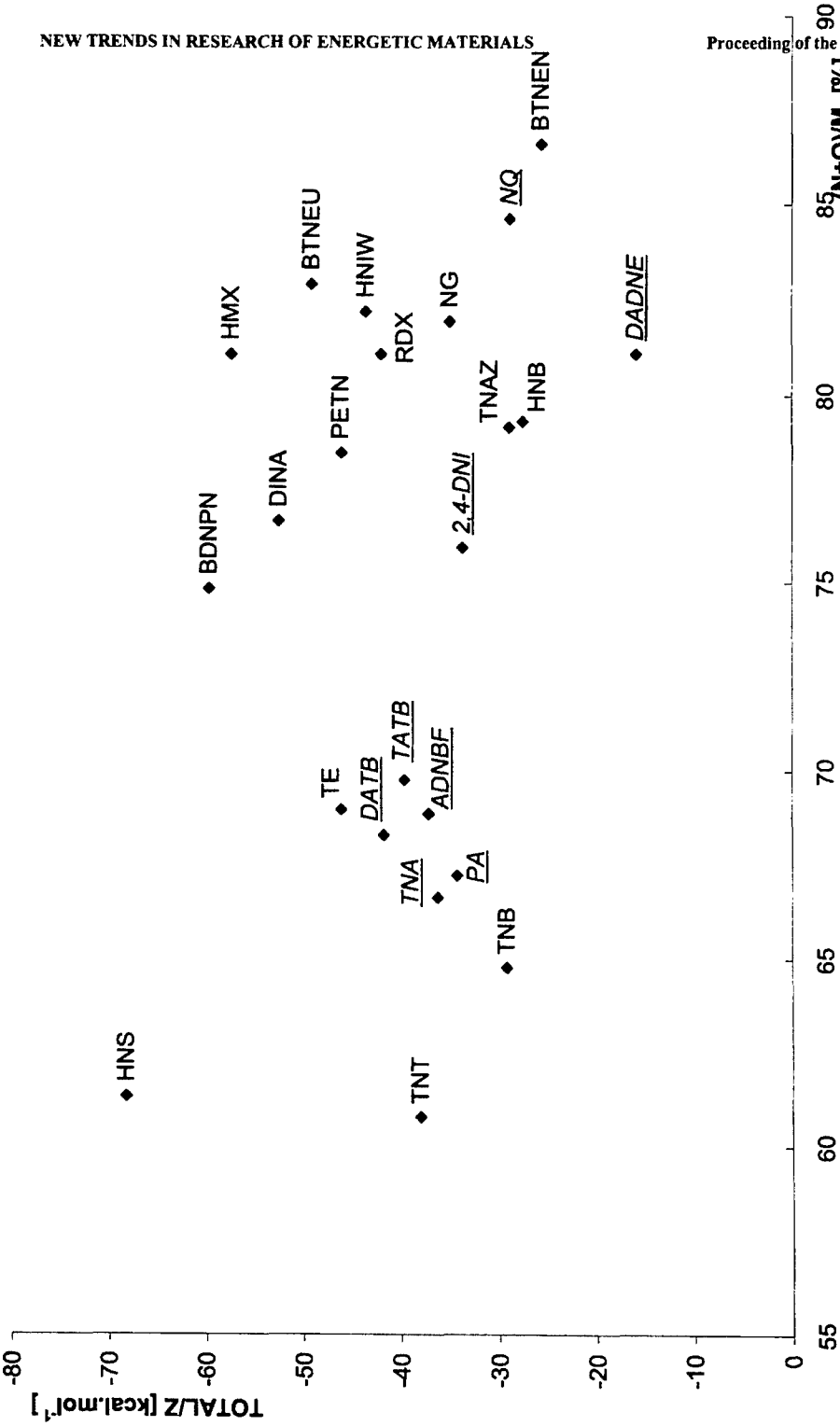


Fig 3. *Relationship content nitrogen and oxygen in molecule - amplitude of intermolecular force*

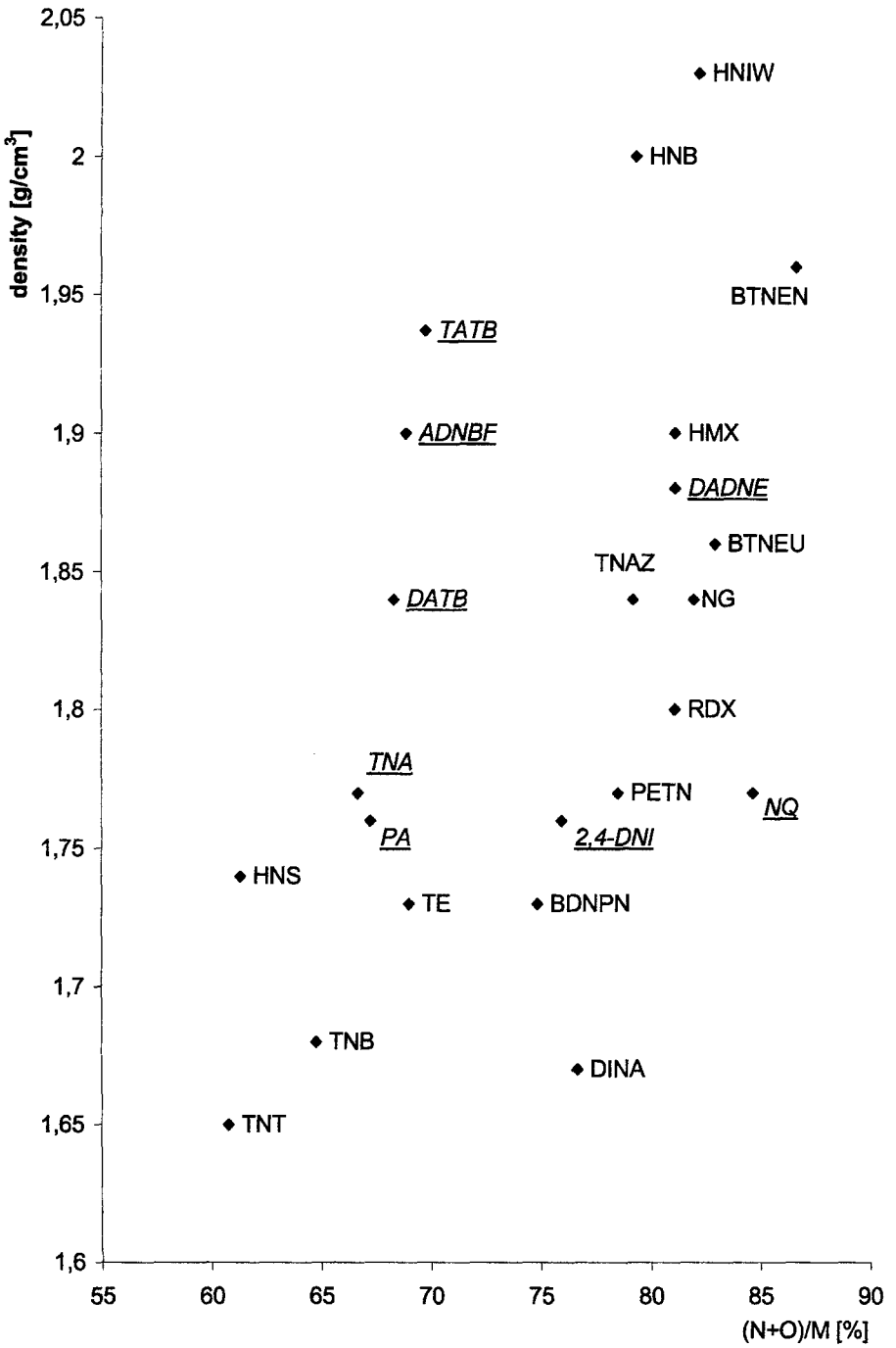


Fig 4. *Relationship density - content nitrogen and oxygen in molecule*

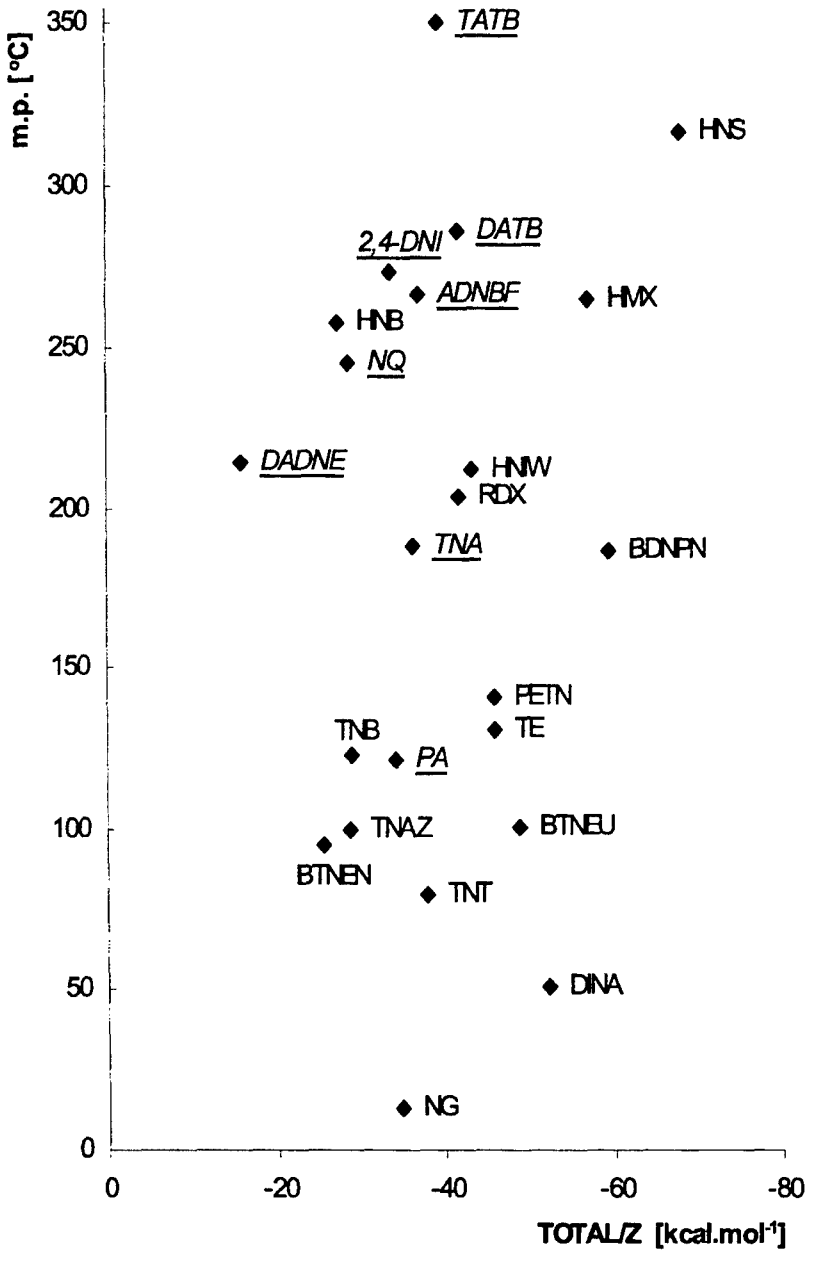


Fig 5. *Relationship melting point - amplitude of intermolecular force*

PERFORMANCE PARAMETERS OF EXPLOSIVES: EQUILIBRIUM AND NONE-EQUILIBRIUM REACTIONS

F. Volk

Fraunhofer Institut Chemische Technologie (ICT)
D-76327 Pfinztal-Berghausen

Abstract:

For the calculation of the performance parameters of combustion processes, equilibrium thermodynamic processes are being taken into account. On the other side, so-called none-equilibrium reactions occur, mostly connected with low pressure burning.
In this paper, several explosives, explosive mixtures, solid and liquid propellants have been calculated. It was shown how energy-output and gas formation is dependent on the O_2-balance and the enthalpy of formation.
It was found that the reason for the higher specific energy of liquid propellants was the increased formation of gases consisting of H_2, N_2 and H_2O, compared with conventional solid propellants based on nitrocellulose and nitroglycerine.
None-equilibrium combustion of solid propellants was found at very low loading densities or pressures lower than 25 bar. In this case, the reaction products measured by mass spectrometry are metastable and highly toxic, producing a much lower heat of explosion compared with equilibrium burning measured and calculated.

1. INTRODUCTION

A precise knowledge of combustion processes of energetic materials is important since the reaction process determines the energy-output and other parameters such as

Enthalpy of reaction

Specific energy

Specific impulse

Reaction temperature and pressure

Reaction products and gas formation and therefore also the degree of the toxicity of the products.

For the theoretical ascertainment of the combustion behavior of energetic materials such as propellants and explosives, in most cases computer codes are being used, which are able to evaluate reaction energy and products on the base of thermo-dynamic equilibrium calculations.

Under the aspect of a critical application of the codes, it is possible to determine not only the combustion energy of a number of explosives, but also the reaction products quantitatively, especially by considering the freeze out reactions of the products. On the other side, it is also possible to avoid some toxic products only by optimization of the components of the propellant or gas generator.

The following contribution shows under which preconditions thermodynamic calculations lead to a good agreement between theory and experiment. But it also points out the limit of the calculation of reactions, which are very strongly dependent on the pressure, so that none-equilibrium reactions occur. In this case we have to analyze the reaction products using experimental methods, or we have to measure the energy output with calorimetric methods.

2. THERMODYNAMIC CALCULATIONS WITH THE ICT-THERMODYNAMIC CODE

The ICT-Thermodynamic Code is based on a method developed by the National Space Administration (NASA) [1,2]. This method uses mass action and mass balance expressions for calculating chemical equilibria. Thermodynamic equilibria can be calculated for constant pressure conditions as well as for constant volume conditions.

In addition to the ideal equation of state (EOS), the Virial EOS can be used and is necessary for the high pressure conditions of gun weapons and closed bombs [3,4]. The calculation of the heat of explosion is of special interest, because the experimental measurement using the closed bomb technique is sometimes difficult due to high temperatures and erosive reaction products.

Finally, the code can be used to determine the parameters of gas detonations, e.g. pressure, temperature and detonation velocity.

The enthalpies of formation, which are necessary for thermodynamic calculations are contained in the ICT-Thermochemical Data Base [5].

2.1 Calculated results of several explosives at constant volume conditions.

For the thermodynamic calculation of energetic materials we usually need the composition and the enthalpy of formation. Then we can decide if the calculation should be for conditions of a constant volume or of constant pressure. The main advantage for a constant volume calculation is that we can evaluate the heat of explosion. This holds for a loading density of 0,1 g/cm^3. Because this value can also be measured experimentally in a calorimetric bomb system at the same loading density, it is possible in this way to compare measured and calculated heat of explosions.

Usually, combustion reactions are dependent not only on the enthalpy of formation. In many cases, the oxygen balance of the energetic component or of the mixture influences much more the energy-output and gas formation. Table 1 contains the results of the calculation of several explosive substances with different oxygen (O_2) balances.

In our case, the O_2-balance is defined as the amount of oxygen we need for a complete combustion of 100g of a substance, or of a mixture of several energetic substances, into CO_2, H_2O and N_2, or in the case of chlorine or aluminium containing systems into HCl and Al_2O_3 etc. This holds for substances which need additional oxygen for a complete combustion. Therefore, the O_2-balance is negative in this case.

Only a few explosive substances exhibit a positive O_2-balance, such as nitroglycerine (+3,5%) or ammonium dinitramide (ADN) with +25,8%. For glycoldinitrate, the O_2-balance is zero.

In Table 1 we see roughly that the highest energy values of specific energy, of heat of explosion and even of the adiabatic temperature are produced during the combustion of substances having a positive or a small negative O_2-balance. But with the increase of the

negative oxygen balance, we see also, together with a decrease of the energy an increase of the mol number. This means that the gas formation of a more negative oxygen balance is normally higher than it is for a better O_2-balance.

We understand also that a combustion of substances with a very negative O_2 -balance such as benzene derivatives cannot be complete: The more CO and H_2 is formed, with a decease of CO_2, the more is the probability of a formation of free carbon, as we see from Table 1. In the same direction, temperature, pressure and both energy parameters are also decreasing.

We should remember, that the specific energy (E_S) can also be evaluated from measurements in a ballistic vessel. Its definition is

$$E_S = n * R * T_{EX}$$

This means that the specific energy is proportional with the gas formation n and the adiabatic temperature T_{EX}.

2.2 Energy of CL 20 with different amounts of PB – binder

The relationship between O_2-balance and energy parameters on the one side and gas formation on the other side will be much more clear when we compare the calculated results of the energetic substance Hexanitrohexaazaisowurtzitane, which we call CL 20, with different amounts of the polybutadiene binder (PB).

From Table 1 and Table 2 we see that CL 20 alone is more energetic than RDX by comparing temperature and heat of explosion. On the other side, combustion pressure and specific energy of RDX is higher. The reason for this behavior is the O_2-balance, which is much more negative for RDX. Therefore RDX produces more gas than CL 20, which increases the product $n * R * T_{EX}$ to a higher value of the specific energy, despite the fact that the adiabatic temperature of RDX is lower.

Together with the PB-binder, the oxygen balance and the enthalpy of formation decrease more and more which is connected with a decrease in pressure, temperature and the energy parameters. Only the mol number and therefore the gas formation increases. In addition, beginning with an O_2-balance of about –57%, the combustion reaction produces more and more carbon soot.

This behavior is typical for the combustion of energetic materials: In many cases we know from experimental investigations that carbon soot is formed from materials with O_2-balances which are more negative than –55%. But we should remember that combustion of energetic materials is very different from detonation processes [6]. In the case of a detonation, much higher pressures will result: they are about 338000 bar for RDX and 190000 bar for TNT. Therefore a lot of carbon monoxide (CO) produced reacts according to the Boudouard equilibrium with the formation of carbon soot and CO_2:

$$2\,CO \Leftrightarrow CO_2 + C; \quad \Delta H = -172{,}4\ kJ/mol$$

Therefore, the carbon soot formation in detonation processes is much higher than in combustion processes. Because of the high energy output of the Boudouard reaction, also the detonation heat is higher than in the case of combustion.

2.3 Energy of Solid Propellants

In connection with the performance of solid propellants, the energy output of some gun propellants is shown in Table 3. With decreasing O_2-balance, we compare energy and gas formation of the four conventional propellants

JA-2 double base propellant

A 5020 single base propellant

M1 single base propellant

P544 triple base propellant with nitroguanidine (Nigu).

with two nitramine containing propellants:

KHP 305 79% RDX, 8,0% TAGN, 13,0% GAP binder,

KHP 168 42,5% RDX, 42,5% Nigu, 4% KNO_3, 11% Polybutadiene binder (PB).

In addition, the energy parameters of RDX, TNAZ (1,3,3-Trinitroazetidine) and CL 20 are also listed in Table 3.

We see that with the decrease of temperature and specific energy the gas formation (mol number n) increases. But it is also of interest that the nitramine propellant KHP 305 containing RDX and a GAP binder exhibits a much higher specific energy (1338 J/g) than the double base propellant JA-2 (1141 J/g).

On the other side, the same composition with respect to RDX and TAGN, but with a polybutadiene binder instead of the GAP binder, produces a much lower specific energy and heat of explosion. The reason for this behavior is that the Glycidylazide Polymer (GAP) has a better oxygen balance (-121,1%) and a more positive enthalpy of formation (H_f = +141,0 kJ/mol), compared with polybutadiene HTPB: O_2-balance = -317,6% and H_f = +2,93 kJ/mol.

So we can conclude that nitramine propellants with GAP- binders exhibit a quite high energy, much higher than the conventional propellants based on nitrocellulose, nitroglycerine and nitroguanidine.

Even when we take into account explosives with the highest energy output, such as 1,3,3-Trinitroazetine (TNAZ) or Hexanitrohexaazaisowurtzitane (CL 20), the specific energy of the pure substances are quite similar to that of the GAP containing nitramine propellant KHP 305, as we see in Table 3.

2.4 Energy of Liquid Propellants

In order to increase the energy output of propellants markedly, we have to use liquid propellants as we see in Table 4:

Very high values of specific energies and of heats of explosion are produced from the hypergolic liquid propellants with hydrazine (N_2H_4) and unsymmetric dimethyl-hydrazine $NH_2 - N - (CH_3)_2$ (UDMH) as fuels and nitrogen tetroxide (N_2O_4) as an oxidizer.

We calculated the following specific energies:

50% N_2H_4 / 50% N_2O_4: 1636 J / g

35% UDMH / 50% N_2O_4: 1536 J / g.

It is clear that these energy values are much higher as the highest energy we can get from solid propellants. In this connection we should remember that the rocket motor of the Apollo 11 Spacecraft Vehicle landing on the moon in July 1969 used UDMH and N_2O_4 as rocket propellant.

The specific energies of the liquid propellants described are higher than those of gun propellants with a similar oxygen balance because of the higher amount of reaction products such as H2, N2 and H2O, and less carbon dioxide. In addition, a less negative enthalpy of formation leads to a higher heat of explosion (Table 5).

Also other fuels such as monomethylhydrazine (MMH) and triethanolamine (TEA) together with nitric acid (HNO_3) as an oxidizer develop quite high energies, see Table 4.

The final liquid propellant system NOS 365, consisting of hydroxyl ammonium nitrate (HAN), isopropylammonium nitrate (IPAN) and water is insofar of interest, as it was tested for a long time as a liquid gun propellant [7, 8]. This fuel combination has the main advantage that only CO_2, N_2 and water is being produced during combustion, without the formation of toxic CO.

2.5 Optimization of Gas Generators for Airbag Systems

Gas generators for airbag systems have to fulfill special requirements with respect to the quality of the combustion products. Especially, the amount of toxic components must be minimized and has to correspond to fixed toxicity limits. Therefore it is very helpful to reduce those toxic products, which can be calculated very accurately such as the CO and NO_X by optimization of the fuel / oxidizer ratio at the manufacturing process [9].

Table 6 makes clear, how the CO content in the reaction products of an airbag propellant consisting of 5-aminotetrazole (5-ATZ) and potassium nitrate (KNO_3) can be minimized only by changing the fuel / oxidizer ratio. We see that the O_2-balance is of great influence on the formation of CO, H_2 and NO. With the increase of the KNO_3 content, this means with improving the O_2-balance, the content of CO and H_2 decreases very strongly. On the other side, the formation of NO increases after attaining the minimum of CO with a further increase of the O_2-balance to positive values.

Therefore it is very important to meet special limits with regard to the fuel / oxidizer ratio during the manufacturing of the propellants for gas generators. Nevertheless, it is very important to measure all the toxic products experimentally by using special trace analysis detectors.

3. NONE EQUILIBRIUM COMBUSTION REACTIONS

Contrary to equilibrium reactions, it is not possible to calculate none equilibrium processes using thermodynamic codes, and for the reaction kinetic procedures, there are not enough correct data for the many reaction rates constants, which we need for a complete calculation of the reaction products. Therefore it is necessary to analyze the combustion products.

In this connection, a lot of investigations have been carried out at the Fraunhofer Institute to learn about the products of propellants, especially formed by low pressure burning [10]. As an example, the reaction behavior of the double base propellant JA-2 was investigated by burning under different pressures (Table 7), at first by burning in a closed vessel with a loading density of 100 g/l (high pressure burning), then by burning with a low loading density of 0,66 g/l. As a result, very different reaction products have been analyzed: The high loading density of 100 g/l leads to a reaction pressure of more than 1200 bar (see also Table 3), compared with only a few bar for the loading density of 0,66 g/l.

Especially of interest is the result of the analysis of the product gas, which was done by mass spectrometry and gaschromatography. The low pressure products are very different from the high pressure burning, which is very similar to the calculated gas composition: A high concentration of NO (18,9 mol%), HCN (1,1 mol%), and carbon soot (13,5 mol%), which are typical for none equilibrium products. There is also a large difference in the heat of explosion: 2488 J/g compared with 4550 J/g. These values have been calculated from the difference of the enthalpies of the reaction products and the propellant components.

A similar influence of the combustion pressure on the reaction products was found for other propellants and explosives such as single base and triple base propellants, but also for all the nitramine containing propellants [11].

4. CONCLUSION

Several explosives have been calculated thermodynamically by using the ICT-Code. It was shown that O_2-balance and enthalpy of formation are the most important parameters, which influence combustion temperature, specific energy, heat of explosion and gas formation.

By comparing the products of liquid propellants and solid propellants having the same O_2-balance, the reason was found why the liquid propellants investigated exhibit a higher specific energy compared with the conventional solid propellants based on nitrocellulose and nitroglycerine. This reason was the increased formation of H_2, N_2 and H_2O, producing much more gas with a lower mean molecular weight.

It was also shown that the ICT-Code is very useful for the optimization of gas generators for airbag systems, especially in connection with the avoiding of toxic products.

In addition it was explained that the limits of thermodynamic calculations are burning reactions at low pressures. In this case, a none-equilibrium burning is responsible for the formation of metastable reaction products, which are very toxic such as NO, N_2O, HCN etc. These products are also the reason that the energy-output is much lower than in the case of an equilibrium burning at pressures higher than 25 bar.

REFERENCES

[1] Zeleznik, F.J., Gordon, S.: An Analytical Investigation of Three General Methods of Calculating Chemical Equilibrium Compositions NASA-TN D-473, 1960

[2] Zeleznik, F.J., Gordon, S. A General IBM 704 or 7090 Computer Program for Computation of Chemical Equilibrium Compositions, Rocket Performance, and Chapman-Jouguet Detonations,NASA-TN D-1454, October 1962

[3] Volk, F., Bathelt, H., Hornberg, H.: Application of the Virial Equation of State in Calculating Interior Ballistics Quantities, Propellants and Explosives 1, (1976), 7-14

[4] The ICT-Thermodynamic Code (ICT-Code), User's manualReport 200626-7, June 2000, Fraunhofer Institut für Chemische Technologie (ICT), D-76318 Pfinztal

[5] Bathelt, H., Volk, F., Weindel, M.: The ICT-Database of Thermochemical Values, Sixth Update, 2001,Fraunhofer Institut für Chemische Technologie (ICT), D-76318 Pfinztal

[6] Volk, F., Schedlbauer, F.: Analysis and Post Detonation Products of Different Explosive Charges, Proceedings of the IV. Seminar "New Trends in Research of Energetic Materials", pp. 352-359, April 11-12, 2001, University of Pardubice, Faculty of Chemical Technology

[7] Leveritt, C.S. and Klein, N.: The Physical Properties and Molecular Structure of the HAN-Based Liquid Gun Propellants, 22nd Intern. Annual Conference of ICT, pp. 74-1-10, 1991

[8] Klein, N., Leveritt, C.S.: The Ignition and Combustion of Liquid Gun Propellants, 22nd Intern. Annual Conference of ICT, pp. 49-1-10, 1991

[9] Volk, F.: Utilization of Propellants for Inflator and belt Restraint Systems Paper for the 4th International Symposium on Special Topics in Chemical Propulsion: Challenges in Propellants and Combustion 100 Years After Nobel, Stockholm, Sweden, May 27-31, 1996

[10] Volk, F.: Analysis of Reaction Products of Propellants and High Explosives, Proceedings Third Symposium on Analysis and Detection of Explosives July 10 – July 13, 1989, Mannheim-Neuostheim Organized by Fraunhofer Institut für Chemische Technologie (ICT)

[11] Volk, F.: Reaction Products of Nitrocellulose and Nitramine Containing Propellants, 22nd International Pyrotechnics Seminar, Fort Collins, Colorado, USA, 1996

Table 1. Influence of Oxygen Balance on Energy Parameters of Explosives

Explosive	ΔHf kJ/kg	O_2-Balance %	Temperature K	Pressure bar	Spec. Energy J/g	Heat of Explosion J/g	Mol number mol/kg	Carbon weight%
Nitroglycerine	-1632	+3,5	3887	1240	1125	6671	31,91	-
Glycoldinitrate	-1596	0,0	3941	1313	1190	7289	32,88	-
Hexanitrobenzene	+420,7	0,0	4509	1283	1154	7203	25,85	-
Nitropenta	-1705	-10,1	3953	1333	1205	6306	34,79	-
CL-20	+921	-10,9	4347	1479	1323	6312	34,22	-
Pentanitrobenzene	-162,9	-13,2	4469	1345	1206	6094	29,69	-
BTTN	-1683	-16,6	3917	1390	1254	6022	37,28	-
TNAZ	+189,5	-16,7	4263	1515	1358	6343	36,39	-
RDX	+301,4	-21,6	4000	1541	1375	5647	40,26	-
NTO	-775	-24,6	2956	1064	945	3148	38,12	-
NC 13,4%N	-2390	-29,2	3388	1218	1094	4409	38,30	-
Nitroguanidine	-893	-30,7	2335	1057	932	3071	46,47	-
1,2,3,5-Tetranitrobenzene	+142,8	-31,0	4298	1431	1277	4941	34,73	-
1,2,3,4-Tetranitrobenzene	+300,2	-31,0	4374	1461	1304	5098	34,73	-
TAGN	-287,9	-33,5	2593	1321	1159	3974	51,90	-
NC 12,6%N	-2598	-34,5	3085	1157	1037	3983	39,69	-
Metriol trinitrate	-1666	-34,5	3497	1409	1260	5053	42,19	-
Nitromethane	-1853	-39,3	3043	1397	1245	4821	47,25	-
DEGN	-2227	-40,8	3083	1320	1178	4566	44,20	-
NC 11,6%N	-2859	-41,2	2683	1063	949	3480	41,17	-
PVN	-1152	-44,9	3388	1430	1269	4781	42,76	-
Tetryl	-69,9	-47,4	3468	1370	1208	4271	40,27	2,2
TATB	-541,4	-55,8	2218	961	838	3062	43,85	4,9
Trinitroaniline	-368,1	-56,1	2663	1096	960	3589	42,26	5,8
1,3,5-Trinitrobenzene	-204,2	-56,3	3017	1196	1050	3963	41,18	6,33
1,2,3-Trinitrobenzene	+25,5	-56,3	3193	1266	1112	4193	41,18	6,4
Triethyleneglycoldinitrate (TEGN)	-2619	-66,6	2025	1025	899	3317	47,50	-
2,4,6-TNT	-295,3	-74,0	2512	1033	908	3766	46,13	11,2
Z-Tacot	+1188	-74,2	3086	1036	924	4121	45,68	16,2
1,3-Dinitrobenzene	-161,8	-95,2	2304	881	782	3519	50,82	19,2
Isopropylnitrate	-2187	-99,0	1723	927	803	3126	53,86	4,1
Nitrobenzene	+78,9	-162,4	1771	590	537	2871	66,12	40,0
Propylene oxide	-2111	-220,4	1371	566	517	2415	74,67	35,2

Table 2. Energy Parameters of CL 20 with Different Amounts of PB

Explosive CL 20 / PB (weight %)	ΔHf kJ/kg	O_2- Balance %	Temperature K	Pressure Bar	Spec. Energy J/g	Heat of Explosion J/g	Mol number mol/kg	Carbon weight%
100 / 0	920,5	-10,95	4347	1479	1323	6312	34,22	-
95 / 5	898,9	-26,4	4206	1565	1392	5453	38,52	-
90 / 10	877,4	-41,8	3751	1550	1366	4780	41,28	-
85 / 15	855,8	-57,2	3167	1450	1263	4579	44,66	3,8
80 / 20	834,3	-72,7	2695	1253	1091	4435	48,23	8,3
75 / 25	812,8	-88,1	2517	1165	1018	4288	51,70	12,6
70 / 30	791,2	-103,5	2355	1083	949	4138	55,08	16,8
65 / 35	769,7	-119,0	2210	1005	884	3985	58,37	20,9
60 / 40	748,1	-134,4	2083	933	824	3829	61,58	24,9
55 / 45	726,6	-149,8	1973	867	769	3670	64,71	28,9

Table 3. Energy Output of Different Solid Propellants

Name	O_2-balance	T (K)	P (bar)	E_S (J/g)	n (mol/kg)	Q_{EX} (J/g)
JA-2	-30,35	3397	1271	1141	40,39	4622
A 5020	-39,67	2916	1131	1011	41,70	3759
M 1	-50,52	2494	1039	921	44,40	3247
P 544	-51,88	2009	907	799	47,83	2841
KHP 305	-35,49	3522	1515	1338	45,69	4828
KHP 305 PB	-61,05	2645	1337	1158	52,67	4098
KHP 168	-55,61	2180	1073	933	51,46	3281
RDX	-21,6	4000	1541	1375	40,26	5647
TNAZ	-16,6	4263	1515	1358	36,39	6343
CL 20	-10,9	4347	1479	1323	34,22	6312

Table 4. Liquid Explosives

	ΔHf kJ/kg	O_2-Balance %	Temperature K	Pressure Bar	Spec. Energy J/g	Heat of Explosion J/g	Mol number mol/kg
N2H4 / N2O4 50 / 50	683,6	-15,15	3725	1835	1636	6822	52,10
UDMH / N2O4 35 / 65	151,6	-29,33	3818	1726	1536	6246	46,87
MMH / HNO3 35 / 65	-1384	-19,51	3496	1572	1414	6076	48,03
TEA / HNO3 35 / 65	-3362	-20,7	3159	1255	1137	4973	43,0
NOS 365 HAN/IPAN/H_2O 60,7/19,3/20,0	-6144	0,01	2480	981	916	4647	44,28

Table 5. Combustion Products of MMH / HNO_3 Compared With the Gun Propellant JA - 2

Loading density: 0,1 g/cm³			
	MMH / HNO3		JA-2
	Analysis	Calculation	Calculation
Oxygen balance in %	-30,0	-30,0	-30,35
Composition in Vol%			
H_2	21,5	22,3	13,6
N_2	26,1	25,9	12,6
CH_4	0,7	0,9	0,6
CO	10,4	10,2	31,8
CO_2	4,7	5,6	18,8
H_2O	36,6	34,8	22,5
Heat of Explosion Q_{EX} (J/g)		5583	4609
Spec. Energy E_S (J/g)		1403	1139
Mol number n (mol / kg)		52,52	40,39
Mean molecular weight (g/mol)		19,04	24,76
Enth. of Formation (kJ/kg)		-1209	-2290

Table 6. Gas Generators Optimization

5-ATZ / KNO3 (weight %)	O_2-Balance %	Temperature K	Heat of Explosion J/g	Mol number mol/kg	CO mol %	H_2 mol %	NO mol %
47,00 / 53,00	-10	2070	3290	32,73	6,90	13,25	-
42,28 / 57,72	-5	2184	3536	30,46	3,86	7,34	-
38,49 / 61,51	-1	2291	3739	28,59	0,85	1,59	-
37,54 / 62,46	0	2300	3790	28,13	0,001	0,001	0,001
36,59 / 63,41	+1	2207	3664	27,85	-	-	0,027
32,80 / 67,20	+5	1843	3161	26,44	-	-	0,061
28,05 / 71,95	+10	1780	2473	22,51	-	-	0,085

Table 7. Reaction Products of Double Base GP JA - 2

(O_2-Balance: -30.2%)	Experiment		Calculation
Loading Density [g/l]	0.66	100	100
Combustion Condition	1 bar	Closed Vessel	-
Products [Mol %]:			
H_2	3.5	14.0	13.6
CH_4	1.0	-	0.7
CO	24.9	32.7	31.2
CO_2	7.0	17.0	19.0
N_2	1.3	12.4	12.6
NO	18.9	0.025*	-
HCN	1.1	-	0.004
NH3	0.8	-	0.08
H_2O	28.0	23.4	22.9
C solid	13.5	0.5	-
Q_{EX} [J/g]	2488	4550	4719
Kp (T)	28.45	3.215	2.765

*(NO)X - Analyzer w265a

non-equil.b equil.b

ENERGETIC MATERIALS FOR INSENSITIVE MUNITIONS

Richard Wild *

Diehl Munitionssysteme GmbH & Co. KG, Werk Maasberg, MML,
D-66620 Nonnweiler, Germany

Abstract:

Worldwide efforts are made to reduce the vulnerability of ammunitions and to bring Insensitive Munitions (IM) in use.
In the past, cure cast PBX was considered to be the only solution for acceptable IM compliant ammunition, especially in strongly confined warheads.
Some years ago we started to use special, pressed plastic bonded explosives for IM also in thick steel shells with IM results similar to cure cast filled warheads.
Basis for our pressed IM are less sensitive Plastic Bonded Explosives with RDX and HMX.
In this paper some of the parameters are discussed, we use to influence the sensitivity of ammunition by the high explosive, by the binder, by the preparation of the PBX and by the manufacturing process of the HE-charge.
The progress of the last 3 years in getting less sensitive moulding powders, can be demonstrated e.g. in the improvements of the impact sensitivity (BAM), in the better compacting behaviour of the granules and the higher initiation threshold of charges.
The Bullet Impact test with a cure cast and a pressed PBX was choosen for an IM comparison of both production methods.

Full paper version wasn't available till the deadline

HEAT CONDUCTIVITY MEASUREMENTS OF EXPLOSIVES

Stephan Wilker, Uldis Ticmanis and Gabriele Pantel

WIWEB Außenstelle Heimerzheim, Großes Cent, 53913 Swisttal, Germany

Abstract:

Chemical stability of explosives, especially nitrocellulose based propellants is of big interest, since from time to time propellant magazines blow off due to autocatalytical self-heating reactions. To avoid danger from exothermal reactions it is important to determine their temperature and time dependence. But as well the thermal transport properties of solid materials are a very important factor, since self-heating processes are only possible when the heat generation rate inside the material is faster than the heat transport to the surface.

In the past the determination of thermal transport properties of solid materials was a time-consuming and quite complicated job. Now, with a newly developed, so-called ‚Hot Disk' method these difficulties are overcome. This apparatus delivers reliable and fast results of heat conductivity and thermal diffusivity and thus of the heat capacity. The measuring principle bases on heating up the sample by 0,2 to 10 K and recording the temperature/time curve by the same sensor that generated the heat. By mathematical treatment of the T/t data the thermal transport properties are available. The sample must not necessarily be a homogeneous block. Also bulk materials and even liquids can be examined by this method. An independent check of the heat capacity by other method(s), e.g. DSC or microcalorimetry guarantees the correctness of the obtained data.

This paper describes the method, its advantages and limitations and gives an overview, how the data can be used for the prediction of the chemical stability of explosives and related items.

1. INTRODUCTION

The decomposition of explosives, especially of nitrate ester based propellants is still of big concern, as it is shown by different blow-offs of ammunition magazines or explosive factories in the last years [1]. The reason for this danger lies in the autocatalytic nature of the chemical reactions that are going on in the propellants. Although the addition of stabilisers usually prevents a blow-off there are still a lot of unstabilised materials around, e.g. during fabrication of propellants.

To make a correct prediction of the thermal runaway we modelled the chemical reactions and simulated the thermal safety [2] using a commercially available program based on the heat transfer model of THOMAS in an extended version of OPFERMANN [3]. The results of these calculations reveal that besides the kinetics of the chemical reactions, a second major influence comes from the thermal transport properties of a material, namely the heat conductivity. Table I summarises the results which were presented at the 32nd ICT conference (2001) [4].

Table 1. Influence of the parameters on critical conditions

Parameter	Influence
Maximum heat generation [μW/g]	Strong
Heat conductivity [W/(cm·K)]	Strong
Loading density [g·cm^{-3}]	Moderately strong
Heat transfer [W/(cm^2·K)]	Weak
Specific heat [J/(g·K)]	Negligible

These results were some kind of surprising, as it was thought before that the heat conductivity was not such an important parameter.

If one looks at literature data only few authors have measured heat transport properties of explosives [5-9]. This is probably due to the complicated and not very reliable methods which were used to determine these parameters in the past. So there are not enough data available in the literature. Because the influence of these parameters is so big it seemed to be necessary to be able to determine the heat conductivity by ourselves.

Just about that time we received the information about a new-developped method to measure the thermal transport properties of solid materials in a very convenient and fast way. This method is also able to determine these parameters on bulk materials and even on semi-liquids [10].

2. PRINCIPLE OF THE METHOD

The measuring principle bases on the so-called Transient Plane Source (TPS) method. This heated plane sensor consists of an electrically conducting thin wire (10 μm) made of Nickel within a thin layer (30 μm) of insulating material (Kapton or Mica). As fig. 1 shows two wires (one of them is acting as heater, the other is acting as resistance sensor) are formed as a double spiral which is sandwiched between two layers of insulating material. This method is called „HOT DISK" [11].

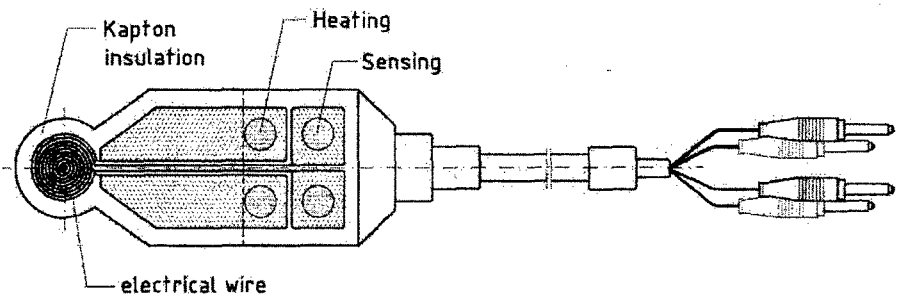


Fig 1. Schematic drawing of the sensor

How does this sensor work ?

It is placed between two pieces of a sample, with their plane surfaces towards the sensor. Then a small current is sent into the wire which causes a temperature increase of the sensor which then also induces a temperature increase of the contacting test material. This small temperature increase (0,2 K to max. 5 K) is measured by the temperature dependence of the resistance of the sensing wire, thus the heat source is placed close to the sensor which records the temperature changes as a function of time.

Before starting a measurement it should be checked that the atmosphere in the metering chamber is stable towards temperature and moisture changes and that the desks do not vibrate.

This method demands of course that the size of the sensor is definitively smaller than the sample itself. For this purpose many different sensor sizes, from 0.5 to 30 mm are available (all values refer to the radii of the wire spiral inside the sensor). It is also necessary to optimise the experimental parameters. Both the output power and the duration of the heating period (= measuring time) can be varied in a wide range. So, for each ‚new' system these conditions must be improved experimentally.

After the measurement (which usually lasts about one half to ten minutes) a mathematical treatment of data is performed, assuming the heat sink to have an infinite thickness. The computer program connected with the sensor calculates the thermal conductivity (λ) and thermal diffusivity (κ) per unit volume. The division of both parameters (λ/κ) delivers the volume specific heat capacity (C_p). If C_p is divided by the loading density of the material, the weight-specific heat capacity is available.

3. FURTHER OPTIONS AND OPPORTUNITIES

From the information given in chapter 2 it can be concluded that only solid, block shaped materials with more or less straight edges can be investigated. But it is also possible that bulk materials or semi-liquid (like rubbers, oils or pastes) and even materials can be analysed. To perform experiments with this kind of materials, special arrangements of the sensor within the material and specific, optimised values for the output power and the duration of the heating period must be found. How these parameters must be changed has to be checked individually for each new experiment.

It is also possible to determine heat transport parameters at other temperatures (up to 1000 K and down to 10 K). Some of these experiments demand other sensor types, but the measuring principle and the data evaluation is completely the same.

If only one sample block is available, a so-called ‚single-sided' experiment can be performed. In this case it is recommended to choose a comparable material on the other side of the sensor. The software can handle (small) differences in λ and κ and evaluate the λ and κ of the sample, but the accuracy of the values is worse compared to the measurement of two identical samples on both sides of the sensor.

4. THEORY

The theory of the method considers a three-dimensional heat flow inside the sample (which can be defined as infinite medium). The measurement must be terminated before the heat boundary reaches the boundaries of the sample.

A typical experimental result is shown in figure 2. It shows the temperature-time graph during the experiment. Each experiment contains 200 equidistant points. Some of them can be excluded from the data evaluation; usually the first 10-20 points are not used for the calculations. See also chapter 5.3.

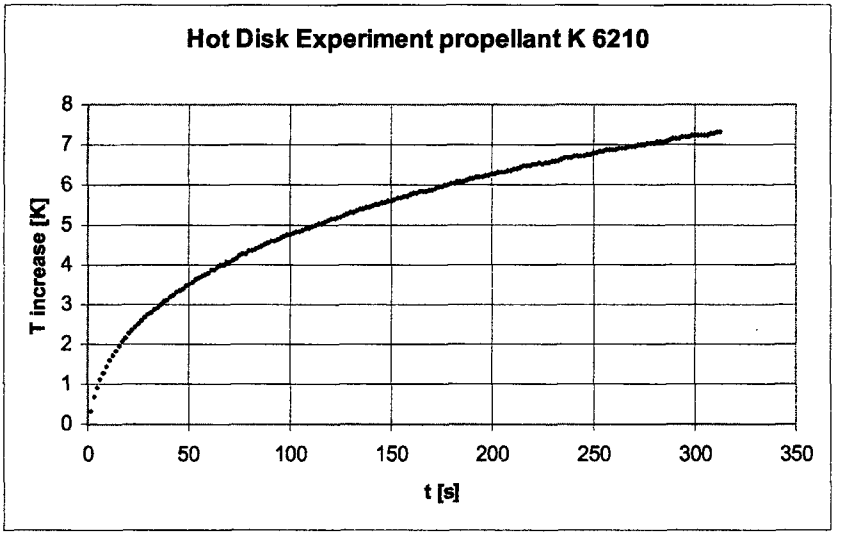


Fig 2. Typical experimental result (ball propellant K 6210)

A 'correct' experiment has a typical temperature increase as depicted in fig. 2. It mainly depends on the power chosen for the experiment. The temperature recorded in fig. 2 is the temperature of the sensor. How the temperature of the sample increases is pointed out in fig. 3.

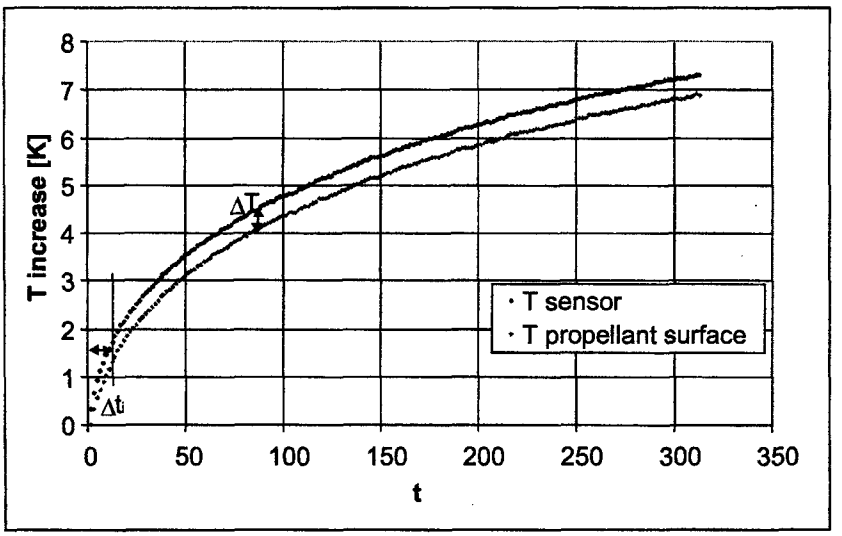


Fig 3. Temperature increase of the sensor and of the sample surface

The temperature difference ΔT between the sensor and the sample surface is – after a short induction period Δt_i – constant. The value of ΔT is a measure of how good the contact between the sensor and the surface is. The time Δt_i until it is reached can be estimated by

$$\Delta t_i = \frac{\delta^2}{\kappa_i}$$

with δ = thickness of the insulating layer and κ_i = thermal diffusivity of the layer material.

The time dependent temperature increase is given by

$$\Delta T(\tau) = \frac{P_0}{\pi^{\frac{3}{2}} * a * \lambda} * D(\tau)$$

where P_0 is the total output of power from sensor (this can be changed individually for each experiment), a is the radius of the disk (there are seven different sizes available), λ is the thermal conductivity and $D(\tau)$ is a dimensionless time dependent function. This variable is defined as

$$\tau = \sqrt{\frac{t}{\Theta}}$$

with t = measuring time and Θ = „characteristic time" (a^2/κ).

The program then starts a plot of the temperature increase ΔT versus $D(\tau)$. A straight line is received with an intercept ΔT_i and a slope $\frac{P_0}{\pi^{\frac{3}{2}} * a * \lambda}$, if measuring times are much longer than Δt_i.

The parameter κ and thus Θ are not known. The program iterates the straight line of the plot from which λ is obtained.

It seems thus to be a little difficult to obtain all the important data like λ or κ by iteration. How can one be sure that the calculated values are correct ?

There are several opportunities to check the correctness of the data. Because the ratio λ/κ is the heat capacity (C_p) of the material there is a good possibility of an independent check of the obtained data, for example a measurement of C_p by DSC [5] or by microcalorimetry [12]. In addition the evaluation program delivers further information about the ratio τ and the temperature increase during the measurement. These indicators and information about the standard deviation of the data points against the theoretical straight line allow a qualitative estimation whether the data are reliable or not.

At last a measurement of standard samples demonstrates the usability of this method. We measured NIST standards (polystyrene blocks) and we found the same λ values as indicated on the package. The reproducibility was very good; the standard deviation was below 1% (17 measurements were perfomed).

A ‚fine tuning' of the evaluation is possible by changing the number of evaluated data points. Usually the first ten or fifteen data points are withdrawn which increases the quality and the reliability of the data markedly. How this influences the results is discussed in chapter 5.3.

5. RESULTS

Influence of input parameters

The influence of the output power and the measuring time on the obtained data are great. In the following examples heat conductivity measurements of a PBX cylinder were performed with a wide variation of output power and measuring time. Figures 4 and 5 show the effects of these parameters on λ, κ and C_p.

The correct value for C_p per unit volume lies in the range of 1,65 to 1,7. With a density of the material of 1,5 g/cm³. This helps to prove how reliable the experimental results are.

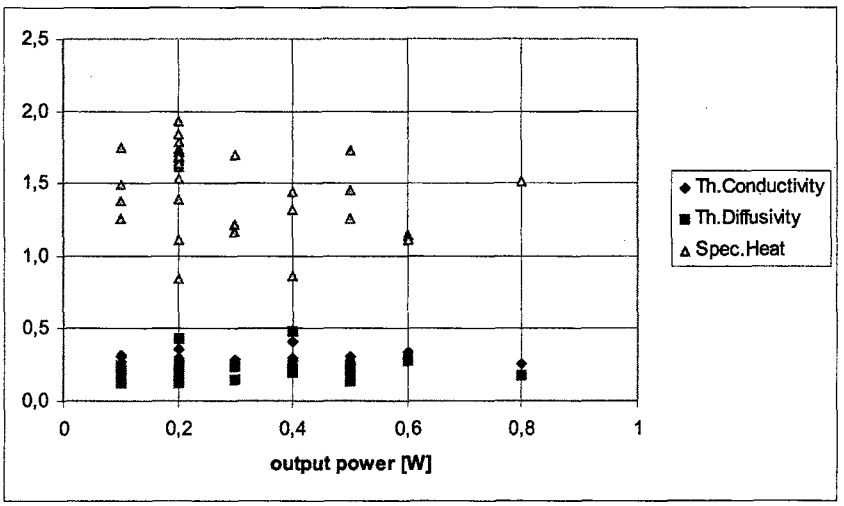


Fig 4. Dependence of λ, κ and C_p from output power (PBX material); measuring time between 5 and 640 s.

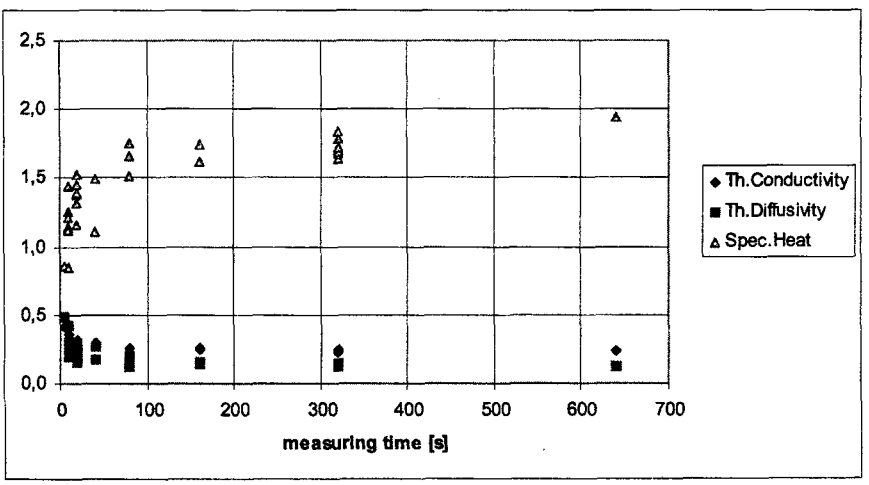


Fig 5. Dependence of λ, κ and C_p from measuring time (PBX material); output power between 0,1 and 0,8 W.

There no significant dependence of λ, κ and C_p on the output power. Correct C_p values can be found either at 0,1, 0,2, 0,3 and 0,5 W. So this parameter does not play an important role for the obtained results.

Figure 5 shows the importance of the parameter ‚measuring time'. Measuring times below 80 seconds lead to definitively too low values for C_p, mainly due to too high values of κ. The values of λ are less dependent on the measuring time, indicating that this parameter is more robust towards changes in the experimental conditions.

This guideline is of course valid for organic materials of bigger dimensions and a low conductivity. For thin samples or materials of high conductivities like metals considerably shorter times should be used.

The reason for this behaviour lies in the evolution of the heated zone within the sample. If this zone is too small (red area, A), the temperature increase is very small and the ratio of measuring time to Δt_i is small. This leads to high values of κ and thus C_p is small. The computer program gives hints in this case. If t/τ is too small, then the effusivity and not κ is measured. The violet area B represents an optimised experiment. The shape of this area is a little bit comparable to a p-electron orbital. If the measuring time is too long, the shape of the heated zone is more sphere-like; in this case the evaluation method is not exactly valid. It must also be stated that the heated front should not reach the closest outer surface of the material.

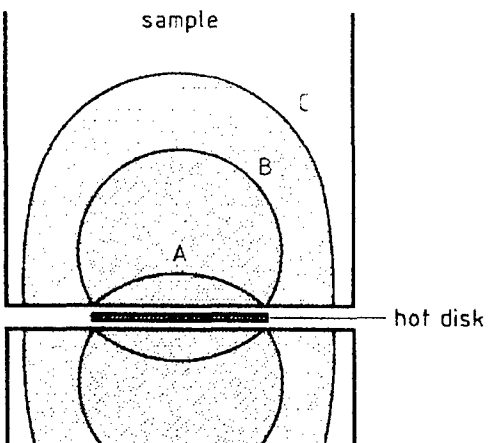


Fig 6. Evolution of the heat front in a sample

Table 2. Dependence of λ, κ and C_p from the input parameters ‚output power' and ‚measuring time' (double base rocket propellant plates)

Output power	Measuring time	Energy	Thermal Conductivity	Thermal Diffusivity	Specific Heat
[W]	[s]	[J]	[W/(m·K)]	[mm²/s]	[J/(K·cm³)]
0,15	80	12	0,239	0,123	1,942
0,20	80	16	0,260	0,129	2,015
0,15	160	24	0,250	0,125	2,008
0,05	**320**	**16**	**0,308**	**0,330**	**0,931**
0,10	320	32	0,243	0,137	1,780
0,15	320	48	0,255	0,130	1,961
0,15	320	48	0,242	0,125	1,928
0,15	320	48	0,257	0,137	1,875
0,15	320	48	0,255	0,131	1,950
0,20	320	64	0,256	0,131	1,948
0,25	320	80	0,247	0,119	2,071
0,25	320	80	0,248	0,122	2,034
0,30	320	96	0,253	0,135	1,880
0,40	320	128	0,254	0,130	1,954
0,50	**320**	**160**	**0,259**	**0,152**	**1,705**
0,50	320	160	0,255	0,125	2,037
0,15	**640**	**96**	**0,254**	**0,188**	**1,350**

Comment to table II: Values marked in bold show too high values for κ and thus too low Cp values.

Influence of sample design

The thermal transport properties are properties of the material itself. But, depending on the contact area the overall transport properties of the bulk material may considerably differ from those of the compact material. To study this in more detail we looked at thermal conductivities of a double base ball propellant (K6210), of a 8 mm thick plate of a double base rocket propellant 1 (91DBE470) and of a big cylinder-shaped double base rocket propellant 2 (D7100), all three with a roughly comparable chemical composition. In addition the thermal transport properties of a single base porous propellant (W6663) are included in table IV.

In a pre-study series we optimised the input parameters for the ball propellant, the porous propellant and for the two rocket propellants. Table III shows the optimised input parameters and the geometrical data of the sample material.

If bulk materials are measured there is a significant influence on the λ and κ values which is depending on the bulk density of the material. A lower bulk density is equivalent to a higher amount of air between the grains which lower the heat conductivity significantly.

Thus multiple determinations on bulk materials may differ from each other when not the same bulk density of the material is achieved.

Table 3. Optimisation of input parameters for the determination of thermal transport properties of nitrocellulose based propellants

Sample	Sample size and geometry	Sensor diameter [mm]	Output power [W]	Measuring time [s]
DB ball propellant	Small grains (1-5 mm). Measurement in a 250 mL beaker	9,734	0,10-0,15	160-320
SB porous propellant	T shaped propellant (grain dimensions 0,3-1,5 mm). Measurement in a 250 mL beaker	9,734	0,025	50-80
Rocket propellant 1	Big plate (170·400 mm; thickness 8 mm)	9,734	0,15-0,30	160-320
Rocket propellant 2	Cylinder (105 mm diam., 80 mm height; inner diam. 35 mm)	9,734	0,15-0,20	160

Table 4. Thermal transport properties of nitrocellulose based propellants

Sample	Heat conductivity λ	Thermal diffusivity κ	Heat capacity C_p
	[W/(m·K)]	[mm²/s]	[J/(K·cm³)]
Ball propellant	0,11	0,12	0,95
Porous propellant	0,10	0,21	0,48
Rocket propellant 1	0,25	0,13	1,94
Rocket propellant 2	0,25	0,15	1,73

This table shows that the heat conductivity rises by the factor of 2,5 when the material is a solid homogeneous block. This table also reveals that κ is increasing with increasing porosity of the material.

Table 5. Input parameters for the determination of thermal transport properties of other explosive materials

Sample	Sample size and geometry	Sensor diameter [mm]	Output power [W]	Measuring time [s]
PBX A	Cylinders of 45 mm diam. and 100 mm height	9,734	0,20-0,30	160-320
PBX B	Cylinders of 21 mm diam. and 50 mm height	3,3	0,10-0,50	40
PBX C	Cylinders of 21 mm diam. and 40 mm height	3,3	0,05-0,30	10-40
composite	Cylinders of 30 mm diam. and 15 mm height	3,3	0,05-0,08	15-30

rocket prop.				
HTPB binder	Cylinders of 50 mm diam. and 15 mm height	9,734	1,6	160-640

Table 6. Thermal transport properties of other explosive materials

Sample	Heat conductivity λ	Thermal diffusivity κ	Heat capacity C_p
	[W/(m·K)]	[mm²/s]	[J/(K·mm³)]
PBX A	0,24	0,14	1,70
PBX B	0,25	0,11	2,17
PBX C	0,58	0,34	1,71
composite rocket propellant	0,83	0,41	2,02
HTPB binder	0,33	0,20	1,65

Note:
PBX A is a pressed HTPB based high explosives with RDX as energetic component
PBX B are pressed Hytemp based high explosives with RDX as energetic component
PBX C is a cast-cured HTPB based high explosive with RDX as energetic component

This table demonstrates that cast-cured materials have much higher λ than pressed materials of comparable composition. Also the filling materials (PBX C and composite propellant contain energetic crystalline material, whereas the HTPB binder (same material) has no filling) have a big influence on λ and on κ.

Influence of evaluation method

As mentioned in chapter 4 it is possible to choose all 200 data points for an evaluation. But in practice it is useful to select the range, by excluding some of the points from calculation. Especially the first 10-20 points are strongly influenced by the heat transport through the contact area and do not describe the evolution of the heat front in the sample.

In figures 7 and 8 it is demonstrated that most of the data points can be excluded without a great effect on the results. This indicates a ‚good' measurement, where most of the data points fit well into the same straight line. If this is not the case, and the calculated values for λ, κ and C_p vary in a wide range when only a few more points are excluded from the evaluation, then the measurement must be repeated with a new set of input parameters.

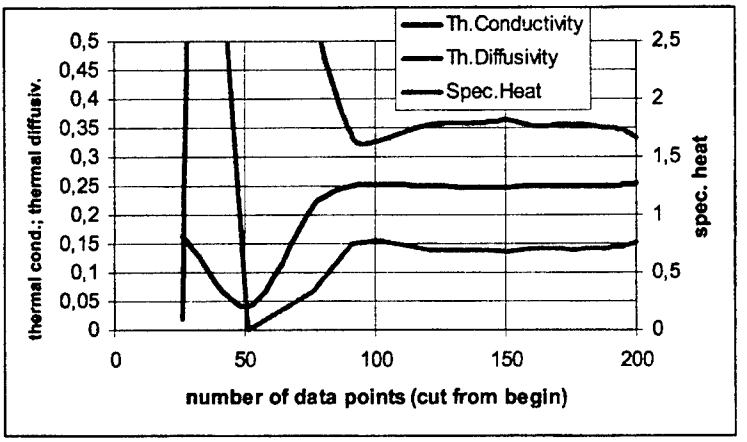


Fig 7. Dependence of λ, κ and C_p from number of evaluated points (PBX material)

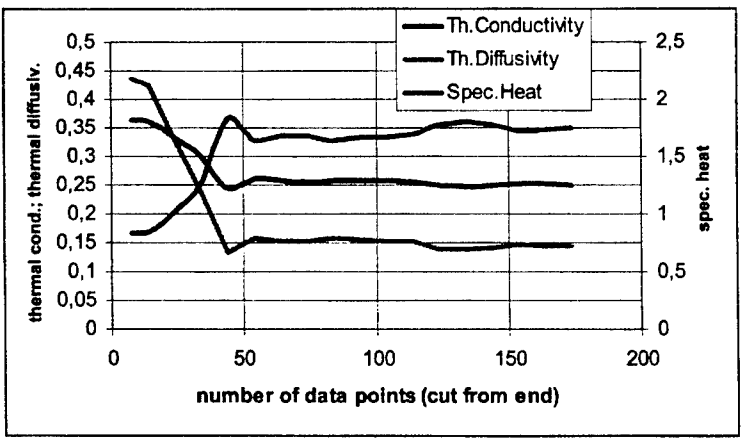


Fig 8. Dependence of λ, κ and C_p from number of evaluated points (PBX material)

Comparison with thermal transport properties data from literature

It is of big importance that the values of λ, κ and C_p are in good correlation with data from literature. As mentioned in the introduction there is not a big data set available, most because the determination of thermal transport properties data is quite difficult. Neverteheless, some authors have measured λ, κ, C_p or all three of them by different methods. Table VI lists the most important figures. Some of the data had to be re-calculated to fit into the SI unit system. It is also necessary to mention the temperature, at which the data were achieved, because the thermal transport properties are temperature-dependent. Some of the references contain the function with which the data at other temperatures can be calculated.

Table 7. Review of literature data

Compound	λ [W/(mK)]	κ [mm²/s]	C_p [J/(cm³K)]	C_p [J/(gK)]	Method	meas. T [°C]	Ref.
Gun propellants							
M10	0,31	0,18	1,75	-	Hot disk analogon	23	6
A5020	0,1322	-	-	1,065	Hollow cylinder	25	14
DB	-	-	-	1,56	HFC	77	11a
DB	0,220	-	-	-	HFC	25	13
M9	0,30	0,13	2,23	-	Hot disk analogon	23	6
JA2	0,29	0,13	2,23	-	Hot disk analogon	22	6
X-14	0,418	-	-	-	mod. DSC	60	5c
K6210	0,135	-	-	1,207	Hollow cylinder	25	14
L5460	-	-	-	1,370	DSC	25	14
TB	-	-	-	1,48	HFC	77	12a
P5430	0,125	-	-	1,417	Hollow cylinder	25	14
Q5560	0,144	-	-	1,185	Hollow cylinder	25	14
M30	0,45	0,15	3,07	-	Hot disk analogon	24	6
XM39	0,25	0,13	1,86	-	Hot disk analogon	22	6
DB rocket propellants							
Different types	0,21-0,24	-	-	-	Thermo -conductometry	48	8a
Composite propellants							
HTPB	0,186	0,137	1,36	-	Hot Disk	25	9
HTPB + NaCl	0,422	0,235	1,85	-	Hot Disk	25	9
HTPB	0,192	0,117	1,65	-	Hot Disk	25	9
HTPB + KCl	1,250	0,656	1,92	-	Hot Disk	25	9
HTPB + KCl	1,070	0,770	1,39	-	Hot Disk	25	9
High explosives and single components							
Comp. B3	0,219	-	1,88	1,14	Hot plate	37	5a
PBX 9010	0,215	-	1,96	1,13	Hot plate	37	5a
PBX 9404	0,385	-	1,86	1,05	Hot plate	37	5a
RDX	-	-	1,89	1,08	Hot plate	37	5a
RDX	0,289	-	-	1,13	DSC	25	14
HMX	-	-	1,95	1,05	Hot plate	37	5a
TNT	0,203	-	-	-	HFC	25	13
TNT	-	-	1,89	1,18	Hot plate	37	5a
PETN	-	-	1,92	1,12	Hot plate	37	5a
NQ	0,425	-	-	1,199	DSC	25	14
NQ	0,424	-	2,02	1,23	Hot plate	37	5a

Explanation to table 7.

It is not possible to give all sample and measurement details in this little overview. The reader is asked to have a look into the original literature for more details, especially of bulk densities and sample sizes.
- not measured or not reported
M10 and A5020 are single base (SB) propellants
M9, JA2, X-14, K6210 and L 5460 are double base (DB) propellants
P5430, Q5560 and M30 are triple base (TB) propellants
XM39 is an RDX containing propellant
All „composite propellants" are „dummy" propellants (not containing high explosives) but with a typical HTPB binder (IPDI hardened)
Comp. B3 contains RDX (60%) and TNT (40%); PBX 9010 (Kel-F-based) contains 90% RDX; PBX 9404 (NC/CEF based) contains 94% HMX

6. DISCUSSION

The literature data of λ, κ and C_p show a wide variety of values, which demonstrate the principal difficulty of the determination of these thermal constants. In general the values of the propellants (which are mostly small grains) vary much more than those of bigger blocks of high explosives or composite propellants, although λ lies in the same magnitude. If we use the C_p values as a guideline then we can distinguish between reliable results and those who may be wrong. But this is only possible if bulk densities are known. This table also shows that many different methods may lead to comparable results, although the TPS (Hot Disk) delivers three parameters in one fast experiment and is thus much more ‚effective' than DSC or Laser flash experiments.

But the Hot Disk can not measure any type of material. Its application ends when inhomogeneous samples are to be measured. In this case it is – depending on the severity of the inhomogenities – hardly possible to detect the thermal transport properties of the pure material. But this can be turned into a big advantage: Because inhomogenities (e.g. lunkers in a composite propellant) lead to a variation of the heat transport properties, Hot Disk is able to detect inhomogenities in a big block of material by the change of λ and/or κ at different spots, which are hardly detectable by any other method.

There are also difficulties to measure samples with a high content of volatiles. During the measurement the material may be dried, but as a consequence, its thermal constants will change as well. But this problem is as well present with any other method mentioned in the literature. Also it is problematic when the sample size is very small. The smallest sensor has a radius of 0,492 mm so the minimum sample size is at least 2 mm.

If the sample size is uneven or if bulk material has to be measured the quality of the measurement may be insufficient. This is mainly due to an undefined contact from the sensor to the sample. But Hot Disk can handle these difficulties much better than any other method mentioned in literature (Laser Flash method e.g. requires polished samples!). It should also be mentioned here that the sensors are quite sensitive towards mechanical damage. A regular check with standard material is recommended.

But in most other cases this new method is very useful and the range of measurable sample types and dimensions is much bigger than with any other method.

7. CONCLUSION

The Hot Disk method is a fast and reliable method to determine the thermal transport properties of explosives. This method does not only have the advantage of a very quick determination of these values; at least as important is the fact that not only solid homogeneous materials can be measured but also bulk materials and even fibers can be measured. Concerning the last two types of materials it must be noticed, that the bulk density and the quality of the contact between sensor and the sample plays an important role on the results. A knowledge of (volumetric or specific) Cp is helpful for the check of the correctness of the evaluated data.

With a little experience it is fairly easy to select optimised input parameters (output power and measuring time) and to choose the correct number of data points for evaluation. This enables the method to become a routine method for a big number of samples of the same type. On the other hand, the wide thermal conductivity range from 0.005 W/(mK) to 500 W/(mK) allows the application of this method for nearly any kind of material.

Acknowledgements

Many thanks go to Dr. Jörg Kübel from C3 Analysentechnik GmbH for fruitful discussions and many hints for better sample handling, for an optimised measuring technique and for the full use of the software features.

REFERENCES AND NOTES

[1] J.-I. Kimura, „Explosion in a Magazine in Tokyo Suburbs on August 12, 2000", *Symp.Chem. Probl. Connected Stabil. Explos.* 12, **(2001)**, in press; I. Tukkanen, „Ammunition Depot Accident in Finland, July 1999", *Symp.Chem.Probl. Connected Stabil. Explos.* 12, **(2001)**, in press.

[2] STANAG 4582, „Explosives, Nitrocellulose Based Propellants, Stability Test Procedure and Requirements using Heat Flow Calorimetry", Final Draft **(02/02)**, U. Ticmanis, G. Pantel, M. Kaiser, „Simulation der chemischen Stabilität eines zweibasigen Kugelpulvers", *2. Int. Workshop Mikrokalorimetrie WIWEB*, p. 182-195 **(1999)**.

[3] P.H. Thomas, *Trans.Faraday Soc.* 54, 60-65 **(1942)**, J. Opfermann, Manual for the Computer Program „Netzsch Thermal Safety Simulation", Edn. **2001**.

[4] U. Ticmanis, G. Pantel, S. Wilker, M. Kaiser, „Precision required for parameters in thermal safety simulations", *Int. Annu. Conf. ICT*, 32, **(2001)**.

The usual method for the determination of C_p of explosives is DSC, see e.g.

[5a] J.F. Baytos, „Specific Heat and Thermal Conductivity of Explosives, Mixtures, and Plastic-Bonded Explosives Determined Experimentally", Techn. Report Los Alamos Scientific Laboratory LA-8034-MS;

[5b] W.P. Brennan, B. Miller, J.C. Whitwell, „Thermal conductivity measurement with the differential scanning calorimeter", *J.Appl.Polym.Sci.* 12, 1800-1802 **(1968)**;

[5c] W.W. Hillstrom, „A Method for the determination of thermal conductivity of propellant materials by DSC", *Proc. Intern.Pyrotech.Sem.* 6, 260-272 **(1978)**;

[5d] T. Boddington, P.G. Laye, „The measurement of thermal conductivity by DSC", *Thermochim. Acta* 115, 345-350 **(1987)**;

[5e] W.W. Hillstrom, „Thermal conductivity of hazardous materials by DSC", *Proc.Intern.Conf.on Thermal Conductivity* 16 (**1979**).

A method similar to the Hot Disk method is described in:

[6] M.S. Miller, A.J. Kotlar, „A new technique for the simultaneous measurement of thermal diffusivity and thermal conductivity of small energetic-material specimens", *USArmy Report* ARL-TR-1321 (**1997**); M.S. Miller, „Thermophysical Properties of Six Solid Gun Propellants", *USArmy Report* ARL-TR-1322 (**1997**).

The Laser flash method to determine κ is described by several authors:

[7] A. Degiovanni, „Correction de longueur d'impulsion pour la mesure de la diffusivité thermique par méthode ‚flash'", *J.Heat Mass Transfer* 30, 2199-2200 (**1987**); A. Degiovanni, „Diffusivity and the flash method", *Rev.Gen.Thermique* 185, 417-419 (**1977**); M. Roux, P. Gillard, F. Marlin, C. Brassy, „Diffusivité thermique de substances explosives", *Rev.Gen. Thermique* 380-381, 427-432 (**1993**); D. Maillet, S. André, A. Degiovanni, „Les erreurs sur la diffusivité thermique mesurée par méthode ‚flash': Confrontation théorie-expérience", *J.Phys. III France* 3, 8783-909 (**1993**).

Other methods for the determination of λ, κ or C_p of explosives are published by:

[8a] Plomann, Kraft, „Bestimmungsmethoden der Wärmeleitfähigkeit von Festtreibstoffen", *E 91-Bericht* 272/64 (**1968**);

[8b] Hu Rongzu, Chen Xuelin, Chu Shijin, Li Nan, Qin Jiao, Yan Zhe, „A new method of determining the thermal conductivities of energetic materials by microcalorimeter", *J.Thermal Anal.* 42, 505-520 (**1994**);

Another method for the simulatneous determination of λ and κ is dynamic AC calorimetry, see:

[8c] A.A. Minakov, Ju.V. Bugoslavskij, C. Schick, „Dynamic heat capacity measurements in advanced AC calorimetry", *Thermochim.Acta* 342, 7-18 (**2000**).

[9] T. Ericson, L. Hälldahl, R. Sandén, „A facile method for the study of thermal transport properties of explosives", *Symp.Chem.Probl.Connected Stabil.Explos.* 11, 185-190 (**1998**).

[10] Further reports about the TPS (Hot Disk) method are mentioned in: S.E. Gustafsson, „Transient plane source (TPS) Technique for thermal conductivity and thermal diffusivity measurements of solid materials", *Rev. Sci. Instrum.* 62, 797-804 (**1990**); M. Gustafsson, E. Karawacki, S.E. Gustafsson, „Thermal conductivity, thermal diffusivity, and specific heat of thin samples from transient measurements with hot disk sensors", *Rev. Sci. Instrum.* 65, 3856-3859 (**1994**); T. Log, S.E. Gustafsson, „Transient plane source (TPS) technique for measuring thermal transport properties of building materials", *Fire and Materials* 19, 43-49 (**1995**); L. Hälldahl, „New technique for thermal analysis", *Symp.Chem.Probl.Connected Stabil.Explos.* 10, 29-34 (**1995**); B.M. Suleiman, S.E. Gustafsson, L. Börjesson, „A practical cryogenic resistive sensor for thermal conductivity measurements", *Sensors and Actuators* A 57, 15-19 (**1996**); F.B. Andersen, L.F. Juhl, „Measurement and theoretical considerations of thermal conductivity of high temperature insulating materials", *Skamol Insulation Application note* (April **1997**).

[11] L. Hälldahl, „Hot Disk Thermal Constants Analyser", Instruction Manual **1999**.

[12a] P.F. Bunyan, „A Technique to measure the specific heat of reactive materials by heat flow calorimetry", *Thermochim.Acta* 130, 335-344 (**1988**);

[12b] B. Löwen, U. Meier, S. Schulz, „Heat capacity measurement of bulk or inhomogeneous materials", *Thermochim. Acta* 229, 111-118 (**1993**);

[12c] B. Löwen, S. Schulz, J. Seippel, „Heat capacity measurements by calibration with dynamic correction of the calorimetric output signal of a thermopile heat conduction calorimeter", *Thermochim. Acta* 235, 147-152 (**1994**).

[13] M. Roux, F. Marlin, C. Brassy, P. Gillard, „Numerical determination of the thermal diffusivity and kinetic parameters of solid explosives", *Propellants, Explosives, Pyrotechnics* 18, 188-194 (**1993**).

[14] G. Krien, „Thermische Analyse von Explosivstoffen", unpublished collection of thermoanalytical data of explosives, *BICT* **1989**.

EFFECT OF MOLDING POWDER PRODUCTION, CHARGE PRESSING AND AGING ON PARTICLE SIZE OF EXPLOSIVES *

Shu Yuanjie, Dong Haishan, Liu Shijun, Liu Yonggang, Song Huajie, Hao Ying, Zhan Chunhong and Chen Jie

Institute of Chemical Materials CAEP, 621900, Mianyang, Sichuan, China

Abstract:

Influence of such processes as molding powder production pellets pressing and aging under different conditions on TATB HMX particle size was experimentally studied. The results obtained showed that particle size of these explosives was greatly changed before and after molding powder production but for different size grade of explosive this change was not the same; pressing process had great effect on explosive particle size also, but before and after ageing process explosive particle size did not change seriously.

Keywords: *Molding powder production, Pressing, Ageing, Particle size, Explosive*

1. INTRODUCTION

Influence of particle size of explosive on energy release, safety performance, detonation performance, mechanical intensity and shell life of the explosive formulation is obvious. Hyoun - Soo Kim[1] pointed out that explosive particle size had great effect on the mechanical performance of explosive formulation when he studied the methods improving mechanical properties by neutral polymer coupling agent. The reason is that the dewetting workτa is the function of explosive particle size .

$$\tau a = 4\pi C_{\tau a} E/3r$$

where $C_{\tau a}$ is the fracture energy per unit area, E- modulus, r- average particle size.

M.J.Gifford et al[2] demonstrated that ultrafine PTEN was more sensitive to [1]short pulse shock wave (laser flyer)than conventional PTEN, while to long pulse (gap test), the result was converse. They also found that explosive particle size greatly affected the properties of deflagration-to-detonation transfer. So, particle size of explosive is one of main factors which should be considered while studying explosive formulations and production process designing.

In this paper effect of such processes as molding powder production, pellets pressing, aging etc on particle sizes of TATB and HMX was studied in order to learn how these processes affect the performance of explosive formulation.

* This project is supported by key fund of CAEP

2. EXPERIMENTAL

2.1 Explosive preparation

TATB (fine TATB, called f-TATB below) was made by ourselves, its average particle size was about 16μm. TATB was milled mechanically (micron TATB, called m-TATB)32hours and average particle size was about 6.2μm. Sub micro TATB was obtained by gas-flow milling and average diameter of which was about 0.5μm (submicron TATB, sub m-TATB).

Fine HMX (named f-HMX) was commercial product , its average diameter was about 16μm; f-HMX was milled mechanically 32hours and its average particle size became 6.7μm (called micron HMX, m-HMX).

2.2 Molding powder production

Binder used was Fluororesin F which could be bought commercially. The molding powder production method was: fluororesin was dissolved by ethyl acetate, then added to mixture of explosive and water at a certain rate. The mixture was agitated, heated. When the diameter of powders was close to the needed value, filtered it and dried it.

2.3 Pellet pressing

The pellet used to study the particle size change of explosive before and after pressing is pressed by machine. Pressing parameters as temperature, pressure and time of keeping pressure were changed to learn the effect of pressing conditions on particle size of explosive.

2.4 Analysis of Particle size

Ethyl acetate and THF were used to dissolve fluororesin in molding powder and pellet. After that, filtered the mixture and measured explosive particle size with Laser particle apparatus.

3. RESULTS AND DISCUSSION

3.1 Explosive particle size obtained by different methods

Explosive particle size obtained by different methods was listed in table 1.

Table 1. Average particle size of TATB and HMX μm

Type	TATB	HMX
Fine	16.45	16.32
Micron	6.164	6.729
Submicron	0.490	/

3.2 Effects of molding powder production on explosive particle size

3.2.1 The particle size change after molding powder production

Molding powder of Several particle grades TATB and HMX were produced and analysis results of particle size were listed in Table 2 and Fig.1.

Table 2. Particle size of TATB, HMX before and after molding powder production

Sample	particle size□μm□	
	Before	After
F-TATB	16.45	13.20
M-TATB	6.164	7.590
Sub m-TATB	0.490	0.779
F-HMX	16.32	34.94
M-HMX	6.729	10.15

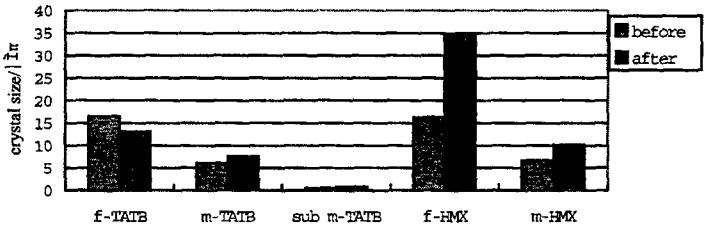


Fig 1. Crystal particle size of TATB and HMX before and after molding powder production

From this table it could be seen that: particle diameter of F-TATB became smaller after production; but the growth of M-TATB and SUB M-TATB was quite large after production; especially submicron TATB grew very seriously.

The crystals sizes of F-HMX grew up twice and M-TATB grew up 1.4 times after becoming molding powder.

3.2.2 Effect of production process conditions on diameter of explosive

The results of effect of production process conditions (temperature , concentration of binder) on diameter of explosive were listed in Table 3 and fig.2.

Table 3. Effects of different molding process conditions to diameter of explosive

Conditions	TATB /μm			HMX /μm	
	P	M	G	P	M
T=70□, C=4%	13.20	7.716	0.490	34.94	9.743
T=70□, C=5%	10.29	7.590	0.779	/	10.15
T=80□, C=4%	12.00	8.736	0.569	47.08	10.49
T=80□, C=5%	13.93	7.373	/	34.85	9.315

Notes: T-bath temperature C- binder concentration

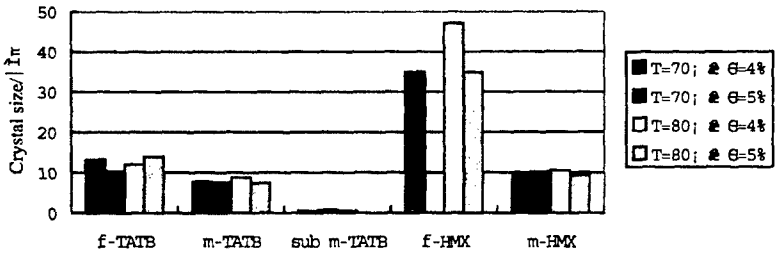


Fig.2. Effect of molding powder production parameters on explosive crystal size

Results showed that production conditions had some effect on gas-flow milled TATB, but there were almost no influences on other explosives.

3.3 Effect of pressing on particles size of explosive

Effect of different pressing conditions (pressure, rate of exerting pressure,temperature) forϕ20mm x 20mm pellets on explosive particle size was studied.

3.3.1 Effect of pressure

Results of effect of pressure were shown in Table 4.

Table 4. Effect of pressing on explosive particle size

Name	Condition	Particle size (μm)
F-HMX	45KN	21.41
F-HMX	55KN	12.91
F-HMX/F	80KN	14.89
F-HMX/F	100KN	10.25
M-HMX/F	80KN	8.001
M-HMX/F	90KN	7.486
F-TATB	85KN	8.341
F-TATB	105KN	7.420
F-TATB/F	85KN	11.17
F-TATB/F	105KN	9.673
M-TATB	85KN	6.903
M-TATB	105KN	6.638
M-TATB/F	85KN	7.091
M-TATB/F	95KN	6.603
Sub m- TATB	85KN	0.510
Sub M-TATB	105KN	0.816
Sub M-TATB/F	85KN	1.393
Sub M-TATB/F	105KN	1.078

From Table 4 it could be seen that for molding powder explosive after pressing explosive particle size became smaller with the increase of pressure, while for neat fine

HMX and TATB it grew after pressing and increased as increase of pressure. This agreed to the conclusion of Mr. Joseph T. Mang et. al[3] when they characterized high-explosive system by small-angle neutron scattering. The reasons were, on one hand, while pressing owing to the high pressure (up to 143MPa even to 334MPa), the explosive particles contacted each other (very high content), which led to explosive crystal and defects inside crystal collapsed. So did the pure explosvies.Therefore explosive particle size decrease with pressure increasing. On the other hand, for submicron TATB, inspite of crystal and inside defects collapse, but the absorption effect and TATB plastical property appeared and were very strong, so explosive particle size increased with the pressure increasing.

3.3.2 Effect of exerting pressure time on explosive particle size

Effect of the time exerting pressure from 0 to the needed pressure on explosive diameter was studied. Results were listed in Table 5.

Table 5. Effects of exerting pressure on particle size

NO.	Name	condition	Particle size (μm)
1.	F-HMX/F	90KN[30-40S]	15.20
2.	F-HMX/F	90KN[70-80S]	18.03
3.	F-HMX/F	90KN[90-100S]	18.01
4.	M-HMX/F	90KN□30-40S□	8.337
5.	M-HMX/F	90KN□70-80S□	8.224
6.	M-HMX/F	90KN□90-100S□	7.669
7.	F-TATB	95KN□30-40S□	7.561
8.	F-TATB	95KN□90-100S□	7.326
9.	Sub M-TATB	95KN□30-40S□	0.503
10.	Sub M-TATB	95KN□90-100S□	0.682
11.	M-TATB	95KN□30-40S□	5.975
12.	M-TATB	95KN□90-100S□	6.240

Results indicated that the influence of exerting pressure time on particle size was very small.

3.3.3 Effects of *pressing* temperature on particle size of explosive

Warm pressing was the case that while pressing the mold and explosive were heated to 70C for 1hr. Othewise pressing at room temperature was called cool pressing. Results of pressing temperature efffect were listed in Table 6 and Fig.3.

Table 6. Effects of press temperature on explosive particle size

NO.	Name	condition	Explosive particle size (μm)
1.	F-HMX/F	90KN	16.49
2.	F-HMX/F	90KN (warm press),	19.84
3.	M-HMX/F	90KN	7.486
4.	M-HMX/F	90KN (warm press),	10.27
5.	F-TATB	95KN	7.883
6.	F-TATB	95KN, (warm press),	8.288
7.	TATB/F	95KN	9.428
8.	TATB/F	95KN ,(warm press),	9.492
9.	M-TATB	95KN	7.459
10.	M-TATB	95KN ,(warm press),	6.344
11.	M-TATB/F	95KN	6.603
12.	M-TATB/F	95KN ,(warm press),	7.025
13.	SUB M-TATB	95KN	0.503
14.	G- TATB	95KN, (warm press),	0.915
15.	SUB M-TATB/F	95KN	0.490
16.	SUB M-TATB/F	95KN (warm press),	0.593

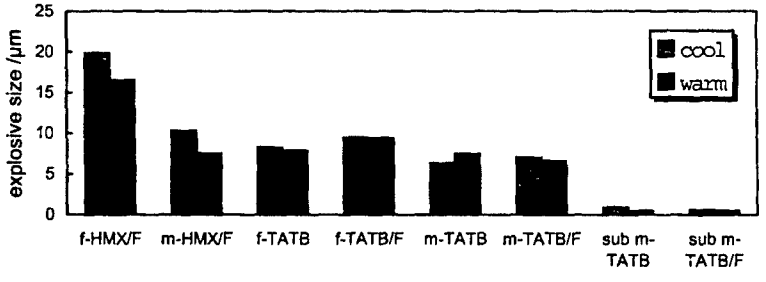


Fig 2. Effects of pressing temperature on particle size of explosive

Results showed that the particle size of warm pressing F-HMX and M-HMX was obviously bigger than that of cool pressing. Press temperature had less influence on F-TATB and M-TATB and their molding powders, but had great influence on submicron TATB and its molding powders.

3.4 Effects of aging on particles size of explosive

The effect of aging of TATB/F for 3 years on explosive particle size was also studied. Result was listed in table 8.

Table 7. Change of particle size of TATB after and before aging for 3years

Aging temperature/□	TATB□□/μm	
	Before aging	Aging for3 years
45	7.561	9.076
55	7.561	9.376
65	7.561	8.392
75	7.561	8.712

Result showed that particle size of TATB after aging 3 years at different temperatures only increased a little, so the influence of aging was not obvious.

4. CONCLUSION

1. The change of particle size of explosive crystal was very obvious after and before molding powder production, but the extent of change was different for explosive with different particle grade.
2. Effect of pressing process on particle size of explosive was very great.
3. Aging did not seriously affect the particle size of F-TATB.

REFERENCE

[1] H. S. Kim, Propellant Explosive Protechnics, 1999

[2] M. J. Gifford, M. W. Greenaway, W. G. Proud & J. Z. Field, Thery and Practice Energetic Materials, Vol. 4,P3-11, IASPEP, 2001,10

[3] Joseph T. Mang et. al, Characterization of high-explosive systems by small-angle neutron scattering, Lansce Division Research Review.

STUDY OF THE IMPACT REACTIVITY OF POLYNITRO COMPOUNDS

PART I.

IMPACT SENSITIVITY AS "THE FIRST REACTION" OF POLYNITRO ARENES.

Svatopluk Zeman and Miloslav Krupka

Department of Theory & Technology of Explosives, University of Pardubice, CZ-532 10 Pardubice, Czech Republic

Abstract:

The impact reactivity („the first reaction") of 20 polynitro arenes was expressed as the drop energy E_d, required for 50 percent initiation probability. Relationships have been found between the E_d valuesand heats of fusion, on the one hand, and ^{13}C NMR chemical shifts of carbon atoms in reaction centers, on the other. On the basis of the said relationships it was stated that the impact reactivity of polynitro arenes molecules depends on the electronic configuration within their reaction centers and intensity of their intermolecular interactions in the molecular crystals.

Key words:
impact sensitivity, polynitro arenes, ^{13}C NMR chemical shifts, heat of fusion

1. INTRODUCTION

Impact sensitivity of energetic materials may result from a combination of three elementary sensitivities [1]: molecular, crystalline and environmental. In the sense of the idea and on the basis of new knowledge about reactivity of nitramines [2-8], conclusions of the said studies have been re-examined in paper [9] by means of the characteristics of nitramines, which could have some relation to the particular sensitivities. The characteristic involved [9] heats of fusion $\Delta H_{m,tr}$, ^{15}N NMR chemical shifts of amino (aza) nitrogen atoms in the corresponding nitramino groupings, and Arrhenius parameters E_a and *log A* of low-temperature thermolysis.

The above-mentioned paper [9] deals with new aspects of the impact reactivity (*sensitivity*) of nitramines, defined as "the first reaction". However, this kind of sensitivity of other classes of polynitro compounds has not been subject to detailed investigation yet. Therefore, this paper focuses on the aspects of "the first reaction" of polynitro arenes in similar way. Heats of fusion, $\Delta H_{m,tr}$, and ^{13}C NMR chemical shifts, δ_C, of carbon atoms at the reaction centres of the said molecules have been applied to this purpose.

2. EXPERIMENTAL

2.1 Impact Sensitivity (Reactivity) Determination

For the impact sensitivity determination in the Budapest laboratory of the Hungarian company GEOINFORM Szolnok, the standard impact tester (*Julius Peters*) was used with exchangeable anvil and the amount of tested substance was 0.25 cm^3 (*refs.* [10,11]); 2 kg and 5 kg weight drop hammers were used [10,11]. For a positive experiment was taken that connected with the first detectable decomposition [10,11] (*"the first reaction", i. e. not only acoustic effect*). Using up-and-down method the obtained sensitivity was expressed as drop energy E_{dr} [10,11] whose values are presented in Table 1.

2.2 Heats of Fusion

The heats of fusion $\Delta H_{m,tr}$, defined in the sense of monograph [12] as the sum of heat of melting and heats of all polymorph transitions, were determined in the Research Department of CHEMKO (*Strážske, The Slovak Republic*) by means of a Perkin-Elmer differential scanning calorimeter Pyris DSC 7. During the measurement, nitrogen was introduced into the furnance of the DSC and the heating rate of 20° min^{-1} was used. Weighed amounts (1 – 2 mg) of crystalline polynitro arenes were placed in aluminium pans fitted with covers. The resulting DSC records were analyzed by means of the Pyris Series DDSC Adv SW Suite (*N537-0613*), which is licensed by Perkin-Elmer. For the compound HNS, whose thermal decomposition already begins in solid phase, the $\Delta H_{m,tr}$ value was predicted on the basis of the published calculated lattice energies using the methods according to refs [13,14]. The obtained $\Delta H_{m,tr}$ values are given in Table 1

2.3 ^{13}C NMR Spectroscopy

Most of the *^{13}C NMR* chemical shifts were taken from patent [15]. They were obtained with the help of an FX-60 JEOL apparatus working at the frequency of 15.04 MHz and with the proton noise decoupling. The polynitro arene samples were measured in the form of solutions in hexadeuteriodimethyl sulphoxide at a concentration of 0.1 mol compound per 1 dm^3. In similar way, but using an AMX-360 apparatus, we have obtained the spectra of DiMeDIPS and BITNT in this work. A survey of the measured and literature data is presented in Table 2.

Table 1. Survey of the polynitro arenes studied, their code designation, ^{13}C NMR chemical shifts, δ_C, in reaction centers of their molecules, heats of fusion $\Delta H_{m,tr}$, and impact sensitivity expressed as the drop energy, E_{dr}, of "the first reaction" [10].

Polynitro arene			^{13}C NMR Chemical shifts in reaction centre			Heat of fusion		Drop energy
Data No.	Chemical name	Code designation	position in molecule	δ_C in ppm	Ref.	$\Delta H_{m,tr}$ in kJ mol^{-1}	Ref.	E_{dr} in J
1	1,3,6-Trinitrobenzene	TNB	1,3,5-	148.3	15	15.69	16	5.90
1.1		TNB				16.74	17	
2	2,2',4,4',6,6'-Hexanitrobiphenyl	HNB	2,2',6,6'-	148.2	15	37.44	16	2.79
3	1,8-Dinitronaphthalene	1,8-DNN	1,8-	145.7	15	35.23	a	18.37
4	1,5-Dinitronaphthalene	1,5-DNN	1,5-	148.2	15	33.03	a	11.02
5	1,4,5-Trinitronaphthalene	1,4,5-TNN	4-	147.6	15	27.49	a	9.52
6	1,4,5,8-Tetranitronaphthalene	TENN	1,4,5,8,-	146.9	15			9.65
7	1-Methyl-2,4,6-trinitrobenzene	TNT	2,6-	150.9	15	19.58	a	>29.43
7.1		TNT						35.86[d]
8	1,3-Dimethyl-2,4,6-trinitrobenzene	TNX	2-	148.5	15	40.87	a	9.91
9	1,3,5-Trimethyl-2,4,6-trinitrobenzene	TNMs	2,4,6-	149.5	15	30.72	a	7.41
10	2,2',4,4',6,6'-Hexanitrobibenzyl	DPE	2,2',6,6'-	150.9	15	43.85	c	5.78
11	3,3'-Dimethyl-2,2',4,4',6,6'-hexanitrobiphenyl	BITNT	2,2'-	151.2	a	33.69	a	7.40
12	2,2',4,4',6,6'-Hexanitrodiphenylsulfide	DIPS	2,2',6,6'-	151.5	15	38.00	a	2.94
13	3,3'-Dimethyl-2,2',4,4',6,6'-hexanitrodiphenylsulfide	DIMEDIPS	2,2'-	151.2	a	57.78	a	29.40
13.1		DIMEDIPS	6,6'-	147.9	a			
14	2,2',4,4',6,6'-Hexanitrodiphenylsulfone	DIPSO	2,2',6,6'-	148.5	15	40.39	c	3.86
15	2,2',4,4',6,6'-Hexanitrostilbene	HNS				40.21	b,13	3.64
16	2,2',4,4',6,6'-Hexanitrodiphenylamine	DPA	2,2',6,6'-	138.7	15	37.38	a	10.16
17	2,2',4,4',6,6'-Hexanitrooxanilide	HNO	2,2',6,6'-	144.7	15			8.70
18	1,3,7,9-Tetranitrophenothiazine-5-oxide	TNPMO	1,9-	137.1	15			7.04
19	1,3,7,9-Tetranitrophenothiazine-5,5-dioxide	TNPTD	1,9-	136.5	15			4.50
20	1,3,7,9-Tetranitrophenoxazine	TENPO	1,9-	141.2	15			9.84

Notes: a) the value resulted from measurements in this paper; b) the value predicted; c) the value calculated by means of relationship for group B in Fig. 1; d) the value calculated by means of relationship for group *IV* in Fig. 2.

Table 2. Table 2: ^{13}C NMR Chemical shifts, δ, of the polynitro arenes studied - taken from Ref. 15.

Chemical name	Position in molecule	δ in ppm	Chemical name	Position in molecule	δ in ppm
			1,3-Dimethyl-2,4,6-trinitro-benzene	α,α'-	13.9
1,3,5-Trinitrobenzene	1,3,5-	148.3		1,3-	129.2
	2,4,6-	123.8		2-	148.5
2,2',4,4',6,6'-Hexanitro-				6,4-	147.4
biphenyl	1,1'-	126.0		5-	121.9
	2,2',6,6'-	148.2	2,2',4,4',6,6'-Hexanitro-		
	3,3',5,5'-	125.2	bibenzyl	α,α'-	27.1
	4,4'-	148.7		1,1'-	133.2
				2,2',6,6'-	150.9
1,8-Dinitronaphthalene	1,8-	145.7		3,3',5,5'-	123.2
	2,7-	127.9		4,4'-	146.6
	3,6-	127.7	3,3'-Dimethyl-2,2',4,4',		
	4,5-	135.4	6,6'-Hexanitrobiphenyl[a]	α,α'-	15.4
	9-	116.1		1,1'-	122.1
	10-	135.7		2,2'-	151.2
				3,3'-	133.7
1,5-Dinitronaphthalene	1,5-	148.2		4,4'-	145.3
	2,6-	125.5		5.5'-	124.2
	3,7-	128.9		6,6'-	150.1
	4,8-	129.1	2,2',4,4',6,6'-Hexanitro-		
	9,10-	126.0	diphenylsulfide	1,1'-	125.7
				2,2',6,6'-	151,5
1,4,5-Trinitronaphthalene	1-	150.6		3,3',5,5'-	124.4
	2-	124.9		4,4'-	147.8
	3-	127.6	3,3'-Dimethyl-		
	4-	147.6	2,2',4,4',6,6'-	α,α'-	15.1
			hexanitrodiphenylsulfide[a]		
	5-	145.9		1,1'-	122.9
	6-	129.4		2,2'-	151.2
	7-	130.8		3,3'-	131.6
	8-	129.2		4,4'-	145.5
	9-	117.0		6,6'-	147.9
	10-	117.4			
1,4,5,8-Tetranitro-			2,2',4,4',6,6'-Hexanitro-		
naphthalene	1,4,5,8-	146.9	diphenylsulfone	1,1'-	121.1
	2,3,6,7-	128.0		2,2',6,6'-	148.5
	9,10-	117.9		3,3',5,5'-	124.1
1-Methyl-2,4,6-trinitro-				4,4'-	143.5
benzene	α–	15.1	2,2',4,4', 6,6'-Hexanitro-		
	1–	133.1	diphenylamine	1,1'-	142.0
	2,6-	150.9		2,2',6,6'-	138.7
	3,5-	122.7		3,3',5,5'-	124.4
	4-	145.8		4,4'-	132.0

Table 2: - continued

Chemical name	Position in molecule	δ in ppm	Chemical name	Position in molecule	δ in ppm
1,3,5-Trimethyl-2,4,6-trinitrobenzene	α,α',α''-	12.6			
	1,3,5-	124.4			
	2,4,6-	149.5			
2,2',4,4',6,6'-Hexanitrooxanilide	carbonyls	157.1	1,3,7,9-Tetranitrophenothiazine-5,5-dioxide	1,9-	136.5
	1,1'-	128.4		2,8-	125.4
	2,2',6,6'-	144.7		3,7-	141.0
	3,3',5,5'-	125.0		4,6-	124.4
	4,4'-	143.6		10,12-	136.7
				13,14-	124.0
1,3,7,9-Tetranitrophenothiazine-5-oxide	1,9-	137.1	1,3,7,9-Tetranitrophenoxazine	1,9-	141.2
	2,8-	123.9		2,8-	117.3
	3,7-	141.2		3,7-	144.6
	4,6-	124.9		4,6-	114.3
	10,12-	135.6		10,12-	142.6
	13,14-	125.8		13,14-	163.4

Note: a) results of the present paper.

3. DISCUSSION

The relationship between the impact sensitivity *("the first reaction")* and the heat of fusion, $\Delta H_{m,tr}$, is presented in Fig. 1. This relationship should especially represent the elementary crystalline sensitivity, i.e. the impact sensitivity as a function of intermolecular interactions in the molecular crystal. The relationship has the same form as that valid for nitramines [9]. However, from the standpoint of molecular structure, the classification of investigated polynitro arenes in its sense is not so strict as that in the case of nitramines. From the point of view of the number of trinitrophenyl units per molecule, particularly group *A* of compounds does not appears to be homogeneous. This is probably connected with the larger variety of inter- and intra-molecular interactions (*particularly the mesomeric effects*) in the investigated arenes as compared with that encountered in the simpler molecules of aliphatic nitramines. Classes *A* and *B* are not homogeneous even from the point of view of the primary splitting in their low-temperature thermolysis: The homolysis of C–NO_2 bond should start the splitting of TNB and HNB, while the primary splitting of the other polynitro arenes consists in the interaction of oxygen atom of nitro group with the hydrogen atom at γ position [18-21] or with the sulphur bridge atom [22,23]. Using the relationship valid for the class *B* compounds we calculated the $\Delta H_{m,tr}$ values for DPE and DIPSO (see Table 1).

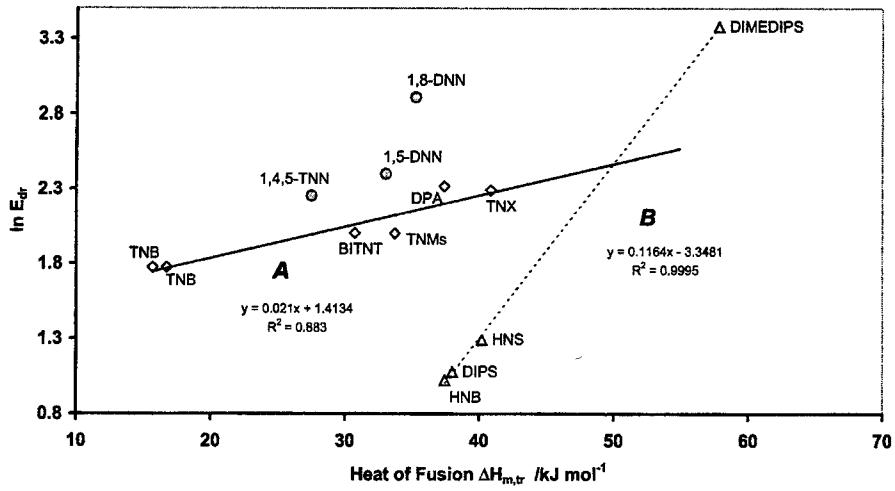


Fig 1. Relationships between impact sensitivity (E_{dr}) and heat of fusion.

It is know that application of ^{13}C and ^{15}N NMR chemical shifts in the study of initiation of polynitro compounds by shock [2], impact [9], electric spark [6] or heat [3] can give very valuable results. Philosophy of this approach is based on the fact that values of these shifts correspond predominantly to the electronic configuration and steric conditions within the reaction center. The papers [2,3,6,9] have been shown that the center should be the same in all the above-mentioned kinds of initiations. Likevise to nitramines [9] a relationship exists between E_{dr} values and chemical shifts of the most reactive nitrogroup "carriers" (*i. e. carbon atoms in the reaction centers of molecule*) in the studied polynitro arenes. As Fig. 2 shows the relationship has again the same form as that valid for nitramines [9].

The classification of compounds in the sense of Fig. 2 is primarily connected with the mechanism of initial fragmentation of their molecules during low-temperature thermolysis. The compounds of group *I* are characterised by the primary decomposition of C–NO_2 bond. This class also involves DIPSO: in its molecule the sulphur hetero-atom is occupied by two bound oxygen atoms, which is why it cannot interact with the oxygen atom of *ortho*-nitro group any more.

Class *II* of compounds in Fig. 2 mostly comprises compounds having a –CH_2– linkage in the molecule. Their thermal decomposition goes by the so-called "tritol mechanism" [18] (i. *e. the already mentioned interaction of oxygen atom of nitro group with hydrogen atom at γ position* [18-21]). In the case of thermal decomposition of DIPS, the primary interaction should involve the oxygen atom of *ortho*-nitro group with the bridge hetero-atom of sulphur [22,23]. The relationship valid for class *II* is excellently obeyed by the data of 1,5-DNN, which means that the thermal decomposition of 1,5-DNN should begin by the interaction of oxygen atom of nitro group with hydrogen atom at *peri*-position.

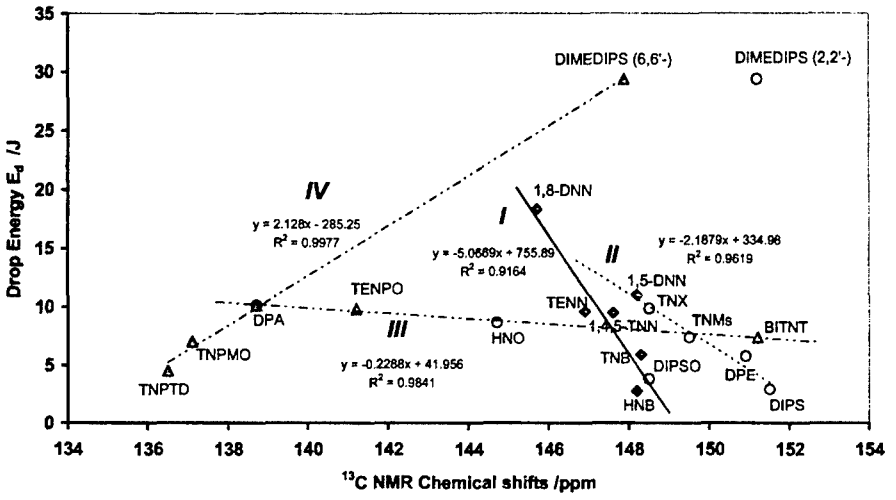


Fig 2. Relationships between impact sensitivity (E_{dr}) and ^{13}C NMR chemical shifts of the carbon atoms in reaction centers of polynitro arenes molecules.

The application of relationships from Fig. 2 to specification of reaction centre of the molecule can also be demonstrated on DIMEDIPS. Theoretically, the molecule of this compound should contain two types of these centres: the sterically hindered nitro groups at 2,2′-positions and the less hindered nitro groups at 6,6′-positions. However, the relationship for compounds of class *IV* in Fig. 2 is excellently obeyed by the data applying to the reaction centre at 6- or 6′-position, which means that the primary splitting of the DIMEDIPS molecule by action of heat (*but also impact, shock or electric spark*) should consist in the interaction between oxygen atom of nitro group at 6- or 6′-position and the bridge sulphur hetero-atom. It must be added that the other compounds in class *IV* but also class *III* in Fig. 2 are characterised by the presence of an hydrogen atom at γ-position with respect to nitro groups. The intensity of non-bonding interaction of these hydrogen atoms with nitro groups in the ground state of molecule can be the reason why there exist these two separate classes of polynitro arenes. It must be added that the interaction in this case corresponds to the state of given molecule in solution.

In the experiments specifying the impact sensitivity of TNT its decomposition did not take place at the conditions applied (*see Table 1*). In comparison with TNB, the TNT molecule shows a strong phlegmatizing effect of methyl group. A distinct phlegmatizing effect of this type is also encountered in DIMEDIPS (*as compared with DIPS*). Therefore, the data of TNT logically belong among the polynitro arenes of class *IV*. On the basis of this consideration it was possible to calculate the real E_{dr} value for TNT (*data 7.1 in Table 1*).

4. CONCLUSION

The relationships between impact sensitivity in sense of "the first reaction" of polynitro arenes and their heats of fusion on the one hand, and the ^{13}C NMR chemical shifts at the reaction centres of their molecules on the other hand, are of the same types as those found for nitramines [9]. That means that the said sensitivity of polynitro arenes also depends on the electron configuration of reaction centre of their molecules and on intensity of intermolecular interactions in their molecular crystals. These factors affect the transfer of impact energy to the reaction centre of molecule. The relationships found make it possible to specify this reaction centre.

Acknowledgements

The authors express their gratitude to former student of their Department, Mr. Zsolt Jermann, for his precise work and high level of results treatment within the framework of corresponding Thesis [10]. The authors also express their gratitude to:

(1) the Hungarian company GEOINFORM Szolnok for affording the impact tester and sponsoring the respective measurements,

(2) the Management of R & D Department of the Slovak firm CHEMKO Strážske and Mrs. Ljubov Tokárová, M.Sc. from the Dept. for affording differential scanning calorimeter Pyris DSC-7 and helping with measurements,

(3) the Ministry of Industry and Commerce of the Czech Republic for support the work within the framework of research project No. FC-M2/05.

REFERENCES

[1] A. Delpuech and J. Cherville, "Relation entre la StrucrureElectronique et la Sensibilité au Choc des Explosivs Swcondaires Nitrés. Critére Moleculaire de Sensibilité. I.", *Propellants, Explos. 3*, 169-175 (1978).

[2] S. Zeman, "Relationship between Detonation Characteristics and ^{15}N NMR Chemical Shifts of Nitramines", *J. Energ. Mater. 17*, 305-330 (1999).

[3] S. Zeman, "Analysis and Prediction of the Arrhenius Parameters of Low-Temperature Thermolysis of Nitramines by Means of the ^{15}N NMR Spectroscopy", *Thermochim. Acta 333*, 121-129 (1999).

[4] Z. Jalový and S. Zeman, "Relationship between the Length of the Longest N-N Bonds and Activation Energies of Low-Temperature Thermolysis of Nitramines", [Proc.] *30th Int. Annual Conf. ICT*, Karlsruhe, 1999, pp. 104/1-104/9.

[5] V. Zeman and S. Zeman, "Relationship between the Electric Spark Sensitivity and Detonation Velocities of Some Polynitro Compounds", [Proc.] *28th Annual Conf. ICT*, Karlsruhe, June 1997, pp. 67/1-67/10.

[6] S. Zeman, V. Zeman and Z. Kamenský, " Relationship between the Electric Spark Sensitivity and the NMR Chemical Shifts of some Organic Polynitro Compounds", [Proc.] *28th Annual Conf. ICT*, Karlsruhe, June 1997, pp. 66/1-66/9.

[7] V. Zeman, J. Kočí and S. Zeman, "Electric Spark Sensitivity of Polynitro Compounds. Part III. A Correlation with Detonation Velocities of some Nitramines", *HanNeng CaiLiao 7,* 127-132 (1999).

[8] S. Zeman and J. Kočí, " Electric Spark Sensitivity of Polynitro Compounds. Part IV. A Relation to Thermal Decomposition Parameters", *HanNeng CaiLiao 8,* 18-26 (2000).

[9] S. Zeman, "New Aspects of the Impact Reactivity of Nitramines", *Propellants, Explos., Pyrotech. 25,* 66-74 (2000).

[10] Z. Jermann, *"Impact Sensitivity of some Explosives",* M.Sc.-Thesis, Univiversity of Pardubice, June, 1994.

[11] *"Testing Methods of Explosives: Testing the Impact Sensitivity with an Impact Tester",* Hungarian Standard No. MSZ 14-05007-87, Jan. 30th, 1987.

[12] A. Bondi, *"Physical Properties of Molecular Crystals, Liquids, and Glasses",* John Wiley & Sons, New York, 1968.

[13] S. Zeman an M. Krupka, "Some Predictions of the Heats of Fusion, Heats of Sublimation and Lattice Energies of Energetic Materials", [Proc.] *4th Seminar "New Trends in Reserach of Energetic Materials",* University of Pardubice, April 2001, pp. 393-401.

[14] S. Zeman and M. Krupka, "Calculated Lattice Energies of Energetic Materials in a Prediction of their Heats of Fusion and Sublimation", *HanNeng CaiLiao 10* (2002) - in press.

[15] S. Zeman, V. Mlynárik, I. Goljer and M. Dimun, "Determination of Heat of Explosion", CS Patent 237 661 (Nov. 30th, 1987); *Chem. Abstr. 108,* 39564k (1988).

[16] S. Zeman, *"Thermostable Polynitro Arenes: Molecular-Structural Aspects of the Chemical and Physical Stabilities",* Ph.D. Thesis, Univ. Pardubice, June 1973.

[17] N. D. Lebedeva, V. L. Ryadenko and I. N. Kuznetsov, „Heats of Combustion and Enthalpies of Formation of some Aromatic Nitro Derivatives" *Zh. Fiz. Khim. 45,* 980-981 (1971).

[18] V. G. Matveev, V. V. Dubikhin and G. M. Nazin, „Soglasovanyi mekhanism razlozheniya aromaticheskikh nitrosoedinii v gazovoy faze (Thermolysis Mechanism of the Aromatic Nitrocompounds in the Gas Phase)", *Izv. Akad. Nauk SSSR, Ser. Khim.* 474-477 (1978).

[19] S. Bulusu, D. I. Weinstein, J. R. Autera, D. A. Anderson and R. W. Velicky, „Deuterium Kinetic Isotope Effect: An Experimental Probe for the Molecular Processes Governing the Initiation of RDX, HMX and TNT", [Proc.] *8th Int. Symp. on Detonation,* Albuquerque, NM, July, 1985.

[20] L. M. Minier and J. C. Oxley, „Thermolysis of Nitroarenes: 2,2',4,4',6,6'-Hexanitrostilbene", *Thermochim. Acta 166,* 241-249 (1990).

[21] J. Wang and H.-Y. Lang, „Mechanistic Study of Polynitro Compounds by XPS: Mechanism of the Thermal Decomposition of Polynitro Phenols", *Science in China, Ser. B 33,* 257-266 (1990).

[22] S. Zeman, M. Dimun and Š. Truchlik, „The Relationship between Kinetic Data of the Low-Temperature Thermolysis and the Heats of Explosion of Organic Polynitro Compounds", *Thermochim. Acta 78,* 181-209 (1984).

[23] S. Zeman, "Modified Evans-Polanyi-Semenov Relationshop in the Study of Chemical Micromechanism Governing Detonation Initiation of Individual Energetic Materials", *Thermochim, Acta 384,* 137-154 (2002).

STUDY OF THE IMPACT REACTIVITY OF POLYNITRO COMPOUNDS PART II.

IMPACT SENSITIVITY AS A FUNCTION OF THE INTERMOLECULAR INTERACTIONS

Svatopluk Zeman and Miloslav Krupka

Department of Theory & Technology of Explosives, University of Pardubice,
CZ-532 10 Pardubice, Czech Republic

Abstract:

Published data of impact sensitivity, detected for sound of 32 polynitro compounds were expressed as the drop energy, E_{dr}, required for 50 percent initiation probability. A logarithmic relationship has been found between the E_{dr} values and heats of fusion of the said compounds. The relationship has been found to be in accordance with the idea of the role of plastic deformations of crystal played in the initiation of energetic materials by impact and shock. An analogous application of heats of sublimation has not given convincing results.

Keywords: *impact sensitivity, heat of fusion, heat of sublimation*

1. INTRODUCTION

The studies of the relationship between molecular structure of energetic materials and their sensitivity to impact, shock, electric spark and heat form an important starting point for study of chemical micromechanism governing detonation initiation of these materials [1-8]. From the results of studies of this type it follows that the intensity of intermolecular interactions in the corresponding crystal represents one of the factors influencing the transfer of initiation energy into the reaction centre of the molecule [1-9]. This fact is documented by the findings obtained from studies of impact [1,3,7,9] or electric spark initiations [4-7] of polynitro compounds.

From among the measurable quantities the heat of sublimation, ΔH_s, is the best parameter as far as the characterisation of the intensity of intermolecular interactions within a crystal is concerned. However, the respective values of many energetic materials have not been published yet. Nevertheless, in some specific cases it is possible to replace the heat of sublimation by the heat of fusion, $\Delta H_{m,tr}$, [1,3,8], determined with the help of DSC. Both the heats of sublimation and fusion of some polynitro compounds were recently also predicted by means of calculated lattice energies [10,11].

In refs [1,3,7,9] conclusions were made on the basis of impact sensitivity defined as the so-called "first reaction". However, the results of estimation of impact sensitivity detected on the basis of sound (*see, e.g., Bruceton method* [12-15]) have not been studied in a similar way yet. Therefore, this work focuses attention on the relationship between the second type of impact sensitivity mentioned and both the heats of fusion and heats of sublimation of some polynitro compounds.

2. EXPERIMENTAL

2.1 Impact Sensitivity (Reactivity) Data

Impact sensitivity data (*the drop heights*) were taken from literature [13-15]. The most of these were measured at Los Alamos National Laboratory and/or Naval Surface Weapons Center, using the Bruceton method [13-15]. Some from them were obtained at other workplaces [26,27,33-35]. The drop heights were re-counted in drop energies, E_{dr}, in this paper. Impact sensitivity data of the studied compounds are presented in Table 1.

2.2 Heats of Fusion

The heats of fusion $\Delta H_{m,tr}$, defined as the sum of heat of melting and heats of all polymorph transitions, were determined in the Research Department of CHEMKO (*Strážske, The Slovak Republic*) by means of a Perkin-Elmer differential scanning calorimeter Pyris DSC 7. The method is described in Part I of this paper [9]. For some compounds, whose thermal decomposition already begins in solid phase, the $\Delta H_{m,tr}$ value were predicted on the basis of the published calculated lattice energies in papers [10,11] or on the basis of comparison analyses [8,9,24]. Some data were taken from literature [16,17,21,22,25,32]. The applied heats of fusion are presented in Table 1.

2.3 Heats of Sublimation

The heats of sublimation, ΔH_s, were partly taken from literature [19,20,23]. For some compounds, whose the ΔH_s values are not published yet, their prediction on the basis of the published calculated lattice energies was made in papers [10,11]. The applied ΔH_s values are presented in Table 1.

3. DISCUSSION

Analysis of the relationship between the impact sensitivity detected for sound and heats of fusion of the studied polynitro compounds gave a logarithmic relationship documented in Figs 1 and 2. Analogous relationship for the impact sensitivity defined as "the first reaction" represents a semi-logarithmic function [3,9]. This difference could be connected with the different mechanisms of transfer of drop energy to the reaction centre of molecule in the case of "the first reaction" as compared with the impact sensitivity detected by sound. The reaction centre is presumed to be represented by that molecular moiety in which the primary chemical changes take place after an external impulse. The papers [1-7,9,41] show that this centre should be the same for the initiation by impact, shock, heat and electric spark. From among all these impulses, the splitting of energetic materials by heat has been studied most thoroughly. As far back as 1976, Kamlet used the findings from this type of splitting for interpretation of some aspects of impact sensitivity of polynitro compounds [13,42]

In the co-ordinate system shown in Fig. 1, the set of polynitro arenes studied falls into several classes. Class *A* includes 1,3,5-trinitrobenzene (TNB) and its derivatives. Except for TNB itself, all the other compounds of this class contain a hydrogen atom standing at a γ-position to a nitro group; the migration of this hydrogen atom to oxygen atom of *ortho*-nitro group is regarded to be the primary step of thermal decomposition of the corresponding molecules [37-40]. Class *D* of polynitro arenes can be regarded a scion of class *A*: it differs from *A* only in the higher energy needed for creation defects in crystal lattice.

Table 1. Survey of the polynitro compounds studied, their code designation, heats of fusion, $\Delta H_{m,tr}$, and sublimation, ΔH_s, and impact sensitivity expressed as the drop energy, E_{dr}.

Polynitro compound			Heat of fusion		Heat of sublimation		Impact sensitivity		
Data No.	Chemical name	Code designation	$\Delta H_{m,tr}$ (kJ mol^{-1})	Ref.	ΔH_s (kJ mol^{-1})	Ref.	$h_{50\%}$ (cm)	E_{dr} (J)	Ref.
1.1	1,3,5-Trinitrobenzene	TNB	15.69	16	107.3	19	100	24.52	13,14
1.2			16.74	17					
2.1	1-Methyl-2,4,6-trinitrobenzene	TNT	21.86	18	118.4	23	160	39.24	13,14
2.2			19.58	a					
3.1	1,3-Dimethyl-2,4,6-trinitrobenzene	TNX	40.87	a	129.8	19	100	24.54	15
4.1	1,3,5-Trimethyl-2,4,6-trinitrobenzene	TNMs	30.72	a	103.6	19	110	27.00	15
5.1	1-Hydroxy-2,4,6-trinitrobenzene	PA	17.41	a	105.1	19	87	21.33	13,14
6.1	1,3-Dihydroxy-2,4,6-trinitrobenzene	TNR	28.80	a	120.8	19	43	10.54	13
7.1	1-Methyl-3-hydroxy-2,4,6-trinitrobenzene	TNCr	26.74	a	111.2	19	191	46.84	13,14
8.1	1-Amino-2,4,6-trinitrobenzene	PAM	28.15	a	125.3	19	177	43.40	13,14
9.1	1,3-Diamino-2,4,6-trinitrobenzene	DATB	35.25	a	140.0	20	320	78.48	13
10.1	1,3,5-Triamino-2,4,6-trinitrobenzene	TATB	56.60	10,11	168.2	20	490	120.17	13
11.1	2,4,6-Trnitrobenzoic acid	TNBA	31.60	a	154.7	10,11	109	26.73	13,14
12.1	2,2‘,4,4‘,6,6‘-Hexanitrobiphenyl	HNB	37.44	16	171.8	10,11	76	18.64	13
12.2							85	20.84	14
13.1	3,3‘-Dimethyl-2,2‘,4,4‘,6,6‘-hexanitrobiphenyl	BITNT	33.69	a	160.8	10,11	135	33.14	13,14
14.1	2,2‘,4,4‘,6,6‘-Hexanitrobibenzyl	DPE	43.85	9			114	27.98	14
15.1	2,2‘,4,4‘,6,6‘-Hexanitrodiphenylsulfide	DIPS	38.00	a	173.4	10,11	38[b]	7.45	29
15.2								6.00	30
16.1	2,2’,4,4’,6,6’-Hexanitrodiphenylsulfone	DIPSO	40.36	9			43[b]	8.44	29
17.1	2,2‘,4,4‘,6,6‘-Hexanitrodiphenylamine	DPA	37.38	a	171.6	10,11	48	11.77	13,14
17.2								7.50	30
18.1	2,2‘,4,4‘,6,6‘-Hexanitrostilbene	HNS	40.21	10,11	179.9	20	39	9.56	13

Table 1 - continued

Polynitro compound			Heat of fusion		Heat of sublimation		Impact sensitivity		
Data No.	Chemical name	Code designation	$\Delta H_{m,tr}$ (kJ mol^{-1})	Ref.	ΔH_s (kJ mol^{-1})	Ref.	$h_{50\%}$ (cm)	E_{dr} (J)	Ref.
19.1	1-(2,4,6-Trinitrophenyl)-5,7-dinitrobenzotriazole	BTX	40.10	21	179.7	10,11	27	6.62	21
19.2							35	8.58	21
20.1	1-(Methylnitramino)-2,4,6-trinitrobenzene	TETRYL	25.85	22	133.8	19	32	7.85	13
21.1	Nitroguanidine	NQ	11.49	a	142.7	19	177	43.45	36
21.2							47[b]	9.22	31
22.1	1,4-Dinitro-1,4-diazabutane	EDNA	23.24	24			34	8.33	14
23.1	2,5-Dinitro-2,5-diazahexane-3,4-dione	DMNO	11.77	24			79	19.37	14
24.1	1,3-Dinitro-1,3-diazacyclobutane	TETROGEN	26.32	24	94.2	10,11		9.97	d
25.1	1,3,3-Trinitroazetidine	TNAZ	30.31	32	106.2	10,11	28	6.90	34
25.2		TNAZ	29.45	25					
26.1	1,3,5-Trinitro-1,3,5-triazacyclohexane	RDX	33.01	24	130.2	20	24	5.88	14
27.1	1,3,5,7-Tetranitro-1,3,5,7-tetraazacyclooctane	β–HMX	32.10	24	175.3	20	26	6.37	14
28.1	*trans*-1,4,5,8-Tetranitro-1,4,5,8-tetraazadecaline	TNAD	46.40	24	154.2	10,11	35	8.58	26
29.1	1,3,5,7,9-Pentanitro-1,3,5,7,9-pentaazacyclodecane	DECAGEN	34.93	1,3	120.0	10,11	20	4.90	27
30.1	4,10-Dinitro-2,6,8,12-tetraoxa-4,10-diazaisowurtzitane	TEX	36.10	8	123.4	10,11	50[c]	24.25	28
30.2		TEX					45.5[c]	23.00	35
31.1	2,4,6,8,10,12-Hexanitro-2,4,6,8,10,12-hezaazaisowurtzitane	ε–HNIW	42.70	8	168.7	10,11	24.2[c]	11.90	33
32.1	2,4,6,8,10,12-Hexanitro-2,4,6,8,10,12-hezaazaisowurtzitane	α–HNIW	42.70	8	168.7	10,11	20.7[c]	10.20	33

Notes:
a) the value resulted from DSC measurements in this paper;
b) determined with a 2 kg hammer;
c) determined with a 5 kg hammer;
d) calculated by means of relationship for group *F* in Fig. 2;

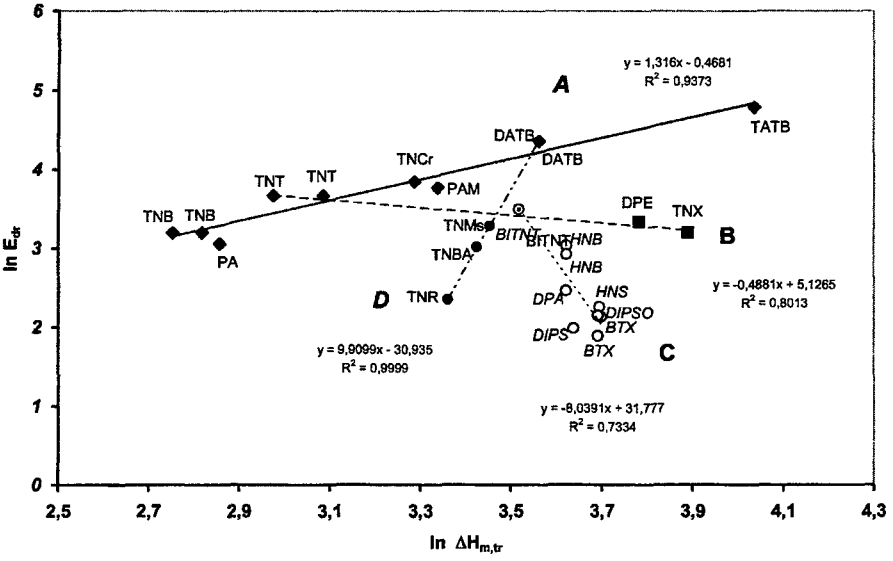


Fig 1. Relationship between the impact sensitivity (E_{dr}) and heat of fusion of polynitro arenes.

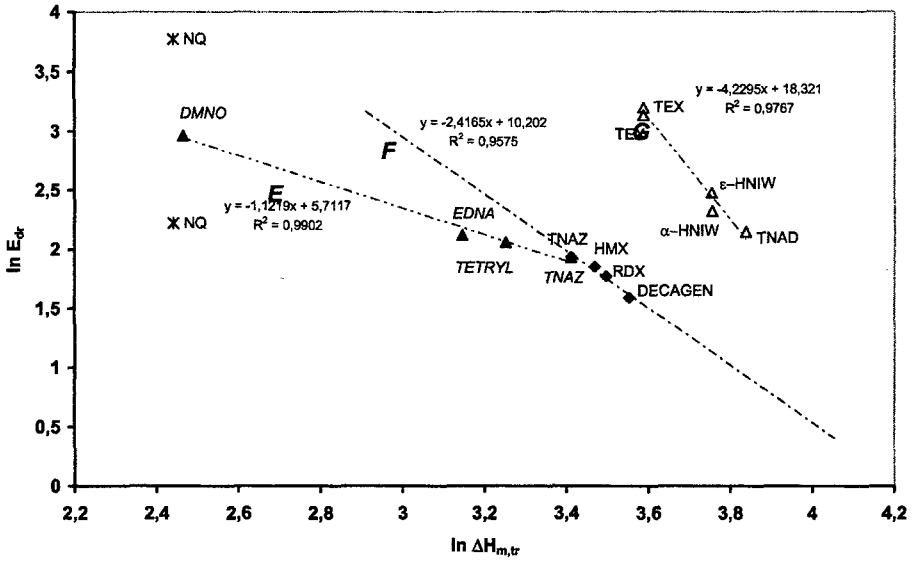


Fig 2. Relationship between the impact sensitivity (E_{dr}) and heat of fusion of nitramines.

A distinct class in Fig. 1 is class *B*. It includes TNT, TNX, TNMs BITNT and DPE. Their molecules contain a $-CH_2-$ linkage. These compounds also form a distinct independent class in terms of the well-known Kamlet relationship between oxygen balance and impact sensitivity of polynitro arenes [13,14]. From the point of view of mechanism of

the primary step of their thermal decomposition (*again migration of a hydrogen atom at γ-position to a nitro group*) this class appears homogeneous.

Class *C* of compounds in Fig. 1 includes binuclear polynitro arenes. The primary step in thermal decomposition of DIPSO and HNB should consist in homolysis of some of the C–NO_2 bonds at the sterically hindered 2,2′,6,6′ positions; in the case of BTX, this primary process should concern the similar bond at 5-position of benzotriazole ring [41]. Migration of hydrogen atom to some of the nitro groups at the 2,2′-positions of the BITNT molecules and 2,2′,6,6′-positions of the DPA and HNS molecules is the starting process of thermolysis of these polynitro arenes. Interaction of oxygen atom of some of the nitro groups at 2,2′,6,6′-positions with the bridge sulphur hetero atom should start the thermal decomposition of DIPS [2].

Figure 2 shows that also the set of nitramines studied falls into several classes in the sense of the relationship found. Sharp molecular structure characterisation is encountered with compounds of classes *F* and *G*. The former includes cyclic structures with methylenenitramine arrangement in their molecules. The relationship is obeyed by the data of TNAZ, which is structurally close to (*not yet synthesised*) Tetrogen. The relationship for the class *F* nitramines was used for calculation of E_{dr} value of Tetrogen. A characteristic feature of the class *G* compounds is the presence of 1,4-dinitro-1,4-diazacyclohexane structure in their rigid molecules. A common feature of the nitramines from classes *F* and *G* is the primary homolysis of N–NO_2 bond during their thermal decomposition (*see refs* [2,3] *and papers cited therein*). The structurally non-uniform class *E* of nitramines should also be non-uniform from the viewpoint of mechanism of thermal decomposition. In the case of EDNA this splitting can begin by a bimolecular mechanism [43]. Figure 2 also documents large differences between the E_{dr} values published for NQ (*Gibbs & Popolato even give the fall height above 320 cm* [44], *i.e. the E_{dr} value above 78.5 J*): the lowest E_{dr} value (data 21.2) might correspond to "the first reaction" [49].

The found relationship, which is presented in Figs 1 and 2, seems to be in accord with the ideas about the decisive role of plastic deformation of crystal played in the initiation of energetic materials by impact or shock [45-48]. These ideas primarily consider lattice and molecular distortions within the crystal due to impact or shock. Heat of fusion represents the work connected with formation of defects in crystal lattice (*ending in its complete collapse*). Therefore, the relationship between impact sensitivity and heat of fusion seems to be logical.

Figures 3 and 4 show a comparison of impact sensitivities (E_{dr}) and heats of sublimation (ΔH_s) of the polynitro compounds studied. As already stated the ΔH_s value characterises best the intra-molecular forces in crystal. Although Fig. 3 indicates certain dependences, the well-known class of polynitro arenes with –CH_2– linkage in the molecule is not clearly delimited (*cf.* Fig. 1). Class *I* of compounds includes the TNB derivatives, and class *II* comprises polynuclear derivatives. The data of TNBA incline to class *II*, which follows from the ability of carboxylic acids to form dimers by means of their carboxyl groups in crystals. As for the nitramines in Fig. 4, it is not possible to make definitive conclusions although the data in class *IV* of substances indicate a certain trend. Class *III* should represent more volatile nitramines but this statement is questionable in the case of NQ. Heats of sublimation do not seem to be very suitable for application to studies of impact sensitivity.

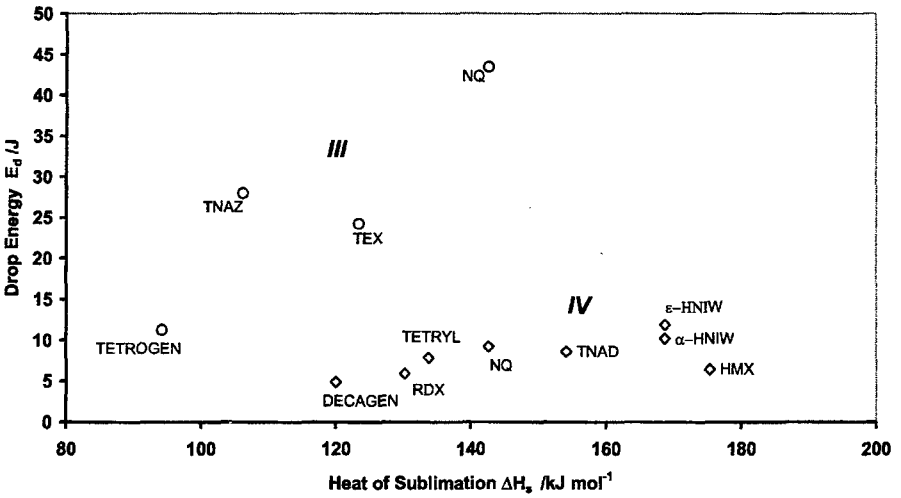


Fig 3. Impact sensitivity (E_{dr}) versus heat of sublimation of polynitro arenes.

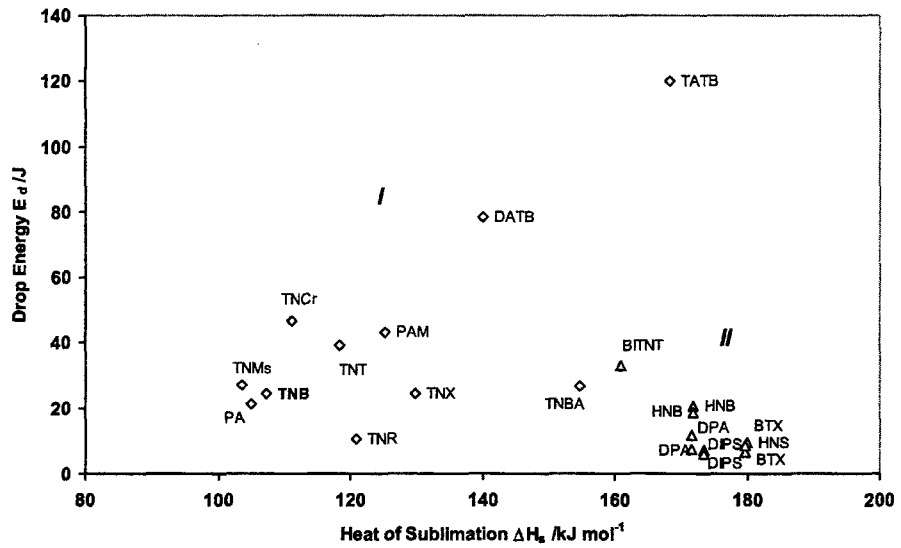


Fig 4. Impact sensitivity (E_{dr}) versus heat of sublimation of nitramines.

4. CONCLUSION

The impact sensitivity is a function of heat of fusion. This applies both to impact sensitivity in the sense of "the first reaction" [1,3,9] and to sensitivity in the sense of the Bruceton method (*a detection of sound*). However, the said function has different general mathematical forms for either of the two types of sensitivity. This difference might be connected with differences in mechanism of transfer of drop energy to the reaction centre of molecule when the individual types of impact sensitivity are determined. As the heat of fusion represents the work needed for formation of defects in crystal lattice, the relationships found seem to stand in accordance with the ideas about the decisive role of plastic deformations of crystal played in the initiation of energetic materials by impact or shock [45-48]

In the sense of the logarithmic relation found in this work (*see Figs 1 and 2*) the set of studied polynitro compounds fell into several classes. A common feature in each of the individual classes lies mainly in factors of molecular structure and much less in the mechanism of primary thermal decomposition. An exception is represented by polynitro arenes with $-CH_2-$ linkage in the molecule, which form an independent class even in the case of the well-known Kamlet [13] relationship between oxygen balance and impact sensitivity, and which have the same mechanism of thermal decomposition, too.

Mutual comparison of impact sensitivities and heats of sublimation of the studied polynitro compounds indicates a division of these compounds into several classes. However, these classes are not identical with the division based on the heats of fusion: in particular the class of polynitro arenes containing the $-CH_2-$ linkage in the molecule is absent.

Acknowledgements

The authors express their gratitude to:

(1) the Management of the R & D Department of the Slovak firm CHEMKO Strážske and Mrs. Ljubov Tokárová, M.Sc. from the Dept. for affording differential scanning calorimeter Pyris DSC-7 and helping with measurements,

(2) the Ministry of Industry and Commerce of the Czech Republic for support the work within the framework of research project No. FC-M2/05.

REFERENCES

[1] S. Zeman, "The impact sensitivity of some nitramines", [Proc]. *10th Symp. Chem. Probl. Connected Stabil. Explos.*, Margretetrop, Sweden, 1995, p. 367-377.

[2] S. Zeman, "Modified Evans-Polanyi-Semenov Relationship in the Study of Chemical Micromechanism Governing Detonation Initiation of Individual Energetic Materials", *Thermochim. Acta 384,*137-154 (2002).

[3] S. Zeman, "New Aspects of the Impact Sensitivity of Nitramines", *Propellants, Explos., Pyrotech. 25*, 66-74 (2000).

[4] V. Zeman, J. Kočí and S. Zeman, "Electric Spark Sensitivity of Polynitro Compounds. Part II. A Correlation with Detonation Velocities of some Polynitro Arenes", *HanNeng CaiLiao 7,* 127-132 (1999).

[5] V. Zeman, J. Kočí and S. Zeman, " Electric Spark Sensitivity of Polynitro Compounds. Part III. A Correlation with Detonation Velocities of some Nitramines", *HanNeng CaiLiao 7,* 172-175 (1999).

[6] S. Zeman and J. Kočí, "Electric Spark Sensitivity of Polynitro Compounds. Part IV. A Relation to Thermal Decomposition Parameters", *HanNeng CaiLiao 8,* 18-26 (2000).

[7] J. Kočí, V. Zeman and S. Zeman, "Electric Spark Sensitivity of Polynitro Compounds. Part V. A Relationship between Electric Spark and Impact Sensitivities of Energetic Materials", *HanNeng CaiLiao 9,* 60-65 (2001).

[8] S. Zeman and Z. Jalový, "Heats of Fusion of Polynitro Derivatives of Polyazaisowurtzitane" *Thermochim. Acta 345,* 31-38 (2000).

[9] S. Zeman and M. Krupka, "Study of the Impact Reactivity of Polynitro Compounds. Part I. Impact Sensitivity as the First Reaction of Polynitro Arenes", [Proc.] *5th Seminar „New Trends in Research of Energetic Materials"*, Univ. Pardubice, April 2002, pp.

[10] S. Zeman and M. Krupka, "Some Predictions of the Heats of Fusion, Heats of Sublimation and Lattice Energies of Energetic Materials", [Proc.] *4th Seminar "New Trends in Reserach of Energetic Materials"*, University of Pardubice, April 2001, pp. 393-401.

[11] S. Zeman and M. Krupka, "Calculated Lattice Energies of Energetic Materials in a Prediction of their Heats of Fusion and Sublimation", *HanNeng CaiLiao 10* (2002) - in press.

[12] E. H. Eyster and L. C. Smith, "*Studies of the ERL Type 12 Dropwieght Impact Machine at NOL*", Report NOLM-10003, NSWC Silver Spring, Jan.1949.

[13] M. J. Kamlet and H. G. Adolph, "The Relationship of Impact Sensitivity with Structure of Organic High Explosives. Part II. Polynitroaromatic Explosives", *Propellants, Explos. 4,* 30-34 (1979).

[14] C. B. Storm, J. R. Stine and J. F. Kramer, "Sensitivity Relationships in Energetic Materials", in S. N. Bulusu (Ed.), "*Chemistry and Physics of Energetic Materials*", Kluwer Acad. Publs., Dordrecht, 1990, pp. 605-639.

[15] D. E. Bliss, S. L. Christian and W. S. Wilson, "Impact Sensitivity of Polynitroaromatics", *J. Energ. Mater. 9,* 319-345 (1991).

[16] S. Zeman, "*Thermostable Polynitro Arenes: Molecular-Structural Aspects of the Chemical and Physical Stabilities*", Ph.D. Thesis, Univ. Pardubice, June 1973.

[17] N. D. Lebedeva, V. L. Ryadenko and I. N. Kuznetsova, "Heats of Combustion and Enthalpies of Formation of some Aromatic Nitro Derivatives" *Zh. Fiz. Khim. 45,* 980-981 (1971).

[18] B. T. Fedoroff, O. E. Sheffield and S. M. Kaye, *"Encyclopedia of Explosives and Related Items"*, PATR 2700, Vol. 7, Picatinny Arsenal, Dover, N. J., 1975, p. H44.

[19] R. B. Cundall, T. F. Palmer and C. E. C. Wood, "Vapor Pressure Measurements on some Organic High Explosives", *J. Chem. Soc., Faraday Trans. 1, 74,* 1339-1345 (1978).

[20] J. M. Rosen and C. Dickinson, "Vapor Pressure and Heats of Sublimation of some High Melting Organic Explosives", *J. Chem. Eng. Data 14,* 120-124 (1969).

[21] J. L. Flippen-Anderson, R. D. Gilardi, A. M. Pitt and W. S. Wilson, "Synthesis and Explosive Properties of Benzotriazoles", *Aust. J. Chem. 45,* 513-524 (1992).

[22] P. G. Hall, "Thermal Decomposition and Phase Transformations in Solid Nitramines", *Trans. Faraday Soc. 67,* 556-562 (1971).

[23] G. Edwards, "The Vapor Pressure of 2,4,6-Trinitrotoluene" *Trans. Faraday Soc. 46,* 423-428 (1950).

[24] S. Zeman, "Some Predictions in the Field of the Physical Stability of Nitramines:, *Thermochim. Acta 302,* 11-16 (1997).

[25] M. Sućeska, M. Rajić, S. Zeman and Z. Jalový, "1,3,3-Trinitroazetidine (TNAZ). Part II. Study of Thermal Behavior", *J. Energ.. Mater. 19,* 259-272 (2001).

[26] R. L. Willer, "Synthesis and Characterization of High Energy Compounds. I. *trans*-1,4,5,8-Tetranitro-1,4,5,8-tetraazadecalin (TNAD)", *Propellants, Explos., Pyrotech. 8,* 65-69 (1983).

[27] T. S. Pivina, M. S. Molchanova, V. A. Shlyapochnikov, D. V. Sukachev, X. Heming, L. De Lu, Y. B. Heng and G. X. Dong, "Hexogen and its Homological Series: Structure, Properties, Perspective", [Proc.] *18th Int. Pyrotech. Seminar,* Breckenridge, Colorado, July 1992, pp. 685-700.

[28] K. Dudek, P. Mareček and P. Vávra, "Laboratory Testing of HNIW Mixtures", [Proc.] *31st Int. Annual Conf. ICT,* Karlsruhe, June 2000, pp. 110/1-110/6.

[29] B. T. Fedoroff and O. E. Sheffield, *"Encyclopedia of Explosives and Related Items"*, PATR 2700, Vol. 5, Picatinny Arsenal, Dover, N. J., 1972, pp. D1478-D1480.

[30] J. Köhler and R. Meyer, *"Explosives"*, 4th Edition, VCH Verlagsgesellschaft mbH, Weinheim, 1993.

[31] B. T. Fedoroff and O. E. Sheffield, *"Encyclopedia of Explosives and Related Items"*, PATR 2700, Vol. 6, Picatinny Arsenal, Dover, N. J., 1974, p. G155.

[32] J. Zhang, R. Hu, Ch. Zhu, G. Feng and Q. Long, "Thermal Behaviour of 1,1,3-Trinitroazetidine", *Thermochim. Acta 298,* 31-35 (1997).

[33] Ou Yuxiang, Wang Cai, Pan Zelin and Chen Boren, "Sensitivity of Hexanitrohexaazaisowurtzitane", *HenNeng CaiLiao 7,* 100-102 (1999).

[34] R. I. Simpson, R. G. Garza, M. F. Foltz, D. I. Ornellas, and P. A. Utriev, *„Characterization of TNAZ"*, Rep. UCRL-ID-119572, Laewrence Livermore Lab., 1994.

[35] J. Vágenknecht, P. Mareček and W. Trzcinski, „Some Characteristics and Detonation Parameters of TEX Explosive", contribution to *J. Energet. Materials.*

[36] R. M. Doherty and R. L. Simpson, „A Comparative Evaluation of Several Insensitive High Explosives". [Proc.] *28th Int. Annual Conf. ICT,* Karlsruhe, June 1997, pp. 32/1-32/23.

[37] V. G. Matveev, V. V. Dubikhin and G. M. Nazin, „Soglasovanyi mekhanism razlozheniya aromaticheskikh nitrosoedinii v gazovoy faze (Thermolysis Mechanism of the Aromatic Nitrocompounds in the Gas Phase)", *Izv. Akad. Nauk SSSR, Ser. Khim.* 474-477 (1978).

[38] S. Bulusu, D. I. Weinstein, J. R. Autera, D. A. Anderson and R. W. Velicky, „Deuterium Kinetic Isotope Effect: An Experimental Probe for the Molecular Processes Governing the Initiation of RDX, HMX and TNT", [Proc.] *8th Int. Symp. on Detonation,* Albuquerque, NM, July, 1985.

[39] L. M. Minier and J. C. Oxley, „Thermolysis of Nitroarenes: 2,2',4,4',6,6'-Hexanitrostilbene", *Thermochim. Acta 166,* 241-249 (1990).

[40] J. Wang and H.-Y. Lang, „Mechanistic Study of Polynitro Compounds by XPS: Mechanism of the Thermal Decomposition of Polynitro Phenols", *Science in China, Ser. B 33,* 257-266 (1990).

[41] S. Zeman, V. Zeman and Z. Kamenský, " Relationship between the Electric Spark Sensitivity and the NMR Chemical Shifts of some Organic Polynitro Compounds", [Proc.] *28th Annual Conf. ICT,* Karlsruhe, June 1997, pp. 66/1-66/9.

[42] M. J. Kamlet, "Relationship between the Impact Sensitivity and Structure of Polynitroaliphatic Organic Compounds", in: A. A. Borisov (Ed.), *"Detonatsiya i vzryvchatye veschestva (Detonation and Explosives)",* Izdat. Mir, Moscow, 1981, pp. 142-159. See also M. J. Kamlet, [Proc.] *6th Symp. (International) on Detonation,* San Diego, Celif., 1976, ONR Rep. ACR 221, p. 312.

[43] A. N. Pavlov, A. A. Fedotov, L. L. Pavlova, Yu. V. Gamera and F. I. Dubovitskii, "Autoprotolytic Mechanism of the Primary Nitramines Thermolysis", in B. V. Novozhilov (Ed.): [Proc.] *9th All-Union Symp. Combust. Explos.,* Suzdal, November 1989, printed by Acad. Sci. USSR, Chernogolovka, pp. 103-107.

[44] T. R. Gibbs and A. Popolato, *"LASL Explosive Property Data"*, Univ. of California Press, Berkeley, 1980, pp. 52-60 and p. 448.

[45] J. E. Field, G. M. Swalowe and S. N. Heavens, "Ignition Mechanism of Explosives During Mechanical Deformation", *Proc. R. Soc. Lond. A 382,* 231-244 (1982).

[46] C. S. Coffey and J. Sharma, "Initiation of Crystalline Explosives due to Energy Dissipated During Plastic Flow", [Proc.] *11th Int. Detonation Symposium*, Snowmass Village, Colorado, August 1998, pp. 66-72.

[47] C. S. Coffey and J. Sharma, "Plastic Deformation, Energy Dissipation, and Initiation of Crystalline Explosives", *Phys. Rev. B: Condens. Mater. Phys. 60,* 9365-9371 (1999).

[48] C. S. Coffey, J. Namkung, J. Sharma and D. W. Edsall, "Plastic Deformation and the Initiation of Explosives", [Proc.] *CPIA Publ., 704 (JANAF 19th Propulsion Systems Hazards Subcom. Meeting, 2000, Vol. 1),* 309-318 (2000).

[49] S. Zeman, "Study of the Impact Reactivity of Polynitro Compounds. Part IV. Allocation of Polynitro Compounds on the Basis of their Impact Sensitivities", [Proc.] *5th Seminar „New Trends in Research of Energetic Materials"*, Univ. Pardubice, April 2002, pp.

STUDY OF THE IMPACT REACTIVITY OF POLYNITRO COMPOUNDS

PART III.

RELATIONSHIP BETWEEN ELECTRONIC CHARGES AT NITROGEN ATOMS OF PRIMARILY SPLIT OFF NITRO GROUPS AND IMPACT SENSITIVITY OF SOME POLYNITRO ARENES

Svatopluk Zeman*, Zdeněk Friedl and Radim Huczala***

* Department of Theory & Technology of Explosives, University of Pardubice, CZ-532 10 Pardubice, Czech Republic

** Faculty of Chemistry, Brno University of Technology, CZ-612 00 Brno, Czech Republic

Abstract:

*Electronic charges q at nitrogen atoms of eight polynitro arenes were calculated by means of ab initio DFT B3LYP/6-31G** and semi-empirical AM1 methods. The relationships have been confirmed between impact sensitivities of the arenes and q-values for primarily split off nitro groups. These relationships directly specify the most reactive nitro groups of molecules with trinitrophenyl and trinitrophenylene building units in the initiation by impact.*

Keywords: *impact sensitivity, polynitro arenes*

1. INTRODUCTION.

It is well known that nitro groups are centres of reactivity in organic polynitro compounds [1-18]. Therefore, it is logical that there exist relationships between the ^{15}N NMR chemical shifts δ_N of nitrogen atoms in nitro groups of nitramines and the Arrhenius parameters of their thermolysis [12,13], impact sensitivity [15,18], electric spark sensitivity [16] and their detonation characteristics [17]. It is also known that the chemical shifts δ_N are connected with electron configurations at the respective nitrogen atoms. Our experiments have confirmed that also the impact sensitivity of polynitro compounds is connected with the electron configuration at the reaction centre of the molecule [15,18]. From what has been said it follows that the impact sensitivity of polynitro compounds should correlate with electronic charges at nitrogen atoms of nitro groups primarily reacting in this type of initiation. Therefore, the present paper deals with the said correlation. For this purpose we chose a group of "genuine" polynitro arenes as model polynitro compounds.

2. DATA SOURCES

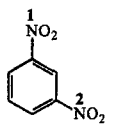
2.1 Impact Sensitivity (Reactivity) Data

Impact sensitivity data (*the drop heights*) were taken from literature [24-27]. Most of them were measured using the Bruceton method [24-27]. The drop heights were re-calculated into the drop energies, E_{dr}, in this paper. The impact sensitivity data of the compounds studied are presented in the following tables (see in 2.2.).

2.2 Electronic charges at nitrogen atoms

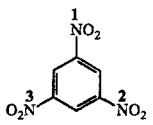
The calculation of electronic charges at nitrogen atoms of nitro groups of the polynitro arenes investigated was carried out by means of the Mulliken and/or NBO (Natural Bond Orbital) population analysis of electron densities (in *e*) obtained both at an *ab initio* level DFT B3LYP/6-31G** and at the semi-empirical level AM1 [19]. A survey of the substances studied, their codes and the results obtained is presented in the following tables:

1,3-Dinitrobenzene (1,3-DNB)				
	Mulliken		NBO	
Nitro group	AM1	B3LYP	AM1	B3LYP
N1	0.571387	0.408809	0.571387	0.514759
N2	0.571387	0.408809	0.571387	0.514759



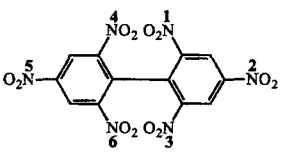
Drop energy 39.0J [27]

1,3,5-Trinitrobenzene (TNB)				
	Mulliken		NBO	
Nitro group	AM1	B3LYP	AM1	B3LYP
N1	0.575496	0.418164	0.575496	0.515373
N2	0.575496	0.418164	0.575496	0.515373
N3	0.575496	0.418164	0.575496	0.515373



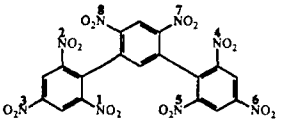
Drop energy 24.64 [24-26]

2,2',4,4',6,6'-Hexanitrobiphenyl (HNB)				
	Mulliken		NBO	
Nitro group	AM1	B3LYP	AM1	B3LYP
N1	0.577910	0.404608	0.577910	0.517751
N2	0.576932	0.411510	0.576932	0.515611
N3	0.577910	0.404608	0.577910	0.517751
N4	0.577910	0.404608	0.577910	0.517751
N5	0.576932	0.411510	0.576932	0.515611
N6	0.577910	0.404608	0.577910	0.517751



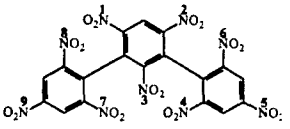
Drop energy 20.92J [25]

2,4,6,4',6',2'',4'',6''-Octanitro[1,1',3',1''] terphenyl (ONT)				
	Mulliken		NBO	
Nitro group	AM1	B3LYP	AM1	B3LYP
N1	0.573071	0.401511	0.573071	0.517520
N2	0.580559	0.397361	0.580559	0.517528
N3	0.576309	0.409777	0.576309	0.515048
N4	0.572976	0.398861	0.572976	0.517297
N5	0.580478	0.395753	0.580478	0.516735
N6	0.576346	0.409986	0.576346	0.515393
N7	0.578274	0.430621	0.578274	0.524186
N8	0.578292	0.430947	0.578292	0.523812



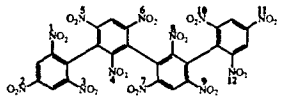
Drop energy 15.73J [25]

2,2',2'',4,4',4'',6,6',6''-Nonanitro[1,1',3',1'']terphenyl (NONA)				
	Mulliken		NBO	
Nitro group	AM1	B3LYP	AM1	B3LYP
N1	0.581734	0.406614	0.581734	0.518912
N2	0.581777	0.408104	0.581777	0.519168
N3	0.582106	0.399252	0.582106	0.525837
N4	0.579877	0.427681	0.579877	0.522453
N5	0.576479	0.412352	0.576479	0.515405
N6	0.575444	0.408234	0.575444	0.519226
N7	0.575387	0.406980	0.575387	0.519226
N8	0.579727	0.426567	0.579727	0.522716
N9	0.576480	0.412133	0.576480	0.515394



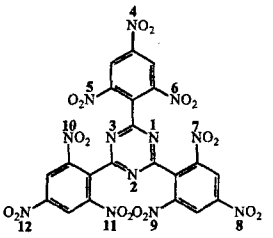
Drop energy 9.10J [25]

2,2',2'',2''',4,4',4'',4''',6,6',6'',6'''-Dodecanitro-[1,3',1',1'']quaterphenyl (DODECA)				
	Mulliken		NBO	
Nitro group	AM1	B3LYP	AM1	B3LYP
N1	0.575822	0.408400	0.575822	0.520247
N2	0.576493	0.408265	0.576493	0.515657
N3	0.579935	0.404754	0.579935	0.520243
N4	0.578834	0.406848	0.578834	0.524370
N5	0.581681	0.414803	0.581681	0.522607
N6	0.581333	0.408594	0.581333	0.521077
N7	0.578476	0.378955	0.578476	0.516247
N8	0.577820	0.416432	0.577820	0.522880
N9	0.582087	0.414743	0.582087	0.522940
N10	0.574580	0.415266	0.574580	0.519840
N11	0.576396	0.412391	0.576396	0.515576
N12	0.579665	0.414463	0.579665	0.521941



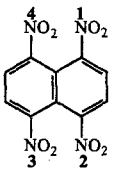
Drop energy 9.85J [25]

2,4,6-tris(2,4,6-Trinitrophenyl)-[1,3,5]triazine (TPT)				
	Mulliken		NBO	
Nitro group	AM1	B3LYP	AM1	B3LYP
N1	-0.134326	-0.406044	-0.134326	-0.464482
N2	-0.140723	-0.407646	-0.140723	-0.466087
N3	-0.143975	-0.398293	-0.143975	-0.463580
N4	0.575113	0.412648	0.575113	0.515421
N5	0.575117	0.441682	0.575117	0.518467
N6	0.574800	0.436213	0.574800	0.517381
N7	0.575784	0.418187	0.575784	0.517353
N8	0.575219	0.410799	0.575219	0.515149
N9	0.575414	0.436912	0.575414	0.518493
N10	0.574505	0.447437	0.574505	0.518875
N11	0.574723	0.434366	0.574723	0.518258
N12	0.574970	0.413166	0.574970	0.515534



Drop energy 22.85J [25]

1,4,5,8-Tetranitronaphthalene (TENN)				
	Mulliken		NBO	
Nitro group	AM1	B3LYP	AM1	B3LYP
N1	0.565289	0.403134	0.565289	0.514654
N2	0.565269	0.403134	0.565269	0.514654
N3	0.565269	0.403134	0.565269	0.514654
N4	0.565289	0.403134	0.565289	0.514654



Drop energy 24,61J [25]

3. DISCUSSION

It is a generally known fact that chemical changes in thermolysis or in initiation of "genuine" polynitro arenes primarily affect nitro groups that are sterically hindered (for discussion of these see Refs [13,20-22]). The results of semi-empirical level AM1 method clearly show that nitrogen atoms of all those nitro groups exhibit the highest positive values of the charge q [20,21]. The analysis of inter-correlation between these q values and the impact sensitivity of the studied polynitro arenes are presented in Fig. 1. Figures 2 and 3 represent analogous relationship resulting from the *ab initio* level DFT B3LYP/6-31G** method. They were, however, derived with the application of the q values of those nitrogen atoms that exhibit the maximum values of this charge according to the AM1 method.

As it follows from papers [15, 18, 23] the impact sensitivity can also be considered a function of intermolecular interactions in the molecular crystal. However, the q values concern the isolated molecules. This disproportion is probably responsible for the fact that the relationships depicted in Figs 1-3 are only valid within very narrow molecular-structure series of compounds, in the present case derivatives having 2,4,6-trinitrophenyl and 2,4,6-trinitrophenylene building units in their molecules (Figs 1 and 3). The disproportion is even more marked in the case of application of B3LYP/Mulliken charges in Fig. 2: here the substances having 2,4,6-trinitrophenylene building units in their molecules (i.e. NONA and DODECA) became separated. Nevertheless, it can be stated that all the calculation methods adopted in this work have led to an identical finding: primary chemical changes in the impact initiation of "genuine" polynitro arenes primarily affect nitro groups that are sterically hindered.

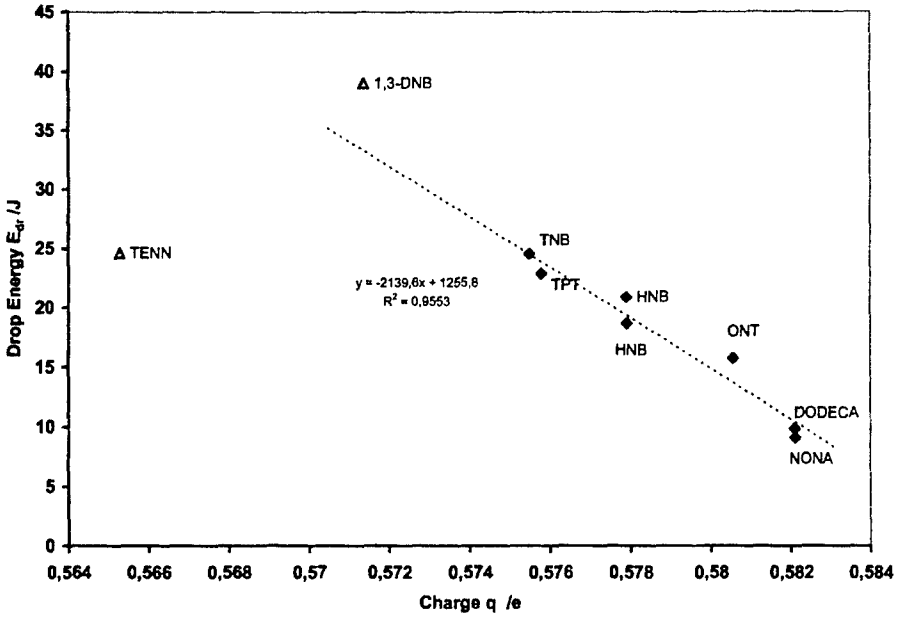


Fig 1. Plot of impact sensitivity of polynitro arenes versus AM1/Mulliken charges.

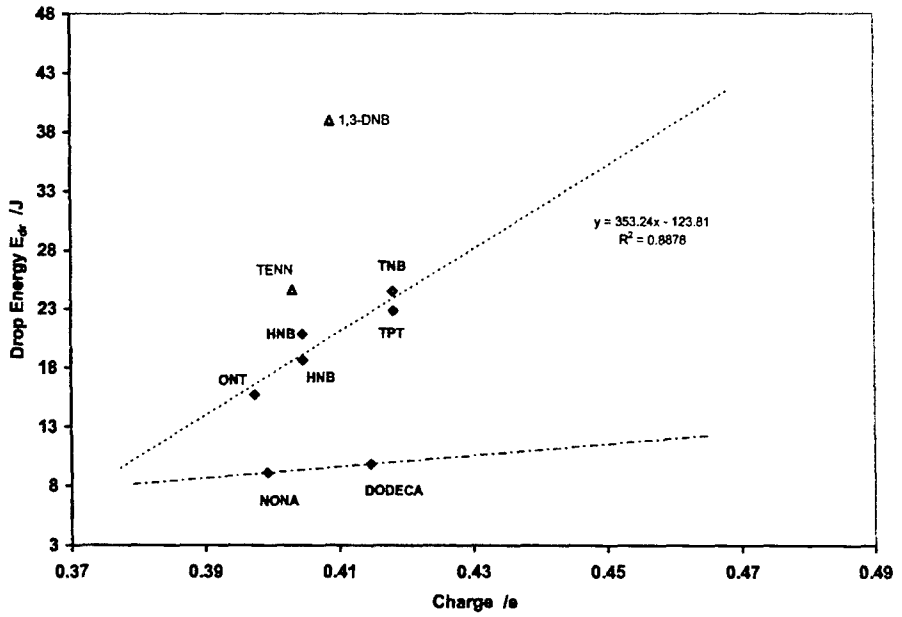


Fig 2. Plot of impact sensitivity of polynitro arenes versus B3LYP/Mulliken charges.

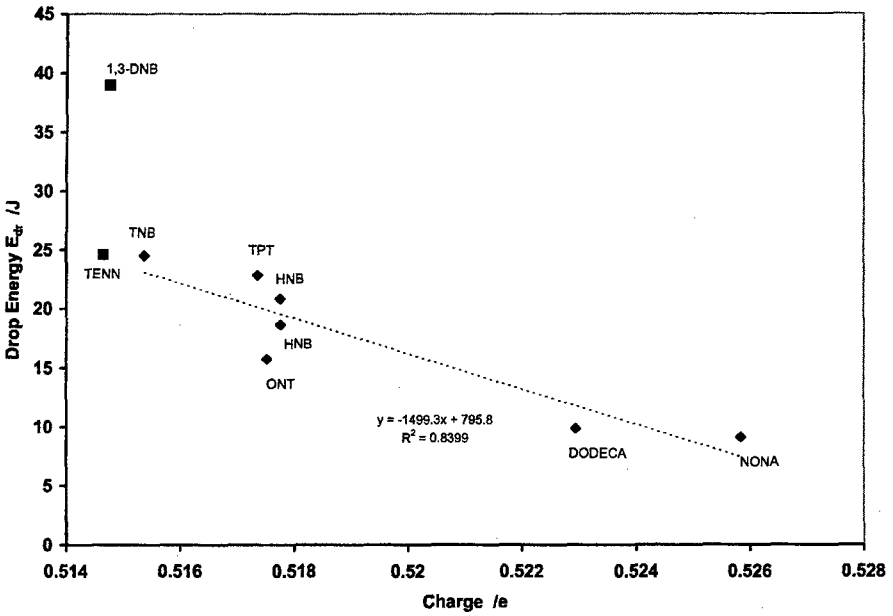


Fig 3. Plot of impact sensitivity of polynitro arenes versus B3LYP/NBO charges.

4. CONCLUSION

It is possible to specify a relationship between the electron charges q and the impact sensitivity of polynitro arenes having trinitrophenyl and trinitrophenylene building units in their molecules. The q values correlating in the sense of this relationship belong to the most sterically hindered nitro groups in the molecule. These nitro groups undergo the primary chemical changes after an impact has affected the molecule. These statements agree with the theoretical findings [2,4-7] concerning shock and impact reactivity of polynitro compounds.

Acknowledgements

The authors express their gratitude to the Ministry of Industry and Commerce of the Czech Republic for support the work within the framework of research project No. FC-M2/05.

REFERENCES

[1] A. Delpuech and J. Cherville, "Application de la Chimie theoretique a la Recherche d'un Critere de Sensibilite des Explosifs" [Proc.], *Symposium H.D.P. "Corportement des Milieux Denses Soushautes Pressions Dynamiques"*, Paris, 27-31 Aout, 1978.

[2] A. Delpuech and J. Cherville, "Relation entre la Structure Electronique et la Sensibilite au Choc des Explosifs secondaries Nitres. Critere Moleculaire de Sensibilite. I", *Propellants Explos. 3*, 169-175 (1978).

[3] A. Delpuech and J. Cherville, "Relation entre la Structure Electronique et la Sensibilite au Choc des Explosifs secondaries Nitres. III", *Propellants Explos. 4*, 61-65 (1979).

[4] F. J. Owens and P. Politzer, *Molecular Orbital Calculation of Indices of Impact and Shock Induced Reactivity in Trinitroaromatic Molecules,* in Shock Waves Condens. Matter, Proc. 4th Am. Phys. Soc. Top. Conf. 1985, Publ. Plenum Press, New York, 1986, pp. 857-861.

[5] Xiao Heming, Wang Zun-Yao and Yao Jian-Min, "Quantum Chemical Study on Sensitivity and Stability of Aromatic Nitro Explosives", *Acta Chim. Sinica 43*, 14-18 (1985).

[6] F. J. Owens, K. Jayasuriya, L. Abrahmsen and P. Politzer, "Computational Analysis of some Properties Associated with the Nitro Groups in Polynitroaromatic Molecules", *Chem. Phys. Letter 116,* 434-438 (1985).

[7] Fan Jianfen and Xiao Heming, "Theoretical Study on Pyrolysis and Sensitivity of Energetic Compounds", *J. Mol. Struct. (THEOCHEM) 365*, 225-229 (1996)

[8] F. J. Owens, "Calculation of Energy Barriers for Bond Rupture in some Energetic Molecules", *J. Mol. Struct. (THEOCHEM) 370,* 11-16 (1996).

[9] J. S. Murray and P. Politzer, "Computational Studies of Energetic Nitramines", in S. N. Bulusu (Ed.): *Chemistry and Physics of Energetic Materials*. Kluwer Acad. Publ., Dordrecht, 1990, pp. 175-193.

[10] P. Politzer, J. S. Murray, P. Lane, P. Sjøberg and H. G. Adolph, "Shock-Sensitivity Relationships for Nitramines and Nitroaliphatics", *Chem. Phys. Letters 181*, 78-82 (1991).

[11] J. S. Murray, P. Lane, P. Politzer and R. Bolduc, "A Relationship Between Impact Sensitivity and the Electrostatic Potentials at the Midpoints of C-NO_2 bonds in Nitroaro*matics", Chem. Phys. Letters 168,* 135-139 (1990).

[12] S. Zeman, "Relationship Between the Arrhenius Parameters of the Low-Temperature Thermolysis and the ^{13}C and ^{15}N Chemical Shifts of Nitramines", *Thermochim. Acta 202,* 191- (1992).

[13] S. Zeman, "Modified Evans-Polanyi-Semenov Relationship in the Study of Chemical Micromechanism Governing Detonation Initiation of Individual Energetic Materials", *Thermochim. Acta 384,*137-154 (2002).

[14] S. Zeman, "Analysis and Prediction of the Arrhenius Parameters of Low-Temperature Thermolysis of Nitramines by Means of the ^{15}N NMR Spectroscopy", *Thermochim. Acta 333,* 121-129 (1999).

[15] S. Zeman, "New Aspect of the Impact Reactivity of Nitramines", *Propellants, Explos., Pyrotech., 25,* 66-74 (2000).

[16] S. Zeman, V. Zeman and Z. Kamenský, "Relationship between Electric Spark Sensitivity and the NMR Chemical Shifts of some Organic Polynitro Compounds", [Proc.] *28th Int. Annual Conf. ICT*, Karlsruhe. 1997, p. 66/1-66/9.

[17] S. Zeman, "Relationship between Detonation Characteristics and ^{15}N NMR Chemical Shifts of Nitramines",. *J. Energet. Mater. , 17,* 305-330 (1999).

[18] S. Zeman and M. Krupka, "Study of Impact Reactivity of Polynitro Compounds. Part I. Impact Sensitivity as the First Reaction of Polynitro Arenes", [Proc.] *5th Seminar „New Trends in Research of Energetic Materials"*, Univ. Pardubice, April 2002, pp.

[19] *PC software TITAN v.1.0.5 (CPU Pentiun4 1.7 GHz, 512 MB RAM, 36 GB SCISI HD).* Wavefunction Inc., Schrödinger Inc., USA , 2000.

[20] R. Huczala, S. Zeman and Z. Friedl, "Relationship between Electronic Charges at Nitrogen Atoms of Primarily Split Off Nitro Groups and Detonation Characteristics of some m-Dinitro-benzopolyazaarenes:, [Proc.] *4th Seminar "New Trends in Research of Energetic Materials"*, University of Pardubice, April 2001, pp. 131-143.

[21] S. Zeman, R. Huczala and Z. Friedl, "The Study of Chemical Micromechanism Governing Detonation Initiation of Some *m*-Dinitrobenzopolyazaarenes", *J. Energ. Mater. 20,* (2002) – in press.

[22] S. Zeman, "Thermal Stabilities of Polynitroaromatic Compounds and their Derivatives", *Thermochim. Acta 31,* 269-283 (1979).

[23] S. Zeman and M. Krupka, "Study of the Impact Reactivity of Polynitro Compounds. Part II. Impact Sensitivity as a Function of Intermolecular Interactions", [Proc.] *5th Seminar „New Trends in Research of Energetic Materials"*, Univ. Pardubice, April 2002, pp.

[24] M. J. Kamlet and H. G. Adolph, "The Relationship of Impact Sensitivity with Structure of Organic High Explosives. Part II. Polynitroaromatic Explosives", *Propellants, Explos. 4,* 30-34 (1979).

[25] C. B. Storm, J. R. Stine and J. F. Kramer, "Sensitivity Relationships in Energetic Materials", in S. N. Bulusu (Ed.), "*Chemistry and Physics of Energetic Materials*", Kluwer Acad. Publs., Dordrecht, 1990, pp. 605-639.

[26] D. E. Bliss, S. L. Christian and W. S. Wilson, "Impact Sensitivity of Polynitroaromatics", *J. Energ. Mater. 9,* 319-345 (1991).

[27] J. Köhler and R. Mayer, "*Explosives*", 4th Edition, VCH Verlagsgesellschaft mbH, Weinheim, 1993.

STUDY OF THE IMPACT REACTIVITY OF POLYNITRO COMPOUNDS

PART IV.

ALLOCATION OF POLYNITRO COMPOUNDS ON THE BASIS OF THEIR IMPACT SENSITIVITIES

Svatopluk Zeman

Department of Theory & Technology of Explosives, University of Pardubice,
CZ-532 10 Pardubice, Czech

Abstract:

A linear relationship has been found between the drop energies of impact sensitivity detected by sound and the drop energies of „the first reaction" for 25 polynitro compounds. In the sense of this relationship, the compounds studied fall into three classes. The reason of the said diversification lies in the decomposition reaction rate at the temperature of beginning thermolysis.

Keywords: *impact sensitivity, polynitro compounds*

1. INTRODUCTION

The impact reactivities of energetic materials have been studied from the point of view of both the quantum chemistry [1-7] and the molecular structure-reactivity relationships [8-15]. Especially recently, new findings have appeared about the impact sensitivity as "the first reaction" [12-14] and the sensitivity detected by sound [15]. However, the interrelation between the two types of sensitivities has not been investigated yet. Therefore, the present paper deals with the said relationship applied to the area of polynitro compounds. Its interpretation has also been supported by some data obtained from the thermal decomposition of the compounds mentioned.

2. DATA SOURCES

2.1 Thermal Decomposition Data

The data on the onset of exothermic decomposition of most polynitro compounds studied were obtained by means of differential thermal analysis (DTA) in the papers [16-18]: these DTA onsets, T_D, correspond to a linear temperature increase of 5 °C min^{-1} and samples of 0.09-0.11 g [16,17] or 0.05 g [18] magnitude.

Table 1. Survey of the studied compounds, their code designations and thermal decomposition data.

Polynitro compound			Thermal decomposition data						
Data No.	Chemical name	Code designation	DTA onsets		Arrhenius parameters				
			T_D in K	Ref.	Method of evaluation	State of decomposition	E_a in kJ mol^{-1}	log A in s^{-1}	Ref.
1	1,3,5-Trinitrobenzene	TNB	580	16	SMM	liquid	180.03	10.9	28
2.1	1-Methyl-2,4,6-trinitrobenzene	TNT	526	16	SMM	liquid	144.44	9.3	28
2.2		TNT			DSC	liquid	143.90	11.4	29
3	1,3-Dimethyl-2,4,6-trinitrobenzene	TNX	521	16	SMM	liquid	146.95	9.1	28
4	1,3,5-Trimethyl-2,4,6-trinitrobenzene	TNMs	488	16	SMM	liquid	185.05	12.3	28
5	1-Methyl-3-hydroxi-2,4,6-trinitrobenzene	TNCr	468	a	SMM	liquid	192.46	15.6	30
6	1,4,5,8-Tetranitronaphthalene	TENN	579	16	DTA	solid	223.05	15.0	31
7	2,2',4,4',6,6'-Hexanitrobiphenyl	HNB	534	16	SMM	liquid	207.24	16.1	32
8	3,3'-Dimethyl-2,2',4,4',6,6'-hexanitrobiphenyl	BITNT	489	16	SMM	solid	106.40	5.3	33
9	2,2',4,4',6,6'-Hexanitrobibenzyl	DPE	514	16	extrapol.	liquid	124.00	6.3	34
10	2,2',4,4',6,6'-Hexanitrostilbene	HNS	544	16	SMM	solid	183.80	12.0	35
11	2,2',4,4',6,6'-Hexanitrodiphenylsulfide	DIPS	525	16	SMM	liquid	131.80	7.4	36
12	2,2',4,4',6,6'-Hexanitrodiphenylsulfone	DIPSO	530	16	SMM	solid	106.76	5.6	37
13	2,2',4,4',6,6'-Hexanitrodiphenylamine	DPA	513	17	TGA	solid	153.30	11.0	38
14	2,2',4,4',6,6'-Hexanitrooxanilide	HNO	550	16	SMM	solid	215.62	16.0	35
15	3-Nitro-1,2,4-triazol-5-one	NTO	507	a	chemilum.	solid	140.00	6.7	39
16	Pentaerythritol tetranitrate	PETN	421	18	SMM	liquid	163.17	15.6	40
17	1,3-Dinitro-1,3-diazacyclobutane	TETROGEN	440	b	calcd.		153.10	14.1[c]	41
18	1,3,5-Trinitro-1,3,5-triazacyclohexane	RDX	478	18	manometr.	solid	198.90	18.5	42
19.1	1,3,5,7-Tetranitro-1,3,5,7-tetraazacyclooctane	β–HMX	509	18	manometr.	solid	220.50	19.5	42
19.2		β–HMX			DSC	solid	214.60	18.8	43
20	1,3,5,7,9-Pentanitro-1,3,5,7,9-pentaazacyclodecane	DECAGEN	475	b	^{15}N NMR	solid	213.50	18.6	44
21	2,4,6,8,10,12-Hexanitro-2,4,6,8,10,12-hexaazaisowurtzitane	ε–HNIW	480	a	TGA	sold	172.00	13.8	45
22	1,4-Dinitrotetrahydroimidazo[4,5-d]imidazol-2,5-(1H,3H)-dione	DINGU	403	18	DSC	solid	217.82	20.9	46

Notices: a) the value resulted from DTA measurements in this paper; b) the predicted value; c) the value taken from ref. 44

Table 2. Survey of the impact sensitivities and calculated logarithms of rate constants for the temperatures of decomposition onsets of the studied compounds.

Polynitro compound				Impact sensitivity data expressed as drop enrgy, E_{dr}, in J, detected as:				Logarithm of the rate constant for temperature T_D (Table 1)
Class of compds. (Fig. 1)	Data No.	Chemical name	Code designation	the first reaction	Ref.	sound effect	Ref.	
A	1	1-Methyl-2,4,6-trinitrobenzene	TNT	35.86	14,23	39.24	9,15	-11.6146
	1.1		TNT					-6.6558
	2	2,2',4,4',6,6'-Hexanitrodiphenylamine	DPA	10.16	14,23	11.81	9,15	-10.6146
	2.1		DPA			7.50	15,47	
	3	2,2',4,4',6,6'-Hexanitrooxanilide	HNO	8.70	14,23	7.50	48	-10.3124
	4	1,3-Dinitro-1,3-diazacyclobutane	TETROGEN	10.78	13	9.97	15	-9.3852
	5	1,3,5-Trinitro-1,3,5-triazacyclohexane	RDX	6.69	13,23	5.90	8,15	-7.4513
	6	1,3,5,7-Tetranitro-1,3,5,7-tetraazacyclooctane	β–HMX	7.59	13,23	6.40	8,15	-7.2047
	6.1		β–HMX					-7.4223
	7	1,3,5,7,9-Pentanitro-1,3,5,7,9-pentaazacyclodecane	DECAGEN	5.90	13	4.90	12,15	-11.2342
	8	Pentaerythritol tetranitrate	PETN	3.59	23	2.90	12	-10.6971
						Average *ln k* value		*-9.2591*
B	9	1,3-Dimethyl-2,4,6-trinitrobenzene	TNX	9.90	14,23	10.46	11,15	-12.9716
	10	2,4,6-Trinitrobenzoic acid	TNBA	8.28	14,23	26.82	9,15	
	11	2,2',4,4',6,6'-Hexanitrodi[henylsulfide	DIPS	2.94	14,23	6.00	15,49	-13.1566
	11.1		DIPS			7.30	15,47	
	12	2,2',4,4',6,6'-Hexanitrodiphenylsufone	DIPSO	3.86	14,23	8.44	15,49	-11.3340
	13	2,2',4,4',6,6'-Hexanitrostilbene	HNS	3.64	14,23	11.50	9,15	-13.0073
	14	1,4,5,8-Tetranitronaphthalene	TENN	9.64	14,23	24.61	10	-11.7967
	15	2,5-Dinitro-2,5-diazahexane-3,4-dione	DMNO	6.94	12,23	19.44	8	
	16	2,4,6,8,10,12-Hexanitro-2,4,6,8,10,12-hexaazaisowurtzitanre	ε–HNIW	5.38	13	11.90	15,50	-11.5954
	16.1		ε–HNIW	4.6±0.6	24			
						Average ln k value		*-12.3103*

Table 2- continued

Polynitro compound				Impact sensitivity data expressed as drop enrgy, E_{dr}, in J, detected as:				Logarithm of the rate constant for temperature T_D (Table 1)
Class of compds. (Fig. 1)	Data No.	Chemical name	Code designation	the first reaction	Ref.	sound effect	Ref.	
C	17	1,3,5-Trinitrobenzene	TNB	5.90	14,23	24.64	9,15	-12.2360
	18	1,3,5-Trimethyl-2,4,6-trinitrobenzene	TNMs	7.41	14,23	20.45	11,15	-17.2880
	19	1-Methyl-3-hydroxi-2,4,6-trinitrobenzene	TNCr	9.40	14,23	47.00	10,15	-13.5431
	20	2,2',4,4',6,6'-Hexanitrobiphenyl	HNB	2.79	14,23	20.92	9,15	-9.6074
	21	2,2',4,4',6,6'-Hexanitrobibenzyl	DPE	5.79	14,23	28.06	10,15	-14.5105
	22	3,3'-Dimethyl-2,2',4,4',6,6'-hexanitrobiphenyl	BITNT	7.40	14,23	33.14	9,15	-13.9674
	23	1,4-Dinitrotetrahydroimidazo[4,5-d]imidazol-2,5(1H,3H)-dione	DINGU	5.55	12	24.61	10	-16.8863
	24	3-Nitro-1,2,4-triazol-5-one	NTO	15.85	23	71.61	10	-17.7858
	25	Nitroguanidine	NQ	9.22	26	43.45	51	
							Average *ln k* value	*-14.4780*

Note: the kinetic parameters of thermal decomposition, which would be compatible with outputs of the Russian manometric method (SMM), are not available for TNBA, DMNO and NQ.

Some of the T_D values were obtained within the work described in this paper. The measurements were carried out on a DTA 550 Ex apparatus [19,20] specially developed for thermal analysis of explosives at our Detp. The apparatus represents a considerably modernised version of one used in the research described in [18]. Te measurements were realised at ambient pressure, the sample being in direct contact with atmospheric air. The weighed sample (0.05 g) was placed in a Simax test tube of 5 mm diameter and 50 mm length. The reference standard was aluminium oxide (0.05 g). The T_D values of the compounds examined are given in Table 1.

The data obtained from Russian manometric method (SMM) [21] formed the main source of the Arrhenius parameters (i.e. E_a and log A) of thermal decomposition of the substances studied. It is possible to apply also these kinetic data from the differential scanning calorimetry (DSC), which are directly compatible with the SMM results in many cases [21,22]. Results of the differential thermal analysis (DTA) and thermo-gravimetric analysis (TGA) can be converted to compatible values by means of the calibration curves [21,22]. The above-mentioned E_a and log A parameters can also be obtained by prediction on the basis of modified Evans–Polanyi–Semenov equation or by means of outputs of the ^{15}N NMR spectroscopy [22]. The said parameters of the compounds studied are given in Table 1.

2.2 Impact sensitivity data.

The results of determination of impact sensitivity detected on the basis of sound (see the Bruceton method) were taken from literature [8-11] and are presented in Table 2 as drop energies, E_{dr}. The sensitivity characteristics of "the first reaction", expressed in the same way, come from papers [12-14, 23]: for this kind of sensitivity determination in the Budapest laboratory of the Hungarian company GEOINFORM Szolnok, the standard impact tester (*Julius Peters*) was used with exchangeable anvil and the amount of tested substance was 0.25 cm^3 (*refs.* [14,23,25]); 2 kg and 5 kg weight drop hammers were used [23,25].

In the case of "the first reaction" of ε-HNIW, Table 2 presents the E_{dr} value predicted for the chemical species [13] along with that determined with a technical sample of this nitramine in Research Institute of Coal (VVUÚ) Ostrava [24].

3. DISCUSSION

The mechanism of transfer of drop energy to the reaction centre of molecule in the case of the impact sensitivity as "the first reaction" should differ from that in the case of impact sensitivity detected by sound [15]. Comparison of the drop energy values (E_{dr}) of the two types of impact sensitivity leads to relationships shown in Fig. 1. In the sense of this diagram, the set of the polynitro compounds studied falls into three classes. Below, the interpretation of this fact is approached starting from findings about primary fragmentation of molecule of energetic materials by action of outer stimuli.

The homolytic fragmentations or reactions of the C–NO_2, N–NO_2, N–NO, and O–NO_2 groupings, or other bearers of explosibility (i.e. explosophores), are common primary fission processes of energetic materials under thermal, impact, shock, and electric spark stimuli (see Ref. [22] and references herein). Therefore, it is natural that there exist relationships between impact sensitivities and characteristics of thermal decomposition of polynitro compounds [12-14, 27]

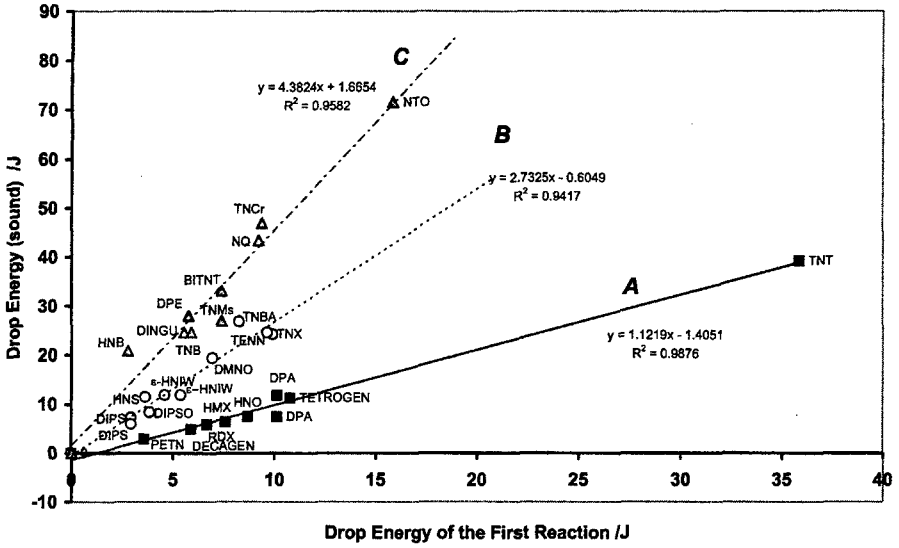


Fig 1. Relationships between impact sensitivity, detected for sound, and the sensitivity, defined as „the first reaction".

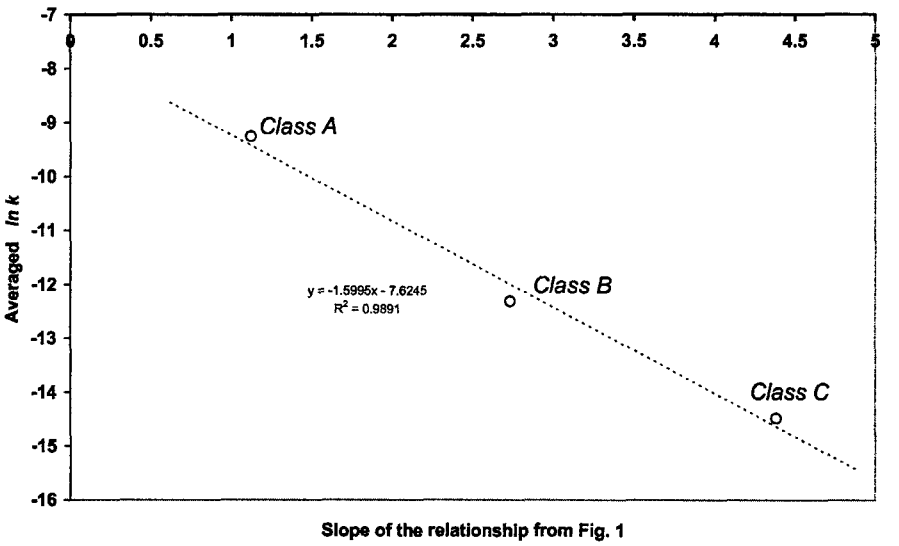


Fig 2. Averaged logarithms of the rate constants, *ln k,* versus slope of the relationships from Fig. 1.

Hence, the interpretation of the relationships shown in Fig. 1 could start from the critical temperature (from Frank–Kamentskii equation – see e.g. [29]), which is an important characteristic of thermal stability of energetic materials. The rate of thermal decomposition of the studied polynitro compounds at the temperature might be the reason of their diversification in the sense of Fig. 1. However, the values of critical temperatures of many compounds from the studied set were not available. Therefore, in the first rough approximation we applied the onset values (T_D) of thermal decomposition of the polynitro compounds. These T_D values (see Table 1) are easily specified by means of simple differential thermal analysis (DTA). From the Arrhenius parameters of thermal decomposition given in Table 1, we then calculated the logarithms of rate constants, ln k, for the temperatures of their decomposition onset T_D. The results are presented in Table 2. There it can be seen that the ln k of the individual compounds in a given class in Fig. 1 have close values (*theoretically, the values should be identical for all substances of a given class*)

As far as the composition of classes of compounds in Fig. 1 is concerned, classes *A* and *C* include the most reactive and the least reactive (*even the LOVA explosives NQ and NTO*) polynitro compounds, respectively. Paradoxically, the drop energies, E_{dr}, of "the first reaction" of the most reactive members of class *A* exceed in their values the energies of sensitivity detected by sound (see Table 2). This can be due to the method adopted for obtaining the first mentioned E_{dr} values [23, 25]. The E_{dr} value of 9.22 J for NQ, taken from ref. [26], corresponds with "the first reaction".

Thus the decomposition reaction rate of the polynitro compounds studied at the critical temperature really appears to be the reason of their diversification in the sense of Fig. 1. The said fact is also documented by mutual comparison of averaged *ln k* values of the individual classes of compounds with the values of slopes of the respective relationships in Fig. 1. Such a comparison is shown in Fig. 2.

4. CONCLUSION

There exists a linear dependence between the drop energies of impact sensitivity detected by sound and those of "the first reaction". The polynitro compounds are diversified in the sense of this relationship and fall into three classes. Each of them includes compounds with close values of thermolysis rate constants of these substances at the temperatures of beginning exothermic decomposition. The given temperatures result from differential thermal analyses of the said compounds. However, the application in the mentioned sense of critical temperatures would be more appropriate.

Acknowledgements

The author expresses his gratitude to his former student, Mr. Zsolt Jermann, for precise work and high level of results treatment within the framework of corresponding Thesis [23]. The author also expresses his gratitude to:

(1) the Hungarian company GEOINFORM Szolnok for affording the impact tester and sponsoring the respective measurements,

(2) the Ministry of Industry and Commerce of the Czech Republic for support the work within the framework of research project No. FC-M2/05.

REFERENCES

[1] A. Delpuech and J. Cherville, "Application de la Chimie theoretique a la Recherche d'un Critere de Sensibilite des Explosifs" [Proc.], *Symposium H.D.P. "Corportement des Milieux Denses Soushautes Pressions Dynamiques"*, Paris, 27-31 Aout, 1978.

[2] A. Delpuech and J. Cherville, "Relation entre la Structure Electronique et la Sensibilite au Choc des Explosifs secondaries Nitres. Critere Moleculaire de Sensibilite. I", *Propellants Explos. 3*, 169-175 (1978).

[3] A. Delpuech and J. Cherville, "Relation entre la Structure Electronique et la Sensibilite au Choc des Explosifs secondaries Nitres. III", *Propellants Explos. 4*, 61-65 (1979).

[4] F. J. Owens and P. Politzer, "Molecular Orbital Calculation of Indices of Impact and Shock Induced Reactivity in Trinitroaromatic Molecules", in [Proc.] *Shock Waves Condens. Matter,. 4th Am. Phys. Soc. Top. Conf. 1985,* Publ. Plenum Press, New York, 1986, pp. 857-861.

[5] Xiao Heming, Wang Zun-Yao and Yao Jian-Min, "Quantum Chemical Study on Sensitivity and Stability of Aromatic Nitro Explosives", *Acta Chim. Sinica 43,* 14-18 (1985).

[6] P. Politzer, J. S. Murray, P. Lane, P. Sjøberg and H. G. Adolph, "Shock-Sensitivity Relationships for Nitramines and Nitroaliphatics", *Chem. Phys. Letters 181,* 78-82 (1991).

[7] J. S. Murray, P. Lane, P. Politzer and R. Bolduc, "A Relationship Between Impact Sensitivity and the Electrostatic Potentials at the Midpoints of C-NO_2 bonds in Nitroaromatics", *Chem. Phys. Letters 168,* 135-139 (1990).

[8] M. J. Kamlet, "Relationship between the Impact Sensitivity and Structure of Polynitroaliphatic Organic Compounds", in: A. A. Borisov (Ed.), *"Detonatsiya i vzryvchatye veschestva (Detonation and Explosives)",* Izdat. Mir, Moscow, 1981, pp. 142-159. See also M. J. Kamlet, [Proc.] *6th Symp. (International) on Detonation,* San Diego, Celif., 1976, ONR Rep. ACR 221, p. 312.

[9] M. J. Kamlet and H. G. Adolph, "The Relationship of Impact Sensitivity with Structure of Organic High Explosives. Part II. Polynitroaromatic Explosives", *Propellants, Explos. 4,* 30-34 (1979).

[10] C. B. Storm, J. R. Stine and J. F. Kramer, "Sensitivity Relationships in Energetic Materials", in S. N. Bulusu (Ed.), *"Chemistry and Physics of Energetic Materials"*, Kluwer Acad. Publs., Dordrecht, 1990, pp. 605-639.

[11] D. E. Bliss, S. L. Christian and W. S. Wilson, "Impact Sensitivity of Polynitroaromatics", *J. Energ. Mater. 9,* 319-345 (1991).

[12] S. Zeman, "The impact sensitivity of some nitramines", [Proc]. *10th Symp. Chem. Probl. Connected Stabil. Explos.*, Margretetrop, Sweden, 1995, p. 367-377 .

[13] S. Zeman, "New Aspect of the Impact Reactivity of Nitramines", *Propellants, Explos., Pyrotech., 25* 66-74 (2000).

[14] S. Zeman and M. Krupka, "Study of the Impact Reactivity of Polynitro Compounds. Part I. Impact Sensitivity as „the first reaction" of Polynitro Arenes", [Proc.] *5th Seminar „New Trends in Research of Energetic Materials"*, Univ. Pardubice, April 2002, pp.

[15] S. Zeman and M. Krupka, "Study of the Impact Reactivity of Polynitro Compounds. Part II. Impact Sensitivity as a Function of Intermolecular Interactions", [Proc.] *5th Seminar „New Trends in Research of Energetic Materials"*, Univ. Pardubice, April 2002, pp.

[16] S. Zeman, "Thermal Stabilities of Polynitroaromatic Compounds and their Derivatives", *Thermochim. Acta 31,* 269-283 (1979).

[17] S. Zeman, "Possibilities of Applying the Piloyan Method of Determination of Decomposition Activation Energies. Part. III. Derivatives Containing Two Picryl Groups in the Molecule, and Melamine derivatives", *J. Thermal Anal. 19,*107-115 (1980).

[18] S. Zeman, J. Fedák and M. Dimun, „Non-Isothermal Defferential Thermal Analysis in the Specification of the Thermostability Threshold of Thermodynamically Unstable Substances of Aliphatic Series", *Zbornik Radova 19*, 71-81 (1983).

[19] M. Krupka, „Thermal Analysis of Selected Organic Nitrocompounds", [Proc.] *2nd Seminar "New Trends in Research of Energetic Materials"*, Univ. Pardubice, April 1999, p. 70-78.

[20] M. Krupka, „Devices and Equipment for Testing of Energetic Materials", [Proc.] *4th Seminar "New Trends in Research of Energetic Materials"*, Univ. Pardubice, April 2001, p. 222-227.

[21] S. Zeman, "Kinetic Compensation Effect and Thermolysis Mechanisms of Organic Polynitroso and Polynitro Compounds", *Thermochim. Acta 290,* 199-217 (1997).

[22] S. Zeman, "Modified Evans-Polanyi-Semenov Relationship in the Study of Chemical Micromechanism Governing Detonation Initiation of Individual Energetic Materials", *Thermochim. Acta 384,*137-154 (2002).

[23] Z. Jermann, *"Impact Sensitivity of some Explosives",* M.Sc.-Thesis, Univiversity of Pardubice, June, 1994.

[24] "Determination of the impact sensitivity of ε–HNIW", *Test report No. A00211-V06246/04/99,* VVUÚ Ostrava-Radvanice, Nov. 11th, 1999.

[25] *"Testing Methods of Explosives: Testing the Impact Sensitivity with an Impact Tester",* Hungarian Standard No. MSZ 14-05007-87, Jan. 30th, 1987.

[26] B. T. Fedoroff and O. E. Sheffield, *"Encyclopedia of Explosives and Related Items",* PATR 2700, Vol. 6, Picatinny Arsenal, Dover, N. J., 1974, p. G155.

[27] M. A. Schrader, M. W. Leeuw and A. C. Van der Steen, "The Thermal Step Test: A Key to High Temperature Behavior of Explosives", [Proc.] *9th Int. Pyrotech. Seminar,* Colorado Springs, Aug. 1984, pp. 881-890.

[28] Yu. Ya. Maksimov, N. V. Polyakova and V. F. Sapranovich, „Nitromethylbenzenes Thermal Decomposition*", Tr. Mosk. Khim.-Tekhnol. Inst. Mendeleeva 83*, 55-60 (1974).

[29] R. N. Rogers, „Thermochemistry of Explosives*", Thermochim. Acta 11*, 131-139 (1975).

[30] Yu. Ya. Maksimov, L. S. Glushetskaya and S. B. Sorochkin, „Termicheskoye razlozheniye i davleniye parov trinitrokrezola i trinitroanizola (Thermal Decomposition and Vapor Pressure of Trinitrocresole and Trinitroanizole*)", Tr. Mosk. Khim.-Tekhnol. Inst. Mendeleeva 104*, 22-27 (1979).

[31] S. Zeman, "Possibilities of Applying the Piloyan Method of Determination of Decomposition Activation Energies. Part. IV. "1,3,5-Trinitrobenzene, 2,2',4,4',6,6'-Hexanitrobiphenyl, 2,2',2'',4,4',4'',6,6',6''-Nonanitro-m-terphenyl, 1,4,5,8-Tetranitronaphthalene and 2,4,6-Tripicryl-1,3,5-triazine", *J. Thermal Anal. 19,* 207-214 (1980).

[32] K. K. Andreev, *„Termicheskoye razlozheniye i goreniye vzryvchatykh veschestv (Thermal Decomposition and Combustion of Explosives)"*, Izdat. Nauka, Moscow, 1966; Transl. as U. S. Govt. Rep. AD-693600, NTIS, Springfield (1969).

[33] Yu. Ya. Maksimov and S. B. Sorochkin, „Termicheskoye razlozheniye 3,3'-dimetilgeksanitrodifenila (Thermal Decomposition of 3,3'-Dimethylhexanitrobiphenyl)*",. Tr. Mosk. Khim.-Tekhnol. Inst. Mendeleeva 112*, 36-39 (1980).

[34] S. Zeman, „Kinetic Data from Low-Temperature Thermolysis in the Study of the Microscopic Initiation Mechanism of the Detonation of Organic Polynitro Compounds", *Thermochim. Acta 49*, 219-246 (1981).

[35] Yu. Ya. Maksimov and E. N. Kogut, „Termicheskoye razlozheniye tverdykh aromaticheskikh nitrosoedinenii (Thermal Decomposition of Aromatic Nitrocompounds in the Solid State)", *Khim. Khim. Tekhnol. 20,* 349- (1977)

[36] Yu. Ya. Maksimov, "O vliyanii agregatnogo sostoyaniya par-zhidkost na skorost termicheskogo raspada aromaticheskikh polinitrosoedinenii (On Vapor-Liquid State Influence on the Thermal Decomposition of Polynitro Arenes)", *Zh. Fiz. Khim. 45,*1193- (1974).

[37] Yu. Ya. Maksimov and L. A. Shipitsin, „O temperaturnom predele primeneniya vzryvchatykh aromaticheskikh nitrosoedinenii v glubokikh skvazhinakh (On the Temperature Threshold of Nitroaromatic Explosives Application in Deep Holes)", *Prikl. Geofiz. 73,* 195-199 (1974).

[38] S. Zeman, „The Thermoanalytical Study of some Aminoderivatives of 1,3,5-Trinitrobenzene", *Thermochim. Acta 216*, 157-168 (1993).

[39] H. Őestmark, H. Bergman and G. Aqvist, "The Chemistry of 3-Nitro-1,2,4-triazol-5-on – Thermal Decomposition", *Thermochim. Acta 213,* 165-175 (1993).

[40] G. B. Manelis, *„Problemy kinetiki elementarnykh khimichaskikh reaktsii (Problems of the Kinetics of Elementary Chemical Reactions):,* Izdat. Nauka, Moscow, 1973, p. 93-108.

[41] M. E. Grice, D. Habibollahzadeh and P. Politzer:, „Calculated Structure, Heat of Formation and Decomposition Energetics of 1,3-Dinitro-1,3-diazacyclobutane", *J. Chem. Phys. 100*, 4706-4707 (1994).

[42] A. J. B. Robertson, "The Thermal Decomposition of Explosives. Part II. Cyclotrimethylenetrinitramine and Cyclotetramethylenetetranitramine", *Trans. Faraday Soc. 45,* 85-93 (1949).

[43] R. N. Rogers, "Differential Scanning Calorimetric Determination of Kinetics Constants of Systems that Melt with Decomposition", *Thermochim. Acta 3*, 437-447 (1972).

[44] S. Zeman, "Analysis and Prediction of the Arrhenius Parameters of Low-Temperature Thermolysis of Nitramines by Means of the ^{15}N NMR Spectroscopy", *Thermochim. Acta . 333,* 121-129 (1999).

[45] S. Lűbbecke, M. A. Bohn, A. Pfeil and H. Krause, "Thermal Behavior and Stability of HNIW (CL-20)", [Proc.] *29th Int. Annual Conf. ICT,* Karlsruhe, 1998, p. 145/1.

[46] S. Zeman, M. Andoga and A. Tall, „Specification of Kinetics Parameters of the Nitramines Thermolysis by means of DSC", [Proc.] *Conf. Thermal Anal., 11th THERMANAL '88,* High Tatras, Slovakia, Sept. 1988, pp. C9-C12.

[47] J. Köhler and R. Meyer, *"Explosives",* 4th Edition, VCH Verlagsgesellschaft mbH, Weinheim, 1993.

[48] S. M. Kaye, *"Encyclopedia of Explosives And Related Items",* Vol. 8, PATR 2700, U. S. Army Armament Res. & Develop. Command, Dover, N. J., 1978, p. O37.

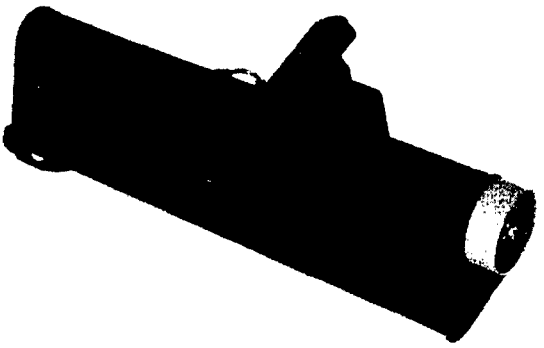
[49] B. T. Fedoroff and O. E. Sheffield, *"Encyclopedia of Explosives and Related Items",* PATR 2700, Vol. 5, Picatinny Arsenal, Dover, N. J., 1972, pp. D1478-D1480.

[50] Ou Yuxiang, Wang Cai, Pan Zelin and Chen Boren, "Sensitivity of Hexanitrohexaazaisowurtzitane", *HenNeng CaiLiao 7,* 100-102 (1999).

[51] R. M. Doherty and R. L. Simpson, „A Comparative Evaluation of Several Insensitive High Explosives". [Proc.] *28th Int. Annual Conf. ICT,* Karlsruhe, June 1997, pp. 32/1-32/23.

OUR GOODS & SERVICES SAVE YOUR LIVES

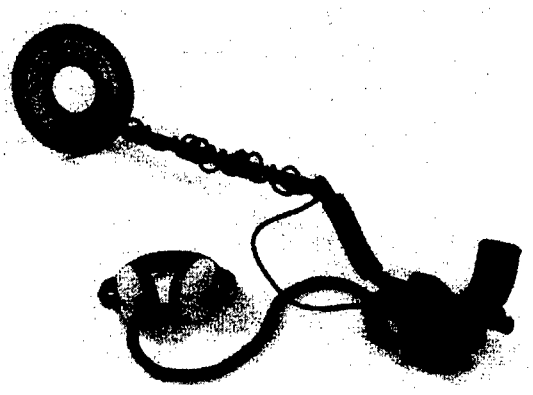
EXPLOSIVE DETECTOR



- Detect all commercial & military explosives, plastic explosives and marking additives
- Accessories for particle detection
- Not required warm-up time
- Can be connect to PC
- Battery life 5,5 hours

METAL DETECTORS

Wide range of metal detectors for field and underwater operations:



- Demining & UXO clearance
- Rivers & fords inspection
- Underwater operations
- Personnel checking
- Deep buried objects locating

SERVICE concerning

Explosives, UXO clearance & Ammunition

- Advice & Consultancy
- Expertises for court purposes
- Research & Development
- EOD training

For more details contact please:

Dr. CHLADEK, E-mail: chladekmail@seznam.cz, fax: +420 2 57922907

zeman®

Jiří Chládek AALL

ZEMAN AM - technical specification

Special boots with protection against anti-personnel contact mines
with charge of **35-50 g High Explosives**

Technical specification of blast protective boots:



- Upper material grain leather, hydrophobic, smooth, thickness of 2.0 - 2.2 mm
- Leather counter
- Double thermal toe puff
- Special lasting insole from ballistic material of the thickness of 7 mm
- Bottom design with use of sewn through technology
- Special rubber sole with the thickness of 20 mm combined with ballistic material while preserving sufficient flexibility
- Closed tongue
- Leather collar bandage
- Sock lining absorbing treading energy in toe
- Lacing - 4 eyelets 5 passes through
- Thread stitching 1000

- **Black colour**
- **Boot height:** 30 cm
- **Weight:** 2980 g
- **Sizes:** 6-12

Producer: **ZEMAN COMPANY**
e-mail:zemanl@zeman.cz
www: www.zemanshoe.com

Technical support: **Dr. Jiri CHLADEK**
e-mail: chladekmail@seznam.cz

Dr. E. Beneše 1029 • 765 02 Otrokovice • Czech republic
ICO: 63481499 • DIC: 346 - 63481499
Phone: +420 67 7923910 • Fax: +420 67 7922024

UP 02-22

ISBN 80-7194-435-1